ASSESSING EARTHQUAKE HAZARDS AND REDUCING RISK IN THE PACIFIC NORTHWEST

Volume 1

U.S. GEOLOGICAL SURVEY PROFESSIONAL PAPER 1560

Cover. *Insert*, ground-shaking damage from the 1949 Puget Sound earthquake to unreinforced masonry in Seattle, Wash. Photograph by George Cankonen, Seattle Times. *Background*, landslide damage to the railbed between Olympia and Tumwater, Wash., in the 1965 Puget Sound earthquake. Photograph by Greg Gilbert, Daily Olympian.

Cover design by Carol A. Quesenberry.

Assessing Earthquake Hazards and Reducing Risk in the Pacific Northwest

Albert M. Rogers, Timothy J. Walsh, William J. Kockelman, *and*
George R. Priest, *Editors*

Volume 1

U.S. GEOLOGICAL SURVEY PROFESSIONAL PAPER 1560

An investigation of the earthquake potential in the Pacific Northwest and examination of the measures necessary to reduce seismic hazards

UNITED STATES GOVERNMENT PRINTING OFFICE, WASHINGTON : 1996

U.S. DEPARTMENT OF THE INTERIOR
BRUCE BABBITT, Secretary

U.S. GEOLOGICAL SURVEY
Gordon P. Eaton, Director

For sale by U.S. Geological Survey, Information Services
Box 25286, Federal Center
Denver, CO 80225

Library of Congress Cataloging-in-Publication Data

Assessing earthquake hazards and reducing risk in the Pacific Northwest / Albert M. Rogers...[et al.], editors.
p. cm.—(U.S. Geological Survey professional paper ; 1560)
Includes bibliographical references.
Supt. of Docs. no.: I 19.16:1560
1. Earthquake hazard analysis—Northwest, Pacific. 2. Earthquakes—Northwest, Pacific. I. Rogers, A.M. II. Series.
QE535.2.U6A825 1997
363.3′495—dc20 95–37559
CIP

PREFACE

To increase knowledge and understanding of geologic hazards and risk in the Pacific Northwest, the U.S. Geological Survey initiated a research program focused on these issues in the late 1970's (volcanic hazards have traditionally been studied separately). This study area was chosen for several reasons. Large, damaging earthquakes are part of the regional documentary record, yet for various reasons we do not have confidence in existing estimates of earthquake hazards. New information has increased our concern about the potential for great subduction-zone earthquakes and large, shallow earthquakes. Furthermore, the rapid increase in population density and urban development in this area during the last decade has increased the seismic risk. For these reasons, funding for these studies was increased in 1987 to support a 5-year accelerated research program under the sponsorship of the National Earthquake Hazards Reduction Program. The studies were primarily conducted under an element of the national program termed "Urban and Regional Hazards Assessment," which previously supported intensive studies in Salt Lake City, Utah, and Los Angeles and San Francisco, Calif. Typically, scientists, engineers, and sociologists from Federal agencies, State geological organizations, universities, and private industry have participated in this research program. Some of the scientific studies from the first 3 years of the program are presented in this professional paper. The overview chapter summarizes the state of knowledge concerning geologic hazards and risk in this region through 1991, including the studies herein and other relevant studies.

The broadest goals of this professional paper are to promote the recognition, assessment, and reduction of earthquake hazards in the Pacific Northwest. Engineers, planners, decisionmakers, and land and building owners should, in the long term, use this information to reduce the effects of expected future earthquakes in Washington, Oregon, northern California, and British Columbia, Canada.

Because persons in many parts of society are responsible for understanding earthquake hazards and making decisions to reduce earthquake effects, we hope this professional paper will have a wide audience. To some extent, the diversity in the contents of the paper reflects the diversity of the audience. Although many of the research reports address specialists having some familiarity with the geologic and geophysical sciences and earthquake-hazard mitigation, the overview chapter and reports on implementation of hazard-reduction techniques (volume 2) are intended to inform both technical and nontechnical readers. To further aid the lay reader, we have defined technical terms used throughout the professional paper in the glossary.

A.M. Rogers
T.J. Walsh
W.J. Kockelman
G.R. Priest

CONTENTS

VOLUME 1

INTRODUCTION

Preceding page. *Insert,* debris left by the April 29, 1965, Seattle, Wash., earthquake. Photograph courtesy of NOAA/EDIS. *Background,* destruction caused by the fall of an unbraced masonry parapet in downtown Klamath Falls, Oreg., during the Sept. 20, 1993, *M* 5.9 and *M* 6.0 earthquakes. Photograph by Lou Sennick of the Herald and News, Klamath Falls, Oreg. (from Dewey, J.W., 1993, Damages from the 20 September earthquakes near Klamath Falls, Oregon: Earthquakes & Volcanoes, v. 24, no. 3, p. 121–128).

EARTHQUAKE HAZARDS IN THE PACIFIC NORTHWEST—AN OVERVIEW

By Albert M. Rogers,[1] Timothy J. Walsh,[2] William J. Kockelman,[3] *and* George R. Priest[4]

ABSTRACT

Scientific research on earthquake hazards in the Pacific Northwest through 1991 suggests that the potential for large earthquakes and losses is greater than has been previously recognized. A great earthquake of magnitude 8 or more on the thrust fault that separates the North America and Juan de Fuca plates (commonly termed the Cascadia thrust or megathrust fault) or a large earthquake of about magnitude 8 or less on shallow faults in the continental crust would produce much greater damage than previously experienced by the modern inhabitants of this region. Furthermore, damaging events similar to the 1949 and 1965 Puget Sound earthquakes, which occurred in the subducted Juan de Fuca plate, are expected to recur. In some circumstances, marginally different locations or larger magnitudes for these earthquakes could substantially increase the levels of damage compared to levels observed historically.

A variety of geologic and geophysical data suggest that great earthquakes (those with magnitudes between 8 and 9.5) have occurred in the last 7,000 years on the Cascadia thrust fault. First, marsh deposits along parts of the Washington and Oregon coast record episodic sudden submergence. The sudden submergence events, which have been inferred from peaty soils overlain by tidal mud deposits in coastal estuaries, have been ascribed to tectonic subsidence associated with past great earthquakes along the Cascadia thrust fault. In some places, the buried peaty soils are capped by thin sand layers that suggest sand-bearing tsunamis caused by some earthquakes coincided with the drowning of tidal wetlands. Second, geodetic measurements suggest that the continental crust in western Washington is undergoing compression, where the direction of maximum compressional increase is parallel to the direction of convergence between the Juan de Fuca and North America plates. Third, Pleistocene and Holocene folding and faulting of offshore and coastal sediments are evidence of deformation that may have accompanied subduction. Fourth, the Cascadia subduction zone has several characteristics similar to those in other subduction zones that have produced great earthquakes historically. And fifth, ground shaking during prehistoric earthquakes may have triggered 13 seafloor turbidite deposits at widely scattered locations along the Cascadia subduction-zone margin. Most scientists believe that these and other data are consistent with continued subduction, and some believe the data are consistent with seismic subduction and great prehistoric earthquakes.

High-precision radiocarbon ages suggest that the last sudden coastal submergence and tsunami occurred about 300 years ago. The time between great earthquakes, however, may range from a few centuries to more than a millennium. At present, a reliable forecast of the time until the next great earthquake is not possible. Nonetheless, because the effects of a great earthquake are likely to be substantial and widespread, such an event should be considered in earthquake risk assessment and disaster planning for the region.

The consequences of a great earthquake on the Cascadia thrust fault are significant because of the large area exposed to most types of earthquake hazards. Damaging shaking may reach across much of western Oregon, western Washington, and northern California. This type of earthquake may also produce widely scattered ground failure in susceptible areas. Tsunami and seiche that may accompany a great earthquake can further compound the levels of damage from ground failure and shaking in coastal areas.

Some scientists, however, think that subduction of the Juan de Fuca plate is aseismic. For example, no great earthquakes have occurred since the arrival of European settlers in the area, nor have sensitive seismographs detected small earthquakes on the Cascadia thrust fault. The case for aseismic subduction is also based on inferences from theoretical modeling about fault-zone properties and slab temperatures that suggest the downdip width of the locked section of the thrust fault is limited. The maximum magnitude of great

[1]U.S. Geological Survey, Box 25046, MS 966, Federal Center, Denver, CO 80225.

[2]Washington Department of Natural Resources, PY-12, Olympia, WA 98504.

[3]Deceased.

[4]Oregon Department of Geoscience, 910 State Office Building, 1400 S.W. 5th Ave., Portland, OR 97201.

Cascadia thrust-fault earthquakes may be limited and, if some model predictions prevail, seismic subduction may even be precluded. It is also argued that some estuary submergence events may have causes other than great earthquakes. For example, the effects of eustatic sea-level rise, dating procedures, and local tectonics cloud the interpretation of some of the submergence events. Yet, the evidence for great earthquakes appears stronger than the evidence against them.

The potential for shallow continental-crust earthquakes of about magnitude 8 or less is also increasingly apparent. New geologic evidence indicates that faults capable of generating large continental-crust earthquakes may exist in western Washington, western Oregon, and northwestern California. These earthquakes have the potential to produce locally higher levels of damage than great subduction earthquakes where they underlie or pass near urban areas. The long-term hazards from earthquakes on these faults are unknown because many shallow faults may be unmapped, and earthquake recurrence rates and maximum magnitudes on these faults are unknown.

Intermediate-depth earthquakes (40–80 km deep in the subducted Juan de Fuca plate), similar to those in 1949 and 1965, are expected to recur. These earthquakes may occur on a shallower part of the subducted plate, may strike closer to urban areas, or may have greater magnitudes than those in the past. A maximum magnitude of about 8 is possible for this type of earthquake. Hence, these earthquakes have the potential to produce greater damage and life loss than has been observed historically. Earthquake risk assessment and disaster-planning efforts should also include these hypothesized earthquakes.

Much new research, presented in this professional paper and other recent studies, stimulates increased awareness of earthquake hazards in the Pacific Northwest and encourages steps to reduce the risk. Such steps should involve hazard prediction, loss estimation, citizen education, disaster management, urban planning, and continued evaluation and enforcement of earthquake building codes.

INTRODUCTION

The Pacific Northwest is a very large region that includes all of Oregon, Washington, northern California, and western British Columbia, Canada. In this professional paper, Pacific Northwest refers primarily to the area west of the Cascade Range in this region, including Vancouver Island (figs. 1 and 2). The study area is large enough to facilitate understanding of earthquake hazards with a tectonic-province perspective. Although our discussion of the Pacific Northwest involves the entire region, much of the research reported in this professional paper necessarily focuses on topical studies within smaller areas, primarily in Washington and Oregon. Unfortunately, the topical and geographic limits of this research currently preclude a full description and understanding of earthquake hazards. Because some issues are complex and cannot be simplified without losing significant understanding, we recommend reading other discussions to further clarify some aspects of the issues or to provide additional detail and a different perspective (for example, Riddihough, 1978; Heaton and Hartzell, 1987; Noson and others, 1988; Rogers, 1988a, 1988b; Shedlock and Weaver, 1991).

Recent research has also exposed several new and significant unresolved issues that continue to be studied and discussed. These issues are to some extent a consequence of the remarkable diversity and complexity of past and present tectonic processes, a fact that may permit multiple interpretations of the same data. But the variety of interpretations also results from scant data and the infancy of scientific research on some topics. Future data collection, new techniques, and continued research will ultimately result in greater understanding of earthquake hazards than is currently possible. The present state of knowledge, however, is sufficient to continue planning and decision making to reduce the risks caused by future earthquakes. Both increasing understanding of the hazards and efforts to reduce them should be viewed as long-term goals spanning decades or more, steps that will ultimately increase the level of protection for urban areas in this region.

ACKNOWLEDGMENTS

The authors are grateful for the exceptionally thorough reviews of this chapter provided by Brian Atwater, Craig Weaver, and Robert Crosson. Their comments helped to significantly improve the clarity, organization, and accuracy of the manuscript. Written comments and discussions provided by William Spence, James Savage, David Perkins, and S.T. Algermissen helped clarify several issues for the authors. We also benefited from discussions, preprints, fault mapping, and partial reviews by Parke Snavely, Jr., Samuel Clarke, Ian Madin, Garry Carver, Alan Nelson, Verne Kulm, R.D. Hyndman, and James Yount. We thank Arthur Tarr for helping to complete the seismicity figure using GIS. We wish to thank Barbara Hillier and John Synnefakis, our U.S. Geological Survey technical editors, for their tremendous efforts in providing each author with final editing copy and for their managing of the details of the completion of this publication. Without their help, this publication would not have been possible.

We deeply regret the untimely death of our co-editor, William J. Kockelman. Bill was a tremendous help in the completion of this paper. The Implementation section of the professional paper could not have been produced without his participation. But beyond this paper, he also contributed significantly to earthquake hazard awareness in the Pacific Northwest, Utah, California, and elsewhere through his

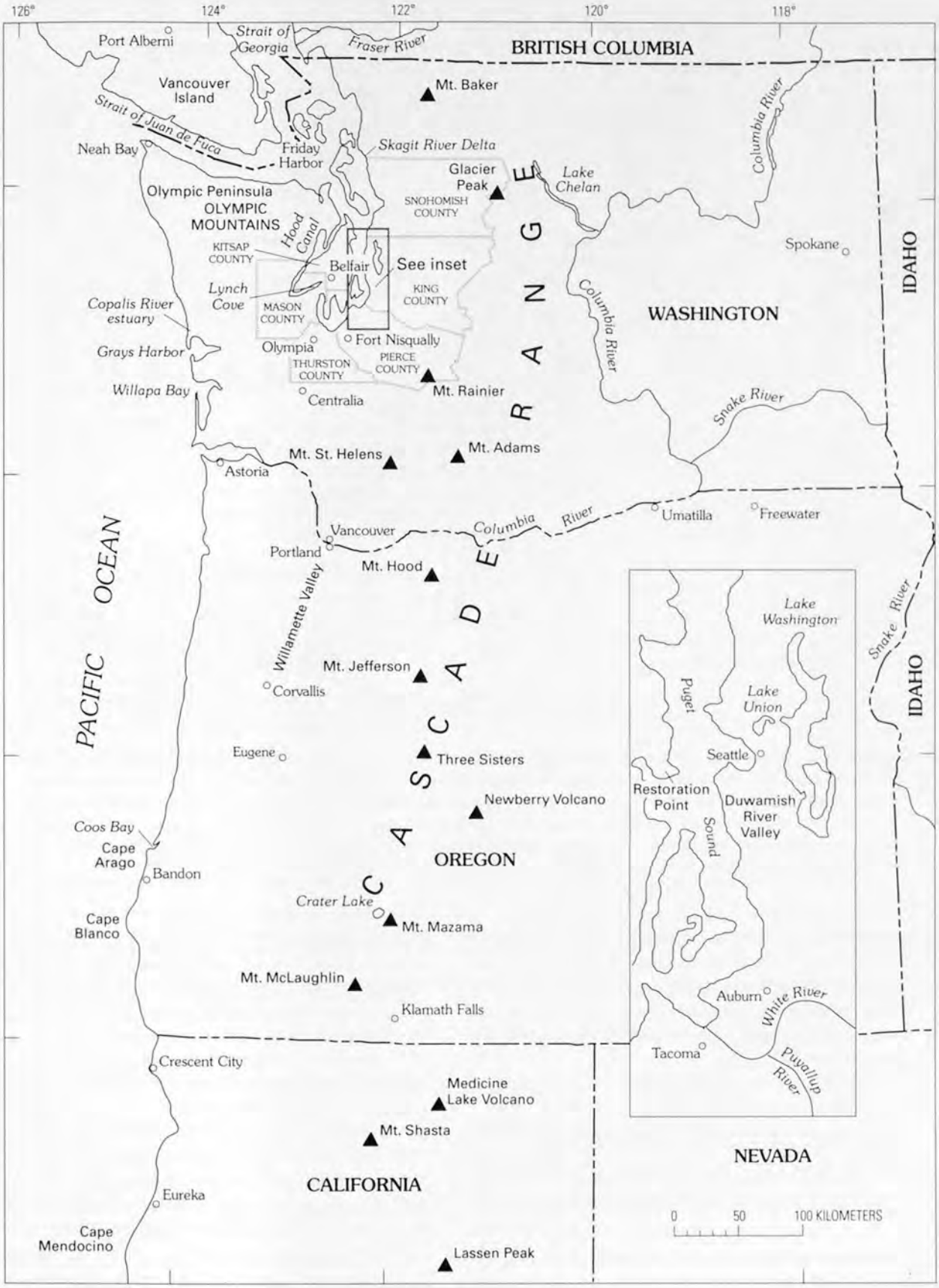

Figure 1. Index map of the Pacific Northwest study area. Triangles show major Quaternary volcanoes.

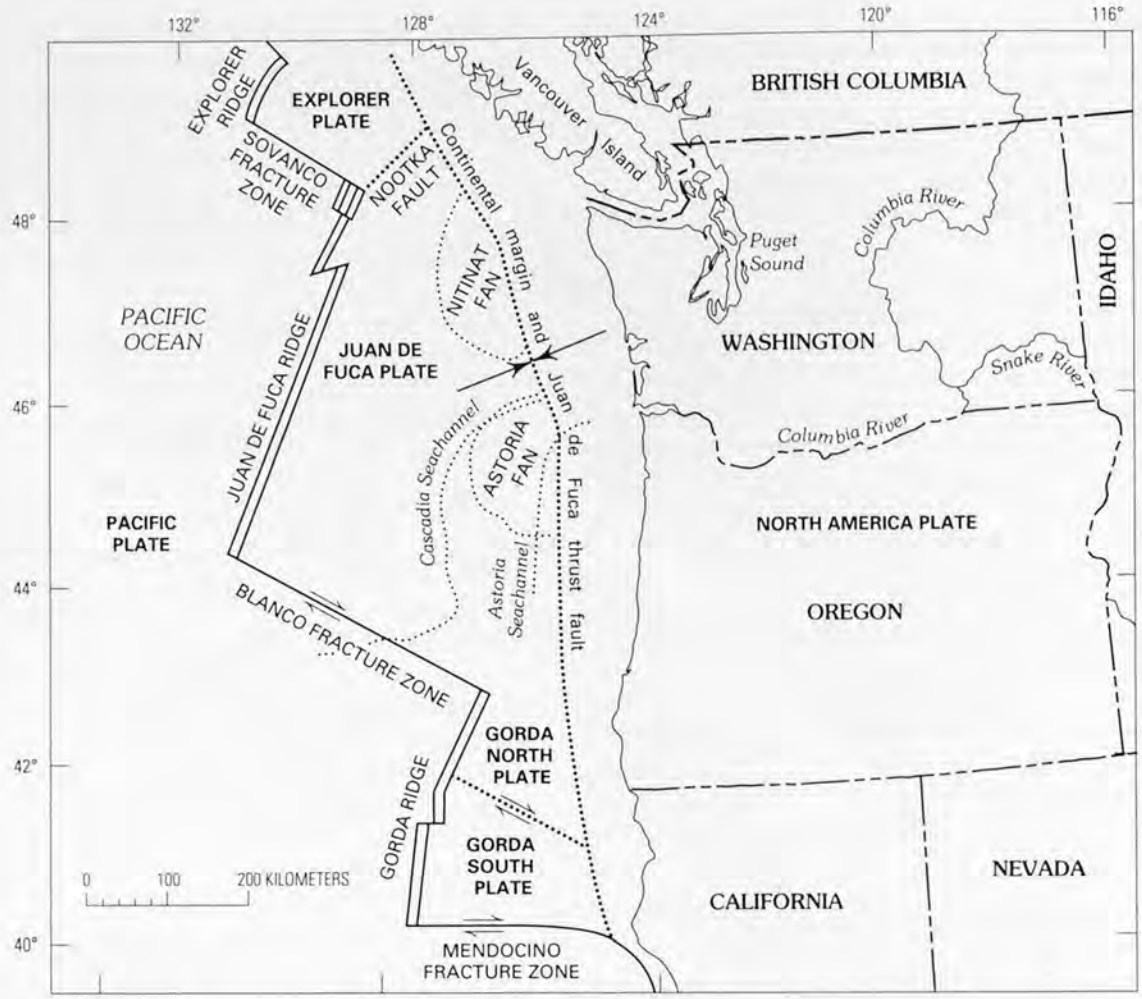

Figure 2. Major geologic features in the Pacific Northwest. Barbs show relative slip directions across fracture zones. The arrows show the direction of relative convergence between the North America and Juan de Fuca plates. Ridges are major fractures in the lithosphere where plates separate and new crustal material is emitted. The fracture zones are strike-slip transform faults that accommodate differential motion between plates. The dotted line marking the continental margin is the western boundary of the main thrust fault where the oceanic plate begins to underthrust or subduct beneath the continental plate.

extensive participation and leadership in workshops on this topic on a number of occasions and his publication contributions. His dedication to increasing public awareness of the earthquake hazard in many regions is widely recognized and appreciated. As a personal friend to each of the co-editors of this paper, he will be missed.

RECOGNIZING POTENTIAL EARTHQUAKE HAZARDS AND RISK IN THE PACIFIC NORTHWEST

The earliest inhabitants of the Pacific Northwest suffered the consequences of a wide range of geologic hazards (Heaton and Snavely, 1985; Grant and Minor, 1991). Even though generations of retelling have left some aspects unclear, stories are still told among native peoples concerning some of these events. Stories told by the Makah and other tribes suggest the occurrence of a large tsunami along the coast of Washington. Yurok mythology relates the existence of a powerful earthquake god (Heaton and Snavely, 1985), and the Chinook have traditions describing earthquakes that shook their houses and raised the ground (Gibbs, 1955); Gibbs (1955) noted evidence for recent raising and lowering of the land at Shoalwater (now Willapa) Bay, Wash., a locale of the Chinook tribe. Recent findings about the geology of the region suggest that at least some of these traditions have basis in fact (for example, Atwater, this volume).

Some early events are unequivocal in the documentary record. A large ash fall between 1770 and the early part of the 19th century contributed to sickness and death in the

Table 1. Large, damaging earthquakes of the Pacific Northwest since 1833.

[Modified Mercalli intensity (MMI) of VII or greater. Intensity values adopted from Algermissen (1983) unless footnoted. Leaders (---), no data available]

Date	Location	Maximum MMI	Surface wave magnitude (M_s)
Dec. 14, 1872	Near Lake Chelan, Wash.	IX[1]	[2]7 – 7.4
Nov. 22, 1873	Southwestern Oregon	VIII	[3]6.7
Oct. 12, 1877	Cascade Range, Oregon	VIII	---
Mar. 7, 1893	Umatilla, Oreg.	VII	---
Apr. 14, 1898	Mendocino County, Calif.	VIII–IX	---
Mar. 17, 1904	About 60 km northwest of Seattle, Wash.	VII	---
Jan. 11, 1909	North of Seattle, near the British Columbia border	VII	---
Dec. 6, 1918	Vancouver Island, British Columbia	VIII[2]	7
Jan. 24, 1920	Strait of Georgia, British Columbia	VII[2]	---
Jan. 22, 1923	Cape Mendocino (offshore), Calif.	VII–VIII	[4]7.3
July 15, 1936	Near Freewater, Oreg.	VII	[2]5.7
Nov. 13, 1939	Northwest of Olympia, Wash.	VII	[2]5.8
Apr. 29, 1945	About 50 km southeast of Seattle, Wash.	VII	---
Feb. 15, 1946	About 35 km north-northeast of Tacoma, Wash.	VII	6.3
June 23, 1946	Vancouver Island, British Columbia	VIII[2]	[5]7.2 – [6,7]7.3
Apr. 13, 1949	Between Olympia and Tacoma, Wash.	VIII	[6,7]7.1
Apr. 29, 1965	Between Tacoma and Seattle, Wash.	VIII	[8]6.5
Nov. 8, 1980	North of Cape Mendocino (offshore), Calif.	VII	[9]7.0 – 7.2
Aug. 17, 1991	Near the coast of northern California	VII[9]	[10]6.2
Apr. 25, 1992	Near the coast of northern California	IX[11]	[11]7.1
Mar. 25, 1993	Near the Washington-Oregon border	VII[12]	[6,12]5.5
Sept. 21, 1993	Near Klamath Falls, Oreg.	VII[13]	[13]5.7 – 5.9

[1]M.G. Hopper, written commun., 1990.

[2]Estimated maximum MMI or magnitude estimated from MMI data. The magnitude of the 1872 earthquake is estimated as M 7.4 (Malone and Bor, 1979), assuming a depth of 60 km; M 7 is estimated from the maximum MMI of IX, itself estimated assuming a shallow crustal depth (M.G. Hopper, written commun., 1990).

[3]Toppozada and others (1981).

[4]Coffman and Hake (1973).

[5]Rogers and Hasegawa (1978).

[6]Body-wave magnitude, m_b.

[7]Abe (1981).

[8]m_b or M_s, Algermissen and Harding (1965).

[9]Person (1981).

[10]U.S. Geological Survey (1991). Several other large earthquakes occurred within a month to several hours of this event; they were farther offshore and did not produce onshore MMIs above V. These earthquakes occurred on July 13 (M_s 6.9, MMI V), August 16 (M_s 6.3, MMI V), and August 17 (M_s 7.1, MMI V).

[11]Oppenheimer and others (1993). This earthquake is significant not only because it produced considerable damage (estimated between $48 and $66 million, but because it may have occurred on the Cascadia thrust fault or a subparallel fault. In either case, it likely indicates active subduction of the Gorda plate. The earthquake was followed by two large aftershocks on April 26 that also caused damage (both M_s 6.6, MMI VIII).

[12]U.S. Geological Survey (1993).

[13]U.S. Geological Survey (1993). An aftershock with about the same magnitude and location occurred about 2 hours after the main shock. Another earthquake in this series that produced MMI VII occurred on December 12.

Sanpoil tribe (possibly several eruptions from Mt. Hood, Glacier Peak, or Mount St. Helens; see fig. 1) (Coombs and others, 1977). The earliest documented earthquake was associated with the 1820 eruption of Mt. Rainier (then called Mt. Tacoma) (Coombs and others, 1977). Settlers at Fort Nisqually, Wash. (fig. 1), felt another earthquake in 1833 (Bradford, 1935). In 1872, European settlers and Indians alike reported the effects of the magnitude (M) 7.4 Lake Chelan earthquake, which was felt from Eugene, Oreg., to British Columbia. The direct and indirect effects of this earthquake caused many deaths among the Indians. Even though no mortality figures exist, multiple accounts mention deaths from rock falls, emissions of poisonous gases, and famine following the earthquake (Coombs and others, 1977). Altogether, at least 57 earthquakes in the Pacific Northwest have been large enough to produce some damage (Modified Mercalli intensity, or MMI, VI or greater; Coffman and Hake, 1973). A few of these earthquakes caused or had potential to cause substantial damage (MMI VII or greater) (table 1; figs. 3–5).

Figure 3. Ground-shaking damage from the 1949 earthquake to unreinforced masonry in Seattle. Photograph by George Cankonen, Seattle Times.

Recently collected geologic and geodetic data (Darienzo and Peterson, 1990; Savage and others, 1991; Adams, this volume; Atwater, this volume; Nelson and Personius, this volume; Peterson and Darienzo, this volume) suggest that the region could have major earthquakes along the Cascadia subduction zone in the future. Future rupture of a 300- to 1,200-km segment of the Cascadia thrust fault would produce a great earthquake of *M* 8–9.5 (Heaton and Hartzell, 1987), which is much larger than any historical earthquake in the region. Although historical earthquakes have had a significant impact on the Pacific Northwest, no great earthquakes (*M* 8 or greater) have occurred in the Pacific Northwest in the 200-year record of European settlement, and none have had the intensity or the geographic extent of damage that is likely in a great Cascadia thrust-fault event.

Unfortunately, little information currently exists concerning great-earthquake characteristics such as frequency, size, expected location, and expected intensity and geographic distribution of ground shaking and ground failure. Furthermore, the frequency of large, damaging earthquakes is low compared with many subduction zones around the world. The apparent discrepancy between the historical and geologic records, differing interpretations of these and other relevant data, and scant data on some of the aspects just noted have produced uncertainty and debate regarding the degree of earthquake hazard from great earthquakes.

It is difficult to establish the full consequences of a great earthquake in this region for several reasons. First, some properties of the earthquake source area, including the lateral and downdip extent of the expected rupture area, are not established; the dimensions of the slipping section of the fault strongly control the magnitude of the expected earthquake and the proximity of the fault section that produces ground shaking in urban areas. If the slipping section of the Cascadia thrust fault is close to urban areas, the hazard will be greater than if it is distant. Second, the attenuation of strong ground shaking in this region is not adequately known for any earthquake source type. Third, the characteristics of ground-shaking effects related to geologic site conditions in urban areas are just beginning to be studied (Wong and others, 1990; Carver and others, volume 2; Madin, volume 2), yet these effects could strongly influence the levels of shaking in urban areas. Until many of these issues are better

Figure 4. Ground-shaking damage from the 1949 earthquake to the brick veneer of a Centralia, Wash., building. The parapet collapse resulted in one death. Photograph from the A.L. Miller Collection, University of Washington archives.

Figure 5. Landslide damage to the railbed between Olympia and Tumwater, Wash., in the 1965 earthquake. Photograph by Greg Gilbert, Daily Olympian.

resolved, our understanding of the level of hazard from an earthquake of this type will remain uncertain.

Should a great earthquake occur, the resulting shaking and ground failure likely will affect a wide region because of the great length and shallow dip of the Cascadia thrust fault; other hazards such as tsunami and seiche are also likely. Thus, in a single great earthquake, this combination of effects could produce concurrent damage in many urban centers along the western regions of Oregon, Washington, northern California, and British Columbia.

Aside from the great-earthquake issue, however, the historical and geologic records tell us that large earthquakes can be expected on faults other than the Cascadia thrust fault. For example, large continental-crust earthquakes have occurred on Vancouver Island and possibly in the northern Cascade Range. Geologic evidence suggests that young, shallow faults may exist close to major population centers in both the Puget Sound and Willamette basin regions (for example, see Wilson and others, 1979; Harding and others, 1988; Bucknam and Barnhard, 1989; Yeats, this volume). Because of the proximity of shallow faults to developed areas, moderate to large earthquakes on these faults might be as damaging in urban areas as more distant earthquakes on the Cascadia thrust fault.

Continued subduction of the section of the lithosphere below the Cascadia thrust fault is likely to produce 1949- and 1965-style earthquakes with no further convergence between the North America and Juan de Fuca plates. The occurrence of earthquakes similar to those in the past, but with slightly different magnitudes or locations, could lead to greater loss of life and property than has been observed historically. Together, the 1949 and 1965 earthquakes in the Puget Sound region caused well over $200 million (in 1984 dollars) in property damage and 15 deaths (May and Noson, 1986). The U.S. Geological Survey (1975) estimated that an earthquake similar to the 1949 event could result in 2,200 deaths, 8,700 serious injuries, and as many as 23,500 homeless in the Washington counties of King, Kitsap, Mason, Pierce, Snohomish, and Thurston (fig. 1). The hypothetical Benioff-zone earthquake (see the glossary) assumed in that study produced effects more severe than the 1949 and 1965 events, for several reasons. The assumed magnitude (M 7.5) was larger, the assumed hypocenter was at shallower depth (50 km), and the assumed epicenter was closer to urban areas than the earlier earthquakes (of the scenarios considered in this study, the greatest life loss and injury was produced by an earthquake hypocenter beneath southern Seattle). Nonetheless, the assumptions are realistic for an earthquake of this type, which was a recognized earthquake source at the time of the study.

Infrastructure and population have significantly increased in Washington and Oregon since the 1975 estimates were made, adding to the number of lives and dollars at risk. May and Noson (1986) estimated that since the U.S. Geological Survey (1975) study, the population in the Puget Sound region alone has increased by 25 percent, and the total assessed value has increased by 240 percent. At present, however, we do not know the effects of these changes on anticipated losses.

Although the documented record of moderate earthquakes in the region has prompted some application of building codes to the development of modern infrastructure, it is possible that the hazards have been underestimated and that existing actions to reduce risk are inadequate, considering much new data. The most populous parts of Washington and Oregon lie within seismic zones 2 and 3 of the Uniform Building Code (International Conference of Building Officials, 1991), classifications that have special earthquake-resistant design requirements for certain types of structures. However, absence of the largest hypothesized earthquakes from the documentary record of the region may weaken the resolve among contemporary citizens to adapt and enforce hazard-reduction techniques. We know, for example, that some municipalities have not strictly enforced earthquake elements of the building codes (May and Noson, 1986). Lack of experience, debate about the level of hazard, and our scant knowledge regarding fundamental aspects of earthquake occurrence in this region hamper efforts to seek hazard-reduction measures.

THE NATURE OF EARTHQUAKE HAZARDS

A large earthquake can cause widespread regional damage resulting from several different geologic and seismic effects. An earthquake occurs when rocks on opposite sides of a fault move or slip abruptly in response to stress that exceeds the strength of the fault. In map view, the fault and associated fractures are commonly confined to a narrow zone a few meters to a few kilometers wide and several meters to a thousand or more kilometers long. The downdip extent of the fault, referred to as the fault width, can range from a few meters for a very small earthquake (magnitude less than 2) to 100 km or more for a very large earthquake (M 7.5 or greater). Not all earthquakes occur on faults that produce slip at the Earth's surface, a fact that damaging earthquakes of the Pacific Northwest commonly demonstrate (for example, see Weaver and Smith, 1983). Nonetheless, faults with surface expression do exist in this region (pl. 1), particularly offshore between the Cascadia thrust fault and the coast, and some of these faults (both onshore and offshore) have the potential to produce earthquakes.

In other areas, fault slip commonly inflicts damage on buildings, roadways, pipelines, or other structures lying within a fault zone that has surface expression. Disruption of lifelines (see the glossary) by faulting can have significant consequences in urban areas (Earthquake Engineering Research Institute, 1986). Young, mappable faults intersect

the land surface in this region in several places, and geophysical data suggest that many such faults may exist that are obscured by sediments (for example, Harding and others, 1988; Finn, 1990; Yount and Gower, 1991).

The destruction from an earthquake, however, commonly extends much beyond the rupture zone. Damaging energy in the form of seismic waves propagates away from the fault to distances as great as several hundred kilometers in a large earthquake. The strong shaking that occurs when the energy reaches the Earth's surface is responsible for the largest property and life loss in most earthquakes (figs. 3–5). Although shaking levels generally decrease with distance from the rupture because of the natural attenuation of the Earth and geometric spreading of seismic waves, levels of ground shaking can increase at sites underlain by soft soils or alluvium and (or) deep sedimentary basins. This effect is commonly termed "site amplification" or simply the "site effect." The phenomenon, which may be enhanced at distant sites by seismic-wave reflections from deep rock layers, was clearly seen in several recent earthquakes such as the 1985 Michoacan, Mexico; 1985 Chile; and 1989 Loma Prieta, Calif., events (Algermissen and others, 1985; Singh and others, 1988; Theil, 1990). In the 1985 Michoacan earthquake, collapsed or damaged buildings in Mexico City were nearly 400 km from the source. Soil amplification was a factor affecting shaking in the 1949 and 1965 Puget Sound earthquakes (Algermissen and Harding, 1965; Mullineaux and others, 1967; U.S. Geological Survey, 1975) and it is expected to be a factor during future earthquakes in the Pacific Northwest (Carver and others, volume 2; Madin, volume 2; Silva, volume 2).

Strong or prolonged shaking also produces other damaging geologic effects such as landslides (fig. 5), liquefaction, and lateral spreading. In some earthquakes, landslides and soil failure may produce greater damage and life loss than ground shaking, particularly for urban areas in mountainous terrain. Noson and others (1988) noted that as many as 14 earthquakes have caused landslides in Washington between 1872 and 1980. The 1949 and 1965 earthquakes triggered at least 105 separate landslides (Chleborad and Schuster, 1989). Potentially disastrous prehistoric landslides are known to have occurred, such as the Osceola mudflow that extended from the slopes of Mount Rainier down the White and Puyallup Rivers as far as the present-day location of Auburn and Tacoma (Crandell, 1971). Earthquake shaking may have induced some prehistoric landslides. For example, about 1,100 years ago, large-scale landsliding submerged blocks along the shore of Lake Washington (Jacoby and Williams, 1990; Jacoby and others, 1992); the timing of these landslides approximately coincides with other regional geologic events that may be earthquake related (for example, see Karlin and Abella, 1992; Schuster and others, 1992).

Liquefaction is a phenomenon wherein soils of certain types lose strength owing to the shaking-induced flow of water from depth towards the surface; lateral spreading is a related characteristic of soils that results in permanent horizontal displacement of the ground. Both phenomena can be destructive to facilities that lie in ground-failure zones. These effects may have caused as much as 25 percent of the damage in the 1949 and 1965 earthquakes in the Pacific Northwest (Grant, 1989).

Ground failure will occur in the future in the Pacific Northwest, induced by both rainfall and earthquake shaking. Schuster and Chleborad (1989), Chleborad and Schuster (volume 2), and Grant and others (volume 2), among others, have discussed the locations of past landslides and the areas susceptible to future landsliding.

Earthquakes and landslides offshore can produce large sea-wave trains, or tsunamis (see McCulloch, 1985, for a review). Tsunamis travel away from the source area at speeds of as much as 800 km/hour (McCulloch, 1985). Their height is low in the open ocean but can reach tens of meters on approaching shore, causing flooding of low-lying areas as much as thousands of kilometers from the source. The outer coasts of Washington, Oregon, and California are not only susceptible to tsunamis generated by earthquakes rupturing the Cascadia subduction zone (Hebenstreit, 1988), but they are also susceptible to smaller waves from distant earthquakes along the Aleutian and Japanese trenches (McCulloch, 1985). The tsunami from the 1964 Alaska earthquake damaged the Alaska, British Columbia, Washington, Oregon, and northern California coasts (including 13 killed and $11 million in damage, primarily at Crescent City, Calif.; McCulloch, 1985). Sand deposits in coastal Washington and Oregon suggest that tsunamis accompanied several large earthquakes on the Cascadia subduction zone in the last 5,000 years (Atwater, 1987; Bourgeois and Reinhart, 1988; Darienzo and Peterson, 1990; Atwater, this volume; Peterson and Darienzo, this volume). Bucknam and Barnhard (1989) and Bucknam and others (1992) found evidence for recent uplift of 7 m at Restoration Point in Puget Sound (fig. 1). If deformation of this type occurs suddenly, it is likely that a tsunami will be generated. In fact, evidence does exist that a tsunami occurred in Puget Sound in association with this uplift (Atwater and Moore, 1992). Permanent modification of the shoreline can also be expected.

Finally, damaging seiches can occur in the Pacific Northwest. A seiche is similar to the resonant sloshing of water in a bucket that has been disturbed. These waves, which are observed in lakes and other bodies of mostly enclosed water, can produce considerable damage and flooding along shorelines. Seiches are commonly induced by the long-period ground shaking that accompanies earthquakes but can also be induced by submarine or shoreline ground failure, sudden uplift or subsidence, or sudden tilt (McCulloch, 1985). Past earthquakes have caused seiches in Lake Washington and Lake Union in Seattle, as well as at other lakes in Washington and Oregon (see Thorsen, 1988, for a summary). It is reasonable to question whether the seismic- or nonseismic-induced collapse of a large delta such as the Skagit River delta (fig. 1) could produce a damaging water wave (McCulloch, 1985; Finn and others, 1989).

PACIFIC NORTHWEST EARTHQUAKES: ORIGIN, LOCATION, SIZE, AND TIMING

Most earthquakes in the Pacific Northwest are either directly or indirectly related to the interaction of the crustal plate system of the region, which includes the Pacific, Juan de Fuca, Gorda North, Gorda South, Explorer, and North America plates (fig. 2) (Atwater, 1970; Fox and Engebretson, 1983; Spence, 1989). Much evidence suggests that these brittle plates converge obliquely along the 1,200-km-long Cascadia subduction zone, causing the oceanic plates to descend, or subduct, beneath the continent (fig. 6). This process can lead to several types of earthquakes at widely separated locations not only offshore but throughout much of the western regions of Washington, Oregon, northern California, and British Columbia (figs. 7 and 8). We classify the earthquakes most likely to affect population centers in this subduction zone into four principal types based on fault location (fig. 6*C*): (1) shallow crustal earthquakes in the North America plate; (2) earthquakes that rupture faults within the subducted oceanic lithosphere below the thrust fault (these earthquakes partly define the dipping Benioff zone and commonly extend from the deepest section (20–30 km) of the locked thrust fault to as much as 80 km deep); (3) earthquakes on the main boundary thrust fault between the oceanic and continental plates (these earthquakes also help define the Benioff zone in some cases but not at the Cascadia subduction zone; and (4) shallow earthquakes within the oceanic plates or along plate margins. Earthquake types that occur on faults within plates are termed "intraplate events," and those along plate boundaries are termed "interplate events." All except type 3 earthquakes have been observed historically in the Pacific Northwest; evidence for this type, however, may exist in the geologic record (for example, Atwater and others, 1991; Atwater, this volume; Peterson and Darienzo, this volume).

In this report, we limit discussion of some earthquake sources because they are of little importance in seismic-hazard evaluation or are outside the study area. For example, significant earthquakes are likely east of the Cascade Range, which could affect urban areas on both sides of the Cascades. The largest historical earthquake in Washington and Oregon (*M* 7–7.4; see table 1) (Milne, 1956; Malone and Bor, 1979; M.G. Hopper, U.S. Geological Survey, written commun., 1989) was in 1872 and probably occurred outside our study region, near Lake Chelan. This was probably a crustal earthquake (Algermissen, 1983), but no surface expression of the fault has yet been found (Shannon & Wilson, Inc., 1977). As recently noted in California, however, shallow earthquakes on some thrust faults (termed blind thrusts) do not always rupture to the surface. Many young crustal faults exist east of the Cascades (pl. 1), and some of these faults may be capable of earthquakes that would affect urban areas on both sides of the Cascades (for example, see Hawkins, Foley, and LaForge, 1989; Peity and others, 1990). Although such faults are not the focus of this report and we do not discuss them further, we should be aware that they do contribute to the potential overall hazard in the study area.

Figure 6 (facing page). The Cascadia subduction zone from three different perspectives, emphasizing one or more aspects discussed in the text. *A*, the relationship between the principal geographic and geologic features in the Pacific Northwest. The shaded region is the contact zone between the North America and Juan de Fuca plates, termed the Cascadia thrust fault. The sloping lines on this fault are drawn primarily to aid in visualization of a three-dimensional effect, but the subducted plate may indeed be broken into one or more sections. MFZ, Mendocino fracture zone. Vertical scale is exaggerated. *B*, roughly east-west cross section through the Earth's crust and upper mantle near the latitude of Puget Sound, showing continental-plate compression and warping that occurs during the periods between great earthquakes and the resulting variability in uplift and tilt that is expected as a function of geographic position. The warping of the upper plate and the arch in the lower plate are greatly exaggerated. The subducted plate has a lower dip along the top of the arch, extending the thrust fault farther inland near Puget Sound than to the north or south. Potential segmentation of the slab may extend into the thrust fault or even into the oceanic lithosphere west of the subduction zone but, at present, no evidence exists to connect potential segmentation offshore with that below the thrust fault. Barbs show relative motion across the segmentation fault, and arrows show relative movement of various parts of the plates. *C*, cross section near the latitude of Puget Sound showing the positions of the most significant types of earthquakes in the Pacific Northwest. The largest historical earthquakes in this region were in the Benioff zone and in the continental crust. Earthquakes in the Benioff zone occur within both the subducted oceanic crust and underlying lithosphere. In most places along the Cascadia subduction zone, the accretionary wedge is nearly aseismic; however, a few historical earthquakes occurred in the younger sections of the accretionary wedge (age increases from west to east), and considerable seismicity occurs in the accretionary wedge west of Vancouver Island and west of the northern California coast (see fig. 7). Many earthquakes also initiate in the oceanic plate in these two areas (west of the region depicted in this drawing). Some scientists suggest that a thin section of soft sediments, not shown here, is subducted along the thrust fault. The brittle-ductile boundary (see the glossary), here arbitrarily drawn at a depth of 25 km, is the probable depth limit for seismic slip on the thrust fault and the depth limit for earthquake occurrence within the continental rocks. In this drawing, the backstop (see the glossary) is approximately coincident with the outer arc ridge (not shown here; see the glossary) (P.D. Snavely, Jr., U.S. Geological Survey, oral commun., 1991; Snavely, 1992). Barbs show relative motion on fault.

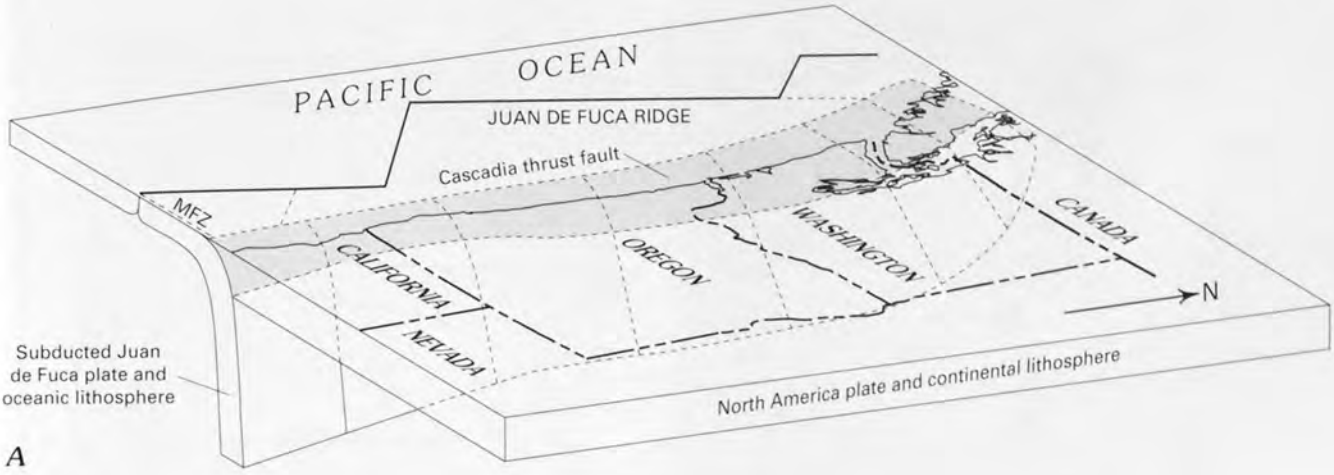
PACIFIC OCEAN
JUAN DE FUCA RIDGE
Cascadia thrust fault
MFZ
CALIFORNIA
OREGON
WASHINGTON
CANADA
NEVADA
N
Subducted Juan de Fuca plate and oceanic lithosphere
North America plate and continental lithosphere

A

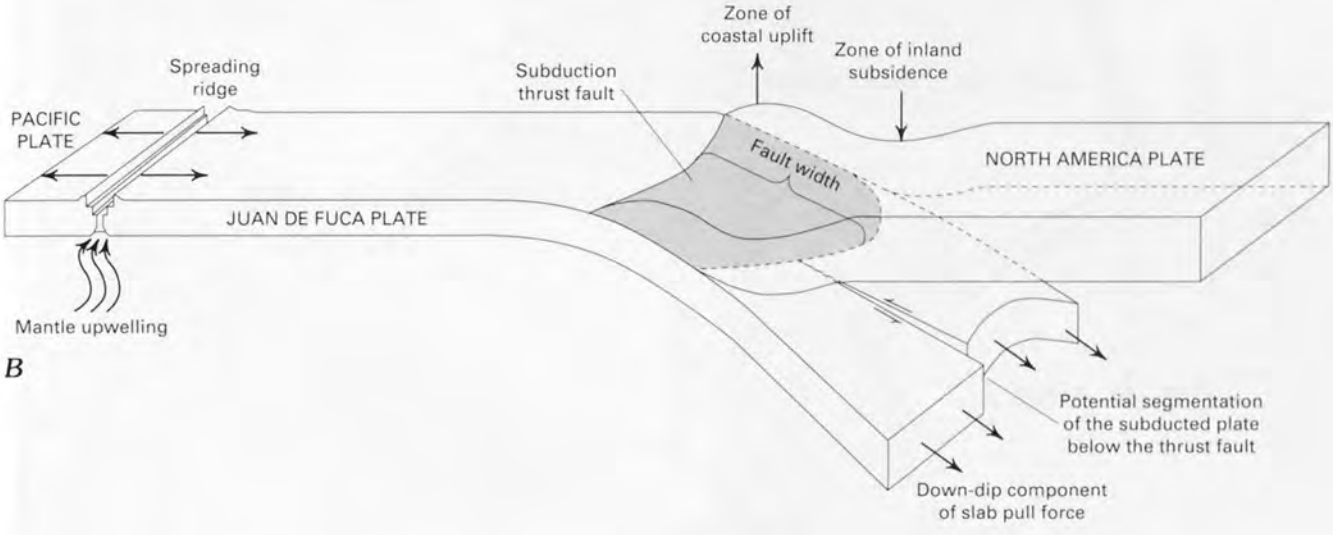
Zone of coastal uplift
Zone of inland subsidence
Spreading ridge
Subduction thrust fault
PACIFIC PLATE
Fault width
NORTH AMERICA PLATE
JUAN DE FUCA PLATE
Mantle upwelling
Potential segmentation of the subducted plate below the thrust fault
Down-dip component of slab pull force

B

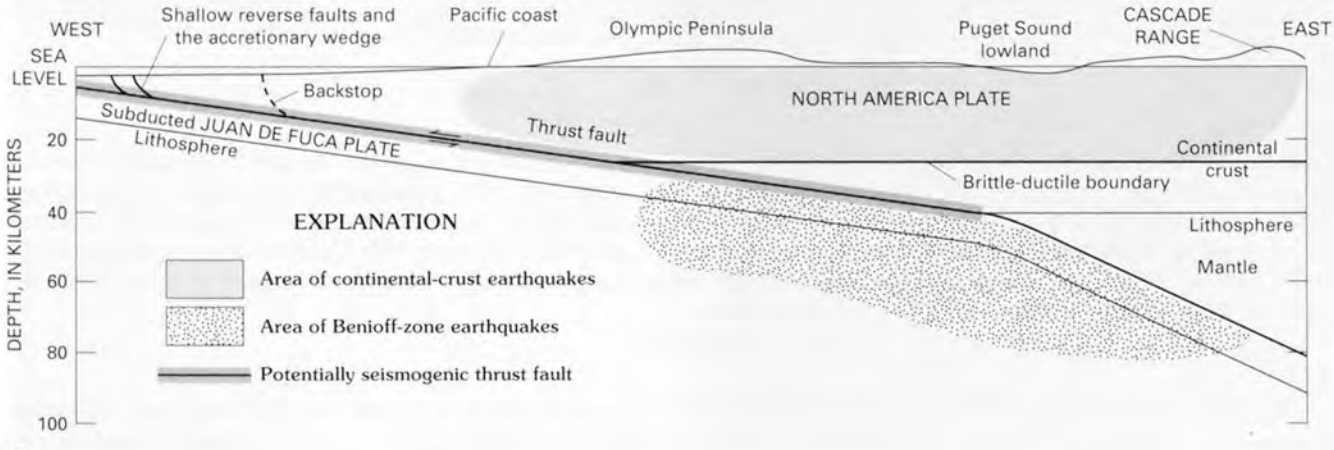
WEST
Shallow reverse faults and the accretionary wedge
Pacific coast
Olympic Peninsula
Puget Sound lowland
CASCADE RANGE
EAST
SEA LEVEL
Backstop
NORTH AMERICA PLATE
Subducted JUAN DE FUCA PLATE
Lithosphere
Thrust fault
Continental crust
Brittle-ductile boundary
Lithosphere
Mantle
DEPTH, IN KILOMETERS
20
40
60
80
100
EXPLANATION
Area of continental-crust earthquakes
Area of Benioff-zone earthquakes
Potentially seismogenic thrust fault

C

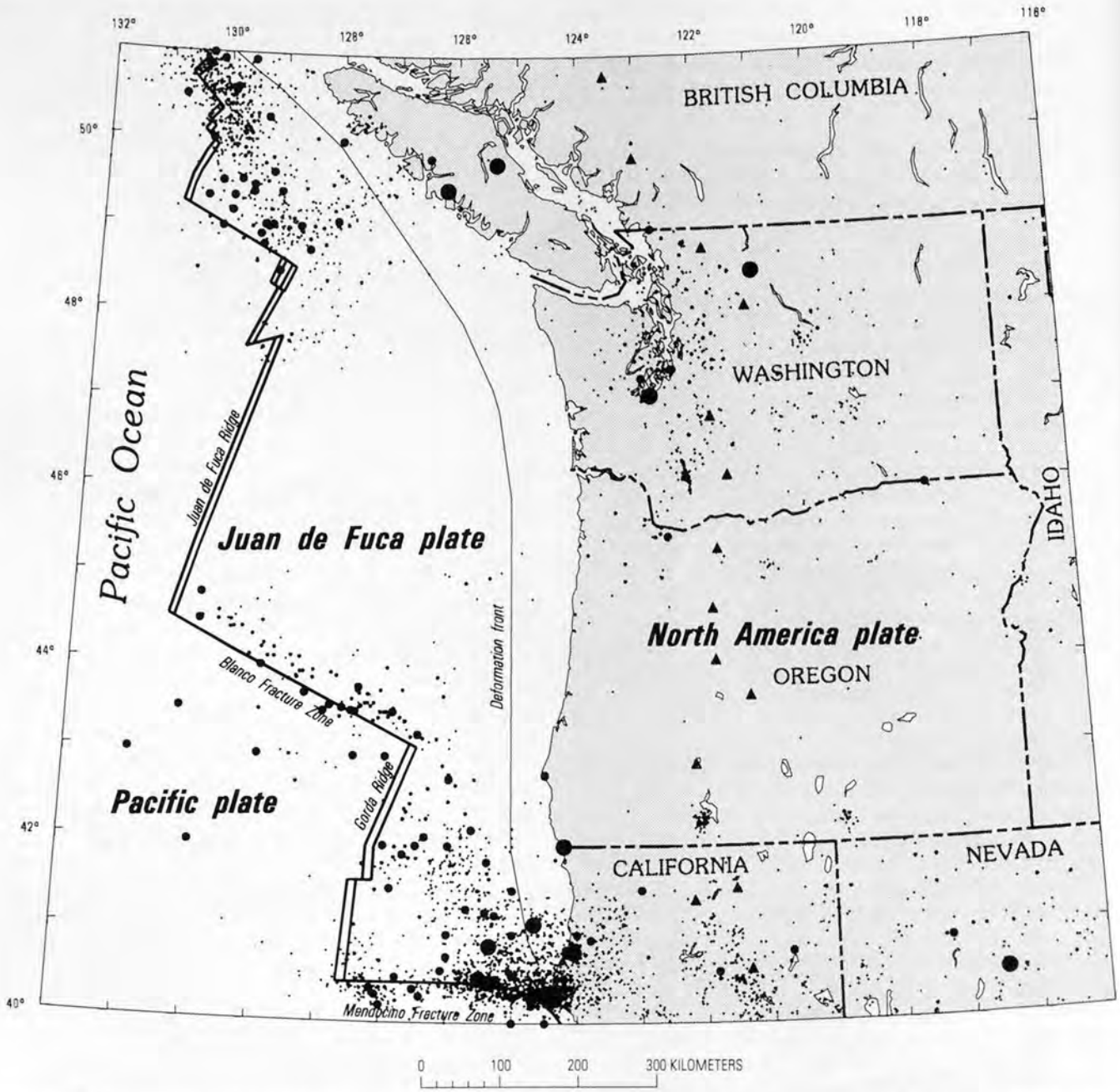

Figure 7. Epicenter map showing the largest earthquakes in the Pacific Northwest for the period 1833 through December 1993 based on the data of Ludwin and others (1991) and U.S. Geological Survey (1991, 1992, 1993). The size of the epicenter symbol is proportional to the earthquake magnitude as follows: $M \geq 7$, largest circle; $6 \leq M < 7$, next smaller; $5 \leq M < 6$, pencil point; $M < 5$, smallest dot. Double lines show oceanic spreading ridges; heavy solid lines show the approximate positions of major transform faults (modified from Riddihough, 1983); the thin solid line indicates the inferred position of the continental margin and, therefore, the westernmost extent of the Cascadia thrust fault (modified from Connard and others, 1984). Triangles are volcanoes.

We also largely ignore the earthquake potential along the spreading ridges in the Pacific Ocean because earthquakes in those areas are too distant from urban areas to cause widespread damage. Earthquakes along the fracture zones, such as the Blanco and Mendocino fracture zones (fig. 2), or within the continental and oceanic plates offshore have produced significant damage in the past. The 1980 earthquake off California (table 1), for example, injured six people, caused a bridge collapse, and produced a maximum MMI VII near Eureka (U.S. Geological Survey and National Oceanic and Atmospheric Administration, 1982). Three earthquakes, ranging in magnitude from 6.0 to 7.1, occurred off

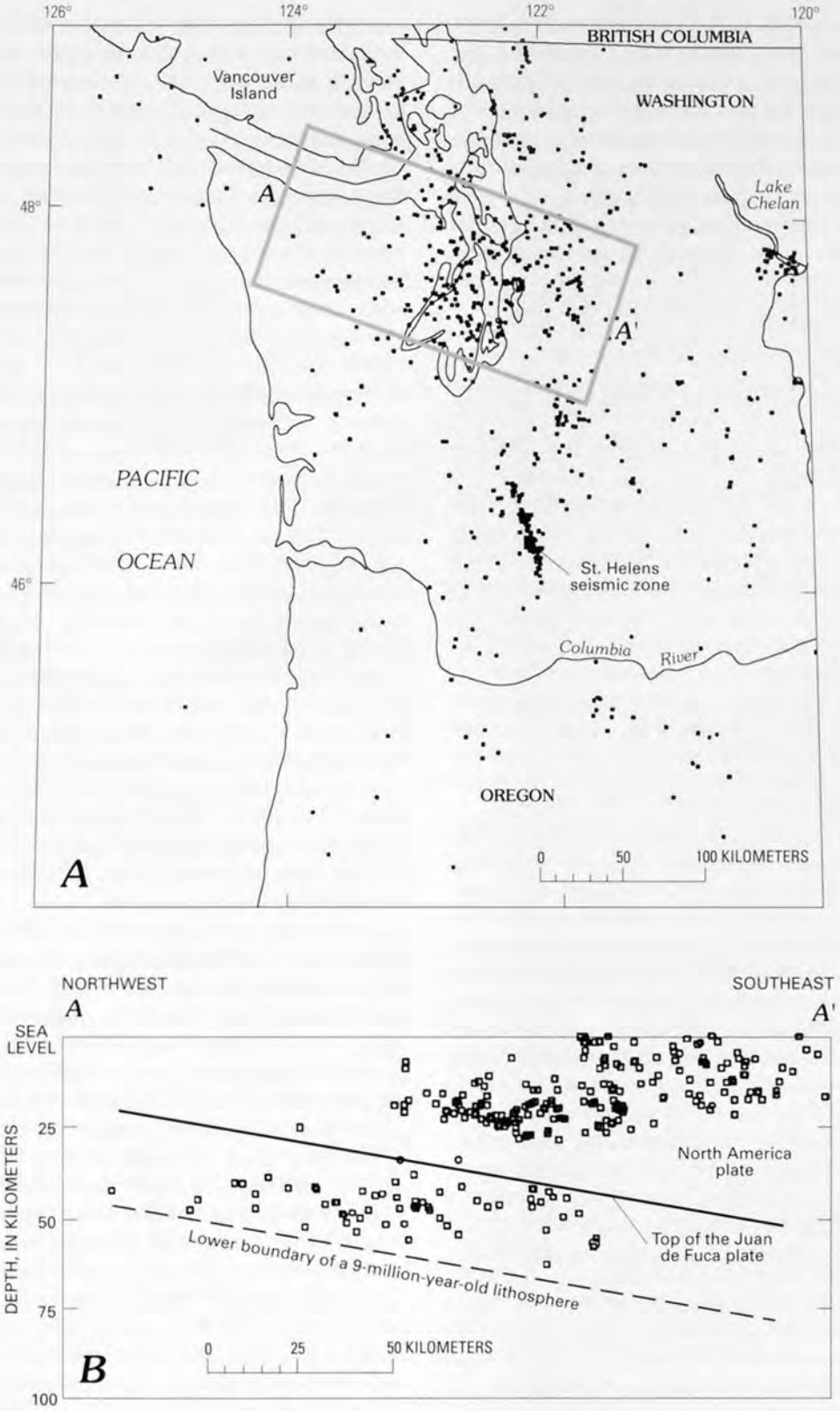

Figure 8. Locations of earthquake epicenters with well-constrained depths in the Pacific Northwest. *A*, epicenters (dots) based on the data of Ludwin and others (1991) and the U.S. Geological Survey (1991). Box shows area of epicenters projected to the plane of cross section *A*–*A'* in part *B*. *B*, cross section *A*–*A'* showing earthquake hypocenters (squares) relative to the position of the top of the subducting oceanic (Juan de Fuca) plate as inferred by Mooney and Weaver (1989).

northern California in 1991 (U.S. Geological Survey, 1991). The smallest of these events, which was near the coast, produced maximum MMI VII in coastal northern California. If the *M* 7.1, 1991 event had occurred close to shore, damage along coastal California and Oregon would have been substantial. Although these offshore structures are important in assessing the earthquake hazards of this region, we do not focus on them in this report. In the following sections of this chapter, we emphasize the potential for damaging earthquakes within the continental crust, within the subducted plate and lithosphere, and on the Cascadia thrust fault.

CONTINENTAL CRUSTAL EARTHQUAKES

Some parts of the continental crust in the Pacific Northwest are clearly seismically active because many historical low-magnitude earthquakes and several historical large earthquakes (fig. 7) occurred in the continental (North America) plate (Ludwin, 1989). Low-magnitude seismicity in the continental plate has defined the north-northwest-striking right-lateral St. Helens seismic zone (fig. 8*A*) (Weaver and Smith, 1983). The 1918 body-wave magnitude (m_b) 7.2 and 1946 m_b 7.3 Vancouver Island earthquakes were also crustal events (Rogers and Hasegawa, 1978; Cassidy and others, 1988). These earthquakes may have a second-order relation to subduction. If the thrust fault is locked, stresses produced by subduction and relative plate motions may be transferred to the continental plate (Fitch, 1972).

Young faults recently recognized by geologists must have produced shallow earthquakes in recent prehistoric time. Plate 1 shows faults with known or suspected Quaternary displacements and geophysically inferred lineaments in the Pacific Northwest (note that the decrease in density of youthful faults in Oregon at the Oregon-California border, apparent on plate 1, is not a tectonic feature but rather an artifact of the greater emphasis on fault mapping in California). Near Puget Sound, the Saddle Mountain East, Saddle Mountain West, and Hood Canal faults are of Holocene age; the Dow Mountain and Cushman Valley faults are of late Quaternary age (Wilson, 1983). Faults within and bounding the Portland basin in Oregon appear to be seismically active (Yelin and Patton, 1991). Evidence exists for as many as three Holocene slip events on the Little Salmon fault zone in northwestern California and for less frequent and smaller events on the nearby Mad River fault zone (Carver, 1987; Carver and Burke, 1987b; Kelsey and Carver, 1988; Carver and others, 1989; Clarke and Carver, 1989; Clarke and Carver, 1992). Bucknam and Barnhard (1989) observed Holocene uplift at Restoration Point on Bainbridge Island and at Lynch Cove near Belfair, Wash. (fig. 1), which may be related to slip on a shallow fault that cuts through postglacial deposits on the floor of Puget Sound (Yount and Gower, 1991). Deformation on local shallow faults may have produced subsidence at Coos Bay, Oreg. (Nelson and Personius, this volume).

Mapping of offshore deposits shows many offshore faults and folds in the continental plate. Snavely (1987) and Snavely and others (1980) discussed Holocene faults both onshore and on the continental shelf that have the potential to produce destructive earthquakes. Clarke (1990, 1992), and Clarke and Carver (1992) mapped many offshore fold and thrust structures. The age of these structures is not precisely known. Because blind thrust faults may not rupture through rocks as young as the age of faulting, some faults may be younger than the youngest rock unit penetrated. Where these faults come ashore, in some places they have been dated as Holocene and Pleistocene (Clarke and Carver, 1989). Clarke (1990) stated that these offshore "* * * structures originated or were reactivated as a consequence of deformation accompanying plate convergence during Pliocene to Holocene time." Offshore faults and folds cutting Holocene sediments are also abundant on the continental margin off Washington (Wagner, 1985; Wagner and others, 1986) and in the Strait of Juan de Fuca (Wagner and Tomson, 1987). Finally, Harding and Barnhard (1987) and Harding and others (1988) discussed features, identified in seismic-reflection profiles, that offset or disturb the sediments on the floor of Puget Sound and Lake Washington. In some places, submarine slumps may produce these offsets, but in other places the depth penetration and dip of the features are evidence of faulting of Holocene age. Some of these faults may represent secondary rupture in response to slip on the Cascadia thrust fault (Clarke and Carver, 1992). The return time for earthquakes on such secondary faults could be linked with the return time for great earthquakes on the Cascadia thrust fault. Slip on some continental faults, however, may be independent of the Cascadia thrust fault.

Whether these faults represent primary or secondary rupture, many are long enough to be considered potential sources of large, damaging earthquakes. On the basis of historical seismic data, a maximum magnitude of 7.4 is possible, if events such as the 1872 Lake Chelan earthquake are possible at other locales west of the Cascade Range. A similar magnitude is suggested by the Vancouver earthquakes (table 1). The St. Helens seismic zone (Weaver and Smith, 1983) produced an earthquake of local magnitude (M_L) 5.5 in 1981. Weaver and Shedlock (1989) suggested that this fault is capable of an earthquake as large as *M* 6.8. Some mapped faults in the region may be capable of maximum magnitudes greater than 7.4. For example, based on fault offsets in Holocene sediments on the Little Salmon, McKinleyville, and Mad River fault zones, Clarke and Carver (1989, 1992) and Dengler and others (1991) inferred prehistoric earthquakes associated with these faults having magnitudes ranging between 7.5 and 8+.

The lack of data hampers establishment of a reliable upper limit for the magnitude of shallow continental-crust earthquakes, which, in any case, should be determined separately for each fault. Despite the evidence cited, little is presently known about the location, size, or recurrence interval

of earthquakes on shallow crustal faults, and it is likely that many shallow faults with the potential to produce large earthquakes have not been recognized. It is not yet possible to state the location of all such earthquakes. Even where the location of surface faulting is known, few data are yet available about the timing of past movement. Nevertheless, existing fault data suggest that large, shallow earthquakes are possible at some locations west of the Cascade Range, and the size and location of these faults suggest that the hazard from continental-crust earthquakes may be as large as or greater than that from other source types.

EARTHQUAKES WITHIN AND BELOW THE SUBDUCTED PLATE

The Benioff zone is the dipping zone of earthquakes, observed in active subduction zones worldwide, that partially defines the subducting oceanic lithosphere. Commonly, this seismic zone includes earthquakes on the thrust fault (interplate) and earthquakes within the subducting oceanic lithosphere below the thrust fault (intraplate). In the Pacific Northwest, the Cascadia thrust fault has not produced detectable earthquakes (Ludwin and others, 1991), therefore, in this region, the Benioff zone is defined only by intraplate earthquakes. Large, damaging intraplate Benioff-zone earthquakes have occurred in the past in this region, and similar events will likely occur in the future. Two of the largest historical earthquakes, which occurred in 1949 (m_b 7.1) and 1965 (m_b 6.5) (table 1) at depths between 50 and 60 km, were intraplate Benioff-zone events. Ludwin and others (1991) suggested that the 1873 earthquake near the Oregon-California border (table 1) may have been an intraplate earthquake because it lacked aftershocks, a feature that is common to many such earthquakes (Astiz and others, 1988). Although seismic evidence for a well-defined Benioff zone in this region was lacking in the past (Crosson, 1972), recent seismic-network upgrades, improved earthquake location techniques, and an extended period of monitoring have shown that a Benioff zone does exist beneath western Washington and western British Columbia and that it is clearly defined by small- to moderate-magnitude earthquakes (Ludwin and others, 1991). Evidence is still lacking for a seismically defined Benioff zone beneath Oregon (discussed below). Strong evidence, however, does exist for the presence of a subducting plate beneath Oregon, Washington, northern California, and western British Columbia from studies of seismic-wave travel times (McKenzie and Julian, 1971; Lin, 1974; Langston, 1981a; Michaelson and Weaver, 1986; Taber and Lewis, 1986; Zervas and Crosson, 1986; Crosson and Owens, 1987; Owens and others, 1988; Rasmussen and Humphreys, 1988).

The downward gravitational pull of the oceanic crust into the Earth's mantle is likely the fundamental process that causes Benioff-zone earthquakes (Spence, 1987; Astiz and others, 1988). The force of gravity not only causes earthquakes in the subducted slab by extensional faulting, but it is also the predominant driving force that produces stress on the thrust fault, which can lead to great subduction-zone earthquakes. The subducted slab can also deform in ways other than by normal faulting. For example, differential extension between faulted segments of the downgoing slab may cause strike-slip faulting (fig. 6*B*) (Taber and Smith, 1985; Baker and Langston, 1987).

Intraplate Benioff-zone earthquakes do not have a well-established upper-bound magnitude. Astiz and others (1988) noted that *M* 8 earthquakes of this type have been observed worldwide, and this magnitude has been suggested by some scientists as a maximum (Coppersmith and Youngs, 1990). The probable thickness of the subducted slab at the Cascadia subduction zone may imply that the slab can sustain intraplate earthquakes no larger than *M* 7.5 (Washington Public Power Supply System, 1988). To compute the probabilistic seismic hazard of the region, Perkins and others (1980) assumed an upper limit of *M* 7.9 for this type of earthquake.

THE POTENTIAL FOR GREAT THRUST-FAULT EARTHQUAKES IN THE CASCADIA SUBDUCTION ZONE

Both prehistoric and future great earthquakes with magnitudes between 8 and 9.5 have been hypothesized for the Cascadia thrust fault on the basis of a wide variety of evidence (Savage and others, 1981; Heaton and Kanamori, 1984; Heaton and Hartzell, 1986, 1987). Scientific controversy exists concerning this hypothesis, however, because no information unequivocally indicates either prehistoric great earthquakes or the preconditions for such an event in the future. Furthermore, the Cascadia thrust fault has not produced detectable earthquakes at any magnitude level during the 90-year instrumental record or the 200-year historical record of the region (Ludwin and others, 1991). The scientific controversy centers on several related questions. First, is the Juan de Fuca plate continuing to subduct beneath North America? Second, is subduction, if ongoing, seismic or aseismic? Third, if seismic subduction is possible, how large can the earthquake be and how likely is it?

In the following sections of this chapter, we discuss the potential for great earthquakes on the Cascadia plate boundary and some aspects of the debate on this topic. The discussion is an outline intended to review and cite the most significant arguments for and against active seismic subduction. Tables 2 and 3 summarize the text discussion that follows in the next several sections. The discussion and citations are not intended to be all inclusive; readers can find a greater level of detail and other arguments about this topic in the references cited.

Table 2. Principal arguments for and against contemporary active and inactive subduction in the Cascadia subduction zone.

[Argument references and additional discussion are found in the text]

Supporting arguments and evidence	Counterarguments
Active subduction	
Seafloor magnetic lineaments indicate spreading of the Juan de Fuca ridge, and global plate-motion reconstruction indicates convergence between the Juan de Fuca and North America plates	The inferred rate of seafloor spreading decreased between 6 Ma and 700 ka, the time of the last magnetic reversal. If seafloor spreading continued to decrease after that, subduction may have ended. Plate-motion reconstructions are presently only loosely constrained
The direction of greatest compressive stress inferred from strain-rate data in Washington is subparallel to the plate-convergence direction, and compressive strain is increasing	The strain rates are low and, hence, the measurement errors may be comparable to the measured strain-rate values
The observed horizontal-strain and coastal-uplift rates are successfully modeled by a locked thrust fault converging at the independently estimated plate-convergence rate	Observed strain rates could be produced by permanent deformation of the continental plate without subduction. The strain measurements may be influenced by processes near the Earth's surface, such as topography or local deformation
A Benioff zone exists beneath Washington and western British Columbia, and seismicity is present along the Mendocino, Blanco, and Nootka fracture zones	A Benioff zone is lacking beneath Oregon and northern California
The presence of normal-fault earthquakes in the Benioff zone suggests active slab pull against a locked thrust fault. Slab pull is the predominant force producing subduction	Normal faulting in the Benioff zone could continue in the subducted slab after the thrust fault had permanently locked
Geophysical data indicate the presence of a subducted slab downdip from the thrust fault, which supports subduction	This evidence supports ancient subduction but is not evidence of current subduction
Offshore and onshore late Pleistocene and probable Holocene folding and faulting are consistent with subduction	Tectonic processes other than subduction could produce some of these structures
Inactive subduction	
Seismicity is lacking on the Cascadia thrust fault and is low at the Juan de Fuca ridge	Seismic gaps exist on many faults that have produced large earthquakes. The Juan de Fuca ridge continues to produce new crust and has heat-flow values comparable to other active ridges. Subduction could continue without active ridge spreading, owing to slab-pull forces and overriding by the continental plate
The direction of greatest compressive stress inferred from earthquake focal mechanisms and borehole breakouts is north-northeast to north-northwest in western Washington, Oregon, northern California, British Columbia, and in the Juan de Fuca plate; this direction is not parallel to the convergence direction (east-northeast)	Active subduction stresses may be in a low-stress phase of the earthquake cycle. Landward counterclockwise rotation of the stress orientation may exist because of permanent deformation of the continental shelf and slope. Or, since the last ancient earthquake on the Cascadia thrust fault, elastic rebound in the continental crust may have produced present-day extensional strain subparallel to the maximum strain-rate direction
Low horizontal-strain rates are observed near Puget Sound and on the Olympic Peninsula, which could indicate low rates of subduction or stopped subduction	Strain rates may change with time. Low strain rates, however, have been predicted on the basis of a locked thrust fault and the convergence of the Juan de Fuca and continental plates
A poorly defined trench could be evidence that subduction has ended	Buoyant oceanic crust that is well coupled but still undergoing active subduction may produce a poorly defined trench based on comparisons with other subduction zones worldwide. High sedimentation rates in the Pacific Northwest obscure the trench by filling it with sediments

SUBDUCTION: ACTIVE OR INACTIVE?

GEOPHYSICAL DATA

Seafloor magnetic lineaments are the principal evidence for active subduction during the last several million years. These lineaments are the remnants of the magnetic field of the Earth and show ancient reversals in this field recorded by ocean-bottom rocks as the rocks cooled after ejection from the oceanic ridges (Raff and Mason, 1961; Vine and Matthews, 1963). These features and other geophysical and geologic data show that the Juan de Fuca ridge (fig. 1) is spreading at a rate of about 3 cm/year in an east-southeast direction with respect to the Pacific plate, whereas the North America plate is moving at about 5.8 cm/year in a southeast direction with respect to the Pacific plate (Atwater, 1970; Nishimura and others, 1984; Riddihough, 1984). These motions resolve into east-northeastward/west-southwestward relative convergence (fig. 2) between the Juan de Fuca and North America plates at about 2.5–4.3 cm/year.

Compelling evidence for active subduction also comes from strain-rate (see the glossary) measurements in Washington. The direction of maximum contraction inferred from geodetic measurements of strain, N. 59±6.6° E. in the Olympic Peninsula, N. 68° E. in Seattle (Savage and others, 1991), and E. 3° S. in western Oregon (Paul Vincent, University of Oregon, written commun., 1991), is subparallel with the convergence direction (N. 68° E.) determined from plate motions and, thus, is consistent with active subduction. Variable measurements from the Vancouver Island area, N. 2±13° E. in Queen Charlotte Strait, N. 18±11° E. at Port Alberni (Dragert, 1991), suggest complexity in the subduction process in the Vancouver Island region but are consistent in magnitude with a locked-thrust-fault model (Dragert, 1991).

Tide-gauge and leveling data indicate gradual uplift of coastal areas in both Washington and Oregon. Savage and others (1991) showed that this observation is consistent with ongoing shortening of the North America plate (fig. 6*B*).

Several investigators (Silver, 1972; Snavely, Wagner, and Lander, 1980; Snavely, 1987; Kelsey, 1990; McInelly and Kelsey, 1990; and Clarke, 1992; among others) concluded, from a variety of offshore geophysical data, that the outer continental margin and coastal regions are undergoing active youthful (Holocene at some localities) folding and faulting consistent with subduction of the Juan de Fuca plate. The north-south extent of the deformation suggests that ongoing subduction also includes the Explorer (Riddihough, 1978; Hyndman and others, 1979, 1990) and North and South Gorda subplates (fig. 2) (Kelsey and Carver, 1988).

SEISMICITY

One of the observations leading to controversy is that no great earthquakes have been detected during the past 200 years on the Cascadia thrust fault (Rogers, 1988a); today, the fault zone is seismically quiet even at the lowest detectable magnitude levels (Crosson, 1972; Crosson, 1983; Ludwin and others, 1991).[5] Also, no earthquakes have been observed in large regions of the offshore continental plate in spite of the youthful faulting and folding of offshore sediments noted above. Seismicity is also absent at the Juan de Fuca ridge and in large sections of the oceanic plate west of the subduction thrust fault (fig. 7), although this observation is common to many subduction zones worldwide (American Association of Petroleum Geologists, 1981). Seismicity does occur, however, along the offshore fracture zones and within the Gorda South plate. We discuss these dilemmas in the following paragraphs.

The lack of historical seismicity on the subduction thrust fault has been interpreted in several ways: (1) the subduction process has stopped, that is, there is no longer any closing motion between the North America and the Juan de Fuca plates, or slab pull (see the glossary) is insufficient to initiate slip on the thrust fault (Crosson, 1972; Farrar and Dixon, 1980); (2) the plates are unlocked and the subduction process is proceeding without generating earthquakes (Ando and Balazs, 1979); and (3) the two plates are strongly locked but converging nonetheless; this condition would lead to compression and bending of the North America plate and storing of elastic energy, to be released in a future great earthquake (Savage and others, 1981; Heaton and Kanamori, 1984). In interpretation 3, the historical period is presumably part of the seismic cycle between great earthquakes.

In simplest terms, the seismic cycle refers to the buildup and release of stress on faults, which results in alternating periods of quiescence and seismicity. The relationship between this cycle and earthquake occurrence is not yet completely clear (Kanamori, 1981). In one model of the seismic cycle, however, motion of crustal plates produces strain accumulation resulting in several seismicity phases. At low strain levels, a few earthquakes may occur at a rate that defines a low, or background, level. As strain accumulates, the rate of earthquake occurrence commonly increases throughout the strained volume of crustal rock. At larger strain levels, some faults or fault segments lock and become

[5]Two earthquakes have occurred recently that may have been produced by slip on or subparallel to the subduction thrust fault. Low-angle nodal planes and thrust-slip style computed for these earthquakes (U.S. Geological Survey, 1991,1992; Oppenheimer and others, 1993) are the basis for this conclusion. The earthquakes occurred on August 17, 1991 (*M* 6.2), and April 25, 1992 (*M* 7.1). The 1992 earthquake has also been discussed by Hubert and Schwartz (1993), Koch (1993), and Graves (1993).

quiet again, although seismicity may continue on surrounding faults. As strain increases further, a sequence of foreshocks may develop within the formerly quiet zone, near the impending mainshock in time and location. When strain reaches a critical level on a given fault, the mainshock earthquake occurs followed by a series of aftershocks, after which the cycle repeats. If the rate of long-term strain accumulation is constant and the fault-zone properties are uniform, the time between mainshocks depends on the amount of slip in the last mainshock (Bufe and others, 1977). Under the conditions of this simplistic model, an earthquake with large slip will be preceded by a longer quiescent period than an earthquake with small slip.

The seismic cycle concept partly stems from the absence of seismicity on some young faults, a commonly observed characteristic (Lay and others, 1982); yet, some of these faults have been seismically active historically. Rogers (1988a) cited the subduction zone in New Zealand near Wellington as an example of a fault that produced a large subduction-zone earthquake in the last century but has no detectable present-day seismicity on the thrust fault. Seismic gaps along other subduction zones may forecast the potential for future large earthquakes (Kelleher, 1970; McCann and others, 1979). Sections of the San Andreas fault in California, although not a thrust fault, suggest another example of the seismic cycle. As noted by Heaton and Kanamori (1984), the section of the fault that ruptured in 1906 is now seismically quiet, whereas the creeping section that has not produced a large earthquake historically is seismically active at low magnitude levels. Thus, we can take neither the presence of small earthquakes as conclusive evidence of the potential for large events nor the absence of small earthquakes as evidence of a fault with no potential for large events (Lomnitz and Nava, 1983). Nevertheless, based on these examples, the Cascadia thrust fault may be in a quiet period of its seismic cycle, considering that other data suggest that plate motions continue.

For example, seismicity occurs on some boundaries of the regional plate system that includes the boundaries between the North America, Juan de Fuca, North and South Gorda, and Explorer plates. Because the Mendocino, Blanco, and Nootka fracture zones (compare figs. 2 and 7) produce earthquakes, it is possible to determine if slip rates inferred from earthquake magnitudes on these boundaries are consistent with independently determined plate-motion rates. Hyndman and Weichert (1983) showed that slip rates calculated from the magnitudes of earthquakes on the plate-boundary faults agree with slip rates based on global plate kinematics. Their result, however, did not resolve which plates are in motion but only showed that relative motion occurs on these faults at rates consistent with plate-motion reconstructions.

Examination of slip directions and stresses derived from earthquake focal mechanisms is another means of observing relative crustal plate motions, but these observations are equivocal regarding active subduction. Focal mechanisms and seismicity alignments indicate right-lateral strike slip on the Mendocino and Blanco fracture zones (fig. 2) (McEvilly, 1968; Spence, 1989). Right-lateral slip on these faults is consistent with either transport of the Juan de Fuca plate into the trench, a fixed Juan de Fuca plate and northwest transport of the Pacific plate, or motion of both plates. Only the first and third alternatives are wholly consistent with active subduction. As noted in the following paragraphs, the second alternative may or may not be consistent with active subduction, depending on other assumptions.

The direction of greatest compressive stress inferred from focal mechanisms is principally north-south in the Pacific Northwest (Spence, 1989). If convergence of the two plates is ongoing and the thrust fault is locked, a more east-northeastward compressive stress direction should be observed, parallel to the convergence direction. Most of the focal-mechanism observations do not confirm this stress direction.

Spence (1989) computed stress directions and magnitudes throughout the Juan de Fuca plate and parts of Washington and Oregon, based on a model that only requires motion of the Pacific and North America plates and a locked subduction zone. This model assumes no motion of the Juan de Fuca plate. The orientation of the greatest compressive stress computed using this model roughly fits the focal-mechanism-inferred direction of greatest compression, north-south. The agreement between modeling and data implies that the Juan de Fuca plate west of the trench is not presently under subducting compression, although the modeling does not preclude subduction in the future (see additional discussion of this modeling in the section "Strain rate measurements, crustal shortening, and focal mechanisms").

Seismic evidence for motion of the subducted slab below the locked zone strengthens the argument for active subduction. Taber and Smith (1985), who studied the focal mechanisms for small earthquakes in the Benioff zone (in locations similar to earthquakes within the subducting lithosphere shown in fig. 8*B*), found that these events were predominantly normal-fault earthquakes with inferred tension stress axes parallel to the downgoing slab. Both the 1965 and 1949 earthquakes also had this stress orientation (Weaver and Baker, 1988). Extension in the Benioff zone is consistent with active subduction because the slab is being pulled into the mantle by gravitational forces. Spence (1989) argued that the slab-pull force extends the downgoing lithosphere, producing normal-fault earthquakes with downdip tension axes because the locked thrust fault pins the slab and resists downdip slab forces. If the thrust fault is unlocked, evidence from other subduction zones suggests that an ongoing series of normal-fault earthquakes should occur out to the trench and farther west (Spence, 1989) as the slab-pull force causes

extension and bending of the oceanic lithosphere. If the thrust fault undergoes a seismic cycle, normal-fault earthquakes near the trench are expected only after a subduction-zone great earthquake permits an extensional stress pulse to move updip past the momentarily unlocked fault. At the Cascadia subduction zone, normal-fault earthquakes do not extend as far as the trench, although they do extend beneath the Olympic Peninsula (Taber and Smith, 1985), suggesting that a part of the thrust fault is locked.

The 1949 earthquake focal mechanism was strike slip rather than normal faulting. From ground-motion modeling studies, Baker and Langston (1987) inferred left-lateral strike slip on an east-west-striking fault for this earthquake. This slip style can be produced by differential motion between different segments of the downgoing slab (fig. 6*B*). Thus, an east-west tear in the slab could result in strike-slip movement on this fault (Baker and Langston, 1987) if the southern segment of the slab moved downdip relative to the northern segment. In any case, this earthquake suggests active subduction.

OTHER VIEWS AND COMPLEXITIES

The interpretation of active subduction is not unquestioned. In earlier studies, Crosson (1972), Milne and others (1978), and Sbar (1983) noted the lack of a distinct Benioff zone and an earthquake-inferred compressive-stress direction different from the convergence direction, whereas for many subduction zones these two directions are approximately equal. From this information, they argued that subduction may have ceased. Since then, however, new data on the seismicity of the region has improved the definition of the Benioff zone beneath Washington (Crosson, 1983; Crosson and Owens, 1987; Ludwin and others, 1991). Yet, the lack of a distinct Benioff zone beneath Oregon (Weaver and Michaelson, 1985) has not been adequately explained. Bolt and others (1968) discussed seismic and geologic evidence that a part of the Gorda and North America plates have formed a single plate owing to the extension of the San Andreas fault to the northwest beyond the Mendocino fracture zone. This hypothesis implies that a southern section of the Cascadia subduction zone is permanently locked.

Other arguments have been made to suggest that subduction has ended. The pattern of ocean-bottom magnetic reversals indicates that the Juan de Fuca ocean-ridge spreading rate decreased during the last 6 million years (Riddihough, 1977, 1984; Carlson, 1981; Duncan and McElwee, 1984). Unfortunately, the last age for which active spreading can be calculated is about 700 ka; thus, the magnetic lineament data give no information on the ridge-spreading rate to the present day. Furthermore, at present, the Juan de Fuca ridge is nearly aseismic, which could imply that spreading has ended. If spreading has slowed and subduction rates are low, the thrust fault could have permanently locked during the last 700,000 years (for example, see Atwater, 1970).

Other evidence or arguments counter the ceased-subduction hypothesis. For example, seismic rates are commonly low along many actively spreading ridges worldwide (American Association of Petroleum Geologists, 1981). And even though the Juan de Fuca ridge is aseismic, tens of kilometers of new crust have formed in some sections of the Juan de Fuca ridge (Delaney and others, 1981; Heaton and Hartzell, 1987) during the last 700,000 years, and heat-flow values over the spreading ridge are comparable to those over other active spreading ridges (Korgen and others, 1971).

Some workers regard the lack of an offshore trench as evidence that subduction has stopped (for example, Riddihough, 1978). However, high sedimentation rates from the Columbia and Fraser Rivers since the last glaciation, a slow subduction rate, and a buoyant oceanic plate may obscure or inhibit development of a prominent trench. Geophysical data support this inference (for example, Kulm and Peterson, 1984). Finally, Heaton and Hartzell (1986) suggested that the poorly defined sediment-filled Cascadia subduction-zone trench is characteristic of youthful, buoyant, strongly locked, active subduction zones worldwide.

In our view, the evidence favors ongoing active convergence across the Cascadia thrust fault. Active slab pull could produce subduction and the eventual occurrence of large earthquakes on the thrust fault (Spence, 1987). The most direct evidence for contemporary subduction is the offshore deformation of young sediments in the accretionary wedge, strain data that indicate active compression of the continental plate, coastal uplift inferred from leveling and sea-level data, and the existence of a Benioff zone having earthquakes with downdip extensional stress axes beneath Washington.

IS THE CASCADIA THRUST FAULT SEISMIC?

Even though active subduction is widely accepted, considerable debate exists about whether the Cascadia thrust fault is capable of producing large earthquakes (for example, Ando and Balazs, 1979; Heaton and Kanamori, 1984, 1985; Acharya, 1985; Byrne and Sykes, 1987; Sykes and Byrne, 1987; Atwater, 1988a; Byrne and others, 1988; Sammis and others, 1988; Washington Public Power Supply System, 1988; West and McCrumb, 1988a, 1988b; Spence, 1989; Sykes, 1989; Coppersmith and Youngs, 1990). In a recent polling of 14 scientists (Coppersmith and Youngs, 1990), estimates were requested about the potential for significant earthquakes (moment magnitude, M_w, greater than 5.0) on the thrust fault. The responses varied widely, from near certainty that such earthquakes would not occur (probability near 0) to near certainty that they would occur (probability near 1). The majority of the respondents, however, assigned a probability between 0.5 and 0.9 for such an earthquake. Significant new data suggesting seismic subduction, discussed in this paper, were not known to these scientists at the time of their evaluation in 1988.

Table 3. Principal arguments for and against contemporary seismic and aseismic subduction in the Cascadia subduction zone.

[Argument references and additional discussion are found in the text. Because a locked thrust fault is a prerequisite for seismic subduction, some arguments center on whether the effects of a locked fault are present in the various observations. Neither arguments nor counterarguments are conclusive at present and, in some cases, further response to counterarguments is possible (see the original studies referenced in the text for this level of detail). **In our view, however, the weight of the evidence favors seismic subduction. In particular, the evidence for sudden subsidence, tsunami deposits atop buried peats, and the modeling of strain data by a locked thrust fault are all highly significant.** Additional work to improve the accuracy of radiocarbon dating and connection of these events with shaking evidence, such as liquefaction and landsliding, could make the case for great subduction earthquakes unequivocal]

Supporting arguments and evidence	Counterarguments
Seismic subduction	
Geologic evidence exists for multiple episodes of sudden prehistoric coastal subsidence	Rapid eustatic changes in sea level could produce similar effects at some locations. Coastal subsidence at some locales may be produced by deformation on shallow or local faults. Coastal submergence may also have occurred during interseismic periods at some locales. The ages of peat burial are not demonstrably equal at all estuaries. Aseismic slip on the plate boundary could produce subsidence
Sand deposits atop peats, buried by rapid coastal subsidence, suggest the occurrence of tsunamis	Over decades following rapid or gradual coastal subsidence, estuary flooding by high tides, unusual river discharge, or tsunamis from distant earthquakes could also produce these layers in some places
Thirteen episodes of submarine turbidites are observed in offshore sea-fan deposits less than 7,500 years old	Turbidites could be triggered naturally by excess sedimentation or by earthquakes other than subduction events
Observed horizontal-strain and coastal-uplift rates are successfully modeled by a locked thrust fault converging at the independently estimated plate-convergence rate	Observed strain rates could be produced by permanent deformation of the continental plate without subduction. The strain measurements may be influenced by processes near the Earth's surface, such as topography or local deformation
Leveling data that show northward tilt in Oregon and eastward tilt of the Coast Ranges in Washington are consistent with a locked thrust fault	None
The Cascadia subduction zone is analogous to subduction zones off southern Chile, Mexico, southwestern Japan, and Colombia	The Cascadia subduction zone has unique features. No other active subduction zone compares exactly with this one
Exceptionally young, buoyant oceanic slab should couple and store stress more effectively with the continental plate. A locked thrust fault is supported by the downdip tension direction in the Benioff zone that results from slab pull against a locked thrust fault and by the presence of seismicity in the continental plate	If the fault locks too strongly or the subducted crust is too buoyant, the slab-pull force may be too small to overcome the frictional stress on the fault. Normal faulting in the Benioff zone could continue in the subducted slab after the thrust fault had permanently locked
Offshore and onshore late Pleistocene and probable Holocene folding and faulting is consistent with subduction	Folding and faulting could also be formed during aseismic subduction processes, particularly in the soft sediments of the accretionary wedge
The mostly consistent compressive-stress direction (north-northeast to north-northwest), inferred from focal mechanisms and well breakouts in both the Juan de Fuca and North America plates, suggests a locked thrust fault. See table 2 for other stress-related arguments that apply	The lack of agreement between this stress direction and the convergence direction suggests that subduction-produced compressive stress is low compared to the compressive stress being produced by the Pacific-North America plate interaction. See table 2 for other stress-related arguments that apply
Known Holocene landslides in the region yield ^{14}C ages similar to those for some inferred subduction earthquakes	Rainfall or local earthquakes could also have produced Holocene landslides

Table 3. Principal arguments for and against contemporary seismic and aseismic subduction in the Cascadia subduction zone—Continued

Supporting arguments and evidence	Counterarguments
Aseismic subduction	
Lack of earthquakes along the thrust fault suggests aseismic subduction	Other active subduction zones are commonly aseismic for some periods of the seismic cycle. If only the offshore section of the thrust fault is locked, it may be difficult to detect small earthquakes in that region using existing onshore seismic networks
Holocene coastal terraces are mostly absent in the region	Terraces may be absent because of repeated coseismic coastal subsidence and the position of the coast relative to the locked thrust fault. Continuing eustatic sea-level rise or high rates of coastal erosion may have obliterated terraces
Low horizontal-strain rates are observed near Puget Sound and on the Olympic Peninsula, possibly indicating low or stopped subduction, especially if the error in strain-rate measurements is comparable to the measurements	Strain rates may change with time. Successful modeling of low strain rates with a locked fault model supports the subduction earthquake hypothesis
In one model, eastward tilt is expected for a zone undergoing aseismic subduction	In other models, either eastward or westward tilt may be observed depending on position relative to the locked thrust fault
High heat flow and high fluid pressure in the accretionary wedge and subducted soft sediments along the thrust fault may prevent accumulation of the required stresses for a great subduction-zone earthquake	Inferences about the temperatures, fluid pressures, rock properties, and presence of subducted soft sediments along the thrust fault are difficult to test and are considered by some to be circumstantial evidence

A locked thrust fault and accumulating stress are prerequisites to large subduction-zone earthquakes, although not all agree on this point (Chen and others, 1982; Washington Public Power Supply System, 1988). Nonetheless, the seismic-aseismic debate about the Cascadia thrust fault centers on data that are relevant to whether the fault is locked and accumulating compressional stress. Unfortunately, these data may lead to equivocal conclusions. Though assessment of the potential for large earthquakes is not completed, we review the principal aspects of the discussion in the following paragraphs. Table 3 also outlines the evidence on both sides of the debate.

One question to be asked is, what constitutes unequivocal evidence for the hypothesis that a great earthquake will occur on the Cascadia thrust fault? On the one hand, the only completely unequivocal evidence is probably a great-earthquake occurrence. On the other hand, reasonably consistent evidence of several types, combined with a model that fits these data well using statistical measures, could produce a high level of confidence in the hypothesis. If this level of confidence is considered high by a group of observers, then most observers would conclude that such earthquakes will occur. For example, if all the following were true, then in our view, confidence in the hypothesis would be high: (1) consistent times of coastal submergence at widely separated localities, so that only slip on the Cascadia thrust fault could have produced the effect; (2) evidence of ground shaking in the form of tsunamis, landslides, liquefaction, and turbidites, each occurring at times consistent with the submergence events; (3) a model of the locked subduction zone that explains the geodetic observations, sea-level changes, and ancient submergence events; and (4) development of a model that permits stick slip over parts of the thrust fault, using inferences about temperatures and pore pressures along the thrust fault. Conversely, the hypothesis might be rejected because of: (1) lack of synchronous occurrence of submergence events along the coast and (or) of submergence events and shaking evidence; and (2) development of models that explain geodetic data, sea-level data, and rapid coastal submergence in terms of aseismic slip. As is shown in the following sections, confidence in the hypothesis is stronger than confidence in its rejection. Arguably, the most significant evidence suggests that at least some segments of the

Cascadia thrust fault are locked, that subduction continues, and that seismic slip on the thrust fault can be expected in the future (Heaton and Hartzell, 1986, 1987; Spence, 1989; Savage and others, 1991; Atwater, this volume).

INFERENCES FROM MODELS OF PLATE AND FAULT-ZONE PROPERTIES

In one model of the plate-boundary thrust fault (Byrne and others, 1988), the fault is characterized by four zones (fig. 6*C*, downdip from the surface trace of the fault): (1) the deformational front (accretionary wedge), or leading edge of the continental plate, where clay-laden sediments are relatively soft and affected by high pore pressure; (2) a zone of igneous rock and dewatered, lithified, consolidated sediments, referred to as the "backstop," that is, strong enough to support stress accumulation; (3) continental crustal rocks; and (4) a thin zone of unconsolidated sediments along the thrust fault that accumulated on the oceanic crust, before their subduction. These unconsolidated sediments form a boundary of variable thickness between the subducted slab and the overlying continental rocks. High fluid pressure and subducted unconsolidated sediments could reduce the area of a locked thrust fault in zones 1 and 2 (Byrne and Sykes, 1987; Sykes and Byrne, 1987; Byrne and others, 1988; Crosson, 1989, 1990; Kulm, 1989; Magee and Zoback, 1989). This model is a hypothesis, and many of its features may be difficult to test. For example, the pore pressure and temperatures at the depth of the thrust fault can only be inferred from shallow measurements and modeling, and the actions of thrust faults under conditions characteristic of subduction are not yet well understood. Finally, some recent geophysical data suggest that sediments are mostly scraped off the downgoing Juan de Fuca plate at some places and are not subducted (Hyndman and others, 1990). The long-term aseismicity of the thrust fault, however, could ultimately validate this hypothesis.

In zones 2 and 3, temperatures on the fault may exceed 300–450°C (Davis and others, 1990; Hyndman and others, 1990), which would prevent stick-slip motion on this section of the fault (Scheidegger, 1984; Byrne and others, 1988; Sammis and others, 1988). Temperature measurements in shallow seafloor boreholes and modeling of thermal characteristics of the crust form the basis of this hypothesis. Under some conditions, which may apply to the Cascadia thrust fault, these effects could reduce the area of potential locked fault zone to zero (Byrne and Sykes, 1987; Sykes and Byrne, 1987; Byrne and others, 1988).

The age and temperature of the downgoing slab form the basis of other hypotheses about subduction in this region. A young, relatively hotter oceanic plate may slow subduction because it is more buoyant, reducing the slab-pull force and increasing interplate coupling (Spence, 1989). In this model, large earthquakes may be possible even with a reduced rate of subduction (for example, see Heaton and Kanamori, 1984; Spence, 1989). Contrary to this interpretation, however, others believe that evidence exists that a very youthful subducting plate and relatively slow rate of subduction could create a condition of aseismic subduction (Kanamori and Astiz, 1985).

COMPARISONS WITH SUBDUCTION-ZONES WORLDWIDE

To various degrees, each subduction zone is unique, as noted by Heaton and Hartzell (1986) and Spence (1989). Nonetheless, one way of assessing the likelihood that the Cascadia subduction zone can produce great earthquakes is to compare its characteristics to other active subduction zones worldwide. Heaton and Kanamori (1984), Heaton and Hartzell (1986, 1987), and Rogers (1988a) found that the Cascadia subduction zone shares many characteristics with subduction zones off southwestern Japan, southern Chile, and Colombia, all zones that have produced great earthquakes historically. Some of these characteristics are: (1) an age and plate convergence rate that, combined, group this zone with others that have produced great earthquakes; (2) lack of an active backarc basin; (3) absence of seismicity in the Benioff zone below about 80 km; (4) lack of a well-defined offshore trench; and (5) a shallow-dipping Benioff zone. These studies give details comparing Cascadia with other subduction zones. We cite the Rivera subduction zone off the west coast of Mexico as an important example having properties very similar to the Cascadia subduction zone. The Rivera and Juan de Fuca plates are similar in size and share several other significant characteristics (table 4). The most significant difference is that the Rivera plate may have produced a surface-wave magnitude (M_S) 8.2 earthquake in 1932 (Singh and others, 1985), yet the Juan de Fuca thrust fault has produced no significant earthquakes in the past 200 years. Unfortunately, this analog is ambiguous because some suggest that the 1932 earthquake occurred on the Cocos thrust fault south of the Rivera plate (Eissler and McNally, 1984; Washington Public Power Supply System, 1988).

ELEVATION CHANGES: SUDDEN SUBMERGENCE AND TILT OF THE EARTH'S SURFACE

In active locked subduction zones, the compression of the continental margin leads to secular changes in elevation and shortening of the crust (fig. 6*B*). Some elevation changes may occur abruptly at the time of a great earthquake. Secular changes in the tilt of the Earth's surface at some locations may also accompany the elevation change. Because of the complexity of elevation and tilt activity as a function of geographic position, the dip of the fault, the position of the locked part of the fault, and the rheological properties of the continental rocks and fault zone, the observations at different

Table 4. Comparison of subduction-zone characteristics of the Juan de Fuca and Rivera tectonic plates.
[From Rogers (1988a)]

Characteristics	Juan de Fuca plate	Rivera plate
Age of subduction plate (millions of years)	7	10
Convergence rate (cm/year)	4.5	2.5
Contemporary seismicity on the thrust fault	Aseismic	Nearly aseismic
Contemporary seismicity on the spreading ridge	Nearly aseismic	Nearly aseismic

locations may appear contradictory, leading to differing interpretations. Progress is being made, however, in developing models that explain the wide range of observations.

The strongest evidence for seismic subduction comes from three sources. First, multiple sequences of buried peats in coastal intertidal lowlands appear to have been caused by sudden submergence of coastal areas (Atwater, 1987; Grant and McLaren, 1987; Atwater, this volume; Peterson and Darienzo, this volume). Second, thin sand layers overlie some peats, suggesting that rapid submergence was followed by a tsunami. Third, as many as 13 episodes of offshore turbidites occur in the Cascadia Seachannel, Astoria Canyon, and at two sites off Cape Blanco, Oreg. (Adams, this volume). Turbidites are slumps of seafloor sediments that liquefy and flow over large distances. Excessive sedimentation or earthquake shaking could trigger turbidite flow (Adams, 1990). The significance of these 13 turbidites is that they all lie above the Mount Mazama ash (a widespread volcanic deposit about 7,500 years old) (Adams, this volume), and they come from Cascadia Seachannel tributaries having widely separated sources, evidence that turbidites occurred at different locations at about the same time. Fourth, landslides or other ground failures occur in several places that may temporally correlate with subsidence (Schuster and others, 1992; Williams and Jacoby, 1989; Jacoby and Williams, 1990).

From studies of estuary deposits, evidence in the form of buried peat deposits has been found at about 50 radiocarbon-dated locations showing that coastal lowlands have undergone episodic, rapid submergence (Atwater, 1987; Atwater, this volume; Peterson and Darienzo, this volume). Some of these locations also have 300-year-old tree stumps and snags now surrounded by salt- and brackish-water tidal marshes. Because these trees must have grown above the reach of salt water, it is likely that sea-level rise or land subsidence killed them. Tree-ring growth patterns and the presence of intact grasses in the buried peat deposits suggest that sudden submergence of coastal lowlands most likely killed these organisms (Atwater and Yamaguchi, 1991).

If the dating of submergence events, turbidite deposits, liquefaction, and ancient landslides showed common ages at many places in a several-hundred-kilometer north-south section of the subduction zone, the evidence for great subduction-zone earthquakes of M 8 or larger might be conclusive. Evidence for ground shaking (in the form of liquefaction, landslides, and turbidity deposits) that was synchronous with rapid coastal elevation changes would be particularly important data supporting earthquake occurrence. As shown by Nelson (1992a) and Atwater (1992), however, carbon-14 ages may differ by centuries, making the temporal correlation of different types of events at many sites hard to test. The combined difficulty of obtaining samples representative of the age of a particular subsidence or ground-failure event and or ambiguity inherent in age-dating techniques produces the observed scatter in the age determinations. Of course, such scatter could, in part, also indicate inadequacy of the earthquake model assumed. Nonetheless, the data suggest a correlation in the time of occurrence of some of these events.

For example, Atwater and others (1991), taking advantage of more accurate age estimates afforded by high-precision carbon-14 dating techniques and tree-ring data, concluded that sudden submergence in areas 55 km apart was the result of coordinated slip on one fault or one system of faults. Because the subduction-zone thrust fault is the only fault recognized as extending through the entire 55-km-long area, Atwater and others (1991) associated the submergence event with a Cascadia thrust-fault earthquake. The high-precision radiocarbon dating fixed the time of this submergence in the interval A.D. 1695–1710 (95-percent confidence interval; 296–281 YBP) (Atwater and others, 1991), referred to below as time A. Less precise ages indicate that sudden submergence occurred about this time at other locations along the Washington and Oregon coast, suggesting that the 300-year-old earthquake ruptured more than 55 km of the thrust fault.

The record of probable tsunami deposits in estuary sediments is important evidence of prehistoric large earthquakes. Modeling the geographic distribution of sand atop the 300-year-old buried peat (time A) at Willapa Bay, Wash., its landward deposition pattern, and amount of sedimentation, Reinhart and Bourgeois (1989) found that a 10-m-high tsunami could have produced this sand deposit, whereas flooding by river discharge was an improbable cause. Atwater and Yamaguchi (1991) argued that the landward thinning

of the sand deposits and their coarseness suggest "an extraordinary, landward-directed surge that comprised pulses and approximately coincided with rapid submergence of coast above the Cascadia subduction zone" (see also Atwater, 1987; Darienzo and Peterson, 1990).

Approximately coincident timing of geologic events older than time A may exist at scattered locations (Williams and Jacoby, 1989). For example, approximate coincidence of several types of geologic events (such as sudden submergence, sudden uplift, landsliding, and sand venting) exists at two separate ages, about 600–1,700 YBP (time B) and 1,400–1,900 YBP (time C, possibly two events in this age range; Atwater, 1992). Although Atwater (1992) quotes an age range for each event, time B has been referred to as the 1,150 YBP event, and event C has been referred to as the 1,700 YBP event (Williams and Jacoby, 1989). Lack of coseismic subsidence at the Copalis River, Wash., estuary (fig. 1) at time B raises a question concerning whether this event was produced by movement on the plate-boundary fault or another fault. Subsidence is observed, however, at other coastal Washington and Oregon sites at time B (Atwater, 1988b; Grant, 1989; Darienzo and Peterson, 1990; Peterson and Darienzo, this volume). The Copalis River site does have evidence for vented sand deposits that are approximately coincident with time B, but Atwater (1992, p. 1917) attributed this to folding and (or) faulting of deep aquifers rather than shaking-induced liquefaction. Landslides also occurred at times B and C at Lake Washington (Williams and Jacoby, 1989; P.L. Williams, Lawrence Berkeley Laboratory, written comm., 1992). Landslides at about time B formed within a 30-km radius of the Saddle Mountain east fault in Washington (Schuster and others, 1992). This fault and others nearby may have also slipped at time B (Wilson, 1983). Uplift at Restoration Point and Lynch Cove occurred at time B (Bucknam and Barnhard, 1989; Bucknam, 1991). These geologic events could have resulted from a subduction-zone earthquake, one or more continental-crust earthquakes, or a temporal clustering of both types of earthquakes.

Geologic data at a few localities suggest that some vertical coastal movements may have interpretations other than great earthquakes. For example, buried estuary peats at some localities can be attributed to localized tectonic processes or sedimentation (Nelson, 1992b; Nelson and Personius, this volume). Muhs and others (1990) also noted that local structures can affect the amount and rate of uplift. Although explanation of these data does not always require great subduction-zone earthquakes, the data do imply that active deformation of coastal regions is ongoing. This deformation is likely to be in response to active subduction.

Much evidence exists for tilting of the Earth's surface in the Pacific Northwest. Geologic evidence exists for long-term eastward tilting of coastal regions (Adams, 1984), and geodetic (for example, Reilinger and Adams, 1982) and sea-level data indicate that eastward tilting of these regions continues at present (Adams, 1984). In earlier studies, Ando and Balazs (1979) interpreted the down-to-the-east tilt of the outer coastal zones in Washington and Oregon, the falling sea level at Neah Bay, Astoria, and Crescent City (fig. 1), and rising sea level at Seattle and Friday Harbor with a model of coastal uplift and inland subsidence that was consistent with aseismic subduction. Their model required down-to-the-west preseismic tilt and subsidence of the leading edge of the continental plate produced by aseismic slip along the thrust fault. They concluded, based on comparison with data from Japan, that landward tilt is inconsistent with seismic subduction.

In contrast to Ando and Balazs (1979), others interpreted the elevation and tilt data to indicate seismic subduction. For example, Adams' (1984) interpretation of these data is for seismic accumulation of inelastic deformation near the plate margin and elastic deformation farther inland, consistent with a locked thrust fault. Savage (1983), Weaver and Smith (1983), and Darienzo and Peterson (1990) suggested that some regions of a coast may undergo preseismic subsidence while other coastal zones rise (fig. 6*B*). The movement in a particular region depends, at least in part, on its location with respect to the crest of the uplift, the geometry of the thrust fault, and the position of the locked zone (Atwater, 1988a; West and McCrumb, 1988b). Savage and others' (1991) modeling of strain and elevation data was based on active subduction and a locked thrust fault (further discussion below) and was in accord with the data. Vincent and others (1989) and Paul Vincent (University of Oregon, written commun., 1991), using a combination of north-south and east-west leveling data, also concluded that these data support subduction with strong interplate coupling.

On some coasts adjacent to other subduction zones, ancient beach erosional features, termed "marine terraces," have been uplifted when large thrust-fault earthquakes occurred. The scarcity of uplifted Holocene marine terraces along the coasts of Oregon and Washington (Lajoie and others, 1982) has been used as an argument that the Cascadia subduction zone is not seismic (West and McCrumb, 1988a; Sykes, 1989). Late Quaternary terraces do exist at some Pacific Northwest locations, such as Cape Blanco, Oreg. (Kelsey, 1990), and the Cape Arago-Bandon region (fig. 1) (McInelly and Kelsey, 1990). Although Kelsey (1990) found evidence of a Holocene uplifted beach berm at Cape Blanco, the five terraces at Cape Blanco and Cape Arago are of late Quaternary age and not Holocene. The terraces were deformed and tilted, and the berm was uplifted as a result of local folding during the Holocene at the two locations. These features may be coseismic, secondary deformation related to subduction, as suggested by McInelly and Kelsey (1990) and Kelsey (1990).

Terraces are not always present at locations having historical great earthquakes, such as southern Chile (Heaton and Hartzell, 1986). Other factors such as high coastal erosion rates in the Pacific Northwest could have obscured

terraces (Heaton and Hartzell, 1987). Furthermore, the position of the crest of uplift at the Cascadia subduction zone may be such that rapid submergence of the coast occurs at some locations at the time of the earthquake, whereas uplift is required to produce marine terraces.

Evidence for past and present changes in elevation and land tilt from geologic and geodetic data strongly suggest, but do not prove, that multiple prehistoric earthquakes alternately gradually uplifted some coastal areas between earthquakes and abruptly submerged the same zones when each earthquake occurred. That measurable ongoing uplift and tilt can be modeled by convergence and a locked thrust fault strongly suggests but does not prove that such events will be repeated.

STRAIN-RATE MEASUREMENTS, CRUSTAL SHORTENING, AND FOCAL MECHANISMS

From stress-orientation and strain-rate measurements, the state of interplate coupling between the Juan de Fuca and North America plates can be inferred. High strain rates and the direction of greatest compressive stress being parallel to the plate convergence would imply converging plates, a locked thrust fault, and the potential for large earthquakes. On the other hand, low strain rates and (or) compressive stress directions not parallel to convergence may imply weak interplate coupling and fewer earthquakes or even aseismic subduction.

Data on stress directions come primarily from three sources: earthquake focal mechanisms, strain measurements, and borehole breakouts. Earthquake focal mechanisms provide an estimate of the principal stress orientations by fitting models of earthquake ground-motion radiation to observed first-motion directions and amplitudes. The average focal-mechanism stress directions are commonly assumed to indicate the principal stress orientations at earthquake depths. "Borehole breakout" is a term that refers to elliptical elongation and cracking of the walls of a borehole under stress. The short and long axes of the ellipse align parallel to the greatest- and least-horizontal compressive stresses, respectively. Like strain measurements, borehole breakouts reflect the stress orientations near the surface.

Savage and others (1991) (see also Savage and others, 1981; Savage, 1989; and Savage and Lisowski, 1991) found that although strain rates are low (lower in fact than indicated by earlier measurements), the strain-rate data from both Puget Sound and the Olympic Peninsula were predicted by a model having the thrust fault locked offshore and about 4 cm/year convergence between the Juan de Fuca and North America plates. This model predicted low strain rates and agreed with the observed uplift rates in western Washington determined from tide gauges. The success in fitting this variety of data is especially significant because parameters used in the model were determined independently, rather than fitting the observations by parameter variation. Still, the observation of low strain rates, the limited geographic extent of strain measurements, and the possibility that permanent deformation of the Olympic Peninsula produces the observed strain effects precludes the unequivocal interpretation of a locked subduction zone.

Other interpretations of the strain data also suggest that the two plates are actively converging and locked. Melosh (1987, 1989), using finite-element techniques, modeled uplift and strain data and concluded that a locked thrust fault and plate convergence fit the data best. Other modeling studies support this conclusion. For example, analog stress modeling (Fox and Engebretson, 1983) of a locked thrust fault predicted some aspects of the young geologic deformation history for the past 7 million years.

On the other hand, Crosson (1986, 1990) and Ma and others (this volume) interpreted observations of low horizontal strain rate, episodic strain rate, and north-south compression in the Puget Sound region as arguments for aseismic subduction. Crosson (1986) also argued that strain-rate error bars are comparable to the observations themselves and, therefore, cannot be used to unequivocally support a locked subduction zone.

Other apparent conflicts arise in the comparison of stress and strain-rate principal stress directions. The direction of compressive stress inferred from focal mechanisms differs substantially from that inferred from strain-rate measurements. The strain-inferred direction of greatest compression approximately parallels the direction of convergence between the Juan de Fuca and North America plates. In contrast, the direction of greatest compressive stress inferred from earthquake focal mechanisms, occurring in either the continental plate or in the Juan de Fuca plate (west of the thrust fault), is commonly perpendicular to the convergence direction. Focal mechanisms for earthquakes in both plates generally support a north-south compressive stress direction that characterizes the interaction between the Pacific and North America plates, as observed along the San Andreas fault in California. This discrepancy has been used to argue against active subduction. Although the discrepancy between the orientation of focal-mechanism stresses and principal strain-rate directions is uncommon in locked subduction zones around the world (Uyeda and Kanamori, 1979), we note one exception to this generality along the Nankai trough off the coast of Japan. Here, the convergence direction between the Eurasia and Philippine plates is northwest, but the compressive stress direction inferred from focal mechanisms, strain rates, and geologic deformation is east-west to east-southeast/west-northwest (Tabei, 1989). This subduction zone, however, has a documented history of great earthquakes. Furthermore, the apparent difference in stress directions may be because we are comparing orientations derived from stress (strain) rates with orientations related to the ambient stress.

This difference was noted by Melosh (1989), who attempted to reconcile the stress-direction conflict with a model involving elastic rebound of the continental crust. In the early to middle phases of the earthquake cycle, the continental plate may be in a state of extension because of elastic rebound of the continental plate following the last earthquake (Ando and Balazs, 1979; Spence, 1987). In this phase of the subduction cycle, the stress orientations would reverse so that the direction of extension is parallel to the direction of convergence, but because convergence continues, a compressional strain rate is observed along the direction of extension. As the cycle continues, the rebound is absorbed as the continental plate recompresses. Late in the cycle, earthquake- and strain-inferred compressive-stress directions would coincide, and a thrust-fault earthquake would ultimately occur.

Spence (1989) suggested that a focal-mechanism-inferred compressive-stress direction not parallel to the convergence direction is the result of temporally varying stress-field superposition. Spence (1989) argued that stresses reflecting the Pacific-Juan de Fuca plate interaction and slab pull are transferred to the North America plate through a locked thrust fault. In stress-field modeling studies, Spence (1989) assumed that the stress produced by the Pacific-North America plate interaction presently predominates over stresses related to slab pull. Spence's (1989) model that best fits observed north-south pressure axes only requires motion of the North America and Pacific plates, with a passive Juan de Fuca plate assumed. Subduction is not required, although the model implicitly permits subduction when stresses induced by slab pull, by accumulation of ridge-spreading forces over time or by overriding of the continental plate, become sufficiently great. This model qualitatively accounts for the differences between strain- and focal-mechanism-inferred pressure orientation.

Because of the complex nature of deformation in a subduction zone, extension commonly occurs in the continental crust during active subduction. Evidence exists that east-west extension and north-south compression may be a pattern that persisted during a significant part of Cenozoic time (62–12 Ma) in Oregon and southern Washington. Wells (1990) interpreted clockwise paleomagnetic rotations of forearc, arc, and backarc rocks with a complex model of clockwise block rotations in the arc and forearc regions. Wells (1990) inferred that, in Oregon, the rotation produced equal amounts of extension and right-lateral shear, whereas in Washington smaller rotations were produced primarily by right-lateral shear. The orientation of the inferred shear is about northwest. Wells (1990) cited the Mount St. Helens seismic zone as an example of contemporary deformation fitting this model. Observed temporal clockwise rotation of dike and normal-fault strike directions into Quaternary time led Priest (1990) to observe that arc extension may continue to the present and that the direction of least compression is about east-west in arc and forearc rocks. If this deformation persists to the present day, one can infer that the North America-Pacific plate interaction dominates the contemporary stress pattern, producing oblique subduction and backarc extension (Wells, 1990).

In our view, the evidence largely favors a locked thrust fault with the potential for a great subduction-zone earthquake. We acknowledge, however, many counterarguments (besides the references cited, see also Washington Public Power Supply System, 1988).

MAXIMUM MAGNITUDE EARTHQUAKE ON THE CASCADIA THRUST FAULT

The question of maximum magnitude (M_{max}, assumed to be the same as M_w) on the Cascadia thrust fault is of vital concern. Earthquake size or magnitude is one of the most significant factors relating the level, duration, and lateral extent of strong shaking. The length and downdip width of the rupture determine the earthquake size and, thus, the level, duration, and geographic extent of shaking. In a worst-case situation, the fault-rupture zone may extend the north-south length of the Cascadia subduction zone and eastward to the Puget Sound-Willamette Valley lowland. Alternatively, if the rupture area is limited in size, the geographic area affected is proportionately reduced and may lie farther from urban areas than in the worst case situation. Because the extent and position of the fault rupture control many aspects of earthquake effects, it is important that the most reliable estimates possible be obtained for this parameter.

The distribution and amount of slip on the fault also control the magnitude, shaking levels, and duration of shaking in an earthquake. These aspects of the earthquake source, however, are difficult to determine before the earthquake occurs. Thus, empirical relations between maximum fault-rupture dimensions and magnitude or other empirical data are commonly used to establish the maximum magnitude.

Differences of opinion exist about M_{max} that are fundamentally related to the interplate coupling of the Juan de Fuca and North America plates, the segmentation of the Cascadia subduction zone, and the length and downdip width of the fault area likely to rupture in a single earthquake. Using worldwide data, the maximum expected magnitude has been empirically related to the subduction rate and age of the subducting plate (Heaton and Kanamori, 1984). High rates and youthful subducting plates are associated with the largest magnitudes. Heaton and Kanamori (1984) used this observation to empirically predict a maximum magnitude of 8.3±0.4 for the Cascadia subduction zone. Noting the similarities between the Cascadia and southern Chile subduction zones, Heaton and Hartzell (1986) concluded that rupture of 1,000 km of the Cascadia subduction zone could produce an earthquake as large as M 9.5. Both Adams (1990) and Rogers (1988a) computed a maximum magnitude of 9.1 for the Juan de Fuca segment using different assumptions. Rogers'

(1988a) estimate is based on fault area and rupture of the Cascadia thrust fault on the 900-km-long Juan de Fuca segment from the Nootka fault (fig. 2) on the north to the Gorda South plate, assuming a 100-km fault width. The magnitude is related to the fault area by an empirical relation (Wyss, 1979). Inclusion of the Gorda South plate in this earthquake raises the maximum magnitude to 9.2. Adams (1990) assumed a convergence rate of 45 mm/year and an average recurrence interval of 590 years to compute an average slip of 26 m per earthquake, if all slip is seismic. He further assumed that the fault would rupture 750 km from the Blanco fracture zone to the Nootka fault with a 100-km width. The magnitude was computed from the definition of earthquake moment and an empirical relation between magnitude and moment. In the following discussion, we review the evidence that could limit the length or downdip width of the fault and, thus, limit the maximum magnitude to values less than those just discussed above.

LIMITS ON MAXIMUM MAGNITUDE RELATED TO FAULT SEGMENTATION

Segmentation refers to the possibility that the downgoing slab west of the thrust fault is composed of two or more plates separated laterally by fracture zones. Segmentation raises the possibility that the plates subduct independently of one another. Variations in interplate coupling along the fault strike may also lead to earthquakes that rupture limited sections of the fault. The zones of strong interplate coupling are termed "asperities," and earthquakes can rupture one or more asperities. This mode of rupture leads to the possibility of a range of possible earthquake sizes, where very large events that rupture through several asperities are the least likely. Commonly, segmented thrust faults rupture only one segment in an earthquake, although earthquakes have occurred with probable multiple-segment rupture in a single large event (Ando, 1975; Kanamori and McNally, 1982), as in the 1,000–km-long 1960 Chile rupture. There are no examples worldwide, however, for the rupture of an entire subduction zone in one earthquake (Spence, 1989). Cases of "fault rupture contagion" (Perkins, 1987) also exist in which rupture of a segment leads to a sequence of ruptures of adjacent segments at time intervals ranging from seconds to centuries (Kelleher, 1970; Mogi, 1974; Ando, 1975). The magnitudes of a sequence of earthquakes that occur over an extended time are likely to be smaller than that of a single synchronous rupture of several segments occurring in several minutes. Although segmentation of the Cascadia thrust fault does not categorically limit the maximum magnitude, it suggests the possibility of a range of earthquake sizes on the fault and, perhaps, less frequent multisegment great earthquakes. Great earthquakes with magnitudes exceeding M 8.0 are possible, however, with the rupture of individual segments.

Some data suggest prehistoric rupture across segment boundaries on the Cascadia thrust fault. For example, 13 turbidite events that occurred after deposition of the Mount Mazama ash on the Juan de Fuca and Gorda plates (Adams, 1990) may have been synchronous, which suggests that widespread shaking triggered these events. Furthermore, the most recent estuary-subsidence events in Washington are approximately synchronous with slip on major onshore faults in northern California (Carver and Burke, 1987a; Carver, 1989). All of these events may be a response to motion on the thrust fault (Clarke and Carver, 1989). If rupture of these and other onshore faults occurred at the same time as abrupt coastal subsidence, the large geographic spacing between the events suggests slip on more than one thrust-fault segment. Of course, several alternative interpretations are also possible, including independent rupture of several segments at about the same time.

The evidence for a segmented Cascadia thrust fault also appears strong. It is likely, for example, that the Gorda plate on the south and the Explorer plate on the north separated from the Juan de Fuca plate about 4 million YBP (Riddihough, 1984). Also, the 750-km-long Juan de Fuca section of the Cascadia thrust fault, which extends from the Nootka fault on the north to the Blanco fracture zone, may be further segmented. Morgan (1968) shows at least five faults in the Juan de Fuca plate offsetting magnetic lineaments. Like the Juan de Fuca ridge and the Cascadia thrust fault, however, these faults, if seismically active, are active at very low rates and (or) low magnitude levels.

A segment boundary may exist at lat 46°N. (Magee and Zoback, 1989; Coppersmith and Youngs, 1990). A change in stress directions and uplift rates has been observed between lat 45°N. and lat 46°N. that could be related to segmentation (Mitchell and others, 1991; Palmer and others, 1991). From borehole breakouts, focal mechanisms, and other data, Weaver and Smith (1983), Zoback and Zoback (1989), and Magee and Zoback (1989) inferred that the directions of greatest horizontal stress and plate convergence are similar in Washington north of lat 46°N. and west of the Cascade Range, indicating a locked thrust fault in that zone. Their data are consistent, however, with a difference between these directions from south of lat 46°N. to the Mendocino fracture zone (fig. 2) (see also Werner and others, 1991), which was inferred to indicate weak interplate coupling between the subducting slab and the continental crust south of lat 46°N. in Oregon. In contrast to this interpretation, Ma and others (this volume) concluded that the data do not require a rotation in the compressive stress orientation south of lat 46°N., although their analysis does not preclude a rotation.

Sidescan sonar, SeaBeam bathymetry, and single multichannel seismic records show three to seven left-lateral strike-slip faults off the coast of central and northern Oregon that may be active segment boundaries in the Juan de Fuca plate (Goldfinger and others, 1990; Kulm and others, 1991; Goldfinger and others, 1992; Goldfinger and others, this

volume). These faults strike N. 62° W. to N. 78° W., subparallel to the Blanco fracture zone, and there is evidence that slip on some of the faults at some places occurred during the Holocene (Kulm and others, 1991). Although Goldfinger and others (this volume) have inferred a block-rotation mechanism for the offshore left-lateral faults, they also note that other interpretations are possible. Much remains unclear about the kinematic significance of these faults. Wells and Coe (1985) interpreted older onshore faults in southwestern Washington of similar orientation and slip style (west-northwest and left lateral) as a secondary response (Riedel shears) to clockwise block rotation within a major system of north-northwest-striking right-lateral faults.

Parts of the Juan de Fuca plate downdip from the thrust fault may also be segmented (Michaelson and Weaver, 1986), although the evidence on this point is not conclusive (Rasmussen and Humphreys, 1988). From seismicity data, the dip direction of the Juan de Fuca plate appears to vary from northeast under northwestern Washington to about east-southeast under southwestern Washington and northern Oregon (Crosson and Owens, 1987; Weaver and Baker, 1988) (fig. 6*A*). These data suggest that the dip angle varies as well, from about 15–20° north and south of an arch in the plate that extends beneath Puget Sound, to about 10–12° along the arch axis. Recent seismic-reflection studies by Hyndman and others (1990) partly confirm this interpretation. In any case, Weaver and Michaelson (1985) interpreted these data as two plate segments separated by a transition zone. In further analyses, Michaelson and Weaver (1986) suggested that the Juan de Fuca plate may be segmented in three sections in Washington and northern Oregon between about lat 43°N. and lat 49°N. Based on these data, the maximum segment length is about 250 km, and rupture of this segment could produce an earthquake of M_{max} 8.25±0.25 (Washington Public Power Supply System, 1988). Rupture of the Gorda South plate segment could produce a M_{max} of 8.4 (Clarke and Carver, 1991, 1992). Unfortunately, we do not know whether segmentation of the slab below the thrust fault implies segmentation of the slab in the locked thrust zone and (or) west of the thrust fault. At present, it is also unclear whether plate geometry, such as the bend in the slab, could control the lateral extent of faulting.

Serial rupture of Cascadia thrust fault segments would produce discordant subsidence that might be detected by high-precision dating if the discordance exceeds a few decades (Atwater and others, 1991). In fact, considerable variability in subsidence-event ages is observed, but the variability among ages at individual localities is commonly as large as the variability among localities (Atwater, 1992; Nelson, 1992a).

Peterson and Darienzo (this volume) argue that the presence of probable tsunami-generated sands only on the tops of buried peats rather than within the intervening bay-mud layers is inconsistent with segmented ruptures because ruptures of adjacent or even more distant segments would likely produce tsunami deposits interspersed in the peat horizons of the nonrupturing segments. We believe, however, that segmented ruptures with close temporal spacing could also produce sands only at the top of the peats, and the rupture of one segment might not produce tsunamis large enough to breach bay-mouth bars in adjacent or distant segments, inhibiting the deposition of tsunami sands in bay-mud deposits of the adjacent segments.

The issue of segmentation and its bearing on maximum magnitude remains unresolved. Although Cascadia thrust-fault segmentation is likely, at present no argument or data preclude rupture of multiple segments. For the present, a maximum rupture length of 800–1,200 km should be considered plausible, but we have little idea of the likelihood of such an event. Conversion of the range of possible segment lengths into expected maximum magnitudes requires other assumptions about the downdip width of the fault and the amount of slip. The maximum expected magnitude, even with segmentation, ranges between 8 and 9+ (Coppersmith and Youngs, 1990; U.S. Nuclear Regulatory Commission, 1991).

WHAT IS THE ANTICIPATED DOWNDIP EXTENT OF RUPTURE?

The width of the fault (fig. 6*B*), namely the downdip extent of rupture and the area over which stick-slip displacement occurs, is not well defined and is an important unresolved issue bearing on the maximum magnitude of earthquakes and the level of strong ground shaking in inland urban areas. The locked section of the fault radiates seismic energy at the time of slip. Several competing views exist concerning the size of the locked section of the thrust fault. The fault could rupture downdip for 100–200 km from the offshore deformation front to the intersection of the thrust fault with the continental crust-mantle boundary at a depth of about 30–40 km (Weaver and Shedlock, 1989). Others suggest that the locked zone may extend from the trench eastward to the continental slope and outer shelf (Davis and others, 1990) or farther eastward to the outer coast (Savage and others, 1981; Weaver and Shedlock, this volume). Some of these models propose the existence of a locked zone and transition zone (Clarke and Carver, 1991; Savage and others, 1991). In the transition zone, which is assumed to exist downdip from the locked zone, both seismic and aseismic slip are expected. In the extreme view, no section of the fault locks (Byrne and Sykes, 1987). We review these hypotheses in the following paragraphs.

Strain data from near Seattle are consistent with a locked thrust fault extending 120 km from the offshore continental margin to about the outer coast (Savage and others, 1981; Weaver and Smith, 1983; Lisowski and others, 1987). Melosh (1987, 1989) discussed finite-element modeling of slip and strain accumulation along the fault that also fits tilt

observations and the record of sudden coastal submergence and gradual uplift. In this model, the eastern limit of the locked fault is west of the outer coast.

In a study based on additional strain-rate data from the Olympic Peninsula, Savage and Lisowski (1991) fitted both the strain-rate and the geologic data (interseismic uplift rates at the coast and coseismic subsidence) well. Their model, which assumed a convergence rate of 4 cm/year, required a locked fault extending from the offshore trace of the thrust fault about 100 km eastward. Farther eastward, the fault is assumed to be unlocked, but the continental crust in this region accumulates compressional strain. The abrupt slip accompanying the earthquake would occur in the locked zone but may propagate into the unlocked zone. In this model, the total downdip extent over which seismic radiating slip occurs is 175 km or less. The zone of seismic slip would be less than 175 km if slip near the updip and downdip tips of the rupture occurred as rapid postseismic creep (J.C. Savage, U.S. Geological Survey, oral commun., 1991). We infer from this model that the energy-radiating section of the fault may extend east of the outer coast, well into the Olympic Peninsula.

Arguments have been made suggesting that the Cascadia thrust fault is unable to sustain stress over sections of the accretionary wedge and at depths below about 20 km owing to properties of the Juan de Fuca plate and conditions along the fault zone. In these interpretations, plastically deforming soft sediments and high pore pressures in the leading edge of the accretionary wedge limit the western extent of faulting (Sykes and Byrne, 1987; Byrne and Sykes, 1987; Byrne and others, 1988), whereas subduction of significant quantities of young sediments and unusually high temperatures of the subducting slab limit the eastern extent of faulting. The youthfulness of the slab and the covering of sediments may produce a slab temperature that prevents stick slip (Scheidegger, 1984; Davis and others, 1990). The volume of sediment deposition in the trench, produced by the Columbia and Fraser Rivers, is greater than that in some active subduction zones considered similar to this one. These young sediments not only thermally insulate the downgoing oceanic plate, but also insulate the accretionary wedge, raising the wedge temperature and, subsequently, the temperature at the thrust-fault boundary. Under such conditions, the shallow section of the thrust fault could slip aseismically. In this case, the locked fault width, if a locked section exists, is limited to the zone between the backstop (relatively more competent continental rocks) and the depth at which the fault crosses the 400°–450°C isotherm (the brittle-ductile boundary, fig. 6*C*). This boundary is estimated to be at a depth of between 20 km (Davis and others, 1990) and 35 km (Byrne and others, 1988). This limited section of the fault zone probably lies beneath the continental slope and the outer continental shelf. The locked section of the fault is narrower or nonexistent, if soft sediments are carried below the backstop (Sykes and Byrne, 1987). These factors could significantly limit the size of earthquakes on the thrust fault or, perhaps, preclude their occurrence.

This model raises several issues. First, Scheidegger (1984) showed a zone of 3.4 km/second-velocity sediments that thicken eastward and overlie the basalt at one locality 30 km west of the base of the slope. He interpreted this high-velocity layer as thermally dewatered sediments, which presumably could sustain shear stress. These and other data argue against subduction of significant quantities of soft sediments at some localities. Second, estimation of the depth and map position of the 450°C isotherm on the top of the subducted slab is highly dependent on a number of assumptions, such as accretion and erosion rates, initial thermal gradient, and frictional heating on the thrust fault (Barr and Dahlen, 1989). Finally, the estimated position of the 450°C isotherm computed by Davis and others (1990) applies only to the region off Vancouver Island. Because of the arch in the subducting slab, the map position of this isotherm on the top of the slab is probably well onshore in the model of Crosson and Owens (1987) or nearshore in the model of Weaver and Baker (1988).

Differences exist concerning the position of the locked thrust fault relative to the backstop in various models. The possible existence of multiple backstops and (or) differing definitions for this term may be responsible for these differences. For example, some suggest that the locked section of the fault lies updip from the backstop (Clarke and Carver, 1991; Savage and others, 1991; Wang and Hyndman, 1991). In these models, the accretionary wedge is aseismic from its leading edge to roughly 20 km downdip. In this zone, the thrust fault also slips aseismically. A locked section lies further downdip that is of variable width as a function of geographic position. Near the Olympic Peninsula, the locked section may extend 95 km downdip (Wang and Hyndman, 1991); in northern California, the locked section may extend 70–80 km downdip (Clarke and Carver, 1991). Downdip from the locked section, a transitional zone may exist that can produce both aseismic and seismic slip. This zone also likely varies in width as a function of latitude but may range between an 80-km length near the Olympic Peninsula to 65 km off Oregon (Wang and Hyndman, 1991), or it may extend to the subducted plate knee bend (Clarke and Carver, 1991) where the plate dip changes from 11° to about 25° (fig. 6*C*).

Definition of the location and downdip width of the locked zone is an important parameter required to model strain and stress data and secular vertical motion of the coastal regions. Definition of the locked section of the fault, however, may not fully specify the fault section that radiates energy at the time of the earthquake (Wang and Hyndman, 1991). The locked section is expected to radiate seismic energy when rupture occurs; however, if the rupture propagates into unlocked fault sections either updip or downdip, these sections may also radiate energy. Thus, the locked fault section may only be a lower bound on the fault dimensions radiating seismic energy. Very little is known about this aspect of subduction-zone earthquakes.

Models that assume that the rupture zone extends to onshore regions implicitly suggest greater hazard to urban areas. Because these models fit several kinds of data, more weight should be accorded them compared to models that are based on indirect evidence and hypothesis. Nevertheless, specification of the fault width is a matter of current debate not yet resolved. Continued monitoring of regional strain rates, broader strain network coverage, and refined modeling techniques are likely to produce more certain estimates of the width and length of the locked fault in the future. Research is also needed, however, to better define the relationship between the size of the locked zone and the section of the fault that radiates energy in subduction-zone earthquakes.

EARTHQUAKE RECURRENCE

Earthquake-recurrence estimates are expressed in several ways. Specification of the precise time, location, and magnitude of the next earthquake is termed "earthquake prediction." Unfortunately, at present, methods of earthquake prediction are still being devised and have not been adequately tested. The next lower level of specification is the calculation of probability of specific earthquake magnitudes on particular faults for a given period. This calculation depends on the historic seismic record, the geologic paleoseismic record of times between events, and the time since the last event. This level of specification of earthquake occurrence has been termed an "earthquake forecast." At present, official earthquake forecasts are only available for selected faults in California (U.S. Geological Survey, 1988). In the Pacific Northwest, studies are underway to determine paleoseismic intervals between events and the time since the last event, data that are the basis of preliminary earthquake forecasts (see below). The lowest level of specification of earthquake recurrence is a mean rate of occurrence for a given magnitude level in a given region. When the logarithm of the mean rate of occurrence is plotted as a function of magnitude, the values form a straight line that is referred to as the Gutenberg-Richter recurrence relationship. In the Pacific Northwest at present, even this level of specification is difficult because the historical record of earthquakes in the region is too short.

It is worth noting that specification of a mean rate of earthquake occurrence, although useful for some applications, does not necessarily describe temporal characteristics of earthquake occurrence in specific cases. That is, although earthquake occurrence may fit the Gutenberg-Richter statistical law in a region that includes multiple faults when averaged over sufficient time, earthquakes in subregions or on specific faults commonly recur with considerable irregularity.

The diverse types of earthquake sources in the Pacific Northwest complicate the estimation of earthquake recurrence in comparison with most other regions of the United States. Thrust-fault earthquakes, oceanic-plate earthquakes, continental-crust earthquakes, and intraslab earthquakes are each likely to have different mean recurrence intervals for a given magnitude. Even for a given source type, subregional recurrence variations likely exist; for example, there are lower seismic rates in western Oregon relative to western Washington and lower rates within the oceanic plates relative to those along their margins.

Although we are very uncertain about the accuracy of seismic rates, we can compute estimates for each source type. At present, we must rely on scanty historical seismic data to estimate recurrence rates of continental-crust earthquakes. Ongoing paleoseismicity studies of individual surface faults may eventually yield recurrence-interval data for crustal prehistoric earthquakes, at least for large events on selected individual faults. Sparse historical earthquakes in the subducted lithosphere provide a small data base for estimation of recurrence rates of Benioff-zone earthquakes. Because no historical seismic data exist for thrust-type subduction-zone earthquakes, estimation of recurrence intervals must rely entirely on plate-convergence-rate estimates and geologic data, such as the time intervals between rapid subsidence events (Atwater, this volume) or submarine slope-failure events (Adams, this volume). These complexities add to our uncertainty about earthquake recurrence for each source type.

Although the recurrence rates for crustal, Benioff zone, and great subduction earthquakes are not yet well established, estimates have been calculated for several source types and source areas (table 5). The earthquake magnitudes in table 5 are the magnitudes at which a given author specified the recurrence rate (in some studies, the author also inferred these magnitudes to be the maximum magnitude; notwithstanding these values, in our view, the discussion of maximum magnitude given above seems most plausible). These recurrence rates give a rough basis for estimating the recurrence of damaging earthquakes for each source type. Large crustal earthquakes (about M 6) have a mean return period of about 200 years (Crosson, 1989) based on seismic data from the Puget Sound region. Note, however, that three to four crustal earthquakes with magnitudes between 7 and 8 have occurred in the Pacific Northwest since the first documented earthquake in 1833 (1872 Washington, probably crustal; 1918 and 1946 Vancouver Island; table 1). Study of ancient earthquakes on several individual faults in northern California and southern Oregon indicates the average return period (M 7.6–7.8) on these faults is about 500–600 years (Carver, 1989; Clarke and Carver, 1989). From the small seismicity data base, M 7.4 earthquakes in the Benioff zone have about a 200-year return period (Crosson, 1989).

On the basis of age dating of buried estuary peats, subduction-zone earthquakes occurred on average every 600 years for the last 3,500 years but had irregular interseismic intervals (see Grant and others, 1989; Yeats, 1989; Atwater, this volume; Darienzo and Peterson, this volume). Turbidite

Table 5. Recurrence intervals for large earthquakes in the Pacific Northwest.

[Values are in years, rounded to the nearest hundred; *M* is the magnitude at which the rate is estimated; leaders (---) indicate no estimate. This table shows the variability in return-periods based on either historical seismicity or geologic or strain data. Earthquakes may not recur at regular intervals; hence, return period is a marginally useful concept. Still, the variability in these values and the range about which these measurements cluster gives a sense of the time between events expected in this region based on these data]

Data source	Intervals determined by geologic studies	Mean intervals determined by seismic studies		
	Subduction earthquakes	Benioff-zone earthquakes	Crustal earthquakes (except subduction)	Benioff-zone and crustal earthquakes
Atwater (this volume), south coastal Washington	300–1,200	---	---	---
Peterson and Darienzo (this volume), central coastal Oregon	300–700	---	---	---
Clark and Carver (1991), Gorda South plate	150–550 (*M* 8.4)	---	---	---
Heaton and Hartzell (1986)[1]	100–250 (*M* 8.5)	---	---	---
	250–500 (*M* 9.5)	---	---	---
Adams (this volume)	600	---	---	---
Adams (1984)	200–500	---	---	---
Based on Juan de Fuca plate convergence rates (see text; and Rogers, 1988a)	400–1,300	---	---	---
Based on strain-rate measurements				
Savage and Lisowski (1991)	400–1,100	---	---	---
50-μstrain accumulations (see text)	550	---	---	---
Crosson (1989), Puget Sound	---	200 (*M* 7.4)	200 (*M* 6.1)	---
Rasmussen and others (1974), Puget Sound	---	---	---	100 (*M* 7.0)
Perkins and others (1980), Puget Sound	---	---	---	100 (*M* 7.0)
Perkins and others (1980), Willamette basin	---	---	---	700 (*M* 7.0)

[1]Rates inferred from strain measurements and (or) comparison with other subduction zones.

deposition during about the last 7,500 years had an average occurrence rate remarkably similar to that deduced from buried estuary peats. The uniform thickness of turbidite deposits suggests that subduction-zone earthquakes happen at relatively uniform intervals of about 590±170 years (Adams, this volume). On the basis of both data sets, the most recent earthquake occurred about 300 years before 1990, although earlier dates do not always coincide for turbidites and subsidence events. Approximate or possible correspondence, however, exists for events at 300, 1,100-1,200, and about 4,300 years ago (Adams, this volume). The lack of accord between event dates over the entire record for the two data sources may be related to their measurement and interpretation. For example, several processes, such as erosion or oxidation, could remove or mask some markers in the subsidence record. It is also plausible that some large earthquakes do not produce uplift at the coast, as has been observed for some events in Chile. Furthermore, estimation of the date of turbidite deposition, based on the thickness of layers that separate turbidite deposits and assumptions about erosion of these layers, is only approximate (Adams, this volume). Nonetheless, the close agreement between the long-term mean rates of event occurrence and the similarity in some of the age estimates from two independent data sets is compelling but still equivocal, evidence that the geologic record marks the effects of paleoseismic earthquakes.

Continued refinement of paleoseismic techniques and extension of the data base to older earthquakes will help test these results. Further study will also clarify the degree to which errors in radiocarbon dating or other errors bias these results and will help determine whether some earthquakes are missing in the geologic record.

If we know the rate at which the Juan de Fuca and North America plates converge and if we know or assume the total slip occurring in a great earthquake, it is possible to calculate the return period between events (return period equals total slip divided by slip rate). Rogers (1988a) estimated the mean repeat time for great earthquakes on the Cascadia thrust fault by combining convergence-rate estimates with assumptions about maximum slip during great earthquakes and the ratio of seismic slip to total slip. Using this technique, return-period estimates range from 400 to 1,300 years for the Juan de Fuca segment of the Cascadia thrust fault. The recurrence intervals obtained using this method for the Explorer plate (100–300 years) and the Gorda plates (70–200 years) are small, leading Rogers (1988a) to suggest that these segments have the highest probability of rupture.

Inference about the time between great earthquakes from strain-rate measurements appears to roughly agree with the geologic data from Washington and Oregon. It is estimated 40–100 μstrain accumulated before fault rupture in other great earthquakes, independent of magnitude (μstrain is a dimensionless quantity referring to deformation of crustal rocks of one part in one million; also, see the definition of strain rate in the glossary) (Sbar, 1983; Adams, 1984; Heaton and Hartzell, 1986). Given the compressional strain

rate of 0.092 μstrain per year (Savage and others, 1991), and a similar strain rate for western Oregon, that is, 0.08 μstrain per year (Paul Vincent, University of Oregon, written commun., 1991), the period between earthquakes is about 400–1,100 years. Repeating the calculation using the 50-μstrain maximum estimated for the great subduction-zone earthquakes in Chile in 1960 and Alaska in 1964 (Plafker and Savage, 1970; Plafker, 1972), the calculated return period is about 550 years, a value approximating the long-term mean rates deduced from geologic data.

Using current estimates of the mean repeat time, the time since the last earthquake, and the standard error in these estimates, the probability of a large earthquake on the Cascadia thrust fault can be forecast for specified time periods. Adams (this volume) used the turbidite recurrence interval to compute a 10-percent probability of a great earthquake in the next 100 years and a 25-percent probability in the next 200 years. He notes that these estimates could be in error by a factor of 2 and does not include the possibility of events clustering in time (Adams, this volume). We consider the values quoted from this study to be preliminary estimates because of present uncertainties in the underlying assumptions and data.

Note that the time since the last great earthquake, based on geologic studies, is about 300 years, whereas the average repeat time is about 600 years. If the repeat times are regular, one could infer that the next earthquake is 300 years hence. If the repeat times vary between 300 and 1,200 years, however, it is difficult to infer the time of the next event with statistical significance or practical utility. Although much is known, many questions remain unanswered concerning the timing and recurrence of great earthquakes.

LOWER SEISMIC RATES IN OREGON

Compared to western Washington, much of western Oregon has lower seismic activity (for example, see Weaver and Michaelson, 1985). Although a subducted plate is present beneath western Oregon, seismicity defining the Benioff zone is absent, and few earthquakes have been detected in the continental crust. The meager number of seismograph stations in Oregon, however, probably reduces our ability to detect earthquakes with magnitudes below some threshold. Nevertheless, it is likely that a difference does exist in the underlying activity rate at magnitude levels where detection is complete. The cause of this difference and its implication for earthquake hazard in Oregon are important problems that have not been satisfactorily addressed. Two simplified hypotheses, similar to those used to explain the lack of seismicity on the thrust fault, may be invoked: (1) the thrust fault is unlocked in the Oregon section, and the continental crust and subducted slab are in a low-stress state that produces few earthquakes (for example, see Magee and Zoback, 1989); (2) the thrust fault and continental faults are locked, but the seismic cycle is such that few earthquakes are presently produced in either the continental crust or the Benioff zone (for example, see Spence, 1989). As with many tectonic issues in this region, existing data do not allow an unequivocal interpretation. The historical aseismicity in western Oregon implies lower short-term hazard compared with western Washington, but the long-term hazard is not necessarily lower. This conclusion would require definitive evidence that the subduction process is aseismic in this section of the Cascadia thrust fault. At present, we consider the long-term earthquake hazard in Oregon comparable to that of other sections of the Cascadia thrust fault because the geologic evidence suggests an active Cascadia thrust fault; furthermore, both offshore and onshore youthful faulting and folding suggest active continental earthquake processes.

In detail, several concepts related to these two hypotheses can or have been considered, but some of these ideas raise further dilemmas. For example, Riddihough (1984) suggested that subduction is slowed in the Oregon section relative to the Washington section because, including the Gorda North plate, the subducting slab adjacent to southern Oregon is younger than that adjacent to Washington. In this model, a young oceanic slab has more buoyancy and locks more effectively with the continental crust, reducing subduction rates (Kanamori, 1971; Uyeda and Kanamori, 1979; Ruff and Kanamori, 1980, 1983). Differences in buoyancy cause the Juan de Fuca plate to pivot about a pole located south of the plate, with slower subduction on the south and faster subduction on the north (Menard, 1978; Riddihough, 1984). In this model, slowed subduction on the southern section of the Juan de Fuca plate could reduce strain and seismic rates in the continental crust of Oregon.

Several issues arise in the consideration of Riddihough's (1984) hypothesis. From earthquake locations (Crosson and Owens, 1987) and travel-time studies (Green and others, 1986; Michaelson and Weaver, 1986; Owens and others, 1988), an arched subducted slab dips more shallowly beneath northern Washington and has steeper dip to the north and south of this section (fig. 6*A*). If the slab beneath Oregon is more youthful (and therefore more buoyant), one might expect the plate dip there to be shallower, not steeper, than that beneath Washington, although other factors such as oblique convergence, varying strike of the Cascadia thrust fault, and plate buoyancy could combine to produce complex plate geometry (Crosson and Owens, 1987).

If the subducted plate is arched, interplate coupling is expected to be greatest where the plate dips more shallowly and to be less in the steeply dipping sections such as beneath Oregon (Weaver and Michaelson, 1985). Decreased interplate coupling of the thrust fault beneath Oregon differs from Riddihough's (1984) model but is also consistent with lower seismic rates in western Oregon. An unlocked thrust fault beneath Oregon would not only permit aseismic subduction but would reduce seismic rates in the continental crust and subducted lithosphere (Rogers,

1985; Weaver and Michaelson, 1985). For example, an unlocked condition would reduce the slab-pull extensional stress necessary to produce Benioff-zone earthquakes.

If motion of the Juan de Fuca plate is independent of the Gorda (North and South) and Explorer plates, the buoyant-plate hypothesis would produce a result diametrically opposed to Riddihough's (1984) conclusion. Rogers (1985) argued that buoyancy was greater on the northern section of the Juan de Fuca plate (considering the Juan de Fuca plate alone, age increases from north to south). This hypothesis differs from Riddihough's (1984) model, which treated the Juan de Fuca and the Gorda North plates as a single plate. In Rogers' (1985) model, the age difference increases the interplate coupling on the north compared with the south. In this interpretation, the section of the trench off the Oregon coast is moving seaward (referred to as trench rollback) at about the same rate as the westward component of North America-Juan de Fuca relative plate motion. Rogers (1985) supported this interpretation by noting that partial compressional unloading of the continental crust in Oregon may have permitted extensional-style volcanism in western Oregon in the last 2.5 million years. Priest (1990) also argued that east-west extension in Oregon and eastward migration of the volcanic arc during the last 4–7 million years supports compressional unloading. Thus, a difference in the style of tectonism between the northern and southern sections of the continental crust adjacent to the Cascadia subduction zone could also result in differential seismic rates.

Other hypotheses have also been suggested. For example, a complete break in the downgoing slab at depths between 40 and 100 km could reduce slab-pull stress (Weaver and Michaelson, 1985; Michaelson and Weaver, 1986; VanDecar and others, 1991). In an extension of Riddihough's (1984) model, the lack of a Benioff zone beneath Oregon might be explained by reduced slab-pull forces owing to the buoyancy of young subducted crust. Spence (1989) argued that a slow subduction rate under Oregon permits the subducted-plate temperature to increase. Under this condition, the density of the downgoing slab beneath Oregon decreases relative to that beneath Washington, reducing the slab-pull force. Spence (1989) used seismic-velocity changes in the slab noted by Michaelson and Weaver (1986) to infer slab density. Neither the lack of slab seismicity nor these models, however, unequivocally indicate that large Benioff-zone earthquakes (similar to those in Washington in 1949 and 1965) or thrust-fault earthquakes are unlikely beneath Oregon.

GROUND-SHAKING-HAZARD ESTIMATION

Accurate estimation of the level of ground shaking in an earthquake requires much information about the earthquake rupture, including its depth, rupture area, orientation, and the slip distribution on the fault. Other factors are equally important, such as the distance between the fault and the site under consideration, the properties of the rock or soil underlying the site (including sediment geometry), and the attenuation of shaking that is expected between the fault and the site. Earthquakes occurring in the continental crust, the Benioff zone, or on the thrust fault must each be treated separately in shaking estimates because of factors such as differences in earthquake depth, expected maximum magnitude, and various source parameters. Much of the data required to estimate earthquake ground motions may not be available until after an earthquake occurs. Uncertainty about the parameters for each of the source types, including the likely position of ruptures both within and between the North America and Juan de Fuca plates, magnifies the difficulty of computing ground-shaking estimates in the Pacific Northwest. Thus, prediction of shaking levels requires estimation of these parameters from scant geologic, geodetic, and seismic information and earthquake activity in other localities.

Ground-shaking estimates can take several forms. For example, some maps depict the geographic variation in ground shaking with measures such as Modified Mercalli intensity, peak acceleration, spectral acceleration, spectral velocity (see the glossary for a definition of these terms), measures of relative motion at sites underlain by soil compared to rock, or some other parameter. Ground-motion maps are useful in the design of ordinary structures, urban planning, earthquake emergency response, zoning, estimation of losses, and so forth. Methods are also available to estimate these ground-motion parameters for specific sites, a practice that is used in the design of high-rise buildings, hospitals, and other critical structures. Site-specific shaking estimates commonly include more detailed information than is feasible for map estimates and, thus, are usually more accurate than map values.

Ground-shaking time series (for example, ground acceleration versus time) and related spectra are commonly estimated from theoretical and hybrid (combinations of empiricism and theory) methods. Estimation of the model parameters is difficult, and intensive computations are required with these methods; thus, this type of prediction is most commonly applied in site studies for critical structures. In the following sections, we review various ground-shaking estimates for hypothetical and historical Pacific Northwest earthquakes to give the reader a sense of the expected levels of shaking for various earthquake types and to outline the uncertainties surrounding these estimates.

PROBABILISTIC GROUND-MOTION ESTIMATES

One type of empirically based ground-motion estimate takes the form of statements about the level of ground shaking that will not be exceeded during a specified exposure period with a specified probability level. Maps of uniform

Table 6. Probabilistic earthquake ground-shaking-hazard estimates for various urban areas.

[Peak horizontal accelerations and velocities, with a 10-percent probability of exceedance in the number of years shown, on firm soil. (>), greater than]

Location	Exposure time			
	Peak acceleration (percent g[1])		Peak velocity (centimeters per second)	
	50 years	250 years	50 years	250 years
Seattle, Wash.	[2,3]30	[3]41–[2]60	[3]17–[2]28	[3]23–[2]52
Portland, Oreg.	[2,3]16	[3]30–[2]36	[3]10–[2]15	[3]15–[2]30
Salt Lake City, Utah	[2]29–[4]35	[2]60–[4]70	[2]22	[2]60
San Francisco, Calif.	[2]80	[2]>80	[2]80	[2]>80
Memphis, Tenn.	[2]30	[2]40	[2]20	[2]40

[1] g, local gravitational acceleration, approximately equal to 980 cm/s^2.
[2] Algermissen and others (1990). Includes uncertainties for some parameters.
[3] Perkins and others (1980). Does not include parameter uncertainties.
[4] Youngs and others (1987). Includes parameter uncertainties.

probabilistic ground-shaking hazard are computed for specified site conditions, commonly firm soil or rock. For example, the mapped parameter may be the peak horizontal acceleration, peak velocity, or spectral acceleration having a 10-percent probability of being exceeded in an exposure period of 50 years. The Applied Technology Council (1978) used such maps (updated every 3 years) for design ground-motion specification included in their proposed seismic regulations for buildings. The National Earthquake Hazards Reduction Program's "NEHRP Recommended Provisions for the Development of Seismic Regulations for New Buildings" (Building Seismic Safety Council, 1992) used similar specifications for ground motion in the 1988 Uniform Building Code (International Conference of Building Officials, 1991).

Computation of probabilistic hazard maps requires (1) the location, depth, orientation, and seismic rate on each active fault for the range of earthquakes capable of generating strong shaking, (2) an estimate of the maximum magnitude for each source, (3) the ground-motion attenuation curve as a function of magnitude and distance from the source, and (4) an estimate of each parameter's variability. In lieu of complete information about specific faults, seismic rates are commonly attributed to source zones that may be composed of a few or no specific faults, "background faults" (a uniformly spaced fault grid of specified orientation and maximum magnitude), and uniformly distributed point sources for earthquakes of magnitude less than about 6–6.5. Seismic rates may be distributed on these elements uniformly or may be apportioned based on seismic observations or geologic constraints. In principal, the maximum magnitude could be defined as the maximum magnitude observed in the source zone or on a specific fault. However, the maximum magnitude for some source zones is unknown because the historical period is too short to have observed the largest earthquake. In such cases, the maximum magnitude may be estimated from the length of young faults in the source zone or from comparison of the tectonic setting with similar circumstances in other places, or it is assumed to be a value arbitrarily equal to or larger than that observed historically. Commonly, the attenuation function is based on historical strong-motion data, which is predominantly composed of records of shallow earthquakes in California.

Past probabilistic ground-shaking-hazard estimates for the Pacific Northwest suggested that the hazard is significant. Estimates such as those by Algermissen and others (1982), Perkins and others (1980), or Algermissen and others (1990) were based on the assumption that damaging future events will recur as they have in the past, that is, as shallow- and intermediate-depth earthquakes no larger than M 8.2. These probabilistic estimates did not incorporate great subduction-zone earthquakes because evidence for such events was not yet recognized. These probabilistic ground-shaking-hazard maps show that levels of shaking that might be exceeded in a 50-year period with a 10-percent probability of exceedance are comparable to those in the Salt Lake City, Utah, area (table 6) or to those in the moderately seismic areas of California, such as the Central Valley and sections of northern California (Algermissen and others, 1990).

Algermissen (1988) also produced preliminary probabilistic hazard estimates that do account for potential subduction-zone earthquakes. He assumed, based on the paleoseismic data, that a subduction-zone earthquake of M 8.5 could have average recurrence intervals of 300, 600, or 900 years, ranges that roughly parallel those suggested by geologic studies. The calculations also account for shallow seismicity and large Benioff-zone earthquakes (M_w 7.5 or less). These calculations did not account for the time since the last earthquake but assumed a Poisson earthquake-occurrence process. Besides the three recurrence intervals

assumed, two fault models were separately applied. In one model, the eastern extent of slip was assumed to be the point at which the fault penetrated to a depth of 20 km, which limits its extent west of the outer coast. In the second model, the eastern extent of slip was assumed to be the point at which the fault penetrated to a depth of 50 km, which permits the rupture to extend as far east as Puget Sound. For the rupture model to 20-km depth, Algermissen (1988) found that the 50-year exposure-time peak acceleration on rock with a 10-percent probability of exceedance was not appreciably different from the value given in table 6 for Seattle. This result held for all three assumed recurrence intervals. For the deeper rupture extending to Puget Sound, the probabilistic peak acceleration and velocity were about equal to that in table 6 when the 900-year average recurrence interval was assumed, but the peak velocity was double the table 6 value when the 300-year recurrence interval was assumed.

More recent modeling (Algermissen and Leyendecker, 1992) of the subduction zone to compute spectral probabilistic ground motions is in general agreement with the peak acceleration results just discussed. These results show that for an exposure time of 50 years, probabilistic spectral accelerations at 0.3 s and 1.0 s (5-percent damping) on stiff soils (S2 classification, Building Seismic Safety Council, 1992) are about 85 cm/s^2 and 35 cm/s^2, respectively, at Seattle. Spectral accelerations for a 250-year exposure time are about double the 50-year values. The spectral values can be approximately converted to peak values by dividing the 0.3-s-period values by 2.12 (Newmark and Hall, 1982). Thus, the peak acceleration expected in Seattle on stiff soils for a model that incorporates all three source types is about 0.4g (g=980 cm/s^2, see the glossary). The spectral values are unchanged at Seattle whether or not the great subduction zone earthquake is included.

The important conclusion is that, if the rupture surface in the subduction zone is more than about 125 km from Seattle and if average recurrence rates of large M_s 8.5 earthquakes equal about 500 years, large subduction-zone shocks have little effect on the maximum probabilistic acceleration (10-percent chance of exceedance) at Seattle for periods of interest (exposure times) of as much as about 250 years.

The result that the probabilistic hazard with and without inclusion of large thrust-fault earthquakes is mostly unchanged for some ground-motion parameters is due in part to the greater distance of the subduction fault rupture from the urban areas of Washington and Oregon relative to faults in the continental plate and Benioff zone and in part to the infrequency of great subduction-zone earthquakes relative to other earthquake sources. This result does not imply that subduction-zone earthquakes are an inconsequential component of the earthquake-shaking hazard. First, strong shaking in a large subduction-zone earthquake will be widespread. Although mapped probabilistic ground-motion estimates would show this fact clearly, point estimates such as those discussed above (Algermissen, 1988) do not delineate the geographic extent of shaking. Furthermore, statements about the probabilistic peak acceleration and to a lesser extent peak-velocity hazard do not adequately represent the hazard due to low-frequency ground motions of long duration that would be of great importance in assessing the effect of this type of earthquake on tall buildings and bridges. The efficiency of a great earthquake in generating low-frequency motions is also of prime importance in increasing the degree and distribution of landsliding and liquefaction. Second, note that probabilistic hazard calculations presently do not fully account for the effects of site geology, which can significantly increase the level of ground shaking at sites underlain by low-velocity sediments or at sites affected by ground-motion focusing due to sediment geometry. Finally, peak acceleration or velocity computed by this method does not necessarily represent the maximum ground motion expected in each source zone. The maximum expected motion can be estimated by deterministic means (see below) or by using probabilistic ground motions for long exposure periods.

Other limitations of probabilistic ground-motion maps are widely recognized. The calculations are no better than the accuracy of the input parameters used in the models. For example, the return period and expected size for each type of earthquake in the Pacific Northwest is poorly determined, particularly for continental-crust earthquakes. Probabilistic maps could understate the hazard for continental-crust earthquakes. Although past probabilistic hazard calculations assumed that large continental-crust earthquakes were possible, it is increasingly apparent that the number of shallow faults capable of producing large earthquakes and the rate of earthquakes on these faults is presently unknown. Stated another way, given the complexity of the deformation in the Pacific Northwest, the historical record probably does not provide an adequate sample of the seismic rate or the modes of deformation, and there is presently no means to entirely account for this fact in probabilistic hazard calculations. On the other hand, McGuire and Barnhard (1981) found in a study of the China earthquake record that the best hazard estimate for the next 50-year interval is the most recent 50-year period, a result that supports the utility of probabilistic forecasts.

The utility of probabilistic hazard maps stems from the need of users to compare the relative hazard across geographic regions using our current state of knowledge in a way that integrates different historical seismic rates, ground-motion attenuation, maximum magnitude, and tectonic style (National Research Council, 1988). The absolute hazard level predicted by these methods is useful only insofar as the parameters incorporated into such maps are an accurate representation of physical earthquake processes; however, the quality of this knowledge itself varies geographically. As we continue to improve our knowledge of earthquake processes, probabilistic estimates of the ground-shaking hazard can serve as a guide in decisions made by designers, code writers, regulators, owners, and public officials. Probabilistic

hazard calculations serve to establish the change in risk incurred for various decisions within the constraints of the models and our present state of knowledge.

Probabilistic hazard calculations are commonly used in infrastructure design decisions and now form the basis for design ground motions in most building codes. Ideally, design levels should vary for buildings of different types. The use of building-design motions corresponding to longer exposure periods, for example, is a conservative approach that can be used for critical facilities to mitigate the effects of imperfect return-period and time-of-occurrence estimates for great subduction-zone earthquakes. The design level may be higher for schools and hospitals, where the risk for loss of life is higher, than for certain types of low-occupancy, low-rise commercial structures. Thus, for a type of structure with low economic value or life-loss risk, a ground motion associated with a 50-year exposure period (or shorter) may be adequate, whereas for a structure with high value, high life-loss risk, and (or) a long projected lifetime, a ground motion associated with a 250-year exposure period (or longer) may be the design motion required to achieve an acceptably low level of risk. The point is that probabilistic estimates of the ground-shaking hazard permit one to assess the relative risk incurred for various design ground-motion decisions.

OTHER EMPIRICAL GROUND-MOTION ESTIMATES

As an example of estimated shaking values in map form, the U.S. Geological Survey (1975) produced maps of expected Modified Mercalli intensities for several hypothesized Benioff-zone earthquakes in Washington. These *M* 7.5 events were separately assumed to initiate at 50-km depth at the location of the 1965 earthquake and at a location near Seattle. Modified Mercalli intensities were estimated for a six-county area that included Seattle, Tacoma, and Olympia. The predicted Modified Mercalli intensities in the Seattle area ranged between VI and IX, depending on near-surface geologic conditions. These maps were the basis of casualty and damage estimates in the six-county region (we summarized the results in the "Recognizing Potential Earthquake Hazards and Risk in the Pacific Northwest" section).

An important method of predicting the ground motion for subduction-zone and Benioff-zone earthquakes is to fit earthquake observations recorded in other subduction zones with an equation that includes terms for magnitude, geometric and anelastic attenuation, and site conditions. This technique has been used in several studies relevant to the Pacific Northwest (Crouse and others, 1988; Youngs and others, 1988; Youngs and Coppersmith, 1989). Although the data distribution and data properties are generally inadequate to independently determine all the coefficients in an equation expressing each of these factors, one or more of the parameters are commonly fixed by theory or other independent information. Furthermore, ground motions generated by individual subduction zones may differ because of unmodeled parameters such as dip of the fault, distribution of slip on the fault, and the type of earthquake (that is, a thrust-fault or Benioff-zone event). Still, these are among the most reliable methods currently available to predict deterministic ground-shaking values. The probabilistic computations also require empirical equations of this type.

Empirical ground-motion values predicted using the relations developed by Youngs and others (1988) and Youngs and Coppersmith (1989) for both great thrust-fault and Benioff-zone earthquakes are summarized in table 7. For a thrust-fault earthquake, we considered two cases. In the first case, we assumed the thrust-fault rupture extends eastward as far as the 40-km-depth contour on the fault. Some disagreement exists concerning the geographic position of the 40-km contour. Crosson and Owens (1987) placed it 35 km west of Seattle, assuming that the thrust fault lies within the seismically quiet zone between the position of the crustal earthquakes and the earthquakes within and below the subducted slab (the seismicity cross section in fig. 8*B* is representative of the data). Weaver and Baker (1988) inferred a position 90 km west of Seattle based on the position of the Benioff zone but assumed that the thrust fault lies along the top of the Benioff-zone seismicity. From refraction profiles and other geophysical data, Mooney and Weaver (1989) placed the 40-km contour about 30 km west of Seattle. These contour locations correspond to a 50–100-km range in closest distance to the fault. Closest distance to the fault (R, table 7) is the equation parameter required in Youngs and others (1988) and Youngs and Coppersmith (1989) formulation. To complete our example calculations, we used the contours of Mooney and Weaver (1989). The shortest distance to the fault is about 50 km to Seattle and 40 km to Portland. In the second case, we assume the thrust fault ruptures to the 20-km depth contour on the fault. The shortest distance to the rupture is about 135 km from Portland and about 160 km from Seattle. We assume that parts of the rupturing segment of the Cascadia thrust fault are adjacent to but west of each city. The magnitude we assume is arbitrary and independent of the implicitly assumed fault length.

The computed results in table 7 illustrate several important points about the ground-shaking hazard at Seattle and Portland from Cascadia thrust-fault earthquakes. First, under any assumption about the position of the rupture, an earthquake of this size is expected to produce damaging ground motion at least as far east as the urban areas of the Puget Sound-Willamette Valley lowland. Second, the ground-motion values expected at Portland are marginally higher than those expected at Seattle. Third, the values at Seattle or Portland under case 2 could be roughly twice the values under case 1. Fourth, based on the Youngs and others (1988) equations, ground-motion values at sites underlain by soil

Table 7. Empirically predicted and observed seismic ground motions for Seattle, Wash., and Portland, Oreg.

[Based on relations developed by Youngs and others (1988) and Youngs and Coppersmith (1989). R, closest distance to the fault. Predicted acceleration is rounded to the nearest 0.05*g*, and predicted velocity is rounded to the nearest 5% *g* (where *g* is approximately 980 cm/s^2). Predicted spectral-acceleration values are computed by the appropriate transformation of spectral velocity given by the relations developed by Youngs and others (1988) and Youngs and Coppersmith 1989]

	M 8.5 thrust-fault rupture								*M* 7.9 Benioff-zone rupture predicted ground motions,[1] R=50 km		*M* 7.1, 1949 earthquake, observed ground motions,[1] R=49 km	*M* 6.5, 1965 earthquake, observed ground motions,[1] R=91 km
	Rupture to the 40-km fault contour				Rupture to the 20-km fault contour							
	Rock		Soil		Rock		Soil					
	R=50 km (Seattle)	R=40 km (Portland)	R=50 km (Seattle)	R=40 km (Portland)	R=165 km (Seattle)	R=145 km (Portland)	R=165 km (Seattle)	R=145 km (Portland)	Rock	Soil	Soil[2]	Soil[2]
Peak ground acceleration (percent *g*)	20	20	30	35	10	10	15	15	25	40	[3]28	[4]20
Five-percent spectral acceleration at 0.3 and 0.7 seconds (percent *g*)	40–30	45–35	70–50	75–55	15–10	20–15	30–20	35–25	50–35	90–60	[5]58–25	[5]42–20
Five-percent spectral velocity at 1-s period (centimeters per second)	30	35	50	55	10	15	20	25	35	60	[5]35	[5]23

[1]Olympia Highway Test Laboratory.
[2]Largest of two horizontal components.
[3]Langston (1981b).
[4]Baker and Langston (1987).
[5]Trifunac (1977).

are as much as twice the values at sites underlain by rock. Other data, however, suggest that rock-soil site-spectral differences can be larger than shown in table 7 for some site types at some periods (for example, Algermissen and others, 1985; Theil, 1990; Rogers and others, 1991).

Calculated ground-motion values using equations developed for Benioff-zone earthquakes by Youngs and others (1988) and Youngs and Coppersmith (1989) are also shown in table 7. To illustrate their equations, we postulate a Benioff-zone earthquake of M 7.9 directly beneath either Seattle or Portland, almost a worst-case hypothesis for an earthquake of this type. Ground motion for this type of earthquake is substantially larger than those expected from the thrust-fault earthquakes. The ground motion values observed in the 1949 and 1965 earthquakes at the Olympia Highway Test Laboratory are included in table 7. Although the observed and predicted values cannot be compared directly because of differences in magnitude and distance, a casual comparison shows that the empirical predictions are reasonable.

Uncertainty about the position of intraplate continental-crust faults and the potential maximum magnitude of earthquakes on these faults precludes estimation of the ground-shaking hazard associated with them. If faults such as the Portland Hills, Hood Canal, and Saddle Mountain, or the geophysically inferred structures beneath Puget Sound, are capable of generating earthquakes, the Seattle and Portland levels of ground shaking from earthquakes on these faults could exceed that from either thrust-fault or Benioff-zone earthquakes.

THEORETICAL GROUND-MOTION ESTIMATES FOR BENIOFF-ZONE EARTHQUAKES

Theoretical estimation of ground shaking for Pacific Northwest earthquakes at specific sites has been attempted for a few scenarios. Ground-motion time histories and spectra at a specific site can be produced using theoretical models that incorporate fault rupture, propagation path, and site properties. For example, Langston (1981b) modeled the velocity and displacement time histories that were recorded during the 1965 Benioff-zone earthquake at Seattle, Tacoma, and Olympia. Significant discrepancies between the modeled and recorded motions were attributed to insufficient knowledge about Earth structure and the source. The inadequacy of this model led to more realistic attempts, such as ray-tracing calculations in a two-dimensional model of the Duwamish River valley (Langston and Lee, 1983). This study predicted that order of magnitude changes in ground-motion displacement are possible over distances of 200 m due to focusing of seismic energy by basin geometry. Langston and Lee (1983) suggested that the geographic variability in ground shaking during the 1965 earthquake could be explained on this basis. A three-dimensional model was also evaluated with ray-tracing techniques (Ihnen and Hadley, 1986) and compared with the records for the 1965 earthquake. In this study, maps of peak acceleration for the Puget Sound region showed variability of a factor of 10 at a given distance from the fault, due primarily to focusing by basin geometry and secondarily to amplification by near-surface low-velocity layers. Their model predicted peak accelerations observed at Seattle and Tacoma reasonably well but underestimated the peak acceleration at Olympia by a factor greater than 4. Ihnen and Hadley (1986) indicated that their results qualitatively agreed with the observed intensity variations in the 1965 earthquake. By way of comparison with the predictions given in table 7, a large fraction of Ihnen and Hadley's ground-motion values grouped in the range between 0.03 and 0.3g at epicentral distances between 0 and 70 km, though some of their predicted values were as large as 0.6g near the mouth of the Duwamish River.

Silva and others (volume 2) used a stochastic ground-motion model and random-vibration-theory techniques to predict the ground motions for the 1949 and 1965 earthquakes. Their computations assumed seismic-energy release at a point on the fault nearest the site, attenuating propagation between source and site, and an attenuating flat-layered near-surface velocity model that approximates the site effect. In these simulations, the known hypocenter for these earthquakes is the assumed point of energy release. The peak acceleration values predicted by this technique compare favorably with the observed values (table 7) except at station OHT (Olympia Highway Test Laboratory) for the 1965 earthquake. For this station, the predicted values are too low by about a factor of 2 (table 8) (Silva and others, volume 2). This discrepancy has been attributed to excessive model attenuation in the near-surface sediments. Silva and others' (volume 2) predicted spectral acceleration curves also compare favorably during most periods with the observed spectral accelerations in the 1965 and 1949 earthquakes at stations in the Olympia Highway Test Laboratory and the Federal office building in Seattle. These comparisons show the value of using this technique for predicting ground motions in this region at other sites or for other types of earthquakes.

THEORETICAL GROUND-MOTION ESTIMATES FOR THRUST-FAULT EARTHQUAKES

The results of three theoretical modeling studies for hypothetical earthquakes on the Cascadia thrust fault are shown in table 8. Silva and others (volume 2) applied the model described in the last section to predict the ground motions for a thrust-fault earthquake. In their simulations, they assumed the point of energy release to be at 70-km hypocentral distance from the Federal office building station in Seattle. Thus, this model simulated rupture to the 40-km-depth contour on the thrust fault (see the discussion in the previous section).

Table 8. Theoretical deterministic ground-motion parameters at Seattle for a Cascadia subduction-zone earthquake.

[Accelerations have been rounded to the nearest 5-percent g (where g is approximately 980 cm/s^2). Leaders (---) indicate no estimate]

References	Magnitude	Closest distance to the fault (kilometers)	Peak ground acceleration (percent g)		Maximum 5-percent spectral acceleration at 0.3 and 0.7 seconds (percent g)	
			Rock	Soil	Rock	Soil
Silva and others (volume 2)	8.5	146	---	15	---	35
Cohee and others (volume 2) Washington model (see text)	8	81	10–15 (deep model)	25 (deep model)	20–10	[2]30
Heaton and Hartzell (1987, 1989)	9.5	68	[1]25		[1]70	

[1]Average of soil- and rock-site records. The values are for Puget Sound rather than Seattle.
[2]Cohee and others (1991).

Cohee and others (volume 2) applied a Green's-function technique (see the glossary), with empirical source functions recorded during the 1985 Chile thrust-fault earthquake at two sites, one underlain by rock and the other by soil. This source function is modified by theoretical functions that simulate the effects of gross crustal structure and geometric attenuation. Two M 8 thrust-fault earthquakes are modeled in this manner, one in Washington and one in Oregon. Each rupture zone had a different length, downdip width, and dip, largely in accord with the plate geometry determined by Weaver and Baker (1988). Ruptures extended to the 40-km-depth fault contour in both cases. The model included the effects of crustal structure and implicitly included near-surface site effects. The calculations separately assumed three distributions of energy release on the fault: shallow (upper one-third of the fault), middle (middle one-third), and deep (lower one-third). The largest accelerations at Seattle and Portland are for both deep-rupture zones because this model places the greatest energy release nearest these urban areas. Peak accelerations at Portland for the deep earthquake (0.1g for rock and 0.2g for soil) were slightly lower than those at Seattle (table 8).

Heaton and Hartzell (1987, 1989) applied an empirical Green's-function technique whereby they added together the radiated ground-shaking contribution of lower magnitude earthquakes distributed on the fault to simulate the radiation of a M 9.5 earthquake. In their study, an assortment of records produced by thrust-fault earthquakes, ranging in magnitude from 7.4 to 8.2, from Japanese and Alaskan subduction zones served as Green's functions. Heaton and Hartzell (1987, 1989) considered three fault models, but the values we quote in table 8 are for the fault model that ruptures from the trench axis east to the coast. In their study and that of Cohee and others (volume 2), the ground-motion values were substantially larger than those shown in table 8 for other cases when the rupture extended eastward to Puget Sound. Extension of the rupture eastward is inferred if the slab is arched into the thrust-fault region, as is suggested by some data sets.

SUMMARY OF GROUND-MOTION ISSUES

Several important factors may control the level of ground shaking in a great subduction-zone earthquake. First, the eastward limit of energy-releasing rupture will have a strong influence on the level of shaking in the urban areas of the Puget Sound-Willamette Valley lowland. If the thrust fault ruptures no farther east than the outer coast, shaking damage will be limited compared with a rupture extending beneath the Olympic Peninsula or farther eastward. A rupture limited to the outer coast would reduce the shaking damage, particularly for low-rise buildings, compared to the effects shown in tables 6–8. Even in this situation, however, the hazard for some classes of structures greater than two to five stories in height may remain high, particularly for those structures underlain by geologic basins or thick sediments. The amplification of long-period ground shaking in sedimentary basins and the lower rate of attenuation of long-period motions with distance could lead to damage of some tall structures. The Michoacan earthquake off the coast of Mexico damaged and collapsed some types of buildings in Mexico City, about 360 km from the epicenter. Buildings of seven to twelve stories were particularly affected at some Mexico City locales because geologic conditions (Singh and others, 1988) increased the level and duration of shaking to damaging levels for buildings in this class (Smolka and Berz, 1989). The 1989 Loma Prieta M 7.1 earthquake also produced damage as much as 80 km from the rupture zone owing to the effects of site geology (for example, see Theil, 1990). Although the most vulnerable geologic conditions in Mexico City and San Francisco are extreme cases, similar deposits are found at some sites in the Pacific Northwest. Furthermore, a Cascadia thrust-fault rupture to the outer coast results in a hypocentral distance to the Puget Sound-Willamette Valley lowland of less than about 160 km, considerably closer than the distance to Mexico City from the Michoacan earthquake.

Table 9. Examples of potential users of earthquake-hazard information in the Pacific Northwest.

City, county, and multicounty government users
Local building, engineering, zoning, and safety departments
City and county offices of emergency services or management
County tax assessors
Mayors and city council members
Multicounty planning, development, and preparedness agencies
Municipal engineers, planners, and administrators
Planning and zoning officials, commissions, and departments
Police, fire, and sheriff's departments
School districts, administrators, and teachers

State government users
Building Codes Agency (Oregon)
Building and Construction Safety Inspection Division (Washington)
Department of Community Development (Washington)
Department of Ecology, Dam Safety Section (Washington)
Department of Energy (Oregon)
Department of Environmental Quality (Oregon)
Department of Education (Washington and Oregon)
Department of Geology and Mineral Industries (Oregon)
Department of Information Services (Washington)
Department of Land Conservation and Development (Oregon)
Department of Transportation (Washington and Oregon)
Department of Water Resources (Oregon)
Division of Energy Management (Washington and Oregon)
Division of Geology and Earth Resources (Washington)
Division of Risk Management (Washington)
Fire Marshall (Oregon)
Fire Protection Services Division (Washington)
Legislature
Museum of Science and Industry (Oregon)
National Guard
Office of the Governor
Utility and Transportation Commission (Washington)

Federal government users
Army Corps of Engineers
Department of Energy
Congress and congressional staffs
Department of Housing and Urban Development
Department of the Interior (Bureau of Land Management, Bureau of Reclamation, U.S. Geological Survey)
Department of Transportation
Environmental Protection Agency
Farmers Home Administration
Federal Emergency Management Agency
Federal Housing Administration
Federal Insurance Administration
Federal Power Commission
Forest Service
General Services Administration
National Institute of Standards and Technology
National Oceanic and Atmospheric Administration
National Security Council
Nuclear Regulatory Commission
Small Business Administration

Other national users
American National Red Cross
Applied Technology Council
American Association of State Highway and Transportation
American Public Works Association
Association of Engineering Geologists
American Association of State Geologists
Earthquake Engineering Research Institute
International Conference of Building Officials
National associations of cities, counties, and States
National Association of Insurance Commissioners
National Center for Earthquake Engineering Research
National Institute of Building Sciences
National Hazards Research and Applications Center

Private, corporate, and quasi-public users
Civic, religious, and voluntary groups
Concerned citizens
Construction companies
Consulting planners, geologists, architects, and engineers
Extractive, manufacturing, and processing industries
Lending and insurance institutions
Landowners, developers, and real-estate salespersons
News media
Professional and scientific societies (including geologic, engineering, architecture, and planning societies)
University departments (including geology, geophysics, environmental, civil engineering, structural engineering, architecture, and urban and regional planning)
Utility districts

Second, the length and downdip width of rupture not only affect the level of shaking at a given location, but they also determine the size of the geographic area affected. An earthquake of M 8–9+ can be expected to produce damage from the outer coastal areas to the urban areas of the Puget Sound-Willamette Valley lowland. Simultaneous damage to a region of this size poses serious problems for emergency response and recovery.

For Benioff-zone earthquakes, an important issue is whether these events are possible at any location in the subducted lithosphere for depths between about 40 and 80 km. If so, then these earthquakes are possible below Seattle, Portland, and other urban areas of the Puget Sound-Willamette Valley lowland (Weaver and Shedlock, this volume). Occurrence of the largest possible Benioff-zone earthquakes, M_{max} 7.5–8 (U.S. Nuclear Regulatory Commission, 1991; Weaver and Shedlock, this volume), at locations near or beneath these urban zones would produce significantly larger ground motions than were observed at the same locations in the 1949 and 1965 earthquakes.

Almost every aspect of continental-crust earthquakes is an issue at present. The potential locations, maximum magnitudes, and shaking attenuation are poorly known for this type of earthquake in this region. Nonetheless, geologic

evidence exists for youthful continental-crust faults, and earthquakes have occurred on such faults in the region historically. Significant damaging ground motions could result from moderate-to-large continental-crust earthquakes occurring near urban areas. Notably, this type of earthquake has the potential to produce more intense damage to structures of all classes than thrust-fault and Benioff-zone earthquakes, if the shallow earthquake occurs within or near an urban area. An earthquake of this type, however, would likely affect a smaller region than a great Cascadia subduction-zone earthquake. Few ground-motion estimates have been produced for this type of earthquake in the Pacific Northwest to date, primarily because of uncertainty about which faults should be considered sources of future earthquakes.

USERS AND USES OF EARTHQUAKE HAZARD INFORMATION

Earthquakes are a recognized hazard in the Pacific Northwest, a fact that has resulted in scientific and engineering studies to assess the hazards. This report contains some of the significant new information produced by these studies. This information, when translated for and transferred to potential users (table 9), should result in the selection and adoption of appropriate earthquake-hazard reduction techniques as, for example, those introduced by Kockelman (volume 2). This report provides an opportunity to build a bridge between the producers and the users of earthquake-hazard information in the Pacific Northwest.

The responsibility for reducing earthquake hazards is shared by all segments of society. Potential users of earthquake-hazard information include many people at community, state, and national levels, both public and private (table 9). These may be scientists and engineers who use the information to resolve scientific or technical questions, planners and decisionmakers who must consider hazards in the context of other land use and development criteria, or just interested citizens who must consider the likelihood of future earthquakes before making personal decisions.

Various levels of government, business, industry, the services sector, voluntary organizations, professional societies, and special-interest groups play important roles in reducing earthquake hazards. Kockelman (volume 2) presents examples of some groups' utilization of earthquake-hazard information to reduce casualties, damage, and socioeconomic interruptions.

CITY, COUNTY, AND AREAWIDE GOVERNMENT USERS

City and county governments are empowered and obligated to provide for the public health, safety, and welfare of their citizens. For example, the Washington State Legislature (1990a, b) requires certain counties and cities to adopt growth regulations precluding land uses or developments that are incompatible with designated "critical areas." The minimum guidelines for classifying critical areas include seismic-hazard areas defined as "areas subject to severe risk of damage as a result of earthquake-induced ground shaking, slope failure, settlement, soil liquefaction, or surface faulting" (Washington State Department of Community Development, 1990). Public liability is an added incentive, as discussed by Perkins and Moy (volume 2). Legislatures commonly authorize and require the adoption and administration of local zoning, subdivision, building, grading, and safety ordinances. For example, recognizing the likelihood and severity of a future earthquake, one of the largest cities in the United States—Los Angeles—inventoried and evaluated its unsafe, unreinforced-masonry bearing-wall buildings. It then enacted an ordinance requiring owners to strengthen or demolish 8,000 such buildings in a 14-year period.

The various plans, codes, and map overlays introduced by Booth and Bethel (volume 2) are particularly good hazard reduction techniques into which earthquake-hazard information can be incorporated. For example, King County's "Sensitive Areas" ordinance can be amended to include more specific earthquake-hazard information, such as ground-shaking severity, landslide potential, and liquefaction potential, as it becomes available.

The principal governmental resource at the site of an emergency or disaster is usually local government agencies. They will necessarily be heavily involved in preparing for, coordinating on-the-scene response to, recovering from, and reconstructing after damaging earthquakes. For example, school preparations have included an earthquake safety program (Martens, 1988), an earthquake emergency planning booklet (Noson and Martens, 1987), and a manual for securing nonstructural building components (Washington State Superintendent of Public Instruction, 1989).

STATE GOVERNMENT USERS

States have the ultimate non-Federal public responsibility for the health, safety, and welfare of their people. For example, the Oregon State Land Conservation and Development Commission (1990, p. 8) adopted statewide mandatory planning goals and suggested guidelines. One of the goals requires that developments "subject to damage or that could result in loss of life shall not be planned or located in known areas of natural * * * hazards without appropriate safeguards." State agencies incorporate their own seismic-safety standards into their operations and also work with local governments to encourage community seismic-safety efforts. California mapped official zones of potentially active fault-rupture areas. It then mandated that all cities and counties require a geologic report for these areas prior to development and a minimum setback from the trace of active faults for most human-occupancy structures.

Officials in almost every State-government agency (table 9) need to consider seismic safety in carrying out their duties. For example, the Washington State Seismic Safety Council (1986) recommended essential actions that both the legislature and eight State agencies should undertake for a long-range seismic-risk-reduction program. In appendixes to its recommendations, the council identified the primary and secondary earthquake hazards, compared its earthquake activities to California's, and discussed potential losses, vulnerability of school buildings, liability, and risk of chemical accidents. The council also inventoried the hazard-reduction activities of selected State agencies.

The Washington State Legislature (1990a) directed the Department of Community Development (which includes the Division of Emergency Management) to create a Seismic Safety Advisory Committee. Funding was provided

> * * * solely for the department to develop a seismic safety program to assess and make recommendations regarding the state's earthquake preparedness. The department shall create a seismic safety advisory board to develop a comprehensive plan and make recommendations to the legislature for improving the state's earthquake preparedness. The plan shall include an assessment of and recommendations on the adequacy of communications systems, structural integrity of public buildings, including hospitals and public schools, local government emergency response systems, and prioritization of measures to improve the state's earthquake readiness * * *.

This advisory committee presently includes participation by 15 State agencies, business and industry representatives, and two local engineering consulting firms. The advisory committee has completed its initial report that recommends priorities for action, including establishment of a seismic-safety oversight committee, improved emergency planning, strengthening of buildings, and strengthening of lifelines (Washington State Seismic Safety Advisory Committee, 1991).

Likewise, in Oregon, Senate Bill 955 was passed in 1989 directing the Department of Geology and Mineral Industries (DOGAMI) to assess and mitigate earthquake hazards. In 1990, the Governor appointed the Seismic Safety Advisory Commission (SSPAC) to provide policy guidance on earthquake-hazard reduction. Also, in 1990, DOGAMI created a new Earthquake Engineer position. In 1991, the legislature established the SSPAC in Senate Bills 96 and 309. Senate Bill 96 also takes the following actions:

- Establishes earthquake drills in public, private, and parochial schools with 50 or more pupils.
- Amends the state building code to:
  1. Evaluate new essential facilities, hazardous facilities, major structures (greater than 6 stories and greater than 60,000 square feet), structures greater than 10 stories, and all parking structures.
  2. Install strong-motion accelerographs in and near selected buildings.
  3. Review geologic and engineering reports for seismic design of new, large, or critical buildings.
  4. File for public use noninterpretive data from seismic site evaluations.
  5. Establish a surcharge of 1 percent of building-permit fees to support the above activities.

Senate Bill 309 authorizes the Oregon Building Codes Agency to adopt regulations to require correction of unsafe conditions caused by earthquakes in existing buildings. The bill also grants building codes inspectors authority to inspect for damage after an earthquake.

Blair and Spangle (1979, p. 24) noted that the "location and construction of public facilities, management of State lands, provision of services, and delegation of powers and responsibilities to local governments should all reflect an awareness that damaging earthquakes are inevitable." Public awareness of the costs of damaging earthquakes, and techniques to reduce such costs, have been addressed in the Pacific Northwest in various ways. These include the Washington State Seismic Safety Council's recommendations (introduced above), bibliography and index to seismic hazards (Manson, 1988), serial publications such as Oregon Geology and Washington Geology (formerly Washington Geologic Newsletter), conferences and workshops (Walsh and others, 1990), outreach programs, and guidebooks (Noson and others, 1988).

FEDERAL GOVERNMENT USERS

The Federal Government is crucial in stimulating State and local governments to improve their seismic-safety efforts. The development and distribution of loss and damage scenarios are a part of its role. For example, the U.S. Geological Survey (1975) prepared a study of potential earthquake losses in the Puget Sound area and is funding an earthquake-hazard assessments program in the Pacific Northwest. Federal efforts to reduce risks have evolved from a national commitment to provide disaster relief to States and local areas devastated by earthquakes. One of these efforts includes the preparation and wide distribution of a series of guidebooks for reducing earthquake hazards (Kockelman, volume 2).

Federal agencies are also responsible for the seismic safety of their own facilities. After the 1971 San Fernando (southern California) earthquake, the U.S. Veterans Administration (1976, 1986) developed earthquake-resistant design requirements for Veterans Administration hospital facilities and established seismic-protection provisions for furniture, equipment, and supplies for these hospitals. In addition, the Government, through the Federal Emergency Management Agency (which carries out the National Earthquake Hazards Reduction Program), formulates plans for national actions in response to catastrophic earthquakes. These plans include large-scale preparedness for, response to, and recovery from major damage or loss of life. Such plans may include search and rescue, evacuation, provision for medical care, food, shelter, police protection, and other emergency help.

The Federal Government, through the U.S. Nuclear Regulatory Commission, is also responsible for the safe siting, design, and operation of nuclear power plants. They

have commissioned many studies by power-plant applicants and engineering firms and reviews on the geologic and seismic hazards that might affect nuclear facilities in the Pacific Northwest (U.S. Nuclear Regulatory Commission, 1991). The U.S. Nuclear Regulatory Commission recently increased the magnitude of the Safe Shutdown Earthquake (the largest earthquake for which major components of the power plant are expected to remain operational) for Cascadia thrust-fault earthquakes to *M* 8.25 (U.S. Nuclear Regulatory Commission, 1991), partly in recognition of work sponsored by the U.S. Geological Survey. The U.S. Nuclear Regulatory Commission also funds an independent research program on earthquake hazards.

The Federal Government is also responsible for the seismic safety of many dams. As part of this responsibility, both the U.S. Army Corps of Engineers and the U.S. Bureau of Reclamation conduct studies concerning the tectonic setting of dams and earthquake and volcanic hazards to these facilities in the Pacific Northwest (for example, see Hawkins, Foley, and LaForge, 1989). The Bureau of Reclamation also recognizes *M* 8.25 as the maximum-magnitude subduction earthquake on the Cascadia thrust fault (Peity and others, 1990).

OTHER NATIONAL USERS

Voluntary organizations (which provide aid to victims of disasters), national institutes, and scientific and professional organizations make major contributions to seismic safety. For example, the American National Red Cross (1986) prepared a resource guidebook that includes strategies on how to identify and use resources, conduct research and evaluations, work with Red Cross and other resources, and develop public relations. The earthquake preparedness program of Snohomish County, Wash., was included as one of 43 examples of Red Cross chapter activities.

Researchers from many disciplines, including seismology, geology, earthquake engineering, and the social sciences, have a major part in reducing earthquake hazards by helping local, State, and Federal planners and decisionmakers formulate and evaluate their plans and programs. Experts from the research community provide technical advice to special advisory groups that prepare model building codes such as the Uniform Building Code by the International Conference of Building Officials (1991). Scientific and professional organizations are major contributors to the worldwide exchange of information through publications and technical meetings.

PRIVATE, CORPORATE, AND QUASI-PUBLIC USERS

The private (including corporate) sector has perhaps the strongest influence on engineering design and land development in the United States. In choosing where to locate and how to construct facilities, industrial and commercial developers are sensitive to tax and other incentives offered by State and local governments to favorable labor and retail markets, to transportation networks, and to terrain and water-resource conditions. Often, natural hazards are not weighted heavily in these development considerations unless they are likely to affect the facilities within their amortized lifetime or period of ownership. According to the U.S. Executive Office of the President (1978, p. 29),

> Business, industry, and the services sector play the lead roles in constructing new buildings and in developing land. Seismic design provisions in local codes * * * are minimum standards. Thoughtful businessmen interested in providing a safe environment for their consumers and employees, and in protecting their capital investment will want to give careful consideration to earthquake hazards in planning, constructing and maintaining their facilities * * *. In some instances short-term profits may be reduced to increase the long-term benefits of saving lives, reducing property damage, and maintaining the functioning of the economy in the face of a major earthquake.

The seismic retrofitting of the Heritage Building and Union Station (Perbix, 1990a, b) in Seattle are good examples of business decisions intended to conserve capital investment and protect the public.

An important but less discussed aspect of engineering design includes the securing of nonstructural building components such as parapets, bookcases, office equipment, light fixtures, and partitions. A particularly good guidebook on reducing nonstructural earthquake damage has been prepared by Reitherman (1985). The hazard-reduction techniques recommended in this guidebook are relatively inexpensive and are fully applicable to the Pacific Northwest.

Kockelman (volume 2) emphasizes evaluation and revision of hazard-reduction techniques. A report on the 1989 Loma Prieta earthquake by the California Association of Hospitals and Health Systems (1990) is similar in scope. This report addresses structural, nonstructural, staffing, communications, cost-reimbursement, media-relations, and research issues. Many recommendations were made to improve building safety, preparedness, response, and recovery. Such studies are needed to effectively update planning for earthquake disaster.

PREREQUISITES FOR USE

The effective use of geologic, seismologic, and engineering information to avoid damage or to reduce loss requires a considerable effort by both the producers and the users of the information. For an integrated hazard-assessment method, see Preuss and Hebenstreit (volume 2). Unless scientific and engineering results are specifically translated, the effective user community is limited to other geologists, seismologists, and engineers. If users do not become proficient in interpreting and applying technical information, the information is likely to be misused or even neglected in the decisionmaking process.

A study by Kockelman (1990) on the use of earth-science information by planners and decisionmakers in Utah showed that the most effective use of hazard information was achieved when maps that clearly depicted the likelihood, location, and severity of the hazards were provided. Furthermore, the use of this information for hazard reduction was more likely when the information was delivered to potential users along with technical assistance and encouragement. The effectiveness of any earthquake-hazard-reduction program is dependent upon the awareness, understanding, and motivation of engineers, planners, and decisionmakers, public and private. May (volume 2) addresses the prospects for hazard reduction in the Pacific Northwest.

SUMMARY

In part, the stimulus for increased earthquake-hazards research funding in the Pacific Northwest was the recognition that this region may have had *M* 8–9.5 earthquakes along the Cascadia thrust fault during the last 7,000 years. Other factors also continue to fuel interest in potential regional earthquake hazards. For example, recent research indicates that large continental-crust earthquakes are possible in or near the principal urban areas of the Pacific Northwest. Given our current level of understanding, it is also likely that Benioff-zone earthquakes similar to the 1965 and 1949 events will recur. Some of these earthquakes could be larger (*M* 8 or less) or could occur closer to urbanized areas of the Puget Sound-Willamette Valley lowland than in the past. Furthermore, this area has also undergone major increases in population and economic value at risk since the last large earthquake in 1965. Together, these considerations provide incentive for continued evaluation of the tectonics and earthquake hazards of the region. The significance of this hazard also provides impetus for continued evaluation of the suitability, level of implementation, and effectiveness of existing plans and regulations to reduce future earthquake effects.

The most important issues regarding the level of earthquake hazard in the Pacific Northwest are summarized as follows:

- Large, shallow crustal earthquakes are likely in the future but, at present, little is known about the recurrence of these events or their potential locations. New geologic data suggest, however, that such earthquakes are possible at locations close to urban areas and that events of this type (not necessarily on the faults near urban areas) could be as large as about *M* 8.
- Great earthquakes are possible on at least some segments of the Cascadia thrust fault, and most scientists believe that these earthquakes could have magnitudes at least as large as 8, although magnitudes as large as 9–9.5 have been suggested.
- Unfavorable ground conditions in the Puget Sound-Willamette Valley lowland are expected to substantially increase the shaking hazard at some sites, particularly for high-rise structures underlain by deep sedimentary basins.
- The extent of downdip rupture in a subduction earthquake on the Cascadia thrust fault will strongly control shaking levels in the principal urban areas. A model fitting both strain and uplift rates suggests that the fault could rupture downdip to points beneath the Olympic Peninsula, which would substantially increase shaking levels relative to models that limit rupture to the Pacific coast or further west.
- Future large Benioff-zone earthquakes are likely, and some scientists believe that these events are possible within the subducted lithosphere from western British Columbia to northwestern California. The probable depth of these earthquakes ranges between 40 and 80 km. Their maximum magnitude is likely to be between 7.5 and 8.0. Thus, earthquakes of this type appear to be possible and have locations and maximum magnitudes that would produce substantially greater damage than the historical Benioff-zone earthquakes.

Progress in understanding the potential for great earthquakes or continental-crust earthquakes will come from continued paleoseismicity studies, instrumental seismicity studies, and expanded geodetic measurements. Much additional work is also needed to produce useful maps that depict the effects of geologic conditions on ground shaking and the areas of various types of ground failure. Although much remains to be done to further our understanding of the earthquake hazard in the Pacific Northwest, progress has been made in several areas, as evidenced by the results presented in this report.

Although this collection of research papers will be of interest to a wide audience, informing a diverse audience is hampered by the complexity of the problem. The controversy surrounding some issues in the Pacific Northwest further complicates communication. These factors prescribe substantial technical discussion to convey both the hazard and the limitations of our present data and methods of analysis. Most important, however, the historical and geologic lessons in hand tell us that earthquake hazards in this region are substantial and that this fact should be made clear to those responsible for the safety of others and the preservation of property in future earthquakes. An important goal of this publication is to provide information to these users and other citizens concerning the scientific state of knowledge about Pacific Northwest earthquake hazards. In addition, clarification of the issues will improve the focus of scientific research on factors that strongly control hazard assessment. This process will lead to increased understanding and recognition of the problem, to more informed decisions by engineers, planners, land and building owners, and public officials and, ultimately, to the adoption of appropriate risk-reduction techniques.

SELECTED REFERENCES

Abe, Katsuyuki, 1981, Magnitudes of large shallow earthquakes from 1904 to 1980: Physics of the Earth and Planetary Interiors, v. 27, p. 72–92.

Acharya, Hemendra, 1985, Comment on "Seismic potential associated with subduction in the northwestern United States" by T.H. Heaton and Hiroo Kanamori: Seismological Society of America Bulletin, v. 75, no. 3, p. 889–890.

Adams, John, 1984, Active deformation of the Pacific Northwest continental margin: Tectonics, v. 3, no. 4, p. 449–472.

———1990, Paleoseismicity of the Cascadia subduction zone—Evidence from turbidites off the Oregon-Washington margin: Tectonics, v. 9, no. 4, p. 569–583.

Algermissen, S.T., 1983, An introduction to the seismicity of the United States: Berkeley, Calif., Earthquake Engineering Research Institute, 148 p.

———1988, Estimation of ground shaking in the Pacific Northwest, *in* Hays, W.W., ed., Proceedings of Conference XLII, Workshop on evaluation of earthquake hazards and risk in the Puget Sound and Portland areas: U.S. Geological Survey Open-File Report 88–541, p. 43–51.

Algermissen, S.T., and Harding, S.T., 1965, Preliminary seismological report, *in* The Puget Sound, Washington, earthquake of April 29, 1965: Washington, D.C., U.S. Coast and Geodetic Survey, p. 1–26.

Algermissen, S.T., Kausel, E., Mueller, C., Borcherdt, R.D., Thenhaus, P.C., and Askew, B., 1985, Preliminary analysis of ground response and observed intensity, *in* Algermissen, S.T., ed., Preliminary report of investigations of the central Chile earthquake of March 3, 1985: U.S. Geological Survey Open-File Report 85–542, p. 117–124.

Algermissen, S.T., and Leyendecker, E.V., 1992, A technique for uniform hazard spectra estimation in the US: Rotterdam, A.A. Balkema, World Conference on Earthquake Engineering, 10th, Madrid, Spain, 1992, v. 1, p. 391–397.

Algermissen, S.T., Perkins, D.M., Thenhaus, P.C., Hanson, S.L., and Bender, B.L., 1982, Probabilistic estimates of maximum acceleration and velocity in rock in the contiguous United States: U.S. Geological Survey Open-File Report 82–1033, 99 p.

———1990, Probabilistic earthquake acceleration and velocity maps for the United States and Puerto Rico: U.S. Geological Survey Miscellaneous Field Studies Map MF–2120, 2 sheets, scale 1:7,500,000.

American Association of Petroleum Geologists, 1981, Plate tectonic map of the Circumpacific region: Tulsa, Okla., American Association of Petroleum Geologists, 6 sheets, scale 1:10,000,000.

American National Red Cross, 1986, Chapter activities in disaster community education—Resource guide: Washington, D.C., American National Red Cross, 122 p.

Ando, Masataka, 1975, Source mechanisms and tectonic significance of historical earthquakes along the Nankai Trough, Japan: Tectonophysics, v. 27, no. 1, p. 119–140.

Ando, Masataka, and Balazs, E.I., 1979, Geodetic evidence for aseismic subduction of the Juan de Fuca plate: Journal of Geophysical Research, v. 84, no. B6, p. 3023–3027.

Applied Technology Council, 1978, Tentative provisions for the development of seismic regulations for buildings: National Science Foundation Publication 78–8, 505 p.

Astiz, Luciana, Lay, Thorne, and Kanamori, Hiroo, 1988, Large intermediate depth earthquakes and the subduction process: Physics of the Earth and Planetary Interiors, v. 53, no. 1/2, p. 80–166.

Atwater, B.F., 1987, Evidence for great Holocene earthquakes along the outer coast of Washington State: Science, v. 236, no. 4804, p. 942–944.

———1988a, Comment on "Coastline uplift in Oregon and Washington and the nature of Cascadia subduction-zone tectonics" by D.O. West and D.R. McCrumb: Geology, v. 16, no. 10, p. 952–953.

———1988b, Geologic studies for seismic zonation of the Puget lowland, *in* Jacobson, M.L., and Rodriquez, T.R., comps., National Earthquake Hazards Reduction Program, Summaries of technical reports, Volume XXV: U.S. Geological Survey Open-File Report 88–16, p. 120–133.

———1992, Geologic evidence for earthquakes during the past 2000 years along the Copalis River, southern coastal Washington: Journal of Geophysical Research, v. 97, no. B2, p. 1901–1919.

Atwater, B.F., and Moore, A.L., 1992, A tsunami about 1000 years ago in Puget Sound, Washington: Science, v. 258, no. 5088, p. 1614–1617.

Atwater, B.F., Stuiver, Minze, and Yamaguchi, D.K., 1991, A radiocarbon test of earthquake magnitude at the Cascadia subduction zone: Nature, v. 353, no. 6340, p. 156–158.

Atwater, B.F., and Yamaguchi, D.K., 1991, Sudden, probably coseismic submergence of Holocene trees and grass in coastal Washington State: Geology, v. 19, no. 7, p. 706–709.

Atwater, Tanya, 1970, Implications of plate tectonics for the Cenozoic tectonic evolution of western North America: Geological Society of America Bulletin, v. 81, p. 3513–3536.

Baker, G.E., and Langston, C.A., 1987, Source parameters of the 1949 magnitude 7.1 south Puget Sound, Washington, earthquake as determined from long-period body waves and strong ground motions: Seismological Society of America Bulletin, v. 77, no. 5, p. 1530–1557.

Barr, T.D., and Dahlen, F.A., 1989, Brittle frictional mountain building, 2—Thermal structure and heat budget: Journal of Geophysical Research, v. 94, no. B4, p. 3923–3947.

Blair, M.L., and Spangle, W.E., 1979, Seismic safety and land-use planning—Selected examples from California: U.S. Geological Survey Professional Paper 941–B, 82 p.

Bolt, B.A., Lomnitz, Cinna, and McEvilly, T.V., 1968, Seismological evidence on the tectonics of central and northern California and the Mendocino escarpment: Seismological Society of America Bulletin, v. 58, no. 6, p. 1725–1767.

Bourgeois, Joanne, and Reinhart, M.A., 1988, Potentially damaging waves associated with earthquakes, coastal Washington, *in* Hays, W.W., ed., Proceedings of Conference XLII, Workshop on evaluation of earthquake hazards and risk in the Puget Sound and Portland areas: U.S. Geological Survey Open-File Report 88–541, p. 96–99.

Bradford, D.C., 1935, Seismic history of the Puget Sound basin: Seismological Society of America Bulletin, v. 25, no. 2, p. 138–153.

Bucknam, R.C., 1991, Puget Sound paleoseismicity, *in* Jacobson, M.L., comp., National Earthquake Hazards Reduction Program, Summaries of technical reports, Volume XXXII: U.S. Geological Survey Open-File Report 91–352, p. 526–527.

Bucknam, R.C., and Barnhard, T.P., 1989, Evidence of sudden late Holocene uplift in the central Puget Lowland, Washington [abs.]: EOS [American Geophysical Union Transactions], v. 70, no. 43, p. 1332.

Bucknam, R.C., Hemphill-Haley, Eileen, and Leopold, E.B., 1992, Abrupt uplift within the past 1700 years at southern Puget Sound, Washington: Science, v. 258, no. 5088, p. 1611–1614.

Bufe, C.G., Harsh, P.W., and Burford, R.O., 1977, Steady-state seismic slip—A precise recurrence model: Geophysical Research Letters, v. 4, no. 2, p. 91–94.

Building Seismic Safety Council, 1992, NEHRP recommended provisions for the development of seismic regulations for new buildings: Washington, D.C., Federal Emergency Management Agency, Part 1—Provisions, FEMA 222, 199 p.; Part 2—Commentary, FEMA 223, 237 p.

Byrne, D.E., Davis, D.M., and Sykes, L.R., 1988, Loci and maximum size of thrust earthquakes and the mechanics of the shallow region of subduction zones: Tectonics, v. 7, no. 4, p. 833–857.

Byrne, D.E., and Sykes, L.R., 1987, Seismic and aseismic subduction, Part 1—The role of young sediments in controlling the mode of slip along the plate boundary [abs.]: EOS [American Geophysical Union Transactions], v. 68, no. 44, p. 1468.

California Association of Hospitals and Health Systems, 1990, Hospital earthquake preparedness, Issues for action—A report on the Loma Prieta earthquake issued October 17, 1990: Sacramento, California Association of Hospitals and Health Systems, 27 p.

Campbell, N.P., and Bentley, R.D., 1981, Late Quaternary deformation of the Toppenish Ridge uplift in south-central Washington: Geology, v. 9, no. 11, p. 519–524.

Carlson, R.L., 1981, Late Cenozoic rotations of the Juan de Fuca ridge and the Gorda rise—A case study: Tectonophysics, v. 77, no. 3/4, p. 171–188.

Carver, G.A., 1987, Late Cenozoic tectonics of the Eel River basin region, coastal northern California, *in* Schymiczek, H., and Suchland, R., eds., Tectonics, sedimentation, and evolution of the Eel River and associated coastal basins of northern California: San Joaquin Geological Society Miscellaneous Publication 37, p. 61–71.

———1989, Paleoseismicity of the southern part of the Cascadia subduction zone [abs.]: Seismological Research Letters, v. 60, no. 1, p. 1.

Carver, G.A., and Burke, R.M., 1987a, Late Holocene paleoseismicity of the southern end of the Cascadia subduction zone [abs.]: EOS [American Geophysical Union Transactions], v. 68, no. 44, p. 1240.

———1987b, Late Pleistocene and Holocene paleoseismicity of Little Salmon and Mad River thrust systems, N.W. California—Implications to the seismic potential of the Cascadia subduction zone [abs.]: Geological Society of America Abstracts with Programs, v. 19, no. 7, p. 614.

Carver, G.A., Vick, G.S., and Burke, R.M., 1989, Late Holocene paleoseismicity of the Gorda segment of the Cascadia subduction zone [abs.]: Geological Society of America Abstracts with Programs, v. 21, no. 5, p. 64.

Cassidy, J.F., Ellis, R.M., and Rogers, G.C., 1988, The 1918 and 1957 Vancouver Island earthquakes: Seismological Society of America Bulletin, v. 78, no. 2, p. 617–635.

Chen, A.T., Frohlich, Clifford, and Latham, G.V., 1982, Seismicity of the forearc marginal wedge (accretionary prism): Journal of Geophysical Research, v. 87, no. B5, p. 3679–3690.

Chleborad, A.F., and Schuster, R.L., 1989, Characteristics of slope failures induced by the April 13, 1949, and April 29, 1965, Puget Sound area, Washington, earthquakes, *in* Hays, W.W., ed., Proceedings of Conference XLVIII, 3d annual workshop on earthquake hazards in the Puget Sound, Portland area: U.S. Geological Survey Open-File Report 89–465, p. 106–113.

Clarke, S.H., Jr., 1990, Map showing geologic structures of the northern California continental margin: U.S. Geological Survey Miscellaneous Field Studies Map MF–2130, scale 1:250,000.

———1992, Geology of the Eel River basin and adjacent region—Implications for late Cenozoic tectonics of the southern Cascadia subduction zone and Mendocino triple junction: American Association of Petroleum Geologists Bulletin, v. 76, no. 2, p. 199–224.

Clarke, S.H., Jr., and Carver, G.A., 1989, Late Cenozoic structure and seismic potential of the southern Cascadia subduction zone [abs.]: EOS [American Geophysical Union Transactions], v. 70, no. 43, p. 1331–1332.

———1991, Tectonics and seismic potential of the southern Cascadia subduction zone [abs.]: EOS [American Geophysical Union Transactions], v. 72, no. 44, p. 315.

———1992, Late Holocene tectonics and paleoseismicity, southern Cascadia subduction zone: Science, v. 255, no. 5041, p. 188–192.

Coffman, J.L., and Hake, C.A. von, 1973, Earthquake history of the United States: Washington, D.C., U.S. Department of Commerce Publication 41–1, Revised edition, 208 p.

Cohee, B.P., Somerville, P.G., and Abrahamson, N.A., 1991, Simulated ground motions for hypothesized M_W=8 subduction earthquakes in Washington and Oregon: Seismological Society of America Bulletin, v. 81, no. 1, p. 28–56.

Connard, G.G., Couch, R.W., Keeling, K.M., Roy, J., and Troseth, S.C., 1984, Abyssal plain and continental net-objective sedimentary thicknesses, *in* Kulm, L.D., and others, eds., Ocean Margin Drilling Program, Regional Atlas Series, Western North American continental margin and adjacent ocean floor off Oregon and Washington, Atlas 1: Woods Hole, Mass., Marine Science International, p. 7.

Coombs, H.A., Milne, W.G., Nuttli, O.W., and Slemmons, D.B., 1977, Report of the review panel on the December 14, 1872, earthquake, *in* Washington Public Power Supply System Nuclear Projects Nos. 1 and 4, Preliminary site analysis report, Amendment 23, v. 2A, subappendix 2R–A, p. 2R–A–i to 31, includes appendixes A–D [a report to the U.S. Nuclear Regulatory Commission]: Available from the U.S. Nuclear Regulatory Commission, Washington, D.C. 20555.

Coppersmith, K.J., and Youngs, R.R., 1990, Probabilistic seismic-hazard analysis using expert opinion—An example from the Pacific Northwest: Geological Society of America, Reviews in Engineering Geology, v. 8, p. 29–46.

Crandell, D.R., 1971, Postglacial lahars from Mount Rainier volcano, Washington: U.S. Geological Survey Professional Paper 677, 75 p., 3 pls., scales 1:48,000 and 1:250,000.

Crandell, D.R., Mullineaux, D.R., and Miller, C.D., 1979, Volcanic hazard studies in the Cascade Range of the Western United States, *in* Sheets, P.D., and Grayson, D.K., eds., Volcanic activity and human ecology: New York, Academic Press, p. 195–219.

Crosson, R.S., 1972, Small earthquakes, structure, and tectonics of the Puget Sound region: Seismological Society of America Bulletin, v. 62, no. 5, p. 1133–1171.

———1983, Review of seismicity in the Puget Sound region from 1970 through 1978, *in* Yount, J.C., and Crosson, R.S., eds., Proceedings of Workshop XIV, Earthquake hazards of the Puget Sound region, Washington: U.S. Geological Survey Open-File Report 83–19, p. 6–8.

———1986, Comment on "Geodetic strain measurements in Washington" by J.C. Savage, Michael Lisowski, and W.H. Prescott: Journal of Geophysical Research, v. 87, no. B7, p. 7555–7557.

———1989, Seismicity of Puget Sound and southern British Columbia, *in* Hays, W.W., ed., Proceedings of Conference XLVIII, 3d annual workshop on earthquake hazards in the Puget Sound, Portland area: U.S. Geological Survey Open-File Report 89–465, p. 31–32.

———1990, Evidence and enigma [letter to the editor]: Science News, v. 137, no. 13, p. 243.

Crosson, R.S., and Frank, D.G., 1975, The Mt. Rainier earthquake of July 18, 1973, and its tectonic significance: Seismological Society of America Bulletin, v. 65, no. 2, p. 393–401.

Crosson, R.S., and Owens, T.J., 1987, Slab geometry of the Cascadia subduction zone beneath Washington from earthquake hypocenters and teleseismic converted waves: Geophysical Research Letters, v. 14, no. 8, p. 824–827.

Crouse, C.B., Vyas, Y.K., and Schell, B.A., 1988, Ground motions from subduction-zone earthquakes: Seismological Society of America Bulletin, v. 78, no. 1, p. 1–25.

Darienzo, M.E., and Peterson, C.D., 1990, Episodic tectonic subsidence of late Holocene salt marshes, northern Oregon central Cascadia margin: Tectonics, v. 9, no. 1, p. 1–22.

Davis, E.E., Hyndman, R.D., and Villinger, Heiner, 1990, Rates of fluid expulsion across the northern Cascadia accretionary prism—Constraints from new heat flow and multichannel seismic reflection data: Journal of Geophysical Research, v. 95, no. B6, p. 8869–8889.

Delaney, J.R., Johnson, H.P., and Karsten, J.L., 1981, The Juan de Fuca ridge—Hot spot—Propagating rift system—New tectonic, geochemical, and magnetic data: Journal of Geophysical Research, v. 86, no. B12, p. 11747–11750.

Dengler, L.A., Carver, G.A., and McPherson, B.C., 1991, Potential sources of large earthquakes in north coastal California [abs.]: EOS [American Geophysical Union Transactions], v. 72, no. 44, p. 315.

Dragert, Herb, 1991, Recent horizontal strain accumulation on Vancouver Island, British Columbia: EOS [American Geophysical Union Transactions], v. 72, no. 44, p. 314.

Duncan, R.A., and McElwee, K.R., 1984, Cenozoic plate reconstructions, *in* Kulm, L.D., and others, eds., Ocean Margin Drilling Program, Regional Atlas Series, Western North American continental margin and adjacent ocean floor off Oregon and Washington, Atlas 1: Woods Hole, Mass., Marine Science International, p. 12.

Earthquake Engineering Research Institute, 1986, Reducing earthquake hazards—Lessons learned from earthquakes: Earthquake Engineering Research Institute Publication 86–02, 208 p.

Eissler, H.K., and McNally, K.C., 1984, Seismicity and tectonics of the Rivera plate and implications for the 1932 Jalisco, Mexico, earthquake: Journal of Geophysical Research, v. 89, no. B6, p. 4520–4530.

Farrar, Edward, and Dixon, J.M., 1980, Miocene ridge impingement and the spawning of secondary ridges off Oregon, Washington and British Columbia: Tectonophysics, v. 69, no. 3/4, p. 321–348.

Finn, Carol, 1990, Geophysical constraints on Washington convergent margin structure: Journal of Geophysical Research, v. 95, no. B12, p. 19533–19546.

Finn, W.D.L., Woeller, D.J., Davies, M.P., Luternauer, J.L., Hunter, J.A., and Pullan, S.E., 1989, New approaches for assessing liquefaction potential of the Fraser River delta, British Columbia, *in* Cordillera and Pacific margin: Geological Survey of Canada Paper 89–1E, p. 221–231.

Fitch, T.J., 1972, Plate convergence, transcurrent faults, and internal deformation adjacent to southeast Asia and the western Pacific: Journal of Geophysical Research, v. 77, no. 23, p. 4432–4460.

Fox, K.F., and Engebretson, D.C., 1983, Horizontal tectonic stress during the late Cenozoic in the northwestern United States, *in* Yount, J.C., and Crosson, R.S., eds., Proceedings of Workshop XIV, Earthquake hazards of the Puget Sound region, Washington: U.S. Geological Survey Open-File Report 83–19, p.141–164.

Geomatrix Consultants, Inc., 1989, Seismotectonic evaluation, Mann Creek Dam site and Mason Dam site, 118 p., 2 maps, scales 1:500,000 and 1:250,000 [final report to the U.S. Bureau of Reclamation under project 1419A]: Available from the U.S. Bureau of Reclamation, Division of Geology, Building 67, Denver Federal Center, Denver, CO 80225–0007.

———1990, Seismotectonic evaluation, Wasco Dam site, 115 p., 2 maps, scales 1:500,000 and 1:250,000 [final report to the U.S. Bureau of Reclamation under project 1421A]: Available from the U.S. Bureau of Reclamation, Division of Geology, Building 67, Denver Federal Center, Denver, CO 80225–0007.

Gibbs, George, 1955, George Gibbs' account of Indian mythology in Oregon and Washington territories, *in* Clark, E., ed., Oregon Historical Quarterly, v. 56, p. 293–325.

Goldfinger, Chris, Kulm, L.D., Yeats, R.S., Appelgate, T.B., MacKay, M.E., and Moore, G.F., 1992, Transverse structural trends along the Oregon convergent margin—Implications for Cascadia earthquake potential and crustal rotations: Geology, v. 20, no. 2, p. 141–144.

Goldfinger, Chris, MacKay, M.E., Kulm, L.D., and Yeats, R.S., 1990, Neotectonics and possible segmentation of the Juan de Fuca plate and Cascadia subduction zone off central Oregon [abs.]: EOS [American Geophysical Union Transactions], v. 71, no. 43, p. 1580.

Gower, H.D., Yount, J.C., and Crosson, R.S., 1985, Seismotectonic map of the Puget Sound region, Washington: U.S. Geological Survey Miscellaneous Investigations Series Map I–1613, 15 p., scale 1:250,000.

Grant, W.C., 1989, More evidence from tidal-marsh stratigraphy for multiple late Holocene subduction earthquakes along the northern Oregon coast [abs.]: Geological Society of America Abstracts with Programs, v. 21, no. 5, p. 86.

Grant, W.C., Atwater, B.F., Carver, G.A., Darienzo, M.E., Nelson, A.R., Peterson, C.D., and Vick, G.S., 1989, Radiocarbon dating of late Holocene coastal subsidence above the Cascadia subduction zone—Compilation for Washington, Oregon, and northern California [abs.]: EOS [American Geophysical Union Transactions], v. 70, no. 43, p. 1331.

Grant, W.C., and McLaren, D.D., 1987, Evidence for Holocene subduction earthquakes along the northern Oregon coast [abs.]: EOS [American Geophysical Union Transactions], v. 68, no. 44, p. 1239.

Grant, W.C., and Minor, Rick, 1991, Paleoseismic evidence and prehistoric occupation associated with late Holocene sudden submergence, northern Oregon coast [abs.]: EOS [American Geophysical Union Transactions], v. 72, no. 44, p. 313.

Grant, W.C., and Weaver, C.S., 1986, Earthquakes near Swift Reservoir, Washington, 1958–1963—Seismicity along the southern St. Helens seismic zone: Seismological Society of America Bulletin, v. 76, no. 6, p. 1573–1587.

Grant, W.P., 1989, Liquefaction hazards in the Pacific Northwest, *in* Hays, W.W., ed., Proceedings of Conference XLVIII, 3d annual workshop on earthquake hazards in the Puget Sound, Portland area: U.S. Geological Survey Open-File Report 89–465, p. 82–83.

Graves, R.W., 1993, Finite-difference modeling of strong ground motions in the Cascadia subduction zone—1992 Cape Mendocino earthquake: EOS [American Geophysical Union Transactions], v. 74, no. 43, p. 200.

Green, A.G., Clowes, R.M., Yorath, C.J., Spencer, C.P., Kanasewich, E.R., Brandon, M.T., and Brown, A.S., 1986, Seismic reflection imaging of the subducting Juan de Fuca plate: Nature, v. 319, no. 6050, p. 210–213.

Harding, S.T., and Barnhard, T.P., 1987, Holocene faulting as indicated from marine seismic-reflection survey in Puget Sound, Washington [abs.]: EOS [American Geophysical Union Transactions], v. 68, no. 44, p. 1240.

Harding, S.T., Urban, T.C., and Barnhard, T.P., 1988, Preliminary evidence of possible Quaternary faulting in Puget Sound, Washington, from a multichannel marine seismic-reflection survey, *in* Hays, W.W., ed., Proceedings of Conference XLII, Workshop on evaluation of earthquake hazards and risk in the Puget Sound and Portland areas: U.S. Geological Survey Open-File Report 88–541, p. 178–193.

Hawkins, F.F., Foley, L.L., and LaForge, R.C., 1989, Seismotectonic study for Fish Lake and Fourmile Lake Dams, Rogue River Project, Oregon, U.S. Bureau of Reclamation Seismotectonic Report 89–3, 26 p.: Available from the U.S. Bureau of Reclamation, Geotechnical Engineering and Geology Division, Building 67, Denver Federal Center, Denver, CO 80225–0007.

Hawkins, F.F., Gilbert, J.D., and LaForge, R.C., 1989, Seismotectonic study for Warm Springs Dam-Vale project and Owhyee Dam-Owhyee project, Oregon, U.S. Bureau of Reclamation Seismotectonic Report 89–6, 35 p., 1 map, scale 1:1,500,000: Available from the U.S. Bureau of Reclamation, Geotechnical Engineering and Geology Division, Building 67, Denver Federal Center, Denver, CO 80225–0007.

Hawkins, F.F., LaForge, R.C., and Gilbert, J.D., 1989, Seismotectonic study for Wickiup and Crane Prairie dams, Deschutes Project, Oregon, U.S. Bureau of Reclamation Seismotectonic Report 89–2, 38 p.: Available from the U.S. Bureau of Reclamation, Geotechnical Engineering and Geology Division, Building 67, Denver Federal Center, Denver, CO 80225–0007.

Heaton, T.H., and Hartzell, S.H., 1986, Source characteristics of hypothetical subduction earthquakes in the northwestern United States: Seismological Society of America Bulletin, v. 76, no. 3, p. 675–708.

———1987, Earthquake hazards on the Cascadia subduction zone: Science, v. 236, no. 4798, p. 162–168.

———1989, Estimation of strong ground motions from hypothetical earthquakes on the Cascadia subduction zone, Pacific Northwest: Pure and Applied Geophysics, v. 129, no. 1/2, p. 131–201.

Heaton, T.H., and Kanamori, Hiroo, 1984, Seismic potential associated with subduction in the northwestern United States: Seismological Society of America Bulletin, v. 74, no. 3, p. 933–941.

———1985, Reply to Hemendra Acharya's comments on "Seismic potential associated with subduction in the northwestern United States": Seismological Society of America Bulletin, v. 75, no. 3, p. 891–892.

Heaton, T.H., and Snavely, P.D., Jr., 1985, Possible tsunami along the northwestern coast of the United States inferred from Indian traditions: Seismological Society of America Bulletin, v. 75, no. 5, p. 1455–1460.

Hebenstreit, G.T., 1988, Tsunami threat analysis for the Pacific Northwest, *in* Jacobson, M.L., and Rodriguez, T.R., comps., National Earthquake Hazards Reduction Program, Summaries of technical reports, Volume XXV: U.S. Geological Survey Open-File Report 88–16, p. 550–555.

Hemphill-Haley, M.A., Page, W.D., Carver, G.A., and Burke, R.M., 1989, Holocene activity of the Alvord fault, Steens Mountain, southeastern Oregon, 38 p. [final unpublished report to the U.S. Geological Survey under Grant No. 14–08–0001–g1333]: Available from the U.S. Geological Survey Library, 12201 Sunrise Valley Drive, Reston, VA 22092–0001.

Howard, K.A., Aaron, J.M., Brabb, E.E., Brock, M.R., Gower, H.D., Hunt, S.J., Milton, D.J., Muehlberger, W.R., Nakata, J.K., Plafker, George, Prowell, D.C., Wallace, R.E., and Witkind, I.J., 1978, Preliminary map of young faults in the United States as a guide to possible fault activity: U.S. Geological Survey Miscellaneous Field Studies Map MF–916, 2 sheets, scale 1:5,000,000.

Hubert, A., and Schwartz, S.Y., 1993, State of stress at the Cape Mendocino triple junction from inversion of focal mechanisms of the 1992 Petrolia, CA earthquake sequence: EOS [American Geophysical Union Transactions], v. 74, no. 43, p. 200.

Hyndman, R.D., Riddihough, R.P., and Herzer, R.H., 1979, The Nootka fault zone—A new plate boundary off western Canada: Royal Astronomical Society Geophysical Journal, v. 58, p. 667–683.

Hyndman, R.D., and Weichert, D.H., 1983, Seismicity and rates of relative motion on the plate boundaries of western North America: Royal Astronomical Society Geophysical Journal, v. 72, p. 59–82.

Hyndman, R.D., Yorath, C.J., Clowes, R.M., and Davis, E.E., 1990, The northern Cascadia subduction zone at Vancouver Island—Seismic structure and tectonic history: Canadian Journal of Earth Sciences, v. 27, no. 3, p. 313–329.

Ihnen, S.M., and Hadley, D.M., 1986, Prediction of strong ground motion in the Puget Sound region—The 1965 Seattle earthquake: Seismological Society of America Bulletin, v. 76, no. 4, p. 905–922.

International Conference of Building Officials, 1991, Uniform Building Code, 1991, 926 p.: Available from the International Conference of Building Officials, 5360 S. Workman Rd., Whittier, CA 90601.

Jacoby, G.C., and Williams, P.L., 1990, Use of temporal correlation to test a proposed seismic origin for giant landslides in Seattle, Washington, *in* Jacobson, M.L., comp., National Earthquake Hazards Reduction Program, Summaries of technical reports, Volume XXX: U.S. Geological Survey Open-File Report 90–334, p. 493–497.

Jacoby, G.C., Williams, P.L., and Buckley, B.M., 1992, Tree ring correlation between prehistoric landslides and abrupt tectonic events in Seattle, Washington: Science, v. 258, no. 5088, p. 1621–1623.

Jennings, C.W., 1985, An explanatory text to accompany the 1:750,000 scale fault and geologic maps of California: California Division of Mines and Geology Bulletin 201, 197 p., 2 sheets, scale 1:750,000.

Kanamori, Hiroo, 1971, Great earthquakes at island arcs and the lithosphere: Tectonophysics, v. 12, no. 3, p. 187–198.

———1981, The nature of seismicity patterns before large earthquakes, *in* Simpson, D.W., and Richards, P.G., eds., Earthquake prediction—An international review, No. 4: Washington, D.C., American Geophysical Union, p. 1–19.

Kanamori, Hiroo, and Astiz, Luciana, 1985, The 1983 Akita-Oki earthquake (M_W 7.8) and its implications for systematics of subduction earthquakes, *in* Kisslinger, Carl, and Rikitake, Tsuneji, eds., Practical approaches to earthquake prediction and warning: Earthquake Prediction Research, v. 3, no. 3/4, p. 305–317.

Kanamori, Hiroo, and McNally, K.C., 1982, Variable rupture mode of the subduction zone along the Ecuador-Colombia coast: Seismological Society of America Bulletin, v. 72, no. 4, p. 1241–1253.

Karlin, R.E., and Abella, S.E.B., 1992, Paleoearthquakes in the Puget Sound region recorded in sediments from Lake Washington, U.S.A.: Science, v. 258, p. 1617–1620.

Kelleher, J.A., 1970, Space-time seismicity of the Alaska-Aleutian seismic zone: Journal of Geophysical Research, v. 75, no. 29, p. 5745–5756.

Kelsey, H.M., 1990, Late Quaternary deformation of marine terraces on the Cascadia subduction zone near Cape Blanco, Oregon: Tectonics, v. 9, no. 5, p. 983–1014.

Kelsey, H.M., and Carver, G.A., 1988, Late Neogene and Quaternary tectonics associated with northward growth of the San Andreas transform fault, northern California: Journal of Geophysical Research, v. 93, no. B5, p. 4797–4819.

Koch, K., 1993, On possible complex source behavior of the 1992 Petrolia earthquake from regional seismograms: EOS [American Geophysical Union Transactions], v. 74, no. 43, p. 200.

Kockelman, W.J., 1990, Reducing earthquake hazards in Utah—The crucial connection between researchers and practitioners: U.S. Geological Survey Open-File Report 90–217, 91 p.

Korgen, B.J., Bodvarsson, Gunnar, and Mesecar, R.S., 1971, Heat flow through the floor of Cascadia basin: Journal of Geophysical Research, v. 76, no. 20, p. 4758–4774.

Kulm, L.D., 1989, Cascadia subduction zone—Structure, tectonics, and fluid process of the accretionary wedge and adjacent abyssal plain, *in* Hays, W.W., ed., Proceedings of Conference XLVIII, 3d annual workshop on earthquake hazards in the Puget Sound, Portland area: U.S. Geological Survey Open-File Report 89–465, p. 38–39.

Kulm, L.D., and Peterson, C.P., 1984, Multichannel seismic records of northern Washington and central Oregon margin, *in* Kulm, L.D., and others, eds., Ocean Margin Drilling Program, Regional Atlas Series, Western North American continental margin and adjacent ocean floor off Oregon and Washington, Atlas 1: Woods Hole, Mass., Marine Science International, p. 28.

Kulm, L.D., Yeats, R.S., and Goldfinger, Chris, 1991, Cascadia subduction zone—Neotectonics of the accretionary wedge and adjacent abyssal plain off Oregon and Washington, Oregon State University College of Oceanography report, 9 p. [report to the U.S. Geological Survey under Grant No. 14–08–0001–G1800]: Available from the U.S. Geological Survey Library, 12201 Sunrise Valley Drive, Reston, VA 22092–0001.

Lajoie, K.R., Sarna-Wojcicki, A.M., and Ota, Yoko, 1982, Emergent Holocene marine terraces at Ventura and Cape Mendocino, California—Indicators of high tectonic uplift rates [abs.]: Geological Society of America Abstracts with Programs, v. 14, p. 178.

Langston, C.A., 1981a, Evidence for the subducting lithosphere under southern Vancouver Island and western Oregon from teleseismic *P* wave conversions: Journal of Geophysical Research, v. 86, no. B5, p. 3857–3866.

———1981b, A study of Puget Sound strong ground motion: Seismological Society of America Bulletin, v. 71, no. 3, p. 883–903.

Langston, C.A., and Lee, J.J., 1983, Effect of structure geometry on strong ground motions—The Duwamish River valley, Seattle, Washington: Seismological Society of America Bulletin, v. 73, no. 6, p. 1851–1863.

Lay, Thorne, Kanamori, Hiroo, and Ruff, Larry, 1982, The asperity model and the nature of large subduction zone earthquakes: Tokyo, Terra Scientific Publishing Co., Earthquake Prediction Research, v. 1, no. 1, p. 3–71.

Lin, J.W., 1974, A study of upper mantle structure in the Pacific Northwest using *P* waves from teleseisms: Seattle, University of Washington, Ph.D. dissertation, 98 p.

Lisowski, Michael, Savage, J.C., Prescott, W.H., and Dragert, Herb, 1987, Strain accumulation along the Cascadia subduction zone in western Washington [abs.]: EOS [American Geophysical Union Transactions], v. 68, no. 44, p. 1240.

Lomnitz, Cinna, and Nava, F.A., 1983, The predictive value of seismic gaps: Seismological Society of America Bulletin, v. 73, no. 6, p. 1815–1824.

Ludwin, R.S., 1989, Earthquake occurrence and hazards in Washington and Oregon, *in* Hays, W.W., ed., Proceedings of Conference XLVIII, 3d annual workshop on earthquake hazards in the Puget Sound, Portland, area: U.S. Geological Survey Open-File Report 89–465, p. 128–140.

Ludwin, R.S., Weaver, C.S., and Crosson, R.S., 1991, Seismicity of Washington and Oregon, *in* Slemmons, D.B., Engdahl, E.R., Blackwell, D.D., and Schwartz, D.P., eds, Neotectonics of North America: Boulder, Colo., Geological Society of America, Decade of North American Geology, v. CSMV–1, p. 77–98.

Madin, I.P., and Pezzopane, S.K., 1990, Quaternary deformation in the Portland metro area, *in* Walsh, T.J., Madin, Ian, Noson, L.L., and Yelin, T.S., eds., Proceedings of Conference LX, 4th annual workshop on earthquake hazards in the Puget Sound and Portland area: U.S. Geological Survey Open-File Report 90–703, p. 4.

Magee, M.E., and Zoback, M.L., 1989, Present state of stress in the Pacific Northwest [abs.]: EOS [American Geophysical Union Transactions], v. 70, no. 43, p. 1332–1333.

Malone, S.D., and Bor, S.S., 1979, Attenuation patterns in the Pacific Northwest based on intensity data and the location of the 1872 North Cascades earthquake: Seismological Society of America Bulletin, v. 69, no. 2, p. 531–546.

Manson, C.J., 1988, Seismic hazards of western Washington and selected adjacent areas—Bibliography and index, 1855–June 1988: Washington Division of Geology and Earth Resources Open-File Report 88–4, 1,039 p.

Martens, Carole, 1988, Perspectives on public information and awareness programs in the Puget Sound, Washington area, *in* Hays, W.W., ed., Proceedings of Conference XLI, A review of earthquake research applications in the National Earthquake Hazards Reduction Program—1977–1988: U.S. Geological Survey Open-File Report 88–13A, p. 75–87.

May, P.J., and Noson, L.L., 1986, Reducing earthquake risks—Seismic safety policy: Seattle, University of Washington, Institute for Public Policy and Management, Washington Public Policy Notes, v. 14, 6 p.

McCann, W.R., Nishenko, S.P., Sykes, L.R., and Krause, J., 1979, Seismic gaps and plate tectonics—Seismic potential for major boundaries: Pure and Applied Geophysics, v. 117, no. 6, p. 1082–1147.

McCulloch, D.S., 1985, Evaluating tsunami potential, *in* Ziony, J.I., ed., Evaluating earthquake hazards in the Los Angeles region—An earth-science perspective: U.S. Geological Survey Professional Paper 1360, p. 375–413.

McEvilly, T.V., 1968, Sea floor mechanics north of Cape Mendocino, California: Nature, v. 220, p. 901–903.

McGuire, R.K., and Barnhard, T.P., 1981, Effects of temporal variations in seismicity on seismic hazard: Seismological Society of America Bulletin, v. 71, no. 1, p. 321–334.

McInelly, G.W., and Kelsey, H.M., 1990, Late Quaternary tectonic deformation in the Cape Arago-Bandon region of coastal Oregon as deduced from wave-cut platforms: Journal of Geophysical Research, v. 95, no. B5, p. 6699–6713.

McKenzie, D.P., and Julian, Bruce, 1971, The Puget Sound, Washington, earthquake and the mantle structure beneath the northwestern United States: Geological Society of America Bulletin, v. 82, no. 12, p. 3519–3524.

Melosh, H.J., 1987, A finite element study of strain accumulation and release in the Pacific Northwest [abs.]: EOS [American Geophysical Union Transactions], v. 68, no. 44, p. 1240.

———1989, Stress and strain in the Cascadia subduction zone [abs.]: EOS [American Geophysical Union Transactions], v. 70, no. 43, p. 1333.

Menard, H.W., 1978, Fragmentation of the Farallon plate by pivoting subduction: Journal of Geology, v. 86, no. 1, p. 99–110.

Michaelson, C.A., and Weaver, C.S., 1986, Upper mantle structure from teleseismic *P*-wave arrivals in Washington and northern Oregon: Journal of Geophysical Research, v. 91, no. B2, p. 2077–2094.

Milne, W.G., 1956, Seismic activity in Canada west of the 113th meridian, 1841–1951: Ottawa, Canada, Dominion Observatory Publication, v. 18, no. 7, p. 119–127.

Milne, W.G., Rogers, G.C., Riddihough, R.P., McMechan, G.A., and Hyndman, R.D., 1978, Seismicity of western Canada: Canadian Journal of Earth Science, v. 15, no. 7, p. 1170–1193.

Mitchell, C.E., Weldon, R.J., II, Vincent, Paul, and Pittock, H.L., 1991, Active uplift of the Pacific Northwest margin [abs.]: EOS [American Geophysical Union Transactions], v. 72, no. 44, p. 314.

Mogi, Kiyoo, 1974, Active periods in the world's chief seismic belts: Tectonophysics, v. 22, no. 3/4, p. 265–282.

Mooney, W.D., and Weaver, C.S., 1989, Regional crustal structure and tectonics of the Pacific coastal states, California, Oregon, and Washington, *in* Pakiser, L.C., and Mooney, W.D., eds., Geophysical framework of the continental United States: Boulder, Colo., Geological Society of America Memoir 172, p. 129–161.

Morgan, W.J., 1968, Rises, trenches, great faults, and crustal blocks: Journal of Geophysical Research, v. 73, no. 6, p. 1959–1982.

Muhs, D.R., Kelsey, H.M., Miller, G.H., Kennedy, G.L., Whelan, J.F., and McInelly, G.W., 1990, Age estimates and uplift rates for late Pleistocene marine terraces—Southern Oregon portion of the Cascadia forearc: Journal of Geophysical Research, v. 95, no. B5, p. 6685–6698.

Mullineaux, D.R., Bonilla, M.G., and Schlocker, Julius, 1967, Relation of building damage to geology in Seattle, Wash., during the April 1965 earthquake, *in* Geological Survey research 1967: U.S. Geological Survey Professional Paper 575–D, p. D183–D191.

National Research Council, 1988, Probabilistic seismic hazard analysis: Washington, D.C., National Research Council, Committee on Seismology, Panel on Seismic Hazard Analysis, National Academy Press, 97 p.

Nelson, A.R., 1992a, Discordant ^{14}C ages from buried tidal-marsh soils in the Cascadia subduction zone, southern Oregon coast: Quaternary Research, v. 48, p. 74–90.

———1992b, Holocene tidal-marsh stratigraphy in south-central Oregon—Evidence for localized sudden submergence in the Cascadia subduction zone, *in* Fletcher, C.P., and Wehmiller, J.F., eds., Quaternary coasts of the United States—Marine and lacustrine systems: Society for Sedimentary Geology (SEPM), Special Publication 48, p. 287–301.

Newmark, N.M., and Hall, W.J., 1982, Earthquake spectra and design: Berkeley, Calif., Earthquake Engineering Research Institute, 103 p.

Nishimura, Clyde, Wilson, D.S., and Hey, R.N., 1984, Pole of rotation analysis of present-day Juan de Fuca plate motion, *in* Special section—S. Thomas Crough memorial: Journal of Geophysical Research, v. 89, p. 10283–10290.

Noson, L.L., and Martens, Carole, 1987, Washington State school earthquake emergency planning: Seattle, University of Washington, School Earthquake Safety and Education Project, 10 p.

Noson, L.L., Qamar, A.I., and Thorsen, G.W., 1988, Washington State earthquake hazards: Washington Division of Geology and Earth Resources Information Circular 85, 77 p.

Oppenheimer, D.H., Beroza, G.C., Carver, G.A., Dengeler, Lori, Eaton, J.P., Gee, Lind, Gonzalez, F.I., Jayko, A.S., Li, W.H., Lisowski, Michael, Magee, M.E., Marshall, G.A., Murray, M.H., McPherson, Robert, Romanowicz, Barbara, Satake, Karji, Simpson, R.W., Somerville, P.G., Stein, R.S., and Valentine, David, 1993, The Cape Mendocino, California, earthquakes of April 1992—Subduction at the triple junction: Science, v. 261, no. 5120, p. 433–438.

Oregon State Land Conservation and Development Commission, 1990, Oregon's statewide planning goals, 1990: Salem, Oregon State Land Conservation and Development Commission, 24 p.

Owens, T.J., Crosson, R.S., and Hendrickson, M.A., 1988, Constraints on the subduction geometry beneath western Washington from broadband teleseismic waveform modeling: Seismological Society of America Bulletin, v. 78, no. 3, p. 1319–1334.

Palmer, R.L., Weldon, R.J., Mitchell, C.E., and Humphreys, E.D., 1991, Modeling of surface strain rates on the Cascadia subduction zone [abs.]: EOS [American Geophysical Union Transactions], v. 72, no. 44, p. 314.

Peity, L.A., LaForge, R.C., and Foley, L.L., 1990, Seismic sources and maximum credible earthquakes for Cold Springs and McKay Dams, Umatilla Project, north-central Oregon: U.S. Bureau of Reclamation Seismotectonic Report 90–1, 62 p.

Perbix, T.W., 1990a, Introduction to a seismic retrofit of older buildings (Heritage Building tour), *in* Walsh, T.J., Madin, Ian., Noson, L.L., and Yelin, T.S., eds., Proceedings of Conference LX, 4th annual workshop on earthquake hazards in the Puget Sound and Portland area: U.S. Geological Survey Open-File Report 90–703, p. 58–60.

———1990b, Seismic retrofit of Union Station (Union Station tour), *in* Walsh, T.J., Madin, Ian, Noson, L.L., and Yelin, T.S., eds., Proceedings of Conference LX, 4th annual workshop on earthquake hazards in the Puget Sound and Portland area: U.S. Geological Survey Open-File Report 90–703, p. 61–63.

Perkins, D.M., 1987, Contagious fault rupture, probabilistic hazard, and contagion observability, *in* Crone, A.J., and Omdahl, E.M., Proceedings of Conference XXXIX, Directions in paleoseismicity: U.S. Geological Survey Open-File Report 87–673, p. 428–439.

Perkins, D.M., Thenhaus, P.C., Hanson, S.L., Ziony, J.I., and Algermissen, S.T., 1980, Probabilistic estimates of maximum seismic horizontal ground motion on rock in the Pacific Northwest and the adjacent outer continental shelf: U.S. Geological Survey Open-File Report 80–471, 40 p.

Person, W.J., 1981, Seismological notes: Seismological Society of America Bulletin, v. 71, no. 5, p. 1677–1684.

Pezzopane, S.K., and Weldon, R.J., 1990, Holocene fault activity between the Basin and Range and high Cascades, Oregon [abs.]: EOS [American Geophysical Union Transactions], v. 71, no. 43, p. 1608.

Plafker, George, 1972, Tectonics, *in* The great Alaska earthquake of 1964—Seismology and geodesy: Washington, D.C., National Academy of Sciences, p. 113–188.

Plafker, George, and Savage, J.C., 1970, Mechanism of the Chilean earthquakes of May 21 and 22, 1960: Geological Society of America Bulletin, v. 81, no. 4, p. 1001–1030.

Priest, G.R., 1990, Volcanic and tectonic evolution of the Cascade volcanic arc, central Oregon: Journal of Geophysical Research, v. 95, no. B12, p. 19583–19599.

Qamar, A.I., and Zollweg, J.E., 1990, The 1990 Deming, Washington earthquakes—A sequence of shallow thrust earthquakes in the Pacific Northwest [abs.]: EOS [American Geophysical Union Transactions], v. 71, no. 41, p. 1145.

Raff, A.D., and Mason, R.G., 1961, Magnetic survey off the west coast of North America: Geological Society of America Bulletin, v. 72, no. 8, p. 1267–1270.

Rasmussen, J.R., and Humphreys, Eugene, 1988, Tomographic image of the Juan de Fuca plate beneath Washington and western Oregon using teleseismic *P*-wave travel times: Geophysical Research Letters, v. 15, no. 12, p. 1417–1420.

Rasmussen, N.H., Millard, R.C., and Smith, S.W., 1974, Earthquake hazard evaluation of the Puget Sound region, Washington State: Seattle, University of Washington Press, 99 p.

Reilinger, R.E., and Adams, John, 1982, Geodetic evidence for active landward tilting of the Oregon and Washington coastal ranges: Geophysical Research Letters, v. 9, no. 4, p. 401–403.

Reinhart, M.A., and Bourgeois, Joanne, 1989, Tsunami favored over storm or seiche for sand deposit overlying buried Holocene peat, Willapa Bay, WA [abs.]: EOS [American Geophysical Union Transactions], v. 70, no. 43, p. 1331.

Reitherman, Robert, 1985, Reducing the risks of nonstructural earthquake damage—A practical guide: U.S. Federal Emergency Management Agency, Earthquake Hazard Reduction Series 1, 87 p.

Riddihough, R.P., 1977, A model for recent plate interactions off Canada's west coast: Canadian Journal of Earth Science, v. 14, no. 3, p. 384–396.

———1978, The Juan de Fuca plate [abs.]: EOS [American Geophysical Union Transactions], v. 59, no. 9, p. 836–842.

———1983, Recent plate motions, Juan de Fuca plate map JFP–9: Canada Geological Survey Open-File Report 83–6, scale 1:2,000,000.

———1984, Recent movements of the Juan de Fuca plate system: Journal of Geophysical Research, v. 89, no. B8, p. 6980–6994.

Rogers, A.M., Perkins, D.M., Hampson, D.B., and Campbell, K.W., 1991, Investigations of peak acceleration data for site effects: Oakland, Calif., Earthquake Engineering Research Institute, Fourth International Conference on Seismic Zonation, Palo Alto, Calif., 1991, Proceedings, p. 229–237.

Rogers, G.C., 1985, Variation in Cascade volcanism with margin orientation: Geology, v. 13, no. 7, p. 495–498.

———1988a, An assessment of the megathrust earthquake potential of the Cascadia subduction zone: Canadian Journal of Earth Sciences, v. 25, no. 6, p. 844–852.

———1988b, Seismic potential of the Cascadia subduction zone: Nature, v. 332, no. 6159, p. 17.

Rogers, G.C., and Hasegawa, H.S., 1978, A second look at the British Columbia earthquake of June 23, 1946: Seismological Society of America Bulletin, v. 68, no. 3, p. 653–675.

Ruff, Larry, and Kanamori, Hiroo, 1980, Seismicity and the subduction process: Physics of the Earth and Planetary Interiors, v. 23, p. 240–252.

———1983, Seismic coupling and uncoupling at subduction zones: Tectonophysics, v. 99, no. 2/4, p. 99–117.

Sammis, C.G., Davis, G.A., and Crosson, R.S., 1988, New perspectives on the geometry and mechanics of the Cascadia subduction zone, *in* Cascadia subduction zone—An evaluation of the earthquake potential and implications to WNP–3, Washington Public Power Supply System response to NRC questions 230.1 and 230.2, 136 p. [unpublished report to the U.S. Nuclear Regulatory Commission]: Available from the Department of Nuclear Resources Library, Geology and Earth Resources Division, Olympia, WA 98504.

Savage, J.C., 1983, A dislocation model of strain accumulation and release at a subduction zone: Journal of Geophysical Research, v. 88, no. 136, p. 4984–4996.

———1989, Interseismic crustal deformation at subduction zones [abs.]: EOS [American Geophysical Union Transactions], v. 70, no. 43, p. 1050.

Savage, J.C., and Lisowski, Michael, 1991, Strain measurements and the potential for a great subduction earthquake off the coast of Washington: Science, v. 252, no. 5002, p. 101–103.

Savage, J.C., Lisowski, Michael, and Prescott, W.H., 1981, Geodetic strain measurements in Washington: Journal of Geophysical Research, v. 86, no. B6, p. 4929–4940.

———1991, Strain accumulation in western Washington: Journal of Geophysical Research, v. 96, no. B9, p. 14493–14507.

Sbar, M.L., 1983, An explanation for contradictory geodetic strain and fault-plane solution data in western North America: Geophysical Research Letters, v. 10, no. 3, p. 177–180.

Scheidegger, K.F., 1984, Thermal evolution of the Juan de Fuca plate, *in* Kulm, L.D., and others, eds., Ocean Margin Drilling Program, Regional Atlas Series, Western North American continental margin and adjacent ocean floor off Oregon and Washington, Atlas 1: Woods Hole, Mass., Marine Science International, p. 8.

Schuster, R.L., and Chleborad, A.F., 1989, Landslides in Washington and Oregon—An overview, *in* Hays, W.W., ed., Proceedings of Conference XLVIII, 3d annual workshop on earthquake hazards in the Puget Sound, Portland area: U.S. Geological Survey Open-File Report 89–465, p. 86–105.

Schuster, R.L., Logan, R.L., and Pringle, P.T., 1992, Prehistoric rock avalanches in the Olympic Mountains, Washington: Science, v. 258, p. 1620–1621.

Shaffer, M.E., and West, M.W., 1989, Quaternary faulting in the Frenchman Hills anticline, Yakima fold belt, central Columbia basin, Washington [abs.]: Geological Society of America Abstracts with Programs, v. 21, no. 5, p. 142.

Shannon & Wilson, Inc., 1977, Geologic studies in the 1872 earthquake epicentral region, *in* Washington Public Power Supply System Nuclear Projects Nos. 1 and 4, Preliminary safety analysis report, Amendment 23, v. 2A, appendix, 2R, subappendix 2R–D, 44 p. [a report to the U.S. Nuclear Regulatory Commission]: Available from the U.S. Nuclear Regulatory Commission, Washington, D.C. 20555.

Shedlock, K.M., and Weaver, C.S., 1991, Program for earthquake assessment in the Pacific Northwest: U.S. Geological Survey Circular 1067, 29 p.

Silver, E.A., 1972, Pleistocene tectonic accretion of the continental slope off Washington: Marine Geology, v. 13, no. 4, p. 239–249.

Singh, S.K., Lermo, J., Dominguez, T., Ordaz, M., Espinosa, J., Mena, E., and Quaas, R., 1988, A study of amplification of seismic waves in the Valley of Mexico with respect to a hill zone site: Earthquake Spectra, v. 4, no. 4, p. 653–673.

Singh, S.K., Ponce, L., and Nishenko, S.P., 1985, The great Jalisco, Mexico, earthquakes of 1932—Subduction of the Rivera plate: Seismological Society of America Bulletin, v. 75, no. 5, p. 1301–1313.

Smolka, A., and Berz, Gerhard, 1989, An analysis of the insured loss and implications for risk assessment: Earthquake Spectra, v. 5, no. 1, p. 223–248.

Snavely, P.D., Jr., 1987, Tertiary geological framework, neotectonics, and petroleum potential of the Oregon-Washington continental margin, *in* Scholl, D.W., Grantz, Arthur, and Vedder, J.G., eds., Geology and resource potential of the continental margin of western North America and adjacent ocean basins—Beaufort Sea to Baja California: Houston, Tex., Circum-Pacific Council for Energy and Mineral Resources, Earth Science Series, v. 6, no. 6, p. 305–335.

———1992, Cenozoic geologic history of the Oregon and Washington continental margin, *in* Lockwood, Millington, and McGregor, B.A., eds., Proceedings of the 1991 Exclusive Economic Zone symposium on mapping and research—Working together in the Pacific EEZ, Portland, Oreg., November 5–7, 1991: U.S. Geological Survey Circular 1092, p. 30–36.

Snavely, P.D., Jr., Niem, A.R., MacLeod, N.S., Pearl, J.E., and Rau, W.W., 1980, Makah Formation—A deep marginal basin sedimentary sequence of upper Eocene and Oligocene age in the northwestern Olympic Peninsula, Washington: U.S. Geological Survey Professional Paper 1162–B, 28 p.

Snavely, P.D., Jr., Wagner, H.C., and Lander, D.L., 1980, Geologic cross section of the central Oregon continental margin: Geological Society of America Map and Chart Series MC–28J, scale 1:250,000.

Spence, William, 1987, Slab pull and the seismotectonics of subducting lithosphere: Reviews of Geophysics and Space Physics, v. 25, no. 1, p. 55–69.

———1989, Stress origins and earthquake potential in Cascadia: Journal of Geophysical Research, v. 94, p. 3076–3088.

Stover, C.W., and Hake, C.A. von, 1982, United States earthquakes, 1980: Golden, Colo., U.S. Geological Survey and U.S. National Oceanic and Atmospheric Administration, 112 p.

Sykes, L.R., 1989, Great earthquakes of 1855 and 1931 in New Zealand—Evidence for seismic slip along downgoing plate boundary and implications for seismic potential of Cascadia subduction zone [abs.]: EOS [American Geophysical Union Transactions], v. 70, no. 43, p. 1331.

Sykes, L.R., and Byrne, D.E., 1987, Seismic and aseismic subduction, Part 2—Aseismic slip at zones of massive sediment supply and nature of great asperities at convergent margins [abs.]: EOS [American Geophysical Union Transactions], v. 68, no. 44, p. 1468.

Tabei, Takao, 1989, Crustal movements in the inner zone of southwest Japan associated with stress relaxation after major earthquakes: Journal of Physics of the Earth, v. 37, no. 2, p. 101–131.

Taber, J.J., and Lewis, B.T.R., 1986, Crustal structure of the Washington continental margin from refraction data: Seismological Society of America Bulletin, v. 76, no. 4, p. 1011–1024.

Taber, J.J., and Smith, S.W., 1985, Seismicity and focal mechanisms associated with the subduction of the Juan de Fuca plate beneath the Olympic Peninsula, Washington: Seismological Society of America Bulletin, v. 75, no. 1, p. 237–249.

Theil, C.C., Jr., 1990, Competing against time [report to Governor George Deukmejian]: North Highlands, State of California Office of Planning and Research, Department of General Services, Publications Section, 264 p.

Thomas, G.C., Crosson, R.S., Dewberry, S., Pullen, J., Yelin, T.S., Norris, R.D., Bice, W.T., Carver, D.L., Meremonte, M.E., Overturf, D.E., Worley, D.M., Sembera, E.D., and MacDonald, T.R., 1993, The 25 March 1993 Scotts Mills, Oregon earthquake—Aftershock analysis from combined permanent and temporary digital stations [abs.]: EOS [American Geophysical Union Transactions], v. 74, no. 43/Supplement, p. 201.

Thorsen, G.W., 1988, Overview of earthquake-induced water waves in Washington and Oregon, *in* Hays, W.W., ed., Proceedings of Conference XLII, Workshop on evaluation of earthquake hazards and risk in the Puget Sound and Portland areas: U.S. Geological Survey Open-File Report 88–541, p. 83–94.

Tolan, T.L., and Reidel, S.P., 1989, Structure map of a portion of the Columbia River flood-basalt province, *in* Reidel, S.P., and Hooper, P.R., eds., Volcanism and tectonism in the Columbia River flood-basalt province: Geological Society of America Special Paper 239, scale 1:500,000.

Toppozada, T.R., Real, C.R., and Parke, D.L., 1981, Preparation of isoseismal maps and summaries of related effects of pre-1900 California earthquakes: California Division of Mines and Geology Open-File Report 81–11, 101 p.

Trifunac, M.D., 1977, Uniformly processed strong earthquake ground accelerations in the western United States of America for the period from 1933 to 1971—Pseudo-relative velocity spectra and processing noise: Los Angeles, University of Southern California, Dept. of Civil Engineering, Report No. CE77–04, 219 p.

U.S. Department of Energy, 1988, Site characterization plan; Reference repository location, Hanford site, Washington [consultation draft]: Washington, D.C., U.S. Office of Civilian Radioactive Waste Management Report DOE/RW–0164, v. 1, p. 1.3.14–1.3.40.

U.S. Executive Office of the President, 1978, The National Earthquake Hazards Reduction Program: Washington, D.C., 30 p.

U.S. Geological Survey, 1975, A study of earthquake losses in the Puget Sound, Washington, area: U.S. Geological Survey Open-File Report 75–375, 298 p.

———1988, Probabilities of large earthquakes occurring in California on the San Andreas fault: U.S. Geological Survey Open-File Report 88–398, 62 p.

———1991, Preliminary determination of epicenters—Monthly listing for August 1991: Washington, D.C., U.S. Government Printing Office, 32 p.

———1991, Preliminary determination of epicenters—Monthly listing for July 1991: Washington, D.C., U.S. Government Printing Office, 32 p.

———1992, Preliminary determination of epicenters [monthly listings for all months]: Washington, D.C., U.S. Government Printing Office.

———1993, Preliminary determination of epicenters [monthly listings for all months]: Washington, D.C., U.S. Government Printing Office.

U.S. Nuclear Regulatory Commission, 1991, Draft safety evaluation by the Office of Nuclear Reactor Regulation relating to geology and seismology, Washington Public Power Supply System, Washington Nuclear Project No. 3 (WNP–3) Docket No. 50–508: Washington, D.C., U.S. Government Printing Office, 31 p.

U.S. Veterans Administration, 1976, Study to establish seismic protection provisions for furniture, equipment, and supplies for VA hospitals: Washington, D.C., U.S. Veterans Administration Office of Construction, 163 p. [Reprinted February 1980].

———1986, Earthquake-resistant design requirements for VA hospital facilities: Washington, D.C., U.S. Veterans Administration Office of Facilities Handbook H–08–8, 14 p.

Uyeda, S., and Kanamori, Hiroo, 1979, Back-arc opening and the mode of subduction: Journal of Geophysical Research, v. 84, no. B3, p. 1049–1061.

VanDecar, J.C., Crosson, R.S., and Creager, K.C., 1991, Tectonic inferences from the three-dimensional upper-mantle velocity structure of the Cascadia subduction zone [abs.]: EOS [American Geophysical Union Transactions], v. 72, no. 44, p. 326.

Vincent, Paul, Richards, M.A., and Weldon, R.J., II, 1989, Vertical deformation of the Oregon Cascadia margin [abs.]: EOS [American Geophysical Union Transactions], v. 70, no. 43, p. 1332.

Vine, F.J., and Matthews, D.H., 1963, Magnetic anomalies over ocean ridges: Nature, v. 199, p. 947–949.

Wagner, H.C., 1985, Preliminary geologic framework studies showing bathymetry, locations of geophysical tracklines and exploratory wells, sea-floor geology and deeper geologic structures, magnetic contours, and inferred thickness of Tertiary rocks on the continental shelf and upper continental slope off southwestern Washington between latitudes 46°N and 47°30'N and from the Washington coast to 125°20'W: Washington State Department of Natural Resources Open-File Report 85–1, 6 p., 5 pls., scale 1:250,000.

Wagner, H.C., Batatian, L.D., Lambert, T.M., and Tomson, J.H., 1986, Preliminary geologic framework studies showing bathymetry, locations of geophysical tracklines and exploratory wells, sea-floor geology and deeper geologic structures, magnetic contours, and inferred thickness of Tertiary rocks on the continental shelf and upper continental slope off southwestern Washington between latitudes 46°N and 48°30'N and from the Washington coast to 125°20'W: Washington State Department of Natural Resources Open-File Report 86–1, 8 p., 6 pls., scale 1:250,000.

Wagner, H.C., and Tomson, J.H., 1987, Offshore geology of the Strait of Juan de Fuca, State of Washington and British Columbia, Canada: Washington State Department of Natural Resources Open-File Report 87–1, 15 p., 7 pls., scale 1:250,000.

Walsh, T.J., and Logan, R.L., 1985, Geological and geophysical expression of the Olympic-Wallowa lineament (OWL) near North Bend, Washington [abs.]: Geological Society of America Abstracts with Programs, v. 17, no. 6, p. 416.

Walsh, T.J., Madin, Ian, Noson, L.L., and Yelin, T.S., eds., 1990, Proceedings of Conference LX, 4th annual workshop on earthquake hazards in the Puget Sound and Portland area: U.S. Geological Survey Open-File Report 90–703, 275 p.

Wang, K., and Hyndman, R.D., 1991, Thermal constraints on the zone of possible major thrust earthquake failure on the Cascadia margin [abs.]: EOS [American Geophysical Union Transactions], v. 72, no. 44, p. 314.

Washington Public Power Supply System, 1988, Cascadia subduction zone—An evaluation of the earthquake potential and implications to WNP–3, Washington Public Power Supply System response to NRC questions 230.1 and 230.2, 136 p. [unpublished report to the U.S. Nuclear Regulatory Commission]: Available from the Department of Nuclear Resources Library, Geology and Earth Resources Division, Olympia, WA 98504.

Washington State Department of Community Development, 1990, Minimum guidelines to classify agricultural, forest, mineral lands, and critical areas: Olympia, Washington Administrative Code, Sec. 365–190–080(4)(e), 13 p.

Washington State Legislature, 1990a, An act creating a Seismic Safety Advisory Committee: Olympia, Washington State Legislature, Washington Laws 1990, chap. 16, sec. 225.

———1990b, An act relating to growth, Substitute House Bill No. 2929: Olympia, Washington State Legislature, Washington Laws 1990, chap. 17, sec. 6.

Washington State Seismic Safety Advisory Committee, 1991, A policy plan for improving earthquake safety in Washington, fulfilling our responsibility: Washington State Department of Community Development, Emergency Management Division, 75 p.

Washington State Seismic Safety Council, 1986, Policy recommendations: Olympia, Washington State Seismic Safety Council, 21 p.

Washington State Superintendent of Public Instruction, 1989, Safer schools—Earthquake hazards, nonstructural, *in* Noson, L.L., ed., School facilities development procedures manual, Part A, 63 p.: Available from the Department of Natural Resources Library, Geology and Earth Resources Division, Olympia, WA 98504.

Weaver, C.S., and Baker, G.E., 1988, Geometry of the Juan de Fuca plate beneath Washington and northern Oregon from seismicity: Seismological Society of America Bulletin, v. 78, no. 1, p. 264–275.

Weaver, C.S., and Michaelson, C.A., 1985, Seismicity and volcanism in the Pacific Northwest—Evidence for the segmentation of the Juan de Fuca plate: Geophysical Research Letters, v. 12, no. 4, p. 215–218.

Weaver, C.S., and Shedlock, K.M., 1989, Potential subduction, probable intraplate, and known crustal earthquake source areas in the Cascadia subduction zone, *in* Hays, W.W., ed., Proceedings of Conference XLVIII, 3d annual workshop on earthquake hazards in the Puget Sound, Portland area: U.S. Geological Survey Open-File Report 89–465, p. 11–26.

Weaver, C.S., and Smith, S.W., 1983, Regional tectonic and earthquake hazards implications of a crustal fault zone in southwestern Washington: Journal of Geophysical Research, v. 88, no. B12, p. 10371–10383.

Wells, R.E., 1990, Paleomagnetic rotations and the Cenozoic tectonics of the Cascade arc, Washington, Oregon, and California: Journal of Geophysical Research, v. 95, no. B12, p. 19409–19417.

Wells, R.E., and Coe, R.S., 1985, Paleomagnetism and geology of Eocene volcanic rocks of southwest Washington—Implications for mechanisms of tectonic rotation: Journal of Geophysical Research, v. 90, no. B2, p. 1925–1947.

Werner, K.S., Graven, E.P., Berkman, T.A., and Parker, M.J., 1991, Direction of maximum horizontal compression in western Oregon determined by borehole breakouts: Tectonics, v. 10, no. 5, p. 948–958.

West, D.O., and McCrumb, D.R., 1988a, Coastline uplift in Oregon and Washington and the nature of Cascadia subduction-zone tectonics: Geology, v. 16, no. 2, p. 169–172.

———1988b, Reply to B.F. Atwater's comment on "Coastline uplift in Oregon and Washington and the nature of Cascadia subduction-zone tectonics": Geology, v. 16, no. 10, p. 952–953.

West, M.W., and Shaffer, M.E., 1989, Late Quaternary tectonic deformation in the Smyrna Bench and Saddle Gap segments, Saddle Mountains anticline, Yakima fold belt, central Columbia basin, Washington [abs.]: Geological Society of America Abstracts with Programs, v. 21, no. 5, p. 157–158.

Williams, P.L., and Jacoby, G.C., 1989, Evaluation of possible seismic triggering of giant landslides in Seattle, Washington [abs.]: EOS [American Geophysical Union Transactions], v. 70, no. 43, p. 1332.

Wilson, J.R., 1983, Relationships between late Quaternary faults and earthquakes in the Puget Sound, Washington, area, *in* Yount, J.C., and Crosson, R.S., eds., Proceedings of Workshop XIV, Earthquake hazards of the Puget Sound region, Washington: U.S. Geological Survey Open-File Report 83–19, p. 165–177.

Wilson, J.R., Bartholomew, M.J., and Carson, R.J., 1979, Late Quaternary faults and their relationship to tectonism in the Olympic Peninsula, Washington: Geology, v. 7, no. 5, p. 235–239.

Wong, I.G., Silva, W.J., and Madin, I.P., 1990, Preliminary assessment of potential strong earthquake ground shaking in the Portland, Oregon, metropolitan area: Oregon Geology, v. 52, no. 6, p. 131–134.

Wyss, Max, 1979, Estimating maximum expectable magnitude of earthquakes from fault dimensions: Geology, v. 7, no. 7, p. 336–340.

Yeats, R.S., 1989, Current assessment of earthquake hazard in Oregon, *in* Hays, W.W., ed., Proceedings of Conference XLVIII, 3d annual workshop on earthquake hazards in the Puget Sound, Portland area: U.S. Geological Survey Open-File Report 89–465, p. 27–30.

Yelin, T.S., and Patton, H.J., 1991, Seismotectonics of the Portland, Oregon, region: Seismological Society of America Bulletin, v. 81, no. 1, p. 109–130.

Youngs, R.R., and Coppersmith, K.J., 1989, Attenuation relationships for evaluation of seismic hazards from large subduction zone earthquakes, *in* Hays, W.W., ed., Proceedings of Conference XLVIII, 3d annual workshop on earthquake hazards in the Puget Sound, Portland area: U.S. Geological Survey Open-File Report 89–465, p. 42–49.

Youngs, R.R., Day, S.M., and Stevens, J.L., 1988, Near-field ground motions on rock for large subduction earthquakes, *in* Von Thun, J.L., ed., Earthquake engineering and soil dynamics, II—Recent advances in ground-motion evaluation: New York, American Society of Civil Engineers, Geotechnical Engineering Division, Proceedings of the Specialty Conference, Park City, Utah, Geotechnical Special Publication 20, p. 445–462.

Youngs, R.R., Swan, F.H., Power, M.S., Schwartz, D.P., and Green, R.K., 1987, Probabilistic analysis of earthquake ground-shaking hazard along the Wasatch Front, Utah, *in* Gori, P.L. and Hays, W.W., eds., Assessment of regional earthquake hazards and risk along the Wasatch Front, Utah: U.S. Geological Survey Open-File Report 87–585, v. 2, p. M1–M110.

Yount, J.C., and Gower, H.D., 1991, Bedrock geologic map of the Seattle 30′ by 60′ quadrangle, Washington: U.S. Geological Survey Open-File Report 91–147, 37 p., 4 sheets, scale 1:100,000.

Zervas, C.E., and Crosson, R.S., 1986, P_n observation and interpretation in Washington: Seismological Society of America Bulletin, v. 76, no. 2, p. 521–546.

Ziony, J.I., and Kockelman, W.J., 1985, Introduction, *in* Ziony, J.I., ed., Evaluating earthquake hazards in the Los Angeles region—An earth science perspective: U.S. Geological Survey Professional Paper 1360, p. 1–22.

Zoback, M.L., and Zoback, M.D., 1989, Tectonic stress field of the continental United States, *in* Pakiser, L.C., and Mooney, W.D., eds., Geophysical framework of the continental United States: Boulder, Colo., Geological Society of America Memoir 172, p. 523–539.

Zollweg, J.E., and Johnson, P.A., 1989, The Darrington seismic zone in northwestern Washington: Seismological Society of America Bulletin, v. 79, no. 6, p. 1833–1845.

GLOSSARY

[Terms set in bold type are defined elsewhere in the glossary. Definitions are modified from Ziony, J.I., ed. 1985, Evaluating earthquake hazards in the Los Angeles region—An earth-science perspective: U.S. Geological Survey Professional Paper 1360, p. 15–22]

Acceleration. The rate of change of **velocity** of a reference point. Commonly expressed as a fraction or percentage of the acceleration due to gravity (g), where $g = 980$ cm/s^2.

Accelerogram. The record from an **accelerograph** showing ground **acceleration** as a function of time.

Accelerograph. A compact, rugged, and relatively inexpensive instrument that records the signal from an **accelerometer**. Film is the most common recording medium.

Accelerometer. A sensor whose output is almost directly proportional to ground acceleration. The conventional strong-motion accelerometer is a simple, nearly critically damped **oscillator** having a **natural frequency** of about 20 Hz.

Accretionary wedge. Sediments that accumulate and deform where oceanic and continental plates collide. These sediments are scraped off the top of the downgoing oceanic crustal plate and are added to the leading edge of the continental plate.

Active fault. A **fault** that is considered likely to undergo renewed movement within a period of concern to humans. Faults are commonly considered to be active if they have moved one or more times in the last 10,000 years, but they may also be considered active when assessing the hazard for some applications even if movement has occurred in the last 500,000 years.

Aftershocks. Secondary tremors that may follow the largest shock of an earthquake sequence. Such tremors can extend over a period of weeks, months, or years.

Alluvium. Loosely compacted gravel, sand, silt, or clay deposited by streams.

Amplification. An increase in seismic-signal **amplitude** within some range of **frequency** as waves propagate through different Earth materials. The signal is both amplified and deamplified at the same site in a manner that is dependent on the frequency band. The degree of amplification is also a complex function of the level of shaking such that, as the level of shaking increases, the amount of amplification may decrease. Shaking levels at a site may also be increased by focusing of seismic energy caused by the geometry of the sediment velocity structure, such as basin subsurface topography, or by surface topography.

Amplitude. Zero-to-peak value of any wavelike disturbance.

Arc. Commonly refers to the chain of volcanoes (volcanic arc) that sometimes form inland and that are produced by **subduction**.

Arias intensity. A ground-motion parameter derived from an **accelerogram** and proportional to the integral over time of the **acceleration** squared. Expressed in units of velocity (meters per second or centimeters per second).

Asperity. A region on a fault of high strength produced by one or more of the following conditions: increased normal stress, high friction, low pore pressure, or geometric changes in the fault such as fault bends, offsets, or roughness. This term is used in two contexts: it may refer to sections of a fault that radiate uncommon seismic energy or it may refer to locked sections of the fault that cause fault **segmentation**.

Aseismic. Refering to a fault on which no earthquakes have been observed. Aseismic behavior may be due to lack of shear stress across the fault, a **locked-fault** condition with or without shear stress, or release of stress by fault **creep**.

Attenuation. A decrease in seismic-signal **amplitude** as waves propagate from the seismic **source.** Attenuation is caused by geometric spreading of seismic-wave energy and by the absorption and scattering of seismic energy in different Earth materials (termed anelastic attenuation). Q and kappa are attenuation parameters used in modeling the attenuation of ground motions.

Backarc. The region landward of the chain of volcanoes (volcanic **arc**) in a subduction system.

Backstop. Continental rocks in the **backarc** that are landward from the trace of the subduction thrust fault and that are strong enough to support stress accumulation. These rocks are both igneous and dewatered, lithified, consolidated sediments that probably were part of the **accretionary wedge**. The softer accretionary-wedge rocks are strongly deformed as they accumulate against the backstop. The exact position and dip direction of the backstop is not well determined, and more than one backstop may exist.

Basement. Igneous and metamorphic rocks that underlie the main sedimentary-rock sequences of a region and extend downward to the base of the **crust**.

Bedrock. Relatively hard, solid rock that commonly underlies softer rock, sediment, or soil.

Benioff zone. A dipping planar zone of earthquakes that is produced by the interaction of a downgoing oceanic crustal plate with a continental plate. These earthquakes can be produced by slip along the subduction thrust fault (sometimes referred to as the thrust interface fault because it is the interface between the continental plate and the oceanic plate) or by slip on faults within the downgoing plate as a result of bending and extension as the plate is pulled into the **mantle**. Slip may also initiate between adjacent segments of downgoing plates. The Benioff zone in the Pacific Northwest is not as well developed as it is in other subduction zones. The earthquakes in this region do not appear to be produced by slip along the thrust fault. Also known as the Wadati-Benioff zone.

Body wave. A seismic wave that propagates through the interior of the Earth, as opposed to **surface waves** that propagate near the Earth's surface. ***P*** and ***S*** **waves** are examples. Each type of wave has distinctive **strain** characteristics.

Brittle-ductile boundary. A depth in the crust across which the thermomechanical properties of the crust change from brittle above to ductile below. A large percentage of the earthquakes in the crust initiate at or above this depth on high-angle faults; below this depth, fault slip may be aseismic and may grade from high angle to low angle.

Bulk density. The weight of a material divided by its volume, including the volume of its pore spaces.

^{14}C age date. A relative age obtained for geologic materials containing bits or pieces of carbon using measurements of the proportion of radioactive carbon (^{14}C) to daughter carbon (^{12}C). These dates are independently calibrated with calendar dates.

Coherent slides. Landslides that consist of a few relatively intact blocks of rock or soil that move together. The basal failure surface of most of these slides is several meters or tens of meters below the land surface.

Cohesionless. Refering to the condition of a sediment whose shear strength depends only on friction because there is no bonding between the grains. This condition is typical of clay-free sandy deposits.

Colluvium. Loose soil or rock fragments on or at the base of gentle slopes or hillsides. Deposited by or moving under the influence of rainwash or downhill creep.

Compressional wave. See ***P*** **wave**.

Convolution. A mathematical operation that describes the action of a linear system on a signal, such as that of a filter on a seismic signal.

Corner frequency. The **frequency** at which the curve representing the **Fourier amplitude spectrum** of a recorded earthquake seismic signal abruptly changes slope. This frequency is a property of the **source function** related to fault size.

Creep. Slow, more or less continuous movement occurring on faults due to ongoing **tectonic** deformation. Also applied to slow movement of landslide masses down a slope because of gravitational forces. Faults that undergo significant and (or) ongoing creep are likely to be **aseismic** or capable of only small or moderate earthquakes. This fault condition is commonly referred to as unlocked (see **locked fault** and **interplate coupling**).

Critical facilities. Structures whose ongoing performance during an emergency is required or whose failure could threaten many lives. May include (1) structures such as nuclear power reactors or large dams whose failure might be catastrophic; (2) major communication, utility, and transportation systems; (3) involuntary- or high-occupancy buildings such as schools or prisons; and (4) emergency facilities such as hospitals, police and fire stations, and disaster-response centers.

Crust. The outermost major layer of the Earth, ranging from about 10 to 65 km in thickness worldwide. The continental crust is about 40 km thick in the Pacific Northwest. The thickness of the oceanic crust in this region varies between about 10 and 15 km. The crust is characterized by ***P*-wave** velocities less than about 8 km/s. The uppermost 15–35 km of crust is brittle enough to produce earthquakes. The seismic crust is separated from the lower crust by the **brittle-ductile boundary**.

Damping. The reduction in **amplitude** of a seismic wave or **oscillator** due to friction and (or) the internal absorption of energy by matter. See **Geometrical attenuation**.

Deformational front. See **Accretionary wedge**.

Design earthquake. The postulated earthquake (commonly including a specification of the **ground motion** at a site) that is used for evaluating the earthquake resistance of a particular structure.

Deterministic methods. Refers to methods of calculating ground motions for hypothetical earthquakes based on earthquake-source models and wave-propagation methods that exclude random effects.

Dip. Inclination of a planar geologic surface (for example, a fault or a bed) from the horizontal.

Dip slip. See **Fault**.

Directivity. An effect of a propagating fault rupture whereby earthquake **ground motion** in the direction of propagation is more severe than that in other directions from the earthquake source.

Displacement. The difference between the initial position of a reference point and any later position. (1) In seismology, displacement is the ground motion commonly inferred from a **seismogram**. For example, it may be calculated by integrating an **accelerogram** twice with respect to time and is expressed in units of length, such as centimeters. (2) In geology, displacement is the permanent offset of a geologic or manmade reference point along a **fault** or a landslide.

Disrupted slides and falls. Landslides that are broken during movement into chaotic masses of small blocks, rock fragments, or individual grains. The basal failure surface of most such slides is within a few meters of the land surface.

Earthquake. Ground shaking and radiated seismic energy caused most commonly by sudden slip on a fault, volcanic or magmatic activity, or other sudden stress changes in the Earth. An earthquake of magnitude 8 or larger is termed a great earthquake.

Earthquake hazard. Any physical phenomenon associated with an earthquake that may produce adverse effects on human activities. This includes **surface faulting**, **ground shaking**, **landslides**, **liquefaction**, **tectonic** deformation, **tsunami**, and **seiche** and their effects on land use, manmade structures, and socio-economic systems. A commonly used restricted definition of earthquake hazard is the probability of occurrence of a specified level of ground shaking in a specified period of time.

Earthquake risk. The expected (or probable) life loss, injury, or building damage that will happen, given the probability that some **earthquake hazard** occurs. Earthquake risk and earthquake hazard are occasionally used interchangeably.

Elastic dislocation theory. In seismology, a theoretical description of how an elastic Earth responds to fault slip, as represented by a distribution of **displacement** discontinuities.

Epicenter. The point on the Earth's surface vertically above the point (focus or hypocenter) in the crust where a seismic rupture nucleates.

F_{max}. The frequency above which little seismic energy is observed at most strong-motion stations. This frequency cutoff may be produced by **attenuation** of shaking by unconsolidated sediments underlying the recording site or may be a property of the **source function**.

Fault. A fracture along which there has been significant **displacement** of the two sides relative to each other parallel to the fracture. Strike-slip faults are vertical (or nearly vertical) fractures along which rock masses have mostly shifted horizontally. If the block opposite an observer looking across the fault moves to the right, the slip style is termed right lateral; if the block moves to the left, the motion is termed left lateral. Dip-slip faults are inclined fractures along which rock masses have mostly shifted vertically. If the rock mass above an inclined fault is depressed by slip, the fault is termed normal, whereas if the rock above the fault is elevated by slip, the fault is termed reverse (or thrust). Oblique-slip faults have significant components of both slip styles.

Fault-plane solution. An analysis using stereographic projection or its mathematical equivalent to determine the attitude of the causative fault and its direction of **slip** from the radiation pattern of seismic waves using earthquake records at many stations. The analysis most commonly uses the direction of **first motion** of ***P* waves** and yields two possible orientations for the fault rupture and the direction of **seismogenic** slip. From these data, inferences can be made concerning the principal axes of **stress** in the region of the earthquake. The principal stress axes determined in this method are the compressional axis (also called the P-axis, the axis of greatest compression, or σ_1), the tension axis (also known as the T-axis, axis of least compression, or σ_3), and the intermediate stress axis (σ_2).

Fault scarp. Steplike linear landform coincident with a **fault trace** and caused by geologically recent slip on the fault.

Fault trace. Intersection of a fault with the ground surface; also, the line commonly plotted on geologic maps to represent a fault.

Filter. In seismology, a physical system or a mathematical operation that changes the waveform or **amplitude** of a signal.

Filtering. **Attenuation** of certain frequency components of a seismic signal and the **amplification** of others. For a recorded signal, the process can be accomplished electronically or numerically in a digital computer. Filtering also occurs naturally as seismic energy passes through the Earth.

First motion. On a seismogram, the direction of **ground motion** as the ***P* wave** arrives at the **seismometer**. Upward ground motion indicates an expansion in the **source** region; downward motion indicates a contraction.

Focal depth. A term that refers to the depth of an earthquake **focus**.

Focal-mechanism solution. See **Fault-plane solution**.

Focus. See **Hypocenter**.

Focusing. See **Amplification**.

Forearc. The region between the trace of the **subduction thrust fault** and the volcanic chain (volcanic arc).

Foreshocks, mainshock, aftershocks. Foreshocks are relatively smaller earthquakes that precede the biggest earthquake in a series, which is termed the mainshock. Aftershocks are relatively smaller earthquakes that follow the mainshock.

Fourier amplitude spectrum. The relative **amplitude** at different component frequencies that are derived from a **time history** by Fourier analysis.

Fourier transform. The mathematical operation that resolves a time series (for example, a recording of ground motion) into a series of numbers that characterize the relative amplitude and phase components of the signal as a function of frequency.

Frequency. Number of cycles occurring in unit time. **Hertz (Hz)**, the unit of frequency, is equal to the number of cycles per second.

Fundamental period. The longest period for which a structure shows a maximum response. The reciprocal of natural frequency.

***G* or *g*.** See **Acceleration**.

Gaussian noise spectrum. The spectrum of a time history whose sample values are generated by random selection from a statistical population that has a specified mean and standard deviation. The values (ordinates) have a bell-shaped distribution about the mean. In earthquake studies, this type of spectrum is commonly multiplied by a theoretical earthquake source spectrum to obtain predicted ground-motion spectra for hypothetical earthquakes.

Geodetic. Refering to the determination of the size and shape of the Earth and the precise location of points on its surface.

Geometrical attenuation. That component of **attenuation** of seismic-wave amplitudes due to the radial spreading of seismic energy with distance from a given source.

Geomorphology. The study of the character and origin of landforms.

Geotechnical. Refering to the use of scientific methods and engineering principles to acquire, interpret, and apply knowledge of Earth materials for solving engineering problems.

Gravity. The attraction between two masses, such as the Earth and an object on its surface. Commonly referred to as the acceleration of gravity. Changes in the gravity field can be used to infer information about the structure of the Earth's lithosphere and upper mantle. Interpretations of changes in the gravity field are generally applied to gravity values corrected for extraneous effects. The corrected values are referred to by various terms, such as free-air gravity, Bouguer gravity, and isostatic gravity, depending on the number of corrections.

Green's function. A mathematical representation that, in reference to earthquake shaking, is used to represent the **ground motion** caused by instantaneous **slip** on a small part of a fault. Green's functions can be summed over a large fault surface to compute the ground shaking for a large earthquake rupturing a fault of finite size. The fractional fault-slip events that are summed can be records from small earthquakes on the fault or they can be theoretically computed small-earthquake records.

Ground failure. A general reference to **landslides**, **liquefaction**, and **lateral spreads**.

Ground motion [shaking]. General term referring to the qualitative or quantitative aspects of movement of the Earth's surface from earthquakes or explosions. Ground motion is produced by waves that are generated by sudden slip on a fault or sudden pressure at the explosive source and travel through the Earth and along its surface.

Halfspace. A mathematical model bounded by a planar surface but otherwise infinite. Properties within the model are commonly assumed to be homogeneous and isotropic, unlike the Earth itself, which is heterogeneous and anisotropic.

Hazard. See **Earthquake hazard**.

Hertz (Hz). A unit of frequency. Expressed in cycles per second.

Holocene. Refers to a period of time between the present and 10,000 years before present. Applied to rocks or faults, this term indicates the period of rock formation or the time of most recent fault slip. Faults of this age are commonly considered active, based on the observation of historical activity on faults of this age in other locales.

Hypocenter. The point within the Earth where an earthquake rupture initiates. Also commonly termed the **focus**.

Intensity. A subjective numerical index describing the severity of an earthquake in terms of its effects on the Earth's surface and on humans and their structures. Several scales exist, but the ones most commonly used in the United States are the Modified Mercalli scale and the Rossi-Forel scale.

Intraplate and interplate. Intraplate pertains to processes within the Earth's crustal plates. Interplate pertains to processes between the plates.

Interplate coupling. The qualitative ability of a **subduction thrust fault** to lock and accumulate stress. Strong interplate coupling implies that the fault is locked and capable of accumulating stress, whereas weak coupling implies that the fault is unlocked or only capable of accumulating low stress. A fault with weak interplate coupling could be aseismic or could slip by **creep**. See **Locked fault**.

Isoseismal. Refering to a line on a map bounding points of equal **intensity** for a particular earthquake.

Kinematic. Refering to the general movement patterns and directions of the Earth's rocks that produce rock deformation.

Late Quaternary. Refering to an age between the present and 500,000 years before the present. Faults of this age are sometimes considered active based on the observation of historical activity on faults of this age in some locales.

Landslide. The downslope movement of soil and (or) rock.

Lateral spreads and flows. Terms refering to **landslides** that commonly form on gentle slopes and that have rapid fluid-like flow movement.

Least-squares fit. An approximation of a set of data with a curve such that the sum of the squares of the differences between the observed points and the assumed curve is a minimum.

Lifelines. Structures that are important or critical for urban functionality. Examples are roadways, pipelines, powerlines, sewers, communications, and port facilities.

Liquefaction. Process by which water-saturated sediment temporarily loses strength and acts as a fluid. This effect can be caused by earthquake shaking.

Lithology. The description of rock composition and texture.

Lithosphere. The outer solid part of the Earth, including the **crust** and uppermost **mantle**. The lithosphere is about 100 km thick, although its thickness is age dependent. The lithosphere below the crust is brittle enough at some locations to produce earthquakes by faulting, such as within a subducted oceanic plate.

Locked fault. A fault that is not slipping because frictional resistance on the fault is greater than the shear stress across the fault. Such faults may store **strain** for extended periods that is eventually released in an earthquake when frictional resistance is overcome. A locked fault condition contrasts with fault-**creep** conditions and an unlocked fault. See **Interplate coupling**.

Love wave. A type of seismic surface wave having a horizontal motion that is transverse to the direction of propagation.

Ma. An abbreviation for one million years ago.

Magnetic polarity reversal. A change of the Earth's magnetic field to the opposite polarity that has occurred at irregular intervals during geologic time. Polarity reversals can be preserved in sequences of magnetized rocks and compared with standard polarity-change time scales to estimate geologic ages of the rocks. Rocks created along the **spreading oceanic ridges** commonly preserve this pattern of polarity reversals as they cool, and this pattern can be used to determine the rate of ocean-ridge spreading. The reversal patterns recorded in the rocks are termed sea-floor magnetic lineaments.

Magnitude. A number that characterizes the relative size of an earthquake. Magnitude is based on measurement of the maximum motion recorded by a **seismograph** (sometimes for earthquake waves of a particular **frequency**), corrected for attenuation to a standardized distance. Several scales have been defined, but the most commonly used are (1) local magnitude (M_L), commonly referred to as "Richter magnitude," (2) surface-wave magnitude (M_S), (3) body-wave magnitude (m_b), and (4) moment magnitude (M_W). Scales 1–3 have limited range and applicability and do not satisfactorily measure the size of the largest earthquakes. The moment magnitude (M_W) scale, based on the concept of **seismic moment**, is uniformly applicable to all sizes of earthquakes but is more difficult to compute than the other types. In principal, all magnitude scales could be cross calibrated to yield the same value for any given earthquake, but this expectation has proven to be only approximately true, thus the need to specify the magnitude type as well as its value.

Mantle. That part of the Earth's interior between the metallic core and the **crust**.

Microzonation. The geographic delineation at local or site scales of areas having different potentials for hazardous earthquake effects, such as **ground shaking** potential. Microzonation for any of the **earthquake hazards** can be produced.

Moho. A discontinuity in seismic velocity that marks the boundary between the Earth's **crust** and **mantle**. Also termed the Mohorovicic′ discontinuity, after the Croatian seismologist Andrija Mohorovicic′ (1857–1936) who discovered it. The boundary is between 25 and 60 km deep beneath the continents and between 5 and 8 km deep beneath the ocean floor.

Moment magnitude. See **Magnitude**.

Natural frequency(ies). The discrete frequency(ies) at which a particular elastic system vibrates when it is set in motion by a single impulse and not influenced by other external forces or by damping. The reciprocal of fundamental period.

Newmark analysis. A numerical technique that models a potential landslide as a rigid block resting on a frictional slope, prescribing dynamic forces on the block from assumed ground shaking records in order to calculate the expected displacement of the block.

Normal stress. That **stress** component perpendicular to a given plane.

Oceanic spreading ridge. A fracture zone along the ocean bottom that accommodates upwelling of mantle material to the surface, thus creating new crust. This fracture is topographically marked by a line of ridges that form as molten rock reaches the ocean bottom and solidifies.

Oceanic trench. A linear depression of the sea floor caused by and approximately coincident with a **subduction thrust fault**.

Oscillator. A mass that moves with oscillating motion under the influence of external forces and one or more forces that restore the mass to its stable at-rest position. In earthquake engineering, an oscillator is an idealized damped mass-spring system used as a model of the **response** of a structure to earthquake **ground motion**. A **seismograph** is also an oscillator of this type.

Outer arc ridge. A zone landward from the trace of the subduction thrust fault of elevated sea floor probably related to the compression of the rocks in the **accretionary wedge**. Also referred to as the outer arc high.

***P* wave.** A seismic **body wave** that involves particle motion (alternating compression and extension) in the direction of propagation.

Paleoseismic. Referring to the prehistoric seismic record as inferred from young geologic sediments.

Peak acceleration. See **Acceleration**.

Pedogenic. Pertaining to processes that add, transfer, transform, or remove soil constituents.

Period. The time interval required for one full cycle of a wave.

Period band. That range of **periods** being considered in an analysis of **ground motion**.

Phase. (1) A stage in periodic motion, such as wave motion or the motion of an **oscillator**, measured with respect to a given initial point and expressed in angular measure. (2) A pulse of seismic energy arriving at a definite time. (3) Stages in the physical properties of rocks or minerals under differing conditions of pressure, temperature, and water availability.

Physiographic. Refering to the character and distribution of landforms.

Plate tectonics. A theory supported by a wide range of evidence that considers the Earth's **crust** and upper **mantle** to be composed of several large, thin, relatively rigid plates that move relative to one another. Slip on faults that define the plate boundaries commonly results in earthquakes. Several styles of faults bound the plates, including thrust faults along which plate material is subducted or consumed in the mantle, **oceanic spreading ridges** along which new crustal material is produced, and **transform faults** that accommodate horizontal slip (strike slip) between adjoining plates.

Pleistocene. The time period between about 10,000 years before present and about 1,650,000 years before present. As a descriptive term applied to rocks or faults, it marks the period of rock formation or the time of most recent fault slip, respectively. Faults of Pleistocene age may be considered active though their activity rates are commonly lower than younger faults.

Poisson distribution. A probability distribution that characterizes discrete events occurring independently of one another in time.

Probabilistic earthquake hazard. See **Earthquake hazard** and **Earthquake risk**.

Pseudorelative acceleration spectrum. See **Response spectrum**.

PSRV. Pseudorelative velocity response spectrum. See **Response spectrum**.

Q. See **Attenuation**.

Quaternary. The geologic time period comprising about the last 1.65 million years.

Radiometric. Pertaining to the measurement of geologic time by the analysis of certain radioisotopes in rocks and their known rates of decay.

Random vibration theory. A theoretical probabilistic formulation that links band-limited **Gaussian noise spectra**, representing the spectra of earthquake ground motions, with corresponding **time history peak values**.

Rayleigh wave. A seismic **surface wave** causing an elliptical motion of a particle at the free surface, with no transverse motion.

Ray-tracing method. A computational method of computing ground-shaking estimates that assumes that the ground motion is composed of multiple arrivals that leave the source and are reflected or refracted at velocity boundaries according to Snell's Law. The amplitudes of reflected and refracted waves at each boundary are recalculated according to the law of conservation of energy.

Recurrence interval. The average time span between events (such as large earthquakes, ground shaking exceeding a particular value, or liquefaction) at a particular site. Also termed **return period**.

Reflection. The energy or wave from a seismic source that has been returned (reflected) from an interface between materials of different elastic properties within the Earth.

Reflector. An interface between materials of different elastic properties that reflects seismic waves.

Refraction. (1) The deflection of the ray path of a seismic wave caused by its passage from one material to another having different elastic properties. (2) Bending of a **tsunami** wave front owing to variations in the water depth along a coastline.

Regression analysis. A statistical technique applied to data to determine, for predictive purposes, the degree of correlation of a dependent variable with one or more independent variables. See **Least-squares fit**.

Relaxation theory. Concept wherein radiated seismic waves of an earthquake result when stored strain within the Earth is released at the time of **slip** along a fault; adjacent fault blocks reach new states of equilibrium.

Rigidity. See **Shear modulus**.

Residual. The difference between the measured and predicted values of some quantity.

Resonance. An increase in the **amplitude** of vibration in an elastic body or system when the **frequency** of the shaking force is close to one or more of the **natural frequencies** of a shaking body.

Response. The motion in a system resulting from shaking under specified conditions.

Response spectrum. A curve showing the mathematically computed maximum response of a set of simple damped harmonic **oscillators** of different **natural frequency(ies)** to a particular record of earthquake ground **acceleration**. Response spectra, commonly plotted on tripartite logarithmic graph paper, show the **oscillator's** maximum **acceleration**, **velocity**, and **displacement** as a function of **oscillator** frequency for various levels of oscillator **damping**. A computational approximation to the response spectrum is referred to as the pseudorelative velocity response spectrum (**PSRV**). These curves are used by engineers to estimate the maximum response of simple structures to complex ground motions. For example, the 5-percent spectral acceleration at 1 second is the maximum acceleration of the top of a structure with 5-percent damping whose natural period of vibration is 1 second when subjected to a given input ground-acceleration record.

Return period. See **Recurrence interval**.

Risk. See **Earthquake risk**.

Rheological properties. The properties of rocks that describe their ability to deform and flow as a function of temperature, pressure, and chemical conditions.

Root mean square. Square root of the mean square value of a random variable.

Rupture front. The instantaneous boundary between the slipping and locked parts of a fault during an earthquake. Rupture in one direction on the fault is referred to as unilateral. Rupture may radiate outward in a circular manner or it may radiate toward the two ends of the fault from an interior point, behavior referred to as bilateral.

Rupture velocity. The speed at which a **rupture front** propagates during an earthquake.

***S* wave.** A seismic **body wave** that involves a shearing motion in a direction perpendicular to the direction of propagation. When it is resolved into two orthogonal components in the plane perpendicular to the direction of propagation, *SH* denotes the horizontal component and *SV* denotes the orthogonal component.

Sand boil. Sand and water ejected to the ground surface as a result of liquefaction at shallow depth; the conical sediment deposit that remains as evidence of liquefaction.

Sea-floor magnetic lineaments. See **Magnetic polarity reversals**.

Secular. Refering to long-term changes that take place slowly and imperceptably. Commonly used to describe changes in elevation, tilt, and stress or strain rates that are related to long-term **tectonic** deformation.

Segmentation. The braking of faults along their length by other faults that cross them or their limitation in length by other factors such as topography or bends in the **strikes** of the faults. Segmentation can limit the length of faulting in a single earthquake to some fraction of the total fault length, thus also limiting the size of the earthquake.

Seiche. Oscillation of the surface of an enclosed body of water owing to earthquake shaking.

Seismic hazard. See **Earthquake hazard** and **Earthquake risk**.

Seismic impedance. Seismic ***P*-wave** velocity multiplied by the **bulk density** of a medium.

Seismic wave. An elastic wave generated by an impulse such as an earthquake or an explosion. Seismic waves may propagate either along or near the Earth's surface (for example, **Rayleigh** and **Love waves**) or through the Earth's interior (***P* and *S* waves**).

Seismicity. The geographic and historical distribution of earthquakes.

Seismic gap. A section of a fault that has produced earthquakes in the past but is now quiet. For some seismic gaps, no earthquakes have been observed historically, but it is believed that the fault segment is capable of producing earthquakes on some other basis, such as plate-motion information or strain measurements. This latter case may apply to the Cascadia thrust fault.

Seismic moment. A measure of the size of an earthquake based on the area of fault rupture, the average amount of **slip**, and the **shear modulus** of the rocks offset by faulting. Seismic moment can also be calculated from the amplitude spectra of seismic waves.

Seismic reflection or refraction line. A set of seismographs commonly distributed along the Earth's surface to record seismic waves generated by an explosion for the purpose of recording reflections and refractions of these waves from velocity discontinuities within the Earth. The data collected can be used to infer the internal structure of the Earth.

Seismic risk. The probability of social or economic consequences of an earthquake. See **Probabilistic earthquake hazard**.

Seismic zonation. Geographic delineation of areas having different potentials for hazardous effects from future earthquakes. Seismic zonation can be done at any scale—national, regional, local, or site. See **Microzonation**.

Seismogenic. Capable of generating earthquakes.

Seismogram. A record written by a seismograph in response to ground motions produced by an earthquake, explosion, or other ground-motion sources.

Seismometer or seismograph. A seismometer is a damped oscillating mass, such as a damped mass-spring system, used to detect seismic-wave energy. The motion of the mass is commonly transformed into an electrical voltage. The electrical voltage is recorded on paper, magnetic tape, or another recording medium. This record is proportional to the motion of the seismometer mass relative to the Earth, but it can be mathematically converted to a record of the absolute motion of the ground. **Seismograph** is a term that refers to the seismometer and its recording device as a single unit.

Separation. The distance between any two parts of a reference plane (for example, a sedimentary bed or a geomorphic surface) offset by a fault, measured in any plane. Separation is the apparent amount of fault **displacement** and is nearly always less than the actual **slip**.

Shear modulus. The ratio of shear stress to shear strain of a material during simple shear.

Shear stress. The stress component parallel to a given surface, such as a fault plane, that results from forces applied parallel to the surface or from remote forces transmitted through the surrounding rock.

Shear wave. See ***S* wave**.

Slab. In this document, slab refers to the oceanic crustal plate that underthrusts the continental plate and is consumed by the Earth's **mantle**. See **Plate tectonics**.

Slab pull. The force of gravity causing the **slab** to sink into the **mantle**. The downdip component of this force leads to downdip extensional stress in the slab and may produce earthquakes within the subducted slab. Slab pull may also contribute to stress on the **subducton thrust fault** if the fault is locked.

Slip. The relative **displacement** of formerly adjacent points on opposite sides of a fault, measured on the fault surface.

Slip model. A kinematic model that describes the amount, distribution, and timing of slip associated with a real or postulated earthquake.

Slip rate. The average rate of **displacement** at a point along a fault as determined from geodetic measurements, from offset manmade structures, or from offset geologic features whose age can be estimated. It is measured parallel to the predominant **slip** direction or estimated from the vertical or horizontal **separation** of geologic markers.

Soil. (1) In engineering, all unconsolidated material above **bedrock**. (2) In soil science, naturally occurring layers of mineral and (or) organic constituents that differ from the underlying parent material in their physical, chemical, mineralogic, and morphologic character because of **pedogenic** processes.

Soil profile. The vertical arrangement of soil horizons down to the parent material or to bedrock. Commonly subdivided into A, B, and C horizons.

Source. (1) The geologic structure that generates a particular earthquake. (2) The explosion used to generate acoustic or seismic waves.

Source function. The ground motion generated at the fault during rupture, usually as predicted by a theoretical model and represented by a **time history** or **spectrum**. The terms Brune spectrum, Aki spectrum, and Haskel model refer to varying representations of the source function, each based on different assumptions, as devised by the scientist for which the model is named.

Spectral acceleration. Commonly refers to either the **Fourier amplitude spectrum** of ground acceleration or the **PSRV**.

Spectral amplification. A measure of the relative shaking **response** of different geologic materials. The ratio of the **Fourier amplitude spectrum** of a **seismogram** recorded on one material to that computed from a seismogram recorded on another material for the same earthquake or explosion.

Spectral ratio. See **Spectral amplification**.

Spectrum. In seismology, a curve showing **amplitude** and **phase** as a function of **frequency** or **period**.

Standard deviation. The square root of the average of the squares of deviations about the mean of a set of data. Standard deviation is a statistical measure of spread or variability.

Standard penetration resistance. A measure of relative density expressed by the number of blows (blow count) needed to push a probe a standard distance into sediment. The standard penetration test determines the number of blows required to drive a standard sampling spoon 1 ft into the sediment by repeatedly dropping a 140-pound weight from a height of 30 in.

Station. A ground position at which a geophysical instrument is located for an observation.

Stick slip. The rapid displacement that occurs between two sides of a fault when the shear stress on the fault exceeds the frictional stress. Stick-slip displacement on a fault radiates energy in the form of seismic waves, creating an earthquake.

Stochastic. Applied to processes that have random characteristics.

Strain. Small changes is length and volume associated with deformation of the Earth by **tectonic** stresses or by the passage of **seismic waves**.

Strain rate. Strain measurements are computed from observed changes in length on the Earth's surface, commonly along multiple paths. Because the changes in length are observed over varying time periods and path lengths, they are expressed as the change in length divided by the measurement distance divided by the measurement time period. This number, which is expressed as the change in length per unit length per unit time, is termed the strain rate. These measurements are used to infer the directions of principal strain and stress rates near the Earth's surface.

Stratigraphy. The study of the character, form, and sequence of layered rocks.

Stress. Force per unit area acting on a plane within a body. Six values are required to characterize completely the stress at a point: three normal components and three shear components.

Stress drop. The difference between the **stress** across a fault before and after an earthquake. A parameter in many models of the earthquake source that has a bearing on the level of high-frequency shaking that the fault radiates. Commonly stated in units termed bars or megapascals (1 bar equals 1 kg/cm^2, and 1 megapascal equals 10 bars).

Strike. Trend or bearing, relative to north, of the line defined by the intersection of a planar geologic surface (for example, a fault or a bed) and a horizontal surface.

Strike slip. See **Fault**.

Strong motion. Ground motion of sufficient **amplitude** and duration to be potentially damaging to a building's structural components or architectural features.

Subduction. A **plate tectonics** term for the process whereby the oceanic **lithosphere** collides with and descends beneath the continental **lithosphere**.

Subduction thrust fault. The fault that accommodates the differential motion between the downgoing oceanic crustal plate and the continental plate as **subduction** occurs. This fault is the contact between the top of the oceanic plate and the bottom of the newly formed continental **accretionary wedge**. Also alternately referred to as the plate-boundary thrust fault, the thrust interface fault, or the megathrust fault.

Surface faulting. Displacement that reaches the Earth's surface during **slip** along a fault. Commonly accompanies moderate and large earthquakes having **focal depths** less than 20 km. Surface faulting also may accompany aseismic **tectonic** creep or natural or man-induced subsidence.

Surface wave. Seismic wave that propagates along the Earth's surface. **Love** and **Rayleigh waves** are the most common.

Surface-wave magnitude. See **Magnitude**.

Tectonic. Refers to rock-deforming processes and resulting structures that occur over regional sections of the **lithosphere**.

Teleseismic. Pertaining to earthquakes at distances greater than 1,000 km from the measurement site.

Tilt. An observed rate of change in the slope of the Earth's surface.

Thrust interface fault. See **Benioff zone** and **subduction thrust fault**.

Time history. The sequence of values of any time-varying quantity (such as a ground-motion measurement) measured at a set of fixed times. Also termed time series.

Transform fault. A special variety of strike-slip fault that accommodates relative horizontal slip between other **tectonic** elements, such as oceanic crustal plates.

Traveltime curve. A graph of arrival times, commonly ***P* or *S* waves**, recorded at different points as a function of distance from the seismic **source**. Seismic velocities within the Earth can be computed from the slopes of the resulting curves.

Tsunami. An impulsively generated sea wave of local or distant origin that results from large-scale seafloor displacements associated with large earthquakes, major submarine slides, or exploding volcanic islands.

Tsunamigenic. Refering to those earthquake **sources**, commonly along major **subduction**-zone plate boundaries such as those bordering the Pacific Ocean, that can generate tsunamis.

Tsunami magnitude (M_t). A number used to compare sizes of tsunamis generated by different earthquakes and calculated from the logarithm of the maximum amplitude of the **tsunami** wave measured by a tide gauge distant from the **tsunami** source.

Turbidites. Sea-bottom deposits formed by massive slope failures where rivers have deposited large deltas. These slopes fail in response to earthquake shaking or excessive sedimentation load. The temporal correlation of turbidite occurrence for some deltas of the Pacific Northwest suggests that these deposits have been formed by earthquakes.

Unlocked fault. See **Locked fault** and **Creep**.

Velocity. In reference to earthquake shaking, velocity is the time rate of change of ground **displacement** of a reference point during the passage of earthquake seismic waves. Commonly expressed in centimeters per second.

Velocity structure. A generalized regional model of the Earth's **crust** that represents crustal structure using layers having different assumed seismic velocities.

Water table. The upper surface of a body of unconfined ground water at which the water pressure is equal to the atmospheric pressure.

Wavelength. The distance between successive points of equal **amplitude** and **phase** on a wave (for example, crest to crest or trough to trough).

YBP. An abbreviation for years before present.

FACTORS FOR CONVERTING METRIC UNITS TO INCH-POUND UNITS

Quantitative information in this professional paper is given in the International System of Units, or metric system. The following table converts the most common metric units to inch-pound units for the convenience of those who prefer or are more familiar with the U.S. Customary System of units. Also included are definitions of geochronologic dating terms used to denote elapsed time from the present to the past.

Multiply metric unit	By	To obtain inch-pound unit
Area		
square meter (m^2)	10.76	square foot (ft^2)
square kilometer (km^2)	0.3861	square mile (mi^2)
Density		
gram per cubic centimeter (g/cm^3)	62.43	pound per cubic foot (lb/ft^3)
Length		
millimeter (mm)	0.03937	inch (in)
centimeter (cm)	0.3937	inch (in)
meter (m)	3.281	foot (ft)
kilometer (km)	0.6214	mile (mi)
kilometer (km)	0.5400	mile, nautical (nmi)
Volume		
cubic centimeter (cm^3)	0.06102	cubic inch (in^3)
cubic meter (m^3)	35.31	cubic foot (ft^3)
cubic kilometer (km^3)	0.2399	cubic mile (mi^3)

Abbreviations: ka, thousand years ago; Ma, million years ago.

TECTONIC SETTING

Preceding page. *Insert,* masonry damage caused by the April 29, 1965, Seattle, Wash., earthquake. Photograph courtesy of NOAA/EDIS. *Background,* damage to unreinforced masonry wall and parapet in downtown Klamath Falls, Oreg., during the Sept. 20, 1993, *M* 5.9 and *M* 6.0 earthquakes (from Dewey, J.W., 1993, Damages from the 20 September earthquakes near Klamath Falls, Oregon: Earthquakes & Volcanoes, v. 24, no. 3, p. 121–128).

AN INTRODUCTION TO EARTHQUAKE SOURCES OF THE PACIFIC NORTHWEST

By Timothy J. Walsh[1]

INTRODUCTION

The identification of earthquake sources, average recurrence intervals, and likely magnitudes is essential for accurate earthquake risk assessment. These are most easily characterized by historical records, but the recorded history of the Pacific Northwest is short. The instrumental record of earthquakes in Washington and Oregon is fairly complete at about the magnitude 4 level only since 1960 (Ludwin and others, 1991). Prior to 1960, only a few large earthquakes had been instrumentally located in Washington and Oregon, and earthquake catalogues rely on felt reports. Felt reports are, unfortunately, sparse and difficult to interpret. Although the rate of seismicity in the Puget Sound area appears to be cyclical (Palmer, 1991), the data base is too small for statistically valid conclusions. In contrast, Hutton and Jones (1991) were able to document changes in rates of seismicity in southern California because they had a large-enough data base to draw statistical inferences. For instance, Townley and Allen (1939) reported 81 earthquakes in Oregon between 1841 and 1928 and 166 earthquakes in Washington between 1833 and 1928 but more than 3,000 earthquakes in California for the same period.

Not only are the earthquake catalogues for the Pacific Northwest short, but they still require significant editing of the preinstrumental entries. Rasmussen (1967) deleted a number of entries in the Townley and Allen (1939) catalogue but still reported more earthquakes (186) in Washington between 1841 and 1928. Ludwin and others (1991) suggested that the catalogue for magnitude 6 and larger earthquakes is probably complete at eight events in the Pacific Northwest, but Ludwin and Qamar (1991), who reviewed newspaper reports as part of a continuing effort to edit the pre-1928 catalogue, rediscovered yet another event of that approximate magnitude.

The sheer number of listings does not give a complete account of the true seismic flux in the region. For instance, California does have substantially more earthquakes than the Pacific Northwest, but because California earthquakes are more likely to be shallow, they are felt at lower magnitude levels, and the catalogue includes a large number of aftershocks as well. This accounts for at least some of the difference.

Another consequence of the shallower seismicity in California is that faults are more likely to rupture to the surface. It has frequently been possible to locate surface faulting after earthquakes in California, whereas this has yet to be accomplished in Washington or Oregon. Confidently relating earthquakes to a causative structure is necessary for site-specific seismic risk assessments. Without this kind of information, engineers in the Pacific Northwest commonly have to rely on "floating earthquakes" (shallow crustal earthquakes that are assumed to be possible anywhere within a geologic or physiographic province) for design specifications. This makes inference of recurrence intervals difficult, at least on a site-specific basis, because seismicity is tied to a region rather than a geologic structure. Therefore, land-use planners, who in Washington are required to zone for seismic risk, are unable to relate seismic risk to causative structures and usually zone only for liquefaction susceptibility.

Thus, the relative paucity of historical information means that earthquake-hazard assessment in the Pacific Northwest must rely more heavily on geologic mapping, geophysical and tectonic modeling, and paleoseismology than on past experience. This volume of the professional paper contains reports that describe earthquake sources in the Pacific Northwest in their tectonic context.

TECTONICS

Snavely and Wells (this volume) summarize the Cenozoic tectonic development of the continental margin of the Pacific Northwest. They show that, throughout Tertiary

[1]Division of Geology and Earth Resources, Washington State Department of Natural Resources, Olympia, WA 98504–7007.

time, oblique subduction produced episodic uplift of the coast ranges, folding and thrusting of accretionary-wedge sediments, and strike-slip faulting. Many of these features are also present in Quaternary sediments. They note several unconformities in Quaternary deposits on the continental shelf that they infer to have been caused by both episodic downwarping and diapiric uplift. Noting several Quaternary faults on the shelf, along the coast, and at the northern end of the Olympic Peninsula, they suggest that Holocene seismicity may have triggered large landslides that have been mapped in the Olympic Mountains.

Yeats and others (this volume) compile the geologic mapping, exploration and water-well-drilling data, and seismic-reflection profiles of Oregon's Willamette Valley and analyze its Cenozoic (particularly post-Miocene) tectonic history. They show that there are at least a dozen post-Miocene crustal faults in the valley, at least one of which (the Mount Angel fault) is active. Because offset in mid-Quaternary sediments is small and mappable length of all structures is short, the authors conclude that slip rates must be small and potential earthquake magnitudes are probably moderate.

Goldfinger and others (this volume) compile the available seismic-reflection data, along with SeaMARC and GLORIA sonar records, SeaBeam bathymetry, and observations from the submersible ALVIN, to map late Cenozoic structures on the central and northern Oregon continental margin. In a controversial interpretation, they map a series of left-lateral strike-slip faults on the abyssal plain and suggest that the faults continue onto the continental slope. These faults trend at high angles to most of the structures in and overlying the Juan de Fuca and Gorda plates (although they are parallel to the major transform faults that offset the Gorda Ridge). At least one of these faults, the Wecoma, shows significant late Quaternary offset and appears still to be active. The authors offer several hypotheses for the formation of these structures but, as yet, their significance is unclear.

Still, very little is known about the seismic capability of these or most other structures in the Pacific Northwest. The above authors, Rogers and others (this volume), and Madin (volume 2) show many suspected active faults, but only the Mount Angel fault (Yeats and others, this volume) has been confidently linked to historical earthquakes. Paleoseismic studies are beginning to link some faults to prehistoric earthquakes (for instance, Wilson and others, 1979; Campbell and Bentley, 1981; Bucknam and Barnhard, 1989), and studies of seismicity have delineated several fault zones (Weaver and Smith, 1983; Zollweg and Johnson, 1989; Yelin and Patton, 1991). However, much remains to be done to assess the risks of shallow crustal faulting.

GEOPHYSICS

Weaver and Shedlock (this volume) summarize the potential seismic source regions associated with oblique subduction in the Pacific Northwest. These regions are (1) the crust of the North America plate, which has produced large earthquakes in Washington in 1872 and in British Columbia in 1946; (2) the subducting slabs of the Juan de Fuca and Gorda plates, which produced large earthquakes in Washington in 1949 and 1965 (and, they suggest, the Port Orford area of Oregon in 1873); and (3) the interface between the two, which has been aseismic in historical time with the possible exception of the 1992 Cape Mendocino earthquake (Michael, 1992).

Ma and others (this volume) analyze a well-constrained data set recorded by the University of Washington seismic net and conclude that the North American crust is responding principally to north-south compression, implying that the contribution of plate convergence to the state of stress must be small in comparison. They also suggest that, although focal mechanisms from the St. Helens seismic zone (Weaver and Smith, 1983) imply a rotation of the regional stress field from north-south compression to compression directed toward N. 30° E., the data also permit an unrotated stress field that takes advantage of a preexisting zone of weakness.

PALEOSEISMICITY

Although no historical subduction-zone earthquakes have occurred in the region, and there is no recognized contemporary thrust seismicity on the subduction interface, recent geodetic studies (Savage and others, 1981, 1991) and comparison with other subduction zones (Heaton and Kanamori, 1984; Heaton and Hartzell, 1987; Rogers, 1988) suggested the possibility of large (M 8+) thrust earthquakes on the Cascadia subduction zone. Because the potential rupture surface is inaccessible, traditional paleoseismology tools such as trenching fault traces are unavailable. In 1985, during a National Earthquake Hazards Reduction Program workshop in Seattle, a meeting was held to plan strategies for testing the hypothesis of the Cascadia subduction-zone megathrust earthquake (Schwartz, 1986). As a result of that meeting, B.F. Atwater of the U.S. Geological Survey sought to test the hypothesis of Ando and Balazs (1979) that aseismic subduction should result in coastal uplift. Instead, he found evidence of sudden submergence, dated at more than 250 years ago, along the southern Washington coast (Atwater, 1987). Because it had been observed that great subduction-zone earthquakes cause both sudden uplift and subsidence (Plafker, 1969; Plafker

and Savage, 1970), this evidence of submergence suggested that great subduction-zone earthquakes may have occurred on the Cascadia subduction zone beyond the historical record of the Pacific Northwest.

Atwater (this volume) presents a pictorial view of the evidence for inferred coseismic subsidence followed by deposition of a sand sheet by a tsunami. At least six peaty soils interpreted to be coseismically subsided lowlands are present in coastal southern Washington.

Peterson and Darienzo (this volume), as in a previous work (Darienzo and Peterson, 1990), also report evidence of sudden submergence in Alsea Bay on the central Oregon coast. They investigate other models for rapid submergence, such as riverine floods, storm waves, and changes in tide range. They conclude that, because the soils are laterally persistent, vertically similar in grain size and organic-carbon content, and commonly overlain by sands inferred to be tsunami deposits, they are most likely due to coseismic subsidence.

However, Nelson and Personius (this volume) examine the record of marsh stratigraphy both in the Pacific Northwest and on nontectonic coasts and conclude that sudden oscillations in sea level accompanied by changes in local sediment influx and irregular compaction can produce a similar stratigraphic record. They argue that only where there is evidence of substantial changes in water depth can coseismic subsidence be confidently inferred.

Adams (this volume) provides permissive evidence for two more missing pieces of the subduction-zone-earthquake puzzle. Examining the record of turbidites in the Cascadia Channel, documented by Griggs (1969) and Griggs and Kulm (1970), he shows that if these turbidites were triggered by earthquakes, as originally inferred by Griggs, they imply some degree of synchroneity over significant distances. Adams (this volume) reports that there are more turbidites per tributary to the Cascadia Channel than there are in the main channel. This implies that turbidity currents from the tributary channels coalesced in the main channel, depositing one turbidite instead of the multiple overlapping ones that would be expected if the turbidity currents arrived at different times.

Although the papers in this volume individually present evidence that in general is merely permissive, collectively they argue persuasively that the Pacific Northwest is at risk from a type of earthquake not seen in historical time. Although much work remains to characterize such an event, it would be prudent to incorporate a subduction-zone earthquake in disaster planning and engineering practice in the Pacific Northwest.

REFERENCES CITED

Ando, Masataka, and Balazs, E.I., 1979, Geodetic evidence for aseismic subduction of the Juan de Fuca plate: Journal of Geophysical Research, v. 84, no. B6, p. 3023–3028.

Atwater, B.F., 1987, Evidence for great Holocene earthquakes along the outer coast of Washington State: Science, v. 236, no. 4804, p. 942–944.

Bucknam, R.C., and Barnhard, T.P., 1989, Evidence of sudden late Holocene uplift in the central Puget Lowland, Washington: EOS [American Geophysical Union Transactions], v. 70, no. 43, p. 1332.

Campbell, N.P, and Bentley, R.D., 1981, Late Quaternary deformation of the Toppenish Ridge uplift in south-central Washington: Geology, v. 9, no. 11, p. 519–524.

Darienzo, M.E., and Peterson, C.D., 1990, Episodic tectonic subsidence of late Holocene salt marshes, northern Oregon central Cascadia margin: Tectonics, v. 9, no. 1, p. 1–22.

Griggs, G.B., 1969, Cascadia Channel—The anatomy of a deep-sea channel: Corvallis, Oregon State University, Ph.D. dissertation, 183 p.

Griggs, G.B., and Kulm, L.D., 1970, Sedimentation in Cascadia deep-sea channel: Geological Society of America Bulletin, v. 81, no. 5, p. 1361–1384.

Heaton, T.H., and Hartzell, S.H., 1987, Earthquake hazards on the Cascadia subduction zone: Science, v. 236, no. 4798, p. 162–168.

Heaton, T.H., and Kanamori, Hiroo, 1984, Seismic potential associated with subduction in the northwestern United States: Seismological Society of America Bulletin, v. 74, no. 3, p. 933–941.

Hutton, L.K., and Jones, L.M., 1991, Changes in the rate of seismicity in southern California between 1932 and 1989 [abs.]: Seismological Research Letters, v. 62, no. 1, p. 47.

Ludwin, R.S., and Qamar, A.I., 1991, 1882 earthquake rediscovered: Washington Geology, v. 19, no. 2, p. 12–13.

Ludwin, R.S., Weaver, C.S., and Crosson, R.S., 1991, Seismicity of Washington and Oregon, *in* Slemmons, D.B., Engdahl, E.R., Zoback, M.D., and Blackwell, D.D., eds., Neotectonics of North America: Boulder, Colo., Geological Society of America, Decade Map Volume 1, p. 77–97.

Michael, Andrew, 1992, Three's a crowd in California: Nature, v. 357, no. 6374, p. 111–112.

Palmer, S.P., 1991, Modified Mercalli intensity VI and greater earthquakes in Washington State, 1928–1990: Washington Geology, v. 19, no. 2, p. 3–7.

Plafker, George, 1969, Tectonics of the March 27, 1964, Alaska earthquake: U.S. Geological Survey Professional Paper 543–I, 74 p.

Plafker, George, and Savage, J.C., 1970, Mechanism of the Chilean earthquakes of May 21 and 22, 1960: Geological Society of America Bulletin, v. 81, no. 4, p. 1001–1031.

Rasmussen, Norman, 1967, Washington State earthquakes 1840 through 1965: Seismological Society of America Bulletin, v. 57, no. 3, p. 463–476.

Rogers, G.C., 1988, An assessment of the megathrust earthquake potential of the Cascadia subduction zone: Canadian Journal of Earth Sciences, v. 25, no. 6, p. 844–852.

Savage, J.C., Lisowski, Michael, and Prescott, W.H., 1981, Geodetic strain measurements in Washington: Journal of Geophysical Research, v. 86, no. B6, p. 4929–4940.

———1991, Strain accumulation in western Washington: Journal of Geophysical Research, v. 96, no. B9, p. 14493–14507.

Schwartz, D.P., 1986, Subduction zone earthquakes in the Pacific Northwest—Evaluating the potential—Thoughts for discussion at the Seattle workshop, *in* Hays, W.W., and Gori, P.L., eds., Proceedings of Conference XXXIII, Workshop on earthquake hazards in the Puget Sound, Washington area: U.S. Geological Survey Open-File Report 86–253, p. 58–68.

Townley, S.D., and Allen, M.W., 1939, Descriptive catalog of earthquakes of the Pacific coast of the United States, 1769 to 1928: Seismological Society of America Bulletin, v. 29, no. 1, p. 1–297.

Weaver, C.S., and Smith, S.W., 1983, Regional tectonic and earthquake hazards implications of a crustal fault zone in southwestern Washington: Journal of Geophysical Research, v. 88, no. B12, p. 10371–10383.

Wilson, J.R., Bartholomew, M.J., and Carson, R.J., 1979, Late Quaternary faults and their relationship to tectonism in the Olympic Peninsula, Washington: Geology, v. 7, no. 5, p. 235–239.

Yelin, T.S., and Patton, H.J., 1991, Seismotectonics of the Portland, Oregon, region: Seismological Society of America Bulletin, v. 81, no. 1, p. 109–130.

Zollweg, J.E., and Johnson, P.A., 1989, The Darrington seismic zone in northwestern Washington: Seismological Society of America Bulletin, v. 79, no. 6, p. 1833–1845.

Paleoseismicity

Preceding page. *Insert,* damage from the 1949 Puget Sound earthquake. Photograph by William P. Conser, by permission of the Olympia Heritage Commission. *Background,* damage to unreinforced masonry wall and parapet in downtown Klamath Falls, Oreg., during the Sept. 20, 1993, *M* 5.9 and *M* 6.0 earthquakes (from Dewey, J.W., 1993, Damages from the 20 September earthquakes near Klamath Falls, Oregon: Earthquakes & Volcanoes, v. 24, no. 3, p. 121–128).

COASTAL EVIDENCE FOR GREAT EARTHQUAKES IN WESTERN WASHINGTON

By Brian F. Atwater[1]

ABSTRACT

Buried marsh and forest soils in southern coastal Washington show that earthquakes of magnitude 8 or larger (great earthquakes) probably occur at the Cascadia subduction zone. Similar soils in Alaska and Chile record lowering of coastal land that accompanied great subduction-zone earthquakes in those regions. Fossil plants show that many of the soils in Washington stood above most or all high tides until the onset of burial, when the soils were frequently submerged by tidal water at least ½ m deep. In some cases, fossil plants further show that this submergence resulted from abrupt lowering of the land, not from gradual rise of the sea. Some of the buried soils are mantled with sand that was probably deposited by tsunamis. Sequences of buried soils give evidence that hundreds of years commonly elapse between great earthquakes in southern coastal Washington.

INTRODUCTION

Coastal geology has provided strong evidence for the past occurrence of great earthquakes at the Cascadia subduction zone (Rogers and others, this volume). Such geologic evidence has been found at many estuaries along the Pacific coast from southern British Columbia to northern California (Atwater and others, 1995). Some of the evidence from coastal Oregon is described in Nelson and Personius (this volume) and Peterson and Darienzo (this volume).

In this chapter, I present mostly pictorial evidence from southern coastal Washington, and I compare this evidence with a few of the geologic effects of great historical earthquakes in Alaska and Chile. The Alaskan and Chilean examples show that a great subduction-zone earthquake can leave geologic records of abrupt land-level change and an ensuing tsunami. I infer that such geologic records are present in southern coastal Washington and that the earthquakes responsible for them occurred hundreds of years apart.

The chapter does not present evidence that seismic shaking accompanied the inferred earthquakes. Strong evidence of this kind was first recognized in 1992, two years after the chapter was mostly completed. The evidence shows that liquefaction accompanied the most recent of the abrupt land-level changes in southern coastal Washington. Details about this evidence have been reported by Obermeier (1994), who discovered it, and Atwater (1994).

ACKNOWLEDGMENTS

I thank Mary Ann Reinhart for contributing figure 22*B*. I am also grateful to Alan R. Nelson, H. Edward Clifton, David K. Yamaguchi, Barbara C. Hillier, John Synnefakis, and Timothy J. Walsh for improving the manuscript through reviews and discussions.

[1]U.S. Geological Survey, Department of Geological Sciences, University of Washington AJ–20, Seattle, WA 98195.

GREAT EARTHQUAKES AT SUBDUCTION ZONES CAN CAUSE SUDDEN COASTAL SUBMERGENCE . . .

Regional lowering of the land commonly accompanies great earthquakes at subduction zones. This subsidence can be viewed as part of a cycle of deformation in the continental plate (fig. 9). Before an earthquake, the continental plate bulges over and behind a stuck patch on the plate boundary. During the earthquake, the bulge collapses and the leading edge of the continental plate stretches and thins from lurching seaward while most of the remainder of the plate stands still. Such elastic thinning can produce a belt of subsidence, as illustrated by great subduction-zone earthquakes in Alaska and Chile (fig. 10).

The subsidence in Alaska and Chile dropped well-vegetated lowlands into the intertidal zone. This submergence led to the widespread deposition of tideflat mud on such lowlands as an Alaskan spruce forest (fig. 11*A*) and a Chilean pasture (fig. 11*B*). The change from well-vegetated lowland to tideflat began immediately after each earthquake. First-year casualties in Alaska included Sitka spruce (Plafker, 1969, figs. 12, 19, 22). Tidal-marsh plants later colonized the post-earthquake tideflats (fig. 11).

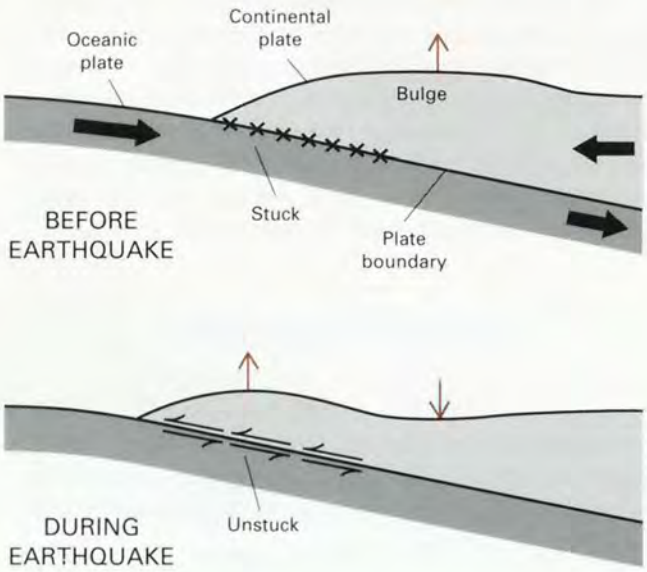

Figure 9. Deformation of a continental plate before and during a subduction-zone earthquake. Black arrows show directions of stress within the plates; colored arrows show exaggerated vertical displacement of the land surface; barbs indicate direction of plate movement. From models of Plafker (1972, p. 913) and Thatcher and Rundle (1984).

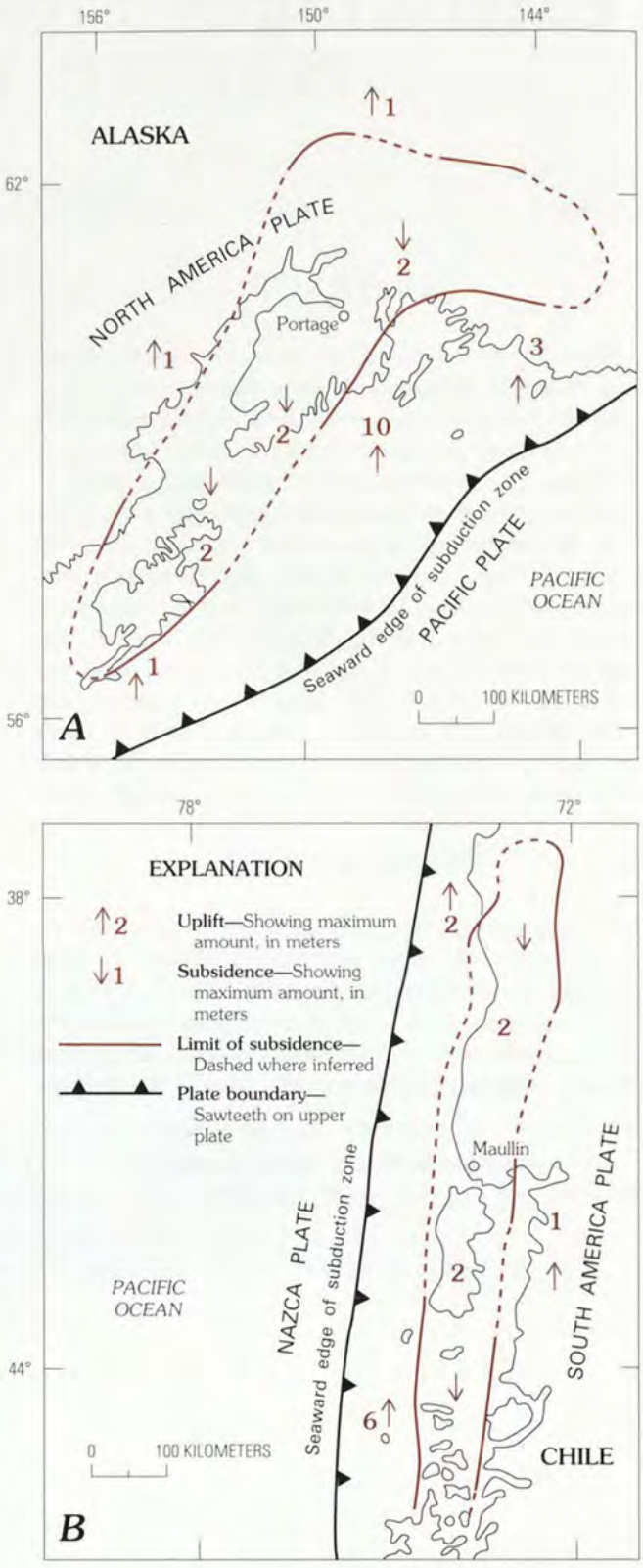

Figure 10 (facing column). Land-level change accompanying two great subduction-zone earthquakes. *A*, Alaska, 1964, magnitude 9.2 (Plafker, 1969). *B*, Chile, 1960, magnitude 9.5 (Plafker and Savage, 1970). Magnitudes are from Kanamori (1977).

. . . AND THE CONSEQUENT BURIAL OF COASTAL LOWLANDS

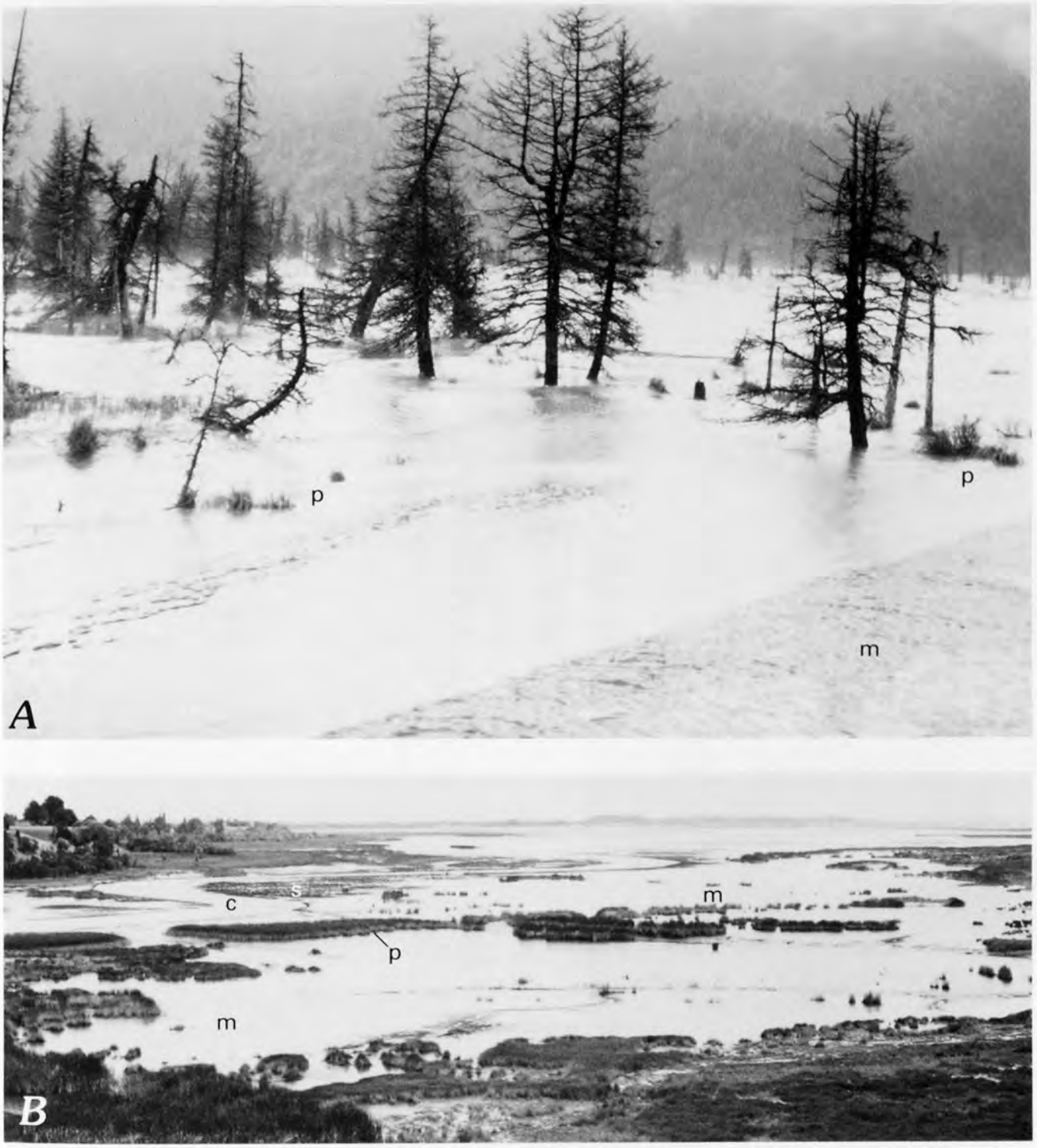

Figure 11. Geologic records of coastal land subsidence from great earthquakes in Alaska and Chile. Tidal-marsh plants (**p**) locally colonize mud (**m**) of post-earthquake tideflats. *A*, dead Sitka spruce forest near Portage, Alaska (fig. 10*A*). Mud 1–2 m thick accumulated on the forest floor between 1964, when the forest became tideflat, and 1973, when the picture was taken (Ovenshine and others, 1976). Photograph by A.T. Ovenshine. *B*, former pasture near Maullín, Chile (fig. 10*B*), mostly covered by mud since subsiding in 1960. Still-exposed soil (**s**) of pre-earthquake pasture undergoes erosion along meandering tidal channel (**c**). Photograph taken at low tide in 1988.

BURIED LOWLANDS ARE COMMON AND CONSPICUOUS IN SOUTHERN COASTAL WASHINGTON

Buried lowlands border all four estuaries of southern coastal Washington—the lower Copalis River, Grays Harbor, Willapa Bay, and the lower Columbia River (fig. 12).

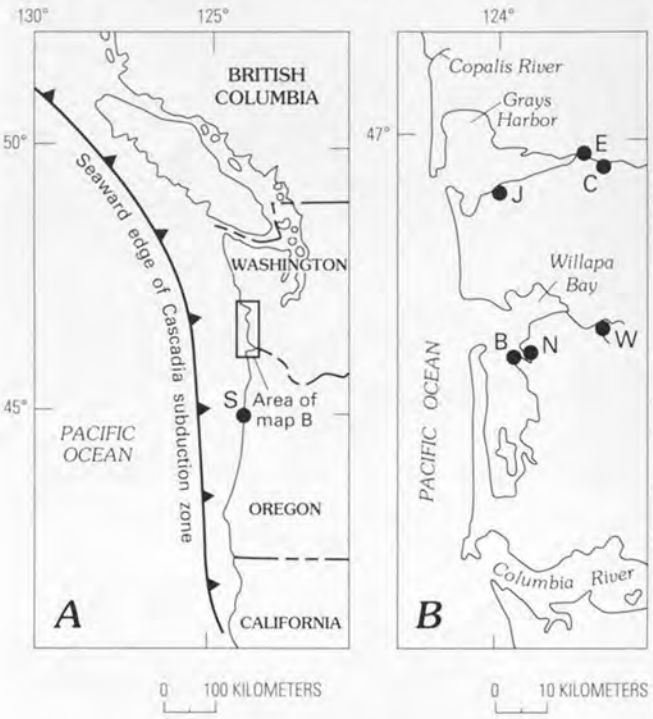

The large dots in figure 12*B* locate examples shown in this chapter.

Many of the buried lowlands retain recognizable lowland features. The soil of the former marsh in figure 13 has lateral extent comparable to that of the modern marsh. Rooted in the buried-marsh soil are fossil stems and leaves of the grass *Deschampsia caespitosa*, which is also the dominant plant of the modern marsh (see detailed photographs in fig. 19).

The most conspicuous buried lowlands are marked by standing dead trunks of western redcedar (fig. 14). Such snags impressed a naturalist on a nineteenth-century railroad survey: "On some of the tide-meadows about Shoalwater [Willapa] bay dead trees of this species only are standing, sometimes in groves * * *" (Cooper, 1860, p. 26). The redcedar snags, mostly rooted below present high tide, are scattered along nearly 100 km of coast from the Copalis River to the Columbia River. The trees died about A.D. 1700 (Yamaguchi and others, 1989; Atwater and others, 1991).

Figure 12 (facing column). The Cascadia subduction zone and southern coastal Washington. *A*, Cascadia subduction zone. Sawteeth are on overriding North America plate. **S** is the Salmon River estuary. *B*, southern coastal Washington. **B** is Bay Center; **C**, Chehalis River and Blue Slough; **E**, Elliott Slough; **J**, Johns River; **N**, Niawiakum River; and **W**, Willapa River.

Figure 13. Soil of a former marsh (**m**), buried and later exhumed along the Johns River, Grays Harbor (fig. 12*B*). Especially resistant to erosion, the soil supports the bench on which the people (**p**) are standing. The water is at low tide; the highest modern tides inundate the live marsh behind the people. Locality 13 of Atwater (1992).

Figure 14. Dead forest of western redcedar (*Thuja plicata*) protruding through a brackish-water tidal marsh along the Copalis River (Atwater, 1992, figs. 2, 5). The floor of the dead forest lies buried below the marsh surface. The live forest in the background occupies the upland above the highest tides.

BURIAL OF LOWLANDS IN COASTAL WASHINGTON RESULTED FROM SUBMERGENCE

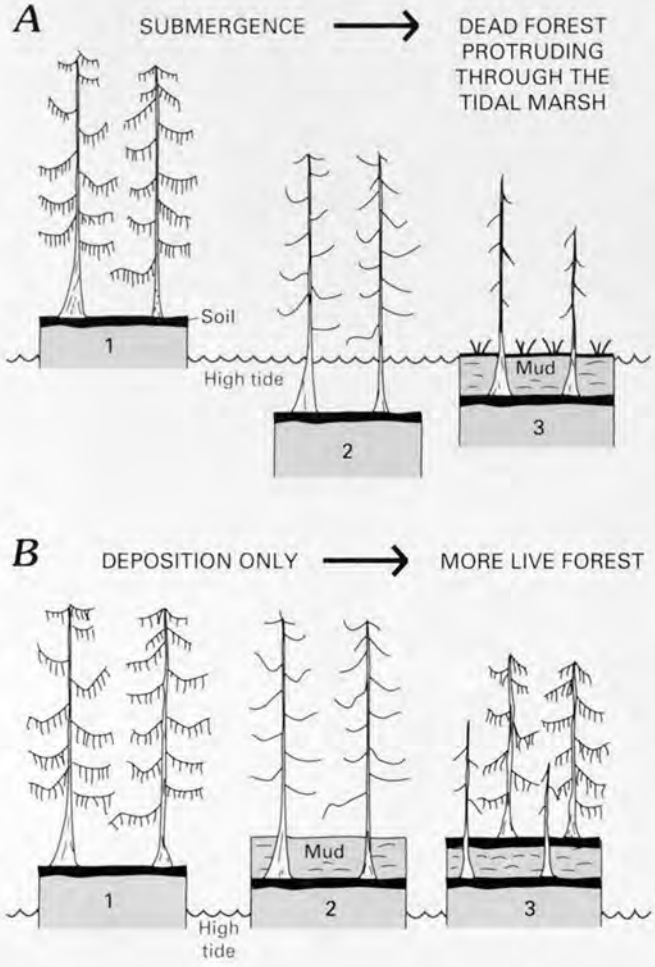

Tidal submergence (fig. 15*A*) led to the demise of the redcedar forest shown in figure 14. Deposition alone—by storm, flood, or tsunami—would not have promoted such submergence (fig. 15*B*).

Buried spruce forests in coastal Washington give further evidence for submergence. Mud just above the soils of these forests commonly contains the below-ground stems (rhizomes) of *Triglochin maritima* or *Carex lyngbyei*, grass-like plants that in coastal Washington are rooted mainly ½ to 1½ m lower in elevation than the lowest Sitka spruce (figs. 16, 17). The spruce stumps and *T. maritima* rhizomes shown in figure 17 thus suggest that the land was lowered about ½ to 1½ m relative to the sea. In comparison, the maximum regional subsidence from great subduction-zone earthquakes in Alaska and Chile caused about 2 m of submergence (fig. 10).

Figure 15 (facing column). Burial of the floor of a coastal lowland forest. *A*, deposition triggered by tidal submergence. The result is a dead forest that protrudes through a tidal marsh, as in figures 11*A* and 14. *B*, deposition by storm, flood, or tsunami without lasting tidal submergence. The forest floor builds farther above high tides, contrary to the result shown in figures 11*A* and 14.

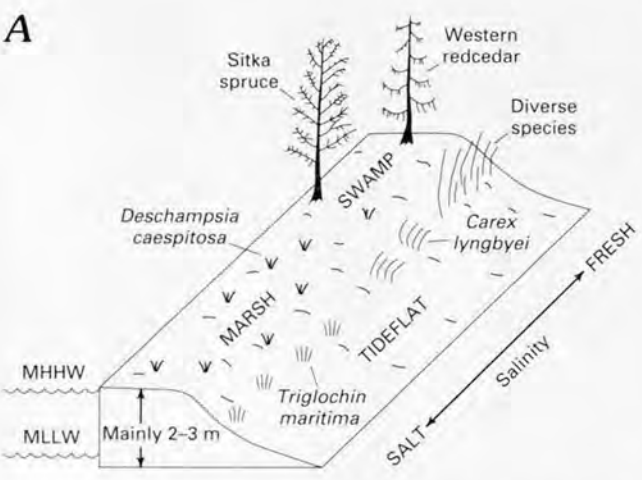

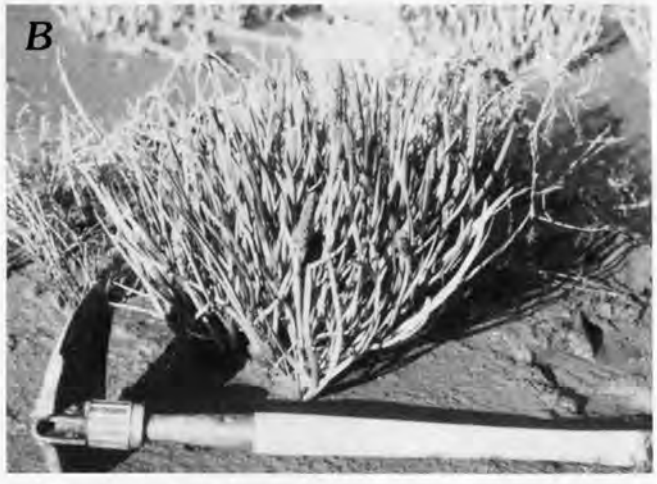

Figure 16. Dominant plants of coastal marshes and swamps in southern Washington. *A*, distribution of plants relative to tides and salinity. MHHW is mean higher high water; MLLW is mean lower low water. From descriptions by Franklin and Dyrness (1973, p. 294–295), Kunze and Cornelius (1982), and Weinmann and others (1984). *B*, *Triglochin maritima* on a muddy tideflat, Willapa Bay. The shovel handle is 0.5 m long.

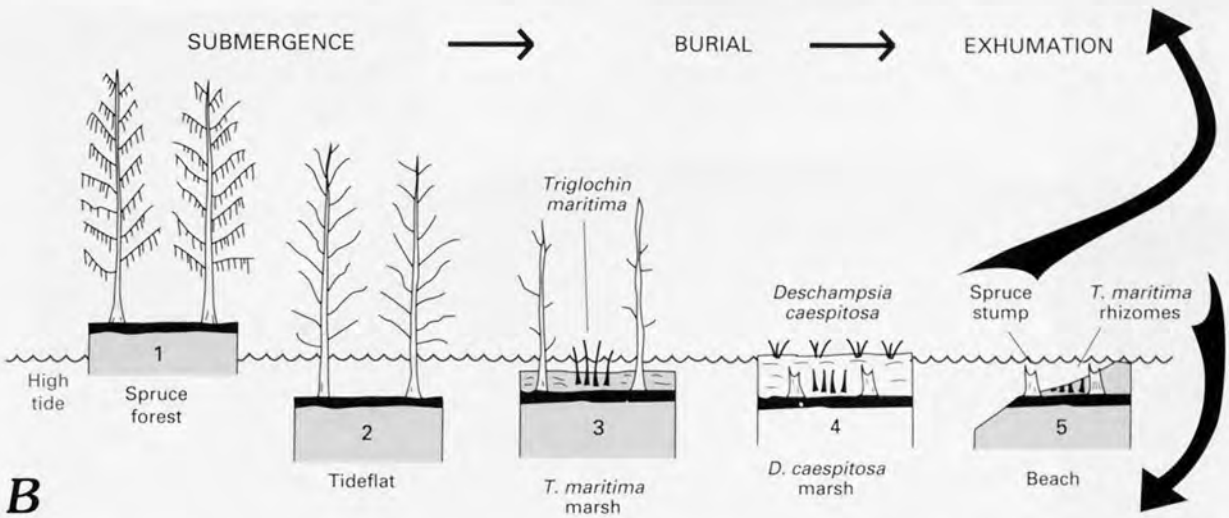

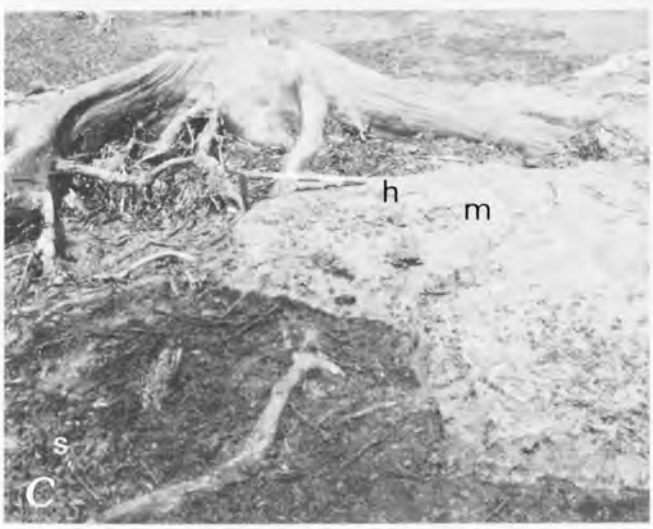

Figure 17. Formerly buried spruce stumps exhumed on a beach at Bay Center, Willapa Bay (fig. 12*B*). The shovel handle (**h**) in *A* and *C* is 0.5 m long. Locality 16 of Atwater (1992). *A*, overview, showing spruce stumps (**a**–**d**) at low tide on the beach. Leaves of eelgrass (**e**, *Zostera marina*), a salt-water aquatic plant, mantle much of the beach and mark the level of highest summertime tides (**t**). *B*, inferred sequence of events leading to burial and exhumation. *C*, detail of stump (**a**) showing peaty soil (**s**) in which the stump is rooted and lowermost 0.3 m of the tideflat mud (**m**) that accumulated on this soil. *D*, vertical view of *Triglochin maritima* rhizomes in mud at lower right in *C*. Individual rhizomes, which include attached leaf bases, are mostly perpendicular to 15-cm scale.

SUBMERGENCE OF BURIED LOWLANDS IN COASTAL WASHINGTON HAPPENED ABRUPTLY

Fossil plants and abrupt tops of buried lowland soils in southern coastal Washington show that submergence of the lowlands happened so quickly that it is better explained by abrupt lowering of the land than by gradual rise of the sea.

Some of the spruce stumps rooted in the youngest buried lowland soil show little or no thinning of outer annual growth rings (fig. 18). This lack of thinning suggests spruce death as sudden as that from earthquake-induced submergence in Alaska (fig. 11*A*). Thinning of outer rings would be expected of trees that suffered slow death from gradual submergence.

Herbaceous plants rooted in some buried lowland soils retain stems and leaves that are entombed in overlying tideflat mud. The most conspicuous of these fossils belong to *Deschampsia caespitosa*, the chief grass in high parts of salt- and brackish-water lowlands in coastal Washington (figs. 16*A*, 19*A–C*). Sudden submergence followed by rapid burial best explains the preservation of the fossil grass (fig. 19*D–F*).

The boundary between buried lowland soil and overlying tideflat mud is typically sharp—evidence that the change from lowland to tideflat happened abruptly (figs. 17*C*, 22*A*, 22*C*, 23*B*). Erosion cannot have caused this abruptness while sparing fossil grass that stands rooted in buried soils (fig. 19).

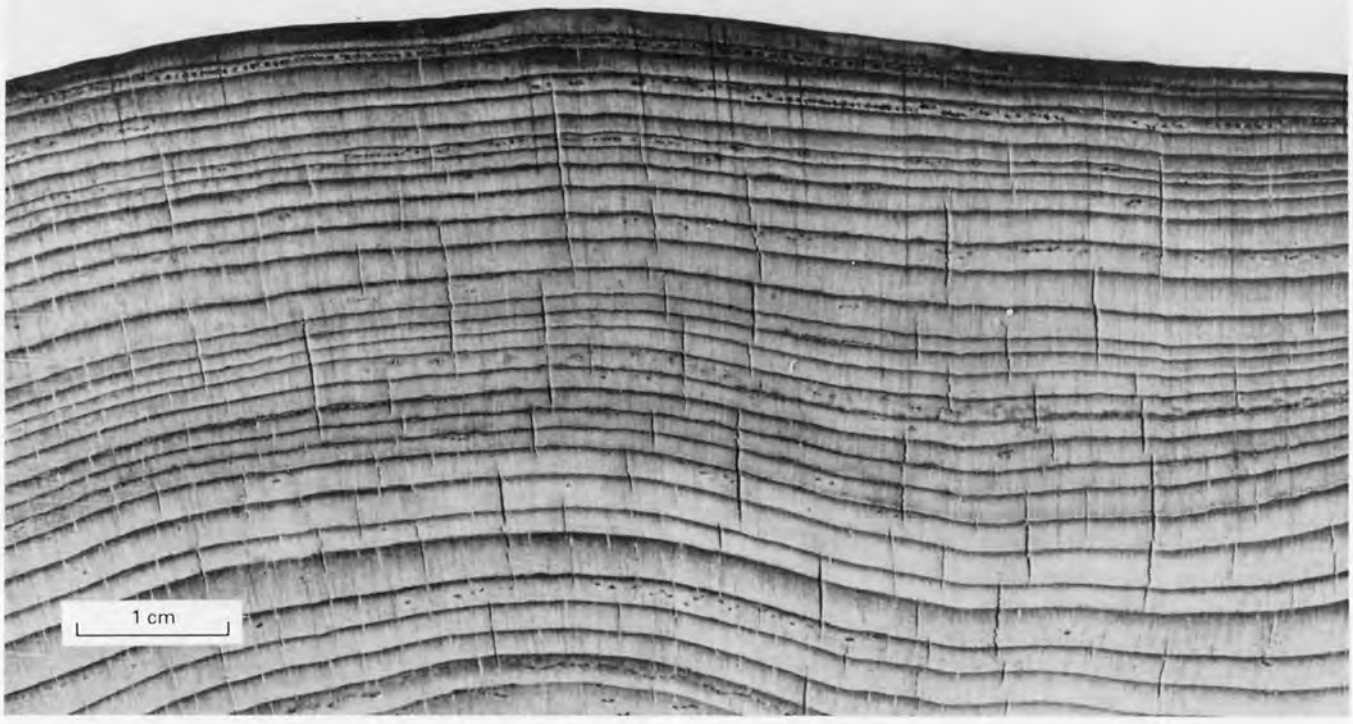

Figure 18. Outermost rings of a Sitka spruce stump rooted in the youngest buried lowland soil at Willapa Bay (fig. 17*A*, stump **b**). The outermost ring is stained from decay of the bark, which fell off during sampling.

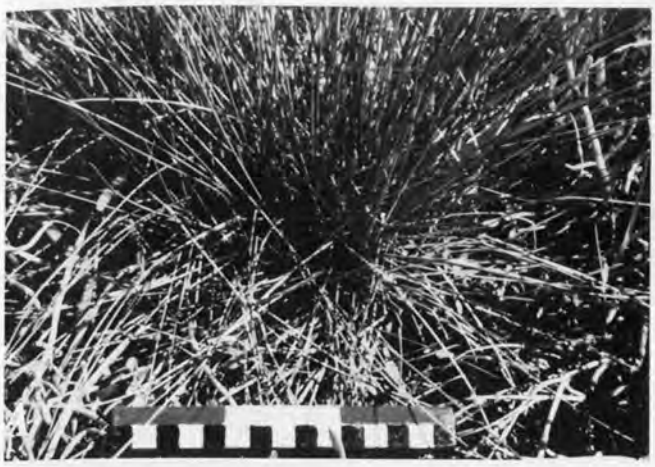

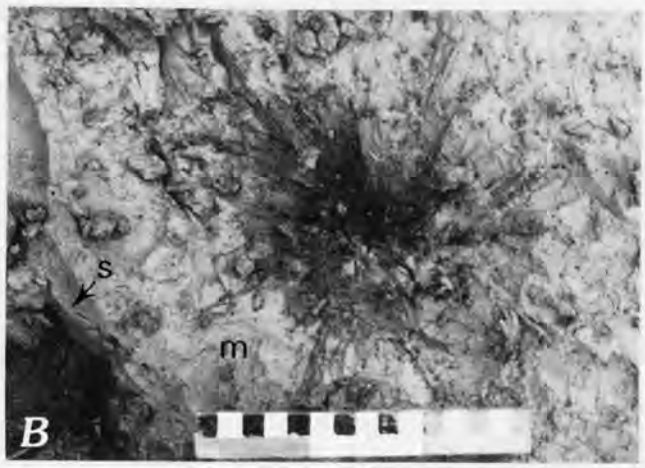

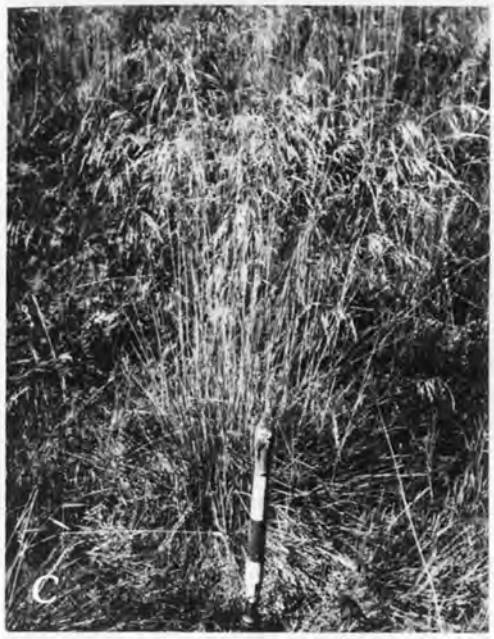

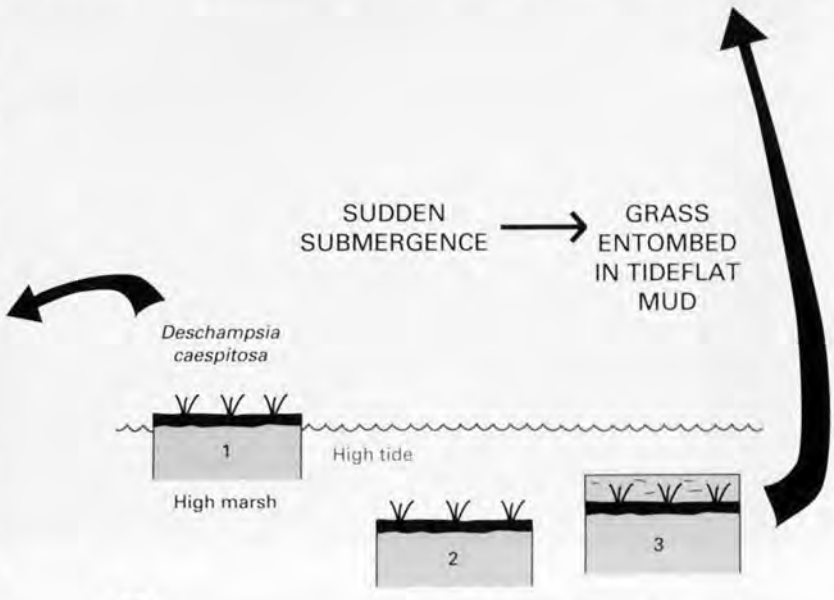

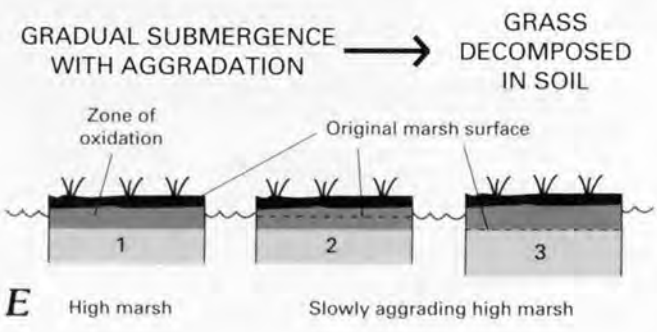

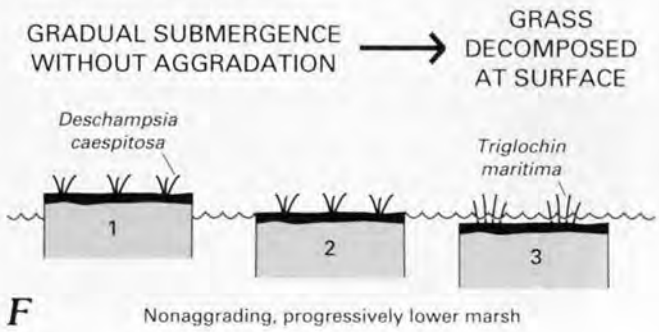

Figure 19. Modern and fossil leaves and stems of the tufted grass *Deschampsia caespitosa* at the Niawiakum River, Willapa Bay (Atwater and Yamaguchi, 1991, fig. 4). *A*, oblique closeup of tufted stems and leaves growing low on a modern plant. The scale is 15 cm long. *B*, vertical view of stems and leaves of a fossil grass tuft surrounded by tideflat mud (**m**). The scale is 15 cm long. The dark soil (**s**) in which the tuft is rooted lies 2–4 cm below most of the surface in view. The probable time of burial was between 1,400 and 1,900 years ago (soil **S**, figs. 24, 25). *C*, a modern plant. Stripes on the scale are 10 cm long. *D*, likely sequence of events that produced the fossil tuft in *B*. *E* and *F*, events unlikely to have produced the tuft shown in *B*.

TSUNAMIS FROM GREAT SUBDUCTION ZONE EARTHQUAKES CAN LEAVE SAND ON COASTAL LOWLANDS . . .

Because a great subduction-zone earthquake usually produces a tsunami (Abe, 1977), coastal lowlands in the region of the earthquake may receive sediment from the train of tsunami waves that comes ashore soon after the earthquake. Such onland deposition followed the 1960 Chile earthquake (Wright and Mella, 1963, p. 1389; Bourgeois and Reinhart, 1989). Near Maullín, Chile (fig. 10*B*), the tsunami-laid sand widely blankets the 1960 soil (fig. 20). The sand, mostly less than 10 cm thick, commonly contains the rooted stems and leaves of herbaceous plants around which the sand accumulated. Locally, the sand contains silty layers that may represent lulls between waves (fig. 20*C*).

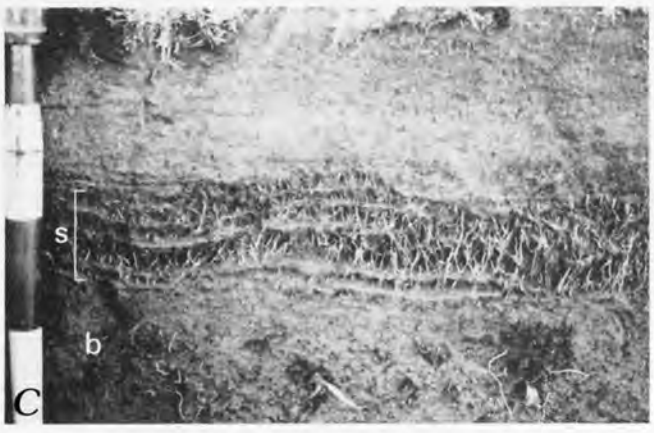

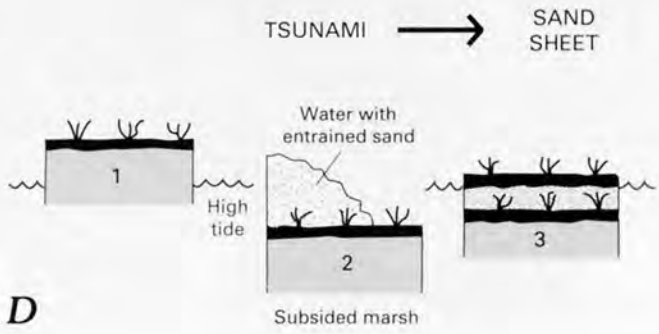

Figure 20. Sand deposited on lowlands near Maullín, Chile (fig. 10 *B*), by the tsunami from the 1960 Chile earthquake. Photographs taken in 1989. Stripes on handle in *B* and *C* are 10 cm long. *A*, two sand beds (lower right) on property of Juan Vera (left), who reported finding tsunami-laid sand in this area in 1960. The upper layer accumulated in 1960, the lower layer during an earlier tsunami. Río Ballenar locality of Atwater and others (1992). *B*, 1960 sand bed (**s**) etched by high tides along an eroding, otherwise peaty bank 1 km west-southwest of locality shown in *A*. *C*, lamination in the 1960 sand bed (**s**) near locality shown in *B*. Resistant laminae are silty, the sand having been etched by tides. Stringy, largely vertical features are roots. Buried 1960 soil (**b**) is not as dark as in *A* because tides have coated it with mud and algae. *D*, sequence of events that produced sandy tsunami deposits on Chilean lowlands in 1960.

. . . AND PROBABLY DID SO IN WASHINGTON AND OREGON

Some of the buried coastal soils in southern Washington and northern Oregon are mantled with sandy deposits that were probably left by tsunamis. Such deposits widely overlie the youngest buried soil (figs. 21, 22). The sand records an unusual event; relative to other sand above the soil, it is exceptionally coarse or thick or both. During the event, the sand moved landward, the direction in which the sand thins and disappears (fig. 22*B*) (Atwater, 1992, fig. 2). Deposition of the sand was interrupted by lulls during which mud settled (fig. 22*A*, *C*). Deposition approximately coincided with sudden subsidence of the land because the sandy interval surrounds rooted tufts of grass that lived on the lowlands at the time of subsidence (fig. 22*C*). Extraordinary, landward directed, interrupted by lulls, and approximately coincident with coastal subsidence in Washington, the event was probably a tsunami from a great subduction-zone earthquake rather than a flood or storm, or a tsunami of some other origin.

Figure 21. Sand bed (s) etched by high tides along the lower Salmon River, northern Oregon (fig. 12*A*) (Grant and McLaren, 1987). Probably analogous with the Chilean sand bed shown in figure 20*B*.

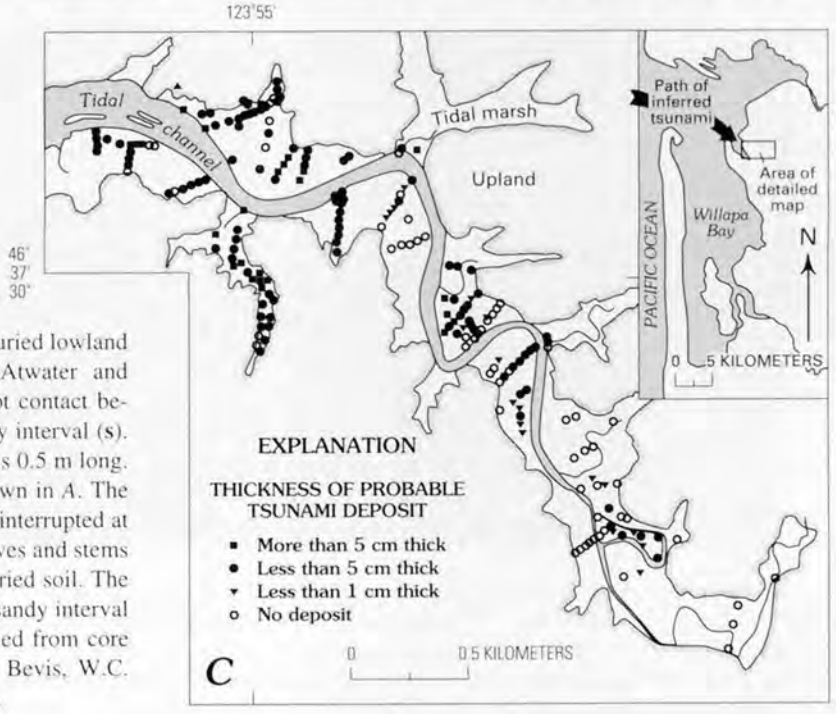

Figure 22. Sandy interval overlying the youngest buried lowland soil along the Niawiakum River, Willapa Bay (Atwater and Yamaguchi, 1991, fig. 5). *A*, outcrop showing abrupt contact between buried lowland soil (dark) and laminated sandy interval (s). Blade of shovel rests on modern tidal marsh; handle is 0.5 m long. *B*, detail of the left part of the sandy interval (s) shown in *A*. The lamina of sand and mud (compare with fig. 20*C*) are interrupted at center left, where they accumulated around tufted leaves and stems of *Deschampsia caespitosa* (fig. 19) rooted in the buried soil. The scale is centimeters. *C*, distribution and thickness of sandy interval shown in *A* (Reinhart and Bourgeois, 1987). Compiled from core logs and outcrop sketches by M.A. Reinhart, K.A. Bevis, W.C. Grant, B.F. Atwater, R.T. Versical, and S. McMullen.

CENTURIES COMMONLY ELAPSE BETWEEN GREAT EARTHQUAKES IN COASTAL WASHINGTON

Sequences of buried lowland soils give clues about how much time may elapse between successive great earthquakes in coastal Washington. The sequences shown in figures 23–25 suggest that the elapsed times commonly span hundreds of years. Earthquakes that incubated longest may be widely marked by peaty forest soils (**Y** and **S** in the figures) beneath which the buried soils (**U** and **N**, respectively) contain little organic matter. Prolonged uplift between earthquakes—the upward bulging in figure 9—may have allowed trees to colonize bold soil **Y** while admitting oxygen into organic matter of soil **U**, which thereby became faint; the same may be true for bold soil **S** and faint soil **N** (fig. 25).

There are many certainties, however, about the history of great earthquakes at the Cascadia subduction zone. One major unknown is the degree to which great earthquakes correspond one-to-one with buried soils. Some buried soils might represent nonseismic changes in tide levels or earthquakes smaller than magnitude 8 (Nelson and Personius, this volume). Other buried soils produced by great earthquakes may have disappeared through decomposition, as shown in figure 25 for a hypothetical correlative of soil **W** (fig. 23*B*).

A second major unknown is the size range of the great earthquakes. Abrupt lowering of coastal land about 300 years ago, during the best understood period of prehistoric plate-boundary seismicity at the Cascadia subduction zone, may record 1,000 km of rupture between southern British Columbia and northern California. However, radiocarbon dating lacks the resolution to show whether this extensive rupture happened piecemeal, during serial earthquakes of magnitude 8, or whether it attended a single earthquake of magnitude 9 (Atwater and others, 1995).

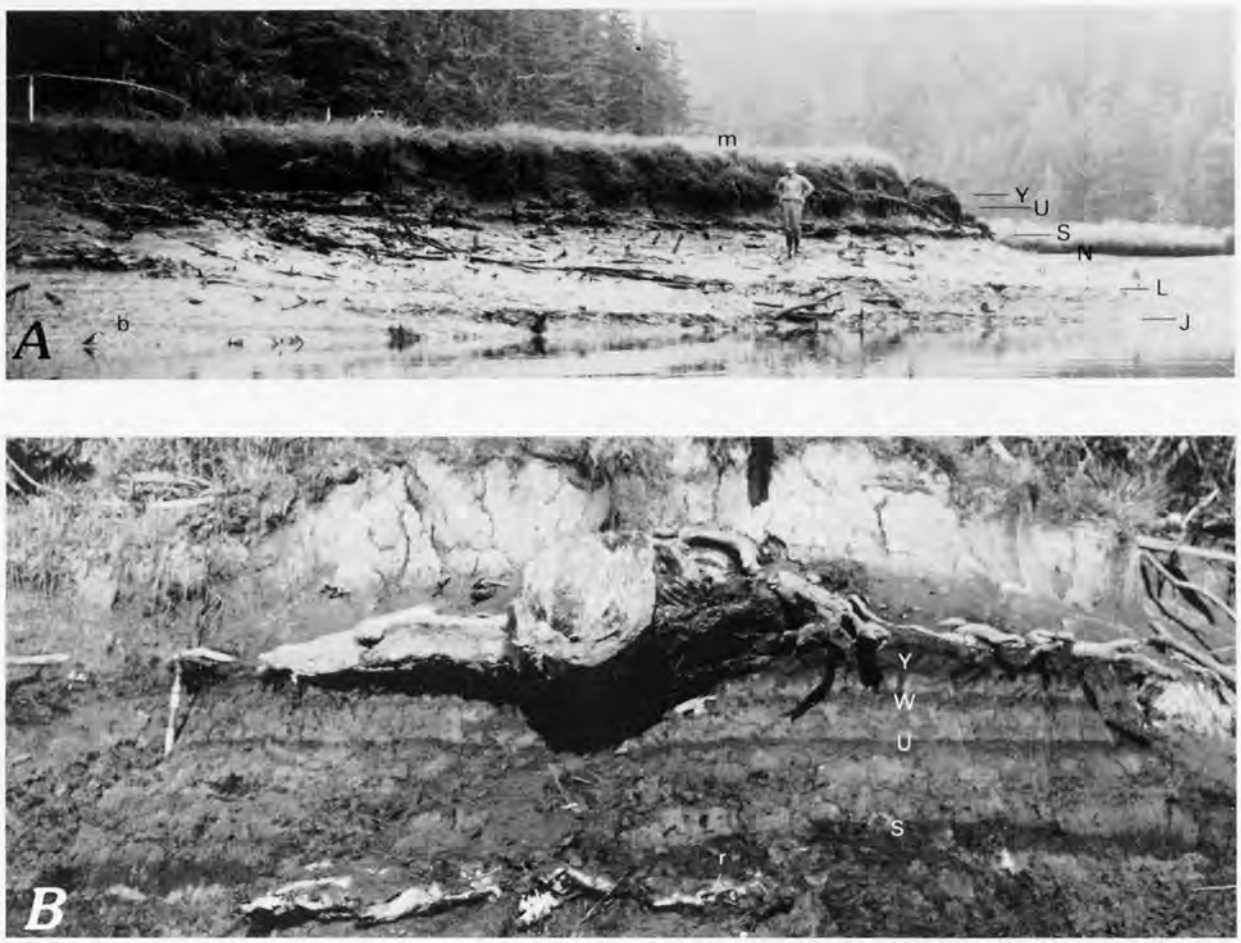

Figure 23. Low-tide outcrops showing successive buried lowland soils in southern coastal Washington. *A*, six buried soils along the Niawiakum River, Willapa Bay. Soils **U** and **N** lack organic matter resistant to erosion. Soils **J** and **L** descend away from Pleistocene bedrock (**b**), probably because of differential settlement. The modern marsh (**m**) extends to the forest, which covers an upland. Locality 17 of Atwater (1992). *B*, four buried soils at the mouth of Elliott Slough, Grays Harbor. Two of the soils contain spruce roots (**r**). The visible part of the shovel handle is 0.4 m long. Locality 9 of Atwater (1992).

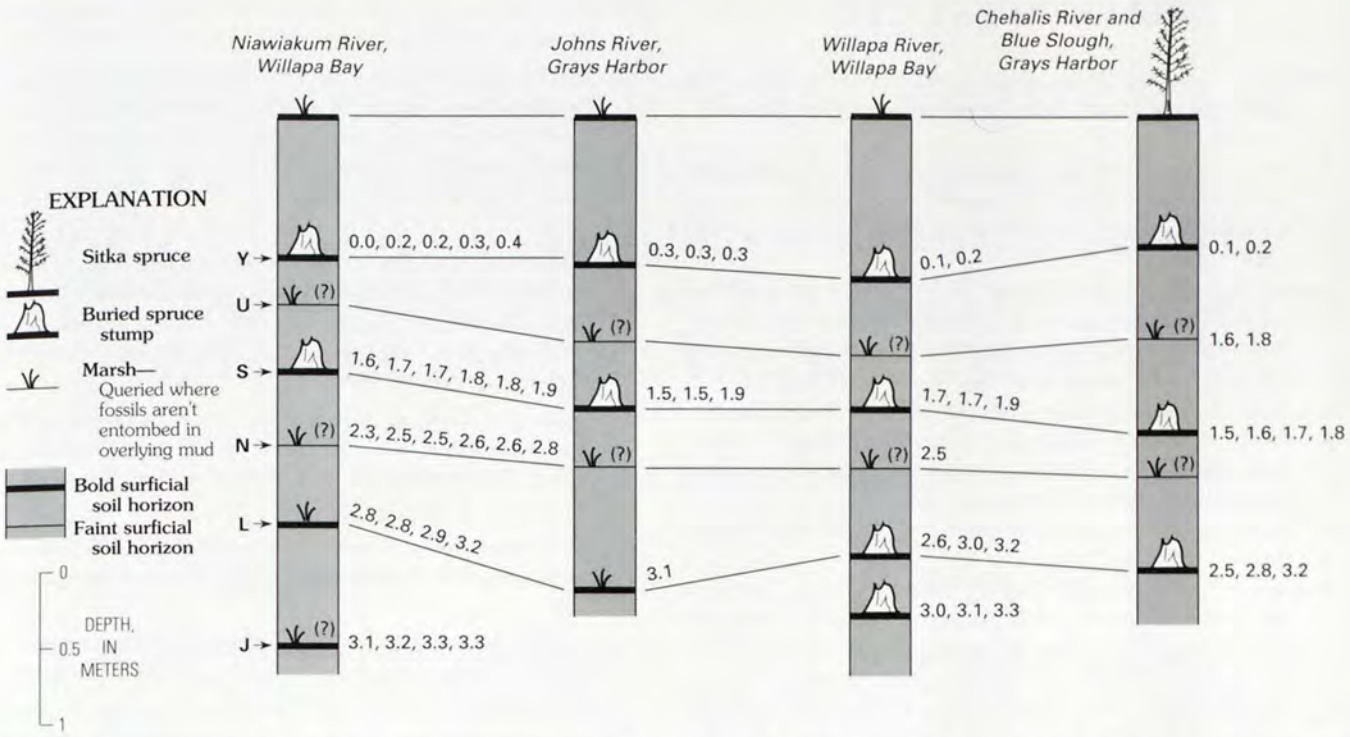

Figure 24. Sequences of buried lowland soils (bold letters) at Grays Harbor and Willapa Bay. The numbers are ages in thousands of radiocarbon years rounded to the nearest hundred. The standard deviation is probably 50–200 radiocarbon years for most ages. The ages were measured on woody roots, sticks, cones, and surficial horizons of soils. Lines between columns link soils that may record a single earthquake or a brief series of earthquakes. Localities of Atwater (1992), from left to right: 17; 14; 15; 10 and 11 combined.

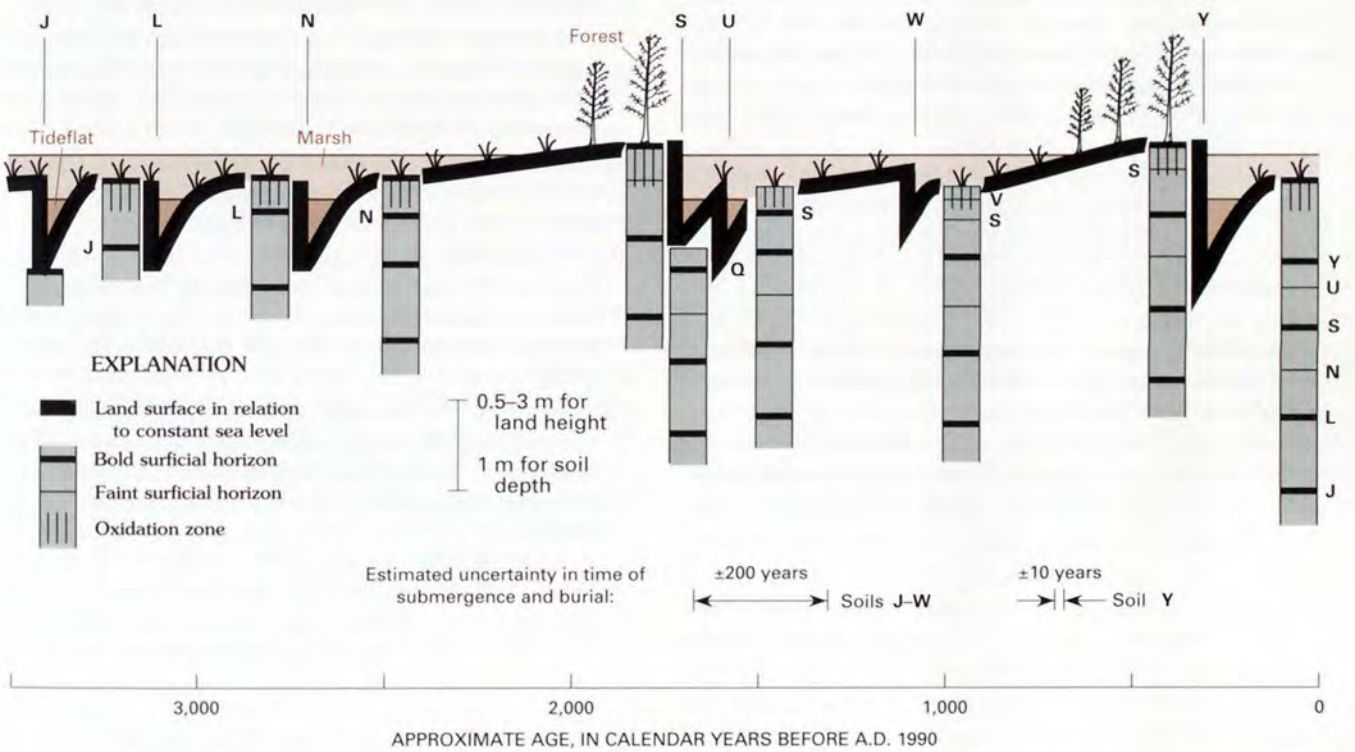

Figure 25. Inferred history of landscape, soils, and earthquakes at the Willapa Bay locality shown in figure 23*A*. Bold letters signify buried soil horizons. Soil **W** is hypothetical at this locality (Atwater, 1992).

REFERENCES CITED

Abe, Katsuyuki, 1979, Size of great earthquakes of 1837–1974 inferred from tsunami data: Journal of Geophysical Research, v. 84, no. B4, p. 1561–1568.

Atwater, B.F., 1992, Geologic evidence for earthquakes during the past 2000 years along the Copalis River, southern coastal Washington: Journal of Geophysical Research, v. 97, no. B2, p. 1901–1919.

Atwater, B.F., comp., 1994, Geology of liquefaction features about 300 years old along the lower Columbia River at Marsh, Brush, Price, Hunting, and Wallace Islands, Oregon and Washington: U.S. Geological Survey Open-File Report 94–209, 64 p.

Atwater, B.F., Jiménez Núñez, Héctor, and Vita-Finzi, Claudio, 1992, Net late Holocene emergence despite earthquake-induced submergence, south-central Chile, *in* Ota, Yoko, Nelson, A.R., and Berryman, K.R., eds., Impacts of tectonics on Quaternary coastal evolution: Quaternary International, v. 15/16, p. 77–85.

Atwater, B.F., Nelson, A.R., Clague, J.J., Carver, G.A., Yamaguchi, D.K., Bobrowski, P.T., Bourgeois, Joanne, Darienzo, M.E., Grant, W.C., Hemphill-Haley, Eileen, Kelsey, H.M., Jacoby, G.C., Nishenko, S.P., Palmer, S.P., Peterson, C.D., and Reinhart, M.A., 1995, Summary of coastal geologic evidence for past great earthquakes at the Cascadia subduction zone: Earthquake Spectra, v. 11, no. 1, p. 1–18.

Atwater, B.F., Stuiver, Minze, and Yamaguchi, D.K., 1991, Radiocarbon test of earthquake magnitude at the Cascadia subduction zone: Nature, v. 353, no. 6340, p. 156–158.

Atwater, B.F., and Yamaguchi, D.K., 1991, Sudden, probably coseismic submergence of Holocene trees and grass in coastal Washington state: Geology, v. 19, no. 7, p. 706–709.

Bourgeois, Joanne, and Reinhart, M.A., 1989, Onshore erosion and deposition by the 1960 tsunami at the Rio Lingue estuary, south-central Chile [abs.]: EOS [American Geophysical Union Transactions], v. 70, no. 43, p. 1331.

Cooper, J.G., 1860, Report on the botany of the route, *in* Reports of explorations and surveys to ascertain the most practicable and economical route for a railroad from the Mississippi River to the Pacific Ocean: U.S. Congress, 36th, 1st session, House of Representatives, Executive Document 56, v. 12, book 2, p. 13–39.

Franklin, J.F., and Dyrness, C.T., 1973, Natural vegetation of Oregon and Washington: U.S. Forest Service, Pacific Northwest Forest and Range Experiment Station, Forest Service Technical Report PNW–8, 417 p.

Grant, W.C., and McLaren, D.D., 1987, Evidence for Holocene subduction earthquakes along the northern Oregon coast [abs.]: EOS [American Geophysical Union Transactions], v. 68, no. 44, p. 1239.

Kanamori, Hiroo, 1977, The energy release in great earthquakes: Journal of Geophysical Research, v. 82, no. 20, p. 2981–2987.

Kunze, L.M., and Cornelius, L.C., 1982, Baseline inventory of rare, threatened and endangered plant species/communities along Washington's Pacific coast: Washington Natural Heritage Program, Coastal Zone Management Grant No. G82–029, Washington Department of Ecology (Olympia, WA 98504–8711), 164 p.

Obermeier, S.F., 1994, Preliminary limits for the strength of shaking for the Columbia River valley and the southern half of coastal Washington for the Cascadia subduction zone earthquake of about 300 years ago: U.S. Geological Survey Open-File Report 94–589.

Ovenshine, A.T., Lawson, D.E., and Bartsch-Winkler, S.R., 1976, The Placer River Silt—An intertidal deposit caused by the 1964 Alaska earthquake: U.S. Geological Survey Journal of Research, v. 4, no. 2, p. 151–162.

Plafker, George, 1969, Tectonics of the March 27, 1964, Alaska earthquake: U.S. Geological Survey Professional Paper 543–I, 74 p.

———1972, Alaskan earthquake of 1964 and Chilean earthquake of 1960—Implications for arc tectonics: Journal of Geophysical Research, v. 77, no. 5, p. 901–925.

Plafker, George, and Savage, J.C., 1970, Mechanism of the Chilean earthquakes of May 21 and 22, 1960: Geological Society of America Bulletin, v. 81, no. 4, p. 1001–1031.

Reinhart, M.A., and Bourgeois, Joanne, 1987, Distribution of anomalous sand at Willapa Bay, Washington—Evidence for large-scale landward-directed processes [abs.]: EOS [American Geophysical Union Transactions], v. 68, no. 44, p. 1469.

Thatcher, Wayne, and Rundle, J.B., 1984, A viscoelastic coupling model for the cyclic deformation due to periodically repeated earthquakes at subduction zones: Journal of Geophysical Research, v. 89, no. B9, p. 7631–7640.

Weinmann, F.C., Boulé, Mark, Brunner, Kenneth, Malek, John, and Yoshino, Victor, 1984, Wetland plants of the Pacific Northwest: Seattle, Wash., U.S. Army Corps of Engineers, 85 p.

Wright, Charles, and Mella, Arnoldo, 1963, Modifications to the soil pattern of south-central Chile resulting from seismic and associated phenomena during the period May to August 1960: Seismological Society of America Bulletin, v. 53, no. 6, p. 1367–1402.

Yamaguchi, D.K., Woodhouse, C.A., and Reid, M.S., 1989, Tree-ring evidence for synchronous rapid submergence of the southwestern Washington coast 300 years B.P. [abs.]: EOS [American Geophysical Union Transactions], v. 70, no. 43, p. 1332.

GREAT-EARTHQUAKE POTENTIAL IN OREGON AND WASHINGTON—AN OVERVIEW OF RECENT COASTAL GEOLOGIC STUDIES AND THEIR BEARING ON SEGMENTATION OF HOLOCENE RUPTURES, CENTRAL CASCADIA SUBDUCTION ZONE

By Alan R. Nelson[1] *and* Stephen F. Personius[1]

ABSTRACT

Fundamental questions in earthquake-hazards research in the Pacific Northwest are concerned with the magnitude and recurrence of great earthquakes in the Cascadia subduction zone (CSZ). Geologic work of the last few years has produced convincing evidence of coseismic subsidence along the Washington and Oregon coasts. Regional subsidence recorded by estuarine deposits suggests that plate-interface earthquakes of at least magnitude 8 with more than 100-km-long ruptures occurred during the late Holocene in northwestern Oregon and southern Washington. Differences in the types of coastal-marsh sequences between northwestern and south-central Oregon, however, suggest that the Oregon coastline did not subside due to regional deformation south of about lat 44°N. North of this latitude, the coast may intersect the seaward edge of a zone of coseismic subsidence that may continue southeastward onshore. Alternatively, the CSZ may be segmented near lat 44°–45°N.; a segment boundary at this location would indicate that plate-interface earthquakes of about magnitude 8 along the central CSZ are more frequent than earthquakes of magnitude 9. South of this boundary, in the Coos Bay region, the tectonic framework developed through mapping and dating of marine and fluvial terraces indicates that at least some episodes of abrupt tidal-marsh burial in south-central Oregon are the product of deformation of local structures. Some of the local deformation could be associated with moderate earthquakes (magnitude less than 6). At most sites in south-central Oregon, however, it is unclear whether the observed deformation is related to local faulting and folding during moderate-magnitude earthquakes, to regional deformation during great plate-interface earthquakes, or to both.

[1]U.S. Geological Survey, Box 25046, MS 966, Federal Center, Denver, CO 80225.

INTRODUCTION

One of the fundamental questions in earthquake-hazards research in the Pacific Northwest is what is the potential for great earthquakes in the Cascadia subduction zone (CSZ), the region shown in figure 26 (Heaton and Hartzell, 1987; Atwater, 1987)? The present seismic quiescence in the region, initially attributed to aseismic subduction (Ando and Balazs, 1979; Acharya, 1981; Reilinger and Adams, 1982), is increasingly regarded as evidence for a locked plate interface where accumulating stress will be released in a great earthquake of moment magnitude (M_w) greater than 8 (Savage and others, 1981; Heaton and Kanamori, 1984; Adams, 1984; Heaton and Hartzell, 1986; Rogers, 1988; Spence, 1989). Recent geologic field studies support the locked plate-interface model (Atwater, 1987; Kelsey and Carver, 1988; Kulm, 1989; Clarke and Carver, 1989; Adams, 1990; Darienzo and Peterson, 1990; Peterson and Darienzo, this volume) but have thus far provided only rough estimates of great-earthquake recurrence and little information on earthquake magnitude.

Resolution of seismic-safety issues in the region requires reasonable estimates of the magnitude, extent, and recurrence of prehistoric plate-interface earthquakes during the last 5,000 years of the late Holocene (Shedlock and Weaver, 1989). A probable locked plate interface, a convergence rate of 30–40 mm/year, and the young age (less than 10 Ma) of the subducting crust suggest plate-interface earthquakes of M_w 8–9 are plausible (Heaton and Kanamori, 1984). But the recurrence and magnitude of these earthquakes probably differs from place to place along the CSZ (Spence, 1988; Weaver and Shedlock, 1989). The temporal and spacial pattern of earthquakes needs to be determined for the last few seismic cycles (Thatcher, 1989) to accurately assess the hazard from great earthquakes (Nishenko, 1989).

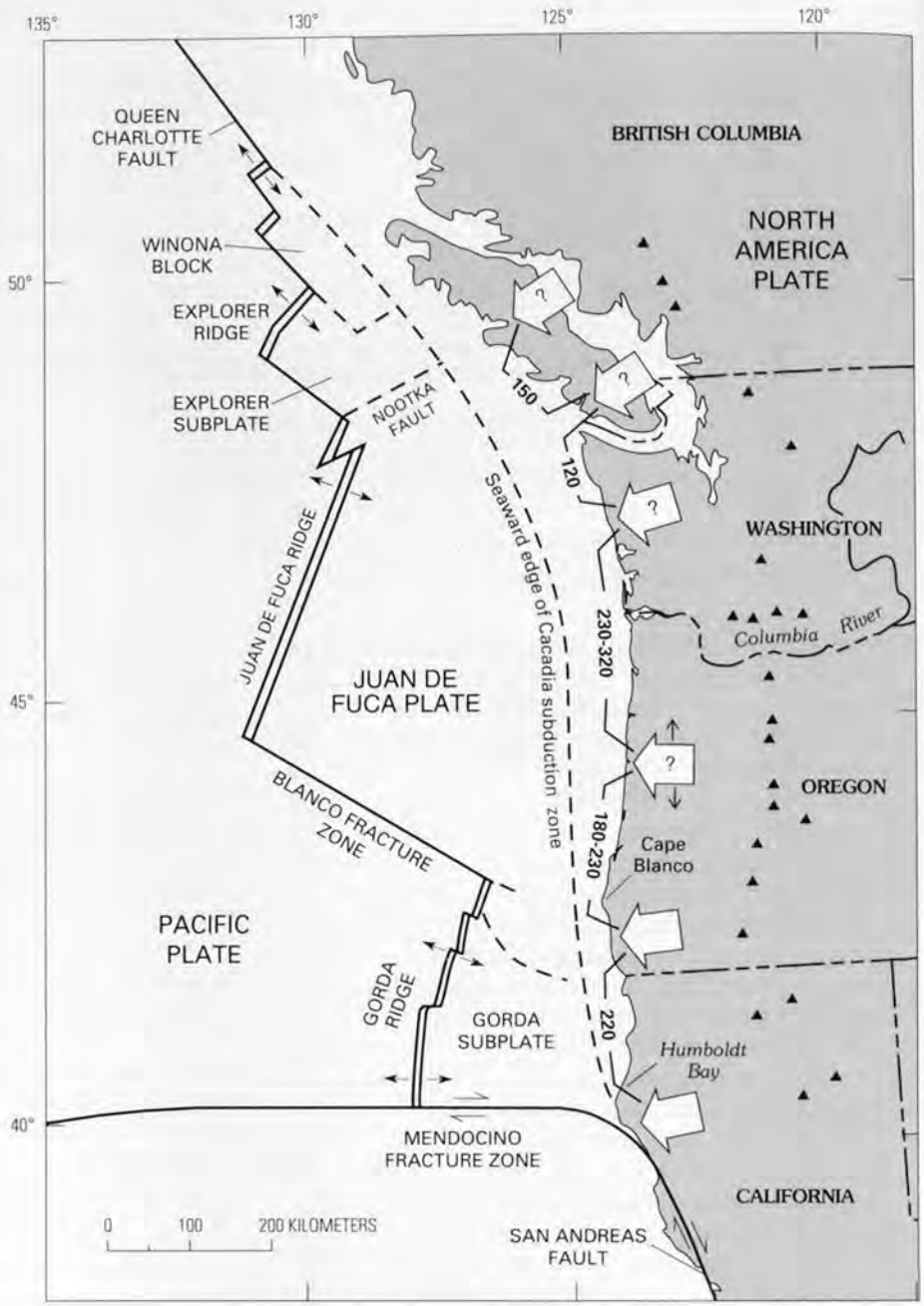

Figure 26. Major features of the Cascadia subduction zone in the northwestern United States and southwestern Canada. Large open arrows, some with queries, mark generalized areas along the coast that coincide with boundaries between tectonic subplates, projections of boundaries between volcanic segments in the Cascade Range (Hughes and others, 1980), or other areas where seismicity and subducting-plate parameters may change, corresponding with boundaries between segments of the Pacific plate as outlined by Spence (1989). No query is shown at the Mendocino fracture zone because its boundary is accurately known. Distances between boundaries (bold numbers, in kilometers) are shown only as ranges of possible segment lengths. The range of distances shown for segments just north and south of lat 44.5°N. reflects several locations for a possible boundary along this part of the coast. We don't know whether most Holocene ruptures along the CSZ have been influenced by these postulated boundaries. Triangles show volcanoes in the Cascade Range; barbs and dark arrows show relative direction of plate movement on faults. Modified from Rogers (1988), Spence (1989), and Wilson (1989).

The degree to which changes in the characteristics of the plate interface along the CSZ control the extent of Holocene ruptures, that is, the extent to which the CSZ is segmented, is critical in determining whether earthquakes of M_w 8 or M_w 9 have occurred more often. Subduction continues at a higher rate beneath Washington than beneath Oregon due to rotation of the Juan de Fuca plate (fig. 26) about a pole in northern California (Nishimura and others, 1984; Riddihough, 1984; Wilson, 1986). The properties of the subducting plate and the width of the locked zone also differ from north to south (Crosson and Owens, 1987; Rasmussen and Humphreys, 1989; Weaver and Shedlock, 1989). Furthermore, the stress regime in the crust throughout the CSZ is dominated by north-south compression due to the interaction of the Pacific, Gorda, Juan de Fuca, and North America plates (Magee and Zoback, 1989; Spence, 1989). The complex interactions of these plates and the limited seismicity data suggest that the CSZ is composed of four to seven segments (Hughes and others, 1980; Weaver and Michaelson, 1985; Heaton and Hartzell, 1986; Rogers, 1988; Weaver and Baker, 1988; Spence, 1989). Although plate-interface properties within areas of high seismic-moment release near segment boundaries may be the primary control on rupture initiation and extent (Thatcher, 1990), the boundaries between these segments probably reflect the endpoints of many plate-interface ruptures during the Quaternary.

We will review some of the preliminary conclusions of geologic field studies that are underway in the coastal areas of Oregon and Washington (as of December 1989) and speculate on some of their implications for the hazards posed by plate-interface earthquakes in the CSZ. Because the record of paleoseismic events is fragmentary, a variety of methods is being used to piece together the late Quaternary tectonic and paleoseismic history of the region. Work in progress is of two kinds—paleoseismology studies of the late Holocene coastal record, and studies of cumulative middle and late Quaternary tectonic deformation as expressed by marine and fluvial terraces.

ACKNOWLEDGMENTS

Our work was supported by the National Earthquake Hazards Reduction Program of the U.S. Geological Survey and by the U.S. Nuclear Regulatory Commission. We thank James Carlton, Paul Rudy, and other staff of the Oregon Institute for Marine Biology, Charleston, Oreg., for providing facilities, logistical support, discussions, and encouragement throughout this study. Michael Graybill strongly encouraged our studies in the South Slough National Estuarine Research Reserve, Coos Bay. Able field assistance was provided by Peter Vetto, William Manley, and Stephen McDuffy. Joint field work and extensive discussions with Curt Peterson and Mark Darienzo were invaluable, as were discussions with Brian Atwater, Gary Carver, Harvey Kelsey, Wendy Grant, Mary Reinhart, William Spence, and Robert Bucknam. Peterson and Darienzo also provided core data from Alsea Bay (discussed extensively in their paper in this volume). Lee-Ann Bradley and Susan Rhea prepared the illustrations. Comments by Brian Atwater, Susan Bartsch-Winkler, and Daniel Muhs significantly improved the manuscript. This is a contribution to IGCP Project 274 (Quaternary Coastal Evolution) and to the INQUA Neotectonics Commission.

HOLOCENE PALEOSEISMOLOGY

RECOGNITION OF COSEISMIC COASTAL DEFORMATION IN WASHINGTON AND OREGON

A linear pattern of coseismic deformation has been observed along subduction-zone coasts during great plate-interface earthquakes (Plafker, 1965; Ando, 1975; reviewed in Lajoie, 1986). Plafker (1969, 1972) developed a model of coseismic deformation, having an elongated zone of uplift and a parallel zone of subsidence, based on mapping of the coseismic deformation in the coastal areas of southern Alaska and south-central Chile after the two largest earthquakes of this century. Uncoupling of the leading edge of the overriding plate during megathrust earthquakes can produce as much as 2 m of regional coseismic uplift in a zone 80–160 km wide. Locally in this zone, as much as 10 m of coseismic uplift can occur by thrusting on small, steep faults in the toe of the overriding plate (Plafker, 1969; Plafker and Rubin, 1978; Yonekura and Shimazaki, 1980). The zone of subsidence, which is landward of the zone of uplift, is commonly wider than the zone of uplift and can be hundreds of kilometers long; maximum regional subsidence can reach 2–3 m during the largest earthquakes (Plafker and Savage, 1970).

INITIAL SEARCH FOR EVIDENCE OF HOLOCENE UPLIFT

Most previous paleoseismology studies along subduction-zone coasts have focused on shoreline features inferred to have been raised by sudden coseismic uplift (reviewed in Lajoie, 1986; Berryman, 1987). Although large storms can deposit terracelike beach berms, flights of Holocene marine terraces along active convergent margins are commonly interpreted to be of coseismic origin. Examples of probable Holocene coseismic terraces from other subduction zones include those in Chile (Kaizuka and others, 1973), Japan (Matsuda and others, 1978), New Zealand (Berryman and others, 1989), the New Hebrides Islands (Taylor and others, 1990), and Alaska (Plafker and Rubin, 1978; Winslow, 1988).

Initial paleoseismic study of the CSZ also focused on a search for features produced by coseismic uplift, but no extensive Holocene terraces were found, even along the southern part of the Oregon coast that lies closest to the subduction-zone trench (the distance from the coast to the edge of the trench at the base of the continental slope is 60–105 km; fig. 27) (Golder Associates, Inc., 1986). West and McCrumb (1988a) interpreted the broad, modern wave-cut platforms and the lack of Holocene marine terraces along the Washington and Oregon coasts as evidence that repeated great plate-interface earthquakes probably had not occurred (at least in central and southern Oregon). They suggested that if plate-interface earthquakes had occurred during the late Holocene, then sea-level rise must have equaled or exceeded the rate of coseismic plus interseismic uplift, or that plate-interface earthquakes were too small to produce significant amounts of coseismic uplift.

In the southernmost part of the CSZ, Holocene marine terraces suggesting uplift rates of 3–4 mm/year have been reported from the plate triple junction area where the Mendocino fracture zone joins the San Andreas fault (fig. 26) (Lajoie and others, 1982; Carver and Burke, 1987; Carver and others, 1989). In addition, Kelsey (1989, 1991) found a single example of a Holocene beach berm of probable coseismic origin near the Elk River, 6 km south of Cape

Blanco on the southern Oregon coast. Cape Blanco is only about 60 km east of the subduction-zone trench and is inferred to lie within a zone of coseismic uplift during plate-interface earthquakes (fig. 28). Rates of late Pleistocene uplift for Cape Blanco are higher than rates to the north and south (West and McCrumb, 1988a; Kelsey, 1990; Muhs and others, 1990). The proximity of Cape Blanco to the trench may thus explain the location of this raised berm along a coastline otherwise devoid of evidence for Holocene uplift.

EVIDENCE FOR COSEISMIC SUBSIDENCE

Heaton and Hartzell (1986), Atwater and Grant (1986), and Atwater (1987) changed the focus of paleoseismicity studies in the Pacific Northwest by proposing that much of the coastline in Oregon and Washington is in a zone of coseismic subsidence rather than uplift during great earthquakes.

Atwater (1987) based his interpretation of repeated coseismic subsidence on the stratigraphy of estuarine deposits in southwestern Washington. He inferred that sudden jerks of subsidence had repeatedly submerged tidal wetland soils on the margins of estuaries during great earthquakes. Plafker (1972, p. 917) had previously suggested the paleoseismic potential of this type of stratigraphic record, and Ovenshine and others (1976), Bartsch-Winkler and others (1983), Combellick (1986), and Bartsch-Winkler (1988) had investigated records of this type in Alaska. However, Atwater (1987) was the first to recognize evidence for coseismic subsidence in the Pacific Northwest and to use stratigraphic methods to show that such subsidence had occurred repeatedly over a large area. Darienzo (1987), Darienzo and Peterson (1987), Peterson and others (1988), and Darienzo and Peterson (1990), working independently in the Netarts Bay estuary in northwestern Oregon, adopted the coseismic-subsidence model to explain similar sequences of interbedded tidal-marsh peat and mud. They and other investigators subsequently found similar evidence for coseismic subsidence in many other estuaries along the Oregon and Washington coasts (Grant and McLaren, 1987; Hull, 1987; Nelson, 1987; Nelson and others, 1987; Grant, 1988; Peterson and Darienzo, 1988a, 1989, this volume; McInelly and others, 1989), as well as in the Humboldt Bay area of California (fig. 26) (Vick, 1988; Carver and others, 1989; Grant and others, 1989).

The repetitive stratigraphy identified by Atwater (1987, 1988d) in tidal-marsh cores and outcrops consists of peaty soils representing densely vegetated wetlands abruptly overlain by intertidal muds. Typically, the peats are thin (0.05–0.2 m), have abrupt upper contacts and gradational lower contacts, are separated by thick (0.5–1.0 m) intervals of intertidal mud, and commonly have spruce or western redcedar stumps rooted in them. Atwater's (1987) evidence that the peaty soils were submerged suddenly due to coseismic subsidence, in some places accompanied by tsunamis, included: (1) the abruptness of the upper contacts of peats,

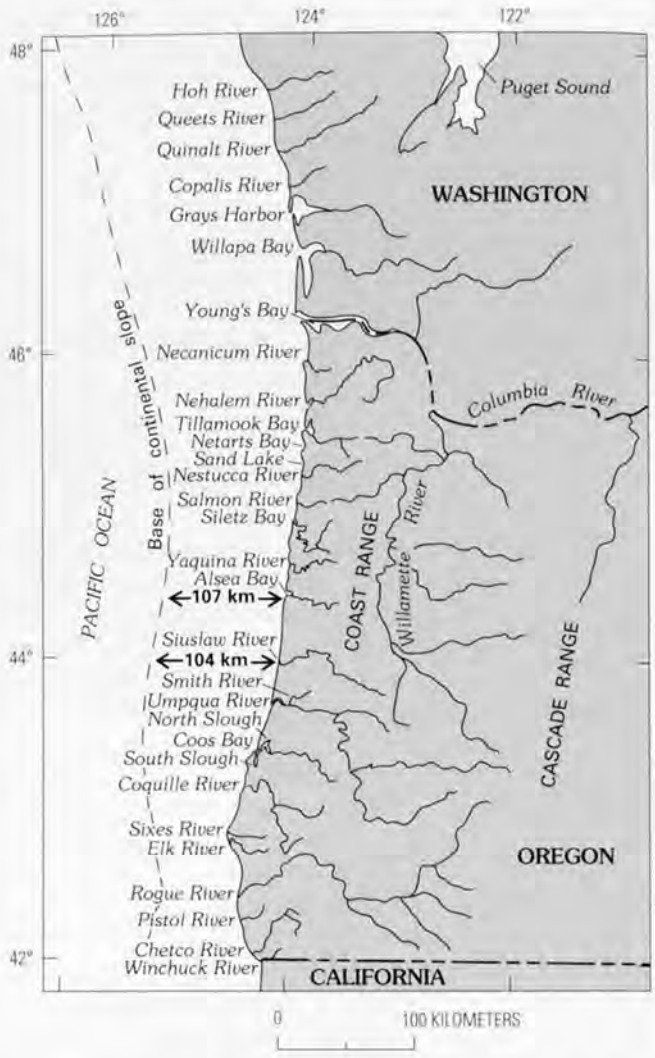

Figure 27. Locations and names of estuaries in Oregon and southern Washington. The distances of the Alsea Bay and Siuslaw River estuaries from the base of the continental slope (eastern edge of the Cascadia subduction-zone trench) are shown in bold.

(2) the amount of submergence (0.5–2.0 m) suggested by plant macrofossils above and below the abrupt contacts, (3) the similar character of the peat-mud couplets both laterally at different sites and in sequence, (4) the presence of continuous peat-mud couplets where these sequences lap up on older, Pleistocene sediments at valley sides, (5) the fining-upward, landward-thinning sand beds capping some peats at sites where no sand is presently being deposited, and (6) the similarity of these sequences to those reported to have been deposited following great earthquakes in Alaska and Chile (Wright and Mella, 1963; Ovenshine and others, 1976). In southwestern Washington, Atwater (1987, 1988c) identified at least eight separate buried peats; the five most widespread peaty soils are dated at less than 3 ka and all are less than 5 ka. Atwater (1987) also used the coseismic-subsidence model to reconcile the relatively slow regional uplift of the

coast (0.1–0.4 mm/year) expressed by raised Pleistocene marine terraces in southwestern Washington with the much higher, regional rate of uplift obtained from tide-gauge records (2–3 mm/year). Periods of jerky subsidence (0.5–2 m), superimposed on a low interseismic uplift rate throughout the late Pleistocene, were hypothesized to yield an even lower net uplift rate.

Because interbedded peat-mud couplets can also be produced by nontectonic processes (discussed below), the most convincing studies of coseismic subsidence focused on evidence suggesting sudden, significant rises in relative sea level (submergence). Rooted stems of herbaceous plants are found locally entombed by overlying estuarine mud at the upper contact of some peaty soils in southwestern Washington (Atwater, 1988e). These fossils provide compelling evidence for sudden submergence because they are generally not preserved at the marsh surface for more than a few years. Tree-ring studies by Yamaguchi and others (1989a) have also shown that redcedar trees rooted in the youngest buried soil at four sites in southwestern Washington probably died suddenly within a few years of each other. In-progress microfossil studies of some peat-mud couplets in south-central Oregon (A.R. Nelson and A.E. Jennings, University of Colorado; and Kaoru Kashima, Kyushu University, unpub. data, 1989), northwestern Oregon (Darienzo, 1987; Peterson, 1989; Darienzo and Peterson, 1990), and southwestern Washington (Hemphill-Haley, 1989) support Atwater's (1987) deduction that the transitions across the upper contacts of the peat-mud couplets represent 0.5–2.0 m of sudden submergence.

Atwater (1987, 1988d) suggested that evidence of sediment deposition by tsunamis, and sediment liquefaction directly overlying the abruptly submerged wetland soils would be compelling evidence of regional coseismic subsidence. Initial mapping of the sand beds that cap some peaty soils in some parts of the marshes bordering tidal streams at Willapa Bay, Wash. (fig. 27) (Atwater, 1987), showed that the sand pinches out landward—the expected result of tsunami deposition. The sand beds were only found capping peaty soils and not within the thick estuarine muds, suggesting that all sand beds were deposited immediately after sudden submergence of the marsh. Similar sand beds capping buried peaty soils at Grays Harbor, Wash. (Reinhart and Bourgeois, 1988), Netarts Bay, Oreg. (Peterson and others, 1988; Darienzo and Peterson, 1990), along the Salmon River, Oreg. (Grant and McLaren, 1987), at Siletz Bay, Oreg. (Peterson, 1989), and at Alsea Bay, Oreg. (Darienzo, 1989; Peterson and Darienzo, this volume), show similar relations and have also been attributed to tsunamis. Field and modeling studies of the sand beds at Willapa Bay (Reinhart and Bourgeois, 1987, 1988, 1989; Bourgeois and Reinhart, 1988) indicate that large, landward-directed surges of sandy water that accompanied some of the subsidence events were locally generated tsunamis rather than storm surges, seiches, or distant tsunamis. Microfossil studies also lend support to the tsunami hypothesis, especially where abrupt peat contacts lack capping sand beds. In estuarine mud directly above an abrupt peat contact in Willapa Bay, Eileen Hemphill-Haley (U.S. Geological Survey, unpub. data, 1989) has found marine diatoms, which are not characteristic of estuarine environments; possibly, these diatoms were transported from the continental shelf by a tsunami.

So far, only one estuarine site in southwestern Washington has yielded definitive evidence of prehistoric sediment liquefaction, but the eruption of a sand blow at this site was not concurrent with a subsidence event (Atwater, 1988c). However, liquefaction features commonly develop in well-sorted fine sand or silt beds that are saturated and confined by overlying finer grained beds (Obermeier and others, 1989). Furthermore, adequate (1–2 m high) vertical exposures where the water table is now below the base of the exposure are required to study such features. No systematic search for liquefaction features has yet been made in sandy areas along the Oregon or Washington coasts, but the continuing rise of late Holocene sea level in the region ensures that any exposures of liquefiable sediments will be difficult to find. Thus, the present lack of well-documented paleoliquefaction sites does not preclude great earthquakes along the CSZ during the late Holocene.

ALTERNATIVES TO THE COSEISMIC–SUBSIDENCE HYPOTHESIS

Much of the initial debate about the applicability of the coseismic-subsidence model to Oregon and Washington has centered on whether observed changes in the sequences of estuarine sediment are distinctive enough to be due to coseismic movements or whether they might have been produced by nontectonic processes. Early investigations (among others, Darienzo, 1987; Darienzo and Peterson, 1987; Reinhart and Bourgeois, 1987) questioned whether at least some of the peat-mud couplets might not result from (1) storm surges, distant tsunamis, or floods coupled with relatively rapid rises in regional sea level, (2) complex patterns of tidal channel cuts and fills, or (3) sudden changes in tidal range caused by migrations of bars near the mouths of tidal inlets. Atwater (1987) argued that storm surges, distant tsunamis, and floods could only raise sea level briefly (less than a few days) and that these processes could not permanently change woody wetlands into intertidal mud flats, as suggested by the lithology and plant macrofossils in the sequences in southwestern Washington. Marsh vegetation should readily incorporate any sediment deposited on the marsh from floods or storms without permanent submergence of the marsh. In support of these arguments, Peterson and Darienzo (1988a, b, this volume) found no evidence of significant sediment deposition in estuarine marsh sequences during either major historic floods or large storm surges in fluvially dominated estuaries in Oregon. Most investigators (for example,

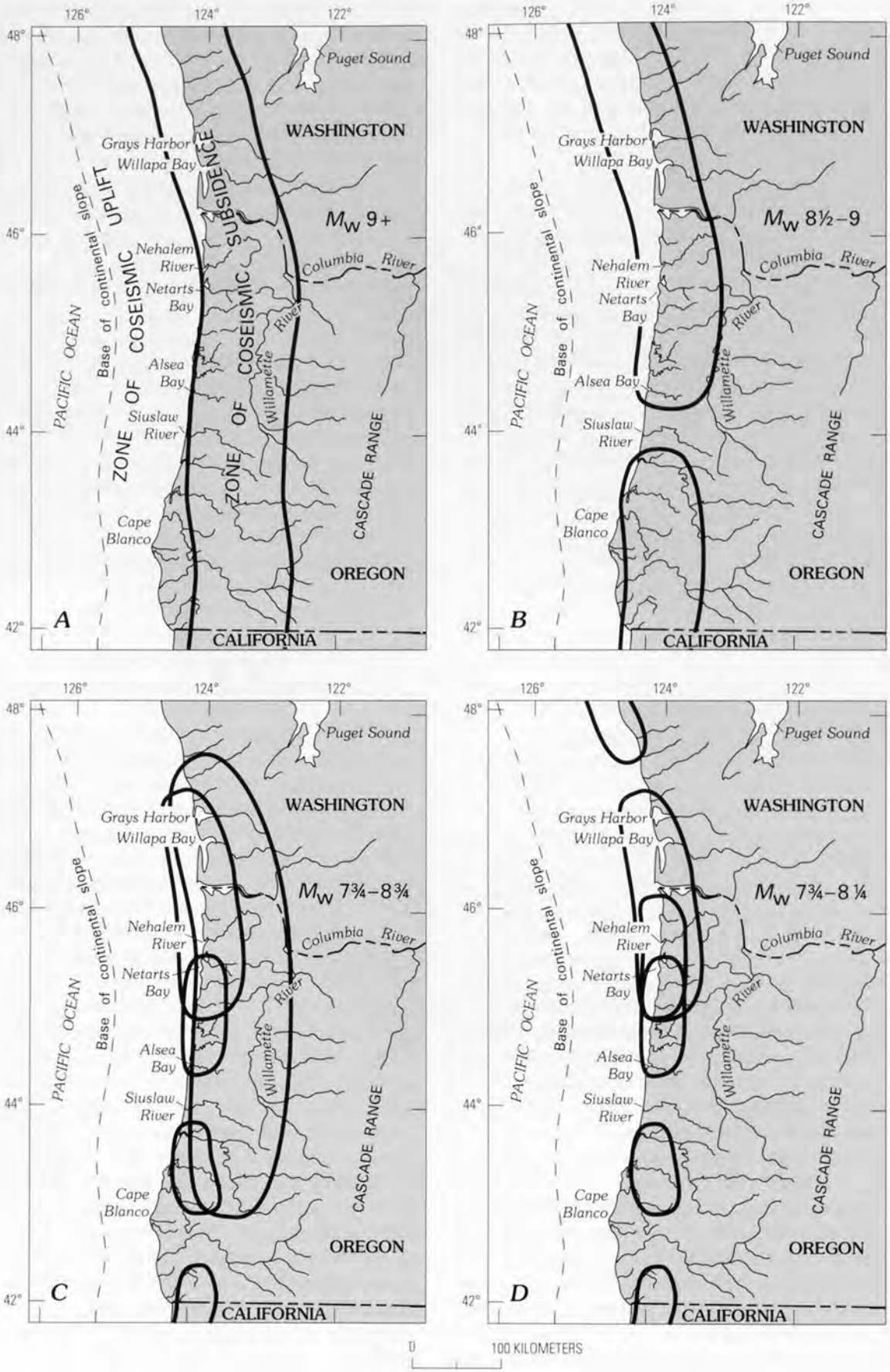
126°
124°
122°
48°
46°
44°
42°
Puget Sound
WASHINGTON
Grays Harbor
Willapa Bay
Nehalem River
Netarts Bay
Alsea Bay
Siuslaw River
Cape Blanco
Columbia River
Willamette River
PACIFIC OCEAN
Base of continental slope
UPLIFT
ZONE OF COSEISMIC SUBSIDENCE
ZONE OF COSEISMIC
CASCADE RANGE
OREGON
CALIFORNIA
A
M_W 9+
B
M_W 8½–9
C
M_W 7¾–8¾
D
M_W 7¾–8¼
0
100 KILOMETERS

Atwater, 1987, 1988e; Darienzo, 1989; Darienzo and Peterson, 1990; Peterson and Darienzo, this volume) also found that the lateral continuity of most of the buried peaty soils (as demonstrated by transects of cores or laterally extensive outcrops) eliminated tidal channel cut-and-fill processes as a possible cause at most sites. The regular sequence of lithologic changes within peat-mud couplets and the changing environments indicated by microfossil assemblages (A.R. Nelson, A.E. Jennings, and Kaoru Kashima, unpub. data, 1989; Hemphill-Haley, 1989) are also incompatible with a channel origin.

Sudden changes in tidal range are more difficult to dismiss as a possible cause of interbedded peat-mud sequences (Darienzo, 1987). In fact, this mechanism is a common explanation of sequences in northwestern Europe (Shennan, 1986) that are similar to the peat-mud couplets in the Pacific Northwest. On the Atlantic coast of the United States, Thomas and others (1989) also suggested this explanation for the sudden changes in lithology and foraminiferal assemblages in cores from a Connecticut salt marsh. Sudden changes in tidal range could explain the burial of some peats in some inlets in the Pacific Northwest, but correlation of similar sequences between sites in inlets of different morphology and tidal characteristics shows that local changes in tidal range cannot have produced most peat-mud couplets.

Figure 28 (facing page). Four models of the locations of zones of coseismic subsidence during plate-interface earthquakes in the central Cascadia subduction zone. Heavy lines are boundaries of areas of coseismic subsidence. *A*, a rupture of more than 700 km of the plate boundary from an earthquake of at least M_w 9 could produce a zone of coseismic uplift extending eastward from the trench and a zone of coseismic subsidence east of the zone of uplift. Estuaries north of the Siuslaw River estuary contain stratigraphic sequences with evidence of coseismic subsidence, whereas the Siuslaw River estuary contains evidence of a slow, uniform rise in relative sea level. Thus, if M_w 9+ earthquakes have occurred, the edge of the zone of coseismic subsidence during these earthquakes may have trended between the Siuslaw River and Alsea Bay estuaries. The eastward extent of the zone of coseismic subsidence for such earthquakes is unknown. *B*, ruptures of 300–600 km of the plate boundary during M_w 8½–9 earthquakes would also produce extensive zones of coseismic subsidence. If these zones were farther west than in *A*, they could not include the Siuslaw River estuary, and the ruptures could not extend north or south of the Siuslaw River. *C*, rupture of single plate-boundary segments or parts of segments during earthquakes of less than M_w 8¼ could produce zones of coseismic subsidence less than 250 km long. These smaller earthquakes might not produce any significant (more than 0.3 m) permanent subsidence and could include the area of the Siuslaw River estuary. Slip along some parts of the plate boundary could also be aseismic (Savage, 1989). *D*, a variation of models *A* and *C* is that earthquakes of M_w 7¾–8¼ could be most common, with rare earthquakes of M_w 8¾ that rupture two segments of the plate boundary. However, in this model, the zone of coseismic subsidence for the rare, largest earthquakes would have to be east of the Siuslaw River estuary.

The weakest part of Atwater's (1987) case for coseismic subsidence was his suggestion that the sequences of interbedded peat and mud so typical of late Holocene estuarine sequences in the Pacific Northwest are characteristic of tectonically active coasts. He argued that on nontectonically active coasts, the slow, uniform rise of sea level during the late Holocene has produced thick, uniform layers of peat like those found in Puget Sound, San Francisco Bay, and Cape Cod marshes (fig. 29, sequence *A*). Using this line of reasoning, the widespread peat-mud couplets in southwestern Washington were thought to be good evidence for the jerky rise of Holocene sea level. Each jerk was inferred to result from an episode of sudden relative sea-level rise due to coseismic subsidence (fig. 29, sequence *B*). But many studies on nontectonic coasts, and particularly those from northwestern Europe, show sequences that are, at least superficially, similar to those in the Pacific Northwest (for example, Devoy, 1987; Tooley and Shennan, 1987). Many of these long-term studies (for example, Jelgersma, 1961; Tooley, 1978; Plassche, 1982; Ters, 1987) are much more extensive than any work so far attempted in the Pacific Northwest and are supported by thousands of ^{14}C ages (for example, see Berendsen, 1984; Shennan, 1987).

The stratigraphy at many individual sites on nontectonic coasts suggests that local rates of sea-level rise have varied markedly (Shennan, 1986); many processes have been invoked to explain these inferred rate changes. Most upper and lower contacts of peaty units in sequences on nontectonic coasts are gradational (fig. 29, sequence *C*) with overlying and underlying intertidal muds, suggesting transitions between upper intertidal and lower intertidal environments that lasted at least tens of years. Oscillations in late Holocene sea level are the most often cited explanation for the interbedded peats and muds on stable coasts (for example, see Rampino and Sanders, 1981; Shennan, 1982, 1986; Fairbridge, 1987; Ters, 1987). Despite the limits of resolution of altitudinal and ^{14}C age data in sea-level studies, some regional oscillations of sea level have been identified (Shennan, 1987), but these oscillations are not necessarily synchronous from region to region (Kidson, 1982). Other processes that may be involved in sea-level changes that produce peat-mud couplets on nontectonic coasts include (1) large storms (Tooley, 1985; Cullingford and others, 1989), (2) long periods with many storm surges (Streif, 1980), (3) changes in the shapes and gradients of estuarine systems due to river changes and rising Holocene sea level (Plassche, 1980), and (4) gradual regional tectonic warping (Newman and others, 1980; Shennan, 1989). However, lithologic changes in the peat-mud sequences may not be direct proxies of small sea-level changes (Orson and others, 1985; Stevenson and others, 1986). Such lithologic changes show, however, that marsh aggradation has not kept up with late Holocene sea-level rise along many nontectonic coasts (Brooks and others, 1979; Kearney and Ward, 1986) and that the lack of thick sequences of peat is not necessarily evidence for tectonic instability.

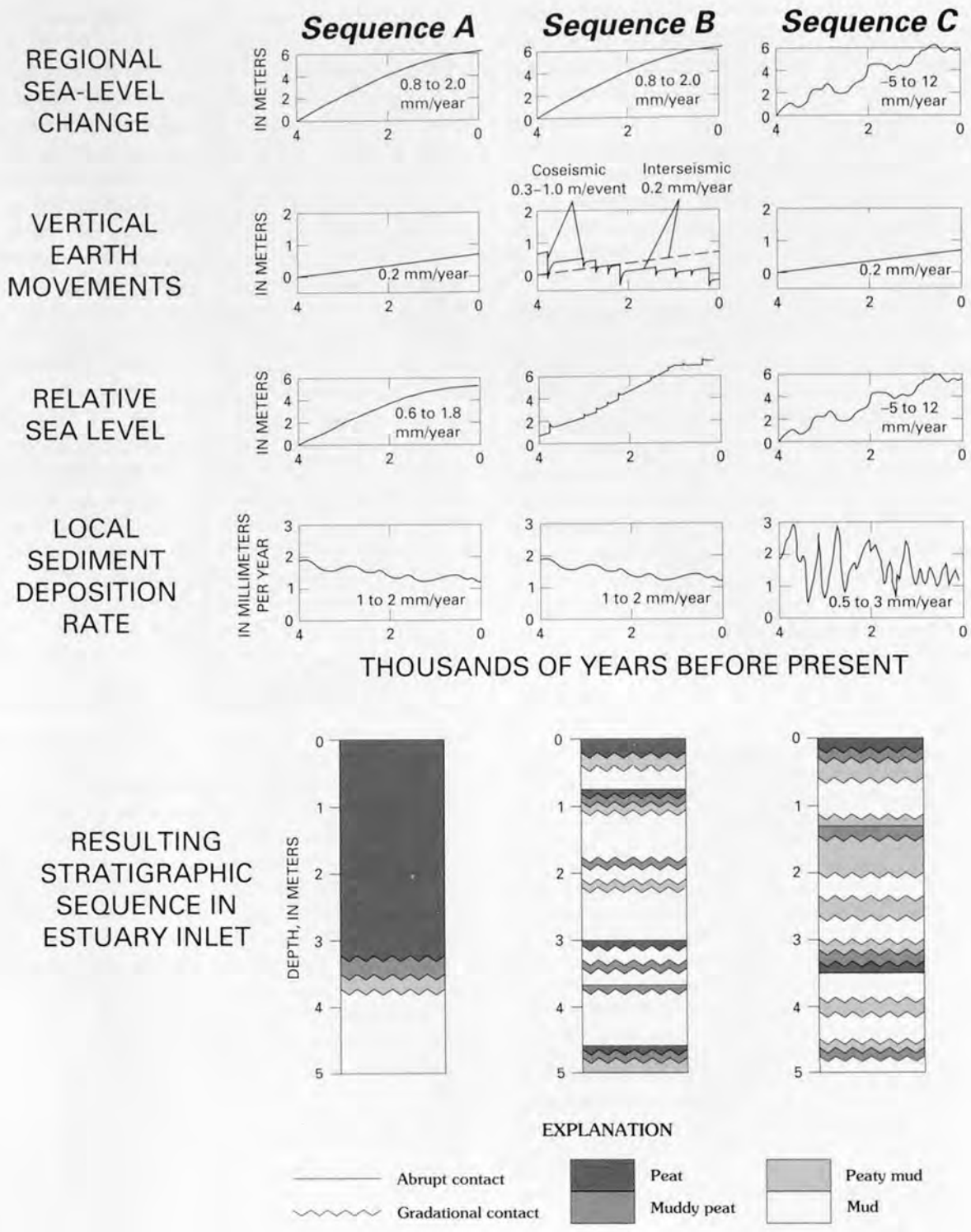

Figure 29. Models of regional sea-level rise, land-level movements, resulting relative sea-level changes, and sediment-deposition rates in tidal inlets in the Pacific Northwest during the late Holocene. The curves illustrate how different but plausible histories of sea-level rise, coastal uplift, and sedimentation rates could produce different types of stratigraphic sequences in these inlets. Sequence *A* could only be produced in an inlet that had not had major (more than 0.3 m) sudden changes in relative sea level. The abrupt upper contacts of the peat units in sequence *B* suggest sudden rises in sea level or erosion. Gradational contacts characterize sequence *C*, which could be produced by fluctuating regional sea level and rapidly changing sedimentation rates. Sequence *B* could easily be confused with sequence *C*, which was produced without any sudden changes in relative sea level.

There have been no detailed studies of Holocene sea level in Oregon and Washington, so the rate and character (smooth vs. oscillatory) of sea-level rise in this region is poorly known. In general, the rate of rise is thought to be similar to that for the United States east coast, about 1–2 mm/year (Peterson and others, 1984, fig. 6; Phipps and Peterson, 1989). However, small (less than 1.0 m), short-term (10–500 years), nontectonic oscillations in regional sea level, combined with changes in local sediment influx and irregular local sediment compaction (Kaye and Barghoorn, 1964), cannot be ruled out as the cause of some peat-mud couplets (fig. 29, sequence *C*). Coseismic subsidence can only be inferred where there is evidence of a sudden, substantial change in water depth across the upper contact of an uneroded peaty soil.

The inability to rule out small regional oscillations in the rate of sea-level rise casts uncertainty on the suggestion that some gradual contacts in marsh sequences in northwestern Oregon were produced by slow accumulation of tectonic strain (Peterson and Darienzo, 1988a; Peterson, 1989; Darienzo and Peterson, 1990). Current models of seismic-strain accumulation, release, and recovery (for example, Savage, 1983; Thatcher, 1984), make a tectonic mechanism for the origin of gradual contacts plausible. However, it is difficult to distinguish the lithology in marsh cores or outcrops resulting from these gradual, tectonically induced changes in regional uplift rate from the lithology resulting from gradual, nontectonic changes in the rate of sea-level rise.

REGIONAL DIFFERENCES IN LATE HOLOCENE TIDAL–MARSH SEQUENCES IN OREGON

Studies of late Holocene tidal-marsh stratigraphy in Oregon and Washington began with Darienzo's (1987) initial field work in 1985 at Netarts Bay (fig. 27). However, most projects are still in progress and only the Netarts Bay work has been published as a full-length paper (Darienzo and Peterson, 1990). Reconnaissance investigations have been made in most of the 27 estuaries along the Oregon and Washington coasts, but detailed work has been completed in fewer than half. Despite the preliminary nature of the interpretations of sequences in many estuaries, there appear to be significant differences in the character of marsh stratigraphic sequences along the Oregon coast.

NORTHWESTERN OREGON

Studies at Netarts Bay (Peterson and Darienzo, 1988a; Peterson and others, 1988; Darienzo and Peterson, 1990) and at the Nehalem River and Salmon River estuaries (fig. 27) (Grant, 1988, 1989) show that late Holocene estuarine sequences in northwestern Oregon contain multiple (3–5) widespread buried tidal-marsh and some spruce-swamp soils abruptly overlain by intertidal muds and, in some places, sand beds. In a reconnaissance survey at the Nestucca River estuary, Peterson and Darienzo (1988a) also found three to five buried peaty soils. The peat-mud couplets in northwestern Oregon are similar to those studied by B.F. Atwater in southwestern Washington, but the peaty horizons are thicker (0.2–1 m) and are separated by thinner intervals of mud (0.3–1.5 m). Stratigraphic relations are more difficult to document in Oregon because the height of tidal outcrops is lower and outcrops are less extensive than in southwestern Washington. Darienzo and Peterson (1990) estimated that the peat-mud couplets at Netarts Bay each represent 1–1.5 m of sudden coseismic subsidence. Thus, similarities in marsh stratigraphy in northwestern Oregon and southwestern Washington suggest recurrent coseismic subsidence of regional (greater than 200 km) extent (Grant, 1989; Darienzo and Peterson, 1990).

CENTRAL OREGON

Few details of marsh-stratigraphy studies at estuaries along the central Oregon coast have been published. Peterson and Darienzo (1988b) reported three to five buried marsh surfaces in the upper 5 m of cores from the Siletz River estuary (fig. 27). More extensive work at the Alsea River estuary showed 3–10 peaty marsh soils in cores 4–7 m deep (Peterson and Darienzo, 1988a, this volume; Darienzo, 1989). Most of the buried peaty soils at Alsea Bay have sharp upper contacts and gradational lower contacts, but peaty units in the upper 2.5 m of most cores are separated by thin (0.02–0.4 m) intervals of mud (fig. 30, core AB8). Buried peaty soils in the lower parts of the cores are separated by greater thicknesses of mud (0.4–1.8 m), similar to the peat-mud couplets in northwestern Oregon. Low outcrops and transects of cores show that many stratigraphic units can be correlated for hundreds of meters across the marsh. Sandy capping beds are less well developed on the buried peaty soils in the fluvially influenced estuaries of the Siletz and Alsea Rivers than they are in the more tidally influenced estuaries such as Netarts Bay (Peterson and Darienzo, 1988a). However, distinctive landward-thinning, sandy capping beds on the peat units in the western Alsea River marshes, combined with the repetitive, abrupt upper contacts of the peats, led Peterson and Darienzo (this volume) to conclude that the contacts were produced by coseismic subsidence accompanied by tsunamis. Based on changes in sediment lithology across the abrupt peat-mud contacts, the amount of subsidence during each event was estimated to be 0.5–1.0 m, less than that estimated for events in northwestern Oregon (Darienzo, 1989; Peterson and Darienzo, this volume).

We found a different type of marsh stratigraphic sequence preserved in the Siuslaw River estuary about 50 km to the south of Alsea Bay (fig. 27). About 3.5–4.0 m of

continuous, uniform tidal-marsh peat overlies tidal sand and mud at an inlet on the south side of the river (fig. 30, core SI–09); 3 km to the north, at the mouth of the North Fork of the Siuslaw River, about 4 m of tidal-marsh peat overlies 3 m of brackish or freshwater peat. The thickness of the tidal-marsh peats and several ^{14}C ages show that the upward growth of the marsh surface was able to keep up with rising sea level during a time span of 2,000 years (fig. 29, sequence *A*). Reconnaissance coring upstream of the sites with thick peat showed interbedded peats (0.05–0.3 m thick) and muds (0.01–0.5 m thick), but contacts are mostly gradational; these contacts suggest gradual rather than sudden submergence. Thus, there may have been gradual changes in the rate of sea-level rise at the Siuslaw River estuary, but the thick peats indicate no significant (more than 0.3–0.5 m), sudden changes in sea level.

Although the types of marsh stratigraphic sequences in the Siuslaw and Alsea River cores differ significantly, the difference is less distinct than the differences between sequences in northwestern Oregon and the Siuslaw River. Perhaps a few of the most gradual contacts in the upper parts of the Alsea Bay cores correlate with some of the subtle, gradual lithologic changes in the thick peats in our cores from the Siuslaw River. If so, we cannot rule out a nontectonic origin for these lithologic changes because they represent smaller water-level changes (probably less than 0.3 m) and are much less abrupt than lithologic changes observed in similar sequences on nontectonically active coasts. Tectonic and nontectonic processes may be producing identical small couplets along the Oregon coast. Present methods of stratigraphic analysis may not be capable of distinguishing between small tectonic components of sea-level change and small oscillations in sea level and sediment input.

SOUTHERN OREGON

South of the Siuslaw River, reconnaissance coring at many sites in the Umpqua River, Coos Bay, and Coquille River estuaries (fig. 27) by Nelson (1987, 1988), Peterson and Darienzo (1989), and Darienzo (1989) showed no consistent regional pattern of multiple abruptly buried peaty soils like those found in northwestern Oregon. Many sequences have a single abruptly buried soil 5–50 cm thick at 0.8–1.5 m depth; the soil at many sites was apparently submerged suddenly and at others more gradually. An outcrop along the Coquille River exposes such a buried soil, which has the trunks of a few small spruce trees rooted in it and is very similar to buried soils in southwestern Washington. This peaty soil is thin (0.05 m), but a possibly correlative soil at North Slough, in northern Coos Bay, is much thicker (0.5 m) and resembles the thick tidal-marsh peat found at the Siuslaw River. The thickness, depth, and organic material

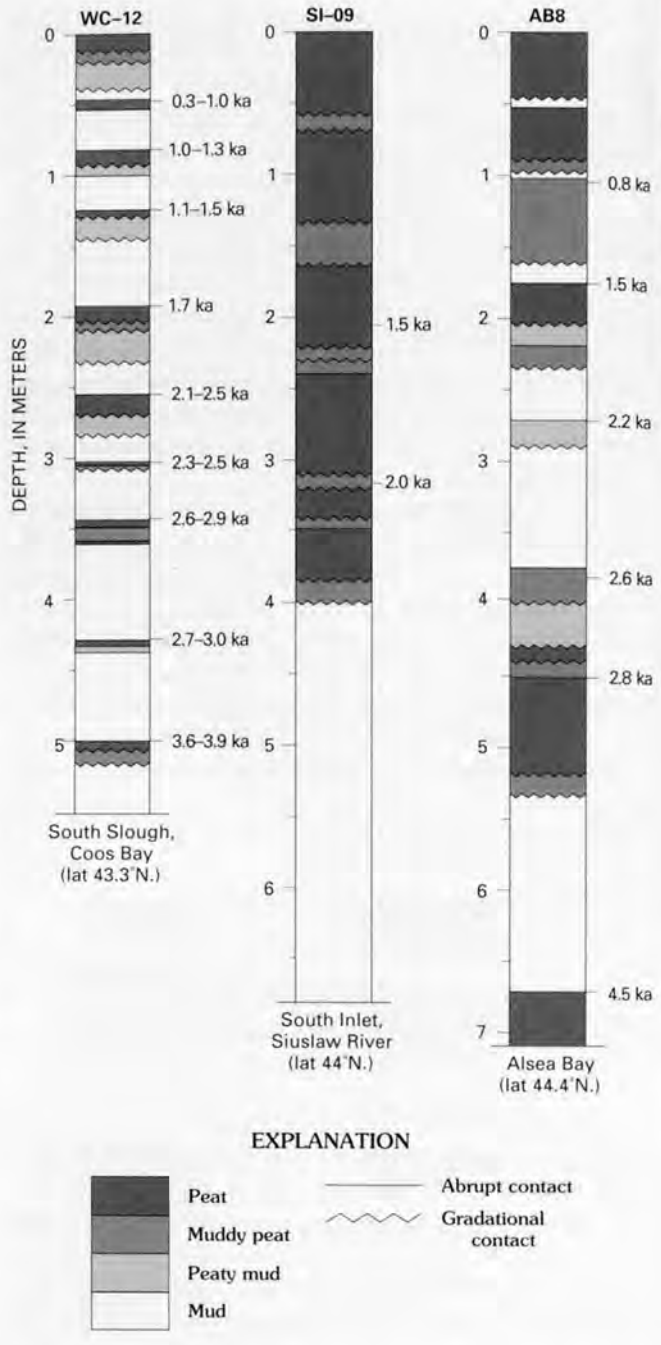

Figure 30. Comparison of typical cores from tidal-marsh sequences at three sites along the south-central Oregon coast. Age estimates for different levels in the cores are based on unpublished ^{14}C ages from these or nearby cores. Core WC–12 contains nine abruptly buried peaty soils, some of which may record coseismic subsidence during movements on local structures. The thick peat in core SI–09 suggests that no sudden changes in relative sea level have occurred since 2.0 ka. The abrupt contacts at the top of peaty soils in core AB8 have been interpreted by Peterson and Darienzo (this volume) as marking coseismic subsidence events of regional extent (0.5–1 m subsidence).

content of uncommon, deeper (greater than 1.5 m depth) peaty soils in the Coos Bay region is highly variable; some soils have abrupt upper contacts and others do not. However, multiple buried peats are rarely found more than 5–10 m from valley side slopes, and few marshes appear to have been as extensive in the past 3,000 years as they are today.

An exception to the lack of widespread, multiple peat-mud couplets in the Coos Bay region is at South Slough (fig. 27), which occupies the axis of an actively deforming north-trending syncline in western Coos Bay. Coring in a small marsh at the south end of the slough revealed as many as 10 buried tidal-marsh surfaces in cores 5–8 m long (fig. 30, core WC–12). At least four of the buried surfaces can be traced in cores across the inlet. Based on lithology, unit thickness, and preliminary foraminiferal and diatom data (A.R. Nelson, A.E. Jennings, and Kaoru Kashima, unpub. data, 1989), these couplets represent about 0.5 m of sudden submergence followed by deposition of 0.3–0.5 m of intertidal sediment. A core from Day Creek, near the middle of South Slough, penetrated a similar sequence of eight buried peaty soils (Peterson and Darienzo, 1989), suggesting about 0.5 m of submergence during these events. Reconnaissance coring by A.R. Nelson (unpub. data, 1988) at other sites in the western part of South Slough showed two to four abruptly buried peats, two of which are capped by thin beds of silty sand.

Nelson (1987), Peterson and Darienzo (1989), Peterson (1989), McInelly and Kelsey (1990), and McInelly and others (1989) suggested that at least some of the submergence events marked by the buried peaty soils at South Slough are the result of coseismic displacement on local structures. Mapping and dating of Pleistocene marine terraces and underlying structures in the Coos Bay region by McInelly and Kelsey (1990) showed that the South Slough syncline is being deformed but that the style of deformation in this region is more complex than previously assumed by Adams (1984). McInelly and Kelsey (1990) have also dated tree stumps in the intertidal zone adjacent to flexure-slip faults within the South Slough syncline, indicating Holocene displacements of these structures. Thus, some of the abruptly buried marsh surfaces in South Slough are probably the result of coseismic displacements due to folding or faulting of the syncline. These displacements are small (about 0.5 m) and cannot easily be correlated with the few buried marsh surfaces found elsewhere in the Coos Bay area.

South of Cape Blanco, the only sizable estuaries in southernmost Oregon are at the mouths of the high-gradient Rogue and Chetco Rivers (fig. 27). Sediments in these two estuaries are predominantly gravel and sand, and only small areas of marsh fringe the rivers. The lack of quiet-water intertidal mud in these estuaries indicates little chance for a well-preserved, unambiguous stratigraphic record of late Holocene sea-level changes.

GREAT-EARTHQUAKE RECURRENCE AND THE LIMITATIONS OF ^{14}C DATING

Until the advent of recent coastal field studies, estimates of the recurrence of great earthquakes in the CSZ were limited to average values, largely based on analogies with other subduction zones. Heaton and Kanamori (1984) used empirical and theoretical relations to calculate an average earthquake of M_w 8.3±0.5 for the Juan de Fuca plate; such an earthquake could recur every 126 to 420 years depending on the ratio of aseismic to seismic slip (Kanamori and Astiz, 1985). Heaton and Hartzell (1986) compared the Juan de Fuca plate to other subduction zones in south-central Chile, southwestern Japan, and southern Alaska. Using these three analogous subduction zones and the convergence rate of the Juan de Fuca plate, they suggested great earthquake recurrences for the Juan de Fuca plate of 250–500 years, 100–250 years, and possibly 1,000 years, respectively. In a study of turbidite deposition on the continental shelf, Adams (1989, 1990) inferred a fairly uniform recurrence of 590±170 years for major earthquakes. However, this study left open questions about the size and location of earthquake sources and whether all turbidites on the shelf were earthquake generated. For example, Thatcher's (1990) recent analysis of great earthquakes in other circum-Pacific subduction zones suggests recurrence of plate-interface earthquakes in the CSZ might be very nonuniform.

A key assumption in initial paleoseismic studies in the Pacific Northwest was that conventional radiocarbon dating could provide fairly accurate estimates of great-earthquake recurrence through analysis of organic materials at or just above the upper contact of abruptly buried peaty soils. It also was hoped that the ages of buried peats were separated by enough time to allow the soils to be correlated from one estuary to another on the basis of conventional radiocarbon dating. However, studies with more than a hundred conventional ^{14}C ages in Washington (Atwater, 1988c; Hull, 1988) and our comparative dating program in southern Oregon showed that conventional ^{14}C ages from the uppermost parts of buried wetland soils vary widely depending on the type of organic material analyzed and how it was prepared prior to analysis (Grant and others, 1989). For example, mean ages from identical splits of the same peat samples from Coos Bay sent to two different laboratories that use different pretreatment methods varied by 100–700 years. Detrital wood picked from some of these same peat samples varied from 100 years older to 1,000 years younger than ages on the bulk samples. More limited data for older peats shows similar variability.

These results indicate that, with the exception of tree trunks well rooted in peaty soils, conventional ^{14}C ages on most materials can only provide a general estimate

(±150–300 years) of the time of peat burial (Grant and others, 1989); most ages from the buried peaty soils are maximum estimates of the time of burial. The wide range in ages from the same peat layers also suggests that many buried peaty soils formed during time intervals of at least 200–1,000 years. Where time intervals between earthquakes are more than 1,000 years, or where multiple ages on different materials above and below the upper contact of peaty soils can be used to constrain the age of the surface of the soil, such as in some of Atwater's (1988c) sites, conventional ^{14}C ages may provide estimates of burial times that are precise enough to allow buried soils to be correlated. However, where the mean earthquake-recurrence interval is less than 500 years and high-quality tree-trunk samples are lacking (central and southern Oregon), conventional ^{14}C ages cannot be used to demonstrate correlations.

Despite these problems, samples from most of the soils inferred to have been buried during as many as 10 late Holocene coseismic events in the coastal Pacific Northwest have been dated by conventional ^{14}C methods (Grant and others, 1989). Atwater (1987, 1988c) collected a variety of materials from above and below the upper contacts of five of the youngest of eight buried wetland soils in southwestern Washington. Mean ^{14}C ages for the subsidence events inferred from these samples were about 0.3, 1.6, 1.7, 2.7, and 3.1 ka. An additional subsidence event about 1.0 ka was identified at the Waatch River estuary near the northwestern tip of Washington and at an inlet on the north side of the mouth of the Columbia River (Atwater, 1988c). Grant (1989) obtained mean ages of about 0.4, 1.0, and 1.6 ka from three buried soils along the Nehalem River and about 0.4 ka from the single buried soil exposed along the Salmon River. Darienzo and Peterson (1990) used peat ages on samples from six buried soils at Netarts Bay to suggest a synchrony of events in northwestern Oregon and Washington about 0.3–0.5, 1.0–1.3, 1.4–1.8, and 3.0–3.3 ka. At Alsea Bay in central Oregon, Peterson and Darienzo (this volume) also dated peat from 6 of 10 peaty soils that were buried within the past 5,000 years. Finally, A.R. Nelson (unpub. data, 1989) used 20 ages on peat and detrital wood from 9 buried soils in a core from the south end of South Slough in Coos Bay to infer times of peat burial at 0.3–1.0 ka, 1.0–1.3 ka, 1.1–1.5 ka, 1.7 ka, 2.1–2.5 ka, 2.3–2.5 ka, 2.6–2.9 ka, 2.7–3.0 ka, and 3.6–3.9 ka (fig. 5, core WC–12). C.D. Peterson and M.E. Darienzo (Geology Dept., Portland State University, unpub. data, 1989) obtained similar ages on six of eight buried soils in a core from central South Slough. But few of the ages from Washington and northwestern Oregon and none from central and southern Oregon are precise enough to allow correlation of most buried soils.

The conventional ^{14}C ages show that recurrence of submergence events at individual sites is nonuniform. Average recurrence intervals are in the range of 400–700 years, but the sites with many ages suggest recurrence intervals as small as 100–200 years and as large as 1,000–1,600 years.

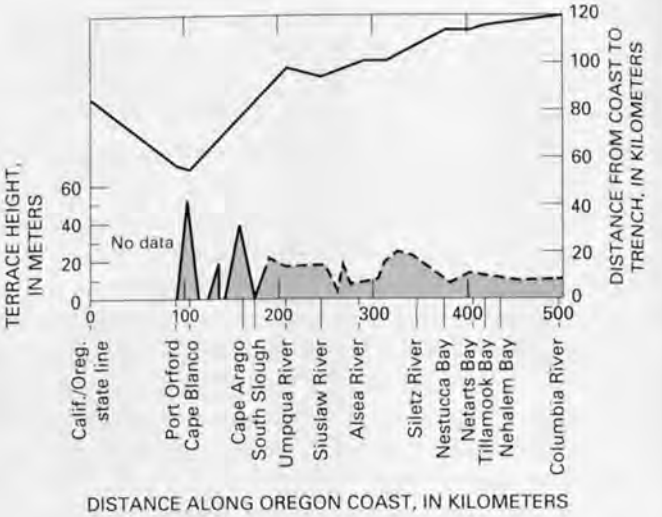

Figure 31. Relation between height of the lowest marine terrace and distance from the Oregon coast to the eastern edge of the Cascadia trench (base of the continental slope). The upper curve shows the distance from the coast to the trench (scale at right), as measured from Peterson and others (1986). The lower curve shows the present height (scale at left) of the lowest (80–125 ka) marine terrace along the Oregon coast between Port Orford and the Columbia River. Solid line elevations in the Cape Blanco-Cape Arago region are from the detailed mapping of Kelsey (1990) and McInelly and Kelsey (1990). Dashed line elevations between South Slough and the Columbia River are derived from West and McCrumb (1988a). Terraces are poorly preserved along much of the Oregon coast, so terrace correlations north of the South Slough area are tentative.

Most ages on the youngest buried soil suggest the latest event occurred during the interval 0.1–0.5 ka, but wide fluctuations in ^{14}C flux in the upper atmosphere during this period (Stuiver and Pearson, 1986) and the large errors on ages from peaty soils make it impossible to determine whether or not the youngest soil was buried about the same time everywhere (Grant and others, 1989).

Tree-ring studies, such as those by Yamaguchi (1988), are the most accurate method of dating subsidence events. Maximum-limiting calendar ages of A.D. 1618–1687 constrain the timing of the most recent subsidence event at four sites that span 100 km of the southwestern Washington coast, but some interpretive problems remain (Yamaguchi and others, 1989b). Unfortunately, this method can only be applied to those few sites with well-preserved fossil redcedar trees, and such sites have been found only in southwestern Washington. High-precision conventional ^{14}C analysis (Pearson, 1979) of large samples of less than 10 rings from large buttress roots (near the base of the trunk) may result in the dating of 1 or 2 earlier events to within a few decades in northwestern Oregon and southwestern Washington where spruce trunks rooted in buried peaty soils are common (Atwater, 1988c, table 2). These are probably the best available methods for testing the synchrony of individual subsidence events along substantial parts of the Pacific Northwest coast.

MIDDLE AND LATE QUATERNARY DEFORMATION

Determination of rates and styles of long-term Quaternary deformation is critical in interpreting evidence of Holocene seismic or aseismic deformation in active subduction zones (Bloom, 1980). Studies of raised marine terraces are the most traditional type of geologic investigation of Quaternary deformation along tectonically active coastlines. Other types of geologic investigations include examination of fluvial-terrace sequences and analysis of regional patterns of river and drainage-basin morphology (Wells and others, 1988; Rhea, 1993; Merritts and Vincent, 1989). These investigations can yield information about the cumulative effects of Quaternary deformation, which may help determine whether a coastal region has been affected by earthquakes of regional or more local extent. Quaternary deformation is commonly quantified through analysis of uplift rates, identification of active structures, and geodetic and geologic analysis of regional tilting. The use of marine and fluvial terraces to describe the nature of these types of Quaternary deformation along the CSZ is discussed below.

UPLIFT RATES

Uplifted marine terraces are found along many tectonically active coastlines. Most Pleistocene marine terraces represent ancient shorelines that were formed during sea-level high stands associated with interglacial periods and subsequent tectonic uplift (Lajoie, 1986). For this reason, terrace studies have been conducted along many tectonically active coastlines around the world (Berryman, 1987); of particular interest are studies in regions undergoing active subduction such as Japan (Yonekura and Ota, 1986), the New Hebrides Islands in the South Pacific (Taylor and others, 1985), and Chile (Hsu and others, 1989). Analysis of uplift rates in other active areas has helped to define the nature of tectonic deformation associated with the CSZ.

Calculation of uplift rates from marine-terrace data requires that the age and highest present elevation of the wave-cut platform be known, as well as the elevation of sea level at the time the terrace was formed. The elevation of a former sea level is determined by comparing the age of the platform to age-elevation curves of sea level derived from well-studied areas such as New Guinea, California, and Japan (Lajoie, 1986). The present elevation of the terrace is then corrected for the elevation of sea level at the time the terrace was formed and for any tilting that may have occurred since the terrace formed. The resulting amount of tectonic uplift can then be used with the age of the terrace to calculate the net rate of uplift since the terrace was formed. Uplift rates are commonly compared from place to place along the coast, and to other active coasts, to identify patterns of regional deformation (Ota and Yoshikawa, 1978).

Pleistocene marine terraces are preserved discontinuously along the Oregon and Washington coasts (fig. 31) but are best developed and have been mapped and dated in the most detail near Cape Blanco and Cape Arago in southern Oregon (Griggs, 1945; Kennedy and others, 1982; Adams, 1984; Golder Associates, 1986; West and McCrumb, 1988a; Kelsey, 1990; McInelly and Kelsey, 1990). A recent detailed study by Muhs and others (1990) used new uranium-series ages and amino-acid and oxygen-isotope data to correlate and date the two lowest terraces at Cape Blanco. Their results indicate uplift rates of about 0.85–1.25 m per thousand years for the 80-ka Cape Blanco terrace and about 0.8–1.5 m per thousand years for the 105-ka Pioneer terrace. These uplift rates are lower than those reported by earlier studies (West and McCrumb, 1988a), but they are still the highest rates reported from marine terraces along the Oregon and Washington coasts.

Muhs and others (1990) also compared their new uplift rates with rates from well-dated terrace sequences at other active subduction zones and concluded that uplift rates at Cape Blanco were not unusually high or low. They also found no clear relation between the style of plate convergence and uplift rates of marine-terrace sequences in other subduction zones. These conclusions conflict with those of West and McCrumb (1988a), who used such a comparison to infer that large plate-interface earthquakes had probably not occurred on the CSZ in late Holocene time.

In addition to marine-terrace studies, we examined fluvial terraces because these features can be useful for measuring incision rates at considerable distances from the coast. In this approach, we consider incision rates to be an indirect measure of uplift rates. Our studies of stream incision along the Siletz, Siuslaw, Smith, and Umpqua Rivers (fig. 27) indicate rates of regional uplift of 0.2–0.8 m per thousand years in the central Oregon Coast Range (fig. 32). These rates are based on terrace heights measured from the modern river level to the stream-cut bedrock bench (strath) underlying each terrace. Terrace ages are derived from radiocarbon dating of Holocene and latest Pleistocene terrace sediments and from thermoluminescence (TL) dating of older terrace deposits. The use of TL dating is relatively new, and our dates are the first such analyses of fluvial sediments in the Pacific Northwest.

DEFORMATION OF QUATERNARY STRUCTURES

The new marine-terrace ages of Muhs and others (1990) were used by McInelly and Kelsey (1990) and Kelsey (1990) to evaluate the amount and style of deformation of specific structures near Cape Arago and Cape Blanco (fig. 31). Kelsey (1990) mapped a prominent west-trending fold (the Cape Blanco anticline) that deforms late Pleistocene marine terraces at Cape Blanco. The uplift rates determined by

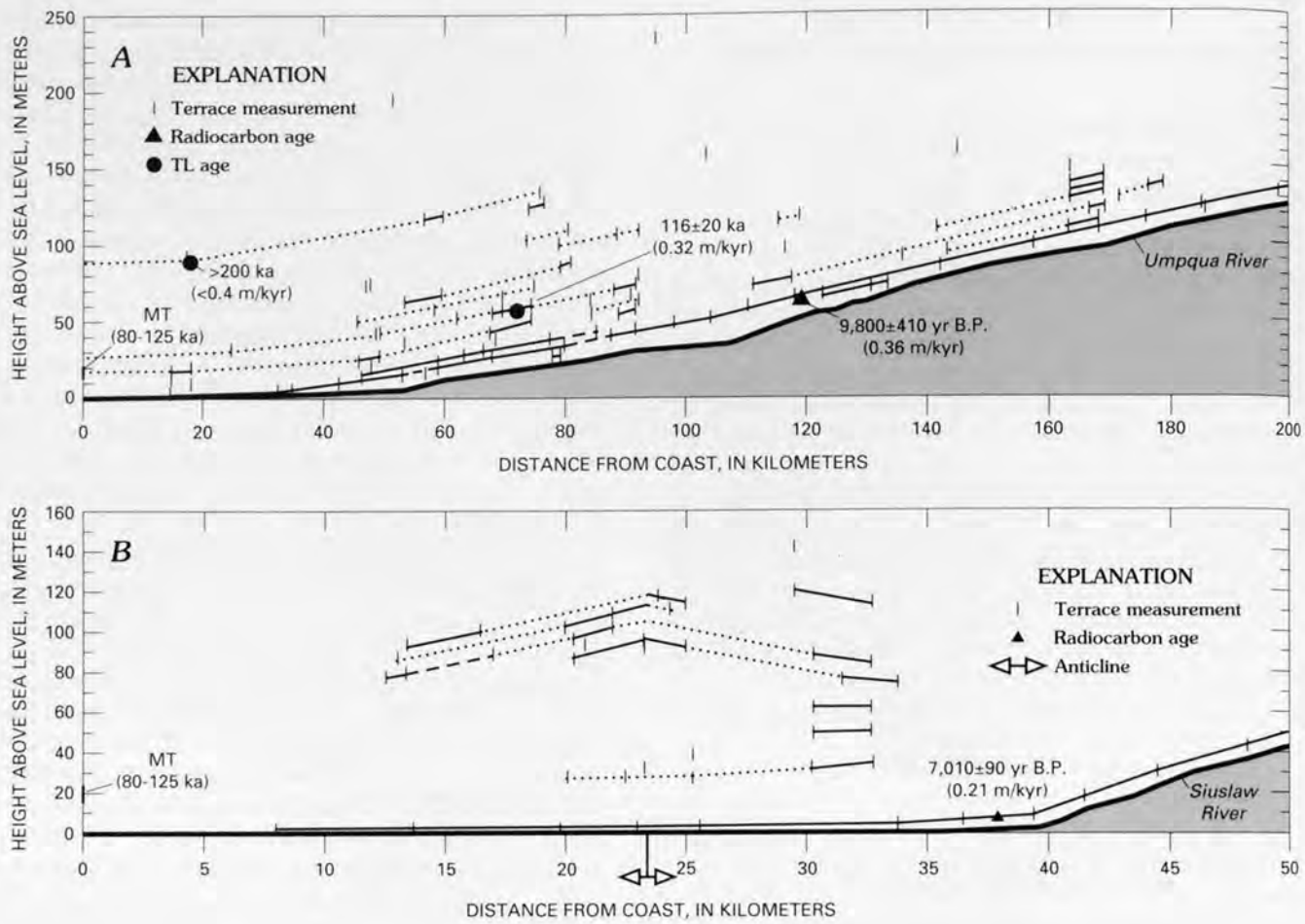

Figure 32. Longitudinal profiles of terraces along the Umpqua and Siuslaw Rivers, central Oregon Coast Range. Heavier solid lines are elevations of the Umpqua and Siuslaw Rivers, and lighter solid lines connect terraces that can be physically correlated; dashed lines connect terraces that are probably correlative, and dotted lines are speculative correlations. Terrace heights may have vertical errors of ±5 m for the higher terraces and ±2 m for the lower terraces. Radiocarbon ages are located with triangles and labeled "yr B.P." (radiocarbon years before 1950); thermoluminescence (TL) ages are located with solid circles and labeled "ka" (thousands of years ago). For comparison, the heights of the lowest marine terraces, labeled "MT," are marked near the mouths of the rivers (heights from Golder Associates, 1986). These marine terraces have been tentatively correlated with one of the oxygen-isotope stage-5 marine terraces near Cape Blanco, Oregon, which have been dated by Muhs and others (1990) and Kelsey (1990) at 80–125 ka. Incision rates, labeled "m/kyr" (meters per thousand years), are calculated from the age determinations and the height of the bedrock benches underlying the fluvial terraces. *A*, longitudinal profiles of terraces along the Umpqua River. Close examination of the nearly continuous early Holocene terrace revealed no evidence of latest Pleistocene folding or faulting along the Umpqua River. *B*, longitudinal profile of terraces along the lower part of the Siuslaw River. Although no age data has been obtained from the pre-Holocene terraces, their relations to the position of the lowest marine terrace and the presence of very well developed soils on the terrace deposits indicate that they were probably formed more than 100 ka. The terrace remnants are clearly modified by an anticline (double arrow symbol below graph) that is present in the underlying Eocene bedrock. We cannot determine if terraces below an elevation of about 50 m have been folded because they are poorly preserved below this height. The nearly continuous early Holocene terrace appears to be undeformed. The large area affected by the folding (more than 20 km wide) indicates that these types of structures should be easy to detect on terrace profiles from other Coast Range rivers.

Muhs and others (1990) in this area were measured along the axis of this anticline. The location of a Holocene beach berm of possible coseismic origin on the south flank of the anticline may indicate that the fold has been active in the late Holocene. Kelsey (1990) also noted several faults that offset Pleistocene marine-terrace surfaces near Cape Blanco, but the apparent association of these structures with major terrane-bounding suture zones may limit their usefulness as indicators of modern stress conditions. Similar studies in the region between Cape Arago and South Slough by McInelly and Kelsey (1990) identified several northwest-trending folds and flexural-slip and high-angle faults. Stratigraphic evidence from marshes in the South Slough syncline may indicate repeated late Holocene coseismic folding and flexural-slip faulting events in this region. The results of these studies indicate that crustal shortening along the southern Oregon coast is the result, at least in part, of the growth of west- and northwest-trending folds and flexure-slip and high-angle faults and is not simply a result of regional uplift.

In our study of fluvial-terrace sequences along the central Oregon coast, we examined a north-trending anticline (previously described by Adams, 1984; and Personius, 1993) that deformed Quaternary deposits along the Siuslaw River (figs. 27 and 32*B*), but we found no evidence of folds or faults with demonstrated Holocene or latest Pleistocene movement. Although we may have missed a few structures, especially where terraces are poorly preserved or where deformation rates are low, the general lack of deformation of local structures indicates that the seismotectonic setting of the central Oregon coast is different from the setting of the Cape Blanco-Cape Arago-South Slough region in southern Oregon.

The recent studies of marine and fluvial terraces summarized above indicate that in the southern part of the CSZ, Quaternary deformation has been dominated by activity of local structures rather than by regional uplift. As suggested by Muhs and others (1990), deformation of local structures may be the most important reason that uplift rates can vary widely along active subduction zones. Variable uplift rates in Oregon (fig. 31) and elsewhere may reflect deformation of local folds and faults rather than changes in the style of plate convergence.

The only other place where onshore Quaternary structures in the forearc of the CSZ have been described in detail are in northern California (Kelsey and Carver, 1988; Carver and others, 1989; Clark and Carver, 1992) near the southern end of the CSZ. Although other small Quaternary structures have been described at scattered locations along the Oregon and Washington coasts (Adams, 1984; McCrory, 1992; Ticknor and others, 1992; Wells and others, 1992), the active structures in the Cape Blanco-Cape Arago region mark a distinct change in style of Quaternary deformation along the CSZ. This change in structural style, near lat 43.5°N., is probably related in part to the central coast's greater distance from the trench (figs. 27 and 31). Maps of latest Quaternary offshore deformation (Clarke and others, 1985; Peterson and others, 1986; Snavely, 1988; Goldfinger and others, 1992) show a fold and thrust belt that appears to trend onshore just north of Coos Bay (Darienzo, 1989; Peterson and Darienzo, 1989). The Quaternary anticline along the Siuslaw River may mark the relatively inactive easternmost part of this fold and thrust belt. Alternatively, the increased structural complexity near Coos Bay may be related to a change in plate-interface geometry or segmentation of the Juan de Fuca plate.

REGIONAL TILTING

Landward-tilted terraces have commonly been observed along active subduction zones (Ota, 1986), so geodetic and geologic evidence for regional tilting has also been used as evidence for subduction at the CSZ (Reilinger and Adams 1982; Adams, 1984; Vincent and others, 1989; Mitchell and others, 1991). Reilinger and Adams (1982) noted that their geodetically measured short-term rates of east-west landward tilt of the Oregon coast were similar to long-term rates of landward tilt calculated from reconnaissance information on marine terraces along the Oregon coast. They interpreted the agreement between long and short-term rates as evidence of aseismic subduction. Adams (1984) discussed this agreement in more detail and calculated crustal shortening rates for the Oregon and Washington coasts using geodetic and limited (and in some places conflicting) geologic tilt data. He noted that the shortening rates suggested coupling of the plate interface during the Pleistocene but concluded that there was insufficient evidence to determine whether present-day subduction was seismic or aseismic. More recent marine-terrace mapping by Kelsey (1990) and McInelly and Kelsey (1990) indicated that landward tilting of marine terraces discussed by Adams (1984) in the Cape Blanco and Cape Arago regions is attributable to deformation of local folds rather than to regional deformation. At Cape Blanco, only the three lowest terraces tilt landward; two higher terraces tilt seaward (Kelsey, 1990). Similarly, our work on fluvial terraces in the Oregon Coast Range has uncovered no evidence of a regional pattern of either landward or seaward tilting as suggested by Adams (1984) but instead indicates uniform east-west uplift of the Coast Range (fig. 32*A*) complicated by movement of local structures such as the anticline on the Siuslaw River (fig. 32*B*). Therefore, shortening across structures in the North America plate in southern Oregon indicates continuing subduction along the CSZ, but terrace tilting and the agreement between geologically and geodetically determined east-west tilt rates in Oregon are not evidence for either seismic or aseismic slip on the plate interface. More recently, Vincent and others (1989) and Mitchell and others (1991) interpreted new geodetic evidence of long-wavelength north-south deformation along the Oregon coast. Repeated leveling surveys between 1941 and 1988 show a broad trough centered between the Yaquina and Tillamook estuaries, Oregon, and upward tilts southward to the Coquille River and northward to the Columbia River. Vincent and others (1989) interpreted these elevation changes as evidence of interseismic deformation due to strong interplate coupling beneath the Yaquina-Tillamook region.

POTENTIAL MAGNITUDE AND RECURRENCE OF PLATE–INTERFACE EARTHQUAKES IN THE CASCADIA SUBDUCTION ZONE

Although the interpretation and implications of the emerging paleoseismic record in the CSZ continue to be debated, the seismic histories of subduction zones that have some characteristics in common with the CSZ limit the probable magnitude and recurrence of future earthquakes in the zone. The results of recent geologic studies suggest some additional constraints on postulated earthquake rupture histories, but several different hypotheses of probable magnitude and rupture extent are permitted by the available preliminary data.

CONSTRAINTS BASED ON OTHER SUBDUCTION ZONES

Several recent geophysical studies (Heaton and Hartzell, 1987; Rogers, 1988; Spence, 1989) concluded that parts of the plate interface in the CSZ are locked and that there is a significant potential for great earthquakes of M_w 7¾–9½. Because no plate-interface earthquakes have been recorded instrumentally in the central CSZ, the magnitude of postulated future great earthquakes seems to depend mostly on the modern analog subduction zone most favored by any particular study. Some subduction zones similar to the CSZ, such as in southwestern Mexico, are characterized by earthquakes of M_w 7¼–8¼ that rupture 60–250 km of the zone (Singh and others, 1981; Nishenko and Singh, 1987). Other zones, however, have had much larger earthquakes, such as the 1960 south-central Chile earthquake of M_w 9.5 that ruptured 900 km of the plate interface (Plafker and Savage, 1970; Nishenko, 1985; Cifuentes, 1989). Studies that propose south-central Chile as a good analogy for the CSZ argue that an M_w 9+ earthquake should be seriously considered (Heaton and Hartzell, 1986; Rogers, 1988). Heaton and Hartzell (1986) also suggested that the largest earthquakes in the Nankai Trough, Japan, or in the subduction zone in western Colombia (M_w 8.5–8.8) may be the best analogies for CSZ earthquakes. In contrast, Kanamori (1986), Rogers (1988), and Spence (1989) suggested that the 1932 Jalisco, Mexico, earthquake (M_w 8.2) on the Rivera plate interface may be the closest analog for plate-interface earthquakes in the CSZ. But Heaton and Hartzell (1986) stated that the low level of modern seismicity at the CSZ ruled out an analogy with southwestern Mexico and other similar subduction zones. Studies of empirical correlations of subduction-zone parameters and modern analogs are limited, however, because there are significant differences between the subduction setting at the CSZ and all suggested analog source zones (Kanamori and Astiz, 1985; Heaton and Hartzell, 1986; Spence, 1989).

In fact, the historical record of subduction-zone earthquakes shows that, although the maximum magnitude of thrust earthquakes depends on plate parameters (Ruff, 1989), earthquakes of variable magnitude typify most subduction zones (Thatcher, 1990). For example, in the Colombian subduction zone, the M_w 8.8 earthquake of 1906 was followed by three M_w 7.6–8.2 earthquakes about 20 years apart (Kanamori and McNally, 1982). Other examples of variable magnitudes are compiled in Nishenko (1989). Thatcher (1989, 1990) argued that great plate-interface earthquakes along segments of subduction zones occur in cycles and that although the magnitude of earthquakes differs from cycle to cycle, the duration of each seismic cycle is similar. Of more importance for evaluating earthquake potential, the earthquakes within each cycle seem clustered near the end of the cycle and tend to occur with increasing rupture length and magnitude in the latter part of the cycle. Reviews by Sykes and Quitmeyer (1981), Kanamori (1986), Ruff (1989), and others show that the majority of subduction zones are characterized by earthquakes closer to M_w 8 than to M_w 9. If these generalizations developed from other subducting circum-Pacific margins apply to the CSZ, earthquakes near M_w 8 and M_w 9 might both be possible, but M_w 8 earthquakes would be much more common than M_w 9 earthquakes and they would tend to cluster near the end of the seismic cycle.

Although the magnitude of plate-interface earthquakes may vary considerably, the location of ruptures along a subduction zone is not random (Thatcher, 1990). Historical (for example, Ando, 1975) and geologic data (for example, Wells and others, 1988; Berryman and others, 1989; Taylor and others, 1990), as well as instrumental records (Sykes and Quitmeyer, 1981), show that subduction zones are segmented by ruptures that tend to fill seismic gaps (Ruff, 1989). Several seismic cycles may be required to fill some gaps, and this timing suggests that asperities (zones of high shear strength on the plate interface) may control the size, timing, and starting points of ruptures (Kanamori, 1986; Ruff, 1989; Thatcher, 1989). Where asperities influence the extent of ruptures through several seismic cycles, the subduction zone is segmented. Identification of potential segment boundaries along a subduction zone is of fundamental importance because the length of segments, their relation to the structural geometry of the convergence zone, and their relation to the recent history of ruptures along the zone, set limits on the possible lateral and down-dip extent of the most probable plate-interface earthquakes.

Although segment boundaries are commonly associated with weak zones between asperities, major zones of faulting or other deformation that divide the subducting plate into subplates also tend to limit the extent of ruptures on the plate interface (Ruff, 1989). At the CSZ, faults dividing the northern and southern ends of the Juan de Fuca plate into subplates (fig. 26) are likely locations for segment boundaries (Spence, 1989). Changes in lower plate dip or the position of the bend within a subducting plate must also have a major effect on the

lateral and down-dip extent of plate-interface ruptures (Kanamori, 1986; Spence, 1987); such changes in the CSZ have been identified at lat 47° and 49°N. (Riddihough, 1984; Michaelson and Weaver, 1986). Hughes and others (1980) noted variations in the alignment and type of volcanoes in the Cascade Range that can be projected to most of the possible segment boundaries (shown by large open arrows in fig. 26). Characteristic seismicity patterns may also serve to identify segments with differing states of stress.

Finally, the instrumental record of earthquakes in subduction zones shows that the rupture process is very complex (Savage, 1989; Thatcher, 1990) and that simple models of fault segmentation and earthquake recurrence may be of limited use in accurately forecasting great earthquakes. Because the physical characteristics of the plate interface and the mechanical properties of asperities within fault segments differ, magnitude and recurrence characteristics of earthquakes during earthquake cycles differ from segment to segment (see Taylor and others, 1990). However, segments may persist on widely ranging time scales. A major fault zone between two subplates might always halt propagating ruptures, whereas a diffuse zone of weakness between asperities or an asperity of moderate size might limit rupture extent only one quarter of the time (Schwartz and Sibson, 1989). For this reason, even for subduction zones that have been characterized by historical earthquakes of relatively moderate magnitude, the rupture of two to five segments in a M_w 9 earthquake cannot be precluded (Heaton and Hartzell, 1986).

CONSTRAINTS BASED ON RECENT GEOLOGIC STUDIES IN OREGON

Although most coastal paleoseismologists now agree that M_w 8+ plate-interface earthquakes have occurred during the late Holocene in the northern half of the Juan de Fuca plate (Atwater, 1987; Grant, 1989; Peterson, 1989; Darienzo and Peterson, 1990; Peterson and Darienzo, this volume), discussions about future earthquakes in the CSZ tend to focus on one of two hypotheses for the recurrence and magnitude of late Holocene plate-interface earthquakes. In the first hypothesis, M_w 9+ earthquakes characterize the CSZ; those earthquakes were accompanied by ruptures that extended for more than 600 km along the Juan de Fuca plate interface and parts of adjacent subplates (fig. 28*A*). Based on analog great earthquakes in other subduction zones and the rate of plate convergence in the CSZ, the recurrence interval of these M_w 9+ earthquakes would be many hundreds of years. In the second hypothesis, the CSZ is segmented in a manner similar to that shown in figure 26, and ruptures of 100–250 km associated with M_w 7¾–8¼ earthquakes (fig. 28*D*) would occur much more frequently than larger earthquakes. Only rarely, perhaps near the end of a long earthquake cycle (Thatcher, 1989), would several segments rupture in an earthquake of about M_w 9 (fig. 28*C*). If the second hypothesis is correct, earthquake recurrence in the CSZ is apparently nonuniform because there have been no great earthquakes on the plate interface in the past 150–200 years. As discussed previously, there are distinct differences in the tidal-marsh sequences attributed to coseismic deformation along the Oregon coast (Peterson, 1989; Darienzo, 1989). These differences are best explained by a segmented subduction zone (most earthquakes less than M_w 8½) rather than an unsegmented zone, but present data do not rule out earthquakes larger than M_w 8½.

The segmented-zone hypothesis requires at least four segment boundaries. Likely segment boundaries for the CSZ (fig. 26) were suggested by Hughes and others (1980) using the distribution and alignment of different types of volcanoes in the Cascade Range and by Spence (1989) using the work of Riddihough (1984), Michaelson and Weaver (1986), and Weaver and Baker (1988). Lateral offsets of some north-south-trending structures in the upper plate on the continental shelf (Snavely, 1988) might also reflect segment boundaries. The independent motions of the Explorer and Gorda subplates show that their plate contacts mark segment boundaries near the northern and southern ends of the CSZ (Spence, 1988). Less certain are differences in seismicity rates within the subducting plates and differences in plate densities and dips in the north-central part of the zone near lat 49°, 48.5°, and 47°N. that may mark segment boundaries. The very low seismicity rate in the south-central part of the zone, our primary area of interest, makes identification of the properties of the subducting Juan de Fuca plate very difficult (for example, see Keach and others, 1989), but Spence (1989) suggested that the low seismicity rate between lat 45°N. and the Blanco fracture zone (lat 43°N.) might also characterize a separate segment of the CSZ.

A segment boundary in central Oregon between lat 44° and 45°N. (fig. 26) that would tend to limit the propagation of plate-interface ruptures is one possible explanation for changes in the types of marsh stratigraphic sequences that occur between northwestern and south-central Oregon. For example, the thick peat sequences in the Siuslaw River estuary may mark the southern extent of late Holocene plate-interface ruptures (figs. 28*B* and 28*D*). The coseismic movements inferred from marsh sequences decrease from as much as 2.7 m of subsidence estimated for some sites in southwestern Washington (Eileen Hemphill-Haley, U.S. Geological Survey, written commun., 1989) to the 0.5–1 m subsidence estimated by Peterson and Darienzo (this volume) in Alsea Bay. Thus, the Alsea Bay sequences may record the southernmost extent of plate-interface ruptures that are hundreds of kilometers long (fig. 28*B*) (Darienzo, 1989). Alternatively, the central Oregon coast may have had only relatively short ruptures (most less than 100–200 km) produced during moderate earthquakes (fig. 28*D*), perhaps with a cycle-ending earthquake of 250–300 km (see Thatcher, 1990). In this case, the size and recurrence of earthquakes in central Oregon would differ from those in northwestern Oregon, but

the Siuslaw River sequences would still mark the southern limit of the long, large-slip ruptures (greater than 0.5 m coseismic subsidence; fig. 28*D*).

An explanation for the variations in the types of marsh sequences that is consistent with the M_w 9 earthquake hypothesis discussed above can be related to the width and location of the zone of subsidence inferred to have been produced during repeated great (M_w 9+) earthquakes (Atwater, 1988b). If the western edge of the zone of subsidence for all these postulated great earthquakes was between Alsea Bay (107 km east of the trench) and the Siuslaw River estuary (104 km from the trench; figs. 27 and 28*A*), only the Alsea Bay sequences would be expected to show evidence of repeated coseismic subsidence. Of course, the length, width, and location of the zone of subsidence varies from earthquake to earthquake but it must always have been east of the Siuslaw River estuary, which shows no evidence of major coseismic-subsidence events.

The differences in the types of marsh records from the Siuslaw River and Alsea Bay sites suggest that these sites are probably on separate late Holocene segments of the CSZ. Both sites are about the same distance from the trench (fig. 27), and the ages of sediments in cores from both estuaries probably span at least the last two to five seismic cycles (2,000–3,000 years). Thus, most earthquakes recorded at Alsea Bay should have been recorded at the Siuslaw River if the ruptures on the plate interface during these earthquakes extended throughout this area. Possibly some long ruptures extended far south of the Siuslaw River (fig. 28*C*) but, if so, the zone of coseismic subsidence was inland of the coast and most of these long-rupture earthquakes were not recorded at Alsea Bay. Unfortunately, the width of the zone of subsidence and its distance from the trench during historic great earthquakes in other subduction zones are sufficiently variable (Atwater, 1988b; West and McCrumb, 1988b) that none of the possible rupture modes in figure 3 can be ruled out using arguments based on analogies with other subduction zones.

It also is unfortunate that stratigraphic studies of the marsh record may not be capable of conclusively distinguishing between the two segmentation hypotheses (figs. 28*A* and 28*D*). In central Oregon, estuaries with marshes of sufficient size to allow the extensive coring needed to document coseismic changes in sea level are spaced 28–50 km apart. Furthermore, in large parts of these estuaries, sequences consist mostly of sandy tidal-channel, eolian, and fluvial sediments in which the record of small sea-level changes is obscure. The size of these river-dominated estuaries (Peterson and others, 1984) and the distribution of their marshes also limits to less than 8 km the length of the east-west-trending zone over which evidence of sea-level changes can be identified. Thus, only four or five estuaries in central Oregon are likely to yield definitive data on coseismic changes in sea level. The distances of potential core sites in these estuaries from the CSZ trench do not differ enough to distinguish between the two segmentation hypotheses discussed above, and there are not enough widely spaced sites within each estuary to determine differences in the amount of coseismic subsidence in an east-west direction. Such differences might be used to better define the position of the zone of subsidence during past earthquakes.

In contrast to the northern and central Oregon coast, the earthquake record of the Coos Bay region appears to be a composite of regional and local earthquakes. Here, the active fold and thrust belt of the overriding plate is well documented by onshore (Kelsey, 1990; McInelly and Kelsey, 1990) and offshore studies (Clarke and others, 1985). Within this tectonic framework, we ascribe some of the multiple, abruptly buried marsh peats in the South Slough syncline to coseismic subsidence during local faulting and folding of the syncline or adjacent anticlines (McInelly and others, 1989; Peterson, 1989). Abrupt burial of some other peaty soils elsewhere in the Coos Bay area may also be due to local deformation of other structures. Lesser amounts of local coseismic deformation could extend as far north as the Siuslaw River (Peterson and Darienzo, 1989), although we have as yet found no evidence of Holocene coseismic deformation there. Although deformation in the Coos Bay region is probably controlled by local structures, plate-interface earthquakes are not precluded because movements on local structures commonly occur during plate-interface earthquakes (Plafker, 1969; Sykes, 1989), and local coseismic deformation could be overprinting regional deformation (Nelson, 1987; McInelly and others, 1989; Peterson and Darienzo, 1989).

A segment boundary north of the Siuslaw River in central Oregon would indicate that the 180- to 230-km-long part of the central CSZ from that boundary south to Cape Blanco consists of one or possibly two segments (Peterson and Darienzo, 1989). For example, between Coos Bay and the Siuslaw River, the submerged mouths of river valleys and the relatively low elevation of Pleistocene marine terraces suggest that this part of the coast has been uplifted at a lower rate than areas to the north and south (Adams, 1984). If this zone of relative submergence is reflecting north-south changes in the properties of the subducting plate, then it could mark a segment boundary. However, because this zone of submergence coincides with the eastern edge of the fold and thrust belt, it is more likely to be related to an east-west structural transition in the overriding North America plate (Peterson and Darienzo, 1989). The change in structural style shown by the marine- and fluvial-terrace studies probably shows the same transition.

Determining the recurrence of prehistoric earthquakes in the fold and thrust belt region of southern Oregon is complicated by the probable composite nature of the paleoseismic record. Analogies with similar areas (Berryman and

others, 1989; Carver and others, 1989) suggest some local earthquakes in the Coos Bay region may have been of small surface-wave magnitudes (M_S less than 7) and were not necessarily triggered by larger plate-interface earthquakes (for a different view, see Sykes, 1989). As argued by Yeats and others (1981) in southern California, earthquakes like those recorded in the South Slough syncline may be very shallow, quite possibly less than M_S 6, and occurring on flexural-slip faults during coseismic folding. Unfortunately, without a means of precisely dating or directly correlating individual submergence events, the possibility seems remote that marsh stratigraphic methods can be used consistently to distinguish local from regional earthquakes on a segment or segments of the CSZ between the Siuslaw River and Cape Blanco.

CONCLUSIONS

Field studies of the past few years have produced convincing evidence of coseismic changes in land level along the Washington and Oregon coasts. Studies of coastal deposits suggest that regional plate-interface earthquakes of at least M_W 8 with more than 100-km-long ruptures have occurred in northwestern Oregon and southwestern Washington.

Differences in the types of tidal-marsh sequences between north and south-central Oregon are consistent with several hypotheses for the recurrence and magnitude of plate-interface earthquakes. We suspect that a segment boundary exists along the CSZ near lat 44°–45°N.; such a boundary would suggest that the CSZ is segmented and, therefore, that plate-interface earthquakes of about M_W 8 along the central CSZ are more frequent than larger earthquakes. Alternatively, the western edge of the zone of coseismic subsidence, due to larger (M_W 9), more infrequent plate-interface earthquakes, may intersect the coast in central Oregon and could produce the observed stratigraphic changes in marsh sequences.

Geophysical and structural studies and mapping of marine and fluvial terraces indicate that many episodes of abrupt marsh burial in south-central Oregon are best interpreted as the products of deformation of local structures. Some of the local deformation could be associated with earthquakes of moderate magnitude (M_S less than 6). At most sites in this area, however, it is still unclear whether coseismic events were responses to local faulting or folding, to regional deformation during great plate-interface earthquakes, or to both. Advances in dating technology and extensive mapping of Pleistocene structures will be needed to distinguish regional from local earthquakes.

REFERENCES CITED

Acharya, Hemendra, 1981, Juan de Fuca plate—Aseismic subduction at 1.8 cm/yr: Geophysical Research Letters, v. 8, no. 11, p. 1123–1125.

Adams, John, 1984, Active deformation of the Pacific Northwest continental margin: Tectonics, v. 3, n. 4, p. 449–472.

———1989, Turbidites off the Oregon-Washington margin record paleo-earthquakes on the Cascadia subduction zone [abs.]: Seismological Research Letters, v. 60, no. 1, p. 1.

———1990, Paleoseismicity of the Cascadia subduction zone—Evidence from turbidites off the Oregon-Washington margin: Tectonics, v. 9, no. 4, p. 569–583.

Ando, Masataka, 1975, Source mechanisms and tectonic significance of historical earthquakes along the Nankai Trough, Japan: Tectonophysics, v. 27, no. 1, p. 119–140.

Ando, Masataka, and Balazs, E.I., 1979, Geodetic evidence for aseismic subduction of the Juan de Fuca plate: Journal of Geophysical Research, v. 84, no. B6, p. 3023–3027.

Atwater, B.F., 1987, Evidence for great Holocene earthquakes along the outer coast of Washington State: Science, v. 236, no. 4804, p. 942–944.

———1988a, Buried Holocene wetlands along the Johns River, southwest Washington [abs.], *in* Holocene subduction in the Pacific Northwest: Seattle, University of Washington, Quaternary Research Center, p. 4.

———1988b, Comment on "Coastline uplift in Oregon and Washington and the nature of Cascadia subduction-zone tectonics" by D.O. West and D.R. McCrumb: Geology, v. 16, no. 10, p. 952–953.

———1988c, Geologic studies for seismic zonation for the Puget lowland, *in* Jacobson, M.L., and Rodriquez, T.R., comps., National Earthquake Hazards Reduction Program, Summaries of technical reports, Volume XXV: U.S. Geological Survey Open-File Report 88–16, p. 120–133.

———1988d, Probable local precedent for earthquakes of magnitude 8 or 9 in the Pacific Northwest, *in* Hayes, W.W., ed., Proceedings of Conference XLII, Workshop on evaluation of earthquake hazards and risk in the Puget Sound and Portland areas: U.S. Geological Survey Open-File Report 88–541, p. 62–68.

———1988e, Subduction-earthquake telltales beneath coastal lowlands, *in* Crone, A.J., and Omdahl, E.M., eds., Proceedings of Conference XXXIX, Directions in paleoseismology: U.S. Geological Survey Open-File Report 87–673, p. 157–162.

Atwater, B.F., and Grant, W.C., 1986, Holocene subduction earthquakes in coastal Washington: EOS [American Geophysical Union Transactions], v. 67, no. 44, p. 906.

Bartsch-Winkler, S.B., 1988, Cycle of earthquake-induced aggradation and related tidal channel shifting, upper Turnagain Arm, Alaska, USA: Sedimentology, v. 35, no. 4, p. 621–628.

Bartsch-Winkler, S.B., Ovenshine, A.T., and Kachadoorian, Reuben, 1983, Holocene history of the estuarine area surrounding Portage, Alaska, as recorded in a 93-meter core: Canadian Journal of Earth Sciences, v. 20, no. 5, p. 802–820.

Berendsen, H.J.A., 1984, Quantitative analysis of radiocarbon dates of the perimarine area in the Netherlands: Geologie en Mijnbouw, v. 63, no. 4, p. 343–350.

Berryman, K.R., 1987, Tectonic processes and their impact on the recording of relative sea-level changes, *in* Devoy, R.J.N., ed., Sea surface studies—A global view: London, Croom Helm, p. 127–161.

Berryman, K.R., Ota, Yoko, and Hull, A.G., 1989, Holocene paleoseismicity in the fold and thrust belt of the Hikurangi subduction zone, eastern North Island, New Zealand: Tectonophysics, v. 163, p. 185–195.

Bloom, A.L., 1980, Late Quaternary sea level change on South Pacific coast—A study in tectonic diversity, *in* Morner, N.-A., ed., Earth rheology, isostasty and eustasy: New York, John Wiley & Sons, p. 505–516.

Bourgeois, Joanne, and Reinhart, M.A., 1988, Potentially damaging waves associated with earthquakes, coastal Washington, *in* Hayes, W.W., ed., Proceedings of Conference XLII, Workshop on evaluation of earthquake hazards and risk in the Puget Sound and Portland areas: U.S. Geological Survey Open-File Report 88–541, p. 96–99.

Brooks, M.J., Colquhoun, D.J., Pardi, R.R., Newman, W.S., and Abbott, W.H., 1979, Preliminary archeological and geological evidence for Holocene sea level fluctuations in the lower Cooper River valley, South Carolina: The Florida Anthropologist, v. 32, p. 85–103.

Carver, G.A., and Burke, R.M., 1987, Late Holocene paleoseismicity of the southern end of the Cascadia subduction zone [abs.]: EOS [American Geophysical Union Transactions], v. 68, no. 44, p. 1240.

Carver, G.A., Vick, G.S., and Burke, R.M., 1989, Late Holocene paleoseismicity of the Gorda segment of the Cascadia subduction zone: Geological Society of America Abstracts with Programs, v. 21, no. 5, p. 64.

Cifuentes, I.L., 1989, The 1960 Chilean earthquakes: Journal of Geophysical Research, v. 94, no. B1, p. 665–680.

Clarke, S.H., Jr., and Carver, G.A., 1989, Late Cenozoic structure and seismic potential of the southern Cascadia subduction zone [abs.]: EOS [American Geophysical Union Transactions], v. 70, no. 43, p. 1331–1332.

Clarke, S.H., Jr., Field, M.E., and Hirozawa, C.A., 1985, Reconnaissance geology and geologic hazards of the offshore Coos Bay basin, Oregon: U.S. Geological Survey Bulletin 1645, 41 p.

Combellick, R.A., 1986, Chronology of late-Holocene earthquakes in south-central Alaska—Evidence from buried organic soils in Turnagain Arm [abs.]: Geological Society of America Abstracts with Programs, v. 18, no. 6, p. 569.

Crosson, R.S., and Owens, T.J., 1987, Slab geometry of the Cascadia subduction zone beneath Washington from earthquake hypocenters and teleseismic converted waves: Geophysical Research Letters, v. 14, no. 8, p. 824–827.

Cullingford, R.A., Caseldine, C.J., Gotts, P.E., 1989, Evidence of early Flandrian tidal surges in Lower Strathearn, Scotland: Journal of Quaternary Science, v. 4, no. 1, p. 51–60.

Darienzo, M.E., 1987, Late Holocene geologic history of a Netarts Bay salt marsh, northwest Oregon coast, and its relationship to relative sea level changes: Eugene, University of Oregon, M.S. thesis, 94 p.

———1989, Evidence for and implications of small-scale (<1 m) tecctonic subsidence in salt marshes of Alsea Bay, Oregon, central Cascadia margin [abs.]: EOS [American Geophysical Union Transactions], v. 70, no. 43, p. 1331.

Darienzo, M.E., and Peterson, C.D., 1987, Episodic tectonic subsidence recorded in late-Holocene salt marshes, northwest Oregon [abs.]: EOS [American Geophysical Union Transactions], v. 68, no. 44, p. 1469.

———1990, Episodic tectonic subsidence of late Holocene salt marshes, northern Oregon central Cascadia margin: Tectonics, v. 9, no. 1, p. 1–22.

Devoy, R.J.N., ed., 1987, Sea surface studies—A global view: London, Croom Helm, 649 p.

Fairbridge, R.W., 1987, The spectra of sea level in a Holocene time frame, *in* Rampino, M.R., Sanders, J.E., Newman, W.S., and Konigsson, L.K., eds., Climate—History, periodicity, and predictability: New York, Van Nostrand Reinhold, p. 127–141.

Golder Associates, 1986, WNP–3 Geologic support services, coastal terrace study: Richland, Wash., Washington Public Power Supply System [unpublished report possibly available from Golder Associates, Redmond, Wash.], 106 p.

Goldfinger, Chris, Kulm, L.D., Mitchell, Clifton, Weldon, Ray, II, Peterson, Curt, Darienzo, Mark, Grant, Wendy, and Priest, G.R., 1992, Neotectonic map of the Oregon continental margin and adjacent abyssal plain: Oregon Department of Geology and Mineral Industries Open-File Report 0–92–4, 2 pls., scales 1:500,000 and 1:1,000,000.

Grant, W.C., 1988, Evidence for late Holocene subduction earthquakes recorded in tidal marsh deposits along the Nehalem and Salmon Rivers, northern Oregon [abs.], *in* Holocene subduction in the Pacific Northwest: Seattle, University of Washington, Quaternary Research Center, p. 10.

———1989, More evidence from tidal-marsh stratigraphy for multiple late Holocene subduction earthquakes along the northern Oregon coast [abs.]: Geological Society of America Abstracts with Programs, v. 21, no. 5, p. 86.

Grant, W.C., Atwater, B.F., Carver, G.A., Darienzo, M.E., Nelson, A.R., Peterson, C.D., and Vick, G.S., 1989, Radiocarbon dating of late Holocene coastal subsidence above the Cascadia subduction zone—Compilation for Washington, Oregon, and northern California [abs.]: EOS [American Geophysical Union Transactions], v. 70, no. 43, p. 1331.

Grant, W.C., and McLaren, D.D., 1987, Evidence for Holocene subduction earthquakes along the northern Oregon coast [abs.]: EOS [American Geophysical Union Transactions], v. 68, no. 44, p. 1239.

Griggs, A.B., 1945, Chromite-bearing sands of the southern part of the coast of Oregon: U.S. Geological Survey Bulletin 945–E, p. 113–150.

Heaton, T.H., and Hartzell, S.H., 1986, Source characteristics of hypothetical subduction earthquakes in the northwestern United States: Seismological Society of America Bulletin, v. 76, no. 3, p. 675–708.

———1987, Earthquake hazards on the Cascadia subduction zone: Science, v. 236, no. 4798, p. 162–168.

Heaton, T.H., and Kanamori, Hiroo, 1984, Seismic potential associated with subduction in the northwestern United States: Seismological Society of America Bulletin, v. 74, no. 3, p. 933–941.

Hemphill-Haley, Eileen, 1989, Investigation into the use of estuarine microfossil zones for determining amounts of coseismic subsidence in southwestern Washington [abs.]: Geological Society of America Abstracts with Programs, v. 21, no. 5, p. 92.

Hsu, G.J.T., Leonard, E.M., and Wehmiller, J.F., 1989, Aminostratigraphy of Peruvian and Chilean Quaternary marine terraces: Quaternary Science Reviews, v. 8, no. 3, p. 255–262.

Hughes, J.M., Stoiber, R.E., and Carr, M.J., 1980, Segmentation of the Cascade volcanic chain: Geology, v. 8, p. 15–17.

Hull, A.G., 1987, Buried lowland soils from Willapa Bay, southwest Washington—Further evidence for recurrence of large earthquakes during the last 5000 years: EOS [American Geophysical Union Transactions], v. 68, no. 44, p. 1468–1469.

———1988, Radiocarbon age of probable coseismic buried soil layers from Washington State, *in* Holocene subduction in the Pacific Northwest: Seattle, University of Washington, Quaternary Research Center, p. 7.

Jelgersma, Saska, 1961, Holocene sea-level changes in the Netherlands: Mededelingen Geologische Stichting, Serie C, v. 6, no. 7, p. 1–100.

Kaizuka, Sohei, Matsuda, Tokhiko, Nogomi, Michio, and Yonekura, Nobuyuki, 1973, Quaternary tectonic and recent seismic crustal movements in the Arauco Peninsula and its environs, central Chile: Tokyo Metropolitan University Geographical Reports, v. 8, p. 1–49.

Kanamori, Hiroo, 1986, Rupture process of subduction-zone earthquakes: Earth and Planetary Sciences Annual Reviews, v. 14, p. 293–322.

Kanamori, Hiroo, and Astiz, Luciana, 1985, The 1983 Akita-Oki earthquake (M_W 7.8) and its implications for systematics of subduction earthquakes, *in* Kisslinger, Carl, and Rikitake, Tsuneji, eds., Practical approaches to earthquake prediction and warning: Earthquake Prediction Research, v. 3, p. 305–317.

Kanamori, Hiroo, and McNally, K.C., 1982, Variable rupture mode of the subduction zone along the Ecuador-Colombia coast: Seismological Society of America Bulletin, v. 72, no. 4, p. 1241–1253.

Kaye, C.A., and Barghoorn, E.S., 1964, Late Quaternary sea-level change and crustal rise at Boston, Massachusetts, with note on the autocompaction of peat: Geological Society of America Bulletin, v. 75, no. 2, p. 63–80.

Keach, R.W., II, Oliver, J.E., Brown, L.D., and Kaufman, Sidney, 1989, Cenozoic active margin and shallow Cascades structure—COCORP results from western Oregon: Geological Society of America Bulletin, v. 101, no. 6, p. 783–794.

Kearney, M.S., and Ward, L.G., 1986, Accretion rates in brackish marshes of a Chesapeake Bay estuarine tributary: Geo-Marine Letters, v. 6, p. 41–49.

Kelsey, H.M., 1989, 3000-year-old elevated beach berm south of Cape Blanco, Oregon—Probable evidence of late Holocene tectonic uplift [abs.]: Geological Society of America Abstracts with Programs, v. 21, no. 5, p. 101.

———1990, Late Quaternary deformation of marine terraces on the Cascadia subduction zone near Cape Blanco, Oregon: Tectonics, v. 9, p. 983–1014.

Kelsey, H.M., and Carver, G.A., 1988, Late Neogene and Quaternary tectonics associated with northward growth of the San Andreas transform fault, northern California: Journal of Geophysical Research, v. 93, no. B5, p. 4797–4819.

Kennedy, G.L., Lajoie, K.R., and Wehmiller, J.F., 1982, Aminostratigraphy and faunal correlations of late Quaternary marine terraces, Pacific coast, USA: Nature, v. 299, p. 545–547.

Kidson, C., 1982, Sea level changes in the Holocene: Quaternary Science Reviews, v. 1, no. 2, p. 121–151.

Kulm, L.D., 1989, Cascadia subduction zone—Structure, tectonics, and fluid processes of the accretionary wedge and adjacent abyssal plain, *in* Hays, W.W., ed., Proceedings of Conference XLVIII, 3d annual workshop on earthquake hazards in the Puget Sound, Portland area: U.S. Geological Survey Open-File Report 89–465, p. 38–39.

Lajoie, K.R., 1986, Coastal tectonics, *in* Active tectonics: Washington, D.C., National Academy Press, p. 95–124.

Lajoie, K.R., Sarna-Wojcicki, A.M., and Ota, Yoko, 1982, Emergent Holocene marine terraces at Ventura and Cape Mendocino, California—Indicators of high tectonic uplift rates [abs.]: Geological Society of America Abstracts with Programs, v.14, p. 178.

Magee, M.E., and Zoback, M.L., 1989, Present state of stress in the Pacific Northwest [abs.]: EOS [American Geophysical Union Transactions], v. 70, no. 43, p. 1332–1333.

Matsuda, Tokihiko, Ota, Yoko, Ando, Masataka, and Yonekura, Nobuyuki, 1978, Fault mechanism and recurrence time of major earthquakes in southern Kanto district, Japan, as deduced from coastal terrace data: Geological Society of America Bulletin, v. 89, no. 11, p. 1610–1618.

McCrory, P.A., 1992, Quaternary deformation along the Washington margin of the Cascadia subduction zone—Evidence from the Raft River area: Geological Society of America Abstracts with Programs, v. 24, no. 5, p. 69.

McInelly, G.W., and Kelsey, H.M., 1990, Late Quaternary tectonic deformation in the Cape Arago-Bandon region of coastal Oregon as deduced from wave-cut platforms: Journal of Geophysical Research, v. 95, no. B5, p. 6699–6713.

McInelly, G.W., Kelsey, H.M., and Nelson, A.R., 1989, Late Pleistocene and Holocene tectonic deformation of the Whiskey Run wave-cut platform in the Cape Arago-Coos Bay area, coastal Oregon [abs.]: Geological Society of America Abstracts with Programs, v. 21, no. 5, p. 115.

Merritts, Dorothy, and Vincent, K.R., 1989, Geomorphic response of coastal streams to low, intermediate, and high rates of uplift, Medocino triple junction region, northern California: Geological Society of America Bulletin, v. 101, no. 11, p. 1373–1388.

Michaelson, C.A., and Weaver, C.S., 1986, Upper mantle structure from teleseismic P-wave arrivals in Washington and northern Oregon: Journal of Geophysical Research, v. 91, no. B2, p. 2077–2094.

Mitchell, C.E., Weldon, R.J., II, Vincent, Paul, and Pittock, H.L., 1991, Active uplift of the Pacific Northwest margin [abs.]: EOS [American Geophysical Union Transactions], v. 72, no. 44, p. 314.

Muhs, D.R., Kelsey, H.M., Miller, G.H., Kennedy, G.L., Whelan, J.F., and McInelly, G.W., 1990, Age estimates and uplift rates for late Pleistocene marine terraces—Southern Oregon portion of the Cascadia forearc: Journal of Geophysical Research, v. 95, no. B5, p. 6685–6698.

Nelson, A.R., 1987, Apparent gradual rise in relative sea level on the south-central Oregon coast during the late Holocene—Implications for the great Cascadia earthquake hypothesis [abs.]: EOS [American Geophysical Union Transactions], v. 68, no. 44, p. 1240.

———1988, Implications of late Holocene salt-marsh stratigraphy for earthquake recurrence along the coast of south-central Oregon, *in* Hayes, W.W., ed., Proceedings of Conference XLII, Workshop on evaluation of earthquake hazards and risk in the Puget Sound and Portland areas: U.S. Geological Survey Open-File Report 88–541, p. 149–151.

Nelson, A.R., Atwater, B.F., and Grant, W.C., 1987, Estuarine record of Holocene subduction earthquakes in coastal Oregon and Washington, USA [abs.]: International Union for Quaternary Research, 12th International Congress, Programme with Abstracts, Ottawa, Canada, 1987, p. 231.

Newman, W.S., Cinquemani, L.J., Pardi, R.P., and Marcus, L.F., 1980, Holocene deleveling of the United States east coast, *in* Morner, N.-A., ed., Earth rheology, isostasy, and eustasy: New York, John Wiley, p. 449–463.

Nishenko, S.P., 1985, Seismic potential for large and great interplate earthquakes along the Chilean and southern Peruvian margins of South America—A quantitative reappraisal: Journal of Geophysical Research, v. 90, no. B5, p. 3589–3615.

———1989, Circum-Pacific seismic potential 1989–1999: U.S. Geological Survey Open-File Report 89–86, 126 p.

Nishenko, S.P., and Singh, S.K., 1987, Conditional probabilities for the recurrence of large and great interplate earthquakes along the Mexican subduction zone: Seismological Society of America Bulletin, v. 77, no. 6, p. 2095–2114.

Nishimura, Clyde, Wilson, D.S., and Hey, R.N., 1984, Pole of rotation analysis of present-day Juan de Fuca plate motion, *in* Special section—S. Thomas Crough memorial: Journal of Geophysical Research, v. 89, p. 10283–10290.

Obermeier, S.F., Weems, R.E., Jacobson, R.B., and Gohn, G.S., 1989, Liquefaction evidence for repeated Holocene earthquakes in the coastal region of South Carolina: New York Academy of Science Annals, v. 558, p. 183–195.

Orson, R.A., Panageotou, William, and Leatherman, S.P., 1985, Response of tidal salt marshes of the U.S. Atlantic and Gulf coasts to rising sea levels: Journal of Coastal Research, v. 1, no. 1, p. 29–37.

Ota, Yoko, 1986, Marine terraces as reference surfaces in late Quaternary tectonics studies—Examples from the Pacific rim, *in* Reilly, W.I., and Harford, B.E., eds., Recent crustal movements of the Pacific region: Royal Society of New Zealand Bulletin 24, Publication 0102, p. 357–375.

Ota, Yoko, and Yoshikawa, T., 1978, Regional characteristics and their geodynamic implications of late Quaternary tectonic movement deduced from deformed former shorelines in Japan: Journal of Physics of the Earth, v. 26, Supplement, p. s379–s389.

Ovenshine, A.T., Lawson, D.E., and Bartsch-Winkler, S.R., 1976, The Placer River Silt—An intertidal deposit caused by the 1964 Alaska earthquake: U.S. Geological Survey Journal of Research, v. 4, no. 2, p. 151–162.

Pearson, G.W., 1979, Precise ^{14}C measurement by liquid scintillation counting: Radiocarbon, v. 21, no. 1, p. 1–21.

Personius, S.F., 1993, Age and origin of fluvial terraces in the central Coast Range, western Oregon: U.S. Geological Survey Bulletin 2038, 56 p.

Peterson, C.D., 1989, Potential evidence of subduction zone tectonics from stacked peat horizons in late Pleistocene coastal terraces of the northern Cascadia margin: EOS [American Geophysical Union Transactions], v. 70, no. 43, p. 1331.

Peterson, C.D., and Darienzo, M.E., 1988a, Episodic tectonic subsidence of late-Holocene salt marshes in Oregon—Clear evidence of abrupt strain release and gradual strain accumulation in the southern Cascadia margin during the last 3,500 years, *in* Hayes, W.W., ed., Proceedings of Conference XLII, Workshop on evaluation of earthquake hazards and risk in the Puget Sound and Portland areas: U.S. Geological Survey Open-File Report 88–541, p. 110–113.

———1988b, Discrimination of flood, storm, and tectonic events in coastal marsh records of the southern Cascadia margin [abs.], *in* Holocene subduction in the Pacific Northwest: Seattle, University of Washington, Quaternary Research Center, p. 11.

———1989, Episodic abrupt tectonic subsidence recorded in late Holocene deposits of the South Slough syncline—An on-land expression of shelf fold belt deformation from the southern Cascadia margin [abs.]: Geological Society of America Abstracts with Programs, v. 21, no. 5, p. 129.

Peterson, C.D., Darienzo, M.E., and Parker, Mike, 1988, Coastal neotectonic field trip guide for Netarts Bay, Oregon: Oregon Geology, v. 50, no. 9/10, p. 99–106.

Peterson, C.D., Scheidegger, K.F., and Schrader, K.J., 1984, Holocene depositional evolution of a small active margin estuary of the northwestern United States: Marine Geology, v. 59, p. 51–83.

Peterson, C.P., Kulm, L.D., and Gray, J.J., 1986, Geologic map of the ocean floor off Oregon and the adjacent continental margin: Oregon Department of Geology and Mineral Industries, Geologic Map Series, GMS–42, scale 1:500,000.

Phipps, J.B., and Peterson, C.D., 1989, General submergence of Grays Harbor, Washington, during the Holocene: EOS [American Geophysical Union Transactions], v. 70, no. 43, p. 1332.

Plafker, George, 1965, Tectonic deformation associated with the 1964 Alaska earthquake: Science, v. 148, no. 3678, p. 1675–1687.

———1969, Surface faults on Montague Island associated with the 1964 Alaska earthquake: U.S. Geological Survey Professional Paper 543–G, p. G1–G42.

———1972, Alaskan earthquake of 1964 and Chilean earthquake of 1960—Implications for arc tectonics: Journal of Geophysical Research, v. 77, no. 5, p. 901–924.

Plafker, George, and Rubin, Meyer, 1978, Uplift history and earthquake recurrence as deduced from marine terraces on Middleton Island, Alaska, *in* Methodology for identifying seismic gaps and soon-to-break gaps: U.S. Geological Survey Open-File Report 78–943, p. 687–721.

Plafker, George, and Savage, J.C., 1970, Mechanism of the Chilean earthquakes of May 21 and 22, 1960: Geological Society of America Bulletin, v. 81, no. 4, p. 1001–1030.

Plassche, Orson van de, 1980, Holocene water-level changes in the Rhine-Meuse Delta as a function of changes in relative sea level, local tidal range, and river gradient: Geologie en Mijnbouw, v. 59, p. 343–351.

———1982, Sea-level change and water-level movements in the Netherlands during the Holocene: Mededelingen Rijks Geologische Dienst, v. 36, no. 1, 93 p.

Rampino, M.R., and Sanders, J.E., 1981, Episodic growth of Holocene tidal marshes in the northeastern United States—A possible indicator of eustatic sea-level fluctuations: Geology, v. 9, no. 2, p. 63–67.

Rasmussen, J.R., and Humphreys, Eugene, 1989, Tomographic image of the upper mantle *P*-wave velocity structure beneath Washington and western Oregon [abs.]: EOS [American Geophysical Union Transactions], v. 70, no. 43, p. 1329.

Reilinger, R.E., and Adams, John, 1982, Geodetic evidence for active landward tilting of the Oregon and Washington coastal ranges: Geophysical Research Letters, v. 9, no. 4, p. 401–403.

Reinhart, M.A., and Bourgeois, Joanne, 1987, Distribution of anomalous sand at Willapa Bay, Washington—Evidence for large-scale landward-directed processes [abs.]: EOS [American Geophysical Union Transactions], v. 68, no. 44, p. 1469.

———1988, Testing the tsunamis hypothesis at Willapa Bay, Washington—Evidence for large-scale landward-directed processes [abs.], *in* Holocene subduction in the Pacific Northwest: Seattle, University of Washington, Quaternary Research Center, p. 9.

———1989, Tsunami favored over storm or seiche for sand deposit overlying buried Holocene peat, Willapa Bay, WA [abs.]: EOS [American Geophysical Union Transactions], v. 70, no. 43, p. 1331.

Rhea, Susan, 1993, Geomorphic observations of rivers in the Oregon Coast Range from a regional reconnaissance perspective: Geomorphology, v. 6, p. 135–150.

Riddihough, R.P., 1984, Recent movements of the Juan de Fuca plate system: Journal of Geophysical Research, v. 89, no. B8, p. 6980–6994.

Rogers, G.C., 1988, An assessment of the megathrust earthquake potential of the Cascadia subduction zone: Canadian Journal of Earth Sciences, v. 25, no. 6, p. 844–852.

Ruff, L.J., 1989, Do trench sediments affect great earthquake occurrence in subduction zones?: Pure and Applied Geophysics, v. 129, no. 1/2, p. 263–282.

Savage, J.C., 1983, A dislocation model of strain accumulation and release at a subduction zone: Journal of Geophysical Research, v. 88, no. 136, p. 4984–4996.

———1989, Aseismic slip in seismic gaps at subduction zones: Seismological Research Letters, v. 60, no. 1, p. 2.

Savage, J.C., Lisowski, Michael, and Prescott, W.H., 1981, Geodetic strain measurements in Washington: Journal of Geophysical Research, v. 86, no. B6, p. 4929–4940.

Schwartz, D.P., and Sibson, R.H., eds., 1989, Proceedings of Conference XLV, Workshop on fault segmentation and controls of rupture initiation and termination: U.S. Geological Survey Open-File Report 89–315, 447 p.

Shedlock, K.M., and Weaver, C.S., 1989, Rationale and outline of a program for earthquake hazards assessment in the Pacific Northwest, *in* Hays, W.W., ed., Proceedings of Conference XLVIII, 3d annual workshop on earthquake hazards in the Puget Sound, Portland area: U.S. Geological Survey Open-File Report 89–465, p. 2–10.

Shennan, Ian, 1982, Problems of correlating Flandrian sea-level changes and climate, *in* Harding, A.F., ed., Climatic change in later prehistory: Edinburgh, Scotland, Edinburgh University Press, p. 52–67.

———1986, Flandrian sea-level changes in the Fenland, II—Tendencies of sea-level movement, altitudinal changes, and local and regional factors: Journal of Quaternary Science, v. 1, no. 2, p. 155–180.

———1987, Global analysis and correlation of sea-level data, *in* Devoy, R.J.N., ed., Sea surface studies—A global view: London, Croom Helm, p. 198–230.

———1989, Holocene sea-level changes and crustal movements in the North Sea region—An experiment with regional eustasy, *in* Scott, D.B., Pirazzoli, P.A., and Honig, C.A., eds., Late Quaternary sea-level correlation and applications: Dordrecht, The Netherlands, Kluwer Academic Publishers, p. 1–25.

Singh, S.K., Astiz, Luciana, Havskov, J., 1981, Seismic gaps and recurrence periods of large earthquakes along the Mexican subduction zone—A reexamination: Seismological Society of America Bulletin, v. 71, no. 3, p. 827–843.

Snavely, P.D., Jr., 1987, Tertiary geologic framework, neotectonics, and petroleum potential of the Oregon-Washington continental margin, *in* Scholl, D.W., Grantz, Arthur, and Vedder, J.G., eds., Geology and resource potential of the continental margin of western North America and adjacent ocean basins—Beaufort Sea to Baja California: Houston, Tex., Circum-Pacific Council for Energy and Mineral Resources, Earth Science Series, v. 6, no. 6, p. 305–335.

Spence, William, 1987, Slab pull and the seismotectonics of subducting lithosphere: Reviews of Geophysics and Space Physics, v. 25, no. 1, p. 55–69.

———1988, Anomalous subduction and the origins of stresses at Cascadia—A review, *in* Hayes, W.W., ed., Proceedings of Conference XLII, Workshop on evaluation of earthquake hazards and risk in the Puget Sound and Portland areas: U.S. Geological Survey Open-File Report 88–541, p. 114–148.

———1989, Stress origins and earthquake potential in Cascadia: Journal of Geophysical Research, v. 94, p. 3076–3088.

Stevenson, J.C., Ward, L.G., and Kearney, M.S., 1986, Vertical accretion in marshes with varying rates of sea level rise, *in* Wolfe, D.A., ed., Estuarine variability: New York, Academic Press, p. 241–259.

Streif, Hansjorg, 1980, Cyclic formation of coastal deposits and their indications of vertical sea-level changes: Oceanis, v. 5, p. 303–306.

Stuiver, Minze, and Pearson, G.W., 1986, High-precision calibration of the radiocarbon time scale, AD 1950–500 BC: Radiocarbon, v. 28, no. 2B, p. 805–838.

Sykes, L.R., 1989, Great earthquakes of 1855 and 1931 in New Zealand—Evidence for seismic slip along downgoing plate boundary and implications for seismic potential of Cascadia subduction zone [abs.]: EOS [American Geophysical Union Transactions], v. 70, no. 43, p. 1331.

Sykes, L.R., and Quitmeyer, R.C., 1981, Repeat times of great earthquakes along simple plate boundaries, *in* Simpson, D.W., and Richards, P.G., eds., Earthquake prediction—An international review: Washington, D.C., American Geophysical Union, Maurice Ewing Series, v. 4, p. 217–247.

Taylor, F.W., Edwards, R.L., Wasserberg, G.J., and Frohlich, Clifford, 1990, Seismic recurrence intervals and timing of aseismic subduction inferred from emerged corals and reefs of the central Vanuatu (New Hebrides) frontal arc: Journal of Geophysical Research, v. 95, no. B1, p. 393–408.

Taylor, F.W., Jouannic, C., and Bloom, A.L., 1985, Quaternary uplift of the Torres Islands, northern New Hebrides frontal arc—Comparison with Santo and Malekula Islands, central New Hebrides frontal arc: Journal of Geology, v. 93, no. 4, p. 419–438.

Ters, Mireille, 1987, Variations in Holocene sea level on the French Atlantic coast and their climatic significance, *in* Rampino, M.R., Sanders, J.E., Newman, W.S., and Konigsson, L.K., eds., Climate—History, periodicity, and predictability: New York, Van Nostrand Reinhold, p. 204–237.

Thatcher, Wayne, 1984, The earthquake deformation cycle, recurrence, and the time-predictable model: Journal of Geophysical Research, v. 89, no. B7, p. 5674–5680.

———1989, Earthquake recurrence and risk assessment in circum-Pacific seismic gaps: Nature, v. 341, no. 6241, p. 432–434.

———1990, Order and diversity in the modes of circum-Pacific earthquake recurrence: Journal of Geophysical Research, v. 95, no. B3, p. 2609–2623.

Thomas, Ellen, Varekamp, J.C., and Plassche, Orson van de, 1989, Late Holocene fluctuations in sea level rise (Clinton, CT)—Marsh foraminifera and geochemical evidence [abs.]: Geological Society of America Abstracts with Programs, v. 21, no. 2, p. 70.

Ticknor, R.L., Kelsey, H.M., and Bockheim, J.G., 1992, Late Quaternary tectonic deformation along the central Oregon portion of the Cascadia margin as deduced from deformation of wave-cut platforms: Geological Society of America Abstracts with Programs, v. 24, no. 5, p. 86.

Tooley, M.J., ed., 1978, Sea-level changes in north-west England during the Flandrian stage: Oxford, Great Britain, Clarendon Press, 235 p.

———1985, Climate, sea-level and coastal changes, *in* Tooley, M.J., and Sheail, G.M., eds., The climate scene: London, George Allen and Unwin, p. 206–234.

Tooley, M.J., and Shennan, Ian, eds., 1987, Sea-level changes: London, Institute of British Geographers Special Publication 20, Basil Blackwell, 397 p.

Vick, G.S., 1988, Late Holocene paleoseismicity and relative sea level changes of the Mad River Slough, northern Humboldt Bay, California: Arcata, Calif., Humboldt State University, M.S. thesis, 87 p.

Vincent, Paul, Richards, M.A., and Weldon, R.J., II, 1989, Vertical deformation of the Oregon continental margin [abs.]: EOS [American Geophysical Union Transactions], v. 70, no. 43, p. 1332.

Weaver, C.S., and Baker, G.E., 1988, Geometry of the Juan de Fuca plate beneath Washington and northern Oregon from seismicity: Seismological Society of America Bulletin, v. 78, no. 1, p. 264–275.

Weaver, C.S., and Michaelson, C.A., 1985, Seismicity and volcanism in the Pacific Northwest—Evidence for the segmentation of the Juan de Fuca plate: Geophysical Research Letters, v. 12, no. 4, p. 215–218.

Weaver, C.S., and Shedlock, K.M., 1989, Potential subduction, probable intraplate, and known crustal earthquake source areas in the Cascadia subduction zone, *in* Hays, W.W., eds., Proceedings of Conference XLVII, 3d annual workshop on earthquake hazards in the Puget Sound, Portland area: U.S. Geological Survey Open-File Report 89–465, p. 10–26.

Wells, R.E., Snavely, P.D., Jr., and Niem, A.R., 1992, Quaternary thrust faulting at Netarts Bay, northern Oregon coast: Geological Society of America Abstracts with Programs, v. 24, no. 5, p. 89.

Wells, S.G., Bullard, T.F., Menges, C.M., Drake, P.G., Karas, P.A., Kelson, K.I., Ritter, J.B., and Wesling, J.R., 1988, Regional variations in tectonic geomorphology along a segmented convergent plate boundary, Pacific coast of Costa Rica: Geomorphology, v. 1, p. 239–265.

West, D.O., and McCrumb, D.R., 1988a, Coastline uplift in Oregon and Washington and the nature of Cascadia subduction-zone tectonics: Geology, v. 16, no. 2, p. 169–172.

———1988b, Reply to B.F. Atwater's comment on "Coastline uplift in Oregon and Washington and the nature of Cascadia subduction-zone tectonics": Geology, v. 16, no. 10, p. 952–953.

Wilson, D.S., 1986, A kinematic model for the Gorda deformation zone as a diffuse southern boundary of the Juan de Fuca plate: Journal of Geophysical Research, v. 91, no. B10, p. 10259–10269.

———1989, Deformation of the so-called Gorda plate: Journal of Geophysical Research, v. 94, no. B3, p. 3065–3075.

Winslow, M.A., 1988, Holocene deformation patterns and paleoseismicity in the eastern Shumagin seismic gap—Southwestern Alaska [abs.]: Geological Society of America Abstracts with Programs, v. 20, no. 7, p. A382.

Wright, Charles, and Mella, Arnoldo, 1963, Modifications to the soil pattern of south-central Chile resulting from seismic and associated phenomena during the period May to August 1960: Seismological Society of America Bulletin, v. 53, no. 6, p. 1367–1402.

Yamaguchi, D.K., 1988, Preliminary tree-ring dating of late-Holocene subsidence along the Washington coast [abs.], *in* Holocene subduction in the Pacific Northwest: Seattle, University of Washington, Quaternary Research Center, p. 8.

Yamaguchi, D.K., Woodhouse, C.A., and Reid, M.S., 1989, Tree-ring dating of late Holocene subsidence along the Washington and Oregon coasts—A progress report, *in* Jacobson, M.L., comp., National Earthquake Hazards Reduction Program, Summaries of technical reports, Volume XXVIII: U.S. Geological Survey Open-File Report 89–453, p. 162–169.

———1989b, Tree-ring evidence for synchronous rapid submergence of the southwestern Washington coast 300 years B.P. [abs.]: EOS [American Geophysical Union Transactions], v. 70, no. 43, p. 1332.

Yeats, R.S., Clark, M.N., Keller, E.A., and Rockwell, T.K., 1981, Active fault hazard in southern California—Ground rupture versus seismic shaking: Geological Society of America Bulletin, v. 92, no. 4, p. 189–196.

Yonekura, Nobuyuki, and Ota, Yoko, 1986, Sea-level changes and tectonics in the late Quaternary, *in* Recent progress of natural sciences in Japan: Tokyo, Science Council of Japan, Quaternary Research, v. 11, p. 17–34.

Yonekura, Nobuyuki., and Shimazaki, K., 1980, Uplifted marine terraces and seismic crustal deformation in arc-trench systems—A role of imbricated thrust faulting [abs.]: EOS [American Geophysical Union Transactions], v. 61, no. 46, p. 1111.

DISCRIMINATION OF CLIMATIC, OCEANIC, AND TECTONIC MECHANISMS OF CYCLIC MARSH BURIAL, ALSEA BAY, OREGON

By Curt D. Peterson[1] *and* Mark E. Darienzo[1]

ABSTRACT

Late Holocene sequences of 2–10 buried peaty horizons (such as wetland soil layers) from marsh cutbanks and from 19 marsh core sites in Alsea Bay, Oreg., have been analyzed for composition, lateral correlation, and radiocarbon age. These analyses are used to discriminate between different mechanisms of marsh submergence and burial including river flooding, ocean set-up, barrier-spit breaching, and coseismic subsidence. System-wide marsh responses to abrupt but persistent submergence events in Alsea Bay are indicated by (1) lateral correlation of key peaty horizons over distances of as much as 3 km, (2) consistent vertical trends in peaty burial units, generally including increasing organic material and decreasing sand content upunit, and (3) close association of anomalous sand-rich tsunami deposits immediately overlying the buried peaty horizons. The study results rule out marsh burial by catastrophic climatic or oceanic processes and argue for episodic coastal submergence forced by abrupt coseismic subsidence in an active subduction zone.

An average recurrence interval of 500 radiocarbon years is estimated from eight repeat intervals of coseismic subsidence between 4,510 and 480 Radiocarbon Years Before Present (RCYBP). By comparison, an average recurrence interval of 340 radiocarbon years is estimated from the three most recent repeat intervals of coseismic subsidence between 1,490 and 480 RCYBP. Recurrence intervals between successive burial events were found to range from 250 to 1,370 years (uncalibrated radiocarbon years). The average minimum range of vertical subsidence in Alsea Bay (0.5–1 m) at lat 44.4°N. is substantially less than that reported for Netarts Bay, Oreg., (1–1.5 m) at lat 45.4°N. but more than that for Siuslaw Bay, Oreg., (0–0.5 m) at lat 44°N. This trend in average coseismic subsidence implies a coastline closure with a zero isobase, that is, a zone of little or no upper lithospheric plate elastic flexure, south of lat 44°N. If confirmed by future work, the position of a zero isobase located at least 90 km landward of the trench in the Cascadia subduction zone would define the landward limit of the locked zone in central Oregon. Finally, a high correspondence between marsh subsidence and tsunami sand-layer deposition was observed in Alsea Bay, even though the estimated amount of local coastal subsidence (0.5–1 m) is small. Such a high correspondence between tsunami sands and coastal subsidence events can be used to test models of potential earthquake rupture length in the central Cascadia subduction zone margin.

INTRODUCTION

Recent reports of episodic burial of marsh and wetland horizons by tidal-flat muds in several tidal basins of Washington and Oregon have greatly increased the controversy over the neotectonic history of the Cascadia subduction zone (CSZ) (Atwater, 1987; Peterson and others, 1988). For example, evidence of alternating coastal uplift and subsidence might indicate active subduction of the oceanic Juan de Fuca tectonic plate under the continental North America plate landward of the sea-floor trench (fig. 33). Such periodic coastal displacements are associated with similar coseismic subduction in the strongly coupled subduction zones of Chile, southeastern Alaska, and Japan (Plafker, 1972; Uyeda and Kanamori, 1979; Heaton and Hartzell, 1986).

Abrupt changes in relative tide level must have produced the catastrophic burials of the supratidal vegetated surfaces by lower intertidal sediments, as observed in some CSZ coastal tidal basins (Atwater, 1987, 1988; Darienzo and Peterson, 1990). However, abrupt increases in the height of relative tide level in some bays might have been caused by

[1]Department of Geology, Portland State University, Portland, OR 97207.

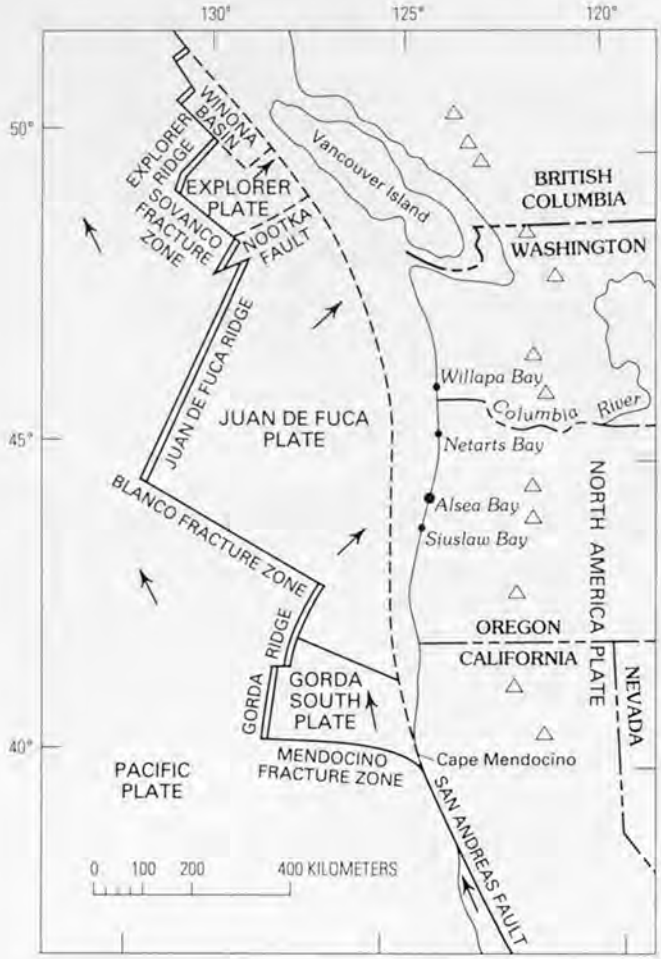

Figure 33. Index map of the Pacific Northwest showing the Alsea Bay study area (large dot) and several other bay wetland areas (small dots) reported to record coastal submergence. The dashed line shows the estimated position of the sediment-filled trench between the subducting Juan de Fuca plate and the overriding North America plate. Arrows show approximate directions of relative plate movement (from Riddihough, 1984). Triangles show volcanoes in the Cascade volcanic arc.

mechanisms unrelated to either local or regional tectonics. Such nontectonic mechanisms might include (1) river flooding, (2) ocean storm surges, (3) anomalous conditions of oceanic circulation, and (4) changes in tidal-inlet morphology and the associated basin tidal prism, that is, the volume of tidal flow in the bays.

As many as six coastal-submergence events have been documented in marsh and wetland deposits from large estuaries in Washington such as Willapa Bay and Grays Harbor (Atwater, 1987, 1988) and from smaller bays, including a barrier lagoon (Netarts Bay) in Oregon (Darienzo and Peterson, 1990; Darienzo, 1991). Buried peaty deposits have also been found in two fluvially dominated estuaries, Nehalem and Salmon Bays, a few tens of kilometers to the north and south of Netarts Bay (fig. 33), respectively (Grant and McLaren, 1987; Grant, 1989). The buried peaty horizons (wetland soils) in these bays have been radiocarbon dated as being of late Holocene age. They range in age from at least 3,300 to about 350 Radiocarbon Years Before Present (RCYBP) in Netarts Bay (Darienzo and Peterson, 1990), and from 5,000 to 300 RCYBP in Willapa Bay (Atwater, 1988). In contrast, relatively long stratigraphic sections of continuous or nearly continuous peaty sediments from 0 to 4 m depth have been observed in Siuslaw Bay (fig. 33) on the central Oregon coast (Nelson, 1987).

Discrimination between tectonic and nontectonic mechanisms of relative sea-level change are critical to the correct interpretation of the submergence events documented in coastal wetlands of the central CSZ margin. Of particular concern to the controversial history of the CSZ is the possible mistaking of tectonic subsidence events for climatic, oceanographic, or spit-breaching rises in tide level. These mechanisms need to be discriminated to confirm possible evidence of regional tectonic subsidence and associated tsunami excitation. Such evidence would clearly indicate the potential for great subduction earthquakes in the central CSZ margin.

In this report, we describe the late Holocene stratigraphy of the Alsea Bay, Oreg., marsh, as documented from cutbank and shallow coring transects (2–7 m depth) that extend across the lower and upper reaches of the estuary. Distinctive horizons in selected marsh cores were analyzed for (1) relative abundance of organic material, (2) sediment grain-size distribution, (3) sand source (marine or fluvial), and (4) radiocarbon age of buried peaty deposits. The results of our study show that the observed marsh stratigraphy in Alsea Bay permits the discrimination of tectonic and nontectonic mechanisms of marsh burial. Due to the wide range of marsh environments in Alsea Bay, we believe that the results of this study site apply to other coastal marsh systems of the central CSZ margin.

ACKNOWLEDGMENTS

We thank Henry Pittock for providing records of wind speed, atmospheric pressure, and corresponding storm-surge levels from Yaquina Bay, Oreg. We appreciate the time Alan Nelson of the U.S. Geological Survey spent in showing us the marsh stratigraphy in Siuslaw Bay. Charles Clough assisted with surveys and lateral correlations of buried peats in cutbanks of Alsea Bay. Larry Kauffman provided us with a boat, motor, and dock facility for the extensive coring and surveying of the Alsea Bay marsh. Margaret Mumford and Carolyn Peterson produced many of the original line drawings. We thank Wendy Grant of the U.S. Geological Survey and Jim Phipps of Grays Harbor College, Aberdeen, Wash., for reviewing this manuscript and providing many suggestions for its improvement. This research was supported by the U.S. Geological Survey under the National Earthquake Hazards Reduction Program, grant number 14–08–0001–G1512, and by National Science Foundation grant EAR–8903903.

Figure 34. The Alsea Bay estuary, showing channel contours of mean lower low water (dashed lines) and the fringing marsh system (plant symbols). More than 90 percent of the sediments flooring this high-gradient, fluvially dominated estuary are in the sand-size range. The bay is roughly divided on the basis of sand source into the marine-dominated lower reaches, the fluvially dominated upper reaches, and the transitional middle reaches (labeled in figure). Line of section *A–A'* at the tide inlet shows cross-section traverses detailed in figure 54.

STUDY-SITE SELECTION

We selected Alsea Bay (fig. 34) as a study area because its physiography was thought to be particularly well suited to the discrimination of potential climatic, oceanic, and tectonic mechanisms of marsh burial. For example, Alsea Bay has marsh deposits that extend continuously across fluvially and tidally dominated estuarine environments (Peterson and others, 1982). The different marsh environments should show either (1) effects from river flooding in the constricted, upper estuary reaches, (2) effects from ocean storm surges in the exposed, broad lower estuary, (3) effects from spit breaching during 1985–1989 (Peterson and others, 1990) in modern marsh deposits, or (4) effects of coseismic coastal subsidence, which should extend across upper and lower estuary marsh environments and which should be absent from historical marsh deposits.

The second reason for selecting this study site is that the hydrography and sedimentology of this small tidal basin have been studied in detail (Goodwin and others, 1970; Boley, 1973; McKenzie, 1975; Peterson and others, 1982; Peterson, and others, 1984; Peterson and others, 1990). Distinctive mineral compositions of river and marine source sands in Alsea Bay (Peterson and others, 1982) are particularly important to the investigations of marsh-burial mechanisms in the estuary. For example, the identification of sand sources (river or ocean beach sand) supplied to the marsh sediments should firmly distinguish between seaward- and landward-directed sediment transport during marsh burial. Finally, buried peaty horizons topped by thin sand layers were known to exist widely in exposed tidal-creek banks of the Alsea Bay marsh (K.F. Scheidegger and C.D. Peterson, unpub. data, 1980).

POTENTIAL MECHANISMS OF MARSH BURIAL

Well-developed salt marshes are present within a restricted range on either side of mean tide level (MTL), roughly 0.5 m below to 2 m above MTL. This range is a function of plant tolerance to local conditions of desiccation, salinity, and substrate stability (Niering and Warren, 1980). Emergence of a salt marsh above the reach of tides results in a transition to upland vegetation (supratidal elevation), whereas submergence to lower intertidal or subtidal levels results in burial by tidal-flat mud.

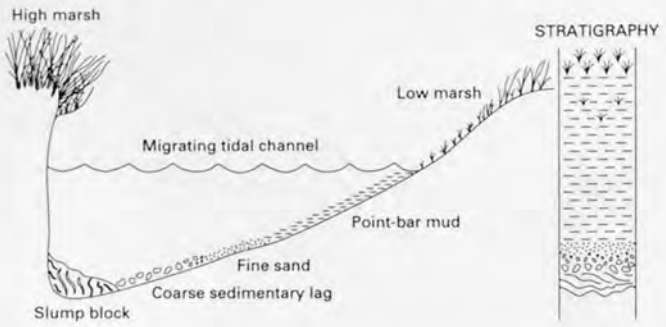

Figure 35. A hypothetical marsh vertical sequence developed within a tidal-creek meander bend. Units in the stratigraphic column correspond to depositional surfaces in the channel cross section. The sequence is produced as the channel migrates laterally, cutting the left bank and building the right bank.

Although meandering tidal channels can produce deposits that mimic emergent tidal-flat to marsh sequences (fig. 35), these channel-fill deposits do not overlie undisturbed marsh surfaces and are only locally developed within the back-filled meander bends of tidal channels. In contrast, broadly defined emergence or submergence records that span intervening tidal creeks indicate changes in MTL relative to the bay marsh system.

Gradual submergence or minor fluctuations in the submergence of late Holocene salt-marsh environments are generally reported from passive continental margins of the eastern and gulf coasts of the United States (Kraft, 1971; Redfield, 1972; Orson and others, 1985). These trends of nearly continuous coastal submergence reflect relatively gradual conditions of eustatic sea-level rise and (or) local subsidence by tectonic warping. In contrast, the episodic events of marsh emergence and submergence observed in some Pacific Northwest coastal bays (Atwater, 1987; Darienzo and Peterson, 1990) must be produced by more dynamic, reversible processes of relative sea-level change. Several possible mechanisms of episodic marsh burial as recorded in coastal deposits of the central CSZ margin are discussed below.

RIVER FLOODING

Tidal basins of the Pacific Northwest coast vary greatly in the relative influence of tidal and river flow. In the fluvially dominated estuaries, the peak river discharge during a given tidal cycle can exceed 50 percent of the basin tidal-prism discharge (Percy and others, 1974). The upper estuarine reaches, often constricted by steep-sided river valleys, are the areas most susceptible to flooding by extreme river

Figure 36. The upper reaches of Alsea Bay showing the central and eastern marsh areas. View is to the east. See figure 34 for the map of the estuary. Photograph by P.D. Komar, College of Oceanography, Oregon State University.

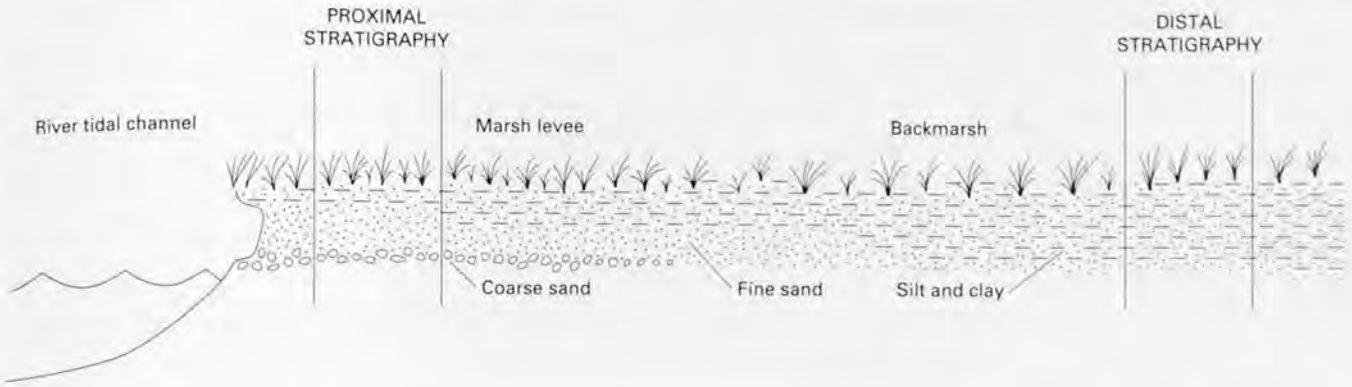

Figure 37. Hypothetical river-flood deposit with proximal (marsh levee) and distal (back marsh) stratigraphic columns showing expected fining-upward sequences. River tidal channels in most of the high-gradient estuaries of the Pacific Northwest are floored by sand and (or) gravel, providing proximal sources of coarse-grained sediments to channel-margin environments during catastrophic floods.

discharge events. For example, extreme river floods (100-year floods) in Alsea Bay that occurred in 1890 and 1964 produced discharges of more than 1,133 m^3/s. These river floods raised the river level about 7 m above the average level (1.5 m at 47 m^3/s) at a gauging station located at the head of tide, a distance of 26 km from the bay mouth (U.S. Geological Survey, 1988). Fine- and coarse-grained sediments are transported down tidal channels of the upper estuary during winter months of maximum rainfall (Peterson and others, 1982). Conceivably, suspended river sediments could bury salt-marsh surfaces in the constricted upper estuary during the most extreme events of river flooding (fig. 36).

The resulting flood sediments, deposited above the peaty marsh horizon, might include fining-upward sequences (fine sand grading upward to silt and clay) (fig. 37) that are typical of flood overbank deposition (Reineck and Singh, 1980, p. 288–291). Also, the coarsest sediments in basal layers above the buried marsh would be expected to diminish in relative abundance with increasing distance from the tidal-channel axis and with increasing distance downstream from the constricted river valley. Finally and most important, marsh-burial deposits of sand should reflect the river-source mineral composition if they are derived from flood overbank deposition.

OCEAN SET-UP

Onshore water-forcing prevails along the Pacific Northwest coast when offshore storms (cyclonic low-pressure centers) approach land from the west or southwest (Smith, 1974). The resulting ocean set-up (increase in sea level) from local storm winds and the associated low atmospheric pressure temporarily increases tide levels within the bays. For example, measured tide levels of at least 1.2 m above predicted tides in Yaquina Bay (15 km north of Alsea Bay) are known to result from extreme onshore winds (as high as 90 knots) that force onshore mass transport of ocean water (fig. 38) (Henry Pittock, College of Oceanography, Oregon State University, unpub. data, 1981). Although the effects of such storm set-up conditions on coastal-marsh systems in the Pacific Northwest have not been reported, hurricanes are known to have produced storm sediment layers 1–3 cm thick in marsh systems of the United States gulf coast (Rejmanek and others, 1988).

Longer periods of episodic sea-level rise can occur from anomalous conditions of climatic-oceanic circulation. Small increases in monthly mean sea level are produced from seasonally persistent conditions of low atmospheric pressure (Huyer and others, 1979; Pittock and others, 1982) and (or) the northward coastal propagation of El Nino Southern Oscillation (ENSO) sea-level bulges (Enfield and Allen, 1980). The ENSO equatorial (eastward) mass transport that results from the relaxation of equatorial trade winds is diverted south and north at the equatorial continental margin. The sea-level bulge then propagates along the margin as a coastal-trapped Kelvin wave. Although the rises in the monthly mean sea levels along the Oregon and Washington coasts have historically been small (10-30 cm) (Enfield and Allen, 1980; Huyer and others, 1983), the long duration (months) of elevated sea level (fig. 39) could conceivably have an impact on tidal marshes, as discussed below.

Conditions of elevated sea level from storm surges and (or) anomalous oceanic circulation would increase the depth and fetch of intrabasin wind waves in the characteristically shallow bays of the Pacific Northwest. The tidal marshes of the broad, lower estuary that are exposed to direct ocean swells or intrabasin wind waves would be the most susceptible to burial by sediments resuspended and deposited during major wind storms. The burial deposits could conceivably contain layered sand and silt (Allen, 1984) resulting from time-variable tidal currents and the storm resuspension of sediments from shallow sand and mud flats (fig. 40). Clay should not constitute a major fraction of the storm-burial layers, as it is likely to be held in suspension during catastrophic wind-storm events. In addition, the immediate

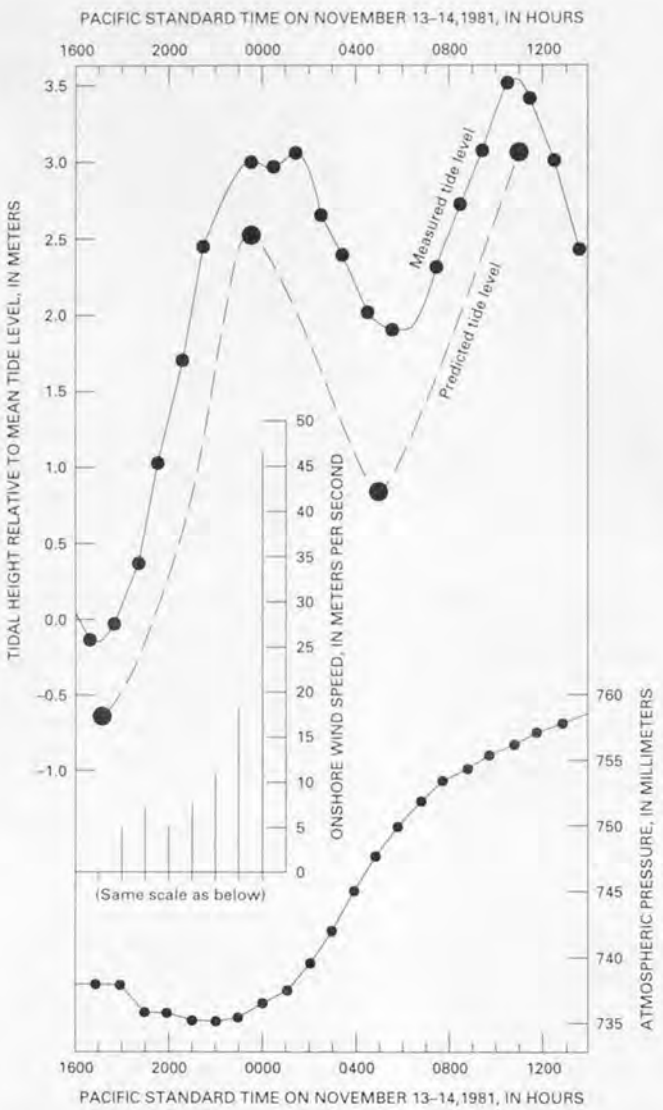

Figure 38. Historical extreme event of ocean set-up from a storm surge in Yaquina Bay, Oreg., 15 km north of Alsea Bay, during November 13–14, 1981. Measured tide level, wind velocity, and atmospheric pressure were recorded simultaneously at the Hatfield Marine Science Center at Yaquina Bay (Henry Pittock, College of Oceanography, Oregon State University, unpub. data, 1981). The measured tide level ranges from 0.5 to 1 m above the predicted tide level during the maximum period of northeasterly to easterly directed wind stress (0000–0800 hours, Nov. 14). Yaquina Bay is similar to Alsea Bay in size and morphology, but a larger tidal entrance to Yaquina Bay probably enhances storm set-up there.

sources of tidal-flat sediments in the fluvially dominated estuaries such as Alsea Bay have a significant beach-sand component (Peterson and others, 1982). The coarse-grained components of the storm deposits should reflect the sand-source mineral composition of the nearby tidal flats from which they would be derived. Finally, marsh environments most sensitive to repeated storm-surge deposition should be dominated by high-energy coarse-grained sediments (sand).

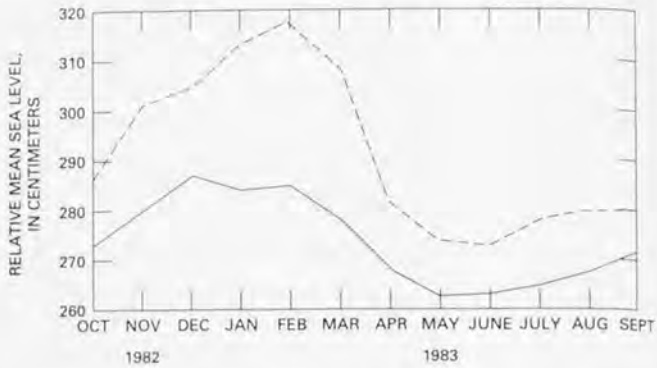

Figure 39. Monthly relative mean sea levels from the Yaquina Bay, Oreg., tide gauge for the 1982–83 El Nino Southern Oscillation (ENSO) period (dashed line), and corresponding 10-year averages (solid line) for the 1971–81 decade (Huyer and others, 1983). The measured increase of monthly mean sea levels peaked at greater than 30 cm above normal for the duration of the 1983 winter, a historically extreme event of intra-annual elevated relative sea level.

BREACHES IN BARRIER SPITS

All of the mechanisms of submergence discussed above involve temporary increases in mean tide level. However, long-term changes in the tide-level range might also impact marsh plant growth and sediment deposition (Clark and Patterson, 1985). Such long-term changes in tide-level range can occur from variations in tidal-inlet morphology that control the tidal flow between the free ocean surface and the inshore tidal basin. Nearly all of the tidal basins on the open coasts of Washington, Oregon, and northern California are fronted by sand-spit barriers (Dingler and Clifton, 1993). Tidal inlets to these bays either cut through the barrier spit or are pinned by the spit against a resistant sea cliff, as in Alsea Bay (fig. 34). The cross-sectional areas of the tidal inlets are generally proportional to the size and corresponding tidal prism of the tidal basin (O'Brien, 1969). The tidal prisms of the larger bays do not allow the spits to completely cut off these estuaries from ocean tide level. However, variable wave climate (energy and direction of surf) and the resulting mobility of littoral sand can cause a net in-filling or erosion of the tidal inlet, thereby reducing or increasing basin tidal flow.

A reduction in tidal flow (choking) across an inlet results in a diminished tidal prism within the tidal basin. For all but the most fluvially dominated estuaries, a decrease in the tidal prism translates into a decreased maximum tide level in the broad lower estuary. Conversely, opening of the inlet (increase of tidal flow) increases the tidal range, thereby increasing the depth but not the period of salt-marsh submergence during high tide. For example, a substantial 50 percent increase in tide-level range above the equilibrium range (2 m) from mean lower low water (MLLW) to mean higher high water (MHHW) (Percy and others, 1974) could add an

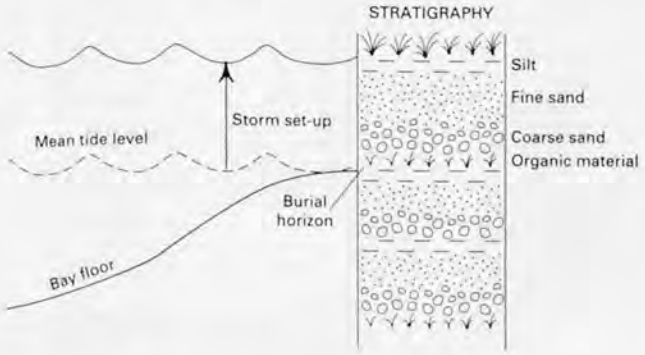

Figure 40. Hypothetical storm deposits composed of cyclic vertical sequences of sand and silt burying marsh horizons. Waning storm conditions might produce fining-upward sequences, whereas variable ocean set-up and tidal cycles might produce more complex layering of sand and silt. The burial of successive supratidal marsh horizons by storm resuspension and deposition would require catastrophic storms superimposed on a longer term trend of coastal submergence.

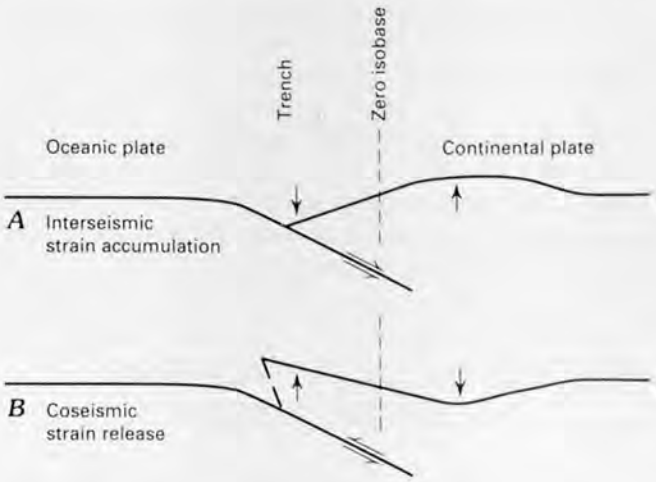

Figure 41. Vertical tectonic relations associated with (*A*) coupled strain accumulation and (*B*) coseismic shear dislocation between a subducting oceanic plate and an overriding continental plate (Ando and Balazs, 1979). The relative position of the coastline and the upper plate flexure line, or zero isobase (Plafker and Kachadoorian, 1966), determines the direction of coastal tectonic displacement during alternating periods of aseismic strain accumulation and coseismic dislocation. Arrows show direction of relative vertical movement on either side of the zero isobase. Barbs show directions of relative plate movement along the fault.

additional 0.5 m of submergence during high tides in Alsea Bay. The effects of a changing tide-level range on existing marsh systems in the Pacific Northwest bays have not previously been examined. However, significant changes in tide range could possibly stress marsh systems, resulting in diminished plant growth and possible burial by sediment.

SUBDUCTION–ZONE TECTONICS

Finally, subduction-zone tectonics might produce episodic marsh emergence and submergence in the convergent-margin setting of the Pacific Northwest. In the CSZ, coastal subsidence or uplift might result from the cyclic strain accumulation and release associated with frictional coupling of the overriding continental plate and subducting oceanic plate (Fitch and Scholtz, 1971; Savage, 1983). The direction of vertical displacement generally depends on the coastline position relative to an elastic flexure line called the zero isobase of vertical deformation (Plafker and Kachadoorian, 1966) (fig. 41). In the case of a coastline position landward of the zero isobase, coastal uplift should be gradual (intersiesmic strain accumulation) whereas coastal subsidence should be abrupt (coseismic strain release). An inverse relation should hold for coastline positions seaward of the zero isobase. However, local upper-plate faults and folds can complicate this deformation pattern (Plafker, 1972; Clarke and Carver, 1992). The tidal-marsh deposits of the central Oregon coast could record abrupt subsidence events if interplate elastic strain is released episodically and the coastal position of the marsh site is landward of the zero isobase.

Marsh-burial sequences produced by coseismic regional subsidence and settling (Plafker and Kachadoorian; 1966) should occur throughout the estuary marsh system and

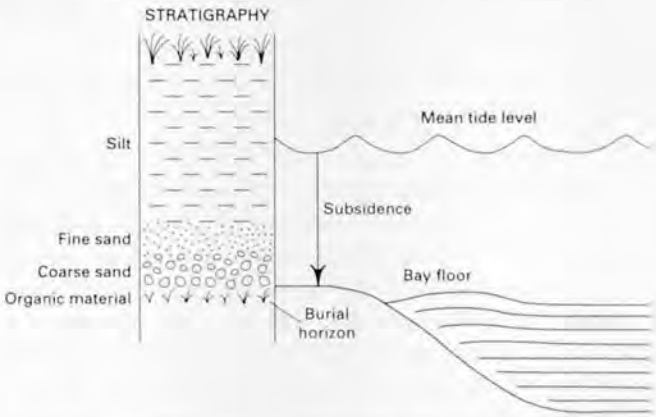

Figure 42. Hypothetical subsidence deposit including a fining-upward vertical sequence of sand to mud and colonizing marsh above the buried preexisting marsh surface. Sand and mud ratios in basal lower-intertidal layers might vary between sites as a function of local sediment supply and resuspension energy. However, the upper-intertidal to supratidal layers should increase in mud and organic material as the depositional surface approaches the maximum reach of high-tide levels.

should consist of low-energy tidal-flat deposits of finely laminated or bioturbated mud overlying the submerged marsh surface (fig. 42). Such laminated or bioturbated muds are most commonly deposited in the protected tidal-flat environments of the Pacific Northwest estuaries (Clifton and Phillips, 1980; Peterson and others, 1982). They indicate prolonged periods of low rates of deposition.

Of particular interest to paleoseismologists is the great potential for tsunami excitation associated with coseismic coastal displacement (Heaton and Hartzell, 1986). Evidence of tsunami sediment deposits immediately above the buried marsh surfaces would indicate marsh burial by coseismic subsidence (Atwater, 1987). Such deposits should reflect a marine-source mineral composition and should diminish in thickness with increasing distance upriver (landward) if they are indeed produced by landward-directed tsunamis.

FIELD AND LABORATORY PROCEDURES

Cutbank exposures of the Alsea Bay marsh in the northern side of the south channel and in both sides of the north channel (fig. 34) were examined for evidence of distinct peaty horizons. The cutbanks (1–1.5 m vertical exposure) are a continuous, circumferential exposure of the shallow stratigraphy of the Alsea Bay marsh system. Two buried peaty horizons and associated sandy sediment capping layers (SCLs) were stratigraphically correlated around the central-marsh and north-channel cutbanks. The subsurface depth of the upper contacts of the two buried peaty horizons were measured in representative stratigraphic sections. A total of 62 shallow stratigraphic sections were measured at spaced intervals around the central-marsh circumference (see fig. 43 for cutbank locations). The marsh-interior stratigraphy was investigated by deeper coring.

A total of 21 cores (19 different sites) were taken from 2–7 m below the surface along a west-east traverse (4 km between sites AB1 and AB13) and two north-south traverses (about 1 km each between sites AB21 and AB18 and between sites AB19 and AB17) (fig. 44). The west-east traverse extends from the middle estuary (exposed to wind-storm processes) to the upper estuary (influenced by river processes) as defined by the hydrography (McKenzie, 1975) and sediment-dispersal patterns (Peterson and others, 1982). The two north-south traverses are oriented perpendicular to the south channel, the major conduit of river-tidal flow in the upper estuary. The Alsea River valley and fringing marshes narrow greatly to the east (upriver) of core site AB12. Core site AB1 (at the western end of the traverse) contains only two thin marsh horizons (25 cm thick) over barren tidal-flat sand, and it probably represents the most westward position attained by the contiguous marsh system in late Holocene time.

Two types of marsh cores were taken in the study area, including continuous cores in ABS plastic pipe (5- and 7.5-cm diameter) and gouge cores (2.5-cm diameter) returned from successively deeper 1-m intervals to depths of as much as 7 m. The uncontaminated continuous cores

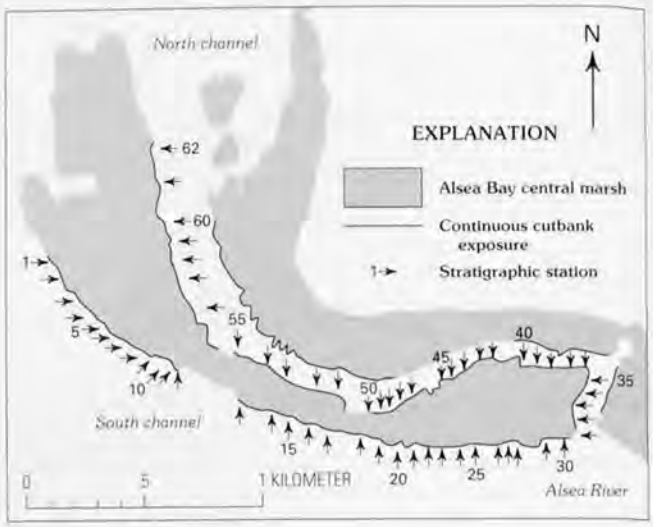

Figure 43. Map of cutbank exposures examined in the middle and upper reaches of Alsea Bay. The solid line represents continuous exposure of two buried peaty horizons. Stratigraphic sections were measured at 62 stations (every fifth station is numbered).

were used for quantitative sediment analyses and for radiocarbon dating of peat horizons. Sediment contamination can occur in gouge cores, but they yield negligible sediment compaction during coring. Gouge cores were generally used for horizon depth control at continuous core sites and for stratigraphic correlation of key horizons between cutbank sites and continuous-core sites.

The core sites were surveyed to the local MTL based on a tidal bench mark (Oreg. No. 9434938) adjacent to core site AB12. Elevation surveys of most core sites and of the modern marsh and tidal flats (adjacent to core sites AB20 and AB17) were made using an autolevel (accuracy, ±0.1 m MTL). The elevations of core sites AB21, AB6, AB12, and AB13 were estimated based on both marsh-surface elevations from adjacent core sites and long-distance sightings with the surveying level (accuracy, ±0.3 m MTL).

Marsh cores were returned to the laboratory for detailed examination, sediment subsampling, and archival in the refrigerated core facility at Oregon State University in Corvallis. Cores were logged to the nearest 1-cm-depth interval in the laboratory. Visual estimates of sediment texture and organic content in cores were calibrated against quantitatively analyzed samples from core sites AB8, AB12, and AB21 (see below). Selected sediment horizons at these three sites were analyzed for sediment dry bulk density after drying at 60°C for 24 hours (Gardner, 1965); relative abundance of organic material, that is, weight loss on ignition at 380°C for at least 10 hours (Andrejko and others, 1983); and relative

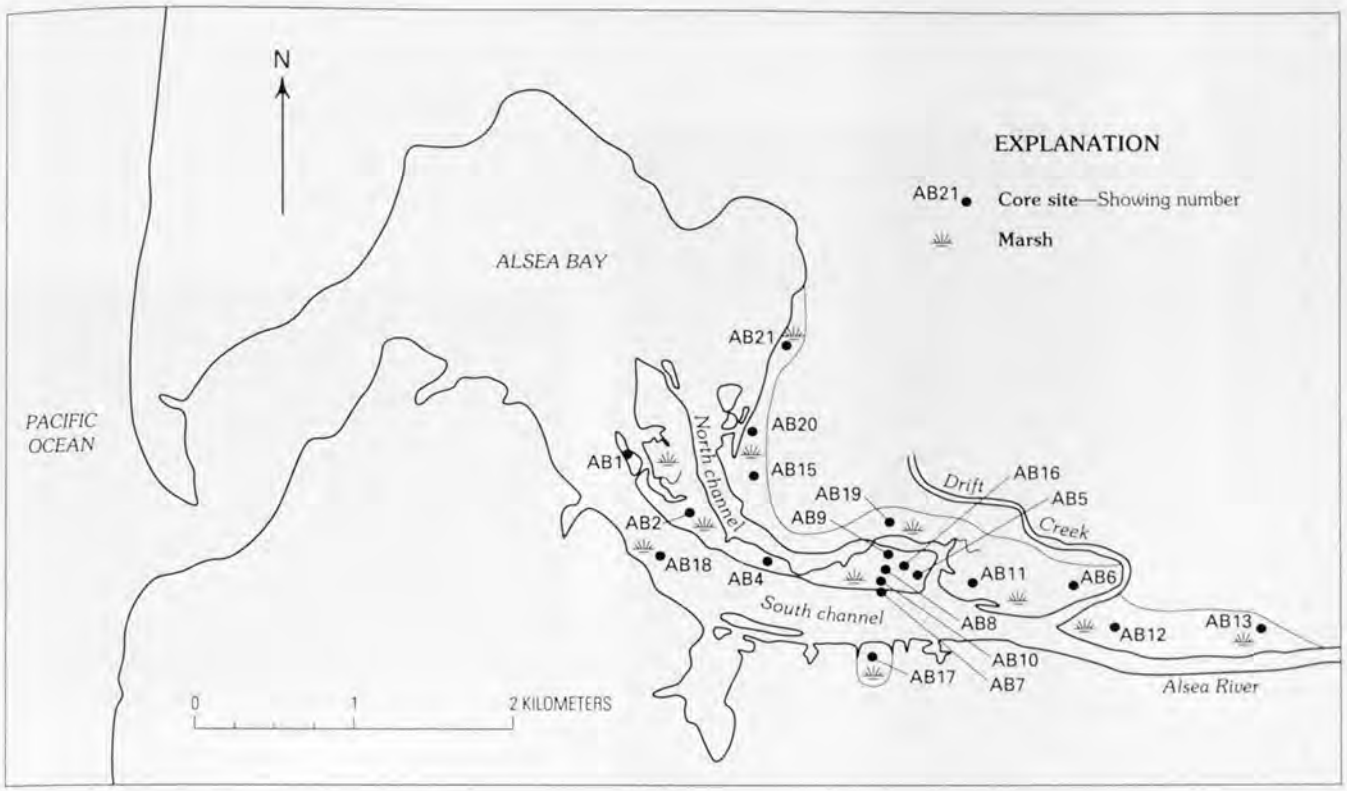

Figure 44. Core sites used to study the Alsea Bay marsh-interior stratigraphy.

abundance of sand (sieve diameter greater than 0.062 mm), silt, and clay after organic oxidation by H_2O_2 (Folk, 1980).

Sand-source mineral composition was established for selected core intervals from sites AB2, AB4, AB9, AB12, AB15, AB18, AB19, and AB21 by petrographic analysis of the heavy-mineral fraction. At least 200 diagnostic mineral grains (pyroxenes) were counted per sample slide to estimate relative abundances of river and beach sand. River pyroxene minerals are angular and consist solely of augite, whereas beach pyroxene minerals are rounded and contain an average hypersthene:augite ratio of 0.60 (Peterson and others, 1982; Peterson and others, 1984). Measurements of grain roundness and hypersthene:augite ratios were normalized to yield percent beach sand and percent river sand.

Approximate ages of marsh-burial events were estimated by radiocarbon dating of the top 5–10 cm of selected buried peats from core site AB9. The peats were hand picked, oven dried, and sent to a commercial firm (Beta Analytic, Inc., Coral Gables, Fla.) for radiocarbon age determination. Standard pretreatment leaches were performed there to remove potential contaminants. Peat ages were adjusted by $^{12}C/^{13}C$ ratios and were calibrated from established tree-ring calibration curves (Stuiver and Reimer, 1986). All peat ages are assumed to predate the corresponding burial events.

STUDY RESULTS

TIDE-ELEVATION RANGES OF THE MODERN MARSH

Modern marsh development in Alsea Bay is clearly zoned with respect to tide levels (Jefferson, 1975). Our observations and measurements of marsh-plant assemblages in Alsea Bay (table 10) indicate that the densely vegetated surfaces of the modern high marsh range between 1.4 and 1.8 m above MTL. High-marsh plants in Alsea Bay include *Deschampsia caespitosa*, *Juncus sp.*, *Potentilla pacifica*, and *Grindelia integrifolia*. Trees (spruce and alder) are presently colonizing the highest marsh upland surfaces (higher than 1.8 m above MTL) on elevated dikes and levees and in landward marsh perimeters.

The lowest tidal elevations of continuous marsh development (low marsh) range from 0.6 to 1.1 m above MTL. The low-marsh plants include, among others, *Salicornia virginica* and *Triglochin maritimum*. Isolated patches of colonizing marsh in protected settings are found between 0.3 and 0.6 m above MTL. Unvegetated tidal-flat sediments in the central and upper reaches of Alsea Bay are typically 0.3–0.6 m higher than MTL. In summary, the laterally continuous development of most of the modern salt marsh in Alsea Bay

Table 10. Modern marsh elevations and tide levels in Alsea Bay.

Marsh type	Tidal stage	Elevation range relative to mean tide level (meters)
High marsh		+1.4 to +1.8
Transitional marsh		+1.1 to +1.4
Low marsh (top)		+1.1
	Mean higher high water (MHHW)	+1.01
	Mean high water (MHW)	+0.80
Low marsh (bottom)		+0.6
Tidal flat		+0.4 to +0.6
Colonizing marsh		+0.3 to +0.6
	Mean tide level (MTL)	0.00
	Mean low water (MLW)	–0.08
	Mean lower low water (MLLW)	–1.01

extends over a tidal range of 1 m (0.6–1.6 m above MTL). However, at least 90 percent of the modern marsh surface is restricted to a much narrower elevation range, that is, high marsh at 1.4–1.8 m above MTL.

The modern marsh surface is a well-constrained tide-level datum. Depths and ages of prehistoric tidal-marsh surfaces record past changes in relative sea-level position. However, specific indicators of high-marsh, low-marsh, and colonizing-marsh settings are needed to establish the elevations of the buried marsh surfaces relative to their corresponding paleotide levels. One such indicator is the relative abundance of peaty material in the marsh subsurface. The organic content of the modern marsh substrate (rooted zone) decreases greatly from the highest marsh elevations to the unvegetated tidal flats in Alsea Bay, as in other Oregon marsh systems (Darienzo and Peterson, 1990).

Generally speaking, as the marsh surface reaches supratidal elevations, the tidal-river supply of inorganic sediments is shut off and the percentage of organic materials (peat) increases. Subsequent oxidation can decrease the relative abundance of organic materials but cannot increase it. Thus, measurements of the percentage of organic material in marsh sediments provides useful criteria for establishing paleotide elevations of prehistoric marsh surfaces. Diatoms and plant macrofossils in marsh sediments can also provide information about paleosalinity and therefore paleotide level in some marsh deposits (Atwater, 1988; Darienzo and Peterson, 1990). However, the abrupt vertical transition from a freshwater diatom flora to an overlying brackish water-marine flora, as seen in Netarts Bay cores (Darienzo and Peterson, 1990), was not observed in Alsea Bay cores. Thus, diatoms were not used as paleotide-level indicators in this study. Plant macrofossils, specifically *Triglochin maritimum* rhizomes (a common tidal-flat colonizer), were identified in some cores at subsurface depths greater than 1.5 m. Their presence at the base of several developed peaty horizons suggests transition from colonizing marsh to high-marsh settings.

For cutbank and core-log descriptions, the relative peat development in the Alsea Bay marshes is defined as follows: peat (greater than 50 percent organic material by dry weight), muddy or sandy peat (25–50 weight percent organics), peaty mud or sand (15–25 weight percent organics), slightly peaty mud or sand (10–15 weight percent organics), rooted or slightly rooted mud or sand (5–10 weight percent organics), and barren mud or sand (less than 5 weight percent organics). Semiquantitative descriptions of the relative abundance of organic materials are based on laboratory comparisons with core samples quantitatively analyzed by dry-sample weight loss on ignition.

Quantitative measurements of organic content from selected marsh horizons in Alsea Bay were performed to (1) establish relative abundances of organic material in modern marsh horizons with known tide elevations, (2) calibrate visual estimates of peat development with measured percentages of organic materials in marsh cores, and (3) document downcore variations in percentages of organic material in marsh cores. Measured organic matter in core samples from modern high-marsh horizons (table 10) contained greater than 25 percent organic material. By comparison, barren-mud deposits in Oregon bays generally contain less than 5 percent organic material (Powell, 1980; Darienzo and Peterson, 1990).

The transition between colonizing-marsh and established low-marsh elevations (table 10) is commonly complicated by the patchy development of colonizing-marsh plants. Therefore, assignment of a representative organic content to this transition zone is somewhat arbitrary. Nevertheless, the examination of marsh cores from Alsea Bay indicates that a minimum value of 10 percent organic material over a 5–10-cm-depth interval can be used to discriminate between established low-marsh horizons and the colonizing marsh or algal mud-flat horizons in Alsea Bay.

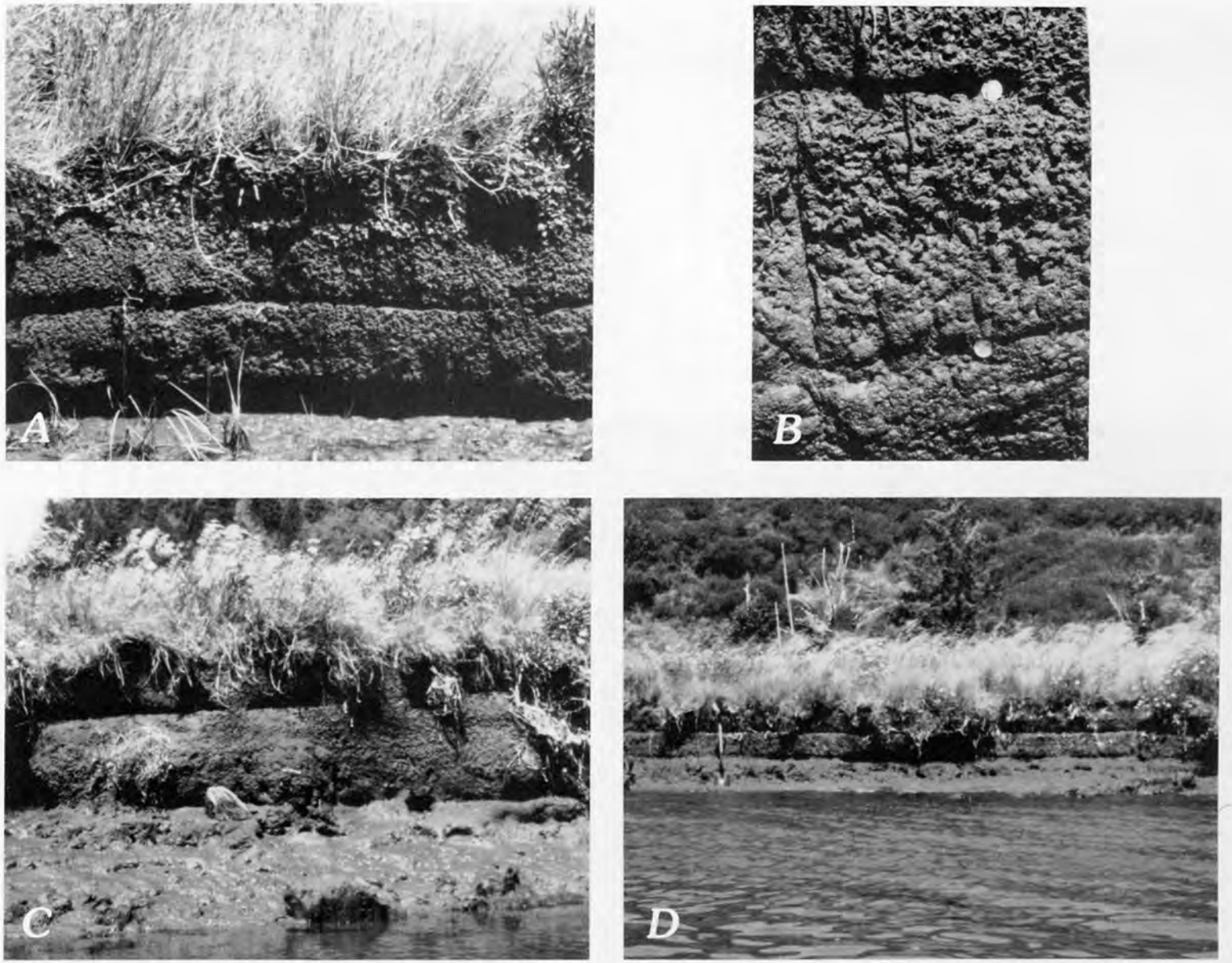

Figure 45. Two buried peaty horizons in cutbank exposures in the Alsea Bay marsh. *A*, northwest cutbank of south channel; *B*, northeast cutbank of south channel; *C*, northeast bank of north channel; *D*, northwest bank of north channel. Sandy layers (generally several centimeters thick) directly above peaty horizons are differentially eroded, producing two shadowed horizontal indentations that correspond to the two peat tops in *A*, *C*, and *D*. Coins mark the tops of the two buried peat horizons in *B*.

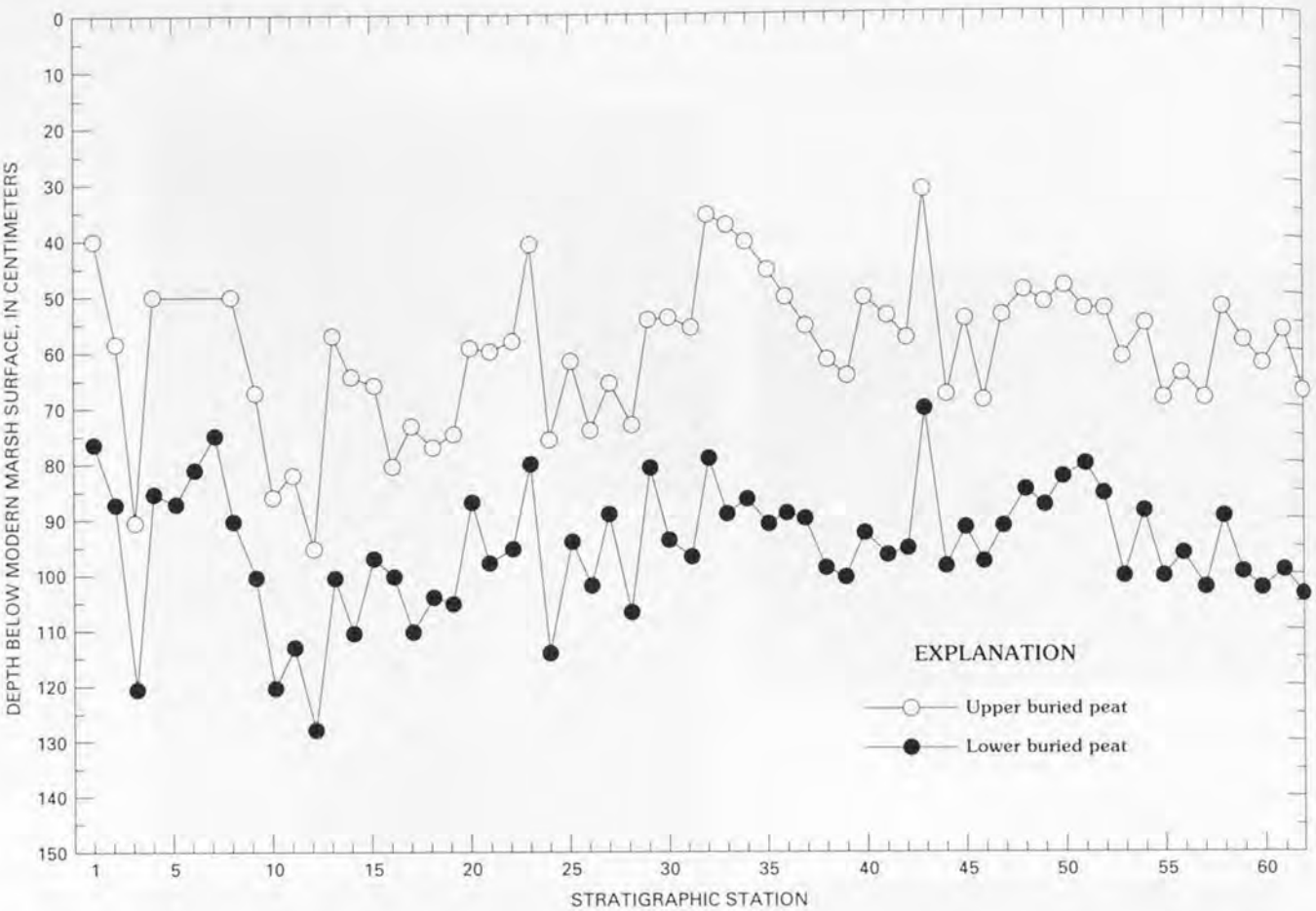

Figure 46. Correlation of two buried peat horizons (buried marsh tops) in 62 measured sections from the central-marsh area in Alsea Bay. Depths of the two buried peat tops below the modern marsh surface are plotted against stratigraphic station number around the central-marsh-island perimeter (a total distance of 4.5 km). The modern marsh surface is arbitrarily set at 0 cm depth for this figure. See figure 43 for stratigraphic station locations and table 11 for corresponding measurements of horizon depth.

CORRELATIONS OF SHALLOW PEATY HORIZONS IN CUTBANKS

The central Alsea Bay marsh is cut by two major tidal channels, the south channel and the north channel (fig. 34). Due to modification of the tidal flow in these channels at their upstream confluence beginning in the early 1900's to divert water first into the north and later into the south channel, the banks of the channels have eroded, exposing the undisturbed marsh stratigraphy. Marsh deposits are very well exposed to 1–1.5 m below the modern marsh surface along the channel cutbanks. Cutbanks are present but are less continuous upstream of the confluence of the north and south channels. The Alsea Bay marsh system possibly is unique within coastal Oregon in containing nearly continuous cutbank exposures of about 13 km in length that extend 6 km east-west, or about one-half the length of the bay. A total of 6.4 km of cutbank exposures in the central-marsh area were mapped for shallow-marsh stratigraphy (fig. 43).

Cutbank exposures in the central Alsea Bay marsh reveal two buried peaty horizons at average depths of about 0.5 m and 1 m below the modern root zone. A third buried peaty horizon was infrequently observed 1–1.5 m below the modern marsh, its exposure being limited by modern sedimentation along the channel banks. The two upper muddy-peat horizons have gradational lower contacts with peaty muds or slightly peaty muds and have sharp upper contacts with thin (1–10 cm thick) sandy layers. The sandy layers above each of the upper buried peats have been differentially eroded by current and wind-wave scour to produce horizontal indentations directly above each buried peaty horizon (fig. 45). An orange-brown oxidized zone (1–2 cm thick) was also rarely observed at a depth of about 0.25 m below the modern marsh surface. No sandy layers were observed directly above this anomalous oxidized zone.

The two upper buried peat horizons were nearly continuously correlated for 4.5 km around the circumference of the central-marsh island (fig. 34) and along 1.9 km of the southern bank of the north channel (figs. 43, 46). The depths

Table 11. Depths of shallow peaty horizons below modern marsh in cutbanks at Alsea Bay.

[See figure 43 for locations of stratigraphic stations]

Stratigraphic station	Depth of upper buried peat (centimeters)	Depth of lower buried peat (centimeters)
AB1	40	76
AB2	58	87
AB3	90	120
AB4	50	85
AB5	eroded	87
AB6	eroded	81
AB7	eroded	75
AB8	50	90
AB9	67	100
AB10	86	120
AB11	82	113
AB12	95	128
AB13	57	100
AB14	64	110
AB15	66	97
AB16	80	100
AB17	73	110
AB18	77	104
AB19	75	105
AB20	59	87
AB21	60	98
AB22	58	95
AB23	41	80
AB24	76	114
AB25	62	94
AB26	74	102
AB27	66	89
AB28	73	107
AB29	55	81
AB30	54	94
AB31	56	97
AB32	36	79
AB33	38	89
AB34	41	87
AB35	46	91
AB36	51	89
AB37	56	90
AB38	62	99
AB39	65	101
AB40	51	93
AB41	54	97
AB42	58	96
AB43	32	71
AB44	68	99
AB45	55	92
AB46	69	98
AB47	54	92
AB48	50	85
AB49	52	88
AB50	49	83
AB51	53	81
AB52	53	86
AB53	62	101
AB54	56	89
AB55	69	101
AB56	65	97
AB57	69	103
AB58	53	90
AB59	59	100
AB60	63	103
AB61	57	100
AB62	68	104

to the tops of the two peat horizons vary from 32 to 95 cm (upper horizon) and from 71 to 128 cm (lower horizon) below the modern marsh surface (table 11). The separation distance between the two buried peaty layers was also found to vary significantly, from 20 to 51 cm. The variation in stratigraphic depth of the buried peaty horizons has resulted from topographic relief of both the paleomarsh and modern marsh surfaces. Such relief is typically on the order of 30–40 cm for the modern high marsh in central Alsea Bay (table 10).

MARSH VERTICAL SEQUENCES

The deeper stratigraphy of the Alsea Bay marsh was determined on the basis of detailed logs taken from a west-east core traverse (fig. 47*A*, *B*) and a north-south core traverse (fig. 47*C*) of the central-marsh system. Maximum core lengths ranged from 2 m (site AB2) to 7 m (sites AB8 and AB9). Our hand-coring devices were unable to penetrate thick sandy horizons (0–1 m below MTL) in either the lower-bay marsh (sites AB1, AB2, AB4, and AB20) or the south-channel banks (sites AB17 and AB18). By comparison, relatively deep cores (–4 to –5.5 m relative to MTL) were consistently obtained from the central marsh (sites AB7, AB8, AB9, AB11, and AB19), which has very fine grain deposits.

All of the analyzed cores from the Alsea Bay central marsh show multiple horizons of peat or peaty mud (5–75 cm thick) that are commonly separated by very low organic (VLO) sediments (fig. 47). The tops of the black, peaty horizons (buried marsh surfaces) generally consist of sharp contacts (less than 1 cm wide) with overlying deposits. In contrast, the contacts between the bottoms of the peaty horizons and the underlying VLO sediments are generally gradational, that is, organic content decreases downcore. An analysis of 95 individual peaty horizons (more than 5 cm thick) from the 19 core sites showed that at least 80 percent of the peat units have sharp upper contacts and gradational lower contacts. These relatively consistent changes in peat development define the tops and bottoms of distinct marsh horizons, even where intervening layers of VLO mud or sand are not present.

The layers of VLO sediments between the peaty horizons are quite variable in thickness and composition. The barren or slightly rooted mud layers are either finely laminated or homogeneous to the naked eye and range from 2 to 125 cm thick (fig. 47). At least 50 laminations (1–5 mm thick) were counted in one VLO mud layer (20 cm total thickness) x-rayed in a thin core slab from site AB4. The VLO layers generally decrease in thickness (50 down to 5 cm thick) from deep core intervals to shallow core intervals. Some of the youngest peaty horizons in the uppermost core intervals are separated by very thin rooted mud or sand layers (1–2 cm thick), such as that shown at about 1 m above MTL at site AB2 (fig. 47*A*). In contrast, thick basal layers (more than 0.5 m thick) of barren sand or muddy sand occur below the peaty marsh deposits in the western core sites (AB2, AB4, AB18, and AB20; see figs. 44 and 47*A*). These VLO basal deposits probably represent barren tidal-flat environments only recently colonized by a prograded marsh.

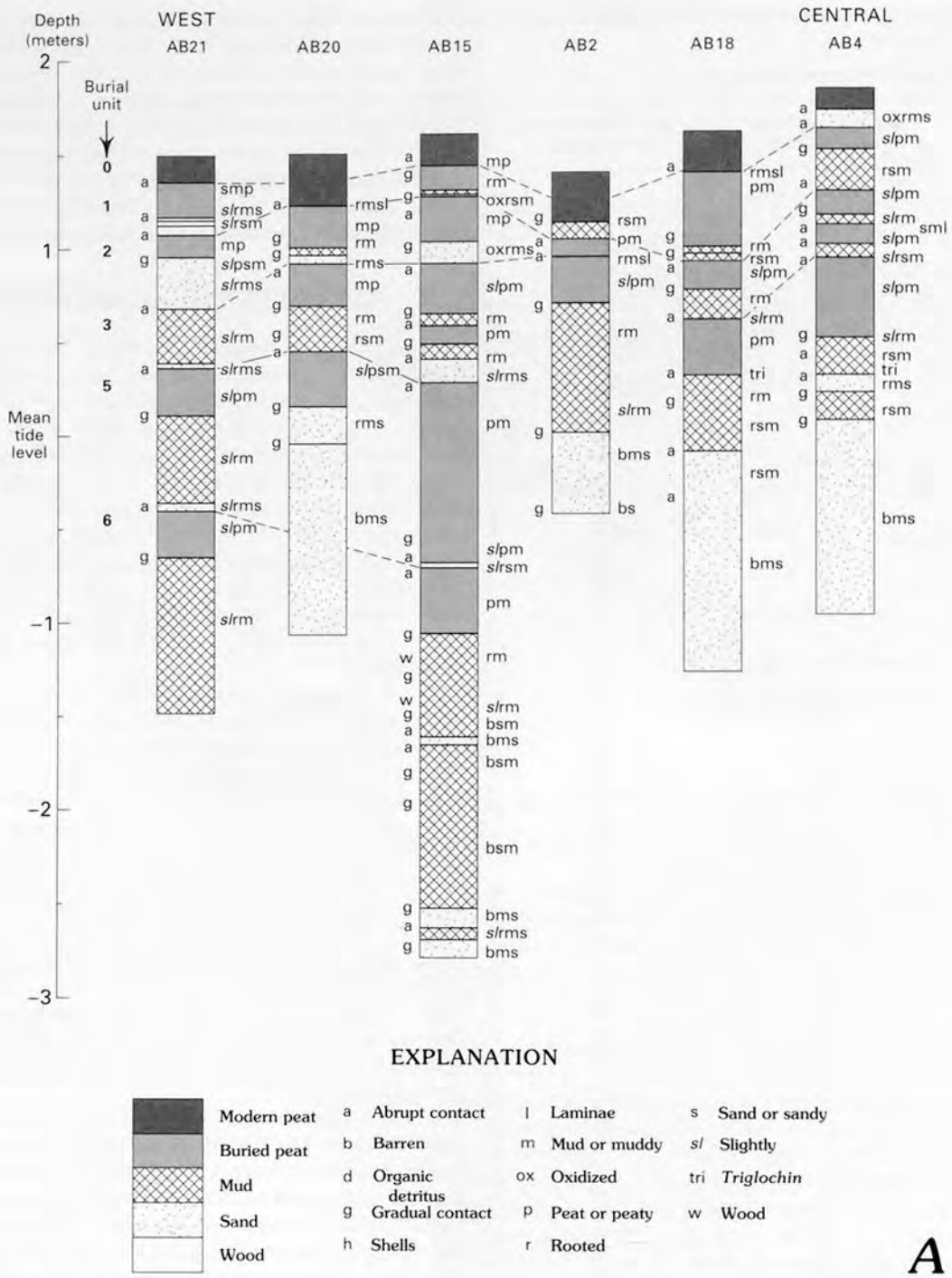

Figure 47 (above and following two pages). Core logs and stratigraphic correlations of key peaty horizons in the Alsea Bay marsh system. *A*, west-central marsh; *B*, east-central marsh; *C*, central marsh (north to south). Solid lines are apparent correlations; dashed lines are less certain correlations. Burial units are numbered 0–10 in core sections from sites AB21, AB12, and AB8. Elevations of sections for cores AB6, AB12, AB13, and AB21 are approximate. Additional quantitative analyses of selected horizons are listed in table 12.

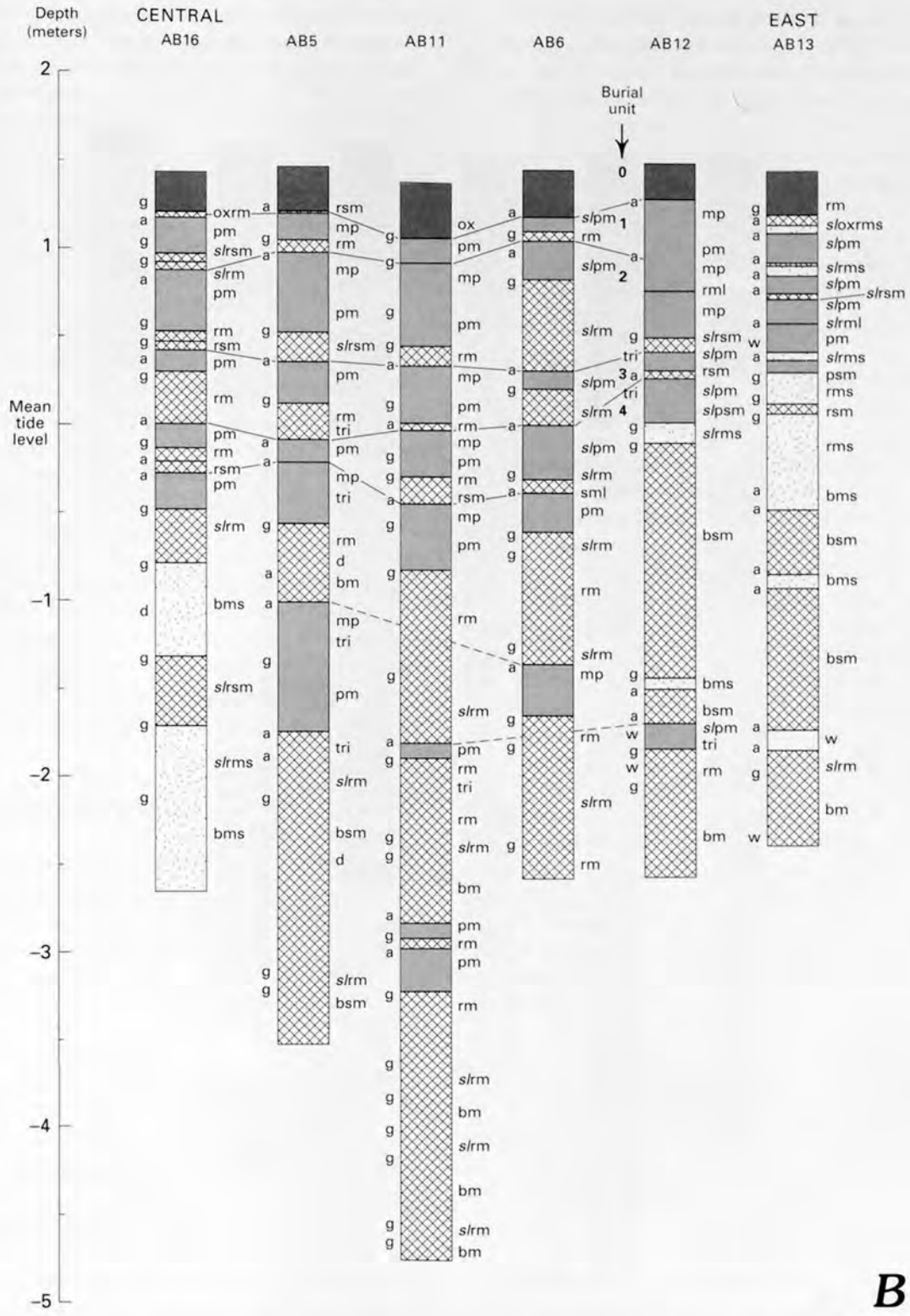

Figure 47. Core logs and stratigraphic correlations of key peaty horizons in the Alsea Bay marsh system—Continued

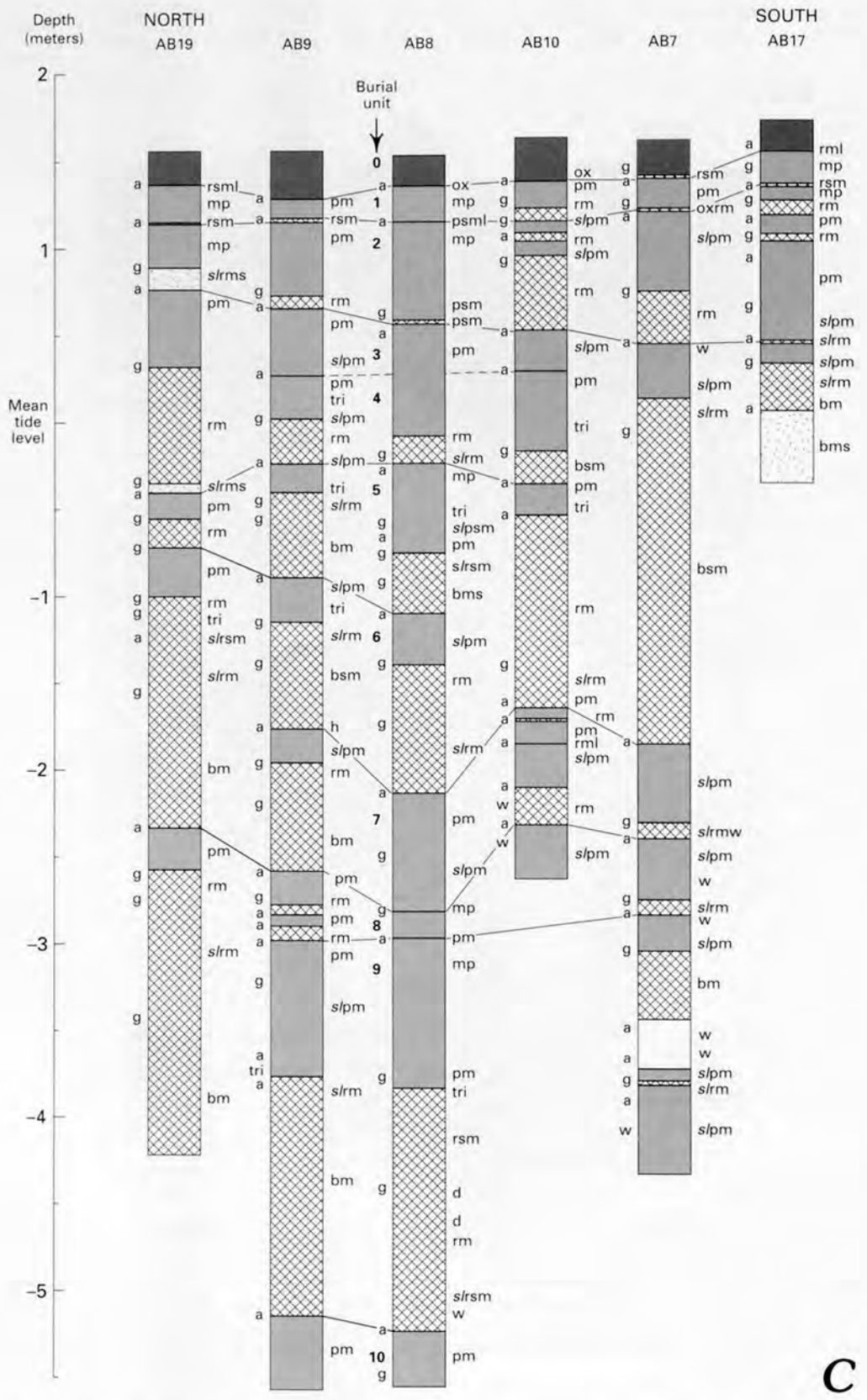

Figure 47. Core logs and stratigraphic correlations of key peaty horizons in the Alsea Bay marsh system—Continued

The bases of some VLO layers and some peat horizons (0.5–1.5 m above MTL) in the western-marsh sites and in sites along the north channel of the central marsh are characteristically enriched in sand (fig. 47). The thin, structureless sands (SCLs) contrast with both the overlying laminated muds or peaty muds and with the underlying peaty horizons. The observed SCLs in the Alsea Bay marsh cores range from 25 cm to less than 1 cm thick. The thicknesses of the SCLs generally decrease with distance from the northwestern bay marsh to the eastern confluence of the north channel, or from site AB21 to site AB16 (figs. 44, 47). Finally, the bases of the two to three uppermost peaty horizons are variably oxidized (orange brown) at many of the marsh core sites (AB4, AB7, AB8, AB10, AB11, AB13, AB15, and AB16), indicating temporary desiccation and exposure to oxidizing conditions.

The vertical sequence of an SCL and (or) VLO layer grading upward into a fully developed peaty horizon represents a complete burial unit. However, some preserved burial units locally do not contain an SCL or thick VLO mud layer. Nevertheless, the vertical repetition of multiple burial units throughout the Alsea Bay marsh represents a repeating sequence of episodic marsh emergence (peat development), then submergence (peat burial by VLO mud). Finally, the dominant contact relations of the buried peaty horizons (gradational lower contacts and sharp upper contacts) indicate that emergence events were generally gradual, whereas submergence events were abrupt.

MARSH STRATIGRAPHIC CORRELATION

Using both the relative depths and numbers of peaty vertical sequences, we correlated key stratigraphic horizons between adjacent core sites. For example, three peat burial units in the uppermost 1.5 m of the central marsh are correlated between sites AB8, AB9, AB10, AB11, AB16, and AB19 (fig. 47*B*, *C*). As described in a preceding section, the upper two units have been traced continuously for several kilometers in exposed cutbanks in the central-marsh area. At least 10 peat burial units were observed to depths of –5.5 m relative to MTL (maximum core penetration) at sites AB8 and AB9 (fig. 47*C*).

Similarly, distinct peaty horizons from the upper 1.5 m of the western and eastern marsh areas are stratigraphically correlated with key horizons of the central marsh (fig. 47). Vertical offsets of 10–30 cm between corresponding peat horizons from nearby core sites are relatively common in the western marsh area. These vertical offsets are consistent with the elevation differences (10–40 cm) of the modern marsh surface (table 10), and they probably reflect the variability of the older marsh elevations prior to burial. By comparison, corresponding peaty horizons in the eastern marsh area are relatively consistent in elevation except for the furthest upriver location (site AB13 in fig. 47*B*).

It is not possible to confidently extend the deeper marsh stratigraphy (0 to –5 m relative to MTL) beyond the central-marsh area because of the shallow depths of core penetration in the sand-rich western sites and the relatively poor preservation of peaty horizons or lack of marsh development below MTL in the western and eastern core traverses. However, the broad correlation of the shallow peat horizons in the top 2 m throughout most of the central, western, and eastern marsh sites provides the necessary control to test several different mechanisms of marsh burial in Alsea Bay. The following sections focus on these uppermost horizons.

QUANTITATIVE ANALYSES OF PEATY UNITS

Quantitative analyses of organic content and sediment grain size in the modern marsh and in burial units were performed on samples from core sites AB21 (western site), AB8 (central site), and AB12 (eastern site) (fig. 44, table 12). Analyses of burial unit marsh tops (MT) and marsh bottoms (MB) or underlying VLO muds are used to verify visual interpretations of core-site stratigraphy as shown in the figure 47 core logs. Due to the wide separation of these three core sites, the quantitative results can be used to compare marsh response to burial processes between tidal- and river-dominated settings. In addition, grain-size analysis was performed on the SCLs from site AB21 to establish the variability of sand-size-fraction abundances between these anomalous sandy layers and the underlying marsh tops. For purposes of clarity, we restate the horizon identification scheme used here. Successively deeper burial units are numbered from 1 to 10 (fig. 47*A*, site AB21; fig. 47*B*, site AB12; fig. 47*C*, site AB8). For example, the top of burial unit 2 is the marsh top (2MT) whereas the bottom of the unit is the corresponding 2SCL. Therefore, 2SCL overlies 3MT, and 2MT underlies 1SCL.

As indicated in the marsh core logs (fig. 47*B*, *C*), the organic content and percentages of sand versus silt-clay (mud) in the inorganic fraction vary systematically downcore in burial units from the central and eastern marshes (table 12). Organic content, established by loss on ignition, increases one- to threefold from the bottom to the top of most burial units from sites AB8 and AB12 (fig. 48). In contrast, the percentage of sand in the inorganic fractions tends to decrease over the same intervals (fig. 49). Organic content and sand percentage show the strongest inverse correlations in the lower stratigraphic sections (burial units 2, 3, and 4). These trends demonstrate a diminishing supply of inorganic sediments, particularly coarse size fractions, relative to organic material in the developing peaty horizons. The increase in relative abundance of organic materials is due to a decrease in the supply of water-borne siliciclastic sediments as the colonizing marsh emerges to supratidal elevations.

Table 12. Organic content and sediment grain sizes of buried layers in three cores from Alsea Bay marshes.

[The burial unit number is followed by the marsh horizon designation: MT, peaty marsh top; MB, peaty marsh bottom; RMT, rooted mud top; RMB, rooted mud bottm; S, very low organic (barren) sediment; SCL, sediment capping layer. The surface is 1.50 m above the mean tide level. (--), no data]

Horizon	Depth relative to mean tide level (meters)	Density (grams/cubic centimeter)	Organic material (percent)	Sand (percent)	Silt and clay (percent)
Core site AB21 (western marsh)[1]					
0MT	1.46	0.28	29.0	10.8	89.2
0MB	1.40	--	34.4	13.0	87.0
1MT	1.34	0.42	41.1	13.0	87.0
1MB	1.25	--	41.8	12.1	87.9
1SCL	1.18	--	--	76.9	23.1
2MT	1.06	--	32.2	8.9	91.1
2MB	1.00	--	10.0	40.0	60.0
2SCL	0.75	1.47	--	88.5	11.5
3RMT	0.63	0.65	7.9	10.8	89.2
3RMB	0.41	--	5.7	0.3	99.7
3SCL	0.35	--	--	58.1	41.9
5MT	0.32	0.53	9.9	0.7	99.3
5S	0.06	--	6.0	4.1	95.9
5SCL	–0.37	--	--	81.8	18.2
6MT	–0.41	0.52	13.0	0.9	99.1
6S	–0.65	--	5.3	1.1	98.9
Core site AB8 (central marsh)					
0MT	1.49	--	43.7	2.2	97.8
0MB	1.43	--	40.0	6.7	93.3
1MT	1.35	0.23	37.6	0.9	99.1
1MB	1.18	--	37.5	1.8	98.2
2MT	1.10	0.26	48.2	0.3	99.7
2MB	0.74	--	12.2	20.8	79.2
3MT	0.55	--	17.1	2.3	97.7
3MB	0.38	--	14.0	1.0	99.0
4MT	0.19	0.29	13.8	0.2	99.8
4S	–0.12	--	6.9	1.9	98.1
5MT	–0.23	0.47	27.6	0.5	99.5
5S	–0.97	0.85	4.3	58.4	41.6
6MT	–1.10	0.53	12.2	5.3	94.7
6S	–1.96	--	6.9	6.8	93.2
7MT	–2.12	0.42	23.7	0.9	99.1
7MB	–2.62	--	10.3	0.8	99.2
8MT	–2.82	--	30.9	1.2	98.8
8MB	–2.86	--	16.4	1.1	98.9
9MT	–3.00	0.33	32.9	4.2	95.8
9S	–4.94	--	7.7	12.4	87.6
10MT	–5.22	0.41	23.9	0.6	99.4
Core site AB12 (eastern marsh)					
0MT	1.46	--	32.1	2.0	98.0
0MB	1.37	--	26.6	5.1	94.9
1MT	1.28	0.30	37.2	5.1	94.9
1MB	1.01	--	24.1	4.8	95.2
2MT	0.94	0.31	30.2	0.8	99.2
2S	0.46	--	6.3	12.5	87.5
3MT	0.38	--	15.4	7.6	92.4
3S	0.32	--	9.0	32.3	67.7
4MT	0.27	0.37	12.4	5.7	94.3
4S	0.03	0.90	7.0	68.5	31.5

[1]Burial unit 4 could not be distinguished in this core.

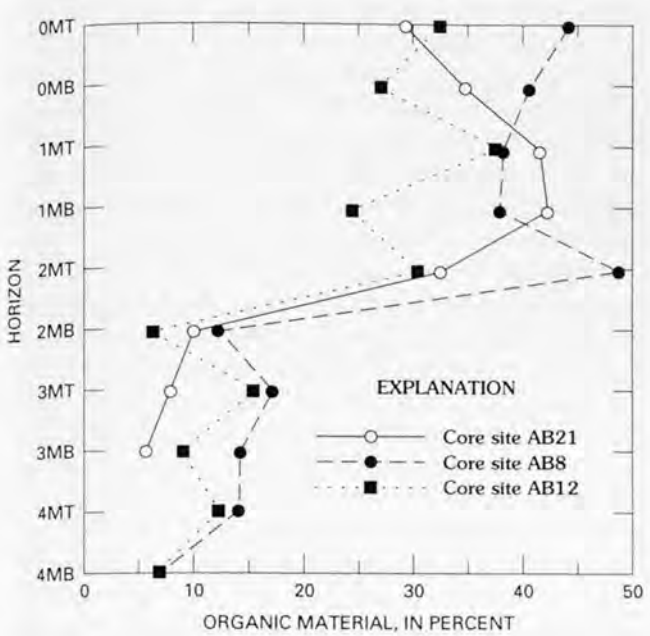

Figure 48. Downcore plots of relative organic-material abundance in peaty horizons of the modern marsh (0 prefix) and four uppermost burial units from three core sites in Alsea Bay. Unit 4 was not found at site AB21. MT, marsh top; MB, marsh bottom. Core sites are shown on figure 44. Measured elevations and additional quantitative data for these horizons are shown in table 12.

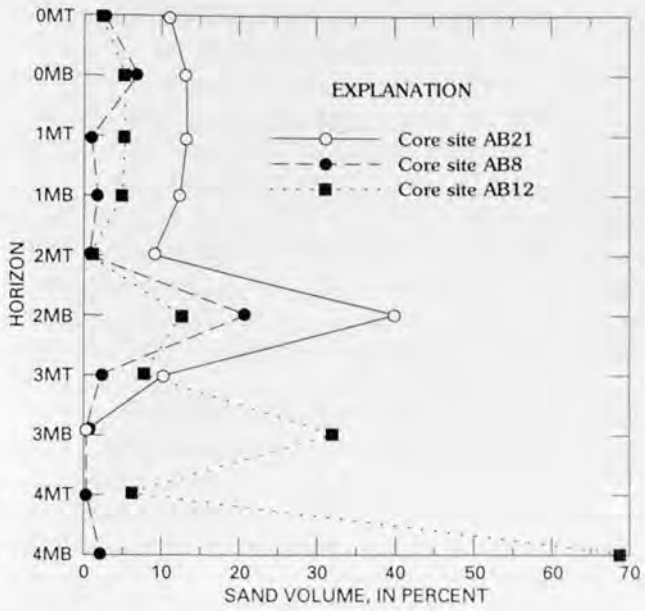

Figure 49. Downcore plots of relative sand abundance in top and bottom peaty horizons of the modern marsh (0 prefix) and four uppermost burial units from three core sites in Alsea Bay. Unit 4 was not found at site AB21. MT, marsh top; MB, marsh bottom. Core sites are shown on figure 44. Measured elevations and additional quantitative data for these horizons are shown in table 12.

By comparison, cyclic variations in either organic content or sand abundance are generally absent from the upper burial units at western-marsh site AB21 (figs. 48, 49). A significant increase in organic content above unit 2MB at site AB21 corresponds to similar increases at central and eastern sites AB8 and AB12, respectively. Whereas the two lower units (3 and 4) generally show upward transitions from colonizing marsh to low marsh (5–15 percent organic material), the upper units (0 and 1) appear to include predominantly high-marsh substrates (24–48 percent organic material). The change in organic content between the 2MT and 2MB horizons at all three core sites indicates a system-wide response to relative sea-level change and further substantiates our stratigraphic correlations of shallow burial units in the Alsea Bay marsh (fig. 47).

Sediment grain-size analyses of the SCLs from site AB21 show substantial differences in the relative sand abundance between the thin SCLs and the underlying peat horizons (table 12). Extreme enrichment of the sand fraction was found at each of the sharp contacts between the SCLs and corresponding buried marsh surfaces (fig. 50). For example, sand abundance increased from 0.9 percent at 6MT to 81.9 percent at 5SCL across this relatively deep contact and from 8.9 percent at 2MT to 76.9 percent at 1SCL across this shallow contact. Relative sand abundance in marsh bottoms or VLO muds from site AB21 are also substantially less than those measured in the SCLs. In summary, the sandy SCLs must have an origin very different from either the peaty horizons or VLO muds that they separate in some intervals of core AB21.

Both the thickness and relative sand percentage in SCLs from central-marsh sites were found to generally decrease with increasing distance up the north channel. For example, 2SCL decreases in thickness from greater than 20 cm at site AB21 to less than 0.5 cm at site AB12, a distance of several kilometers (fig. 47*A*, *B*). The SCLs also decrease in thickness with increasing distance away from the north-channel axis. For example, 2SCL is greater than 5 cm thick at AB19 but is not found at AB10, a distance of 200 m from the channel (figs. 44, 47*C*).

The SCLs are identified here by their relative enrichment of sand. However, some silt-rich laminae (less than 1 cm thick) directly overlie buried peaty horizons in the central- and eastern-marsh areas, such as above 3MT at sites AB8 and AB9 (fig. 47*C*). These anomalous, silty laminae likely correspond to sand-rich SCLs above 3MT at the western-marsh sites. Finally, there is no evidence of SCLs above either 1MT or 4MT within the central-marsh area. The lack of an SCL above the 1MT horizon is possibly consistent with the lack of definition or continuity of the 1MT upper contact with 0MB. In contrast, the 4MT upper contact is well defined at the central-marsh sites, and the lack of a corresponding 3SCL makes the 4MT horizon particularly distinctive in Alsea Bay.

MINERALOGY OF SEDIMENT CAPPING LAYERS

The heavy-mineral assemblages of selected SCLs were investigated to establish the sources (river or marine) of these anomalous sand layers. The thickest SCLs (1SCL above 2MT, 2SCL above 3MT, and 4SCL above 5MT) are found along the northeastern bay margin (sites AB21, AB20, and AB15) and up the north channel (site AB19) (fig. 47*A*, *C*). Heavy-mineral separates from fine-sand-size fractions of these SCLs were analyzed for river and beach sands. The end-member sources were discriminated on the basis of two independent methods—hypersthene:augite ratios and relative grain rounding (Peterson and others, 1982). Heavy-mineral analyses of the sand fractions from underlying marsh tops were also performed to identify any differences in sand source between the anomalous SCLs and the buried peaty horizons.

Sand-source analyses were performed on representative cores from the north channel (sites AB21, AB15, and AB19) and from the south channel (sites AB18, AB4, and AB12). The results of the analyses show striking variations in sand-source composition between SCLs and the underlying buried marsh tops at northern marsh sites AB21, AB15, and AB19 (the contact at site AB12 was also observed under microscope, but only river sand grains constituting less than 1 weight percent of the sediment mass were found) (table 13, fig. 51). Although river sand predominates in all of the analyzed sand fractions (53–100 percent river sand), the SCLs of the northern bay sites are substantially enriched in beach sand. For example, the SCLs range from 14 to 47 percent beach sand at western sites AB15 and AB21, respectively. In contrast, none of the underlying marsh-top horizons or SCLs from the southern bay sites (AB18 and AB4) exceed 10 percent beach sand.

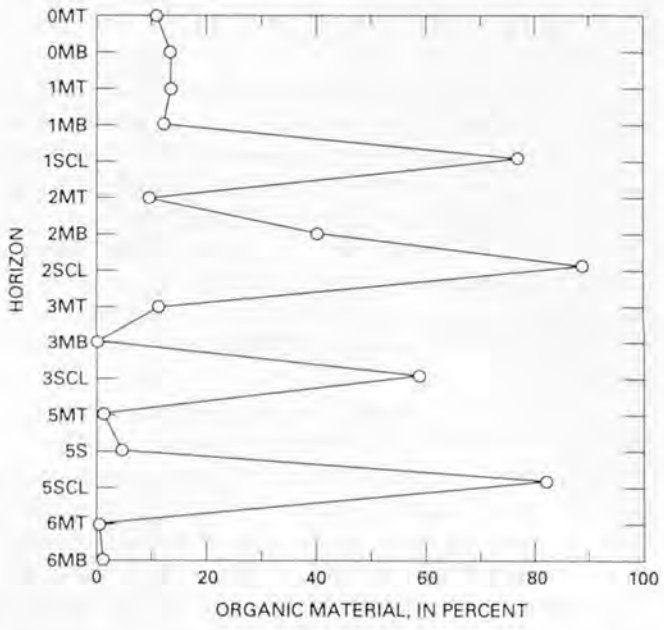

Figure 50. Downcore plot of relative sand abundance in peaty horizons and anomalous sand-rich sediment capping layers (SCLs) that directly overlie the buried peaty horizons at core site AB21 in Alsea Bay. Unit 4 was not found at site AB21. MT, marsh top; MB, marsh bottom; S, very low organic (barren) sediment. Measured elevations of the SCLs are provided in table 12.

Plots of relative abundance of beach sand in SCLs along north channel sites AB21, AB15, and AB19 show that the percentage of beach sand in each of three analyzed SCLs decreases with increasing distance landward (fig. 51). The beach-sand percentages of 2SCL at sites AB21, AB15, AB19, and AB12 are shown in figure 52 along with modern sand-composition contours in the bay, as previously reported in Peterson and others (1982). The high abundance of beach sand (31–47 percent) at marsh sites AB15 and AB21 contrasts sharply with adjacent tidal-flat sands, averaging less than 20 percent beach sand (fig. 52). The nearest possible sand source (greater than 50 percent beach sand) for 2SCL (which has as much as 47 percent beach sand) is 1.5 km due west (seaward) of site AB21. The decreasing beach-sand percentages up the north channel correspond to the decreasing total-sand percentages and decreasing sand-layer thicknesses of the SCLs (fig. 47).

The three trends in SCL deposition, that is, the layer thickness, sand percentage, and sand mineralogy independently confirm a diminishing transport energy with increasing distance landward in Alsea Bay. The SCLs were deposited by marine surges that entered the Alsea Bay mouth and propagated (mostly) up the north channel. The landward attenuation of surge-SCL deposition occurs within a distance of about 7 km from the mouth of Alsea Bay (fig. 52). However, this distance represents more than 75 percent of the length of this small bay.

RADIOCARBON AGES OF PEATY HORIZONS

Selected intervals of buried marsh tops at core site AB9 (figs. 44, 47*C*) and stratigraphic station 41 (fig. 43) from the central marsh were analyzed for radiocarbon age. The radiocarbon-dated marsh tops (intervals 5–10 cm thick) correspond to burial-unit horizons 1MT to 10MT. A total of eight bulk-peat radiocarbon ages and one radiocarbon age from a detrital wood fragment (from interval 2MT) are shown on figure 53. As should be expected, the analyses show increasing age (480 RCYBP to 4,510 RCYBP) with increasing depth (1.1 m to –5.1 m relative to MTL).

The uppermost buried marsh interval yielded a relatively young radiocarbon age (160±50 RCYBP; fig. 53) below the anomalous 1MT upper contact, a noncontinuous, weakly-oxidized horizon. To date the second buried marsh interval, a detrital wood fragment (2 cm diameter) was

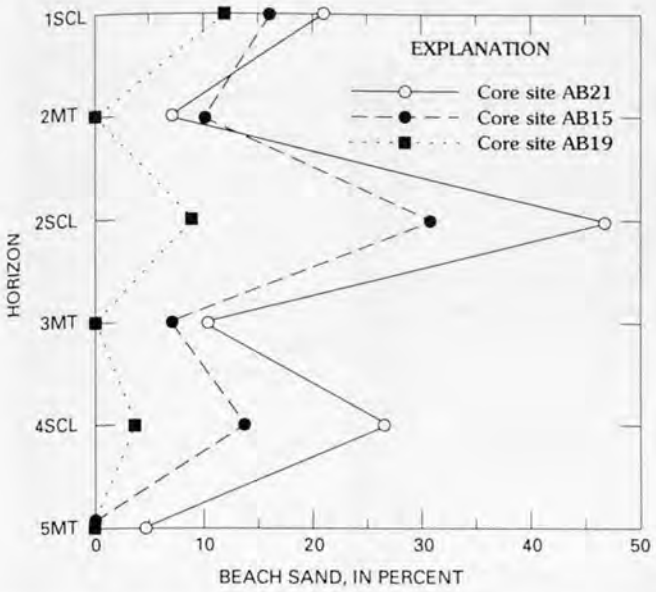

Figure 51. Downcore plot of relative abundance of beach-source component in analyzed sand fractions (0.06–0.25 μm) from sediment capping layers (SCLs) and marsh-top (MT) horizons at core sites AB21, AB15, and AB19 in Alsea Bay (sand fractions were also analyzed from site AB12 and found to contain no beach sand). Beach- and river-source components total 100 percent by volume abundance. The measured elevations of SCLs and marsh-top horizons are shown in table 12 and figure 47.

collected from buried marsh top 2MT at stratigraphic station 41 (fig. 43, table 11). The choice of the detrital wood fragment circumvented the problem of modern root contamination in this shallow, buried marsh horizon. The ages of the wood fragment and the dated peaty intervals are assumed to predate the time of the corresponding events of marsh submergence and burial by sediments. The fourth buried marsh top (4MT) was not radiocarbon dated due to potential contamination via descending roots from the overlying peat horizon. The deepest peat horizon cored (10MT, at –5.12 m relative to MTL) represents the oldest buried marsh (5,319–4,869 cal yr BP) to be reported in the central Oregon coast. Its date extends the known period of episodic marsh burial in this region back to middle Holocene time. The total of at least nine marsh subsidence events that occurred during the period from 4,510 to 480 RCYBP indicates an average recurrence interval of about 500 years.

DISCUSSION

SYSTEM-WIDE RESPONSE TO MARSH-BURIAL EVENTS

Multiple horizons of buried peat or peaty mud are widely preserved in cutbanks and interior sites throughout the central-marsh system of Alsea Bay (figs. 43, 45–47). The total number of peaty horizons (3–10) at each core site is generally proportional to the corresponding maximum depth of core penetration (–0.5 to –5.5 m relative to MTL). Although the successive development and preservation of peaty horizons must indicate an overall condition of relative sea-level rise, the distinct marsh burial units reflect reversing episodes of relative sea-level change. At least 80 percent of the individual peaty horizons analyzed contain both gradational lower contacts (gradual marsh emergence) and sharp upper contacts (rapid marsh submergence and burial). The vertical sequences of marsh burial are largely defined by this asymmetry of marsh development, particularly in the youngest burial units that lack substantial VLO layers.

The mash burial sequences, commonly including distinctive SCLs, provide key stratigraphic horizons that are correlated throughout the central-marsh area (figs. 45–47). For example, two buried marsh tops (2MT and 3MT) and their overlying SCLs (1SCL and 2SCL) are traced around 6.4 km of exposed cutbanks in the central-marsh area (fig. 43).

Table 13. Relative abundance of beach sand in analyzed sand fractions from buried marsh sediment capping layers along the north channel of Alsea Bay.

[SCL, sediment capping layer; MT, peaty marsh top]

Horizon	Amount of beach sand (percent)			
	Site AB21	Site AB15	Site AB19	[1]Site AB12
1SCL	21	16	12	0
2MT	7	10	0	0
2SCL	47	31	9	0
3MT	10	7	0	0
4SCL	27	14	4	0
5MT	5	0	0	0

[1]The bases of burial units at site AB12 are used for mineral analysis to represent equivalent SCL horizons sampled at core sites AB21, AB15, and AB19.

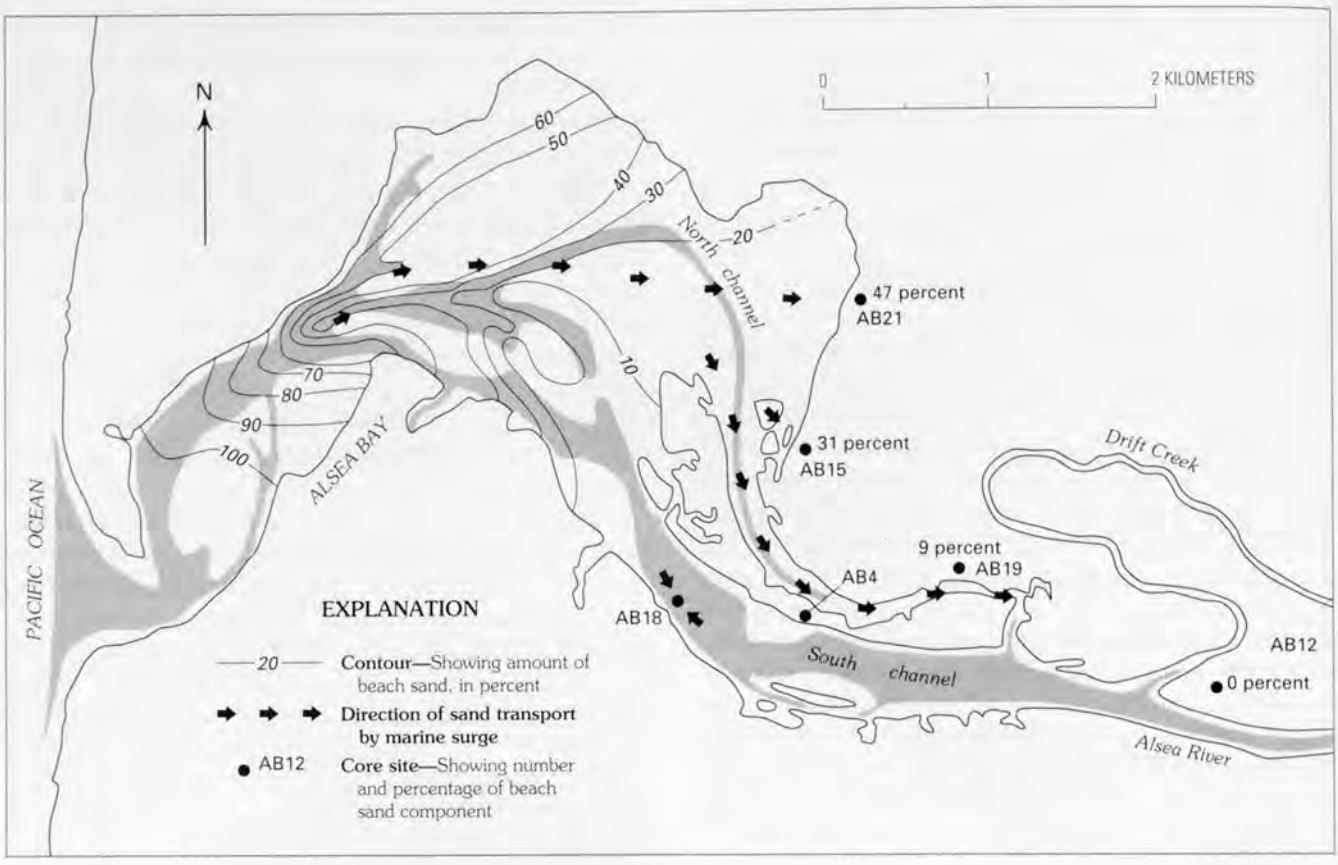

Figure 52. Percentage of beach-sand component in sand fractions from modern estuary sediments (contours) and in the 2SCL horizon at core sites AB21, AB15, AB19, and AB12 at Alsea Bay. Arrows show inferred landward direction of marine surge. Gray shading indicates the area of mean lower low water. The sand mineralogy (10 percent beach sand) for the 2SCL horizon at core site AB18 (south channel) indicates a proximal channel source, so it could not be used to discriminate transport direction.

The lateral continuity of key burial units in cutbanks substantiates the stratigraphic correlations of the 4–5 uppermost buried marsh surfaces identified in the upper 2 m of marsh cores. Several factors indicate a system-wide response to catastrophic events of marsh burial, including (1) continuous lateral correlation of two peaty horizons (2MT and 3MT) in cutbanks of the central-marsh system, (2) a similar number of downcore burial sequences at equivalent depths at most adjacent core sites, and (3) the similarity of generally sharp upper contacts and gradational lower contacts of the peaty horizons at most marsh core sites.

Quantitative analyses of sediment composition in vertical profiles of representative cores from sites AB21, AB8, and AB12 (fig. 44) from the central marsh confirm the stratigraphic interpretations above. For example, inverse relations between the percentages of organic material and river sand from sites AB8 and AB12 indicate successive cycles of low-marsh to high-marsh transition (figs. 48, 49). These vertical depositional sequences suggest episodes of marsh submergence relative to MTL, as reported for other tidal basins of southwestern Washington (Atwater, 1987; 1988) and northwestern Oregon (Peterson and others, 1988; Darienzo and Peterson, 1990). Below, we evaluate the evidence of several potential mechanisms of episodic marsh burial recorded in Alsea Bay.

RIVER-FLOOD PROCESSES

River flooding is an important means of sediment transport down the Alsea River channel in winter months of high river discharge (Peterson and others, 1982). However, predicted stratigraphic features of catastrophic-flood overbank deposition (fig. 37) were not observed in the upper estuary core sites (fig. 47). What was observed was a gradual decreasing percentage of sand upward within each of the burial units. As the marsh system emerged above lower intertidal levels, it rose above the reach of the higher velocity currents that are capable of suspending sand (table 12, figs. 48 and 49). These results indicate long periods of marsh accretion from tidal-cycle deposition rather than catastrophic marsh burial from great river floods. Furthermore, the SCLs

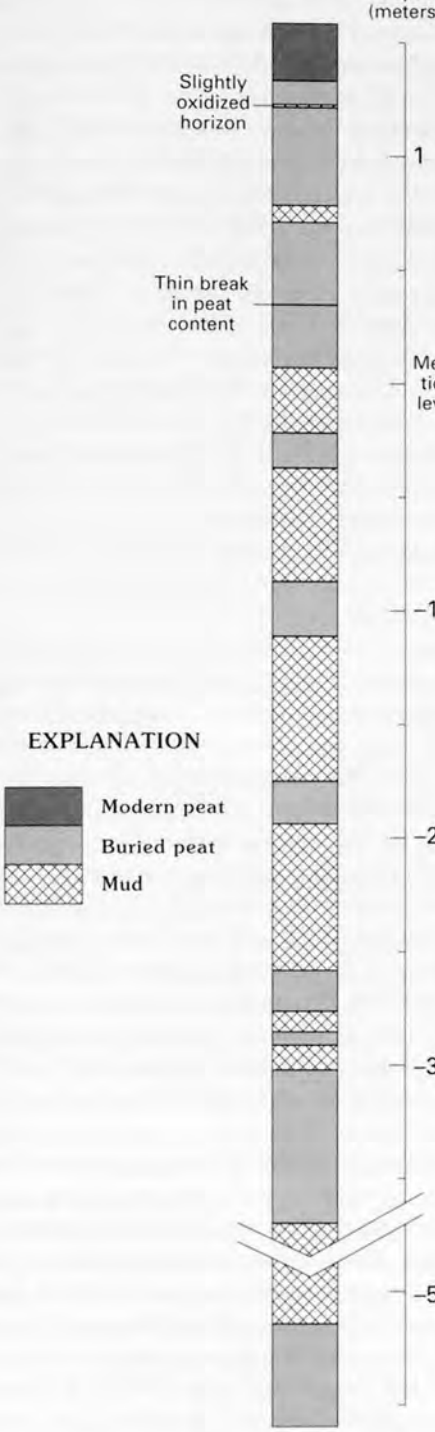

Depth (meters)	Horizon elevation (meters)	Sample no.	Horizon	Age RCYBP	Age C13 adj	Age cal. BP
	1.27	27182	MT1	160±50	120±50	0–290
	1.14	39181	MT2	480±60	500±60	474–645
	0.64	27184	MT3	800±80	760±80	561–903
	0.25	--	MT4	not dated	not dated	not dated
	−0.18	26791	MT5	1,490±80	1,450±80	1,260–1,530
	−0.87	27185	MT6	2,210±80	2,200±80	1,999–2,349
	−1.68	26792	MT7	2,620±60	2,570±60	2,479–2,783
	−2.57	27186	MT8	2,890±70	2,830±70	2,779–3,205
	−3.05	38861	MT9	3,140±50	3,070±80	3,168–3,389
	−5.12	26790	MT10	4,510±80	4,480±80	4,869–5,319

Figure 53. Core log and radiocarbon ages from core site AB9 and one detrital wood fragment from stratigraphic station 41 in Alsea Bay. Radiocarbon dating was performed by Beta Analytic, Inc., of Coral Gables, Fla., and corresponding lab numbers are shown for each sample. Peat ages are shown in radiocarbon years before present (RCYBP, one standard deviation); ^{13}C adjusted ages (C13 adj) are based on measured sample $^{12}C/^{13}C$ ratios; and calibrated ages before present (cal. BP) using 2 units of standard deviation about the ^{14}C calibration curves are established from tree-ring dating (Stuiver and Reimer, 1986). The poor separation of 4MT from 3MB did not allow dating by bulk-carbon methods at the time the testing was performed. The peat tops, used for radiocarbon dating, predate each associated marsh submergence and burial and possibly are older than the ages of the subsidence events.

of the western and central core sites could not have been supplied by river floods because they contain substantial amounts of beach sand (fig. 51).

The lack of catastrophic river-flood deposition in the high tidal marshes of Alsea Bay is explained, in part, by reduced river-flood levels in the estuary. Relative to the constricted river valleys of the tributaries, the tidally dominated estuary is characterized by large areas of intertidal and lower supratidal surfaces (Percy and others, 1974). Consequently, high river stages have much-reduced effects in these areas where river-flood waters are spread out over the broad surfaces. Also, high-marsh flooding is limited to relatively brief intervals of high tide level, which might not coincide with peak river discharge. However, the most important obstacle to high-marsh burial by river floods is the confinement of coarse-grained sediments to the channels.

Sediments carried down the channels of the bay tributaries are likely to settle out of suspension during the period of decelerating river flow that leads to flood-tide slack water. As a result, the coarser river sediments, particularly sand, are unlikely to be deposited over the high-marsh surfaces, which undergo the greatest submergence only during maximum high-tide level. Sediment resuspension in channels is likely to lag the onset of ebb tidal flow, therefore reaching maximum concentrations during falling tidal level. Whereas coarse-grained river sediments move down the upper estuary along channel bottoms, the finest grained sediments remain in suspension. Clay and fine silt are either deposited on the high marshes and protected tidal flats or are effectively transported down the estuary to be dispersed offshore (Peterson and others, 1984).

In summary, catastrophic river flooding as the mechanism of salt-marsh burial in Alsea Bay is contradicted by the following observations: (1) the lack of thick overbank flood deposits at the marsh channel levees, (2) the upward decrease in percentage of river sand within burial units, indicating gradual transitions from low intertidal to supratidal elevations, (3) the general thickening of SCLs, including marine-sand components, with increasing distance from the river source, and (4) diminished effects of salt-marsh submergence and burial by high river discharge due to hydrographic constraints in tidal basins.

OCEAN SET–UP PROCESSES

An alternative means of marsh submergence and burial might be ocean set-up resulting from extreme ocean storm surges and (or) anomalous oceanic circulation. Ocean storm surges are generally short lived in the Pacific Northwest (fig. 38), but they coincide with periods of maximum wind-wave generation over some tidal flats. The combination of elevated tide levels and wave oscillatory currents have undoubtedly added sand to the westernmost marsh core sites (AB1, AB2, and AB21 in fig. 44). For example, the top intervals of the four youngest marsh horizons (0MT, 1MT, 2MT, and 3MT) at core site AB21 generally exceed 10 percent sand (fig. 50 and table 12), whereas corresponding marsh tops from protected interior sites AB8 and AB12 average only 2.5 percent sand in 11 analyzed horizons. Mineralogical analyses of the sands from the upper four marsh tops (peaty deposits) in western site AB21 indicate a proximal source from the nearby tidal flats (figs. 51 and 52), confirming the gradual addition of sand by storm wind-wave resuspension.

In contrast, the coarse-sediment fractions in the peaty horizons and muds, excluding the SCLs, from the central- and eastern-marsh core sites (AB19 and AB12) are almost exclusively composed of river-supplied sand (tables 11 and 12). Ocean storm surges have been incapable of adding any significant amounts of tidal-flat sand, identified by beach-sand minerals, to high-marsh peaty horizons of the central- or eastern-marsh core sites. Also, the sediments of the VLO horizons in the central-marsh sites consist mostly of silt and clay (mud) but not of the coarser size fractions (sand) that are assumed to be resuspended from sand tidal flats during major storms (fig. 40).

In summary, no apparent storm-surge deposits of bay tidal-flat sands were found in peaty horizons from the interior core sites of the central- or eastern-marsh areas. The lack of storm-surge deposition within the last several thousand years rules out catastrophic storm-surge events as mechanisms of system-wide marsh submergence and burial in Alsea Bay. Pacific Northwest storms are frequent but of short duration, with relatively low wind velocities that are generally well under 100 knots (fig. 38). Furthermore, the narrow continental shelf and small tidal basins do not amplify effects of storm-induced ocean set-up along this coast. We conclude that midlatitude ocean storms of the central CSZ margin are not of sufficient magnitude to transport and deposit substantial sediment layers over broad high-marsh surfaces at sites distant from the tidal inlet or open-bay reaches.

By comparison, longer periods (months) of elevated mean sea level might have a more significant impact on marsh development and (or) burial due to the additive effects of submergence during spring-tide extremes and to extended submergence during winter storms and high river discharge. The largest measured increase of monthly mean sea level (30 cm above a 10-year mean) occurred very recently (winter and spring of 1983) as a result of the 1982–83 El Nino Southern Oscillation (ENSO) event (fig. 39) (Huyer and others, 1983). This was also a year of above-average precipitation and high river discharge. However, close examination of the modern marsh horizon (0MT) at all of the Alsea Bay core sites showed no anomalous sedimentation or decrease in the percentage of organic material resulting from this most recent ENSO event. The 0.3 m rise in mean sea level did not result in marsh deterioration in Alsea Bay. Thus, this value provides a lower limit of the amount of submergence that is required to drown and bury a high marsh in this tidal basin.

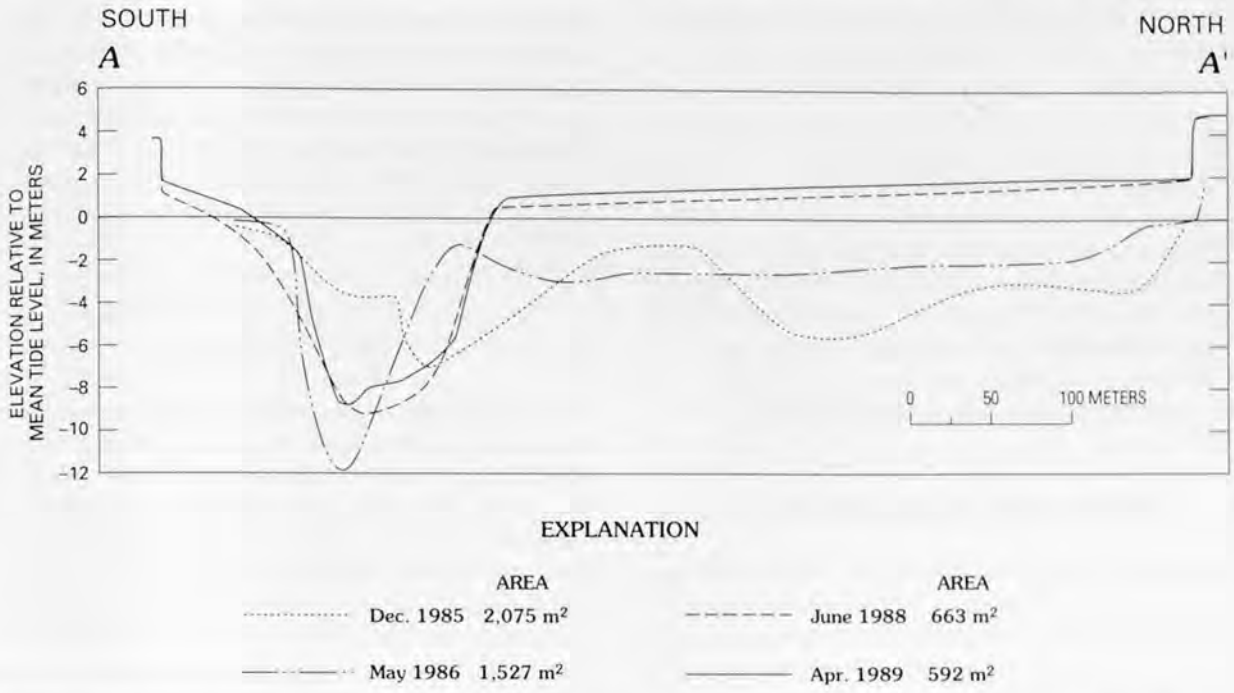

Figure 54. Changes in the shape and cross-sectional area of Alsea Bay inlet between 1985 and 1989 as a result of a spit breach in 1985 and recovery by 1989 (Peterson and others, 1990). Vertical exaggeration is ×12. Location of the line of section is shown in figure 34.

That is to say, more than 0.3 m of abrupt and persistent sea-level rise is needed to kill and bury a high salt marsh in the central CSZ margin.

Whereas ENSO events are possibly capable of producing sea-level rises in excess of 30 cm, their durations are limited to relatively brief intervals of relaxed trade-wind stress and corresponding Kelvin-wave transport (Enfield and Allen, 1980). Furthermore, the ENSO events are unlikely to produce the strong asymmetry in abrupt submergence and gradual emergence found in the marsh records. Also, it seems very unlikely that major ENSO events would coincide with single catastrophic storm surges to yield the nearly one-to-one correspondence between SCLs and marsh burial units in Alsea Bay. However, the strongest evidence against regional ENSO forcing of salt-mash burial in Alsea Bay is the lack of such burial events in the western marshes of Siuslaw Bay (Nelson, 1987), located just 45 km south of Alsea Bay.

BARRIER-SPIT BREACHES

Marsh growth in Alsea Bay could potentially be impacted by variations in tide-level range due to changes in the bay barrier-spit morphology. Sandy tidal inlets do not completely block estuaries that have tidal-prism and river-discharge volumes as large as those in Alsea Bay (O'Brien, 1969; Percy and others, 1974). However, adjustments in barrier-spit morphology can result in significant constriction or widening of the tidal inlets, producing corresponding changes in the tidal prism. For example, major changes in the cross-sectional area of the Alsea Bay tidal inlet occurred in association with an anomalous breaching and recovery of the Alsea Bay spit from 1985 to 1987 (Jackson and Rosenfeld, 1987; Peterson and others, 1990). The total cross-sectional area of the inlet increased from about 600 m^2 (prior to 1985) to at least 2,000 m^2 (December 1985). The tidal inlet and spit finally returned to the pre-1985 size and shape by 1989 (fig. 54). This unusual event was initiated by beach-sand displacement during the 1983 ENSO period (Komar, 1986). It provides an excellent example of the effects of a spit breach and associated inlet widening on mean tide levels within the bay, particularly in terms of the impacts of increased tide-level range on the bay marsh system.

The 400-percent increase in tidal-inlet cross-sectional area in 1985 is estimated to have produced a greater than 60-percent increase in peak tidal flow through the Alsea Bay inlet (Jackson and Rosenfeld, 1987). The greater tidal flow increased the estimated bay:ocean surface-level ratio from 0.71 (pre-1985) to 1.00 (1985). The nearly 30-percent increase in peak tide levels in Alsea Bay could yield an additional 0.7 m of marsh submergence during maximum high tides (Jackson and Rosenfeld, 1987). This is a very substantial increase of peak tidal submergence considering that the equilibrium MHHW–MLLW tidal range in Alsea Bay is only 2 m (table 10).

However, close examination of the modern marsh horizons (0MT) at all of the core sites revealed no observable effects of this major change in tide-level range on plant growth or on the fine-scale stratigraphy of the modern marsh top. For example, there was no evidence of SCL deposition or any increase in sand deposition from storm wind-wave resuspension over the marsh surface at the western core-sites. This major spit breach (fourfold increase in tidal inlet cross-sectional area) did not significantly influence the tidal marshes in Alsea Bay. These results show that prehistoric events of inlet breaching or widening could not have produced the effects of catastrophic marsh submergence and burial that are recorded throughout the bay marsh system.

COSEISMIC SUBSIDENCE

Perhaps the strongest evidence against the burial of the Alsea Bay marsh by relatively brief periods of ocean set-up, anomalous oceanic circulation, or changing tide-level range is the observed asymmetry of peat development. More than 80 percent of the peaty horizons from the Alsea Bay core sites have both sharp upper contacts (marsh tops) and gradational lower contacts (lower-marsh or colonizing-marsh substrates). These vertical trends in peat development indicate conditions of abrupt marsh submergence (upper contacts) followed by gradual marsh emergence (lower contacts). This strong asymmetry of peat development is remarkably consistent throughout the entire marsh system in Alsea Bay (fig. 47). Such asymmetry is consistent with coseismic tectonic subsidence alternating with sedimentation and (or) gradual tectonic uplift (figs. 41, 42) landward of the upper-plate zero isobase.

Specifically, the gradual accumulation of clay and silt, as shown by the finely laminated or bioturbated muds, indicates long-term deposition in low-energy estuarine environments. These burial deposits demonstrate many low-energy depositional cycles as opposed to one high-energy depositional event. Rather than succumbing to catastrophic burial by storm or river floods, the marsh plant growth was terminated or diminished by abrupt and persistent marsh submergence relative to MTL. Although not present in Alsea Bay, high-marsh emergence to forested wetlands is recorded in buried-marsh stratigraphy at northern Oregon bays including Netarts Bay (Darienzo and Peterson, 1990). Wetland emergence above tide level requires an element of tectonic uplift, because tidal sediments cannot be transported above the reach of tides. Episodic events of coseismic subsidence and interseismic uplift that are superimposed on long-term eustatic sea-level rise are the unique mechanisms that account for the buried-marsh stratigraphy in Alsea Bay.

MAGNITUDE OF VERTICAL DISPLACEMENT

The tectonic displacements needed to lower the high-marsh surfaces to intertidal levels of barren tidal flats or colonizing-marsh substrates are on the order of 1 m in Alsea Bay (table 10). However, the apparent marsh transitions over burial units 2–4 (low-marsh to colonizing-marsh tidal flat) and the transitions over burial units 1–2 (predominantly high marsh to upper low marsh) suggest smaller vertical displacements, that is, as little as 0.5 m (fig. 48). Although horizon 1MT might indicate marsh burial, it lacks evidence of abrupt burial by coseismic subsidence, so it is not included in average displacement estimates for Alsea Bay.

Vertical displacement due to sediment compaction is assumed to be small as compared to the coseismic subsidence displacement in Alsea Bay. This assumption is partly based on the relatively small changes in bulk density downcore, which are further decreased when normalized against percent inorganic content (table 12). However, stronger evidence lies in the comparison of marsh stratigraphic elevations that overlie a shallow bench of consolidated Pleistocene deposits and thick, unconsolidated Holocene deposits in the axial river valley. Specifically, elevations of burial-unit horizons (1MT–5MT) vary by a total of about 0.6 m between core site AB21 and sites AB8, AB9, and AB10 (figs. 44, 47). The higher buried-marsh elevations occur at site AB21, which bottoms out only a few meters above consolidated Pleistocene deposits (Peterson and others, 1984). The deeper buried-marsh horizons occur at sites AB8, AB9, and AB10, which overlie 30–50 m of unconsolidated Holocene fill. The total offset of 0.6 m averages only 15 cm of differential subsidence settling for each of the last four subsidence events between the very shallow and very deep fill areas.

Table 14. Minimum subsidence estimated for the four most recent subsidence events in three Oregon bays along the Cascadia subduction zone margin.

[Seq., transition sequence in marsh environment due to subsidence; Displ., coseismic vertical displacement, in meters; VHM, very high marsh; TF, tidal flat; HM, high marsh; LM, low marsh; MM, undefined marsh elevation; (--), no subsidence reported. Netarts Bay data from Darienzo and Peterson (1990). Siuslaw Bay data from Nelson (1987)]

Tidal basin	Distance to subduction zone trench (kilometers)	Event 1		Event 2		Event 3		Event 4		Avg. displacement range (meters)
		Seq.	Displ.	Seq.	Displ.	Seq.	Displ.	Seq.	Displ.	
Netarts Bay	110	VHM–TF	1.5	HM–TF	1–1.5	HM–TF	1–1.5	VHM–TF	1.5	1–1.5
Alsea Bay	100	HM–HM	0.5	HM–LM	0.5–1	LM–TF	0.5–1	LM–TF	0.5–1	0.5–1
Siuslaw Bay	90	MM–MM	0–0.5	--	--	--	--	--	--	0–0.5

The vertical displacements of tectonic subsidence that are estimated for Alsea Bay (0.5–1.0 m subsidence) are substantially smaller than those reported for Netarts Bay (1–1.5 m subsidence) in northwestern Oregon (fig. 33, table 14) (Darienzo and Peterson, 1990). By comparison, the 0.5–1.0 m vertical displacements in Alsea Bay are apparently greater than those 45 km to the south in Siuslaw Bay (0–0.5 m subsidence), where there are minor or no significant breaks in peat development at the western end of the bay (Nelson, 1987).

The 90–120-km distance of the central Oregon coast from the subduction-zone trench (Peterson and others, 1986) (fig. 33) indicates the coastline's proximity to the upper-plate zero isobase (fig. 41), based on coseismic displacements from other subduction zones. For example, coseismic coastal subsidence occurred along the coasts of Japan (1944 and 1946), Southern Chile (1960), Alaska (1964), and Colombia (1979); each subsidence zone was located 100–130 km landward of a subduction-zone trench (Heaton and Hartzell, 1986; West and McCrumb, 1988).

The coast-to-trench distances of marsh systems in Netarts, Alsea, and Siuslaw Bays (fig. 33), and the corresponding marsh coseismic vertical displacements (table 14), are compared in figure 55. The plots show a positive correlation between decreasing distance from the trench and decreasing magnitudes of vertical coastal displacement. The upper-plate flexure line, or isobase of zero displacement (Plafker and Kachadoorian, 1966), for the CSZ margin is estimated to be about 90 km east of the trench, intercepting the coastline at lat 43.5°–44°N. (fig. 56).

An additional indication of the relative landfall position of the zero isobase is the trend of interseismic uplift, which reaches a maximum some distance landward of the zero isobase (fig. 41). The buried wetlands in southern Washington, which are most distant from the trench (about 140 km), commonly reach and exceed supratidal elevations, that is to say, forest soils are commonly developed prior to coseismic subsidence (Atwater, 1988). By comparison, only two of the last four burial units in Netarts Bay (110 km from the trench) emerged above the reach of tides (table 14) (Darienzo and Peterson, 1990). Alsea Bay, at a distance of 100 km from the trench, does not contain any wetland burial sequences that reached fully supratidal elevations, such as shrub-forest soils. Thus, there was insufficient interseismic tectonic uplift to raise tidal-marsh surfaces above the reach of tides in Alsea Bay, further supporting the bay's relatively close proximity to the zero isobase.

The position of the zero isobase is important in constraining the landward termination of the seismogenic locked zone. The width of the locked zone partly determines the magnitude of the megathrust earthquake and the distance between coastal population centers and the earthquake epicenter. Additional studies are underway by these authors to confirm the location of the landfall of the upper plate zero isobase along the central Oregon coast.

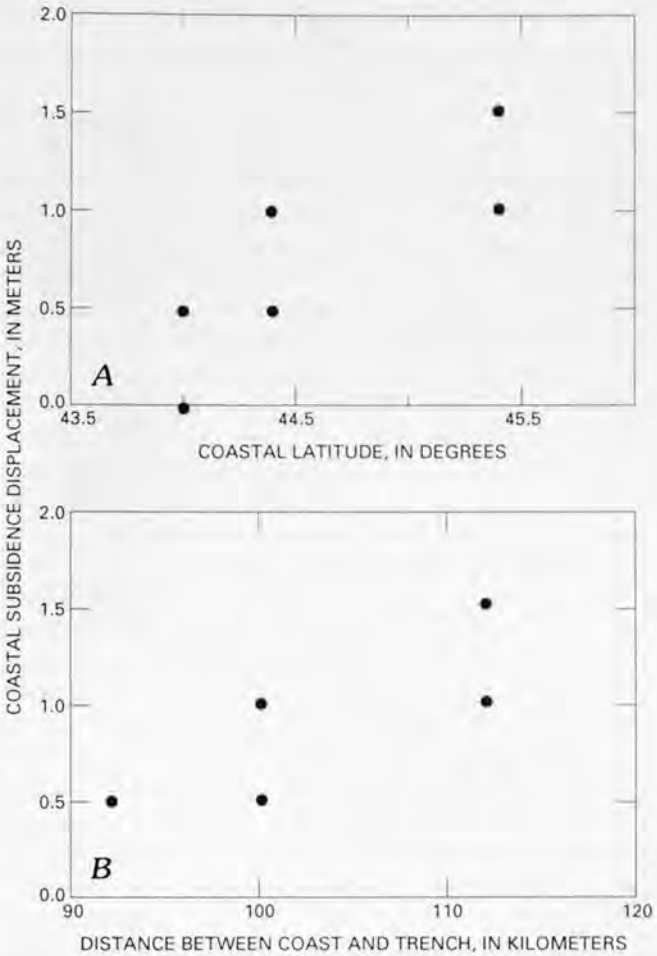

Figure 55. Estimated range of minimum coastal subsidence of marsh systems in Siuslaw, Alsea, and Netarts Bays, Oreg. *A*, subsidence in relation to coastal latitude. *B*, subsidence related to the distance between coast and subduction-zone trench. See table 14 for basis of subsidence magnitude estimates.

TSUNAMI DEPOSITS

The clearest evidence of abrupt tectonic subsidence in the Alsea Bay marsh is the catastrophic burial of the west-central marsh peats by the anomalous SCLs (fig. 47*A*, *C*). Landward-directed marine surges carried beach and (or) tidal-flat sands at least 1.5 km eastward to the westernmost marsh core site, AB21, and deposited thin, sand-rich SCLs over marsh surfaces of the northern bay margin and along the north channel (figs. 51, 52). The SCLs show no evidence of bioturbation or internal cross stratification, but some faint layering is observed at some sites. SCL sands appear to have been deposited directly out of turbulent suspension. These characteristics, taken altogether, indicate sediment suspension, landward transport, and catastrophic deposition by tsunami waves (Atwater, 1987; Reinhart and Bourgeois, 1989; Darienzo and Peterson, 1990). The direct correspondence

between marsh subsidence and SCL deposition in Alsea Bay indicates that these tsunamis were generated by tectonic displacements in the CSZ margin.

Although the Alsea Bay tsunami deposits thin with increasing distance landward, the thicker tsunami sands of the western marsh were generally deposited on low marsh surfaces (fig. 47*A*). In addition, the tsunami surges that flowed up the north channel were insufficient to cross over the narrow marsh at core site AB4 (figs. 44, 52). We interpret these patterns of SCL deposition to indicate that tsunami surges flowed through the bay mouth and then due east to the northeastern bay margin. At this point, the surges deposited relatively thick layers of sand and muddy sand over the marsh-top horizons (2MT, 3MT, and 5MT). The tsunami surges continued up the north channel but rapidly diminished in flow energy, depositing only thin sandy mud or silty mud layers in the central-marsh sites. The inundation of broad tidal flats and marsh surfaces between core sites AB1 and AB5 (figs. 34, 36, and 44) would have greatly reduced the mass and associated momentum of the landward-directed surges. The landward attenuation of tsunami deposition in Alsea Bay is apparently due to the flooding of broad intertidal areas in the middle estuary.

The record of tsunami sedimentation in Alsea Bay provides some important constraints on local tsunami deposition in the CSZ margin. For example, a similarity in tsunami-deposited layer thickness (1–25 cm) occurs between Alsea Bay and Netarts Bay even though their vertical subsidence values differ by a factor of two. The small subsidence displacements in Alsea Bay (0.5–1 m in fig. 55) did not preclude the sedimentation and preservation of associated tsunami deposits. Although some SCLs do thicken over lower marsh settings in Alsea Bay, the greatest variation in tsunami-deposit thickness is controlled by the landward attenuation of the surges (figs. 47, 52). The apparent independence of tsunami deposition and the magnitude of local, coseismic subsidence means that large CSZ-generated tsunamis should be capable of leaving distinct tsunami deposits on marsh surfaces that have experienced little or no corresponding coseismic subsidence.

The observed SCL deposits in Alsea Bay are only associated with events of marsh subsidence apparently caused by coseismic plate deformation. A similar observation in Netarts Bay was used to infer that the preserved tsunami deposits there were produced by locally generated tsunamis and not by distantly produced tsunamis from other Pacific-rim margins (Peterson and others, 1988). Taking this approach a step further, it might be possible to use the correspondence between tsunami deposits and coseismic subsidence in a marsh record to establish whether a tsunami was generated within a particular segment of the CSZ margin.

A simple test of regional versus local segment rupture is provided by high-resolution records of coastal subsidence and tsunami deposition. If tsunami deposits are recorded in marsh sequences that do not show corresponding coastal subsidence, then it can be assumed that the tsunamis were generated outside of the local segment. For example, such records of independent tsunami deposits would be expected in Alsea Bay if small segments of the CSZ margin were released at times other than those in the Alsea Bay area (fig. 57). In contrast, if the marsh stratigraphy only shows tsunami deposition with local coastal subsidence, then the local subsidence must be part of a much larger (regional) tectonic displacement. Indeed, the observed marsh records in Alsea Bay do not show any evidence of tsunami deposits independent of coastal subsidence. A nearly one-to-one correlation of SCL development and local marsh subsidence is recorded for the last half-dozen subsidence events (fig. 47). This high correlation could imply synchronous coseismic displacement over large areas of the CSZ margin. We are currently

Figure 56. Predicted upper-plate flexure line, or zero isobase, in the Cascadia subduction zone, based on an assumed trench-parallel orientation and a coastal interception point between lat 43.5°N. and lat 44°N. The trench position in the south-central continental margin is approximated from the mapped base of the continental slope (Peterson and others, 1986). Five bay marsh systems that have recorded episodic, abrupt coastal subsidence (Atwater, 1987; Grant and McLaren, 1987; Darienzo and Peterson, 1990) are shown north of Siuslaw Bay. All are east of the trend of the predicted zero isobase.

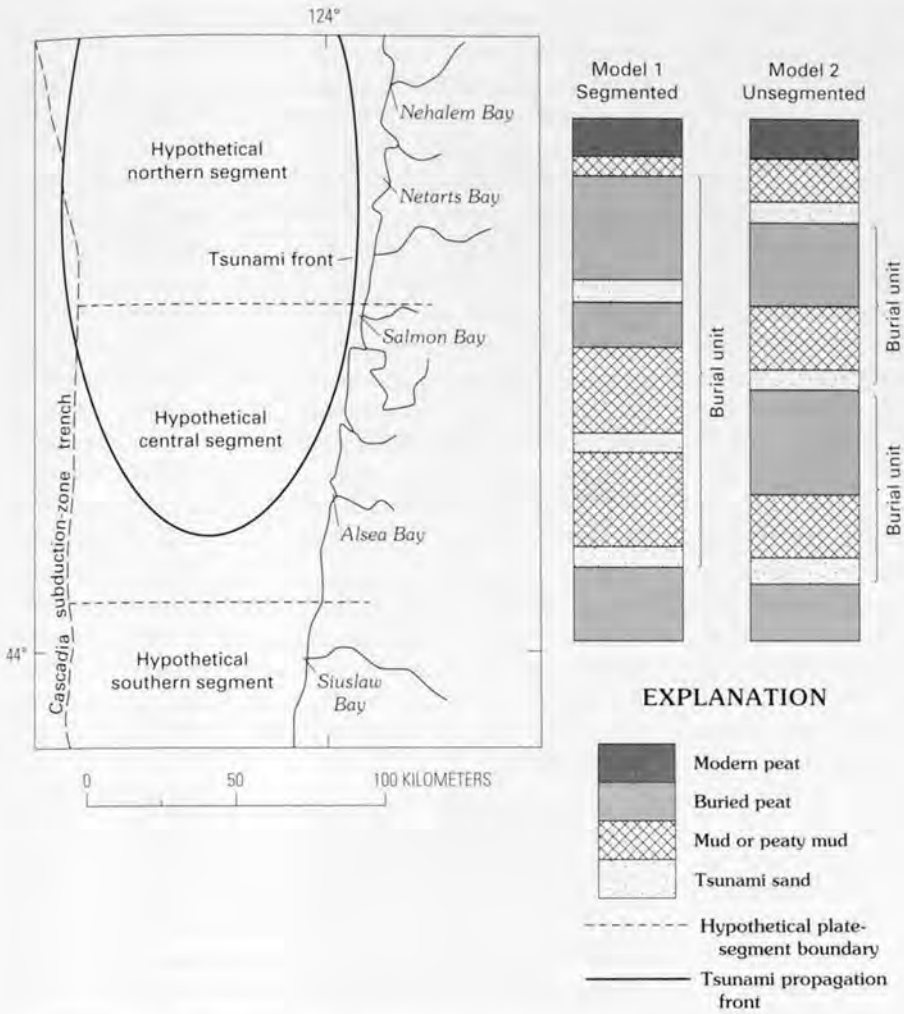

Figure 57. Models of segmented and unsegmented interplate dislocation in the north-central Cascadia subduction-zone margin (northern Oregon). In the segmented margin (model 1), tsunami generation occurs in a ruptured segment and the tsunami waves propagate into aseismic segments. The tsunami surges deposit distinct sandy layers within marsh burial units in the aseismic segments. These layers would not directly overlie buried marsh tops. In the unsegmented margin (model 2), tsunami generation and coastal subsidence are simultaneous throughout all adjoining or nearby coastal areas. Resulting tsunami deposits are only associated with the tops of buried marsh or wetland horizons, indicating contemporaneous coastal subsidence. Model 2 is favored for the Alsea Bay region due to a strong correspondence between the anomalous sandy layers and buried marsh tops.

investigating whether similar one-to-one correspondences of tsunami deposition and coastal subsidence are found in other tsunami-sensitive bays along the northern Oregon coast.

CHRONOLOGY OF BURIAL EVENTS

Significantly, the youngest peat top coseismically subsided in Alsea Bay (2MT interval) has a radiocarbon age (480 RCYBP, fig. 53) that is consistent with the radiocarbon ages of other youngest buried peats and forest soils reported for northern Oregon (Darienzo and Peterson, 1990; Darienzo, 1991) and Washington (Atwater, 1988). A more accurate age of the most recent event of coseismic subsidence in southwestern Washington (about A.D. 1700) is provided by tree-ring dates of cedar snags killed by their submergence to intertidal levels (Yamaguchi and others, 1989). Unfortunately, tree trunks suitable for tree-ring dating have yet to be identified in buried peats of the Alsea Bay marsh.

The next youngest buried horizon in Alsea Bay (3MT) has an intriguing date of 800 RCYBP (561–903 Before Present in calibrated age). This was the first indication of coastal subsidence in the central and northern Oregon coast having occurred during this time period. Additional stratigraphic work in northern Oregon bays (Peterson and others, 1993) has shown that a tsunami produced from this event affected widespread areas north of Alsea Bay, but subsidence from the same event has not been observed north of Yaquina Bay.

Recurrence intervals between successive subsidence events in Alsea Bay were found to range from as little as 250 years (horizons 9MT–8MT, fig. 53) to as much as 1,370 years (horizons 10MT–9MT), based on corresponding, uncalibrated peat radiocarbon dates. Dating errors of as much as several hundred years have resulted from radiocarbon dating of individual CSZ coastal-subsidence events (Atwater, 1988; Peterson and Darienzo, 1990). However, the accuracy of estimating average recurrence intervals is increased over longer time periods as random errors are canceled by the larger number of subsidence events. For example, the average recurrence interval of the three youngest subsidence events (5MT–2MT horizons) from 1,490 to 480 RCYBP is estimated to be about 340 years. By comparison, the average recurrence interval of the next three youngest subsidence events (8MT–5MT horizons) from 2,890 to

1,490 RCYBP is estimated to be about 470 years. The average recurrence interval for the longest period of record (4,510 to 480 RCYBP) is estimated to be about 500 years for eight subsidence events.

Generally, the older stratigraphic intervals show larger recurrence intervals, probably resulting from the declining record-preservation potential with greater age. For example, burial units become increasingly difficult to correlate at depths below MTL in Alsea Bay due to missing marsh horizons at adjacent core sites. At the central-marsh sites, burial unit 6 is missing at sites AB10 and AB7, whereas burial unit 7 is apparently missing at AB19 (fig. 47*C*). Finally, a possible burial unit at a depth of 4 m below MTL at core site AB7 is absent from AB8 and AB9. The absence of this unit at radiocarbon-dated site AB9 might account for the anomalously long period (roughly 1,500 years) between 9MT and 10MT (fig. 53). In Alsea Bay, the most reliable stratigraphic interval for estimating an average recurrence interval is thought to be between 5MT and 2MT, the shallow buried-marsh horizons near or above MTL. Using our calibrated radiocarbon date of 1,530–1,260 years Before Present for 5MT and the reported 300 Calendar Years Before Present date for 2MT (Yamaguchi and others, 1989; Atwater and others, 1991), we estimate an average recurrence interval of 320–410 years for the last three coseismic subsidence events in Alsea Bay.

The long-term average recurrence interval of coastal subsidence events in Alsea Bay, about 500 years, is not significantly different from that reported for Netarts Bay (Darienzo and Peterson, 1990; Darienzo, 1991). The similarity of these long-term intervals implies regional linking of coastal subsidence events in the north-central CSZ margin. However, the relative inaccuracies of radiocarbon dating prohibit regional correlations of individual subsidence events solely on the basis of radiocarbon age. The long-term average recurrence interval of coastal subsidence in Alsea Bay is somewhat less than the average recurrence interval of possible coseismic turbidity flows (590 years) reported for the CSZ continental slope (Adams, 1990). However, we stress that average recurrence intervals measured over shorter and younger time spans in Alsea Bay imply substantially shorter average recurrence intervals, such as 400 years or less, between coseismic subsidence events.

CONCLUSIONS

The broad correlation of key peaty horizons in the top 2 m of the Alsea Bay marsh, and the similar nature of marsh-burial sequences throughout the Alsea Bay estuary, show episodic events of coastal submergence in late Holocene time. Peat-burial sequences in Alsea Bay do not reflect catastrophic burial by brief climatic or oceanic events; rather, they demonstrate rapid and persistent subsidence followed by gradual deposition of suspended material and associated marsh emergence. Furthermore, historical extreme events of river floods, storm surges, and tidal-inlet changes in Alsea Bay have not produced changes in mean tide level or tide range that were sufficient to have significantly impacted modern marsh development.

Coseismic coastal subsidence appears to be the unique mechanism capable of producing the observed records of episodic marsh burial in Alsea Bay. Specifically, the cyclic episodes of gradual coastal uplift and sedimentation followed by abrupt coastal subsidence in several bays of the central CSZ margin reflect alternating periods of crustal strain accumulation (gradual) and strain release (abrupt) in an active tectonic setting. Comparisons of the vertical movements in Alsea Bay with other Oregon marsh systems show similar trends in the asymmetry of vertical motions. However, along margin trends of decreasing tectonic subsidence and uplift with decreasing distance from the trench imply regional rather than local tectonic control of the observed coastal subsidence. These regional trends of tectonic coastal displacements are consistent with upper-plate flexure in a strongly coupled subduction zone. Furthermore, they possibly indicate the relative position of an upper-plate flexure line or zero isobase intersecting the central Oregon coast near lat 44°N.

Coseismic subsidence of the preexisting marsh surfaces in Alsea Bay is indicated by several independent lines of evidence for contemporaneous tsunami deposition. Tsunami deposits (SCLs) above buried marsh surfaces are anomalously sand rich. Also, they contain elevated abundances of marine-source sand relative to adjacent tidal-flat or river-channel deposits. Both the relative thickness and beach-sand content of the SCLs indicate landward-directed attenuation of marine-surge transport. Although the SCLs lie directly above subsided peats, the small magnitude of estimated subsidence in Alsea Bay does not preclude their deposition or preservation. A nearly one to one correlation between tsunami deposition and coastal subsidence recorded in the upper four burial units from Alsea Bay might indicate synchronous coseismic displacements over substantial lengths of the central Oregon margin.

We find that the age of the most recent coseismically subsided marsh top at Alsea Bay (480 RCYBP) is consistent with reported ages of the most recent coseismic subsidence (300 Calendar years Before Present) at other CSZ marsh systems in Oregon and Washington. Average recurrence intervals for the youngest three coseismic-subsidence events in Alsea Bay are estimated to be between 320 and 410 years, based partly on calibrated radiocarbon dates. By comparison, an average recurrence interval of 500 years is estimated for the longest period of record (4,510–480 RCYBP) in Alsea Bay. This interval is similar to long-term recurrence intervals reported from other CSZ marsh systems, implying regional linking of coastal subsidence in the north-central Cascadia subduction-zone margin of northern Oregon and southern Washington.

REFERENCES CITED

Adams, John, 1990, Paleoseismicity of the Cascadia subduction zone—Evidence from turbidites off the Oregon-Washington margin: Tectonics, v. 9, no. 4, p. 569–583.

Allen, J.R.L., 1984, Sedimentary structures, their character and physical basis: New York, Elsevier, 663 p.

Ando, Masataka, and Balazs, E.I., 1979, Geodetic evidence for aseismic subduction of the Juan de Fuca plate: Journal of Geophysical Research, v. 84, no. B6, p. 3023–3028.

Andrejko, M.J., Fiene, Faith, and Cohen, A.D., 1983, Comparison of ashing techniques for determination of inorganic content of peat, *in* Jarrett, P.M., ed., Symposium on testing of peats and organic soils, Ontario, Canada, June 23, 1982: American Society for Testing and Materials, Special Technical Publication 820, p. 5–20.

Atwater, B.F., 1987, Evidence for great Holocene earthquakes along the outer coast of Washington State: Science, v. 236, no. 4804, p. 942–944.

_____1988, Geologic studies for seismic zonation of the Puget lowland, *in* Jacobson, M.L., and Rodriguez, T.R., comps., National Earthquake Hazards Reduction Program, Summaries of technical reports, Volume XXV: U.S. Geological Survey Open-File Report 88–16, p. 120–133.

Atwater, B.F., Stuiver, Minze, and Yamaguchi, D.K., 1991, Radiocarbon test of earthquake magnitude at the Cascadia subduction zone: Nature, v. 353, no. 6340, p. 156–158.

Boley, S.L., 1973, Discharge coefficient of an estuarine entrance: Corvallis, Oregon State University, M.S. thesis, 83 p.

Clark, J.S., and Patterson, W.A., III, 1985, The development of a tidal marsh—Upland and oceanic influences: Ecological Monographs, v. 55, p. 189–217.

Clarke, S.H., Jr., and Carver, G.A., 1992, Late Holocene tectonics and paleoseismicity, southern Cascadia subduction zone: Science, v. 255, no. 5041, p.188–192.

Clifton, H.E., and Phillips, R.L., 1980, Lateral trends and vertical sequences in estuarine sediments, Willapa Bay, Washington, *in* Field, M.E., Bouma, A.H., Colburn, I.P., Douglas, R.G., and Ingle, J.C., eds., Quaternary depositional environments of the Pacific coast: American Association of Petroleum Geology, Society of Economic Paleontology and Mineralogy, Pacific Section, Pacific Coast Paleogeography Symposium, 4th, Bakersfield, Calif., April 9, 1980, p. 55–71.

Darienzo, M.E., 1991, Late Holocene paleoseismicity along the northern Oregon coast: Portland, Oreg., Portland State University, Ph.D. dissertation, 167 p.

Darienzo, M.E., and Peterson, C.D., 1990, Episodic tectonic subsidence of late Holocene salt marshes, northern Oregon central Cascadia margin: Tectonics, v. 9, no. 1, p. 1–22.

Dingler, J.R., and Clifton, H.E., 1993, Barrier systems of California, Oregon and Washington, *in* Davis, R.A., ed., Coastal barriers of the United States: New York, Springer-Verlag, 58 p.

Enfield, D.B., and Allen, J.S., 1980, On the structure and dynamics of monthly mean sea level anomalies along the Pacific coast of North and South America: Journal of Oceanography, v. 10, p. 557–578.

Fitch, T.J., and Scholz, C.H., 1971, Mechanism of underthrusting in southwest Japan—A model of convergent plate interactions: Journal of Geophysical Research, v. 76, no. 29, p. 7260–7292.

Folk, R.L., 1980, Petrology of sedimentary rocks: Austin, Tex., Hemphill Publishing Co., 185 p.

Gardner, W.H., 1965, Water content, *in* Methods of soil analysis, Part 1: Madison, Wis., American Society of Agronomy (Agronomy, no. 9), p. 82–127.

Goodwin, C.R., Emmett, E.W., and Glenne, B., 1970, Tidal study of three Oregon estuaries: Corvallis, Oregon State University, Engineering Experiment Station, Bulletin 45, 32 p.

Grant, W.C., 1989, More evidence from tidal-marsh stratigraphy for multiple late Holocene subduction earthquakes along the northern Oregon coast [abs.]: Geological Society of America Abstracts with Programs, v. 21, no. 5, p. 86.

Grant, W.C., and McLaren, D.D., 1987, Evidence for Holocene subduction earthquakes along the northern Oregon coast [abs.]: EOS [American Geophysical Union Transactions], v. 68, no. 44, p. 1239.

Heaton, T.H., and Hartzell, S.H., 1986, Source characteristics of hypothetical subduction earthquakes in the northwestern United States: Seismological Society of America Bulletin, v. 76, no. 3, p. 675–708.

Huyer, A., Gilbert, W.E., and Pittock, H.L., 1983, Anomalous sea levels at Newport, Oregon, during the 1982–1983 El Nino: Coastal Oceanography and Climatology News, v. 5, p. 37–39.

Huyer, A., Sobey, E.J.C., and Smith, R.L., 1979, The spring transition in currents over the Oregon continental shelf: Journal of Geophysical Research, v. 84, p. 6995–7011.

Jackson, P.L., and Rosenfeld, C.L., 1987, Erosional changes at Alsea Spit, Waldport, Oregon: Oregon Geology, v. 49, p. 55–59.

Jefferson, C.A., 1975, Plant communities and succession in Oregon coastal salt marshes: Corvallis, Oregon State University, Ph.D. dissertation, 192 p.

Komar, P.D., 1986, The 1982–83 El Niño and erosion on the coast of Oregon: Shore and Beach, v. 54, p. 3–12.

Kraft, J.C., 1971, Sedimentary facies patterns and geologic history of a Holocene transgression: Geological Society of America Bulletin, v. 82, p. 2131–2158.

McKenzie, D.R., 1975, Seasonal variations in tidal dynamics, water quality and sediments in the Alsea estuary: Corvallis, Oregon State University, M.S. thesis, 252 p.

Nelson, A.R., 1987, Apparent gradual rise in relative sea level on the south-central Oregon coast during the late Holocene—Implications for the great Cascadia earthquake hypothesis [abs.]: EOS [American Geophysical Union Transactions], v. 68, no. 44, p. 1240.

Niering, W.A., and Warren, R.S., 1980, Vegetation patterns and processes in New England salt marshes: Bioscience, v. 30, p. 301–307.

O'Brien, M.P., 1969, Equilibrium flow areas of inlets on sandy coasts: Journal of Waterways and Harbors Division, American Society of Civil Engineers, no. WWI, February issue.

Orson, R.A., Panageotou, William, and Leatherman, S.P., 1985, Response of tidal salt marshes of the U.S. Atlantic and Gulf coasts to rising sea levels: Journal of Coastal Research, v. 1, no. 1, p. 29–37.

Percy, K.L., Sutterlin, C., Bella, D.A., and Klingeman, P.C., 1974, Oregon's estuaries: Corvallis, Oregon State University, Sea Grant College Program, 294 p.

Peterson, C.D., Darienzo, M.E., Burns, S.F., and Burris, K., 1993, Field trip guide to Cascadia paleoseismic evidence along the northern Oregon coast—Evidence of subduction zone seismicity in the central Cascadia margin: Oregon Geology, v. 55, p. 99–114.

Peterson, C.D., Darienzo, M.E., and Parker, Mike, 1988, Coastal neotectonic field trip guide for Netarts Bay, Oregon: Oregon Geology, v. 50, no. 9/10, p. 99–106, 117.

Peterson, C.D., Jackson, P.L., O'Neil, D.J., Rosenfeld, C.L., and Kimerling, A.J., 1990, Littoral cell response to interannual climatic forcing 1983–1987 on the central Oregon coast, USA: Journal of Coastal Research, v. 6, p. 87–110.

Peterson, C.D., Scheidegger, K.F., and Komar, P.D., 1982, Sand-dispersal patterns in an active-margin estuary of the Northwestern United States as indicated by sand composition, texture and bedforms: Marine Geology, v. 50, p. 77–96.

Peterson, C.D., Scheidegger, K.F., and Schrader, H.J., 1984, Holocene depositional evolution of a small active-margin estuary of the Northwestern United States: Marine Geology, v. 59, p. 51–83.

Peterson, C.P., Kulm, L.D., and Gray, J.J., 1986, Geologic map of the ocean floor off Oregon and the adjacent continental margin: Oregon Department of Geology and Mineral Industries, Geologic Map Series, GMS–42, scale 1:500,000.

Pittock, H.L., Gilbert, W.E., Huyer, A., and Smith, R.L., 1982, Observations of sea level, wind and atmospheric pressure at Newport, Oregon, 1967–1980: Corvallis, Oregon State University, School of Oceanography, Data Report Reference 82–12, 158 p.

Plafker, George, 1972, Alaskan earthquake of 1964 and Chilean earthquake of 1960—Implications for arc tectonics: Journal of Geophysical Research, v. 77, no. 5, p. 901–925.

Plafker, George, and Kachadoorian, Reuben, 1966, Geologic effects of the March 1964 earthquake and associated seismic sea waves on Kodiak and nearby islands, Alaska: U.S. Geological Survey Professional Paper 543–D, 46 p.

Powell, H., 1980, Decomposition of organic matter in estuarine sediments by sulfate reduction—A field study from Yaquina Bay and sediment incubation experiments: Corvallis, Oregon State University, M.S. thesis, 173 p.

Redfield, A.C., 1972, Development of a New England salt marsh: Ecological Monographs, v. 42, p. 201–237.

Reineck, H.E., and Singh, I.B., 1980, Depositional sedimentary environments: New York, Springer-Verlag, 549 p.

Reinhart, M.A., and Bourgeois, Joanne, 1989, Tsunami favored over storm or seiche for sand deposit overlying buried Holocene peat, Willapa Bay, WA [abs.]: EOS [American Geophysical Union Transactions], v. 70, no. 43, p. 1331.

Rejmanek, Marcel, Sasser, C.E., and Peterson, G.W., 1988, Hurricane-induced sediment deposition in a gulf coast marsh: Estuarine, Coastal and Shelf Science, v. 27, p. 217–222.

Riddihough, R.P., 1984, Recent movements of the Juan de Fuca plate system: Journal of Geophysical Research, v. 89, no. B8, p. 6980–6994.

Savage, J.C., 1983, A dislocation model of strain accumulation and release at a subduction zone: Journal of Geophysical Research, v. 88, no. 136, p. 4984–4996.

Smith, R.L., 1974, A description of current, wind and sea level variations during coastal upwelling off the Oregon coast, July-August 1972: Journal of Geophysical Research, v. 79, no. 3, p. 435–442.

Stuiver, Minze, and Reimer, P.J., 1986, A computer program for radiocarbon age calibration, *in* Stuiver, Minze, and Kra, Renee, eds., Calibration issue: Radiocarbon, v. 28, no. 2B, p. 1022–1030.

U.S. Geological Survey, 1988, Water resources data, Oregon water year 1988, Portland, Oregon: U.S. Geological Survey, Water Resources Division, Water Data Report OR–1988.

Uyeda, S., and Kanamori, Hiroo, 1979, Back-arc opening and the mode of subduction: Journal of Geophysical Research, v. 84, no. B3, p. 1049–1061.

West, D.O., and McCrumb, D.R., 1988, Coastline uplift in Oregon and Washington and the nature of Cascadia subduction-zone tectonics: Geology, v. 16, no. 2, p. 169–172.

Yamaguchi, D.K., Woodhouse, C.A., and Reid, M.S., 1989, Tree-ring dating of late Holocene subsidence along the Washington and Oregon coasts—A progress report, *in* Jacobson, M.L., comp., National Earthquake Hazards Reduction Program, Summaries of technical reports, Volume XXVIII: U.S. Geological Survey Open-File Report 89–453, p. 162–169.

GREAT EARTHQUAKES RECORDED BY TURBIDITES OFF THE OREGON-WASHINGTON COAST

By John Adams[1]

ABSTRACT

Piston cores from the Cascadia Seachannel contain sequences of turbidites that can be correlated and dated by using glass shards from the Mount Mazama, Oregon, eruption of about 6,850 years ago as a common datum. Turbidity currents in the channel's tributary canyons appear to have occurred simultaneously and then merged, depositing single turbidite units in the main channel. In the Cascadia Seachannel and at 3 other places along the base of the Oregon-Washington continental slope, there are 13 turbidites that postdate the Mount Mazama eruption. Thin layers of pelagic deposits on each successive turbidite suggest that in each place, the 13 turbidity currents occurred every 590±170 years, on average. The best explanation of the spatial and temporal distribution of the turbidites is that the turbidity currents were triggered by 13 great Cascadia subduction zone earthquakes. The thickness of the topmost pelagic layers suggests that the youngest turbidite was deposited 300±60 years ago, a time consistent with the most recent sudden-subsidence event on the Oregon-Washington coast. The turbidite evidence implies appreciable near-term risk of a great earthquake (magnitude 8 or greater) that might rupture the Cascadia subduction zone from Vancouver Island, British Columbia, to Cape Blanco, Oregon, or even farther south.

INTRODUCTION

About 15 years ago, perceptions of the nature of the subduction zone beneath southern British Columbia, Washington, and Oregon began to change (for example, see Riddihough and Hyndman, 1976). Earlier work had established that the Juan de Fuca plate was converging on North America. However, the lack of seismicity on the interface between the Juan de Fuca and the North America plates led some workers to consider that the subduction was occurring extremely slowly or had stopped.

More recent studies of the deformation front at the base of the continental slope (for example, Barnard, 1978), of geodetic deformation rates on land (Ando and Balazs, 1979; Reilinger and Adams, 1982; Holdahl and others, 1989), and of onshore tectonic deformation such as warped terraces (Adams, 1984) have confirmed that the Oregon-Washington continental margin is being deformed at rates as rapid as those at other subduction zones. Heaton and Kanamori (1984) and Rogers (1988) assessed similarities between the Cascadia subduction zone and other zones worldwide and concluded that the Cascadia subduction zone could generate earthquakes of magnitude 8.3+.

The chief hypothesis of my work is that great earthquakes, should they occur on the Cascadia subduction zone, would be extremely catastrophic events and would leave their mark, not only in the onshore geological record but also in the offshore record. In 1984 and 1985, I suggested that the simplest way to reconcile the discrepancies between long-term and short-term evidence for deformation, strain accumulation, and stress directions was with a great-earthquake cycle of long duration (Adams, 1984, 1985). I discussed how an analysis of landslides, landslide-dammed lakes, drowned trees below sea level, and uplifted beaches could be used to determine evidence for past great earthquakes and I stated that turbidite units deposited by turbidity currents in the Cascadia Seachannel, as described by Griggs and Kulm (1970), could indicate a minimum recurrence interval for such earthquakes.

Earthquakes have long been known to cause submarine turbidity currents (Heezen and Ewing, 1952), but because the very frequent turbidity currents off some deltas (every few years off the Magdalena and Congo Rivers) suggested that many currents were caused by sediment instability due to rapid sedimentation, the role of infrequent earthquakes was less easy to assess. The present chapter was written in parallel with a full paper (Adams, 1990) and updates a summary work (Adams, 1989) that showed that the turbidite record provides strong evidence for great earthquakes occurring about every 600 years. The turbidite evidence complements the large body of onshore research into paleoseismicity that has been conducted since 1986 (for

[1]Geophysics Division, Geological Survey of Canada, 1 Observatory Crescent, Ottawa K1A 0Y3, Canada.

example, Atwater, 1987a, b) and is thus important for the current debate (for example, see Heaton and Hartzell, 1987) about the level of seismic hazard in the Pacific Northwest.

ACKNOWLEDGMENTS

This study would not have been possible without the meticulous work of G.B. Griggs, his fellow Ph.D. students, and their supervisor, La Verne Kulm. I thank Mitch Lyle and the College of Oceanography, Oregon State University, for their cooperation and for making the core logs available. David Piper assisted with technical advice regarding the behavior of turbidity currents, and B.F. Atwater pointed out the importance of the bias in the uncalibrated radiocarbon ages. Permission of the American Geophysical Union to reuse material from Adams (1990) is gratefully acknowledged. I thank B.F. Atwater, P.W. Basham, M.J. Berry, L.D. Kulm, D.J.W. Piper, and G.C. Rogers for valuable critical comments on early reports of this study, and Hans Nelson and Mark Holmes for thoughtful reviews. This paper is Geological Survey of Canada Contribution 45389.

CAN THE CASCADIA SEACHANNEL TURBIDITES BE CORRELATED?

For the past 7,000 years, suspended sediment from the Columbia River has been carried north along the continental shelf and deposited on the shelf and the edge of the continental slope (fig. 58) (Barnard, 1978; Sternberg, 1986). The sediment accumulates as a thin sheet of mud until slope failure occurs, and then it flows down the various submarine canyons and channels as a muddy turbidity current (fig. 59). Griggs and Kulm (1970) calculated that each major turbidity current takes about 2 days to travel the 735-km length of the Cascadia Seachannel and carries about 525×10^6 m^3 of sediment in a flow as large as 17 km wide and 100 m high. The predominantly muddy sedimentation in the channel and the similarity of Cascadia Seachannel piston cores suggests that many of the cores represent a complete record of turbidity currents in the Holocene. By contrast, only two turbidites deposited after the Mount Mazama eruption in southwestern Oregon extend the length of the Astoria Seachannel (fig. 58) (Nelson, 1968, 1976; Nelson and others, 1988), perhaps because of the northward drift of sediment away from Astoria Canyon.

Because large turbidity currents travel the length of the Cascadia Seachannel, turbidites along the length of the channel should correlate. A unique event in the last 10,000 years was the eruption of Mount Mazama at 6,845±50 radiocarbon years before present (Bacon, 1983). Though little if any of the air-fall tephra fell as far west as the coastal ranges (fig. 58), much fell in the drainage basin of the Columbia River and was washed into the ocean and deposited on the continental shelf, apparently mostly north of the river mouth. When this shelf-edge deposit slumped, the turbidity current carried the tephra-rich sediment down into the seachannels.

Because of the presence of this tephra, the oldest turbidite with abundant glass can be traced down the Cascadia Seachannel, and the mean period between turbidity currents can be calculated. The position of the glass in three piston cores from the middle and lower Cascadia Seachannel supports Griggs' (1969) assertion that not only must the lowest turbidite containing Mount Mazama tephra correlate between cores, but so must each of the 12 overlying turbidites (that is, the 13 turbidites in the cores represent the same 13 turbidity currents). The correlation is further supported by the similar pattern of bioturbation in the top eight layers of pelagic sediment in cores 6509–27, 6609–24, and 6509–26 (fig. 58) from a 65-km-long section of the lower Cascadia Seachannel (fig. 60) (Griggs and others, 1969). Although the pattern of bioturbation is distinctive in these three cores, it is unlikely that the correlations could be extended to the cores from the tributary channels discussed below because those cores are uniformly more bioturbated. Also, until the reasons for the degrees of bioturbation are fully understood, Cascadia Seachannel cores cannot be correlated on this basis alone with cores from off southern Oregon.

DO SINGLE TURBIDITES RESULT FROM SIMULTANEOUS TURBIDITY CURRENTS IN SEPARATE TRIBUTARIES?

Core 6508–K1 (fig. 58) is from the Cascadia Seachannel downstream of the confluence of two main tributary channels, the northern from the Juan de Fuca and nearby canyons and the southern from Willapa, Grays, and Quinault Canyons. In the northern tributary, core from site 6705–6 has 14 turbidites deposited since the Mount Mazama eruption, the same number as was found in cores from below the confluence. Farther upchannel from core 6705–6, core 6705–2 contains 16 turbidites deposited after the Mount Mazama eruption (according to Griggs and Kulm, 1970); by inference, 2 small turbidity currents did not flow down the channel as far as core 6705–6. In Quinault Canyon, core 53–18 contains "at least 14" turbidites deposited after the Mount Mazama eruption (Barnard, 1978, p. 111). Further downchannel, in the main Willapa Canyon, core 6705–5 has 15 turbidites since the Mount Mazama eruption; one explanation for this discrepancy is that one small turbidity current did not flow downchannel as far as the confluence and core 6508–K1.

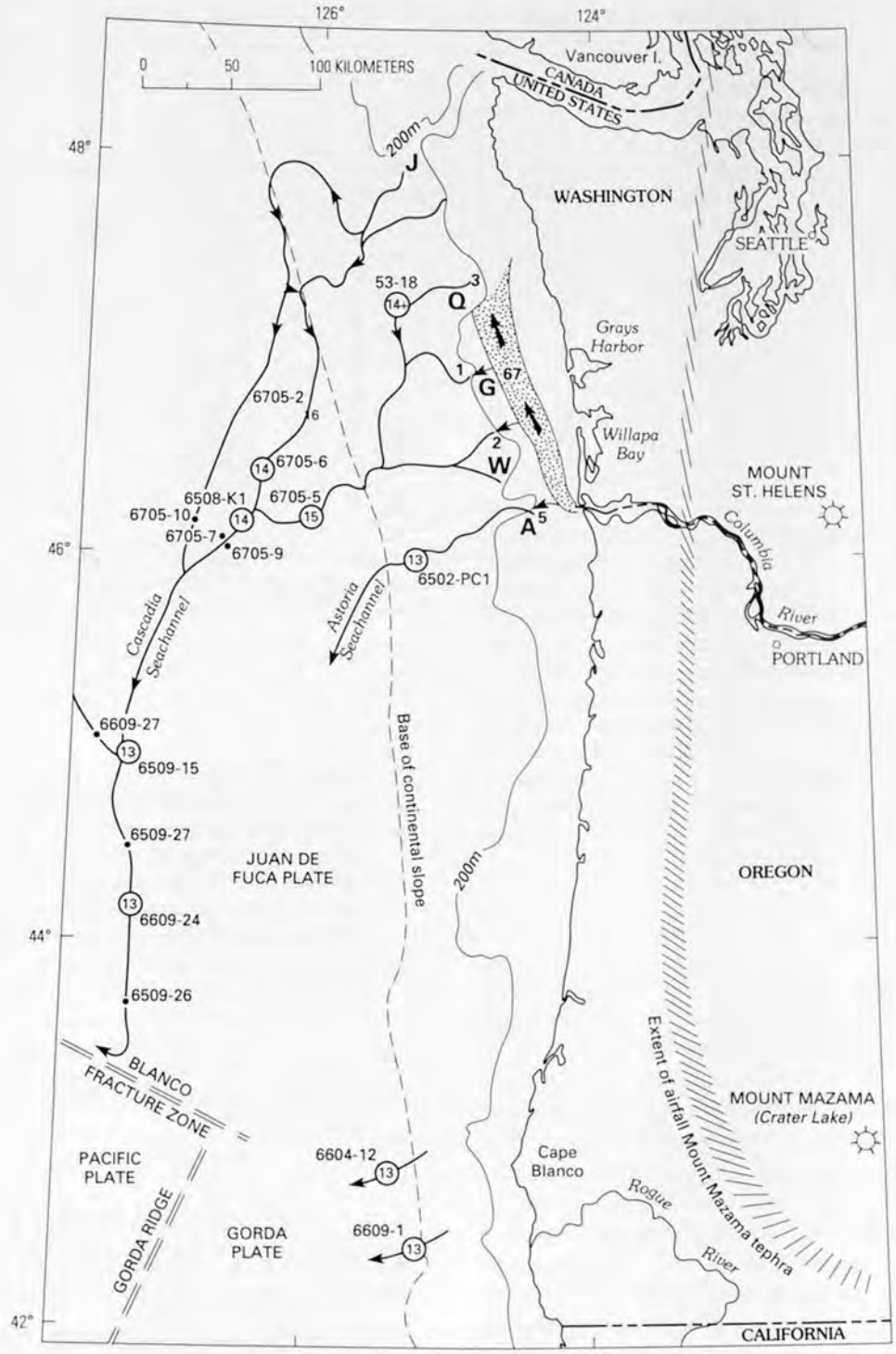

Figure 58. Map of the Oregon-Washington continental margin showing the extent of the airfall Mount Mazama tephra (Fryxell, 1965), the pattern of sediment dispersal north from the Columbia River (stippled area with heavy arrows; numbers show amounts of sediment as a percentage of the river output, from Sternberg, 1986), canyons on the Washington continental slope (J, Juan de Fuca; Q, Quinault; G, Grays; W, Willapa; and A, Astoria), submarine channels leading to the deep-sea floor (lines with arrows), the sites of piston cores described in the text (circles and dots; all from Oregon State University except core 53–18, which is from the University of Washington), and the number of turbidites deposited after the Mount Mazama eruption (numbers within the circles) as discussed in the text. From Adams (1990, fig. 1).

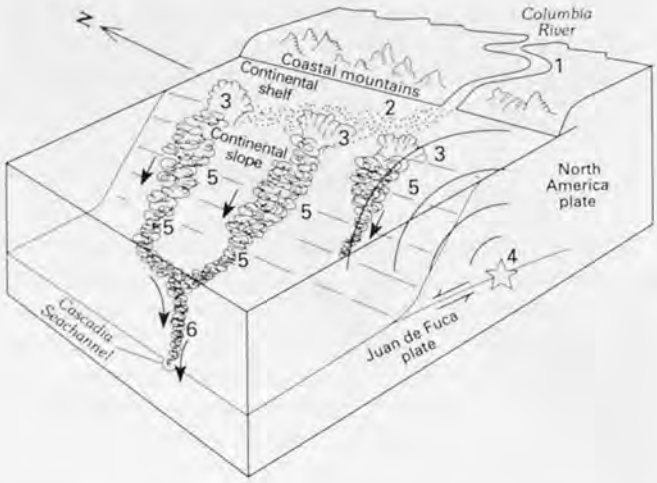

Figure 59. Schematic diagram showing the proposed genesis of turbidity currents in the Cascadia Seachannel. Sediment is carried down the Columbia River (1), drifts north along the continental shelf (2), and accumulates at the top of the continental slope in the heads of deep-sea canyons (3). According to the hypothesis presented in this paper, a great thrust earthquake on the Cascadia subduction zone (4) strongly shakes the shelf and slope (barbs show direction of relative movement across fault plane). The shaking causes sediment liquefaction and slumping simultaneously at many places along the slope. The resultant massive undersea debris flows mix with the water to become a series of turbidity currents traveling simultaneously down separate channels (5). At junctions, the tributary turbidity currents coalesce to travel down the Cascadia Seachannel as one large turbidity current (6). From Adams (1990, fig. 2).

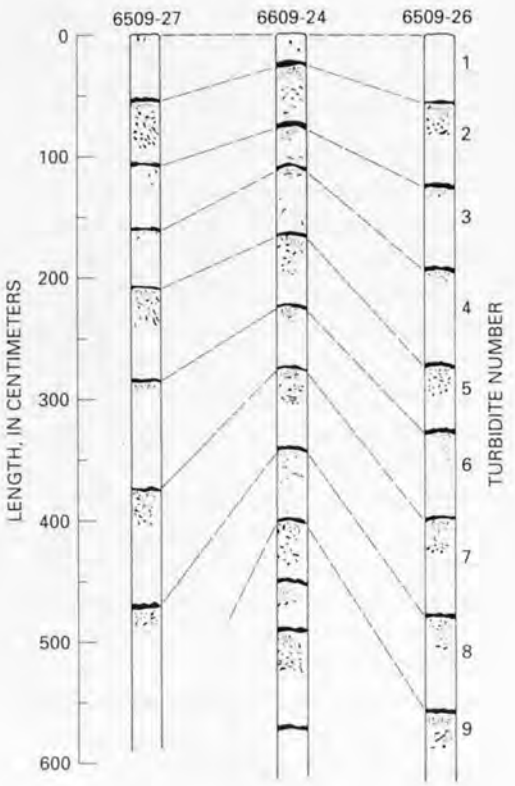

Figure 60. Three cores from the Cascadia Seachannel showing how different degrees of bioturbation in the pelagic sediments confirms the stratigraphic correlation of the turbidites. Core sites are shown in figure 58. The pelagic layers are shown in solid black. Note the uniform thickness of the turbidites. In core 6609–24, the earliest Mount Mazama glass is in the 13th turbidite (not shown) from the top of the core. Redrawn (with changes) with permission from Deep-Sea Research, v. 16, Griggs, G.B., Carey, A.G., and Kulm, L.D., "Deep-sea sedimentation and sediment-fauna interaction in Cascadia Channel and on Cascadia Abyssal Plain," copyright 1969, Pergamon Press PLC.

The cores from the tributaries suggest that a few (2 or 3 of a maximum of 16) small turbidity currents may have been generated that resulted in less extensive deposits than the 13 turbidity currents in the lower channel. Therefore, the remarkable inference can be made that pairs of turbidity currents were generated in the two tributaries at the same time. Had the 15 turbidites deposited in the Willapa Seachannel and the 14 in the northern channel occurred independently, there would be 29 turbidites below the confluence instead of the 14 that have been found. Therefore, I conclude that turbidity currents were generated simultaneously in two independent channels and that each pair of small currents merged to form one large turbidity current.

That only 14 turbidites were found in the main channel implies that every single turbidity current in the two tributaries occurred at the same time, that is, simultaneous occurrence was the rule rather than the exception. Similar merging of turbidity currents from multiple sources to form a single turbidity current has been documented from the Mediterranean Sea and from the Puerto Rico Trench (Pilkey, 1988) and has also been interpreted to represent the effects of a simultaneous regional trigger.

HOW FAR ALONG THE CONTINENTAL MARGIN CAN THE 13 DEPOSITIONAL EVENTS SINCE THE MOUNT MAZAMA ERUPTION BE TRACED?

Besides the cores discussed above, there are many others from sites off Oregon and Washington that contain the Mount Mazama glass and varying numbers of overlying turbidites. Figure 58 shows three core sites outside the Cascadia Seachannel, one at Astoria Canyon and two off Cape Blanco.

Astoria Canyon, off the Columbia River mouth (fig. 58), was a major conduit for sediment until 7,000 years

Table 15. Sediment-layer thicknesses in selected Cascadia subduction zone piston cores.

[Numbers are mean values per layer. Summarized from Adams (1990, table 1). (>), greater than]

Core	Number of turbidites[1]	Turbidites		Pelagic deposits	
		Mean thickness (millimeters)	Variability[2] (percent)	Mean thickness (millimeters)	Variability[2] (percent)
6705–2	16	115	50	62	63
6705–6	14	155	69	55	44
6705–5	15	355	73	31	49
[3]6508–K1	14	360	86	33	26
6509–15	13	65	44	15	36
6509–27	>8	1,060	33	28	44
[3]6609–24	13	450	28	55	35
6509–26	>10	660	17	41	32
6502–PC1	13	130	47	148	24
[3]6604–12	13	420	44	105	61

[1]Since eruption of Mount Mazama (6,845±50 radiocarbon years before the present).

[2]Standard deviation expressed as a percentage of the mean thickness.

[3]Mean pelagic-layer thickness excludes two abnormally thin layers immediately above the first turbidite containing Mount Mazama glass.

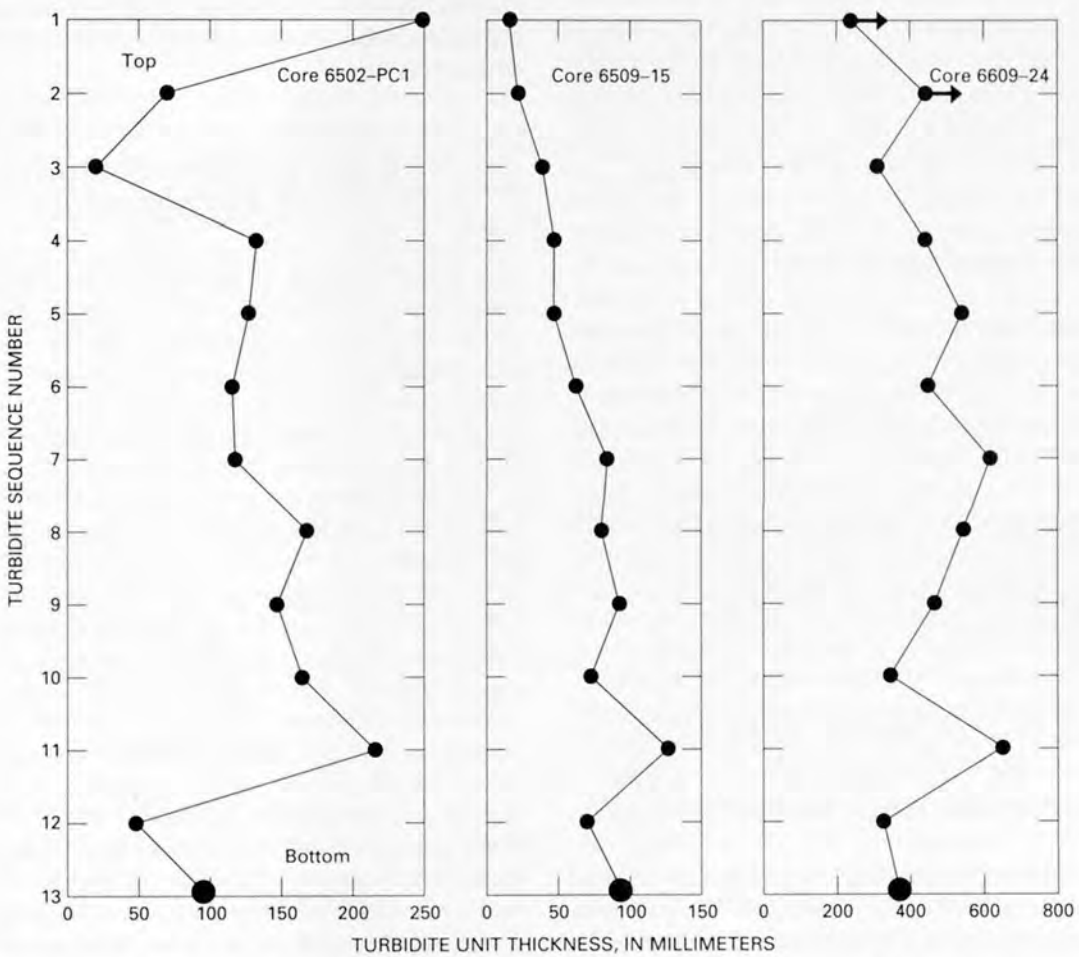

Figure 61. Thicknesses of turbidite units in three cores from off the Oregon-Washington coast (core sites shown in fig. 58). Large dots denote the oldest turbidite containing Mount Mazama glass; arrows show that plotted values are minimum thicknesses. Although some thickness variations may correlate (such as near the base of each graph), such correlations are not obvious.

ago. Although the lower Astoria Seachannel has been less active since two 200–500-mm-thick turbidites were deposited soon after the Mount Mazama eruption (Nelson and others, 1988), core 6502–PC1 shows that 13 thin (average thickness of 130 mm) turbidites were deposited in Astoria Canyon after the eruption (Carlson, 1968). Apparently, these small turbidity currents did not travel all the way down the Astoria Seachannel.

Both the site off Cape Blanco (core 6604–12) and the one off the Rogue River (6609–1) are remote from the Columbia River mouth, and heavy-mineral analysis of the cores shows that, at least since the Mount Mazama eruption, their sediment has come from the Klamath Mountains (Duncan and Kulm, 1970), which are inland and south of Cape Blanco. Despite their remoteness from the Cascadia Seachannel and Astoria Canyon systems, each core contains 13 turbidites deposited after the eruption.

The distance from Juan de Fuca Canyon to Quinault Canyon (fig. 58) is at least 50 km; the distance across the Quinault-Willapa Canyon system is 100 km; on to Astoria Canyon is 30 km; from there to Cape Blanco is 350 km; and to the Rogue River is another 50 km. All 5 parts of the margin have had 13 turbidity currents since the Mount Mazama eruption. The simplest explanation for the simultaneous currents in neighboring tributaries and the same numbers of currents at sites 580 km apart is a series of great earthquakes.

As noted by Griggs (1969) and Griggs and Kulm (1970), the turbidites in the Cascadia Seachannel system have generally similar thicknesses and are separated by intervals of pelagic deposits, also of generally constant thickness. Pelagic and turbidite thicknesses for 10 cores are given in Adams (1990), from which the summary statistics in table 15 are derived. The rather similar turbidite thicknesses within each core (fig. 61) suggest that the volume of each turbidity current was similar. A plot of cumulative pelagic thickness versus turbidite sequence number (Adams, 1990, fig. 5) was previously used to demonstrate that the 13 events affecting the continental margin were fairly regular in time and thus that the mean thickness interval between events is a realistic measure of the event timing.

WHAT IS THE MEAN INTERVAL BETWEEN THE DEPOSITIONAL EVENTS?

The Mount Mazama eruption is well dated by multiple carbon-14 dates at 6,845±50 radiocarbon years before present (Bacon, 1983), though Brown and others (1989) suggested 6,480±60 radiocarbon years before present might be a better estimate. The radiocarbon age is equivalent to 7,620 $^{+159}_{-51}$ calibrated years before 1950 (at the 2σ confidence level using version 2.0 of the computer program of Stuiver and Reimer, 1986). The difference between the +159 year and –51 year errors is small relative to the stochastic error discussed below, so adjusting for the 40 years since the 1950 reference date gives 7,660±100 calibrated years before 1990. Like the St. Helens tephra (Sternberg, 1986), the Mount Mazama tephra was probably carried rapidly to the continental shelf edge and was available for slumping almost immediately after eruption. When did the next turbidity current occur? For 13 turbidity currents, the mean return period is about 600 years, so the next one would probably have been 300±300 years later. Therefore, 7,360±400 years before 1990 is adopted as the age of the oldest turbidite with Mount Mazama tephra.

Since the oldest turbidite, there have been 12 turbidites, 12 between-turbidite intervals, and a period of time since the youngest turbidite. The length of the last period is not known, so it is taken as a 0.5±0.5 interval, for a total of 12.5±0.5 intervals. The mean interval between turbidites is then 7,360±400 years divided by 12.5±0.5 intervals, or 590±50 years (for comparison, the Brown and others (1989) age for the Mount Mazama eruption gives a mean interval of 570±60 years).

WHAT IS THE VARIABILITY OF THE MEAN?

The above error on the mean return period does not measure the variability of turbidity-current timing, which can be estimated by examining the thickness variations of the deposited layers. Table 15 shows the mean accumulation per event and the standard deviation expressed as a percentage of the mean for turbidite and pelagic deposits in some of the Cascadia Seachannel cores. The extremely low variability for the turbidite thicknesses in core 6509–26 (±17 percent; table 15, fig. 60) suggests a very regular series of events including constant sediment accumulation on the continental shelf, rhythmic triggering, and consistent turbidity-flow characteristics that include the amount of erosion. For the pelagic layers, accumulation rates and their variability are generally largest near shore, whereas the deeper cores show more even thicknesses, ±26 percent in 6508–K1 and ±32 percent in 6509–26. If the cores record the same 13 events, those with the more variable pelagic thicknesses must include a larger amount of variance due to measurement errors and erosion and so provide poor estimates of the variability of event timing. Therefore, the average variability for the three lowest variability cores (1σ =28 percent) is chosen as the representative variability of event timing. For a 590-year recurrence interval, this translates to a variability of about 170 years and an implied standard error on the mean

of 50 years. Thus, if the intervals are normally distributed, there is one chance in two that 1 of the 12 intervals would lie outside $\mu \pm 1.7\sigma$, or outside the range of 300–900 years.

WHAT PHENOMENA COULD TRIGGER THE TURBIDITES?

Although Gary Griggs (then at Oregon State University) originally believed that earthquakes were the cause of the turbidity currents (L.D. Kulm, Oregon State University, oral commun., 1988), the lack of large earthquakes nearby made this position difficult to support in the middle to late 1960's. Griggs and Kulm (1970) noted that if sediment is supplied by the Columbia River at a constant rate, it would accumulate in the offshore canyon heads until there was enough to trigger collapse, whereupon the cycle would start again. Such a self-triggering system would tend to repeat itself and would generate similar-size turbidites in the offshore channel system. Of course, triggering by external events of a cyclic nature (such as great earthquakes) would also tend to displace similar masses of sediment and produce similar-size turbidites. Perhaps the strongest argument against the self–triggering hypothesis is that similar numbers of events are noted at widely separated places along the continental margin where sediment accumulation amounts are variable; it would be highly improbable that every canyon would have the same temporal response to the varying rates of sedimentation that occur along the margin. Therefore, I conclude that the triggering events have occurred more frequently than the time needed to accumulate the critical mass required for collapse in most canyons and so the events would preempt the endogenic slumping process.

For a similar reason, events local to one canyon head (such as a magnitude 6.5 earthquake within 50 km) do not sufficiently explain simultaneous turbidity currents in separate tributaries and the same number of events along the continental margin. Therefore, any cause of the simultaneous events must be external to the canyon heads and must affect the Oregon-Washington margin as a whole. Three such external triggers with the required spatial extent are tsunamis, wave-induced slumping during large storms, and great earthquakes on the Cascadia subduction zone.

TSUNAMIS

The most recent damaging tsunami on the Oregon-Washington coast was generated by the 1964 Alaska earthquake, the second largest earthquake of this century. It did not trigger one of the 13 great turbidity currents in the Cascadia Seachannel because both the thickness of pelagic sediment found on top of the cores and the amount of animal life seen on the channel floor during the 1965–67 research cruises (for example, see Griggs and others, 1969) are too large for such a recent turbidity current. Tsunami-generating earthquakes are relatively common around the Pacific Ocean, and if the large tsunami in 1964 did not trigger a turbidity current, it seems unlikely that a coupling of multiple independent tsunami sources with the time-dependent stability changes in the canyon heads would give both long recurrence intervals and the same number of events along the continental margin.

WAVE-INDUCED SLUMPING

The case for wave-induced slumping on such a large scale is poorly documented, and computations suggest that for all but the steepest slopes, wave loading does not influence slope stability in water depths greater than 120 m (Moran and Hurlbut, 1986), which is shallower than most of the offshore canyon heads. Physical parameters constrain the maximum size of storms and storm-generated waves so that an extremely rare storm is not much larger than a more common storm. Therefore, the 100- and 1,000-year storms would have rather similar effects, the sediments probably would need to be close to failure anyway, and so, collapse would happen at different times for different places. Like tsunamis, the process would be unlikely to give both long recurrence intervals and the same number of events for the whole continental margin.

EARTHQUAKES

Earthquakes are unusual natural phenomena in that the strength and duration of ground shaking continues to increase dramatically as the probability of occurrence drops. Thus, a great earthquake is so overwhelmingly large that it would trigger collapse of both marginally and otherwise normally stable canyon-head deposits. Great earthquakes, should they occur on the Cascadia subduction zone, would probably have a long return period and, indeed, return periods of several hundred to a thousand years have been estimated by Adams (1984) and Heaton and Hartzell (1986) based on the rate of geodetic strain accumulation. As a first approximation, plate-boundary earthquakes occur fairly regularly and tend to have a characteristic size. For such characteristic earthquakes, there may be a scale-independent variability in timing amounting to about one-fifth of the mean recurrence interval (Nishenko and Buland, 1987), hence 120 years for a 590-year recurrence interval. This variability is close to the 20–30 percent variability in pelagic deposit thicknesses found in the cores (which includes not only variability due to the earthquake cycle but also that due to variable partial erosion and measurement errors in determining the thickness of the pelagic layers).

HOW DOES THE TURBIDITE EVIDENCE COMPARE WITH ONLAND EVIDENCE OF GREAT EARTHQUAKES?

Evidence that the 13 turbidity currents indeed represent earthquakes is circumstantial, and establishing proof is unlikely in the near future. Nevertheless, because a great thrust earthquake is an extremely large and relatively rare event, it should cause simultaneous effects throughout the coastal Pacific Northwest. Such confirmatory past evidence would include sudden coastal subsidence or uplift, landslides, sediment liquefaction and sand volcanoes, sediment slumping in large lakes, and submarine debris flows. Other less direct effects would be abnormal sedimentation events, deformed tree growth, abandonment of prehistoric Indian settlements, and secondary faulting on crustal faults. Although the turbidite record may well be complete because of the muddy nature of the sediments, the inferred earthquake record might be incomplete because subsequent nearby earthquakes (a second main shock or large aftershock) soon after a great earthquake would probably not generate their own turbidity current(s), all of the unstable sediments having already slumped.

The first onshore evidence inferred to indicate past great Cascadia subduction zone earthquakes was reported by Atwater (1987a), who ascribed buried Holocene marshes in coastal Washington to sudden coseismic subsidences of the coast. His most recent work (Atwater, 1988) suggests five subsidence events and one shaking event in the last 3,100 years. Corresponding evidence comes also from eight buried soils in about 5,000 years at another coastal Washington site (Hull, 1987), seven buried marshes in about 3,550 years in northern Oregon (Peterson and others, 1988), and eight buried marshes in about 5,000 years in southern Oregon (Nelson and others, 1989). At the southern end of the Cascadia subduction zone, Carver and Burke (1987) deduced recurrence intervals of about 600 years for earthquakes on thrust faults in the accretionary prism just north of Cape Mendocino, Calif. Equivalent evidence is described in the other chapters of this volume. In each place, the implied recurrence interval is about 500–600 years, in close agreement with the mean recurrence interval and spatial extent established for the turbidity currents (fig. 62*A*).

B.F. Atwater (U.S. Geological Survey, written commun., 1988) has also drawn my attention to the coincidence between the age of 4,290±80 radiocarbon years before present for the eighth peat at Willapa Bay (sample H1–B of Atwater, 1988) and the age of 4,645±190 radiocarbon years before present for plant fibers in the eighth turbidite of core 6509–27 (Griggs and others, 1969). The fibers had accumulated in the offshore canyon heads for about 600 years prior to the dated turbidity current, so subtracting 300 years (half the inferred accumulation time) from the core date brings the two ages into remarkable agreement. This agreement is all the more significant because each date is on the eighth event, suggesting a one-to-one correspondence between turbidites and subsidence events and reinforcing the argument made from the mean recurrence intervals discussed above.

WHAT ARE THE IMPLICATIONS FOR GREAT THRUST EARTHQUAKES ON THE CASCADIA SUBDUCTION ZONE?

The inferred occurrence of 13 great thrust earthquakes, their mean return period of 590 years, a variability of 170 years, and the 580-km extent of triggered turbidity currents (and, hence, inferred strong ground motion) constrain the slip, rupture dimensions, magnitude, and style of rupture of the margin. Subduction of the Juan de Fuca plate at 45 mm/year and the mean return period of 590 years results in 26 m for the average slip per earthquake if all the slip is seismic. A 26-m slip for the 750-km-long Juan de Fuca plate north of the Blanco fracture zone and a fault width of 100 km could produce an earthquake of moment magnitude (M_w) 9.1, which is in accord with the maximum size proposed by Rogers (1988). A variability of 28 percent in earthquake timing would lead to slip displacements of between 19 and 33 m but a variability in magnitude of only ±0.1 magnitude unit.

Would a rupture of the Cascadia subduction zone extend south of the shoreward extension of the Blanco fracture zone? Core 6604–12, which came from the extension of the fracture zone, and core 6609–1 from the subducting Gorda plate (fig. 58) contain 13 turbidites deposited after the Mount Mazama eruption, which are presumed to represent great earthquakes on the Juan de Fuca part of the Cascadia subduction zone. If the Gorda plate had a history of independent subduction (such as M_w 8.3 earthquakes; see Rogers, 1988), core 6604–12 is close enough to have shown additional turbidity currents that might have been generated by earthquakes either to the north or south. Therefore, the indication of only 13 turbidites in these 2 cores suggests that either every Cascadia subduction zone rupture extends past the Blanco fracture zone (indicating at least M_w 9.2 earthquakes) or the earthquakes on the Gorda plate segment are synchronized with those on the Juan de Fuca plate segment (a zipper effect in which an earthquake on one segment triggers earthquakes on adjacent segments in succession a few hours to years later; hence, no sediment would be left to be triggered by the second earthquake).

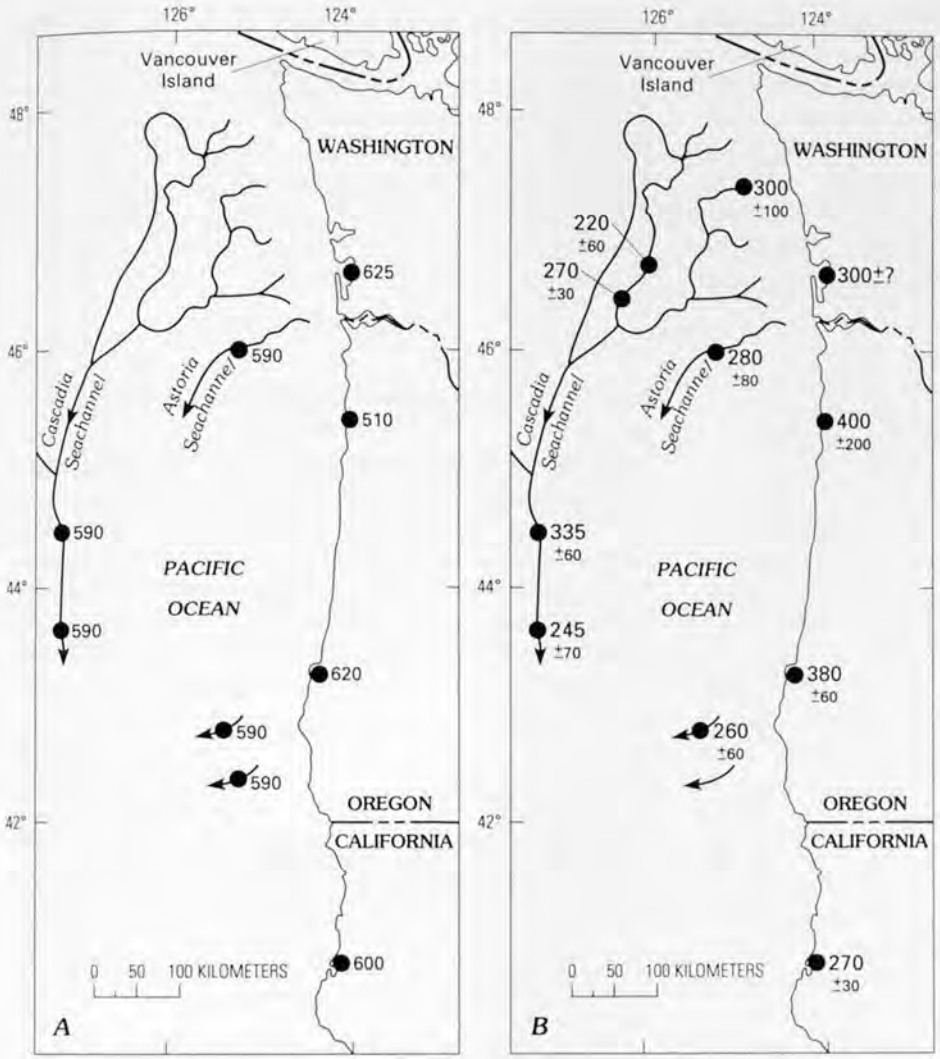

Figure 62. Spatial distribution of age evidence for great earthquakes in the Cascadia subduction zone, coastal Oregon and Washington. *A*, mean recurrence intervals for turbidites and onshore subsidence events, in years. *B*, age of the youngest turbidite, submarine slumping, or onshore subsidence event, in years before 1990. Heavy lines with arrows are submarine canyons and channels leading to the deep-sea floor. From Adams (1990, fig. 6).

WHEN WAS THE LAST EARTHQUAKE?

The age of the last earthquake can be estimated roughly from the thickness of pelagic sediment on top of the youngest turbidite relative to the mean sediment accumulation rate. From six cores (table 16), an age of about 300±60 years (before 1995) is estimated. This age is consistent with the lack of a great earthquake in the 150-year historical record but may be a biased underestimate if some sediment has been washed out from the top of each core. It is noteworthy that both the Astoria Canyon core and the core from off Cape Blanco give similar ages (to within the poor resolution) as the four Cascadia Seachannel cores, thereby showing that the youngest turbidite in each place did not occur at greatly different times.

A date for the youngest turbidite can also be derived from the amount of sediment that has accumulated in the submarine canyons since the sediment last slumped away (for example, see Barnard, 1978, p. 111), but estimates range from 100 to 400 years because the sediment accumulation rates are uncertain. The estimates weakly support the inference that about 300 years have elapsed since the last earthquake. Tree-ring dates on drowned trees at six sites in coastal Washington suggest that the youngest rapid submergence event was about 300 years ago (Yamaguchi and others, 1989). Comparable dates for the youngest buried marsh soil suggest that the youngest subsidence event occurred about 300 years ago in southwestern Washington (Atwater and others, 1987), less than 400±200 years ago in northern Oregon (Peterson and others, 1988), less than 380±60 years ago in southern Oregon (Nelson and others, 1989), and 270±30 years ago in northern California (Gary Carver, Humboldt State University, oral commun., 1989); these dates are consistent with the preceding analysis (fig. 62*B*) and suggest a regional earthquake (or closely spaced series of earthquakes) that affected almost the whole Cascadia subduction zone.

Working from the pelagic thicknesses in core 6508–K1 (fig. 58) (chosen because its pelagic thicknesses are the most regular), assuming that no sediment has been eroded by the overlying turbidite, and adopting 300 years

for the age of the last earthquake, the following dates for the last five earthquakes are deduced: A.D. 1,690±60, A.D. 1,300±130, A.D. 800±200, 180±450 B.C., and 790±520 B.C. (Adams, 1990, table 3). The slow accumulation rates of the pelagic sediments and the disturbance by the coring equipment make these dates rather imprecise, with the errors accumulating for the older dates. However, these dates should prove useful to other researchers seeking to match their discovered onshore events to the record of great earthquakes indicated by the turbidites.

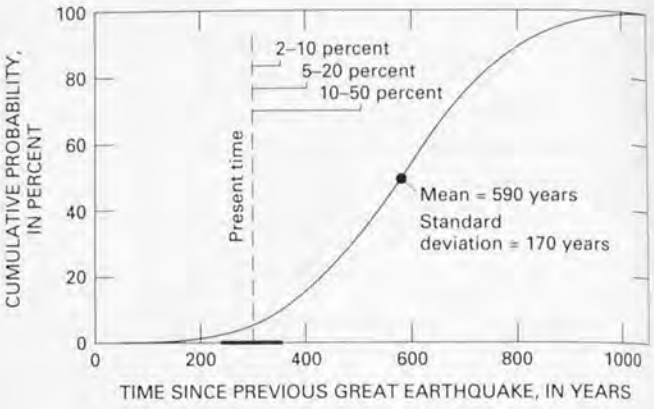

Figure 63. Cumulative normal probability distribution with a mean age of 590 years and a standard deviation of 170 years, as inferred for great earthquakes on the Cascadia subduction zone. The thick bar on the abscissa at 300±60 years is an estimate of where the present time is relative to the last earthquake, and the range of conditional probabilities of the next earthquake for the next 50, 100, and 200 years are illustrated by the values at the top. From Adams (1990, fig. 7).

WHAT IS THE PROBABILITY OF THE NEXT EARTHQUAKE?

From the mean interval between events (590 years), the standard deviation of the mean (about 170 years), the time since the youngest event (about 300 years), and a normal-distribution model for simple recurrent ruptures without clustering, the likelihood of the next great Cascadia subduction zone earthquake can be estimated (fig. 63). At present, there is about a 5 percent chance that the next earthquake should have already happened. For the future, the conditional probabilities are (crudely) 0.1 percent in the next year, 5 percent in the next 50 years, 10 percent in the next 100 years, and 25 percent in the next 200 years. These values are probably correct to only a factor of 2 and need to be refined using a revised date for the last earthquake and perhaps a lognormal distribution model (following Nishenko and Buland, 1987).

Some of the uncertainty arises from the possibility that the earthquakes cluster in time (say, three events in one millennium, followed by long quiescence) and from the still-unknown mode of failure of the subduction zone. Although the same number of turbidites in the Cascadia Seachannel, Astoria Canyon, and at the sites off Cape Blanco strongly suggests simultaneous turbidity currents, a zipper effect whereby smaller earthquakes rupture the plate boundary in a short-term sequence cannot yet be ruled out. Such multiple modes of rupture—sometimes single great earthquakes, sometimes sequences of smaller earthquakes—would complicate the paleoseismic history and are probably beyond the resolving power of the turbidite record. However, the mode of rupture could be resolved through onshore investigations using dendrochronology or other precise dating of earthquake effects.

Even if the rupture mode is complex, the net effect on hazard estimates may not be great because circumstantial evidence suggests that the (hypothetical) rupture segments would need to "stay in step" and the time since the last earthquake is already close to half the estimated mean recurrence interval. In addition, the damage implications for any place

Table 16. Age of the youngest turbidite in selected Cascadia subduction zone piston cores.

[Age estimated from the thickness of the overlying pelagic sediment. From Adams (1990, table 2)]

Core	Pelagic-layer thickness[1] (millimeters)	Accumulation rate[2] (millimeters/event)	Age of youngest turbidite[3] (years)
6705–2	23±6	62	220±60
6705–6	25±3	55	270±30
6509–26	17±5	41	245±70
6509–27	16±3	28	335±60
6502–PC1	70±20	148	280±80
6604–12	47±10	105	260±60
		Mean age	[4]270±60

[1](±), possible error in 1965–67.
[2]From table 15; mean event spacing is 590 years.
[3]Relative to 1965–67; add 30 years for years before 1995.
[4]Or about 300 years before 1995. May be biased towards being too young because of washouts at top of core.

along the continental margin are not greatly different between the single magnitude 9 or multiple magnitude 8 earthquake scenarios, though it is clear that should one magnitude 8 earthquake happen somewhere on the subduction zone, the likelihood of others in the near future would be greatly increased because of the temporal clustering implied by the alternative hypothesis.

CONCLUSIONS

Turbidites in the Cascadia Seachannel and at other places along the Oregon-Washington continental margin were deposited from turbidity currents probably triggered by 13 great Cascadia subduction zone earthquakes since the Mount Mazama eruption. Earthquakes of the order of magnitude 9 have occurred every 590 years on average, an interval that agrees well with the mean interval between known coastal subsidence events. Analysis of the pelagic-sediment intervals between the turbidites suggests that the earthquakes occurred fairly regularly, with a standard deviation of 170 years or less for the earthquake timing, a variability similar to that for great earthquake cycles elsewhere.

The thickness of the topmost pelagic layer suggests that the last earthquake was 300±60 years ago. This age is consistent with the youngest subsidence event discovered on the Washington coast and implies appreciable near-term risk of a great earthquake in the Pacific Northwest.

Rhythmic triggering of turbidity currents by great earthquakes may be a much more common phenomenon than hitherto realized and might be expected at other continental margins such as Alaska, Japan, New Zealand, and Chile, where great thrust earthquakes with a long return period are combined with a moderate supply of sediment to the edge of the continental shelf. If sampled correctly, the turbidite record can provide a quick estimate of the paleoseismicity of a continental margin and so guide confirmation by onshore paleoseismology studies.

REFERENCES CITED

Adams, John, 1984, Active deformation of the Pacific Northwest continental margin: Tectonics, v. 3, no. 4, p. 449–472.

———1985, Deformation above the Juan de Fuca subduction zone—Some enigmas with bearing on great-earthquake risk: EOS [American Geophysical Union Transactions], v. 66, p. 1071.

———1989, Turbidites off the Oregon-Washington margin record paleo-earthquakes on the Cascadia subduction zone, *in* Current research, Part F: Geological Survey of Canada, Paper 89-1F, p. 37–43.

———1990, Paleoseismicity of the Cascadia subduction zone—Evidence from turbidites off the Oregon-Washington margin: Tectonics, v. 9, no. 4, p. 569–583.

Ando, Masataka, and Balazs, E.I., 1979, Geodetic evidence for aseismic subduction of the Juan de Fuca plate: Journal of Geophysical Research, v. 84, no. B6, p. 3023–3028.

Atwater, B.F., 1987a, Evidence for great Holocene earthquakes along the outer coast of Washington State: Science, v. 236, no. 4804, p. 942–944.

———1987b, Subduction-earthquake telltales beneath coastal lowlands, *in* Crone, A.J., and Omdahl, E.M., eds, Proceedings of Conference XXXIX, Directions in paleoseismology: U.S. Geological Survey Open-File Report 87–673, p. 157–162.

———1988, Geologic studies for seismic zonation of the Puget lowland, *in* Jacobson, M.L., and Rodriguez, T.R., comps., National Earthquake Hazards Reduction Program, Summaries of technical reports, Volume XXV: U.S. Geological Survey Open-File Report 88–16, p. 120–133.

Atwater, B.F., Hull, A.G., and Bevis, K.A., 1987, Aperiodic Holocene recurrence of widespread, probably coseismic subsidence in southwestern Washington: EOS [American Geophysical Union Transactions], v. 68, no. 44, p. 1468.

Bacon, C.R., 1983, Eruptive history of Mount Mazama and Crater Lake caldera, Cascade Range, U.S.A.: Volcanology and Geothermal Research Journal, v. 18, p. 57–115.

Barnard, W.D., 1978, The Washington continental slope—Quaternary tectonics and sedimentation: Marine Geology, v. 27, p. 79–114.

Brown, T.A., Nelson, D.E., Mathewes, R.W., Vogel, J.S., and Southon, J.R., 1989, Radiocarbon dating of pollen by accelerator mass spectrometry: Quaternary Research, v. 32, p. 205–212.

Carlson, P.R., 1968, Marine geology of Astoria submarine canyon: Corvallis, Oregon State University, Ph.D. dissertation, 259 p.

Carver, G.A., and Burke, R.M., 1987, Late Holocene paleoseismicity of the southern end of the Cascadia subduction zone [abs.]: EOS [American Geophysical Union Transactions], v. 68, no. 44, p. 1240.

Duncan, J.R., and Kulm, L.D., 1970, Mineralogy, provenance, and dispersal history of late Quaternary deep-sea sands of Cascadia basin and Blanco fracture zone off Oregon: Journal of Sedimentary Petrology, v. 40, p. 874–887.

Fryxell, R., 1965, Mazama and Glacier Peak volcanic ash layers—Relative ages: Science, v. 147, p. 1288–1290.

Griggs, G.B., 1969, Cascadia Channel—The anatomy of a deep-sea channel: Corvallis, Oregon State University, Ph.D. dissertation, 183 p.

Griggs, G.B., Carey, A.G., and Kulm, L.D., 1969, Deep-sea sedimentation and sediment-fauna interaction in Cascadia channel and on Cascadia abyssal plain: Deep-Sea Research, v. 16, p. 157–170.

Griggs, G.B., and Kulm, L.D., 1970, Sedimentation in Cascadia deep-sea channel: Geological Society of America Bulletin, v. 81, no. 5, p. 1361–1384.

Heaton, T.H., and Hartzell, S.H., 1986, Source characteristics of hypothetical subduction earthquakes in the Northwestern United States: Seismological Society of America Bulletin, v. 76, no. 3, p. 675–708.

———1987, Earthquake hazards on the Cascadia subduction zone: Science, v. 236, no. 4798, p. 162–168.

Heaton, T.H., and Kanamori, Hiroo, 1984, Seismic potential associated with subduction in the Northwestern United States: Seismological Society of America Bulletin, v. 74, no. 3, p. 933–941.

Heezen, B.C., and Ewing, Maurice, 1952, Turbidity currents and submarine slumps, and the 1929 Grand Banks earthquake: American Journal of Science, v. 250, p. 849–873.

Holdahl, S.R., Faucher, F., and Dragert, Herb, 1989, Contemporary vertical crustal motion in the Pacific Northwest, *in* Cohen, S.C., and Vanicek, P., eds., Slow deformation and transmission of stress in the Earth: American Geophysical Union Geophysical Monograph 49, p. 17–29.

Hull, A.G., 1987, Buried lowland soils from Willapa Bay, southwest Washington—Further evidence for recurrence of large earthquakes during the last 5000 years: EOS [American Geophysical Union Transactions], v. 68, no. 44, p. 1468–1469.

Moran, K., and Hurlbut, S.E., 1986, An analysis of potential slope instability due to wave loading on the Nova Scotian shelf: St. John's, Newfoundland, Canadian Conference on Marine Geotechnical Engineering, 3d, Proceedings, p. 980–999.

Nelson, A.R., Personius, S.F., and Rhea, Susan, 1989, Earthquake recurrence and Quaternary deformation in the Cascadia subduction zone, coastal Oregon, *in* Jacobson, M.L., comp., National Earthquake Hazard Reduction Program, Summaries of technical reports, volume XXVIII: U.S. Geological Survey Open-File Report 89–453, p. 481–484.

Nelson, C.H., 1968, Marine geology of Astoria deep-sea fan: Corvallis, Oregon State University, Ph.D. dissertation, 287 p.

———1976, Late Pleistocene and Holocene depositional trends, processes, and history of Astoria deep-sea fan, northeast Pacific: Marine Geology, v. 20, p. 129–173.

Nelson, C.H., Carlson, P.R., and Bacon, C.R., 1988, The Mount Mazama climactic eruption (≈6900 yr B.P.) and resulting convulsive sedimentation on the Crater Lake floor, continent, and ocean basin, *in* Clifton, H.E., ed., Sedimentologic consequences of convulsive geologic events: Geological Society of America Special Paper 229, p. 37–57.

Nishenko, S.P., and Buland, R.P., 1987, A generic recurrence interval distribution for earthquake forecasting: Seismological Society of America Bulletin, v. 77, p. 1382–1399.

Peterson, C.D., Darienzo, M.E., and Parker, Mike, 1988, Coastal neotectonic field trip guide for Netarts Bay, Oregon: Oregon Geology, v. 50, no. 9/10, p. 99–106, 117.

Pilkey, O.H., 1988, Basin plains: giant sedimentation events, *in* Clifton, H.E., ed., Sedimentologic consequences of convulsive geologic events: Geological Society of America Special Paper 229, p. 93–99.

Reilinger, R.E., and Adams, John, 1982, Geodetic evidence for active landward tilting of the Oregon and Washington coastal ranges: Geophysical Research Letters, v. 9, no. 4, p. 401–403.

Riddihough, R.P., and Hyndman, R.D., 1976, Canada's active western margin—The case for subduction: Geoscience Canada, v. 3, p. 269–278.

Rogers, G.C., 1988, An assessment of the megathrust earthquake potential of the Cascadia subduction zone: Canadian Journal of Earth Sciences, v. 25, no. 6, p. 844–852.

Sternberg, R.W., 1986, Transport and accumulation of river-derived sediment on the Washington continental shelf: Geological Society of London Journal, v. 143, p. 945–956.

Stuiver, Minze, and Reimer, P.J., 1986, A computer program for radiocarbon age calibration, *in* Stuiver, Minze, and Kra, Renee, eds., Calibration issue: Radiocarbon, v. 28, no. 2B, p. 1022–1030.

Yamaguchi, D.K., Woodhouse, C.A., and Reid, M.S., 1989, Tree-ring evidence for synchronous rapid submergence of the southwestern Washington coast 300 years B.P.: EOS [American Geophysical Union Transactions], v. 70, no. 43, p. 1332.

Tectonics and Geophysics

Preceding page. *Insert,* rescue of a motorist trapped by fallen bricks moments after the April 29, 1965, Seattle, Wash., earthquake. Photograph by Ken Harris of the Seattle Post-Intelligencer. *Background,* damage to unreinforced masonry wall and parapet in downtown Klamath Falls, Oreg., during the Sept. 20, 1993, *M* 5.9 and *M* 6.0 earthquakes (from Dewey, J.W., 1993, Damages from the 20 September earthquakes near Klamath Falls, Oregon: Earthquakes & Volcanoes, v. 24, no. 3, p. 121–128).

CENOZOIC EVOLUTION OF THE CONTINENTAL MARGIN OF OREGON AND WASHINGTON

By Parke D. Snavely, Jr.,[1] *and* Ray E. Wells[2]

ABSTRACT

The Cenozoic tectonic and depositional history of the Oregon and Washington continental margin was marked by underthrusting, transcurrent faulting, and extension during oblique convergence of the North America plate and oceanic plates to the west. Sedimentation, punctuated by episodes of volcanism, was essentially continuous in the forearc basin whose axis lay along the present inner continental shelf. The oldest rocks in the Oregon-Washington Coast Range are Paleocene and lower Eocene oceanic basalt capped in places by islands and seamounts. They most likely formed by in-place eruptions (62-56 Ma) during oblique rifting and extension of the continental margin. These basalts were erupted adjacent to the continental margin, as evidenced by locally interbedded terrestrial sediments. A thick lower Eocene siltstone and middle Eocene turbidite sequence buried the islands while the basin was subsiding. The middle Eocene turbidite strata overlap both oceanic basalt and pre-Tertiary rocks of the Klamath Mountains in southwest Oregon, establishing that suturing of the Coast Range-Olympic Mountains terrane to North America occurred at about 50 Ma. Continued high rates of moderately oblique convergence may have caused strike-slip faulting and tectonic rotations along the continental margin. The north-trending Fulmar fault on the Oregon continental shelf juxtaposes lower Eocene graywacke on the west against lower Eocene oceanic crust of the Coast Range and is interpreted as a right-lateral fault with a minimum offset of 200 km. Eruption of upper middle and upper Eocene tholeiitic and alkalic basalts suggests a transtensional tectonic environment toward the coast. Reduction of the rate of convergence between the Farallon and North America plates after 49 Ma was followed by Cascade arc volcanism (about 44 Ma) and, ultimately, the demise of the right-lateral Fulmar fault, as recorded by the onlap of uppermost Eocene strata. Deposition of Oligocene tuffaceous marine strata in the forearc signaled the beginning of voluminous Cascade arc volcanism at about 35 Ma and contemporaneous subsidence of the forearc. Although rift volcanism characterized the forearc during the late Eocene and early Oligocene, there is evidence for late Eocene underthrusting in the Olympic Mountains accretionary wedge. Major uplift of the Oregon and Washington continental margin occurred in the late middle Miocene, as indicated by a regional unconformity on the continental shelf and by strongly deformed rocks of the Miocene Astoria Formation and the Columbia River Basalt Group in the Coast Range. Offshore, Oligocene and Miocene mélange wedges are overlain by as much as 2,000 m of upper Miocene and Pliocene strata that are folded and thrust faulted. Oblique convergence continues today and has caused Quaternary strata to be episodically folded and thrust along the deformation front on the continental slope. Along the coast, marine terraces have been tilted during uplift of the central and southern Oregon Coast Range. At the strandline, Holocene marsh deposits record several episodes of rapid coastal subsidence, possibly related to earthquakes on the thrust interface with the downgoing plate. Late Cenozoic faults along the coast are adjacent to subsiding regions, and some of these faults show Quaternary displacement.

INTRODUCTION

Sedimentary and volcanic rocks in the Coast Range of Oregon and Washington, in the Olympic Mountains, and on the adjacent continental margin contain a nearly continuous record of Cenozoic sedimentation and tectonism along the oblique convergent margin between the oceanic and North America plates. Although subduction has played a major part in the evolution of the convergent margin, the geologic record indicates a complex history that includes strike-slip faulting, block rotation, extension, and magmatism, along with typical convergent-margin processes of thrusting, underplating, and development of a major accretionary wedge. In this article, we summarize the onshore and

[1]U.S. Geological Survey, MS 999, 345 Middlefield Rd., Menlo Park, CA 94025–3591.

[2]U.S. Geological Survey, MS 975, 345 Middlefield Rd., Menlo Park, CA 94025–3591.

offshore Cenozoic geologic framework of the continental margin, building on previous syntheses by Snavely (1987) and Wells and others (1984). We emphasize the geologic history, regional structure, and offshore evidence for neotectonics to set the stage for evaluation of earthquake potential along this active margin.

ACKNOWLEDGMENTS

We thank Exxon Company, U.S.A., for generously making available their seismic-reflection profile off the mouth of the Columbia River, as this profile clearly images the structure of this segment of the Oregon continental margin. Weldon W. Rau and David Bukry provided the biostratigraphic framework for the Tertiary sequence that is the basis for timing of most geologic events. John G. Vedder, Alan R. Niem, and Timothy Walsh reviewed the manuscript and offered suggestions that improved its quality. The writers are particularly grateful to Diane L. Minasian, who drafted the illustrations and critically reviewed the manuscript.

CENOZOIC GEOLOGIC HISTORY

PALEOCENE TO MIDDLE EOCENE

ORIGIN OF THE COAST RANGE OCEANIC BASEMENT

The oldest rocks of the Oregon and Washington Coast Range are tholeiitic pillow basalt and interbedded breccia and marine sedimentary rocks (fig. 64, × pattern) (Duncan, 1982; Bukry and Snavely, 1988). These oceanic basalts, capped in places by islands and seamounts, include the Siletz River Volcanics in Oregon (Snavely and others, 1968), the Crescent Formation in Washington (Arnold, 1906; Brown and others, 1960; Cady, 1975), and the Metchosin Volcanics on southern Vancouver Island, British Columbia (Clapp, 1917; Muller, 1977). Although several models have been proposed for the origin of these basalts (for example, Duncan, 1982; Wells and others, 1984), we prefer the model of rifting and volcanism along the leading edge of the continental margin of western North America during a period of rapid, highly oblique northeast motion (with respect to the North America plate) of the Kula and Farallon plates that was initiated in the Paleocene (fig. 65) (Wells and others, 1984; Snavely, 1987).

The western boundary of the Coast Range oceanic basement is a north-south-trending fault on the Oregon continental shelf that has been delineated by aeromagnetic data, seismic reflection, and deep test wells (table 17). This fault was named the Fulmar fault by Snavely, Wagner, and Lander (1980) and is interpreted to have at least 200 km of dextral-slip motion, based on the juxtaposition of lower Eocene turbidite sandstone west of the Coast Range oceanic basement.

The Fulmar fault is thought to be the western boundary of the oblique marginal rift basin that is floored by the Paleocene to lower Eocene tholeiitic pillow basalt. Along with other dextral faults farther to the east, it formed a transtensional zone of right-lateral shear along the Eocene continental margin of Oregon and western Washington. The major movement along the Fulmar fault most likely ended by late Eocene time because on the Oregon shelf, this fault is overlapped by strata of latest Eocene age (about 37 Ma) (Snavely, Wagner, and Lander, 1980). However, minor movement has occurred subsequently, as overlying strata as young as Pleistocene show small vertical offsets on seismic-reflection profiles.

BASIN FILLING AND DEFORMATION

Within the rift basin, a 3,000-m-thick sequence of siltstone, turbidite sandstone, and conglomerate of early Eocene age was deposited adjacent to the volcanic high areas. The configuration of the basin was likely inherited from the relief on the Siletz River and Crescent volcanic piles because nearshore deposits as old as early Eocene unconformably onlap these volcanic highs (Bukry and Snavely, 1988; Snavely, 1991). Convergence between the Kula-Farallon and North America plates in late early Eocene time (about 52 Ma) deformed the island chain and overlying marine sedimentary rocks against the North America buttress. In the southern part of the Oregon Coast Range, a set of southeast-dipping imbricate thrust sheets and fault-propagation folds deformed the Paleocene and lower Eocene oceanic basalts and overlying lower Eocene sedimentary rocks (Baldwin, 1974; Heller and Ryberg, 1983; Molenaar, 1985; Wells and Heller, 1988; Niem and Niem, 1990). In the central part of the Coast Range, the Siletz River Volcanics were faulted and folded prior to rapid downwarping and the deposition of the overlying mildly deformed Tyee Formation of early middle Eocene age (Snavely and others, 1976a; Bukry and Snavely, 1988).

This compressional event also deformed and uplifted continental terranes adjacent to the rift basin and accelerated erosion of pre-Tertiary rocks in the Klamath Mountains to the south and on Vancouver Island to the north. Debris flows and conglomerate derived from the Klamath Mountains occur along the southern margin of the Coast Range basin. In the southern Oregon part of the forearc basin, 2,000 m of

Figure 64 (facing page). Generalized onshore geologic map of western Oregon, western Washington, and southern Vancouver Island, British Columbia, with inferred locations of major faults on the adjacent continental shelf. Offshore faults concealed by younger strata are indicated by short dashes. Outcrops of middle Miocene basalt are not shown in the Willamette Valley; upper middle Eocene volcanic rocks are not shown in the eastern part of Puget Sound. Modified from Snavely (1987).

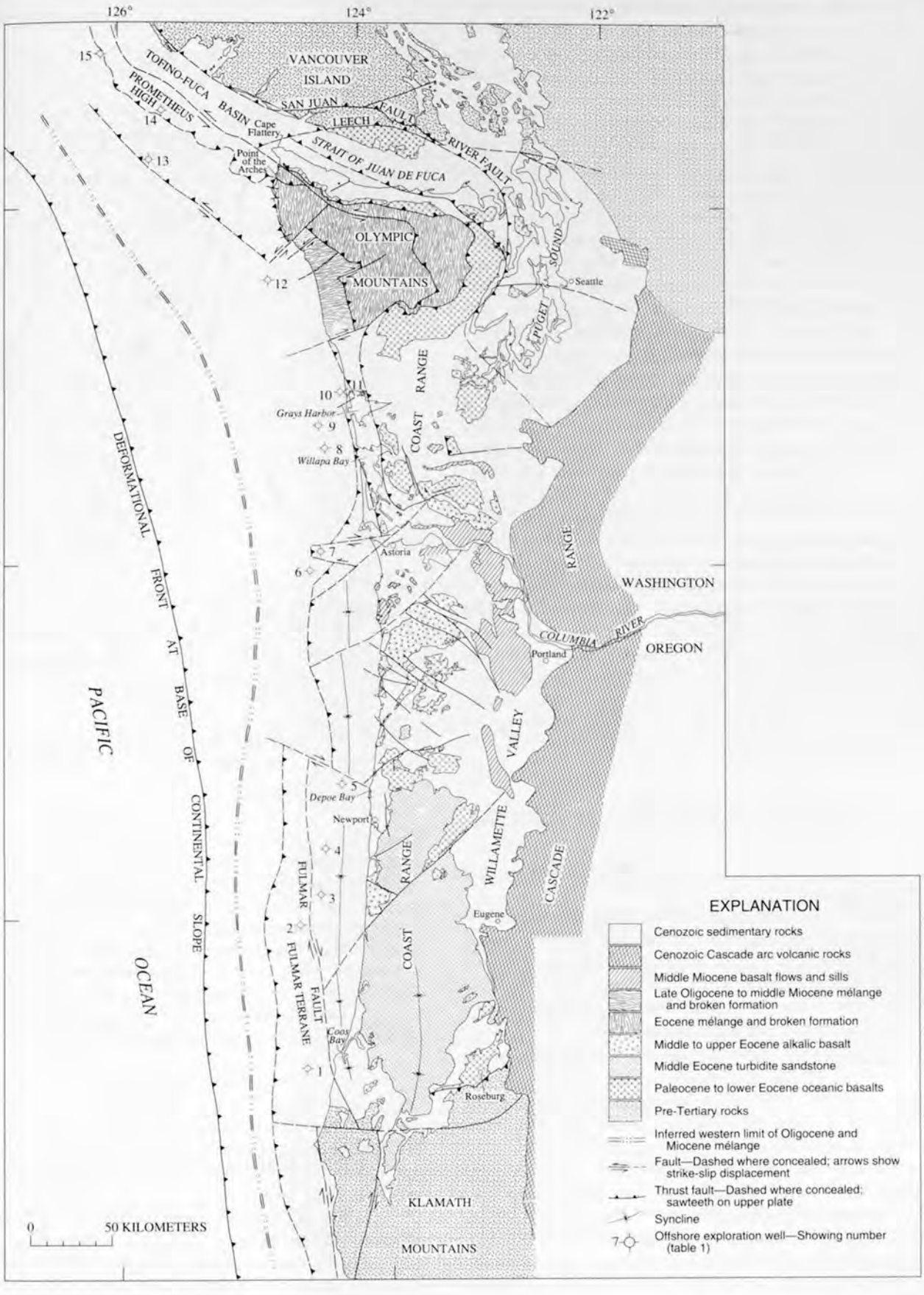
126°
124°
122°
48°
46°
44°
42°
VANCOUVER ISLAND
TOFINO-FUCA BASIN
PROMETHEUS HIGH
SAN JUAN FAULT
LEECH RIVER FAULT
Cape Flattery
Point of the Arches
STRAIT OF JUAN DE FUCA
OLYMPIC MOUNTAINS
PUGET SOUND
Seattle
COAST RANGE
Grays Harbor
Willapa Bay
Astoria
CASCADE RANGE
WASHINGTON
COLUMBIA RIVER
Portland
OREGON
WILLAMETTE VALLEY
DEFORMATIONAL FRONT AT BASE OF CONTINENTAL SLOPE
PACIFIC OCEAN
Depoe Bay
Newport
FULMAR FAULT
FULMAR TERRANE
Coos Bay
Eugene
Roseburg
KLAMATH MOUNTAINS
0 50 KILOMETERS
EXPLANATION
Cenozoic sedimentary rocks
Cenozoic Cascade arc volcanic rocks
Middle Miocene basalt flows and sills
Late Oligocene to middle Miocene mélange and broken formation
Eocene mélange and broken formation
Middle to upper Eocene alkalic basalt
Middle Eocene turbidite sandstone
Paleocene to lower Eocene oceanic basalts
Pre-Tertiary rocks
Inferred western limit of Oligocene and Miocene mélange
Fault—Dashed where concealed; arrows show strike-slip displacement
Thrust fault—Dashed where concealed; sawteeth on upper plate
Syncline
Offshore exploration well—Showing number (table 1)

arkosic, lithic, and feldspathic turbidite sandstone and siltstone of the lower middle Eocene Tyee Formation (Snavely and others, 1964; Lovell, 1969; Baldwin, 1974; Chan and Dott, 1983) was derived in part from an uplifted Klamath terrane and from the Idaho batholith and adjacent terranes (Heller and others, 1985), buried preexisting volcanic highs, and deformed lower Eocene sedimentary rocks. This sedimentary sequence laps across the tectonic boundary between the Klamath pre-Tertiary rocks and the Eocene oceanic basalts to the north and indicates that the Coast Range oceanic basement was accreted to the North America plate in early middle Eocene time (about 50 Ma). Thick-bedded lithic quartzose sandstone and conglomerate of early middle(?) Eocene age in the Olympic Mountains core rocks (Tabor and Cady, 1978a; Snavely and others, 1986) represent material eroded from an uplifted pre-Tertiary terrane of Vancouver Island and the northern Cascade Range. In the Puget Sound area, streams transported large quantities of arkosic and lithic sand into the northern part of the basin across broad low-lying flood plains. The coal-bearing continental fluvial deposits, represented by the lower part of the Puget Group (Wolfe and others, 1961), the Chuckanut Formation (McLellan, 1927; Johnson, 1984), and the Swauk Formation (Russell, 1900; Tabor and others, 1984), formed in lowland areas. Part of this coarse clastic material may have been transported westward through submarine channels into the deeper parts of the basin to form turbidite fans. Some highly deformed lower and middle Eocene thick-bedded carbonaceous, lithic, and arkosic sandstone units within the Olympic Mountains core rocks (Tabor and others, 1972; Tabor and Cady, 1978b) and in the Cape Flattery, Wash., coastal area (fig. 64) (Snavely and others, 1986) may be marine counterparts of these continental deposits.

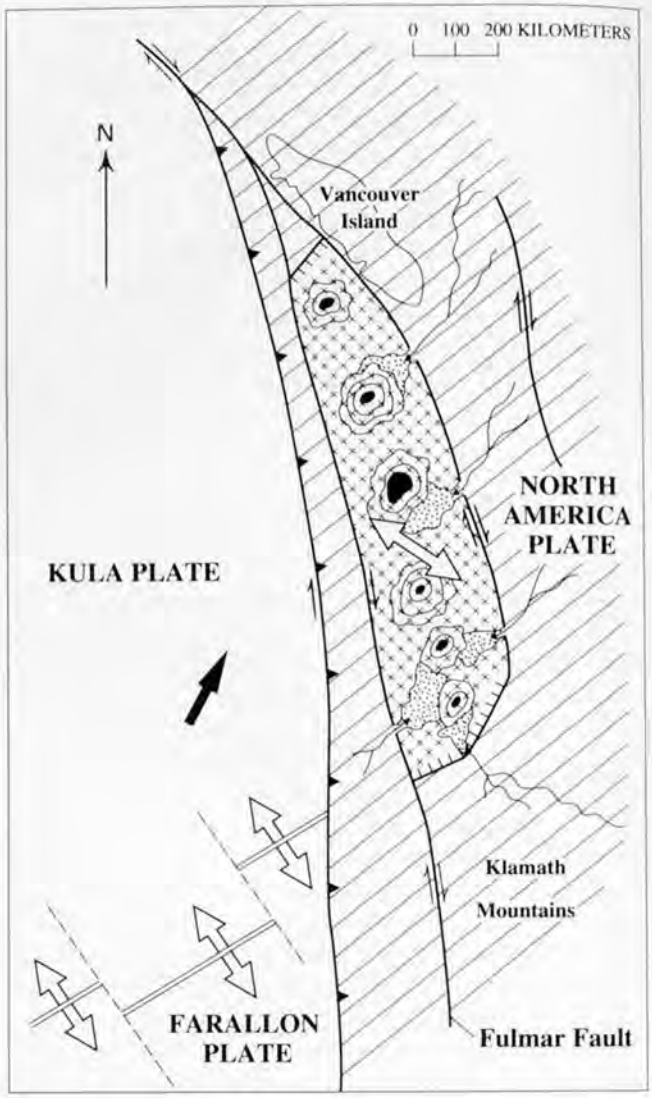

Figure 65. Diagram showing inferred continental-margin-rifting model for the origin of the Paleocene to lower middle Eocene oceanic basalt (× pattern), oceanic islands (circular areas with black subaerial caps), and continental crust (diagonal pattern) in western Oregon and Washington. Large black arrow denotes direction of movement of the Kula plate relative to the North America plate (Engebretson and others, 1985); large open arrows show local spreading direction. Heavy lines are faults, with sawteeth on upper plate and ticks on downthrown block; arrows show lateral movement. Rivers and marine sediments (stipple pattern) are shown schematically.

LATE MIDDLE EOCENE TO LATE EOCENE

CONTINENTAL-MARGIN MAGMATISM

Tholeiitic volcanism continued along the continental margin between 44 and 37 Ma, although the major volcanic centers became restricted to southwest Washington and the northern and central Oregon Coast Range (MacLeod and Snavely, 1973). The lavas were erupted from regional dike swarms that trended northeast before rotation. This orientation suggests a transtensional relationship to the right-lateral Fulmar fault (Wells and others, 1984). The basalts are chiefly subaerial; however, pillow lava and breccia in the lower parts of these units intertongue laterally with deep-water siltstone of the upper middle Eocene Yamhill and the upper Eocene Nestucca Formations (Snavely and others, 1990b). These basalt flows and breccia include the Grays River volcanic rocks of southwest Washington (Livingston, 1966; Wells, 1981; Walsh and others, 1987) and the Tillamook Volcanics in northwest Oregon (Warren and others, 1945; Snavely and others, 1969; Magill and others, 1981; Wells and others, 1983; Niem and Niem, 1985). They were followed closely by the Yachats Basalt (Snavely and MacLeod, 1974) and the basalts of Cascade Head (Snavely and Vokes, 1949; Snavely and others, 1990a) in central coastal Oregon. The volcanic rocks are commonly porphyritic and range widely in composition, from tholeiitic to alkalic basalt, basaltic andesite, and dacite. This compositional range suggests that the basaltic magma that produced these volcanic rocks was differentiated in high-level magma chambers before extrusion.

Table 17. Locations, depths, and oldest rock penetrated in exploratory wells drilled on the Oregon and Washington continental shelf and selected wells drilled on the shelf off southern Vancouver Island, British Columbia.

Well no.[1]	Company and name of well	Year drilled	Location		Total depth (meters)	Oldest rock penetrated
			Latitude (North)	Longitude (West)		
1	Pan American Oil Co. No. 1, P–0112	1967	43°04.8'	124°35.6'	1,873	Lower Eocene arkosic wacke (Snavely and others, 1982)
2	Union Oil Co. Fulmar P–0130	1966	44°03.6'	124°38.8'	3,744	Lower Eocene arkosic wacke (Snavely and others, 1982)
3	Shell Oil Co. P–087 1ET–2ET	1965	44°13.3'	124°28.2'	2,546	Lower(?) Eocene basalt (Snavely and others, 1982)
4	Union Oil Co. Grebe P–093	1966	44°29.8'	124°24.9'	3,051	Lower(?) Eocene basalt (Snavely and others, 1982)
5	Standard Oil Co. Nautilus No. 1 PO–0103	1965	44°51.5'	124°16.7'	3,849	Middle to upper Eocene basalt(?) (Snavely and others, 1982)
6	Shell Oil Co. P–072 1ET	1966	46°02.8'	124°29.9'	2,505	Upper Oligocene to middle Miocene mélange(?)
7	Shell Oil Co. P–075 1ET	1966	46°09.1'	124°24.5'	3,097	Middle(?) Eocene diabase sill
8	Shell and Pan American Oil Co. P–0150	1966	46°43.5'	124°21.3'	4,017	Upper Oligocene to lower Miocene mélange and broken formation
9	Shell Oil Co. P–0155 1ET	1967	46°51.2'	124°24.5'	3,402	Upper Oligocene mélange (Snavely and Wagner, 1982)
10	Union Oil Co. Tidelands State No. 2	1962	47°03.22'	124°12.81'	1,546	Lower to middle Miocene mélange and broken formation
11	Sunshine Mining Co. Medina No. 1	1962	47°03.03'	124°10.02'	1,262	Lower Miocene mélange (onshore well produced 12,000 barrels of oil)
12	Pan American Oil Co. P–0141	1967	47°39.7'	124°47.5'	3,160	Middle to upper Eocene mélange (Snavely and Kvenvolden, 1989)
13	Shell Canada Ltd. Anglo Cygnet J–100	1969	48°19.67'	125°43.96'	2,460	Lower to middle Miocene (Snavely and Wagner, 1981; Shouldice, 1971)
14	Shell Canada Ltd. Anglo Prometheus H–68	1967	48°48.9'	125°39.6'	2,335	Lower(?) Eocene part of Crescent Formation (Shouldice, 1971)
15	Shell Canada Ltd. Anglo Zeus I–65	1968	48°54.6'	126°09.15'	3,042	Lower(?) Eocene arkosic wacke (Shouldice, 1971)

[1] See figure 64 for mapped locations of wells.

BASIN FORMATION AND SEDIMENTATION

Although differential uplift occurred in the areas of subaerial volcanism such as the Heceta Head-Cape Perpetua area on the central Oregon coast (Snavely and MacLeod, 1974), regional downwarping occurred in most places in the forearc basin. Bathyal thin-bedded siltstone and sandstone were unconformably deposited on lower Eocene oceanic basalt and sedimentary rocks. The geometry of post-middle Eocene deposits was controlled in part by the distribution of thick upper Eocene volcanic sequences. For example, a west-trending ridge of the Yachats Basalt separates the Coos Bay basin from the Newport embayment to the north. Other coastal basins appear to be fault controlled. The Tillamook

embayment in northwest Oregon is bordered by a major northwest-trending en-echelon fault zone that traverses the entire Coast Range (Wells and others, 1983).

In the northern part of the Olympic Peninsula, the middle and upper Eocene siltstones of the Aldwell Formation (Brown and others, 1960) overlap older sedimentary rock to rest unconformably upon basalt of the lower Eocene Crescent Formation. The basal contact is marked in places by beds 10–30 m thick of cobble and boulder conglomerate derived from the underlying Crescent Formation. In the north-central part of the Oregon Coast Range, bathyal siltstone of the upper middle Eocene Yamhill Formation (Baldwin and others, 1955; Bukry and Snavely, 1988) unconformably overlaps folded strata of the Tyee Formation to rest upon basalt of the Siletz River Volcanics (Wells and others, 1983; Snavely, 1987). In the northern part of the Oregon Coast Range, the Yamhill Formation intertongues with pillow lavas and breccia of the middle Eocene Tillamook Volcanics (Wells and others, 1983; Snavely and others, 1990b).

A water-laid dacitic tuff bed as much as 30 m thick occurs at or near the base of the Yamhill Formation in the central part of the Oregon Coast Range. This tuff unit is locally exposed from Florence northward to Dolph, a distance of more than 150 km. The source of ash that forms this tuff bed was most likely vents along an ancestral Cascade arc. If this interpretation is correct, volcanism in the Oregon Cascades started about 44 Ma.

During the middle and late Eocene, streams transported large quantities of arkosic sand to a broad, low-lying coastal plain that bordered the eastern and southern parts of the forearc basin. Coal-bearing continental beds greater than 3,500 m thick are represented by the Puget Group (Wolfe and others, 1961) and the Cowlitz and Skookumchuck Formations (Snavely and others, 1958) in Washington and the Coaledo Formation (Allen and Baldwin, 1944; Dott, 1966) in southwest Oregon. Some of this coarse clastic material undoubtedly was transported along channels into shelf basins and formed submarine fans and turbidite deposits. These continental beds interfinger with both Cascade-arc-derived lavas and with coastal tholeiitic lavas, thus tying the middle Eocene tholeiites to the continental shelf.

FOREARC DEFORMATION

In the latest Eocene (about 37 Ma), the forearc basin was deformed across a broad front by oblique convergence between the North America and Farallon plates. Regional uplift that accompanied this event segmented and shoaled the forearc region to produce a number of shelf basins that deepened westward. Erosion of uplifted middle and upper Eocene subaerial volcanic piles, such as the Tillamook Volcanics and the Yachats Basalt, produced thick deposits of fossiliferous basaltic sandstone and conglomerate that fringed the basalt highlands (Bukry and Snavely, 1988; Snavely and others, 1990a, b). In the northernmost part of the forearc basin, two contrasting styles of deformation seem to support oblique subduction as the driving force. The first is north-south compression, as documented by major thrust faulting in the late middle Eocene along the Crescent and other major faults (fig. 66) (MacLeod and others, 1977; Snavely and others, 1986). This transpression resulted from northward movement of the Olympic Mountains-Coast Range Paleogene terrane against the buttress of pre-Tertiary rocks of Vancouver Island. Resulting erosion of uplifted pre-Tertiary terranes on southern Vancouver Island supplied coarse clastic debris to the northern part of the forearc basin to form the conglomerate-rich upper Eocene Lyre Formation (Brown and others, 1956; Snavely and others, 1986, 1989) along the northern Olympic Peninsula. The second deformation style, which occurred at about the same time, formed mélange and broken formation of late Eocene age that were underthrust along the west side of the Olympic Peninsula (Snavely and Kvenvolden, 1989), implying continued subduction during north-south compression of the Coast Range.

Seismic-reflection profiles and subsurface data from deep test wells on the Oregon continental shelf (Snavely, Wagner, and Lander, 1980; Snavely and others, 1982) also show a regional unconformity at the base of upper Eocene lower Refugian siltstone. These strata unconformably overlie folded and faulted rocks as old as early Eocene and overlap the Fulmar fault (Snavely, Wagner, and Lander, 1980; Snavely, 1984). Also, in several areas in the northwesternmost part of the Olympic Peninsula, strata of early Refugian age onlap mélange and broken formation of middle and late Eocene age (Snavely and others, 1986).

OLIGOCENE TO MIDDLE MIOCENE

BASIN DEVELOPMENT

Rapid subsidence occurred in the forearc basin during Oligocene and early Miocene time, and more than 2,500 m of bathyal tuffaceous siltstone and arkosic sandstone were deposited in axial parts of the basin. On the Oregon continental margin, these strata are represented by tuffaceous siltstone of the Alsea Formation of Oligocene age (Snavely and others, 1975) and the Nye Mudstone of early Miocene (Saucesian Stage) age (Vokes and Snavely, 1948; Snavely and others, 1964). In the late Oligocene, high-energy deltaic deposits of pumiceous, coarse-grained sandstone such as the Yaquina Formation (Snavely and Wagner, 1963; Goodwin, 1973) were deposited in places along the eastern margin of the basin. In the deep marginal Tofino-Fuca basin along the north side of the Olympic Peninsula, more than 2,500 m of turbidite sandstone and siltstone of the Makah and Pysht Formations were deposited from the Oligocene to the early Miocene (Snavely and others, 1978; Snavely, Niem, and others, 1980; Snavely and others, 1986). The Makah Formation

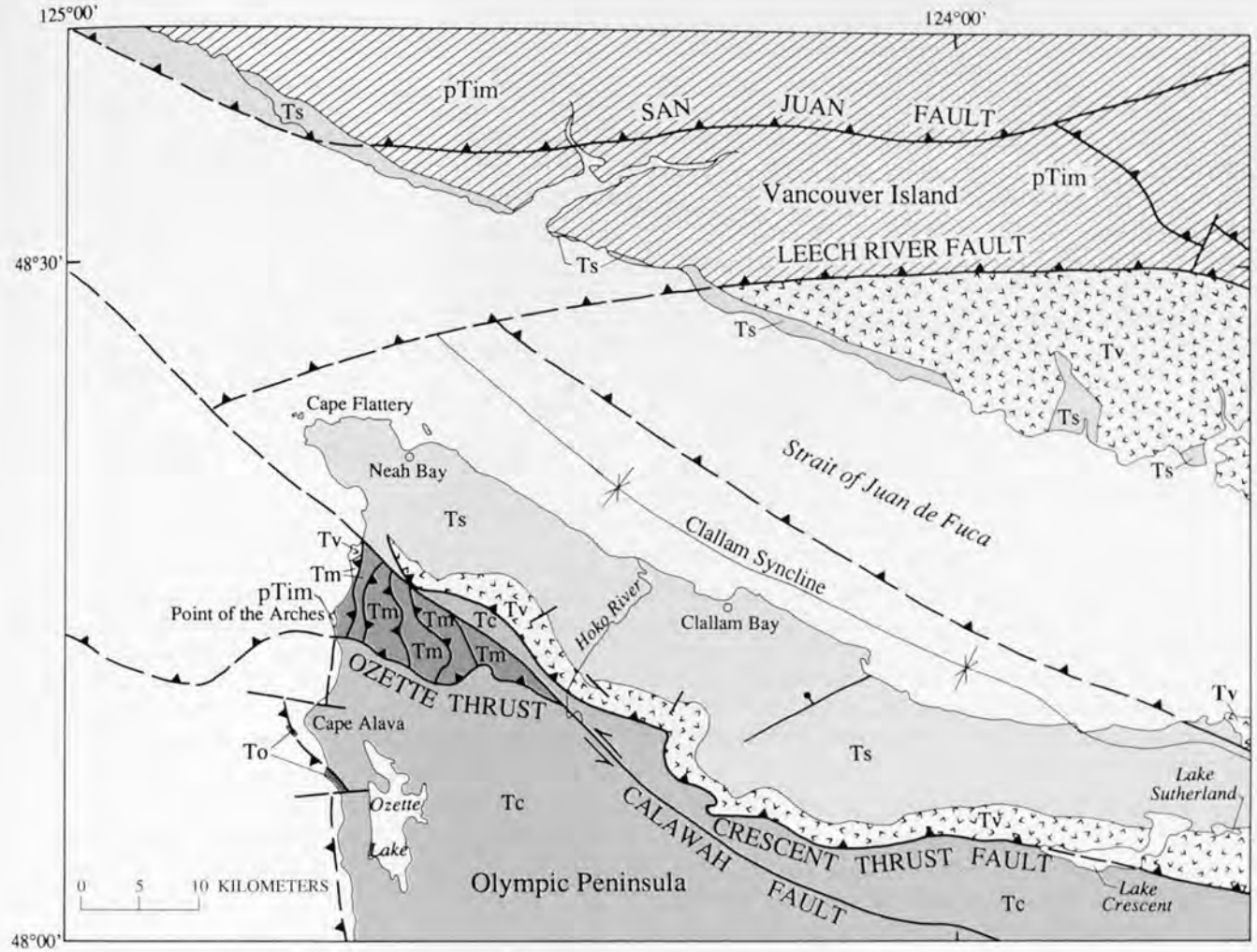

Figure 66. Generalized geologic map of the region adjacent to Cape Flattery, Wash., showing locations of major onshore faults and their offshore extensions. Ts, Tertiary sedimentary rocks, undivided; To, upper Oligocene sandstone and conglomerate; Tm, overthrust pre-Tertiary to upper Eocene broken formation above Ozette thrust; Tc, highly deformed Eocene sandstone and siltstone and other rocks of the Olympic core; Tv, Eocene pillow basalt, breccia, and associated dikes and sills of the Metchosin Volcanics (Clapp, 1917) on Vancouver Island and the Crescent Formation in Washington; pTim, pre-Tertiary igneous and metamorphic rocks, undivided, on Vancouver Island and Point of the Arches, Wash. Faults are dashed where concealed; arrows show strike-slip displacement; sawteeth are on upper plate of thrust fault; bar and ball are on downthrown side of fault. Modified from MacLeod and others (1977) and unpublished maps by P.D. Snavely, Jr.

includes a major submarine landslide deposit (the Jansen Creek Member) that is composed of sediments derived from southern Vancouver Island (Niem and others, 1989). This basin shoaled in the early Miocene, and nearshore coal, sandstone, and conglomerate of the Clallam Formation were deposited (Gower, 1960; Addicott, 1976).

CONTINENTAL-MARGIN MAGMATISM

Volcanic activity in the Cascade arc contributed large quantities of ash and pumiceous tuff breccia to the forearc basin. Cascade-derived Oligocene mudflow conglomerate and thick (10 m) pumice beds occur as far west as the present coastline (Snavely and others, 1975). Close to the late Eocene to middle Oligocene strandline, which lay near the present foothills of the Oregon Cascade Range, andesitic and dacitic tuff breccia and volcaniclastic beds are complexly intercalated throughout much of the marine sequence.

In the central Oregon Coast Range, small volumes of highly evolved magmas were erupted and intruded into the marine strata. Camptonites, nepheline syenites, and ferrogabbros were emplaced between 34 and 30 Ma, roughly contemporaneous with the end of major late Eocene dextral slip faulting along the Fulmar fault and related faults to the east. This magmatism represents the final episode of rift-related magmatism in the Coast Range.

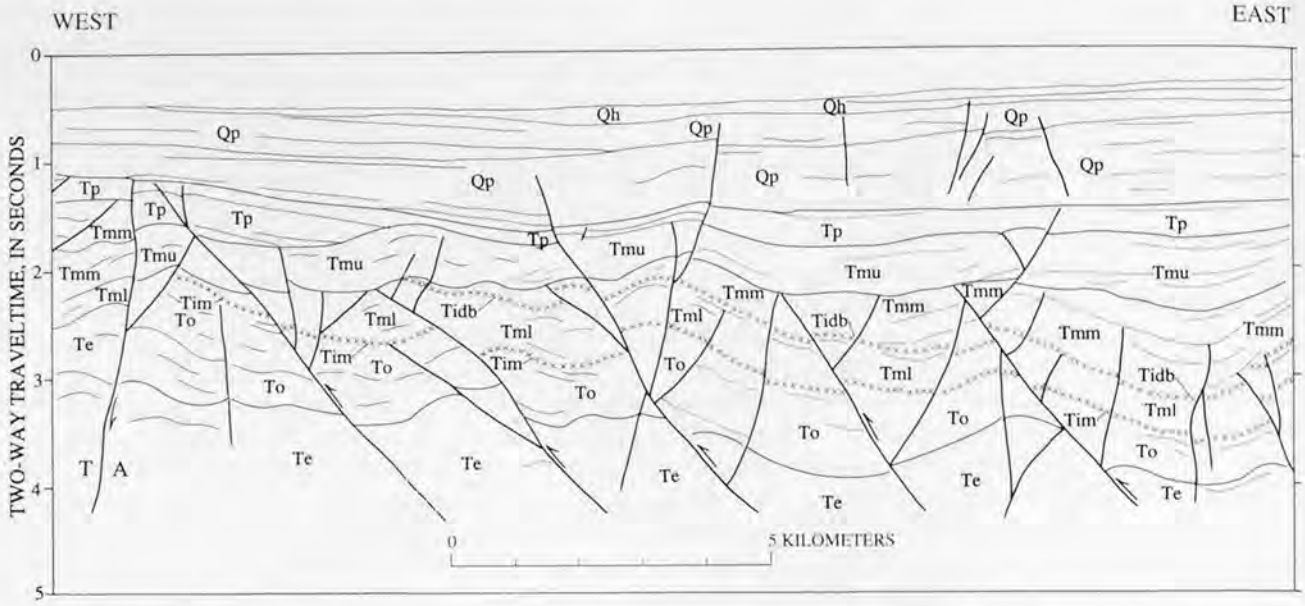

Figure 67. Geologic interpretation of a 24-channel seismic-reflection profile (USGS line WO77–11) collected off the central Oregon coast near lat 45°N. The family of east-dipping thrust faults form fault-propagation folds that are considered to be normal faults reactivated during late middle Miocene transpression. Qh, Holocene units; Qp, Pleistocene units; Tp, Pliocene units; Tmu, upper Miocene units; Tmm, middle Miocene units; Tml, lower Miocene units; To, Oligocene units; Te, late Eocene units; Tidb, basalt flow; Tim, basalt sill. Heavy lines are faults; arrows show direction of movement on thrust faults; on vertical strike-slip faults, T denotes movement toward viewer and A is movement away from viewer. Light lines are form lines showing structure in the sedimentary sequence. Vertical exaggeration is approximately 2:1.

DEFORMATION

Onshore deformation during the Oligocene and early Miocene occurred throughout western Oregon and Washington and was probably most intense in the Olympic Mountains. Potassium-argon dating of low-grade metamorphic rocks from the Olympic core rocks by Tabor (1972) suggests regional uplift at about 29 Ma. A mudflow unit of late Oligocene age that contains olistostromal blocks of basalt and graywacke derived from the Olympic core rocks provides evidence of this episode of uplift. The unit can be traced intermittently along the west side of the Olympic Peninsula from near Taholah northward to the Point of the Arches, a distance of more than 100 km (P.D. Snavely, Jr., unpub. mapping, 1969). However, in the Tofino basin along the north side of the peninsula, deposition appears to have been continuous during the late Oligocene and early Miocene, with lenticular channel-fill deposits that contain conglomerate clasts derived from Vancouver Island (Snavely, Niem, and others, 1980).

Along the central Oregon coast, two tholeiitic basalt units are interbedded with middle Miocene sandstone and siltstone. The oldest—the Depoe Bay Basalt—is petrochemically identical to the Grande Ronde Basalt, and the younger Cape Foulweather Basalt is petrochemically identical to the Frenchman Springs Member of the Wanapum Basalt of the Columbia River Basalt Group (Snavely and others, 1973). The Depoe Bay Basalt extends more than 16 km seaward and was penetrated in several of the test wells at depths of as much as 2,500 m (Snavely, 1984). The Cape Foulweather Basalt, however, is restricted to the inner shelf. Sills and flows of the Depoe Bay Basalt are widespread in the northern Oregon Coast Range and on the continental shelf (Snavely and Wells, 1984; Snavely and McClellan, 1987; Niem and others, 1990). The stratigraphic and petrologic similarity between the coastal basalts and correlative units on the Columbia Plateau led some workers (Beeson and others, 1979) to suggest that the coastal basalts are invasive tongues of the Columbia River Basalt Group that erupted on the plateau. This theory may explain most of the coastal Miocene basalt outcrops, although it is hard to explain intrusions of the Depoe Bay Basalt into volcanic rocks as old as early Eocene in the central coastal area of Oregon (Snavely and others, 1990b).

Regional uplift in the forearc basin in the early Miocene (about 20 Ma) restricted marine deposition to the west flank of the Oregon Coast Range and the adjacent continental shelf and to the Coos Bay, Newport, Astoria, Grays Harbor, and Tofino-Fuca structural embayments (fig. 64). Nearshore deltaic and strandline sandstone and siltstone deposits of the lower and middle Miocene Astoria Formation (Cooper, 1981) grade westward into predominantly bathyal siltstone in the deep marginal basin off Oregon (Snavely and others, 1982). Along the central and northern Oregon coast, the

Astoria Formation rests on strata ranging in age from late Eocene to early Miocene. In the deep marginal basin on the Oregon continental shelf, seismic-reflection profiles and drill-hole data indicate that sedimentation was virtually continuous, and siltstone strata correlative with the Nye Mudstone and Astoria Formation form a single rock-stratigraphic unit (Snavely, Wagner, and Lander, 1980).

On the Olympic Peninsula, lower and middle Miocene thick-bedded sandstone and thin-bedded siltstone and conglomerate of both shelf and bathyal depositional environments lap onto Eocene mélange and broken formation (Rau, 1975, 1979; Snavely and Kvenvolden, 1989). These deposits were intensely folded and faulted during plate convergence in the late middle Miocene.

LATE MIDDLE MIOCENE TO PLIOCENE

Regional deformation occurred in western Oregon and Washington and on the adjacent continental shelf in the late middle Miocene, between 15 and 10 Ma. Uplift of the Coast Range and Olympic Mountains formed highland areas that were rapidly eroded and supplied large amounts of clastic debris to elongate basins on the continental shelf. On the Oregon inner shelf, strata as young as middle Miocene were folded and uplifted, truncated by erosion, and subsequently downwarped and overlapped unconformably by upper Miocene strata (Snavely, Wagner, and Lander, 1980). Uplift was greatest on the Olympic Peninsula, perhaps partly owing to isostatic uplift of the thick prism of mélange and broken formation that was subducted during the late middle Miocene and partly owing to northward motion of the Coast Range. Alternatively, Brandon and Calderwood (1990) suggested that uplift of the core rocks may be a response to development of a flexure in the subducting slab beneath the Olympic Mountains.

Normal faults on the Oregon shelf were reactivated as thrust faults during late middle Miocene transpression and formed a family of landward-dipping fault-propagation folds (fig. 67). Although most folds were truncated by the late Miocene unconformity, movement on some faults gently folded strata as young as Pleistocene.

BASIN DEVELOPMENT

In the late Miocene and Pliocene, episodic downwarping of a deep marginal basin off Oregon was virtually continuous, and more than 2,000 m of sand and silt were deposited. Upper Miocene and Pliocene deposits thin against the eastern border of the marginal basin and against older midshelf structural highs (Snavely, Wagner, and Lander, 1980; Clarke and others, 1981). Shelf basins formed landward of folded and thrust-faulted late Oligocene to late middle Miocene mélange welts. On the central and southern Washington shelf, as much as 2,000 m of upper Miocene and Pliocene sediment accumulated on a thick accretionary wedge of mélange and broken formation of late Oligocene(?) to late middle Miocene age (Rau, 1975, 1979; Snavely and Wagner, 1982). The Miocene and Pliocene strata thin against growing anticlines or diapirs, the cores of which consist of upper Oligocene to middle Miocene mélange and broken formation. Adjacent to these diapiric structures, numerous unconformities, growth faults, and gravity slides occur within younger strata, all of which likely reflect episodic uplift (fig. 68) (also see Snavely and Wagner, 1982).

Off northwest Washington and southern Vancouver Island, upper Miocene strata rest unconformably on older Tertiary rocks (Shouldice, 1971; Snavely and Wagner, 1980). Although most strata of this age are restricted to the shelf, upper Miocene shallow-water sandstone and siltstone occur in a small isolated basin along the west side of the Olympic Peninsula in the lower Bogachiel River Valley (Rau, 1979) and in fault-bounded blocks along the coast north of Taholah (Rau, 1970, 1975). Upper Miocene strata also crop out on the southern Oregon coast near Coos Bay (Addicott, 1976; Armentrout, 1980).

In a filled trench along the base of the slope (fig. 69), about 3,500 m of strata occur above an upper Miocene oceanic crust (Kulm and Fowler, 1974; Snavely, Wagner, and Lander, 1980; Carlson and Nelson, 1987; Snavely, 1987). From analysis of the seismic velocities of the sediments, it is estimated that as much as half of this fill is of late Miocene and Pliocene age.

PLEISTOCENE TO HOLOCENE

Pleistocene and Holocene sediments extend across most of the continental shelf of Oregon and Washington, and Neogene strata are exposed on the sea floor only on large banks such as Stonewall, Heceta, and Nehalem (Kulm and Fowler, 1974; Snavely and Wagner, 1980; Snavely, Wagner, and Lander, 1980; Clarke and others, 1981; Carlson and Nelson, 1987; Snavely and McClellan, 1987). These Quaternary deposits of fine sand and silt are thickest (about 500 m) on the inner shelf and in basins between compressional folds on the outer shelf and lower slope. Several unconformities occur within this sequence, indicating episodic downwarping of the basins as well as uplift of diapiric structures during deposition (fig. 68). On the abyssal plain, more than 1,800 m of strata are most likely of Pleistocene and Holocene age (Kulm and Fowler, 1974; Snavely, Wagner, and Lander, 1980; Carlson and Nelson, 1987).

Pleistocene uplift of the Olympic Mountains and the Oregon and Washington Coast Ranges shed coarse clastic debris that overwhelmed hemipelagic sediments along the eastern flanks of the marginal shelf basin. Uplifted Pleistocene channel-fill deposits along the coast are as much as 60 m thick and contain beds of peat (Snavely, 1948). Glaciofluvial sand and gravel from alpine glaciers in the Olympic Mountains and from the Fraser lobe (Easterbrook, 1969) of the continental ice sheet were deposited along the seaward margin of the Olympic Peninsula and extend onto the inner shelf.

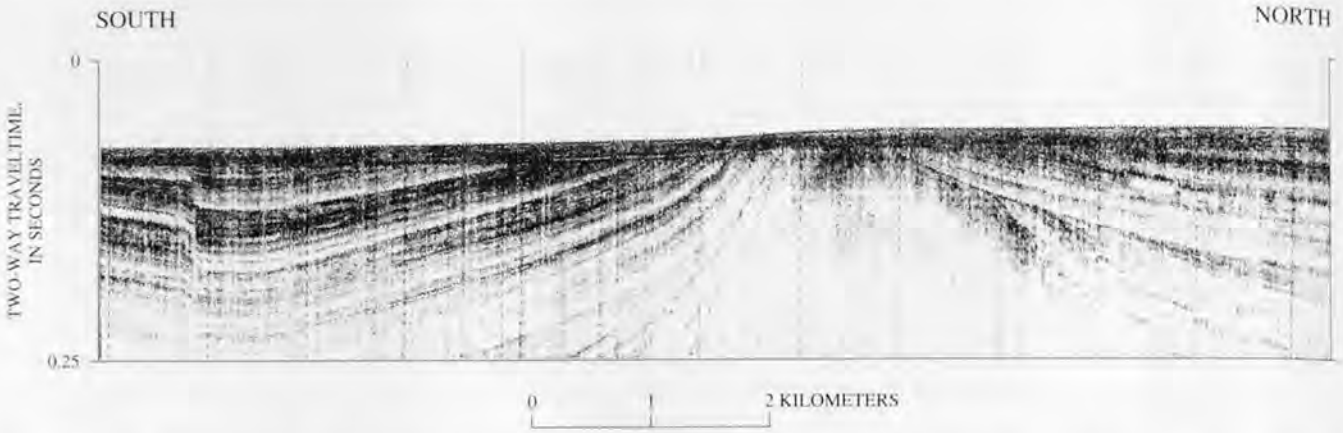

Figure 68. High-resolution single-channel seismic-reflection profile (USGS line WO80–18) across an asymmetric diapiric structure off the mouth of the Columbia River, Oregon and Washington. Strata of Pleistocene age lap onto and thin against this growing structure. The marked unconformity on the north side of the diapiric structure reflects episodic uplift of the core, which appears to be bounded by a growth fault on its south side. Note the fault near the south side of the profile that offsets uppermost Pleistocene strata but not sea-floor sediments. Vertical exaggeration is approximately 12:1. From Snavely (1987).

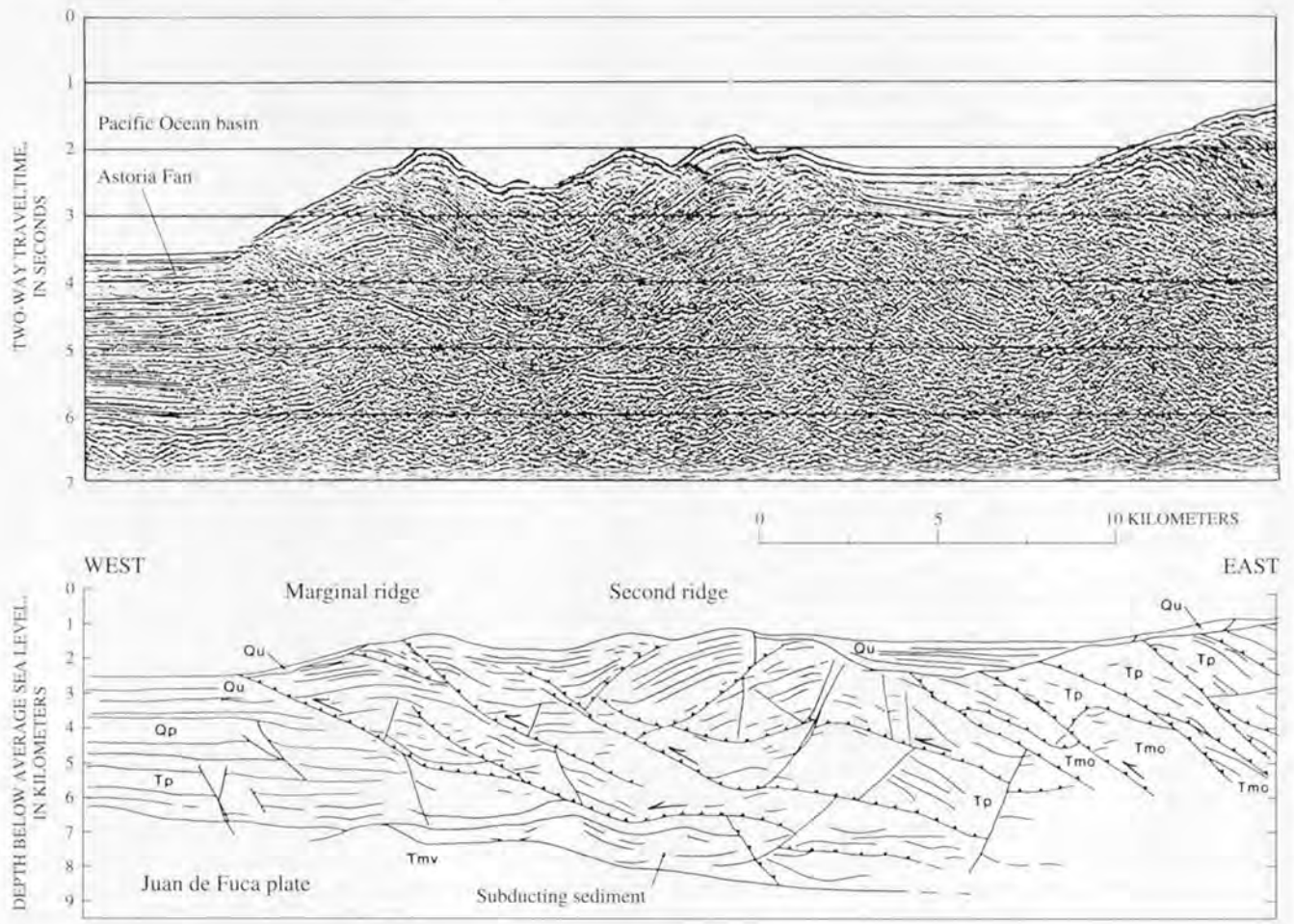

Figure 69. Geologic interpretation of a migrated 24-channel seismic-reflection profile (USGS line WO76–5) across the lower continental slope of central coastal Oregon showing filled-trench deposits and a deformation front consisting of a family of fault-propagation folds. Qu, Holocene units; Qp, Pleistocene units;, Tp, Pliocene units; Tmv, upper Miocene oceanic crust; Tmo, Oligocene to middle Miocene mélange and broken formation. In the lower panel, thrust faults are indicated with sawteeth on the upper plate; arrows show direction of relative movement. Vertical exaggeration is 2.4:1 in the upper panel. Lower panel from Snavely and others (1987).

REGIONAL STRUCTURE

The convergent margin of Oregon and Washington consists of three major tectonic elements (fig. 64): (1) the Coast Range terrane, an oceanic basalt-floored terrane that comprises most of the onshore region between Vancouver Island and the Klamath Mountains and extends westward beneath the inner continental shelf; (2) the Fulmar terrane, a fault sliver on the outer continental shelf, possibly of continental derivation, that is emplaced seaward of the oceanic terrane; and (3) the accretionary assemblage, an imbricate structural complex of offscraped and underplated sedimentary rocks that makes up the continental slope and outer shelf. The structure and arrangement of these terranes reflects a long history of oblique convergence during which margin-parallel strike slip, oblique extension, and continental-margin compression have all been a part. The importance of dextral-slip faulting along the Pacific Northwest convergent margin has only recently been realized with the discovery of offshore faults like the Fulmar fault (Snavely, Wagner, and Lander, 1980; Snavely, 1987) and abundant paleomagnetic evidence for clockwise rotation of coastal regions (see Wells and Heller, 1988; and Wells, 1989, for summary).

COAST RANGE TERRANE

The structure of the Coast Range terrane is largely the result of the Paleocene to early Eocene oblique rifting of the margin (fig. 65), which produced the oceanic basalt basement of the terrane, and the subsequent Eocene compressional event that folded the basalts against the continental margin. On the continental shelf, the tectonic boundary between the tholeiitic basalt Coast Range basement and the pre-Tertiary continental rocks is exposed near Roseburg in the southern Oregon Coast Range and at the southern tip of Vancouver Island (fig. 64). At Roseburg, the Paleocene pillow basalts and overlying lower Eocene turbidites are folded and thrust southeastward beneath pre-Tertiary accreted terranes marginal to the Klamath Mountains (Baldwin, 1974; Heller and Ryberg, 1983; Niem and Niem, 1990). The northeast-trending folds and faults are unconformably onlapped by gently dipping middle Eocene turbidites of the Tyee Formation, thus limiting the time of compression to about 50 Ma. On Vancouver Island, lower Eocene tholeiitic basalts of the Metchosin Formation are thrust to the northeast beneath the Leech River Schist along the Leech River fault (Clowes and others, 1987). The schist has a late middle Eocene potassium-argon cooling age of about 42 Ma, which has been interpreted as the time of accretion of the oceanic terrane to the continent (Fairchild and Cowan, 1982). This age is much younger than that inferred from stratigraphic relationships in the southern Oregon Coast Range and Klamath Mountains and implies a complex tectonic history for the Oregon-Washington continental margin.

The western boundary of the oceanic basement is the Fulmar fault on the outer continental shelf of Oregon. It is presumed to extend at least 200 km north-south on the basis of a linear aeromagnetic gradient (Bond and Zeitz, 1987) that Snavely, Wagner, and Lander (1980) interpreted to be the western edge of Coast Range basaltic basement. Seismic-reflection profiles and offshore deep test wells (Snavely and others, 1982) confirm that a steep fault separates lower Eocene oceanic basalt on the east from lower Eocene quartzose lithic sandstone of continental source on the west. The Fulmar fault is interpreted to be a major Eocene right-lateral strike-slip fault that formed the western margin of an oblique pull-apart basin in which the Coast Range basalts were erupted (Wells and others, 1984; Snavely, 1984, 1987). To the south, the fault intersects the coast south of Coos Bay just north of Five Mile Point and is inferred southward into northern California either along the Coquille River fault (Snavely, 1987) or on the continental shelf (Clarke, 1992). Interpretation of multichannel seismic-reflection profiles indicates that the fault extends along the middle shelf northward to about lat 45°N., where displacement may have been transferred toward the coast to a comparable fault bounding the eastern margin of the Coast Range basement. However, the eastern boundary of the Coast Range basement is covered by younger volcanic rocks of the Cascade arc.

DEFORMATION OF THE COAST RANGE TERRANE

Folds and faults that formed during accretion of the Coast Range basement to the continent have systematic trends that have partly controlled the structural grain of later deformation. Fold axes in uplifts of pillow-basalt basement generally trend northeast in Oregon and northwest in Washington, apparently reflecting subsequent, greater clockwise tectonic rotation of Oregon (70°) as compared to Washington (about 30°) (see Wells, 1989, for a summary). Some of these transverse folds and related thrust faults have been active into the late Cenozoic and possibly are boundaries for tectonically rotated blocks (Wells and Coe, 1985). In southwest Washington, northwest-trending folds and thrust faults extend eastward into the western Cascade Range where they deform rocks as young as Miocene (Snavely and others, 1958; Walsh and others, 1987). The northwest-trending folds are compatible with moderate shortening of the forearc during oblique convergence of the Farallon plate. In Oregon, northeast-trending folds and boundary faults largely became inactive after Eocene time and have been overprinted by Neogene north- to northwest-trending faults and folds (Wells and others, 1983; Niem and Niem, 1985; Snavely and others, 1990b).

Late Cenozoic north-south compression of the Coast Range-Olympic terrane is suggested by widely spaced east-west reverse faults and related folds in rocks as young as Quaternary. These structures include (among others) the

Clallam syncline and parallel, tight asymmetric folds along the north flank of the Olympic Mountains (Brown and others, 1960; Gower, 1960), the Doty-Grays River-Columbia River fault zone in southwest Washington (Pease and Hoover, 1957; Snavely and others, 1958; Wolfe and McKee, 1968, 1972; Wells, 1981), and the Cape Falcon fault zone in northwest Oregon (Niem and Niem, 1985) that deforms middle Miocene flows of the Columbia River Basalt Group.

A coastal system of northwest-trending dextral faults and local conjugate northeast-trending sinistral faults is consistent with north-south compression of the Oregon-Washington Coast Range terrane (Snavely and others, 1976a–c; Wells and others, 1983; Niem and Niem, 1985; Wells and Coe, 1985). However, the smooth increase in clockwise rotation toward the coast (Wells, 1989) also suggests that the coastal region is under dextral shear, probably as a result of long-term oblique subduction along the plate boundary. Block rotation is probably accommodated by the abundant west-northwest- and northwest-trending sinistral faults mapped along the coast (see Wells and Coe, 1985; Snavely and others, 1990a, b). These faults cut the youngest units (Pomona Member of the Saddle Mountains Basalt of the Columbia River Basalt Group, dated at 12 Ma) and commonly have well-developed subhorizontal slickensides. Regionally significant dextral faults extend eastward into the Yakima foldbelt just east of the Cascade arc (Tolan and Reidel, 1989). Fault displacements are difficult to determine, but the increase in tectonic rotation of the Columbia River Basalt Group toward the plate boundary (fig. 70) suggests that cumulative dextral slip after 15 Ma may exceed 100 km between the coast and the unrotated Columbia Plateau 300 km to the east (England and Wells, 1991). Apparently, much of the late Cenozoic margin parallel component of oblique subduction is being converted to strike-slip deformation and northward transport of the continental margin.

Definitive evidence for north-south transpression during the Quaternary is documented in roadcut exposures along U.S. Highway 101 on the east side of Morse Creek, 6 km east of Port Angeles, Wash. Here, Oligocene siltstone beds of the Twin River Group are thrust northward over early(?) Pleistocene alpine drift (Brown and others, 1960; Snavely and others, 1978). This poorly bedded alpine drift, which is overturned and dips about 40° to the south, in turn is unconformably overlain by north-dipping (30–50°), moderately well bedded sand, gravel, and till with scattered clasts of Oligocene siltstone eroded off the fault scarp. Broadly channelized flat-lying outwash gravels of the Fraser continental glacier lobe unconformably overlie the northward-dipping outwash and till unit. In the Strait of Juan de Fuca, Wagner and Tomson (1987) used seismic-reflection data to map numerous west-trending folds and faults that involve sediments as young as Holocene. These structures reflect deformation of a northward-moving coastal block against the pre-Tertiary Vancouver Island buttress (Snavely, 1987).

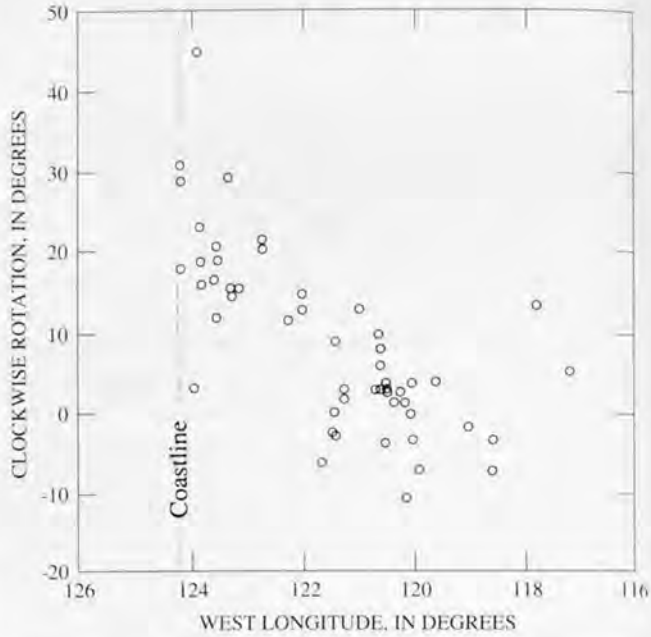

Figure 70. Clockwise paleomagnetic rotation of samples of the Miocene Columbia River Basalt Group in Oregon and Washington plotted on an east-west profile. Rotations increase westward from the Columbia Plateau toward the North America plate boundary, implying a driving force acting along the plate boundary. From England and Wells (1991).

The late Cenozoic north-south compression is compatible with compression axes determined from present-day crustal earthquakes and well-bore breakouts in the Pacific Northwest (Werner and others, 1988; Zoback and Zoback, 1989; Ludwin and others, 1991) and suggests growing influence of the Pacific plate during late Cenozoic deformation of western Oregon and Washington (Spence, 1989).

FULMAR TERRANE

The composition and extent of the Fulmar terrane can only be inferred from the seismic, aeromagnetic, and deep-well data. It is thought to be a continental fragment that has been displaced northward, seaward of the Coast Range oceanic basement. It may represent a piece of southern Oregon or northern California emplaced during regional dextral-slip faulting along the continental margin. The Fulmar fault (fig. 64) conforms to a regional pattern of latest Cretaceous to Eocene right-lateral faulting throughout the Pacific Northwest (Davis and others, 1978; Ewing, 1980; Tabor and others, 1984) and northern California (Blake and Jayko, 1986). Displacement on the Fulmar fault may be at least 200 km, based on the northward extent of the Fulmar terrane; however, geochemical similarities between Coast Range basalts and age-equivalent lower Eocene tholeiites from the allochthonous Yakutat block in the Gulf of Alaska (Davis and

Plafker, 1986) suggest that larger displacements may be possible. Movement along this fault is contemporaneous with the formation of the Kula plate (fig. 65) and its rapid northward motion with respect to North America (Engebretson and others, 1985). The late Eocene end of motion on the Fulmar fault may correlate with the demise of the Kula plate at about 43 Ma, or it may record the northward migration of the triple junction of the Kula, Farallon, and North America plates along the continental margin. More head-on convergence of the Farallon plate may have ended large-scale transcurrent motions and caused thrusting of the marginal basin floor and its sedimentary cover beneath the continental margin. The younger apparent ages for accretion of the oceanic basement in southern Vancouver Island may reflect progressive accretion of the marginal basin to the continent in the wake of the northward-moving triple junction.

ACCRETIONARY-WEDGE TERRANE

An imbricate stack of thrust-bounded folds of highly deformed Cenozoic sedimentary rocks forms the outermost tectonic belt, the accretionary wedge, of the Oregon-Washington convergent margin (fig. 69). The majority of this assemblage is offshore, and its structure is inferred from seismic-reflection profiles and a few deep test wells. However, in the Olympic Mountains, the accretionary assemblage extends onshore, where it can be studied with traditional field techniques (for example, see Stewart, 1974; Tabor, 1975; Rau, 1975, 1979; Tabor and Cady, 1978a; Snavely and others, 1986; Snavely and Kvenvolden, 1989).

The subduction complex of the Olympic Mountains forms the core of a broad anticlinal uplift in which imbricate assemblages of Eocene to Miocene turbidite rocks are thrust beneath oceanic basalts of the Crescent Formation (fig. 64). The boundary between the oceanic basement and the accretionary wedge is a major thrust fault that juxtaposes middle(?) Eocene mélange and broken formation of the Needles-Gray Wolf assemblage to the west against coherent strata of the peripheral rocks to the east (Tabor and Cady, 1978a; Snavely and others, 1986; Brandon and others, 1988). Reflection and refraction profiles interpreted from the Canadian lithoprobe program indicate that these Eocene strata underplate the lower Eocene Metchosin Formation and pre-Tertiary rocks on southern Vancouver Island (Clowes and others, 1987). The thrust-bounded sedimentary assemblages are younger to the southwest, and the upper Oligocene to lower Miocene rock assemblage is exposed along the coast (Rau, 1975, 1979; Snavely and Kvenvolden, 1989). In the northwest Olympic Mountains, two coherent terranes were thrust beneath the basalts of the Crescent Formation in the late middle Eocene—the Ozette terrane and the pre-Tertiary Point of the Arches terrane (Snavely and others, 1986).

TECTONIC UNDERPLATING

Geologic mapping in accretionary assemblages of the western Olympic Mountains (Snavely and others, 1986, 1989; Snavely and Kvenvolden, 1989) and interpretation of seismic profiles on the Vancouver Island margin (Snavely and Wagner, 1981; Clowes and others, 1987; Davis and Hyndman, 1989), on the Washington continental shelf (Snavely and Wagner, 1982), and on the Oregon continental slope (Snavely and others, 1985, 1987) indicate that strata ranging in age from middle Eocene to Pliocene have underplated older rocks along the convergent margin.

Reconnaissance geologic mapping along the west side of the Olympic Peninsula and interpretation of seismic profiles and subsurface data in the Pan American Oil Co. P-0141 well (table 17, well no. 12) on the shelf led Snavely and Kvenvolden (1989) to speculate that the middle to upper Eocene Calawah mélange and broken formation underplate the lower and middle Miocene rocks of the Hoh mélange along the coast. Farther south on the middle shelf off Grays Harbor, the upper Oligocene and middle Miocene rocks of the Hoh mélange are interpreted from seismic-reflection profiles to underplate upper(?) Miocene and younger strata along a master shear zone or décollement as shown on figure 71. On the inner shelf, however, the upper Oligocene and middle Miocene rocks of the Hoh mélange appear to underplate middle Eocene basalt(?) and middle and upper Eocene(?) strata as shown on the eastern part of the profile. Diapiric structures that originate from overpressured mélange developed below this megashear zone intrude the overlying upper(?) Miocene and Pliocene strata. A land-sea geologic cross section drawn just south of Grays Harbor (Snavely and Wagner, 1982) also shows that the upper Oligocene and middle Miocene rocks of the Hoh mélange underplate older rocks near the coastline and may extend eastward beneath Grays Harbor basin.

FAULT-PROPAGATION FOLDS AND BLIND THRUSTS

Northeastward oblique subduction of the Juan de Fuca plate has shortened the accretionary-wedge strata younger than Miocene(?), producing a group of fault-propagation folds. These fault-bounded folds are well imaged on seismic profiles across the deformation front (fig. 64) along the continental slope of Oregon and Washington. In Oregon, the vergence of these thrusts is eastward, whereas along the Washington slope the vergence is westward (Snavely, 1987). The change in the direction of vergence occurs just south of the Columbia River.

A west-trending multichannel seismic-reflection profile across the deformation front at the base of the slope off the mouth of the Columbia River (fig. 72) was generously made available to P.D. Snavely, Jr., by Exxon Company,

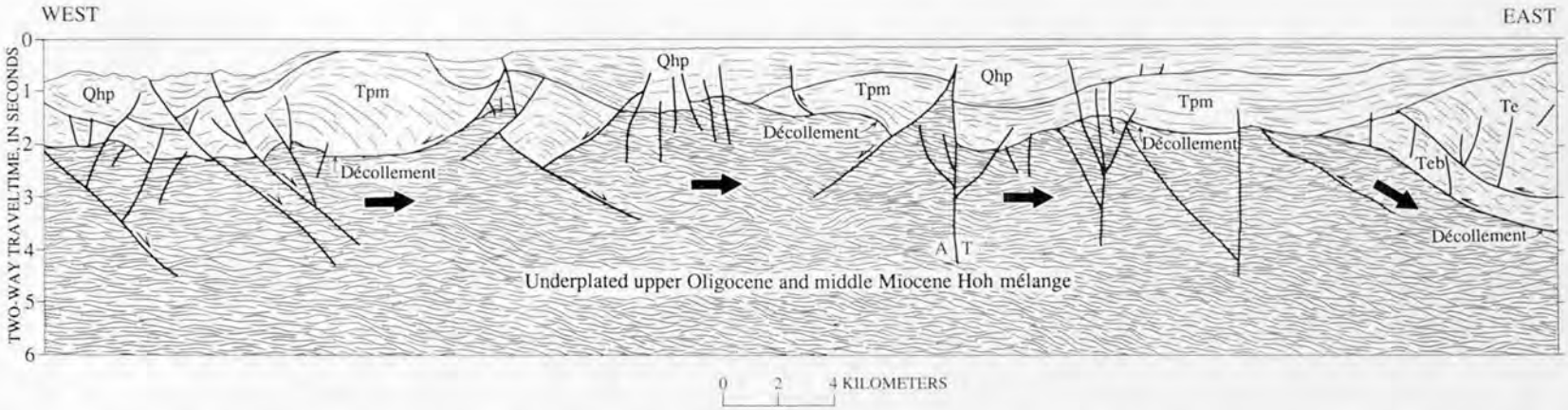

Figure 71. Interpreted time section of migrated multichannel seismic-reflection profile of the continental shelf off Grays Harbor, Wash. The upper Oligocene and middle Miocene Hoh mélange is inferred to underplate broadly folded strata of late Miocene and Pliocene age. Near the eastern edge of the profile, the Hoh mélange appears to underplate middle(?) Eocene basalt and upper Eocene(?) strata. Qhp, Pleistocene and Holocene sediments, undivided; Tpm, upper Miocene and Pliocene strata, undivided; Te, upper Eocene strata; Teb, middle Eocene basalt. Large arrows show direction of tectonic underplating. Heavy lines are faults; arrows show direction of relative movement; T denotes movement toward the viewer and A is movement away from the viewer. Light lines are form lines showing structure in the sedimentary sequence. Vertical exaggeration is about 2.6:1.

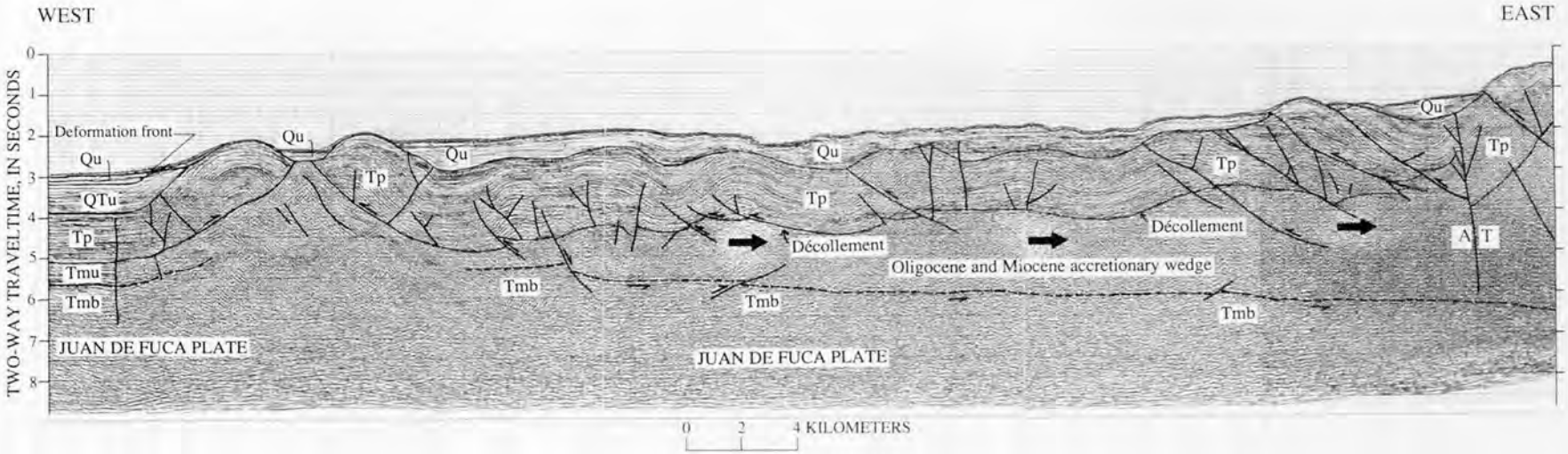

Figure 72. Migrated multichannel seismic-reflection profile across the deformation front on the lower continental slope off northwest Oregon. The fold-thrust belt of uplifted abyssal strata of Pliocene and early Pleistocene age is underplated by an eastward-thickening accretionary wedge of late Oligocene(?) and Miocene age. The top of the subducting Juan de Fuca plate can be traced from the base of the slope eastward for about 55 km. Qu, Quaternary sediments, undivided; Qtu, Tertiary and Quaternary sediments, undivided; Tp, Pliocene strata; Tmu, upper Miocene strata; Tmb, Miocene oceanic basalt. Heavy lines are faults; arrows show direction of relative movement; T denotes movement toward the viewer and A is movement away from the viewer. Large arrows show direction of underplating. From Exxon Company, U.S.A., with permission.

U.S.A., for inclusion in this report. This profile clearly images a group of fault-propagation folds on the continental slope in strata of Pliocene and early(?) Pleistocene age. This fold-thrust belt is interpreted to be underplated by an eastward-thickening mélange wedge of late Oligocene to late Miocene age. The décollement between the Pliocene and Pleistocene sequence and the mélange is sharply defined and truncates folds and faults in the upper plate. Most likely, truncation of upper plate structures was by processes of subduction erosion as defined by Scholl and others (1980). The mélange wedge overlies the gently dipping (about 3°), subducting Juan de Fuca plate that can be traced from the base of the slope eastward for about 55 km. The thrust faults on the lower slope dip eastward, whereas the youngest thrust at the base of the slope at the west end of the profile dips westward. Snavely (1987) speculated that the change in direction of vergence of thrust faults along the continental slope of Oregon and Washington may have been controlled by the slope of the backstop against which the mélange wedge accreted. A steep backstop is inferred to result in seaward vergence, whereas a gently dipping backstop results in landward vergence. In figure 72, the steep backstop formed by the strike-slip(?) fault near the eastern end of the profile produced thrusts with seaward vergence, whereas the gently dipping backstop along the base of the slope produced the landward vergence of the westernmost thrust.

Fault-propagation folds also occur east of the accretionary wedge on the Oregon continental shelf, where numerous blind thrust faults offset rocks as young as middle Miocene (fig. 67). These blind thrusts die out in fault-propagation folds, some of which gently warp strata as young as Pleistocene. One such fold in the deep marginal basin off central Oregon was the exploration target for the Standard Oil Co. Nautilus No. 1 PO-0103 well (table 17, well no. 5), drilled in 1964 (Snavely, Wagner, and Lander, 1980; Snavely, 1987).

Critical to the timing of formation of the blind thrusts and other structures on the continental shelf are widespread subaerial basalt flows of middle Miocene age (about 16 Ma) assigned to the Depoe Bay Basalt (Snavely and others, 1973). These rapidly erupted flows can be traced westward from the coast over a wide area of the Oregon continental shelf (Snavely and Wells, 1984) and probably flowed onto the shelf from coastal vents during a global eustatic lowstand (between cycles 2.3 and 2.4 of supercycle TB2 of Haq and others, 1987). Therefore, using the Depoe Bay flows as a time horizon, an episode of major transpressional tectonics that occurred on the Oregon continental margin can be documented after middle Miocene time and prior to the regional unconformity at the base of upper Miocene strata (about 10.5 Ma). In addition, middle Miocene basalt sills and dikes are common both onshore and offshore (Niem and others, 1990).

Several seismic profiles that cross the upper continental slope also indicate that the shelf margin has collapsed along west-dipping listric faults (fig. 71). Narrow extensional half-graben basins bounded by these faults have been progressively infilled with upper Miocene(?) and Pliocene(?) sediments (Snavely and McClellan, 1987). Unconformities between these sequences most likely reflect episodes of downslope movement along basin-bounding listric faults owing to sediment loading.

NEOTECTONICS

The intense deformation recognized in Cenozoic strata of the Oregon-Washington convergent margin clearly records a prolonged history of episodic tectonism along the active plate boundary. The numerous unconformities on growing structures, the record of giant modern and ancient submarine slides such as the Oligocene Jansen Creek Member of the Makah Formation (Snavely, Niem, and others, 1980; Niem and others, 1989), and abundant debris flows in basin-filling sequences all infer a history of seismic events. There is ample evidence that this episodic deformation continues in the Quaternary.

OFFSHORE STRUCTURES

Seismic-reflection profiles across the deformational front along the continental slope of Oregon and Washington show that episodic underthrusting of the Juan de Fuca plate beneath the North America plate has produced a series of north- to north-northwest-trending elongate en-echelon anticlinal ridges bounded by thrust faults (Silver, 1972; Carson, 1977; Snavely, Wagner, and Lander, 1980; Snavely, 1987). These ridges have bathymetric expression, and they uplift Pleistocene abyssal sediments as much as 1,100 m (fig. 69) (Byrne and others, 1966; Carson and others, 1974; Kulm and Fowler, 1974; Snavely, Wagner, and Lander, 1980; Snavely and Wagner, 1981).

The profile off central Oregon (fig. 69) indicates that two lower slope basins formed landward of anticlinal folds in Pleistocene strata. The larger basin, which is near the base of the upper slope, contains as much as 800 m of Quaternary sediments and an unconformity within these basin deposits, thus indicating two distinct periods of uplift of the fault-propagation fold that bounds the basin on the west. Along the axis of the deep marginal shelf basin off central Oregon, numerous unconformities occur in the Neogene sequence. Of particular interest is the fact that the sea floor itself is also downwarped along the axis of the basin. A family of north-trending faults along the eastern margin of the basin offsets the sea floor and coastal terrace deposits. We speculate that transpression across the basin episodically was relieved along this set of faults to produce the stacked unconformities along the axial part of the basin (fig. 73).

Other recent deformation on the Oregon shelf suggests a complex relationship between normal faulting and growth of diapirs. A high-resolution profile (fig. 74) on the inner

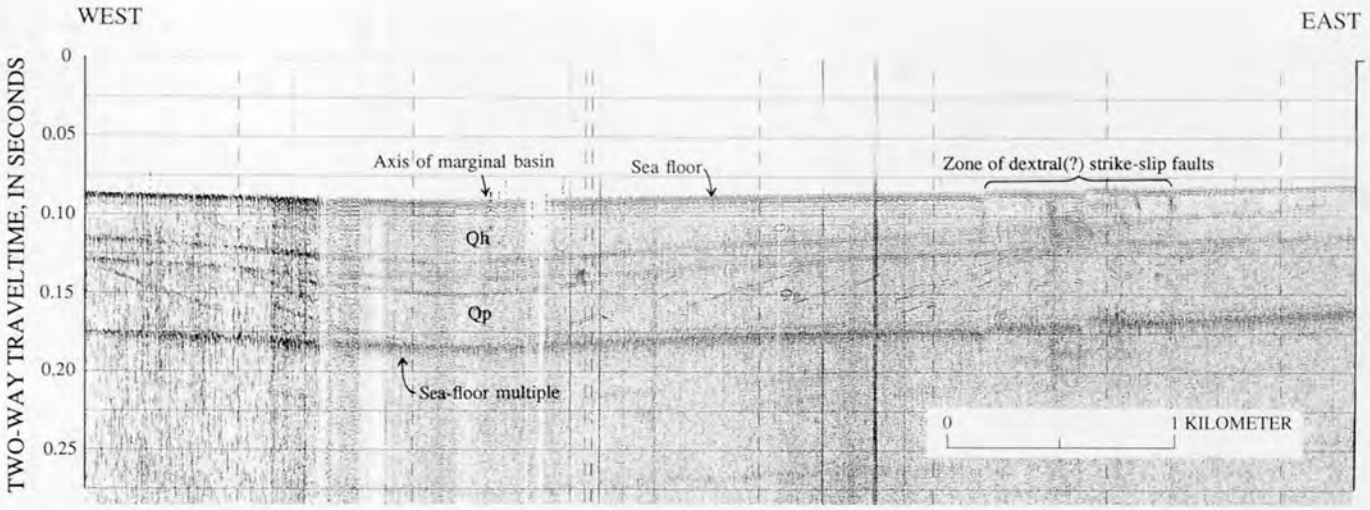

Figure 73. High-resolution seismic-reflection profile extending westward just south of Newport, Oreg., across the axis of the deep marginal basin on the inner shelf. Stacked unconformities (best shown on the west side of the marginal basin) are due to episodic periods of downwarping. The sea floor also appears to be downwarped, indicating a present transpressional regime. A 1/2-km-wide zone of faulting is present along the eastern margin of the basin. These north-trending faults are interpreted to be dextral strike-slip faults along which the northeast-to-southwest transpression was released, perhaps resulting in recent small-magnitude earthquakes along this segment of the Oregon coast. Qh, Holocene strata; Qp, Pleistocene strata. The sea-floor multiple is an acoustical artifact that represents a repeat of the sea-floor acoustical signal.

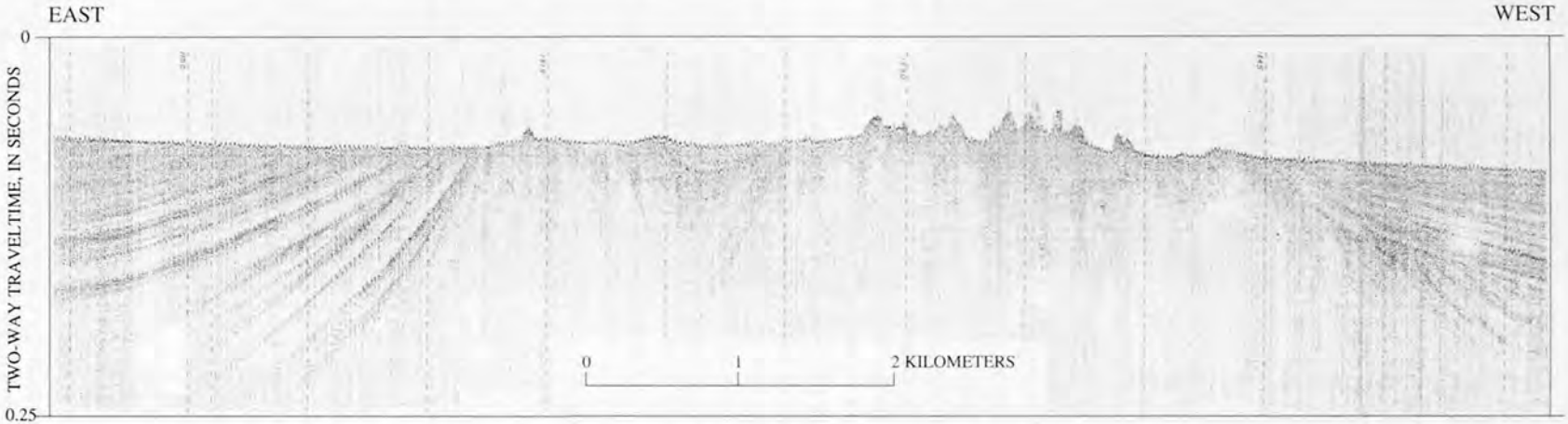

Figure 74. West-trending high-resolution seismic-reflection profile across the inner shelf off northwest Oregon, just south of the Columbia River. The broad diapiric fold in the west-central part of the profile is capped by pinnaclelike features that rise 5–15 m above the sea floor. Vertical dashed lines are 5-minute seismogram time ticks.

shelf off northwest Oregon shows a broad 2-km-wide uplift of Pliocene(?) strata capped by a group of pinnaclelike features that rise 5–15 m above the sea floor. Observations during a submersible dive by L.D. Kulm (Oregon State University, written commun., 1988) indicate that the walls of these features are nearly vertical and that rockfall debris is not present on the intervening flat floors. Also, there apparently is little evidence of erosion that could have carved this topography, and the surface of some blocks have vertical striations (slickensides?). A multichannel profile across this pinnacle-crested fold indicates that this feature is a faulted diapiric structure bounded on the east by a normal (growth) fault. Our interpretation is that the crest of this diapir has been subjected to extension over the 2 km fold, resulting in the development of horst and graben structures along the crest of the fold. The lack of significant erosion on the walls of these blocks and the fact that they have been uplifted above the level of the surrounding flat erosion surface, which most likely was beveled during the late Pleistocene lowstand of sea level, all point to recent uplift and attendant tensional faulting.

Multichannel seismic-reflection profiles off southern Vancouver Island are similar to those off Oregon in that sediments of the Cascadia forearc basin have been uplifted as much as 600 m. The seaward segment of a profile that crosses the base of the slope clearly shows a major northeast-dipping thrust fault (fig. 75, fault A) that uplifts virtually the entire section of strata above upper Miocene oceanic crust. Fault A is overlain by a small basin that contains about 120 m of upper Pleistocene(?) and Holocene sediments. The 120-m section of sediment that overlies fault A indicates that this fault has been inactive since late(?) Pleistocene time. Thrust-fault B, which lies seaward (southwest) of the principal fault A, also is overlain by a thick sequence of late Pleistocene and Holocene sediments. As the imbricate thrust faults along the outer shelf and slope of Oregon and Washington have migrated seaward with time, the next major displacement may be along fault B. This relation of upper Pleistocene sediments deposited over the trace of fault A in figure 75 and folded or tilted unconformities in lower slope basins (fig. 69) suggests episodic rather than continuous underthrusting at the base of the continental slope.

ONSHORE FEATURES

Major landslides such as those in the Olympic Mountains that divided ancient Lake Crescent into the present two lakes—Lake Crescent on the west and Lake Sutherland on the east (Brown and others, 1960; Tabor, 1975)—may have been initiated by an earthquake during late Holocene time. A Quilleute Indian legend purports that during a great battle between the Clallam and Quilleute Indians, Mount Storm King (on the south side of ancient Lake Crescent) became angry and took a great piece of rock from his crest and hurled it down the valley, killing all who were fighting (Tabor, 1975). Although the debris that forms the older and major landslide came largely from the north, a large slide also originated from the ridge just east of Mount Storm King (Brown and others, 1960). The youthful nature of the older landslide, which is indicated by the lack of a thick soil zone on the landslide debris and hummocky topography with closed depressions that contain little recent fill, suggests that the older slide may have occurred relatively soon after the melting of the ice lobe that occupied the Lake Crescent-Lake Sutherland valley. Studies on the Lake Crescent landslide dam by Logan and Schuster (1991) support a Holocene age for the landslide. They reported a 500- to 550-year-old tree growing on rocks that form the dam. A submerged tree on the west side of the older landslide, apparently in an upright (growth) position in Lake Crescent, has a ^{14}C age of 350 yr. B.P. (Snavely, 1987). However, this tree was probably transported into the lake by the younger slide, perhaps the one witnessed by the Indians.

Pleistocene and Holocene faults are present along the coastal zone and on the continental shelf. In the western part of the Olympic Peninsula, upper Pleistocene glacial drift is sheared and tectonically interleaved with siltstone beds of Eocene age (Snavely, 1983). North of Ozette Lake, a Holocene soil zone on upper Pleistocene outwash gravels is offset as much as 2 m. To the southwest, on the continental shelf off Grays Harbor, Wash., sea-floor sediments are offset about 7 m by a trap-door type of fault (Snavely and others, 1977). On the inner shelf and coastal zone of central Oregon, a 75-km-long north-trending zone of steeply dipping normal faults offsets Holocene(?) sediments (Snavely, Wagner, and Lander, 1980); onshore, these faults offset upper Pleistocene marine-terrace deposits (Snavely and others, 1976a, c). These faults are downthrown to the east toward the uplifted Coast Range rather than toward the offshore marginal basin, as one would expect for seaward-verging thrust faults or gravity faults. Several earthquakes with Modified Mercalli intensities of III to IV have occurred in the vicinity of Newport (Berg and Baker, 1963) and may have been generated by movement along faults within this zone.

EARTHQUAKE POTENTIAL

Although present seismic activity is low along the continental margin of Oregon and Washington, this region lies along a major subduction zone where the Juan de Fuca and North America plates are converging at 3.5 cm per year (Riddihough, 1977). In most subduction zones, episodic strain release has generated large earthquakes (Plafker, 1972; Kanamori, 1977; Heaton and Kanamori, 1984), but the absence of a well-defined megathrust along the Washington and Oregon convergent margin has perplexed geologists and seismologists. They have proposed several models to account for the seismically quiescent plate boundary:

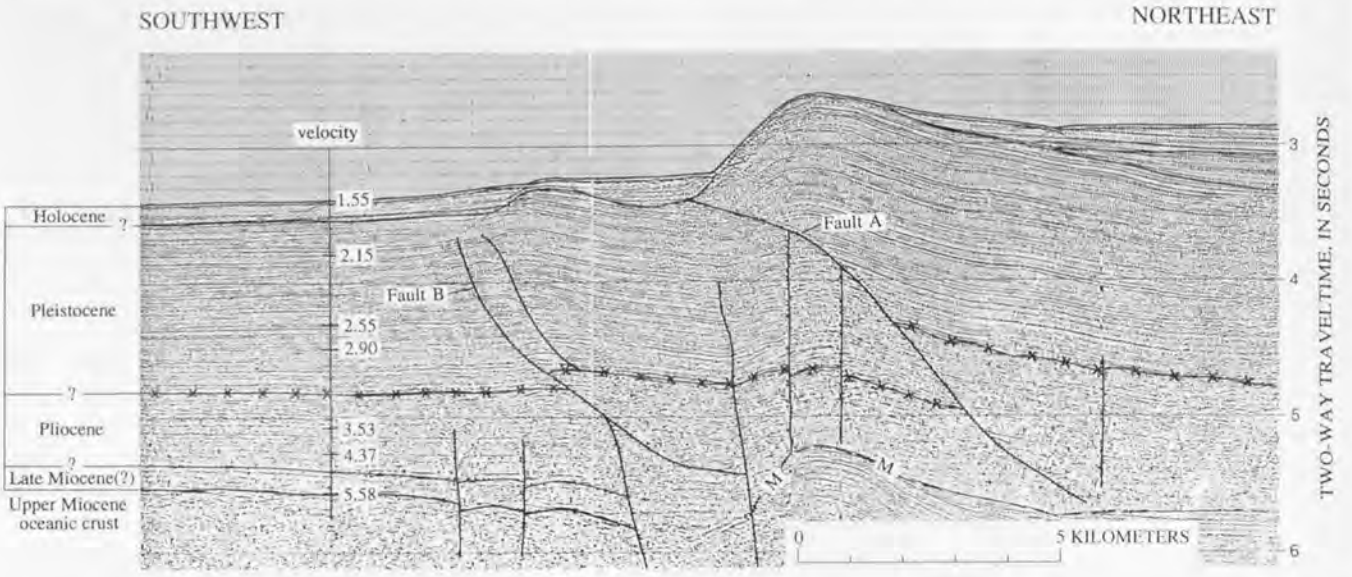

Figure 75. Twenty-four-channel seismic-reflection profile (USGS line 80–7) across the abyssal plain and lower continental slope off southwestern Vancouver Island, British Columbia. Landward-dipping thrust-fault A has folded and uplifted 700-m-thick Pliocene and Pleistocene abyssal sediments. This fault apparently has been inactive during the Holocene because deposits of Holocene age in the small basin southwest of the thrust fold are not offset by fault A. The existence of fault B indicates that the deformation front at the base of the slope is migrating seaward. Velocities (kilometers per second) are based on sonobuoy refraction data. M, sea-floor multiple. Heavy lines are faults. Line of x's shows probable contact between Pliocene and Pleistocene deposits. Vertical exaggeration is about 3:1.

1. Convergence has ceased between the Juan de Fuca and North America plates.

2. Convergence is occurring along the plate boundaries but is aseismic because a young, warm, plastic oceanic crust is being subducted with ductile rather than brittle deformation of the plate boundary.

3. The Juan de Fuca and North America plates presently are strongly coupled, forming a seismic gap along this segment of the northeast Pacific Ocean.

Geodetic measurements by Savage and others (1981) indicated that crustal strain is accumulating in the Puget Sound area and has an average principal direction of contraction of N. 71± 6° E. This direction of contraction is in general agreement with the N. 50° E. direction of relative motion between the Juan de Fuca and North America plates. It also agrees closely with the direction of tectonic transport during the late middle Miocene period of plate convergence, as deduced from drag folds in the upper plate of the Ozette thrust fault in the northwesternmost part of the Olympic Peninsula (fig. 66, unit Tm) (Snavely and others, 1986).

Landward tilting in the Oregon and Washington Coast Range and the Olympic Peninsula has been documented by using tide gauges and by geodetic leveling of uplifted marine terraces (Adams, 1984). This landward tilt, along with crustal shortening shown by thrust faults and folds on the outer shelf and slope of Oregon (Kulm and Fowler, 1974; Seely, 1977; Snavely, Wagner, and Lander, 1980; Snavely, 1987) and on the slope, continental shelf, and coastal zone of Washington (Silver, 1972; Rau, 1975, 1979; Carson, 1977; Snavely and Wagner, 1982; Snavely and others, 1986; Wells, 1989), is characteristic of many other subduction zones where major thrust earthquakes have occurred.

Detailed stratigraphic studies of buried upper Holocene estuarine deposits in westernmost Washington led Atwater (1987; this volume) to conclude that coseismic subsidence is responsible for their burial. At least six episodes of coseismic subsidence may have occurred in the last 7,000 years. Individual episodes of subsidence extended for many tens of kilometers along the coast and at least 30 km inland, implying large Cascadia subduction-zone earthquakes. Similar investigations of coastal salt marshes in Oregon by Peterson and Darienzo (1988) have established late Holocene episodic tectonic subsidence that is interpreted as evidence of abrupt strain release and intervening gradual strain accumulation along the southern Cascadia subduction zone during the last 3,500 years.

The episodic subsidence of coastal lowlands and the evidence for episodic thrust faulting along the deformation front may both reflect intermittent coupling between the Juan de Fuca and North America plates. Presently, the thrust interface may be strongly coupled, and elastic strain may be accumulating across the continental margin (Heaton and Kanamori, 1984). Based upon their interpretation of earthquake focal-mechanism data, Weaver and Smith (1983) also concluded that the subduction zone is locked. As there is no historical record of large, shallow earthquakes along the subduction zone, a 900-km-long seismic gap seems to be present along the subduction zone off Oregon and Washington—the most remarkable gap to be found in the circum-Pacific seismic belt (Heaton and Kanamori, 1984). Despite the fact that present-day seismic activity is low, the potential for a major subduction-type earthquake cannot be discounted.

REFERENCES CITED

Adams, John, 1984, Active deformation of the Pacific Northwest continental margin: Tectonics, v. 3, no. 4, p. 449–472.

Addicott, W.O., 1976, Molluscan paleontology of the lower Miocene Clallam Formation, northwestern Washington: U.S. Geological Survey Professional Paper 976, 44 p.

Allen, J.E., and Baldwin, E.M., 1944, Geology and coal resources of the Coos Bay quadrangle, Oregon: Oregon Department of Geology and Mineral Industries Bulletin 27, 160 p.

Armentrout, J.M., 1980, Cenozoic stratigraphy of Coos Bay and Cape Blanco, southwestern Oregon, *in* Oles, K.F., Johnson, J.G., Niem, A.R., and Niem, W.A., eds., Geologic field trips in western Oregon and southwestern Washington: Oregon Department of Geology and Mineral Industries Bulletin 101, p. 175–216.

Arnold, Ralph, 1906, Geological reconnaissance of the coast of the Olympic Peninsula, Washington: Geological Society of America Bulletin, v. 17, p. 451–468.

Atwater, B.F., 1987, Evidence for great Holocene earthquakes along the outer coast of Washington State: Science, v. 236, no. 4804, p. 942–944.

Baldwin, E.M., 1974, Eocene stratigraphy of southwestern Oregon: Oregon Department of Geology and Mineral Industries Bulletin 83, 40 p.

Baldwin, E.M., Brown, R.D., Jr., Gair, J.E., and Pease, M.H., Jr., 1955, Geology of the Sheridan and McMinnville quadrangles, Oregon: U.S. Geological Survey Oil and Gas Investigations Map OM–155, scale 1:62,500.

Beeson, M.H., Perttu, R.K., and Perttu, Janice, 1979, The origin of the Miocene basalts of coastal Oregon and Washington—An alternative hypothesis: Oregon Geology, v. 41, no. 10, p. 159–166.

Berg, J.W., Jr., and Baker, C.D., 1963, Oregon earthquakes, 1841 through 1958: Seismological Society of America Bulletin, v. 53, no. 1, p. 95–108.

Blake, M.C., Jr., and Jayko, A.S., 1986, Tectonic evolution of northwest California and southwest Oregon: Geological Society of France Bulletin, ser. 8, t. 2, no. 6, p. 921–930.

Bond, K.R., and Zeitz, Isidore, 1987, Composite magnetic anomaly map of the conterminous United States west of 96° longitude: U.S. Geological Survey Geophysical Investigations Map GP–977, 2 sheets, scale 1:2,500,000.

Brandon, M.T., and Calderwood, A.R., 1990, High-pressure metamorphism and uplift of the Olympic subduction complex: Geology, v. 18, no. 12, p. 1252–1255.

Brandon, M.T., Miller, D.S., and Vance, J.A., 1988, Fission-track dates for initiation and uplift of the Cenozoic subduction complex of the Olympic Mountains, northwest Washington [abs.]: Geological Society of America Abstracts with Programs, v. 20, p. 145.

Brown, R.D., Jr., Gower, H.D., and Snavely, P.D., Jr., 1960, Geology of the Lake Crescent-Port Angeles area, Washington: U.S. Geological Survey Oil and Gas Investigations Map OM–203, scale 1:62,500.

Brown, R.D., Jr., Snavely, P.D., Jr., and Gower, H.D., 1956, Lyre Formation (redefinition), northern part of Olympic Peninsula, Washington: American Association of Petroleum Geologists Bulletin, v. 40, no. 1, p. 94–107.

Bukry, David, and Snavely, P.D., Jr., 1988, Coccolith zonation for Paleogene strata in the Oregon Coast Range, *in* Filewicz, M.V., and Squires, R.L., eds., Paleogene stratigraphy, west coast of North America: Society of Economic Paleontologists and Mineralogists, Pacific Section, West Coast Paleogene Symposium, v. 58, p. 251–263.

Byrne, J.V., Fowler, G.A., and Maloney, N.M., 1966, Uplift of the continental margin and possible continental accretion off Oregon: Science, v. 154, no. 3757, p. 1654–1656.

Cady, W.M., 1975, Tectonic setting of the Tertiary volcanic rocks of the Olympic Peninsula, Washington: U.S. Geological Survey Journal of Research, v. 3, no. 5, p. 573–582.

Carlson, P.R., and Nelson, C.H., 1987, Marine geology and resource potential of Cascadia basin, *in* Scholl, D.W., Grantz, Arthur, and Vedder, J.G., eds., Geology and resource potential of the continental margin of western North America and adjacent ocean basins—Beaufort Sea to Baja California: Houston, Tex., Circum-Pacific Council for Energy and Mineral Resources, Earth Science Series, v. 6, no. 6, p. 523–535.

Carson, Bobb, 1977, Tectonically induced deformation of deep-sea sediments off Washington and northern Oregon—Mechanical consolidation: Marine Geology, v. 24, no. 4, p. 289–307.

Carson, Bobb, Yan, Jennwei, Myers, P.B., Jr., and Barnard, W.D., 1974, Initial deep-sea sediment deformation at the base of the Washington continental slope—A response to subduction: Geology, v. 2, no. 11, p. 561–564.

Chan, M.A., and Dott, R.H., Jr., 1983, Shelf and deep-sea sedimentation in Eocene forearc basin, western Oregon—Fan or non-fan?: American Association of Petroleum Geologists Bulletin, v. 67, no. 11, p. 2100–2116.

Clapp, C.H., 1917, Sooke and Duncan map area, Vancouver Island, British Columbia: Geological Survey of Canada Memoir 96, 445 p.

Clarke, S.H., Jr., 1992, Geology of the Eel River basin and adjacent region—Implications for late Cenozoic tectonics of the southern Cascadia subduction zone and Mendocino triple junction: American Association of Petroleum Geologists Bulletin, v. 76, no. 2, p. 199–224.

Clarke, S.H., Jr., Field, M.E., and Hirozawa, C.A., 1981, Reconnaissance geology and geologic hazards of offshore Coos Bay basin, central Oregon continental margin: U.S. Geological Survey Open-File Report 81–898, 84 p.

Clowes, R.M., Brandon, M.T., Green, A.G., Yorath, C.J., Brown, A.S., Kanasewich, E.R., and Spencer, C.P., 1987, Lithoprobe—Southern Vancouver Island—Cenozoic subduction complex imaged by deep seismic reflections: Canadian Journal of Earth Sciences, v. 24, no. 1, p. 31–51.

Cooper, M.D., 1981, Sedimentation, stratigraphy, and facies variations of the lower to middle Miocene Astoria Formation in Oregon: Corvallis, Oregon State University, Ph.D. dissertation, 524 p.

Davis, A.S., and Plafker, George, 1986, Eocene basalts from the Yakutat terrane—Evidence for the origin of an accreting terrane in southern Alaska: Geology, v. 14, no. 11, p. 963–966.

Davis, E.E., and Hyndman, R.D., 1989, Accretion and recent deformation of sediments along the northern Cascadia subduction zone: Geological Society of America Bulletin, v. 101, no. 11, p. 1465–1480.

Davis, G.A., Monger, J.W.H., and Burchfiel, B.C., 1978, Mesozoic construction of the Cordilleran collage, central British Columbia to central California, *in* Howell, D.G., and McDougall, K.A., eds., Mesozoic paleogeography of the Western United States: Society of Economic Paleontologists and Mineralogists, Pacific Coast Paleogeography Symposium No. 2, p. 1–32.

Dott, R.H., Jr., 1966, Eocene deltaic sedimentation at Coos Bay, Oregon: Journal of Geology, v. 74, no. 4, p. 373–420.

Duncan, R.A., 1982, A captured island chain in the Coast Range of Oregon and Washington: Journal of Geophysical Research, v. 87, no. B13, p. 10827–10837.

Easterbrook, D.J., 1969, Pleistocene chronology of the Puget lowland and San Juan Islands, Washington: Geological Society of America Bulletin, v. 80, no. 11, p. 2273–2286.

Engebretson, D.C., Cox, Alan, and Gordon, R.G., 1985, Relative motions between oceanic and continental plates in the Pacific Basin: Geological Society of America Special Paper 206, 59 p.

England, P.C., and Wells, R.E., 1991, Neogene rotations and quasi-continuous deformation of the Pacific Northwest continental margin: Geology, v. 19, no. 10, p. 978–981.

Ewing, T.E., 1980, Paleogene tectonic evolution of the Pacific Northwest: Journal of Geology, v. 88, no. 6, p. 619–638.

Fairchild, L.H., and Cowan, D.S., 1982, Structure, petrology, and tectonic history of the Leech River complex northwest of Victoria, Vancouver Island: Canadian Journal of Earth Sciences, v. 19, no. 9, p. 1817–1835.

Goodwin, C.J., 1973, Stratigraphy and sedimentation of the Yaquina Formation, Lincoln County, Oregon: Corvallis, Oregon State University, M.S. thesis, 121 p.

Gower, H.D., 1960, Geology of the Pysht quadrangle, Washington: U.S. Geological Survey Geologic Quadrangle Map GQ–129, scale 1:62,500.

Haq, B.U., Hardenbol, Jan, and Vail, P.R., 1987, Chronology of fluctuating sea levels since the Triassic: Science, v. 235, no. 4793, p. 1156–1167.

Heaton, T.H., and Kanamori, Hiroo, 1984, Seismic potential associated with subduction in the Northwestern United States: Seismological Society of America Bulletin, v. 74, no. 3, p. 933–941.

Heller, P.L., Peterman, Z.E., O'Neil, J.R., and Shafiqullah, Muhammad, 1985, Isotopic provenance of sandstones from the Eocene Tyee Formation, Oregon Coast Range: Geological Society of America Bulletin, v. 96, no. 6, p. 770–780.

Heller, P.L., and Ryberg, P.T., 1983, Sedimentary record of subduction to forearc transition in the rotated Eocene basin of western Oregon: Geology, v. 11, no. 7, p. 380–383.

Johnson, S.Y., 1984, Evidence for a margin-truncating transcurrent fault (pre-late Eocene) in western Washington: Geology, v. 12, no. 9, p. 538–541.

Kanamori, Hiroo, 1977, Seismic and aseismic slip along subduction zones and their tectonic implications, *in* Talwani, M., and Pittman, W.C., III, eds., Island arcs, deep sea trenches and back-arc basins: Washington, D.C., American Geophysical Union, Maurice Ewing Series 1, p. 173–174.

Kulm, L.D., and Fowler, G.A., 1974, Oregon continental margin model, *in* Burk, C.A., and Drake, C.L., eds., The geology of continental margins: New York, Springer-Verlag, p. 261–283.

Livingston, V.E., Jr., 1966, Geology and mineral resources of the Kelso-Cathlamet area, Cowlitz and Wahkiakum Counties, Washington: Washington Division of Mines and Geology Bulletin 54, 110 p.

Logan, R.L., and Schuster, R.L., 1991, Lakes divided—The origin of Lake Crescent and Lake Sutherland, Clallam County, Washington: Washington Geology (formerly Washington Geologic Newsletter), v. 19, no. 1, p. 38–42.

Lovell, J.P.B., 1969, Tyee Formation—Undeformed turbidites and their lateral equivalents, mineralogy, and paleogeography: Geological Society of America Bulletin, v. 80, no. 1, p. 9–22.

Ludwin, R.S., Weaver, C.S., and Crosson, R.S., 1991, Seismicity of Washington and Oregon, *in* Slemmons, D.B., Engdahl, E.R., Zoback, M.D., and Blackwell, D.D., eds., Neotectonics of North America: Boulder, Colo., Geological Society of America, Decade of North America Geology, Decade Map Volume 1, p. 77–98.

MacLeod, N.S., and Snavely, P.D., Jr., 1973, Volcanic and intrusive rocks of the central part of the Oregon Coast Range: Oregon Department of Geology and Mineral Industries Bulletin 77, p. 47–74.

MacLeod, N.S., Tiffin, D.L., Snavely, P.D., Jr., and Currie, R.G., 1977, Geologic interpretation of magnetic and gravity anomalies in the Strait of Juan de Fuca, U.S.-Canada: Canadian Journal of Earth Sciences, v. 14, no. 2, p. 223–238.

Magill, J.R., Cox, Allan, and Duncan, R.A., 1981, Tillamook Volcanic Series—Further evidence for tectonic rotation of the Oregon Coast Range: Journal of Geophysical Research, v. 86, no. B4, p. 2953–2970.

McLellan, R.D., 1927, The geology of the San Juan Islands: Washington University Publications in Geology, v. 3, 180 p.

Molenaar, C.M., 1985, Depositional relationships of the Umpqua and Tyee Formations (Eocene), southwestern Oregon: American Association of Petroleum Geologists Bulletin, v. 69, no. 8, p. 1217–1229.

Muller, J.E., 1977, Evolution of the Pacific margin, Vancouver Island, and adjacent regions: Canadian Journal of Earth Sciences, v. 14, no. 9, p. 2062–2085.

Niem, A.R., and Niem, W.A., 1985, Oil and gas investigation of the Astoria basin, Clatsop and northernmost Tillamook Counties, northwest Oregon: Oregon Department of Geology and Mineral Industries, Oil and Gas Investigations Map OGI–14, 8 p., correlation chart, scale 1:100,000.

———1990, Geology and oil, gas, and coal resources, southern Tyee basin, southern Coast Range, Oregon: Oregon Department of Geology and Mineral Industries Open-File Report 0–89–3, 3 pls, 11 tables.

Niem, A.R., Snavely, P.D., Jr., Chen, Ying, and Niem, W.A., 1989, Jansen Creek Member of the Makah Formation—A major Oligocene submarine landslide or slump deposit from the Vancouver shelf in the Juan de Fuca deep marginal basin, NW Olympic Peninsula, Washington [abs.]: Geological Society of America, Abstracts with Programs, v. 21, no. 5, p. 123.

Niem, A.R., Snavely, P.D., Jr., and Niem, W.A., 1990, Onshore-offshore geologic cross section from the Mist gas field, northern Oregon Coast Range, to the northwest Oregon continental shelf and slope: Oregon Department of Geology and Mineral Industries Continental Margin Transect OGI–17, 46 p., 1 pl.

Pease, M.H., and Hoover, Linn, 1957, Geology of the Doty-Minot Peak area, Washington: U.S. Geological Survey Oil and Gas Investigations Map OM–188, scale 1:62,500.

Peterson, C.D., and Darienzo, M.E., 1988, Episodic tectonic subsidence of late-Holocene salt marshes in Oregon—Clear evidence of abrupt strain release and gradual strain accumulation in the southern Cascadia margin during the last 3,500 years, *in* Hays, W.W., ed., Proceedings of Conference XLII, Workshop on evaluation of earthquake hazards and risk in the Puget Sound and Portland areas: U.S. Geological Survey Open-File Report 88–541, p. 110–113.

Plafker, George, 1972, Alaskan earthquake of 1964 and Chilean earthquake of 1960—Implications for arc tectonics: Journal of Geophysical Research, v. 77, no. 5, p. 901–925.

Rau, W.W., 1970, Foraminifera, stratigraphy and paleoecology of the Quinault Formation, Point Grenville-Raft River coastal area, Washington: Washington Division of Mines and Geology Bulletin 62, 40 p.

———1975, Geologic map of the Destruction Island and Taholah quadrangles, Washington: Washington Division of Geology and Earth Resources Geologic Map GM–13, scale 1:62,500.

———1979, Geologic map in the vicinity of the lower Bogachiel and Hoh River Valleys, and the Washington coast: Washington Division of Geology and Earth Resources Geologic Map GM–24, scale 1:62,500.

Riddihough, R.P., 1977, A model for recent plate interactions off Canada's west coast: Canadian Journal of Earth Science, v. 14, no. 3, p. 384–396.

Russell, I.C., 1900, Geology of the Cascade Mountains in northern Washington: U.S. Geological Survey Annual Report 20, pt. 2, p. 83–210.

Savage, J.C., Lisowski, Michael, and Prescott, W.H., 1981, Geodetic strain measurements in Washington: Journal of Geophysical Research, v. 86, no. B6, p. 4929–4940.

Scholl, D.W., Huene, Roland von, Vallier, T.L., and Howell, D.G., 1980, Sedimentary masses and concepts about tectonic processes at underthrust ocean margins: Geology, v. 8, no. 12, p. 564–568.

Seely, D.R., 1977, The significance of landward vergence and oblique structural trends on trench inner slopes, *in* Talwani, M., and Pitman, W.C., III, eds., Island arcs, deep sea trenches and back-arc basins: Washington, D.C., American Geophysical Union, Maurice Ewing Series 1, p. 187–198.

Shouldice, D.H., 1971, Geology of the western Canadian continental shelf: Canadian Petroleum Geology Bulletin, v. 19, no. 2, p. 405–436.

Silver, E.A., 1972, Pleistocene tectonic accretion of the continental slope off Washington: Marine Geology, v. 13, no. 4, p. 239–249.

Snavely, P.D., Jr., 1948, Coquille Formation in the Nestucca Bay quadrangle, Oregon: Geological Society of Oregon, Geological News Letter, v. 14, no. 2, p. 11–12.

———1983, Peripheral rocks—Tertiary geology of the northwestern part of the Olympic Peninsula, Washington, *in* Muller, J.E., Snavely, P.D., Jr., and Tabor, R.W., eds., The Tertiary Olympic terrane, southwest Vancouver Island and northwest Washington: Geological Association of Canada, Mineralogical Association of Canada, Canadian Geophysical Union Field Trip Guidebook, Trip 12, p. 6–31.

———1984, Sixty million years of growth along the Oregon continental margin, *in* Clarke, S.H., ed., U.S. Geological Survey highlights in marine research: U.S. Geological Survey Circular 938, p. 9–18.

———1987, Tertiary geologic framework, neotectonics, and petroleum potential of the Oregon-Washington continental margin, *in* Scholl, D.W., Grantz, Arthur, and Vedder, J.G., eds., Geology and resource potential of the continental margin of western North America and adjacent ocean basins—Beaufort Sea to Baja California: Houston, Tex., Circum-Pacific Council for Energy and Mineral Resources, Earth Science Series, v. 6, no. 6, p. 305–335.

———1991, The Salmon River Formation—A lower Eocene sequence in the central Oregon Coast Range, *in* Stratigraphic notes, 1989–90: U.S. Geological Survey Bulletin 1935, p. 1–4.

Snavely, P.D., Jr., Brown, R.D., Jr., Roberts, A.E., and Rau, W.W., 1958, Geology and coal resources of the Centralia-Chehalis district, Washington: U.S. Geological Survey Bulletin 1053, 159 p.

Snavely, P.D., Jr., and Kvenvolden, K.A., 1989, Geology and hydrocarbon potential, *in* Preliminary evaluation of the petroleum potential of the Tertiary accretionary terrane, west side of the Olympic Peninsula, Washington: U.S. Geological Survey Bulletin 1892A, p. 1–17.

Snavely, P.D., Jr., and MacLeod, N.S., 1974, Yachats Basalt—An upper Eocene differentiated volcanic sequence in the Oregon Coast Range: U.S. Geological Survey Journal of Research, v. 2, no. 4, p. 395–403.

Snavely, P.D., Jr., MacLeod, N.S., and Minasian, D.L., 1990a, Preliminary geologic map of the Neskowin quadrangle, Tillamook County, Oregon: U.S. Geological Survey Open-File Report 90–413, scale 1:24,000.

———1990b, Preliminary geologic map of the Nestucca Bay quadrangle, Tillamook County, Oregon: U.S. Geological Survey Open-File Report 90–202, scale 1:24,000.

Snavely, P.D., Jr., MacLeod, N.S., Niem, A.R., and Minasian, D.L., 1986, Geologic map of Cape Flattery area, northwestern Olympic Peninsula, Washington: U.S. Geological Survey Open-File Report 86–344B, scale 1:48,000.

Snavely, P.D., Jr., MacLeod, N.S., and Rau, W.W., 1969 [1970], Summary of the Tillamook area, northern Oregon Coast Range, *in* Geological Survey research 1969: U.S. Geological Survey Professional Paper 650–A, p. A47.

Snavely, P.D., Jr., MacLeod, N.S., Rau, W.W., Addicott, W.O., and Pearl, J.E., 1975, Alsea Formation—An Oligocene marine sedimentary sequence in the Oregon Coast Range: U.S. Geological Survey Bulletin 1395–F, 21 p.

Snavely, P.D., Jr., MacLeod, N.S., and Wagner, H.C., 1968, Tholeiitic and alkalic basalts of the Eocene Siletz River Volcanics, Oregon Coast Range: American Journal of Science, v. 266, no. 6, p. 454–481.

———1973, Miocene tholeiitic basalts of coastal Oregon and Washington and their relations to coeval basalts of the Columbia Plateau: Geological Society of America Bulletin, v. 84, no. 2, p. 387–424.

Snavely, P.D., Jr., MacLeod, N.S., Wagner, H.C., and Rau, W.W., 1976a, Geologic map of the Cape Foulweather and Euchre Mountain quadrangles: U.S. Geological Survey Miscellaneous Investigations Series Map I–868, scale 1:62,500.

———1976b, Geologic map of the Waldport and Tidewater quadrangles, Lincoln, Lane, and Benton Counties, Oregon: U.S. Geological Survey Miscellaneous Investigations Series Map I–866, scale 1:62,500.

———1976c, Geologic map of the Yaquina and Toledo quadrangles: U.S. Geological Survey Miscellaneous Investigations Series Map I–867, scale 1:62,500.

Snavely, P.D., Jr., and McClellan, P.H., 1987, Preliminary geologic interpretation of USGS *S.P. Lee* seismic-reflection profile WO 76–7 on the continental shelf and upper slope, northwestern Oregon: U.S. Geological Survey Open-File Report 87–612, 12 p.

Snavely, P.D., Jr., Niem, A.R., and MacLeod, N.S., 1989, Geology of the coastal area between Cape Flattery and Cape Alava, northwest Washington: U.S. Geological Survey Open-File Report 89–141, scale 1:24,000.

Snavely, P.D., Jr., Niem, A.R., MacLeod, N.S., Pearl, J.E., and Rau, W.W., 1980, Makah Formation—A deep marginal basin sedimentary sequence of upper Eocene and Oligocene age in the northwestern Olympic Peninsula, Washington: U.S. Geological Survey Professional Paper 1162–B, 28 p.

Snavely, P.D., Jr., Niem, A.R., and Pearl, J.E., 1978 [1979], Twin River Group (upper Eocene to lower Miocene)—Defined to include the Hoko River, Makah, and Pysht Formations, Clallam County, Washington, *in* Sohl, N.F., and Wright, W.B., eds., Changes in stratigraphic nomenclature by the U.S. Geological Survey, 1977: U.S. Geological Survey Bulletin 1457–A, p. A111–A120.

Snavely, P.D., Jr., Pearl, J.E., and Lander, D.L., 1977, Interim report on petroleum resources potential and geologic hazards in the outer continental shelf—Oregon and Washington Tertiary province: U.S. Geological Survey Open-File Report 77–282, 64 p.

Snavely, P.D., Jr., and Vokes, H.E., 1949, Geology of the coastal area from Cape Kiwanda to Cape Foulweather, Oregon: U.S. Geological Survey Oil and Gas Investigations Preliminary Map 97, scale 1:62,000.

Snavely, P.D., Jr., Huene, Roland von, and Miller, John, 1987, The central Oregon margin lines WO76–4, *in* Huene, Roland von, ed., Seismic images of convergent margin tectonic structure: American Association of Petroleum Geologists Studies in Geology 26, p. 24–27.

Snavely, P.D., Jr., and Wagner, H.C., 1963, Tertiary geologic history of western Oregon and Washington: Washington Division of Mines and Geology Report of Investigations 22, 25 p.

———1980, Generalized isopach map of Tertiary sedimentary rocks, western Oregon and Washington and adjacent continental margin: U.S. Geological Survey Open-File Report 80–889, scale 1:1,000,000.

———1981, Geologic cross section across the continental margin off Cape Flattery, Washington, and Vancouver Island, British Columbia: U.S. Geological Survey Open-File Report 81–978, 6 p.

———1982, Geologic cross section across the continental margin of southwestern Washington: U.S. Geological Survey Open-File Report 82–459, 10 p.

Snavely, P.D., Jr., Wagner, H.C., and Lander, D.L., 1980, Geological cross section of the central Oregon continental margin: Geological Society of America Map and Chart Series MC–28J, scale 1:250,000.

———1985, Land-sea geologic cross section of the southern Oregon continental margin: U.S. Geological Survey Miscellaneous Investigations Series Map I–1463, scale 1:125,000.

Snavely, P.D., Jr., Wagner, H.C., and MacLeod, N.S., 1964, Rhythmic-bedded eugeosynclinal deposits of the Tyee Formation—Oregon Coast Range, *in* Symposium on cyclic sedimentation: Kansas Geological Survey Bulletin 169, p. 461–480.

Snavely, P.D., Jr., Wagner, H.C., and Rau, W.W., 1982, Sections showing biostratigraphy and correlation of Tertiary rocks penetrated in wells drilled on the southern Oregon continental margin: U.S. Geological Survey Miscellaneous Field Studies Map MF–1482.

Snavely, P.D., Jr., and Wells, R.E., 1984, Tertiary volcanic and intrusive rocks on the Oregon and Washington continental shelf: U.S. Geological Survey Open-File Report 84–282, 17 p.

Spence, William, 1989, Stress origins and earthquake potential in Cascadia: Journal of Geophysical Research, v. 94, p. 3076–3088.

Stewart, R.J., 1974, Zeolite facies metamorphism of sandstone in the western Olympic Peninsula, Washington: Geological Society of America Bulletin, v. 85, no. 7, p. 1139–1142.

Tabor, R.W., 1972, Age of the Olympic metamorphism, Washington—K/Ar dating of low-grade metamorphic rocks: Geological Society of America Bulletin, v. 83, no. 6, p. 1805–1816.

Tabor, R.W., 1975, Guide to the geology of Olympic National Park: Seattle, University of Washington Press, 144 p.

Tabor, R.W., and Cady, W.M., 1978a, The structure of the Olympic Mountains, Washington—Analysis of a subduction zone: U.S. Geological Survey Professional Paper 1033, 38 p.

———1978b, Geologic map of the Olympic Peninsula, Washington: U.S. Geological Survey Miscellaneous Investigations Series Map I–994, scale 1:125,000.

Tabor, R.W., Frizzell, V.A., Jr., Vance, J.A., and Naeser, C.W., 1984, Ages and stratigraphy of lower and middle Tertiary sedimentary and volcanic rocks of the central Cascades, Washington—Application to the tectonic history of the Straight Creek fault: Geological Society of America Bulletin, v. 95, no. 1, p. 26–44.

Tabor, R.W., Yeats, R.S., and Sorensen, M.L., 1972, Geologic map of the Mount Angeles quadrangle, Clallam and Jefferson Counties, Washington: U.S. Geological Survey Geologic Quadrangle Map GQ–958, scale 1:62,500.

Tolan, T.L., and Reidel, S.P., 1989, Structure map of a portion of the Columbia River flood-basalt province, *in* Reidel, S.P., and Hooper, P.R., eds., Volcanism and tectonism in the Columbia River flood-basalt province: Geological Society of America Special Paper 239, scale 1:500,000.

Vokes, H.E., and Snavely, P.D., Jr., 1948, The age and relationships of the Eugene and Fisher Formations: Geological Society of the Oregon Country News Letter, v. 14, no. 5, p. 38–41.

Wagner, H.C., and Tomson, J.H., 1987, Geologic history and hazards geology within the Strait of Juan de Fuca: Washington Division of Geology and Earth Resources Open-File Report 87–1, 15 p., 7 pls.

Walsh, T.J., Korosec, M.A., Phillips, W.M., Logan, R.L., and Schasse, H.W., 1987, Geologic map of Washington—Southwest quadrant: Washington State Department of Natural Resources Geologic Map GM–34, scale 1:250,000.

Warren, W.C., Grivetti, R.M., and Norbisrath, Hans, 1945, Geology of northwestern Oregon west of Willamette River and north of latitude 45°15': U.S. Geological Survey Oil and Gas Investigations Preliminary Map 42, scale 1:145,728.

Weaver, C.S., and Smith, S.W., 1983, Regional tectonic and earthquake hazards implications of a crustal fault zone in southwestern Washington: Journal of Geophysical Research, v. 88, no. B12, p. 10371–10383.

Wells, R.E., 1981, Geologic map of the eastern Willapa hills, Cowlitz, Lewis, Pacific, and Wahkiakum Counties, Washington: U.S. Geological Survey Open-File Report 81–674, scale 1:62,500.

———1989, Mechanisms of Cenozoic tectonic rotation, Pacific Northwest convergent margin, U.S.A., *in* Kiessel, Catherine, and Laj, Carlo, eds., Paleomagnetic rotations and continental deformation, "NATO Advanced Study Institute Series C, 254": Dordrecht, The Netherlands, Kluwer Academic Publishers, p. 313–325.

Wells, R.E., and Coe, R.S., 1985, Paleomagnetism and geology of Eocene volcanic rocks of southwest Washington—Implications for mechanisms of tectonic rotation: Journal of Geophysical Research, v. 90, no. B2, p. 1925–1947.

Wells, R.E., Engebretson, D.C., Snavely, P.D., Jr., and Coe, R.S., 1984, Cenozoic plate motions and the volcano-tectonic evolution of western Oregon and Washington: Tectonics, v. 3, no. 2, p. 275–294.

Wells, R.E., and Heller, P.L., 1988, The relative contribution of accretion, shear, and extension to Cenozoic tectonic rotation in the Pacific Northwest: Geological Society of America Bulletin, v. 100, no. 3, p. 325–338.

Wells, R.E., Niem, A.R., MacLeod, N.S., Snavely, P.D., Jr., and Niem, W.A., 1983, Preliminary geologic map of the west half of the Vancouver (Washington-Oregon) 1° by 2° quadrangle, Oregon: U.S. Geological Survey Open-File Report 83–591, scale 1:250,000.

Werner, K.S., Graven, E.P., Berkman, T.A., and Parker, M.J., 1988, Direction of maximum horizontal compression in western Oregon determined by borehole breakouts: EOS [American Geophysical Union Transactions], v. 69, no. 44, p. 1455.

Wolfe, E.W., and McKee, E.H., 1968, Geologic map of Grays River quadrangle, Wahkiakum and Pacific Counties, Washington: Washington Division of Mines and Geology Map GM–4, 6 p.

———1972, Sedimentary and igneous rocks of the Grays River quadrangle, Washington: U.S. Geological Survey Bulletin 1335, 70 p.

Wolfe, J.A., Gower, H.D., and Vine, J.D., 1961, Age and correlation of the Puget Group, King County, Washington, *in* Short papers in the geologic and hydrologic sciences, articles 147–292: U.S. Geological Survey Professional Paper 424–C, p. C230–C232.

Zoback, M.L., and Zoback, M.D., 1989, Tectonic stress field of the continental United States, *in* Pakiser, L.C., and Mooney, W.D., eds., Geophysical framework of the continental United States: Boulder, Colo., Geological Society of America Memoir 172, p. 523–540.

TECTONICS OF THE WILLAMETTE VALLEY, OREGON

By Robert S. Yeats,[1] Erik P. Graven,[1, 2] Kenneth S. Werner,[1, 3] Chris Goldfinger,[1] *and* Thomas A. Popowski[1]

ABSTRACT

The Willamette Valley is a lowland separating the Oregon Coast Range from the Cascade Range. Three separate basins within this lowland were studied: the southern Willamette Valley south of and including the Salem and Waldo Hills, the northern Willamette Valley between the Salem and Waldo Hills and the Chehalem Mountains, and the Tualatin basin northeast of the Chehalem Mountains and southwest of the Tualatin Mountains.

The rocks of the Willamette Valley are similar to those of the Coast Range, beginning with oceanic basalt of the Siletz River Volcanics of early and middle Eocene age and deep-water turbidite strata of the Tyee Formation of middle Eocene age. Overlying strata of late Eocene and early Oligocene age grade westward from volcanogenic rocks to deep-water sedimentary rocks, showing that arc volcanism east of the Willamette Valley may have begun as early as 47 Ma but not as early as 50 Ma, the age of the Tyee Formation. Nonmarine and marine strata as young as early Miocene were tilted westward prior to 16–14.5 Ma, when flows of the Columbia River Basalt Group moved through a lowland in the Cascade Range, across the northern Willamette Valley, and thence to the coast as intracanyon flows. The Columbia River Basalt Group is overlain, locally with angular unconformity, by fluvial deposits of the proto-Willamette River and its tributaries, the first strata to be limited to the modern Willamette Valley. These deposits are poorly dated but may range in age from late Miocene to Pleistocene. In the northern Willamette Valley, these strata are overlain by vents and intruded by small stocks of the Boring Lavas. After a period of erosion, the fluvial deposits were succeeded by glacial-outwash deposits of the Rowland Formation and by catastrophic flood deposits of the Willamette Formation, both of late Pleistocene age.

Faults and folds began to develop in Eocene time, accompanying clockwise rotation of crustal blocks. Most prominent of these early structures is the Corvallis fault, a low-angle thrust fault with horizontal separation estimated to be 11–13 km. Faults and folds affecting the Columbia River Basalt Group and younger fluvial deposits include a high-angle reactivation of the Corvallis fault, the Owl Creek fault, the Harrisburg anticline, the Mill Creek fault, the Waldo Hills range-front fault, the Gales Creek-Mount Angel structural zone, the Yamhill-Sherwood structural zone, the Northern Willamette downwarp, the Beaverton and Helvetia faults in the Tualatin valley, and faults at the northern margin of the Willamette Valley probably related to emplacement of Boring Lavas.

Faults postdating the Columbia River Basalt Group trend predominantly northwest and northeast, and folds trend predominantly east-west, compatible with the modern stress field in which maximum horizontal compressive stress is oriented north-south. Limited evidence suggests relatively low slip rates, probably less than 0.5 mm/year. Individual faults are relatively short, but brittle crust may extend to depths as great as 30 km, indicating a capability of generating moderate-size earthquakes with long recurrence intervals.

INTRODUCTION

The Willamette Valley is part of a broad lowland separating the Oregon Coast Range from the Cascade Range (fig. 76). The lowland is 120 km long and extends north from Eugene, Oreg., to about 30 km north of Vancouver, Wash. The lowland is more than 60 km wide at the latitude of Portland, where it includes the Portland and Tualatin basins, and only 30 km wide in the southern Willamette Valley south of Albany (fig. 77). The lowland contains four metropolitan areas, Portland-Vancouver, Salem, Corvallis-Albany, and Eugene-Springfield, and many smaller towns. The lowland is divided into separate basins by narrow ridges underlain by the Miocene Columbia River Basalt Group (fig. 77). The Tualatin Mountains (Portland Hills) separate the Portland

[1]Department of Geosciences, Oregon State University, Corvallis, OR 97331.

[2]Unocal Corp., Anchorage, AK 99519.

[3]Unocal Corp., Lafayette, LA 70505.

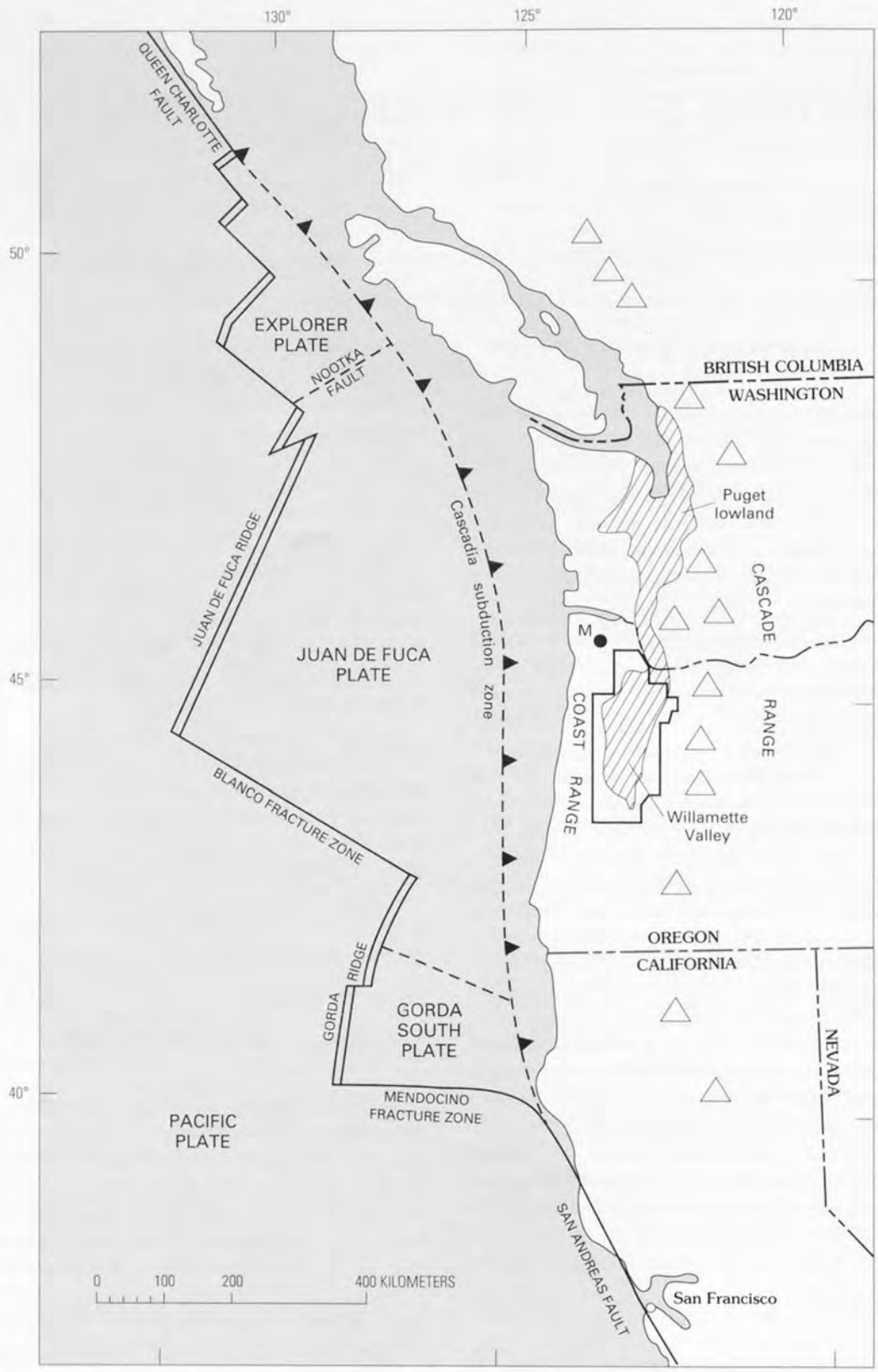

Figure 76. Plate boundaries of the Pacific Northwest showing locations of tectonic features and the Willamette Valley study area. Heavy line, study-area boundary; hatched area, Willamette Valley and Puget lowland; sawteeth denote upper plate of thrust fault. Major stratovolcanoes are shown by open triangles. Dot labeled "M" in northwestern Oregon is the Mist gas field.

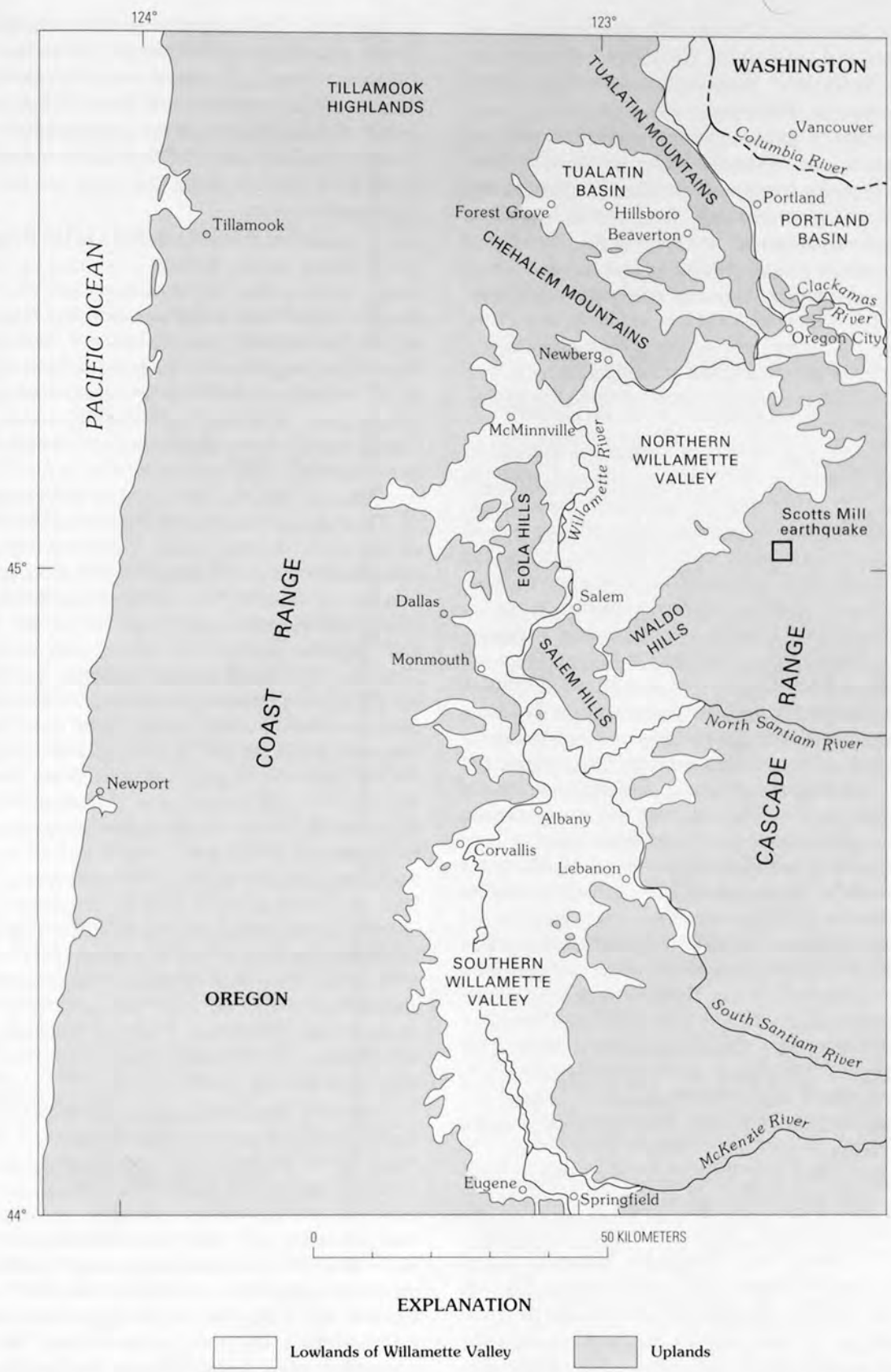

Figure 77. Geographic and physiographic features of the Willamette Valley and Portland and Tualatin basins, northwestern Oregon. The square indicates the epicenter of the March 25, 1993, Scotts Mills earthquake.

and Tualatin basins, the Chehalem Mountains separate the Tualatin basin and the northern Willamette Valley, and the Salem and Waldo Hills separate the northern Willamette Valley and southern Willamette Valley.

With respect to the Cascadia subduction zone and Cascade volcanic arc, the Willamette Valley has the same structural position as the Puget lowland (fig. 76), but the two lowlands are not connected (fig. 77). North of Vancouver and south of Eugene, east-dipping rocks of the Coast Range abut directly against and are overlain by rocks of the Cascade Range. The pre-middle Miocene stratigraphic sequence underlying the Willamette Valley is similar to that of the Coast Range, the upper part of the section containing a higher percentage of volcanic and volcaniclastic rocks than the lower part, reflecting the proximity of the valley to Cascade arc volcanoes.

The structure of northwestern Oregon is dominated by a broad, north-plunging anticlinorium centered over the Coast Range. The western flank of this anticlinorium, including the Oregon coast, contains strata of the same age as those of the eastern flank dipping into the Willamette Valley. The strata dip east across the Willamette Valley and into the western Cascade Range, so that most of the strata that predate the Columbia River Basalt Group of the Willamette Valley are older than rocks of the western Cascade Range. The north plunge of the anticlinorium permits correlation of strata as young as Miocene across the Coast Range near the Columbia River (Niem and Niem, 1985). Smaller scale structures include faults and open folds in both the Coast Range and Willamette Valley. Some of these structures involve the Miocene Columbia River Basalt Group and younger strata, but other structures formed mainly in Eocene time.

The oldest exposed rocks in the region are the Siletz River Volcanics, which are basalt flows and breccias of early and middle Eocene age. The lavas are similar in composition to ocean-ridge or oceanic-plateau basalt and are interpreted to be a result of rifting and extension of an elongate basin prior to the deposition of the Tyee Formation of middle Eocene age (Wells and others, 1984). The Tyee Formation, derived from pre-Tertiary plutonic rocks and a volcanic-arc terrane to the south, prograded northward along a basin axis centered on the Coast Range. The Tyee consists of distal turbidites in the latitude of the southern Willamette Valley (Chan and Dott, 1983).

The lower part of the upper Eocene Yamhill Formation, largely fine grained, overlaps the Tyee Formation to rest directly on the Siletz River Volcanics. It is the oldest formation in the Willamette Valley that grades eastward into volcanic rocks possibly related to the early western Cascade Range (Baker, 1988). In the northern Coast Range, the Yamhill is overlain by and possibly interbedded with the Tillamook Volcanics (Wells and others, 1983). In the Willamette Valley, the Yamhill is overlain by the sand-rich upper Eocene Spencer Formation, which grades northward into the Cowlitz Formation and southeastward into the volcanic-rich Fisher Formation. The overlying marine Eocene and Oligocene Eugene Formation and the marine and nonmarine Oligocene and early Miocene Scotts Mills Formation grade southeastward into volcanic rocks of the western Cascade Range and rest unconformably on western Cascade volcanic rocks. The equivalents of the Eugene and Scotts Mills formations on the coast are the Alsea and Yaquina Formations.

About 16–14.5 Ma, basalt flows of the Columbia River Basalt Group moved through a lowland in the Cascade Range between the Columbia River and the Clackamas River into the northern Willamette Valley (Beeson, Tolan, and Anderson, 1989). The N_2 flows of the Grande Ronde Basalt and Ginkgo flows of the Frenchman Springs Member of the Wanapum Basalt have identical counterparts on the Oregon coast, indicating that these flows also crossed the Coast Range, probably as intracanyon flows (Beeson, Tolan, and Anderson, 1989).

Alluvial deposits that postdate the Columbia River Basalt Group are the oldest strata to be confined principally to the present lowland areas. These deposits include the lacustrine (informal) Monroe clay of late Miocene to early Pliocene age (Roberts, 1984; Roberts and Whitehead, 1984) in the southern Willamette Valley and the Helvetia Formation (Schlicker and Deacon, 1967), Sandy River Mudstone (Trimble, 1963), and Troutdale Formation (Lowry and Baldwin, 1952) in the northern Willamette Valley; the Troutdale Formation was derived in large part from the ancestral Columbia River. In late Pliocene to Pleistocene time, the Boring Lavas were erupted from vents in the Portland basin, Tualatin basin, and northernmost Willamette Valley (fig. 77) (Allen, 1975). Some volcanic centers in the western Cascade Range are also of this age.

The Quaternary history of the area is characterized by alluvial deposits and land surfaces influenced by glaciation in the Cascade Range and changes in sea level or in the longitudinal profile of the Columbia River (McDowell, 1991). Near the end of Pleistocene time, catastrophic glacial-outburst floods from the Columbia River repeatedly inundated the Willamette Valley as far south as Eugene and deposited the Willamette Formation (Balster and Parsons, 1969; Allison, 1978).

We have compiled and field checked existing bedrock mapping (pl. 2) in and around the Willamette Valley lowland except for the Portland basin, which is being described separately by the Oregon Department of Geology and Mineral Industries. We mapped the subsurface geology of the lowland itself using data from oil-exploration wells (plotted on pl. 2A and 2B) and multichannel seismic profiles that were part of an exploration campaign in the 1970's and 1980's together with a network of gravity stations, the data from which were already in the public domain. The subsurface interpretation of sediments younger than the Columbia River Basalt Group is based largely on data from water wells and boreholes drilled for engineering purposes by the Oregon Department of Transportation.

Responsibilities for individual parts of the geologic map (pl. 2) are: southern Willamette Valley, E.P. Graven; Corvallis fault, Chris Goldfinger; northern Willamette Valley, K.S. Werner; and Tualatin valley, T.A. Popowski. A more detailed description of the geology is in Goldfinger (1990), Graven (1990), Werner (1990), and Popowski (1995).

ACKNOWLEDGMENTS

This project was supported by grant 14-08-0001-G1522 from the Earthquake Hazards Reduction Program, U.S. Geological Survey. Additional funding was provided by ARCO Oil and Gas Co. and the Peter P. Johnson Scholarship Committee. We thank ARCO Oil and Gas Co., Northwest Natural Gas Co., Mobil Oil Corp., and Seismological Data Services for allowing us to use proprietary data, including seismic profiles. Oil-exploration-well records were provided by the Oregon Department of Geology and Mineral Industries, supplemented by data from individual operators. Water-well records were obtained from the Oregon Department of Water Resources. Core holes through the alluvial deposits that postdate the Columbia River Basalt Group were provided by the Oregon Department of Transportation. Aerial photographs taken in 1980 were provided by the Environmental Remote Sensing Applications Laboratory at Oregon State University. Synthetic seismograms are based on a program written by John Shay. Drafting was done by independent contractors Paula Pitts and Linda Haygarth, and by Camela Carstarphen and Margaret Mumford of Oregon State University.

We benefited much from discussions of Coast Range stratigraphy with Jack Meyer, Alan Niem, Wendy Niem, Ulrich Franz, and Ray Wells; of Columbia River Basalt Group distribution with Marvin Beeson; of western Cascade Range geology with George Priest, David Sherrod, and Edward Taylor; of Portland basin and eastern Tualatin basin geology with Ian Madin; of Willamette Valley alluvial stratigraphy with Marshall Gannett, Bernard Kleutsch, and Patricia McDowell; and of Willamette Valley gravity data with Richard Couch, Robert O'Malley, and Gerald Connard. Marvin Beeson, Ian Madin, and George Priest reviewed the manuscript.

STRATIGRAPHY

Correlation of stratigraphic units (fig. 78) is based on radiometric ages, benthic foraminifers, and calcareous nannoplankton. Nannoplankton are correlated to zones that are widely distributed in the northern Pacific Ocean and are believed to be close to contemporaneous throughout this region. A preliminary zonation for Paleogene strata based on coccoliths (Bukry and Snavely, 1988) shows some discordance with zonation based on benthic foraminifers. Benthic foraminiferal zones shown here are those of Kleinpell (1938) and Mallory (1959) and are based on stratigraphic sections in California. These zones are strongly influenced by bathymetry and sedimentary environments. Comparisons with open-ocean planktic zones show that the benthic zones are time transgressive within California basins (Crouch and Bukry, 1979; Poore, 1976, 1980); extension of these zones to Oregon adds additional uncertainty in time correlation. Nonetheless, most of the fossils found in northwest Oregon are benthic foraminifers, hence the Kleinpell and Mallory benthic zones are the only ones available for biostratigraphic correlations of most surface and subsurface sections.

SILETZ RIVER VOLCANICS

Oceanic basalts and interbedded basaltic sedimentary rocks assigned to the Siletz River Volcanics and dated as 58.1±1.5 to 50.7±3.1 Ma (Duncan, 1982) form the basement that underlies the Tertiary rocks of the Coast Range and Willamette Valley. The formation was originally named the Siletz River Volcanic Series by Snavely and Baldwin (1948) for exposures on the Siletz River and its tributaries in the central Oregon Coast Range. Snavely and others (1968) renamed the formation the Siletz River Volcanics and divided it into a lower unit consisting of submarine tholeiitic, fine-grained, amygdaloidal pillow basalt and breccia and an upper unit of submarine and subaerial alkali basalt, with the upper unit of much smaller volume than the lower unit. Sedimentary interbeds yielded marine microfossils that Snavely and others (1968) and McWilliams (1980) referred to the Penutian and Ulatisian benthic stages of Mallory (1959), in general agreement with the radiometric ages. Coccoliths from this formation in the Coast Range west of the Willamette River are referred to Subzone CP 10, estimated as about 55.3–53.7 Ma (Bukry and Snavely, 1988).

The Siletz River Volcanics exposed northwest of Corvallis belong mainly to the lower unit of the formation as described by Snavely and others (1968). The volcanic rocks are overlain by, and partly interbedded with, as much as 1,000 m of thin-bedded brown to gray tuffaceous marine siltstone and shale called the Kings Valley Siltstone Member (of the Siletz River Volcanics) by Vokes and others (1954). The Kings Valley Siltstone Member contains thin lenses of basaltic sandstone, a few thin layers of white tuff, and rare foraminifers and carbonaceous debris. The sandstone lenses contain clasts of basalt together with a terrigenous component derived from the east. Coccoliths from the Kings Valley Siltstone Member, as well as similar strata farther west, are referred to Subzone CP 11, estimated as about 53.7–52.5 Ma (Bukry and Snavely, 1988).

Northwest of McMinnville, the Siletz River Volcanics consist of vesicular basalt flows, pillow basalt, flow breccia, and tuff breccia with interbeds of red to green calcareous sandy tuff (Baldwin and others, 1955). The top of the unit contains medium- to dark-gray, calcareous, tuffaceous shale, siltstone, and sandstone (Brownfield and Schlicker, 1981a; Brownfield, 1982b).

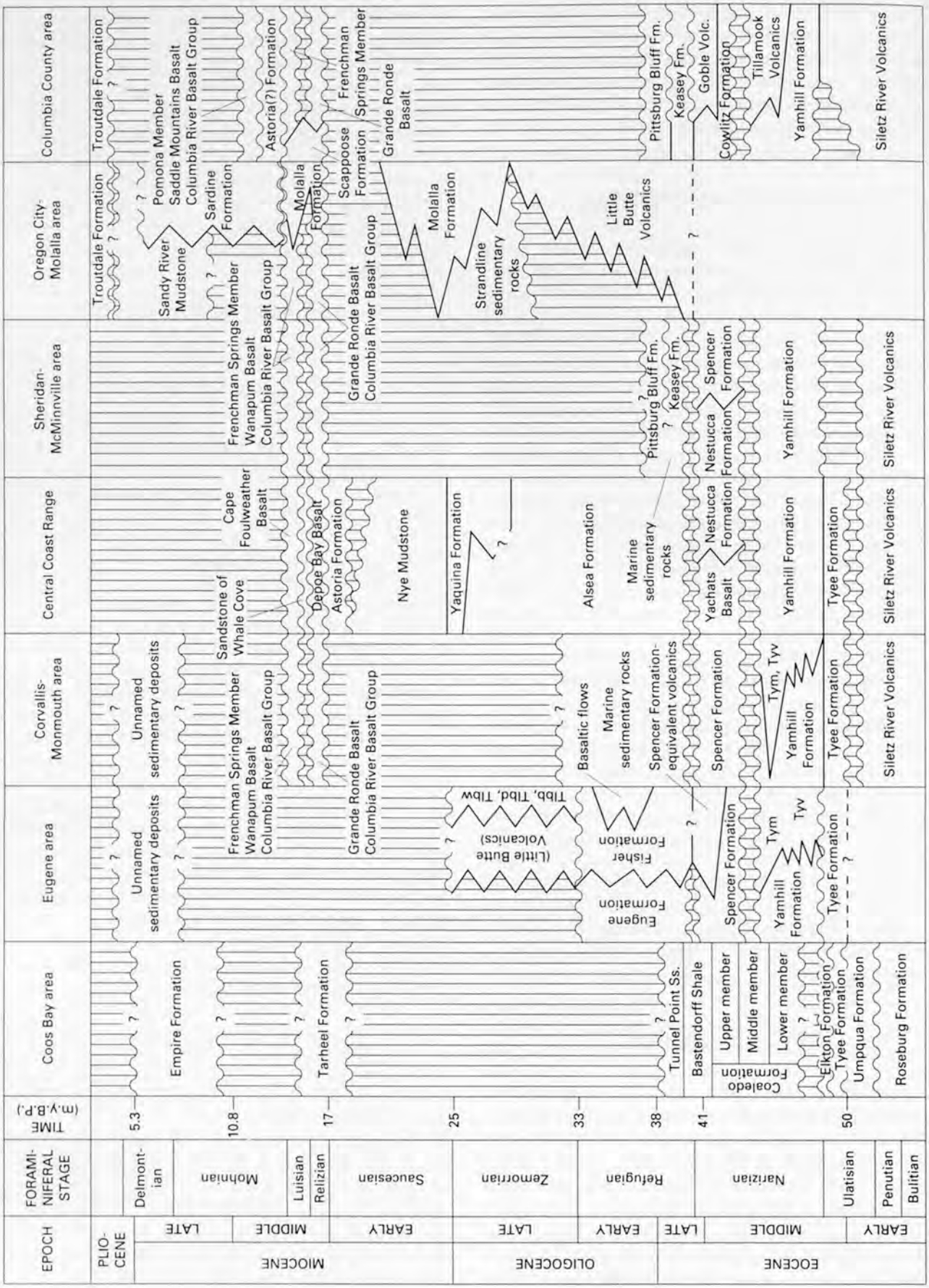
EPOCH
FORAMINIFERAL STAGE
TIME (m.y.B.P.)
Coos Bay area
Eugene area
Corvallis-Monmouth area
Central Coast Range
Sheridan-McMinnville area
Oregon City-Molalla area
Columbia County area
PLIOCENE
MIOCENE
OLIGOCENE
EOCENE
LATE
MIDDLE
EARLY
Delmontian
Mohnian
Luisian
Relizian
Saucesian
Zemorrian
Refugian
Narizian
Ulatisian
Penutian
Bulitian
5.3
10.8
17
25
33
38
41
50
Empire Formation
Tarheel Formation
Tunnel Point Ss.
Bastendorff Shale
Upper member
Middle member
Lower member
Coaledo Formation
Elkton Formation
Tyee Formation
Umpqua Formation
Roseburg Formation
Unnamed sedimentary deposits
Frenchman Springs Member
Wanapum Basalt
Columbia River Basalt Group
Grande Ronde Basalt
Eugene Formation
Fisher Formation
(Little Butte Volcanics)
Tlbb, Tlbd, Tlbw
Spencer Formation
Tym
Tyv
Yamhill Formation
Tyee Formation
Siletz River Volcanics
Sandstone of Whale Cove
Cape Foulweather Basalt
Depoe Bay Basalt
Astoria Formation
Nye Mudstone
Yaquina Formation
Alsea Formation
Basaltic flows
Marine sedimentary rocks
Spencer Formation-equivalent volcanics
Tym, Tyv
Marine sedimentary rocks
Yachats Basalt
Nestucca Formation
Spencer Formation
Yamhill Formation
Tyee Formation
Siletz River Volcanics
Troutdale Formation
Pomona Member
Saddle Mountains Basalt
Columbia River Basalt Group
Sandy River Mudstone
Sardine Formation
Astoria(?) Formation
Molalla Formation
Scappoose Formation
Frenchman Springs Member
Grande Ronde Basalt
Columbia River Basalt Group
Molalla Formation
Strandline sedimentary rocks
Little Butte Volcanics
Pittsburg Bluff Fm.
Keasey Fm.
Goble Volc.
Cowlitz Formation
Tillamook Volcanics
Yamhill Formation
Siletz River Volcanics

The Siletz River Volcanics were found in the Gulf Porter 1 and Humble Miller 1 exploratory wells (pl. 2B) in the southern Willamette Valley, where they contain interbeds of marine strata 3–30 m thick. In the northern Willamette Valley, the Reichold Finn 1 well (pl. 2A) contains 1,110 m of the Siletz River Volcanics, predominantly gray tuff, tuffaceous shale, siltstone, and sandstone with Ulatisian (including late Ulatisian) microfossils indicating lower middle bathyal to tropical inner neritic bathymetry (McKeel, 1984). The Siletz River Volcanics in the Reserve Bruer 1 well (pl. 2A) consist of volcanic breccia and red and green tuff. Synthetic seismograms of the Reserve Bruer 1 and Reichold Finn 1 wells show an abrupt increase in sonic velocity at the top of the Siletz River Volcanics and a gradual increase below, except for a sharp increase at the top of the volcanic breccia (Werner, 1990). The seismic expression of the top of the Siletz River Volcanics is irregular or discontinuous, possibly due to preservation of original flow tops or to erosion, as suggested for field exposures by Brownfield (1982b).

The base of the Siletz River Volcanics is neither exposed nor found in wells, so the thickness of the unit is unknown, although Snavely and others (1968) proposed that its thickness exceeds 6 km. An east-west seismic profile in the southern Willamette Valley near Bellfountain shows a zone of horizontal to gently west-dipping reflectors beneath the Siletz River Volcanics, suggesting a maximum thickness of 8 km, thinning eastward beneath the Willamette Valley (Keach and others, 1989). The Siletz River Volcanics have resistivities of around 100 ohm-meters; this resistive unit is underlain by a near-horizontal unit of low resistivity (Wannamaker and others, 1989). If this low-resistivity unit is not part of the Siletz River Volcanics, the thickness of the Siletz River could be as little as 2 km.

The Siletz River Volcanics are correlative with basalts of the Roseburg Formation (Baldwin, 1974) in southern Oregon, the Crescent Formation of Washington, and the Metchosin Volcanics of southern Vancouver Island (Snavely and others, 1968; Tabor and Cady, 1978); volcanic rocks at the northern and southern ends of the outcrop areas of these units are older than those closer to the Columbia River (Duncan, 1982). Taken together, these volcanic formations are considered to be part of a seamount chain (Siletzia) accreted to North America prior to deposition of the Tyee Formation of middle Eocene age (Duncan, 1982) or, alternatively, they are basalts erupted during oblique rifting of allochthonous terranes now found in southern Alaska (Wells and others, 1984). The location of the eastern boundary of this seamount terrane is unknown; it may lie beneath the western Cascade Range. A linear zone of high-frequency magnetic anomalies beneath the western Cascade Range foothills (Committee for the Magnetic Anomaly Map of North America, 1987) is similar to the magnetic signature of ophiolite and thus may be caused by mafic and ultramafic rocks marking the suture zone between Siletzia and North America (Johnson and others, 1990).

TYEE FORMATION

Sandstone that forms the Tyee Formation, first described by Diller (1896) in the southern Oregon Coast Range, extends for more than 260 km along the Coast Range from the Rogue River north to the latitude of Salem (Molenaar, 1985). The Tyee Formation consists of a deltaic facies to the south and a deep-sea fan facies to the north (Lovell, 1969; Chan and Dott, 1983; Heller and Dickinson, 1985). Its thickness is 1,200 m near Eugene and decreases northward to 500 m west of Dallas, where mudstone and thin-graded sandstone and siltstone of the Tyee Formation abut a highland underlain by the Siletz River Volcanics. Farther north, the Tyee is overlapped by the Yamhill Formation. The thickness of the Tyee Formation also decreases eastward in the southern Willamette Valley to 315 m in the Gulf Porter 1 well and 51 m in the Humble Miller 1 well (pl. 2B). In the Gulf Porter 1 well, strata assigned to the Yamhill Formation may be fine-grained equivalents of the Tyee Formation in the Coast Range. The Mobil Ira Baker 1 well was terminated after penetrating 92 m of fossiliferous siltstone and arkosic sandstone correlated with the Tyee Formation. The age of the Tyee is Ulatisian or middle Eocene (Molenaar, 1985), and microfossils in its most distal northern exposures indicate deposition in at least middle bathyal water depths (McKeel, 1985; Heller and Dickinson, 1985). Coccoliths from the Tyee Formation in the Coast Range west of the Willamette Valley are referred to Subzones CP 12a and 12b, resulting in an age estimate of 52.5–50 Ma for the Tyee (Bukry and Snavely, 1988).

The Tyee Formation is derived from the south, and it shows no evidence of Cascade volcanism to the east. The source was largely plutonic but included a volcanic arc, also south of the Coast Range (Chan and Dott, 1983). Snavely and others (1964) suggested that the source of Tyee sandstones was the Klamath Mountains of southern Oregon and northern California. Heller and others (1985) subsequently found evidence of a Precambrian crustal component in Tyee sedimentary materials, and they concluded that the major source of the Tyee was the Idaho batholith, now far away to the east but presumably closer to the Oregon Coast Range prior to clockwise rotation of the Coast Range (Wells and Heller, 1988).

Figure 78 (facing page). Stratigraphic correlation chart for Tertiary rocks of western Oregon. Foraminiferal stages from Kleinpell (1938) and Mallory (1959). Tym, Miller sand of the Yamhill Formation; Tyv, volcanic rocks of the Yamhill Formation; MOd, dacite and rhyodacite of the Little Butte Volcanics; MOb, basalt and basaltic andesite of the Little Butte Volcanics; MOt, welded to nonwelded ash-flow tuff of the Little Butte Volcanics; m.y.B.P., million years before present. Modified from Armentrout and others (1983).

YAMHILL FORMATION

The Yamhill Formation was named by Baldwin and others (1955) for exposures in Mill Creek, a tributary of the South Yamhill River southwest of Sheridan. In the type locality, the formation consists of 150 m of tuffaceous siltstone and shale overlain by 150 m of basaltic sandstone and siltstone and 1,050 m of micaceous mudstone and siltstone. In the subsurface of the northern Willamette Valley, the Yamhill Formation consists largely of shale and siltstone with minor tuffaceous strata and fine-grained graded sandstone showing partial Bouma sequences (Richard E. Thoms, Portland State University, oral commun., 1991). The Yamhill thickens eastward across coeval normal faults to at least 932 m thick in the Reichold Bagdanoff 23–28 well (pl. 2A), where it includes basalt and tuff.

The Yamhill Formation includes the informally named Miller sand of Bruer and others (1984), known only from the subsurface in the Willamette Valley south of Salem. This is a sandy to conglomeratic volcaniclastic unit overlain by and interfingering northwestward with faintly bedded micaceous siltstone and mudstone (Baker, 1988). The Miller sand pinches out to the northwest, suggesting coeval displacement on the nearby Corvallis fault. The Miller sand increases in thickness southeastward as an underlying mudstone unit decreases in thickness, although the overall thickness of the Yamhill Formation increases as well. Farther southeast, both the Miller sand and the underlying mudstone grade into a volcanic facies. The Gulf Porter 1 well (pl. 2B) penetrated 1,055 m of volcaniclastic sandstone and siltstone and basaltic conglomerate, and the Mobil Ira Baker 1 well (pl. 2B) contains 1,961 m of basalt, andesite, dacite, tuff, and minor tuffaceous mudstone, siltstone, volcaniclastic sandstone, and breccia, all probably equivalent to the Yamhill.

The Miller sand contains microfossils indicating shallow-marine deposition, whereas the overlying and underlying mudstone members of the Yamhill Formation were deposited in upper to middle bathyal water depths (McKeel, 1984, 1985). Foraminiferal assemblages in the type section of the Yamhill are assigned to the early Narizian stage (McWilliams, 1980; Brownfield, 1982b; D.R. McKeel, written comm., 1987). Foraminifers in the Reserve Bruer 1 and Reichold Finn 1 wells in the northern Willamette Valley are early Narizian in age at the base of the Yamhill and Narizian in age for the remainder of the formation. The Yamhill in the Reichold Bagdanoff 23–28 well yielded early Narizian to late Ulatisian foraminiferal assemblages (McKeel, 1984). In the Coast Range south of Eugene, the Elkton Formation and Lorane Siltstone (Bird, 1967; Heller and Dickinson, 1985) have Ulatisian and early Narizian foraminifers. Coccoliths from the Yamhill Formation in the Coast Range west of the northern Willamette Valley are referred to Subzone CP 13c and CP 14a, the ages of which are estimated as 47 Ma to about 42.5 Ma (Bukry and Snavely, 1988). However, coccoliths from the Elkton Formation and Lorane Siltstone are referred to Subzone CP 12b, close to the age of the Tyee Formation (Bukry and Snavely, 1988), suggesting that these formations are older than the Yamhill Formation despite the presence of Ulatisian and early Narizian foraminifers in all three formations. The Yamhill changes facies eastward in the subsurface of the Willamette Valley to arclike volcanic rocks (Baker, 1988), suggesting either that the Cascade arc began to develop earlier than the 43–41 Ma (Lux, 1982; Priest and Vogt, 1983; Verplanck and Duncan, 1987; Taylor, 1990) or 35 Ma (Priest, 1990) ages that are generally accepted based on surface geology or that the volcanism that produced the Clarno Formation, widespread in eastern Oregon, extended this far to the west.

In the Coast Range west of the Tualatin valley, the Yamhill Formation interfingers with and is overlain by the Tillamook Volcanics (Wells and others, 1983). The Yamhill is intruded by a sill of zeolitized gabbro with a potassium-argon age on plagioclase of 43.2±1.8 Ma (L.G. Pickthorn, *in* Bukry and Snavely, 1988). Strata with Narizian microfossils underlying the Cowlitz Formation in the Mist gas field (fig. 76) are also referred to the Yamhill Formation by Bruer and others (1984), but these beds contain late Narizian microfossils and overlie the Tillamook Volcanics; they were described by Niem and Niem (1985) as their informal Hamlet formation. The Yamhill Formation in the northern Willamette Valley, where volcanics are not present, may include in its upper part strata equivalent to the informal Hamlet formation of the northern Oregon Coast Range, although no late Narizian microfossils have been found in the Yamhill Formation.

TILLAMOOK VOLCANICS

The Gales Peak area (pl. 2A) west of the Tualatin basin is underlain by basalt correlated by Wells and others (1983) with the Tillamook Volcanics of the northern Coast Range. Contact relations with adjacent sedimentary rocks are unclear due to faulting and poor exposure. In the Nahama and Weagant Klohs 1 well (pl. 2A) in the Tualatin basin, Refugian strata overlie zeolitized basalt that is interbedded with unfossiliferous marine siltstone, claystone, and minor sandstone; this basalt may either be the Tillamook Volcanics, Goble Volcanics, or basalt of Waverly Heights. The Yamhill Formation and Tillamook Volcanics may be interbedded in the Texaco Cooper Mountain 1 well (pl. 2A) between 945 and 2,823 m well depth. The volcanic rocks below 2,124 m in the Richfield Barber 1 well (pl. 2A) may be the Tillamook Volcanics.

In the Tillamook Highlands (fig. 77), the Tillamook Volcanics consist of a lower unit of submarine basalt with sedimentary interbeds containing early Narizian microfossils (W.W. Rau, *in* Wells and others, 1983) overlain by mostly subaerial basalt. Potassium-argon ages from the middle and lower parts of the sequence are 46.0±0.9 to 42.7±0.5 Ma (Magill and others, 1981); an age of 33.4±0.5 Ma is reported in Wells and others (1983).

BASALT OF WAVERLY HEIGHTS

At Waverly Heights in Milwaukie, along the Willamette River south of Portland, the Columbia River Basalt Group is underlain with angular unconformity by a sequence of subaerial basalt flows and associated sedimentary rocks, probably marine (Beeson, Tolan, and Madin, 1989). The top of the unit is marked by a thick soil zone. Potassium-argon ages from two flows are dated about 40 Ma (R.A. Duncan, *in* Beeson, Tolan, and Madin, 1989), younger than the Siletz River Volcanics, and the unit is probably correlative with the Tillamook Volcanics. This unit may be present in wells in the Tualatin basin, but its presence has not been confirmed.

SPENCER FORMATION AND CORRELATIVE UNITS (COWLITZ AND NESTUCCA FORMATIONS)

The Spencer Formation, named by Turner (1938) for exposures near Eugene, crops out along the western edge of the Willamette Valley from south of Eugene north to the Chehalem Mountains adjacent to the Tualatin basin. Microfossils are referred to the late Narizian. The Spencer is divided into two members (Al Azzaby, 1980; Baker, 1988; Richard E. Thoms, Portland State University, oral commun., 1991). The lower member consists of micaceous, arkosic sandstone, siltstone, and minor coal deposited in a strandline to middle-shelf environment. West of the Tualatin basin, the lower member ranges in thickness from 60 m near Henry Hagg Lake to about 300 m of predominately clean arkosic sand south of Patton Valley (Richard E. Thoms, Portland State University, oral commun., 1991). In the Quintana Gath 1, Linn County Oil Barr 1, American Quasar Hickey 9–12, and Mobil Ira Baker 1 wells (pl. 2B) in the southern Willamette Valley, this member changes to tuffaceous strata eastward and interfingers and grades upward into volcanic rocks of Cascade Range origin. In the American Quasar Wolverton 13–31 and Humble Miller 1 wells (pl. 2B) north of Albany, the lower member includes basalt, andesite, and tuff. Microfossils studied by McKeel (1984, 1985) indicate middle to inner neritic water depths along the western side of the valley and inner neritic water depths to possibly nonmarine along the eastern edge of the valley (Hickey 1 well). Thicknesses in the southern Willamette Valley vary from 230 m in the Reichold Northwest Natural Gas Merrill 1 and Oregon Natural Gas Independence 12–25 wells (pl. 2B) to 310 m in the American Quasar Wolverton 13–31 well.

The upper member consists of mudstone, siltstone, and subordinate sandstone, grading eastward to tuffaceous strata and volcanic rocks (American Quasar Wolverton 13–31 and Gulf Porter 1 wells, pl. 2B). Along the eastern edge of the valley (Quintana Gath 1, American Quasar Hickey 9–12, Linn County Oil Barr 1, and Mobil Ira Baker 1 wells, pl. 2B), the upper member consists of volcanic and volcaniclastic strata correlative in part with the lower part of the Fisher Formation in the Eugene area. The mudstone and siltstone of the upper member of the Spencer Formation in the southern Willamette Valley were deposited in upper bathyal water depths deepening upsection to middle bathyal depths (McKeel, 1984, 1985). The thickness of the upper member in the southern Willamette Valley ranges from 100 m in the American Quasar M & P Farms 33–24 and American Quasar Wolverton 13–31 wells to 178 m in the Gulf Porter 1 well (pl. 2B).

Near the Corvallis fault, the Spencer Formation overlies the Tyee Formation directly with an angular unconformity of as much as 90° difference in dip. The Spencer Formation, where it is in fault contact with the Siletz River Volcanics along the Corvallis fault between Corvallis and Philomath, consists of fossiliferous tuffaceous, basaltic sandstone and conglomerate with clasts as much as 2 m in diameter derived from the Siletz River Volcanics.

The Spencer Formation also consists of a lower (predominantly sandstone) member and an upper (siltstone and mudstone) member in the northern Willamette Valley. The formation thins northward from 760 m near Dallas to 490 m in Yamhill and Washington Counties, and it thins eastward from 325 m in the Reserve Bruer 1 well to 45 m in the Oregon Natural Gas DeShazer 13–22 well (pl. 2A). In the Tualatin basin, the Spencer Formation is 400 m thick near Henry Hagg Lake. North of Forest Grove, strata correlative with the Spencer Formation are referred to the Cowlitz Formation, which rests unconformably on the Tillamook Volcanics. The Cowlitz comprises a lower unit consisting of a basal conglomerate overlain by siltstone (the informal Hamlet formation of Niem and Niem, 1985), the C&W sandstone of local usage that produces gas in the Mist gas field, and an upper siltstone member. The upper two members may be present in the Texaco Cooper Mountain 1 well (pl. 2A).

The Nestucca Formation, originally described by Snavely and Vokes (1949), overlies the Yamhill Formation with angular unconformity in the Coast Range west of McMinnville. It appears to be a deeper water facies equivalent of the Spencer Formation and correlates with the informal Hamlet formation of the northern Coast Range of Oregon. The Nestucca Formation consists of tuffaceous shale and siltstone and thin-bedded sandstone with interbeds of pillow basalt, breccia, and tuff (Baldwin and others, 1955) grading into the Yachats Basalt and the basalt of Cascade Head. Foraminifers are assigned to the late Narizian (W.W. Rau, *in* Wells and others, 1983), and coccoliths are assigned to Subzones CP 15a and CP 15b, giving an age estimate by Bukry and Snavely (1988) of about 38.5–36.7 Ma.

FISHER FORMATION

Nonmarine volcaniclastic strata and interfingering flows in the Eugene area as far north as Cox Butte, west of Junction City, are mapped as the Fisher Formation (Vokes and others, 1951). This formation is 1,680 m thick and consists of andesitic lapilli tuff and breccia, tuffaceous sandstone and siltstone, and pebble to boulder conglomerate interbedded with flows of predominantly andesite and subordinate basalt and dacite (Hoover, 1963). These rocks extend south of Eugene and may be stratigraphically equivalent to the Calapooya Formation and Colestin Formation of the southern Oregon Cascade Range (Wells and Waters, 1934; Peck and others, 1964). They make up unit T_5 of Sherrod and Smith (1989), with an age estimated as 45–35 Ma.

Fossil leaves in the lower part of the Fisher Formation south of Cottage Grove (25 km south of Eugene) suggest a late Eocene age (R.W. Brown, *in* Hoover, 1963). Radiometric ages from basalt and basaltic andesite near the top of the formation are 40–35 Ma (Lux, 1982), close to the youngest age inferred for the Narizian stage of Mallory (1959). The Fisher appears to interfinger northward with the marine Eugene Formation of latest Eocene (Narizian) and Oligocene (Refugian) age (Vokes and others, 1951). The basalt flows dated by Lux (1982) were considered by Vokes and others (1951) to overlie the Fisher and Eugene Formations unconformably, but Walker and Duncan (1989) suggest that these flows are age equivalents of (and thus part of) the Fisher Formation.

In the subsurface of the southern Willamette Valley, the Mobil Ira Baker 1 well (pl. 2B) penetrated 143 m of volcanic and volcaniclastic rocks overlying Narizian marine strata. Between the Salem Hills and Tualatin basin, the marine equivalents of the Fisher Formation are notably free of volcanic rocks. In the Quintana Gath 1 well (pl. 2B), a 440-m-thick volcanic unit bracketed by strata with late Narizian and Refugian microfossils may be equivalent to the Fisher Formation. Still farther north, the Goble Volcanics are interbedded with the Cowlitz Formation; the Goble Volcanics, like the Fisher Formation, are arc-related rocks (Phillips and others, 1989).

EOCENE AND OLIGOCENE MARINE STRATA

North and west of the Tualatin basin, marine strata of Eocene and Oligocene age are mapped as the Keasey Formation and the overlying Pittsburg Bluff Formation (Wells and others, 1983). The Keasey Formation is predominantly thick, light-gray tuffaceous claystone and siltstone with minor mudstone and sandstone; foraminifers are late Narizian and early Refugian in age (McWilliams, 1968, 1973; Brownfield and Schlicker, 1981a). North of Henry Hagg Lake, the Pittsburg Bluff Formation consists of as much as 1,400 m of greenish-gray to gray, tuffaceous, glauconitic and basaltic litharenite sandstone, siltstone, and minor conglomerate with foraminifers of the Refugian Stage (Richard E. Thoms, Portland State University, oral commun., 1991).

West of the Eola Hills, the Keasey Formation consists of sandy tuffaceous siltstone, and the Pittsburg Bluff Formation consists of tuffaceous sandstone, tuff, and tuffaceous shale and siltstone deposited in shallower water than the Keasey Formation. The Reichold Werner 14–21 and Oregon Natural Gas Werner 34–21 and DeShazer 13–22 wells (pl. 2A) in the northern Willamette Valley document an angular unconformity between the Keasey Formation and the Pittsburg Bluff Formation. The two units together are about 715 m thick in the Eola Hills near Amity (Brownfield, 1982b).

In the southern Willamette Valley, feldspathic, tuffaceous sandstone and siltstone containing Refugian foraminifers of Eocene and Oligocene age constitute the Eugene Formation. The formation is 550 m thick in the hills east of Coburg, which includes 343 m of strata penetrated in the Mobil Ira Baker 1 well, more than 800 m thick in the Lebanon area, including strata in the American Quasar Hickey 9–12 well, and 780 m thick beneath the Salem Hills, based on data from the Oregon Natural Gas Independence 12–25 and Reichold Northwest Natural Gas Merrill 1 wells (pl. 2B). The formation is best exposed in the hills east of Coburg, at Peterson Butte, and at the base of the Salem Hills. To the south, the Eugene Formation interfingers with the nonmarine Fisher Formation.

LITTLE BUTTE VOLCANICS

The Little Butte Volcanic Series of Wells (1956) and Peck and others (1964), which is here renamed the Little Butte Volcanics in accordance with Article 38 of the (1983) North American Stratigraphic Code, makes up the base of the exposed western Cascade Range sequence on the eastern margin of the southern Willamette Valley, where it overlies the Eugene Formation, and the northern Willamette Valley, where it is overlain unconformably by the Oligocene and Miocene Scotts Mills Formation and the Miocene Columbia River Basalt Group (Miller and Orr, 1988).

We subdivide the Little Butte Volcanics into basalt and basaltic andesite flows of Walker and Duncan (1989), porphyritic andesite flows of Hampton (1972), dacite to rhyodacite vent complexes of Walker and Duncan (1989) and Bristow (1959), and welded ash-flow tuff in the foothills of the Cascade Range northeast of Eugene (Walker and Duncan, 1989). The age range of the Little Butte Volcanics is 35–17 Ma (Sutter, 1978; Lux, 1982; Walker and Duncan, 1989), corresponding to the T_4 and T_3 time units of Sherrod and Smith (1989). However, many of the rocks in the Eugene area described as Little Butte Volcanics by Lux (1982) yield radiometric ages older than 35 Ma. Lux (1982) reported radiometric ages of 41.5±0.9 Ma and 39.2±0.5 Ma east of Lebanon. However, Verplanck (1985) redated a sample from one of these localities as 31.7±0.4 Ma.

In the Eugene area, Little Butte Volcanics unconformably overlie the Eocene and Oligocene Fisher and Eugene Formations (W.N. Orr, *in* Armentrout and others, 1983). However, Peck and others (1964) found tongues of Eugene Formation interfingering with Little Butte Volcanics south of Brownsville, Beaulieu (1974) noted similar relations to the north in Linn County, and the Quintana Gath 1 well in southwestern Marion County near Salem contains volcanic rocks interbedded with the Eugene Formation. These volcanic rocks are more likely correlated to the Fisher Formation discussed above rather than to the Little Butte Volcanics. The volcanic rocks are not found in the Reichold Northwest Natural Gas Merrill 1, Oregon Natural Gas Independence 12–25, and Erntson Schermacher 1 wells (pl. 2B) to the west. Following eruption, the Little Butte Volcanics were tilted gently to the east and eroded prior to deposition of the Scotts Mills Formation in the northern Willamette Valley (discussed below). Peck and others (1964) considered the volcanic sequence to be between 1,300 and 2,600 m in thickness throughout most of the western Cascade Range. The volcanic rocks appear to thin to the west. Near Washburn Butte, about 750 m of volcanic rocks lie between the Eugene Formation and Miocene-Pliocene andesite that probably overlies the Little Butte Volcanics with angular unconformity. The Humble Wicks 1 well, 10 km southeast of Silverton, penetrated 1,830 m of volcanic rocks, which may include units other than the Little Butte Volcanics.

Sedimentary formations correlative with the Little Butte Volcanics include the Alsea Formation and Yaquina Formation near Newport and the informally named Oswald West formation of Niem and others (1985) of the northern Oregon coast. These formations are older than 25 Ma and thus fall within the time range of the Little Butte Volcanics. The Alsea Formation is referred to Coccolith Zone CP 16 of 36.5–35 Ma age (Bukry and Snavely, 1988). The Scotts Mills Formation and Molalla Formation (Lowry and Baldwin, 1952) are late Oligocene and early Miocene in age (Miller and Orr, 1988), also within the time range of the Little Butte Volcanics. However, these formations overlie the Little Butte Volcanics unconformably in the Molalla and Silverton areas (Miller and Orr, 1988).

INTRUSIVE ROCKS OF THE COAST RANGE

Gabbroic sills, dikes, and laccoliths are common in the central and northern Oregon Coast Range. The best known is the Marys Peak sill, 390 m thick, which intrudes the Tyee Formation near its basal contact with the Kings Valley Siltstone Member of the Siletz River Volcanics. The sill is a highly differentiated, titanium-rich body of granophyric gabbro and granophyric diorite with abundant aplite dikes near its upper chilled contact (Roberts, 1953). The Marys Peak sill was dated as 29.7±1.2 Ma (middle Oligocene) (P.D. Snavely, Jr., *in* Clark, 1969). Other large intrusive bodies of similar lithology are found south of Philomath and at Bald Hills, Dimple Hill, Vineyard Hill, Coffin Butte, Logsden Ridge, and Witham Hill (Snavely and Wagner, 1961; Snavely and others, 1980). The remanent magnetization of the Marys Peak sill is normally polarized (Clark, 1969), as it is for all the other intrusions field checked in the Corvallis and Albany area, supporting the suggestion of Snavely and Wagner (1961) that the middle Oligocene intrusive episode was of short duration. Elongate dikes striking west to west-northwest are found near the Corvallis fault. Northeast-striking dikes intrude the fault, and northeast-striking sills occupy fold hinges parallel to the fault in the Tyee and Spencer Formations, indicating that strong folding predated intrusion. A dike intrudes the west-northwest-striking Philomath fault that offsets the Corvallis fault, but no other intrusions were found associated with other northwest-striking faults offsetting the Corvallis fault.

Sills, presumably of Eocene age, intrude Eocene marine strata of the Willamette Valley as young as the Eugene Formation. In the southern Willamette Valley, a sill intruding at the Spencer-Yamhill Formation contact was found in the Gulf Porter 1 well (pl. 2B) and is marked by a high-amplitude reflector on a seismic profile. There are dikes in several of the buttes on the eastern edge of the valley. An intrusion at Skinner Butte in Eugene was dated at 30.3±0.9 and 29.4±0.9 Ma (J.G. Smith, *in* Walker and Duncan, 1989), the same age as the Marys Peak sill. Intrusions along the eastern edge of the valley are mapped as Oligocene to Miocene in age (Beaulieu, 1974; Walker and Duncan, 1989) and presumably fed volcanic rocks of the western Cascade Range.

SCOTTS MILLS FORMATION

Marine and nonmarine strata of the Scotts Mills Formation (Miller and Orr, 1988) of late Oligocene and early Miocene age are exposed in the Cascade Range foothills east of Silverton adjacent to the northern Willamette Valley. Miller and Orr (1988) divide the Scotts Mills Formation into the Marquam Member, 300–500 m thick, overlain by and interfingering with the Abiqua Member, 300 m thick, which grades laterally into the Crooked Finger Member, 200 m thick. The Marquam Member unconformably overlies the Little Butte Volcanics on a surface with regional relief of as much as 100 m. The marine Marquam Member includes cross-stratified barnacle limestone, fossiliferous conglomerate, burrowed claystone, tuffaceous sandstone, and graded mudstone, indicating deposition along a rocky coast (Miller and Orr, 1988). The Abiqua Member is composed of marine and nonmarine volcanic arkose, and the Crooked Finger Member consists of nonmarine volcanic conglomerate and mudstone. The three members constitute a prograding delta complex that developed southwest of a volcanic headland underlain by the Little Butte Volcanics. The Scotts Mills

Formation is found in two wells drilled in the Waldo Hills, the Humble Wicks 1 well (pl. 2B) that penetrated 239 m of volcanic rocks, claystone, siltstone, sandstone, and rare volcanic conglomerate and the RH Exploration Anderson 1 well (pl. 2A), which penetrated 140 m of an upward-coarsening sequence of sandstone, siltstone, and claystone with volcanic fragments. These strata overlie the Little Butte Volcanics in both wells. The absence of the Scotts Mills in other wells to the west is probably due to eastward tilting and erosion prior to deposition of the Columbia River Basalt Group.

It is unclear how the Scotts Mills Formation is related to other formations of the same age in western Oregon.

MOLALLA FORMATION

The Molalla Formation (Harper, 1946; Lowry and Baldwin, 1952) consists of about 300 m of nonmarine tuffaceous conglomerate, sandstone, siltstone, and water-laid tuff with paleosols in the foothills of the northern Willamette Valley east of Silverton. The Molalla Formation is exposed in stream valleys in the Waldo Hills; it is not found in any exploratory wells. The lower part of the Molalla Formation rests unconformably on the Little Butte Volcanics, is interbedded with the upper members of the Scotts Mills Formation, and is overlain unconformably by the Columbia River Basalt Group (Miller and Orr, 1988), volcanic rocks of the Sardine Formation, and the upper part of the Molalla Formation. Strata included in the upper part of the Molalla Formation appear to be interbedded with the Columbia River Basalt Group (Miller and Orr, 1988). Fossil leaves in the Molalla Formation were dated as early Miocene (J.A. Wolfe, *in* Peck and others, 1964). Radiometric ages of tuff beds in the Molalla are 15.9±1.0 Ma and 15.0±0.7 Ma (Fiebelkorn and others, 1983). Thus, the age of the Molalla Formation ranges from perhaps as old as late Oligocene to middle Miocene. Conglomerate mapped as part of the Troutdale Formation by Peck and others (1964) in this area is considered to be part of the Molalla Formation.

SCAPPOOSE FORMATION

Fine-grained shallow marine sedimentary deposits interfingered with fluvial sandstone, coal-bearing mudstone, and conglomerate make up the middle Miocene Scappoose Formation (Van Atta and Kelty, 1985). The weakly consolidated strata are commonly exposed in steep slopes capped by the resistant Columbia River Basalt Group. More than 275 m of Scappoose strata disconformably overlie the Keasey and Pittsburg Bluff Formations north of the Tualatin basin, and at least 335 m overlie Pittsburg Bluff strata on the western flank of the Chehalem Mountains.

The Scappoose Formation was deposited in an estuarine or deltaic to shallow-marine environment over a dissected paleotopography with relief of as much as 245 m. Basaltic conglomerate derived from low-magnesium flows of the Grande Ronde Basalt commonly occurs near the base of the formation. The upper contact is conformable with the Columbia River Basalt Group; Scappoose strata frequently are intercalated with Grande Ronde flows and overlain by flows of either the Grande Ronde Basalt or Wanapum Basalt (Frenchman Springs Member) (Van Atta and Kelty, 1985).

The Scappoose Formation is probably entirely middle Miocene in age, based on the occurrence of clasts of the Grande Ronde Basalt within the basal conglomerate and flows of the Columbia River Basalt Group overlying the unit. Partly correlative strata in the northern Coast Range and northern Willamette Valley are the Astoria and Scotts Mills Formations, respectively.

COLUMBIA RIVER BASALT GROUP

Flood-basalt flows of the Columbia River Basalt Group were erupted from fissures in eastern Oregon and Washington and western Idaho from 16.5–6 Ma. Some of these flows traversed the Cascade Range via the Columbia trans-arc lowland, which extended from the Columbia River 60 km south to the Clackamas River (Beeson, Tolan, and Anderson, 1989; Beeson and Tolan, 1990) and reached as far as the present-day Pacific coast, where they are interbedded with marine strata. As noted by Beeson and others (1975) and Beeson, Tolan, and Anderson (1989), some of the broad folds and faults of the Oregon Cascade Range and Willamette Valley were active during the emplacement of the Columbia River Basalt Group. These folds and faults include the Portland Hills-Clackamas River structural zone that limited some of the flows of the Grande Ronde Basalt and Wanapum Basalt into the Portland basin and the lower reaches of the Columbia River, and the Gales Creek-Mount Angel structural zone, which formed a barrier to some flows of the Wanapum Basalt. Only the R_2 and N_2 flows of the Grande Ronde Basalt (about 16–15.6 Ma) and the basalts of Ginkgo, Silver Falls, Sand Hollow, and Sentinel Gap of the Wanapum Basalt (about 15.3 Ma; Beeson and others, 1985) crossed the Portland Hills-Clackamas River structural zone and entered the northern Willamette Valley.

The Columbia River Basalt Group underlies nearly all of the Portland, Tualatin, and northern Willamette Valleys. Water wells penetrate more than 200 m of basalt beneath parts of the Tualatin basin (Popowski, 1995). Erosionally resistant basalt comprises most of the exposures in the Waldo, Salem, and Eola Hills, the Red Hills of Dundee, the Tualatin Mountains (Portland Hills), Petes Mountain, Parrett Mountain, Cooper and Bull Mountains, and the Chehalem Mountains. The Grande Ronde Basalt makes up most of the volume of the Columbia River Basalt Group west of the

Cascade Range, as it does in the Columbia Plateau to the east, extending into the Willamette Valley as far south as Franklin Butte, 3 km southeast of Scio. There were no active Cascade Range volcanic centers in the lowland through which the flows of the Grande Ronde Basalt crossed the Cascades (Beeson, Tolan, and Anderson, 1989). Whereas the flows of the Grande Ronde Basalt blanketed most of the northern Willamette Valley, some of the flow units of the Wanapum Basalt tended to follow channels. One channel of the Ginkgo flows crossed the Cascade Range beneath the future site of Mt. Hood and followed the southward-convex arc of the Waldo, Salem, and Eola Hills (Beeson, Tolan, and Anderson, 1989). Basalt on the Oregon coast near Newport is geochemically identical to the Ginkgo flows, suggesting that the Ginkgo flows continued across to the coast prior to most of the uplift of the Coast Range. Another Ginkgo flow passed north of the Willamette Valley in such a way that the intervening northern Willamette Valley contains no flows of the Wanapum Basalt, only those of the Grande Ronde Basalt (Beeson, Tolan, and Anderson, 1989; Tolan and others, 1989; Wells and others, 1989). Similarly, the Wanapum Basalt is absent in the Tualatin basin. The Silver Falls and Sand Hollow basalt flows moved southwest along the axis of the Waldo Hills, and the basalt of Sand Hollow at Hungry Hills is the southernmost exposure of the Columbia River Basalt Group in the Willamette Valley (Beeson and others, 1985; Beeson, Tolan, and Anderson, 1989). The Waldo, Salem, and Eola Hills show a reversal in topography because they were a low area during the time of Ginkgo eruptive activity. The Columbia River Basalt Group is 100–180 m thick in the Salem Hills.

The Columbia River Basalt Group rests with angular unconformity on older units: the Molalla Formation and Scotts Mills Formation east of the Willamette Valley and the Eocene and Oligocene marine sequence in the Salem and Eola Hills. Thus, the homocline composing the western Cascade Range dipped east prior to the eruption of the Columbia River Basalt Group (Priest, 1990).

SARDINE FORMATION

Volcanic and volcaniclastic rocks of the western Cascade Range, erupted after emplacement of the Columbia River Basalt Group, were called the Sardine Formation by Peck and others (1964). The volcanic rocks postdate a period of relative quiescence in the Cascade Range between 17 and 13.5 Ma (Sherrod and Smith, 1989), between Episodes 1 and 2 of Priest (1990). The Sardine Formation is regarded as Miocene and Pliocene in age. The formation is equivalent to the Sardine Series of Thayer (1939) and includes rocks described as the Fern Ridge Tuffs by Thayer (1939), the Rhododendron Formation by Hodge (1933), and the Outerson Basalt by Hammond (1979) and Hammond and others (1980). In the study area, the Sardine Formation includes basalt at Marks Ridge northeast of Sweet Home, basaltic andesite at Washburn Butte, nonmarine tuffaceous strata overlying the Columbia River Basalt Group in the Waldo Hills, and volcanic and volcaniclastic rocks resting on east-dipping rocks of the Little Butte Volcanics southeast of the Waldo Hills. Adjacent to the northern Willamette Valley, breccia and tuff of the Rhododendron Formation are overlain unconformably by pyroxene andesite flows, with the unconformity marked by a laterite (Hampton, 1972). This volcanism was more calc-alkaline than that prior to eruption of the Columbia River Basalt Group, and it consists of lava flows and debris flows of intermediate composition with locally abundant basalt and basaltic andesite (Priest and Vogt, 1983). The basalt at Marks Ridge was dated at 4.5±0.28 Ma (Episode 3 of Priest, 1990), and the basaltic andesite at Washburn Butte was dated at 11.9±0.3 Ma (Verplanck, 1985; Episode 2 of Priest, 1990).

NONMARINE FINE-GRAINED SEDIMENTARY DEPOSITS

In the Portland, Tualatin, and Willamette basins, the Columbia River Basalt Group and older rocks were deeply eroded, developing a topographic surface with as much as 250 m relief. These rocks are overlain unconformably by moderately to poorly lithified siltstone, sandstone, mudstone, and claystone with common wood fragments and local volcanic ash and pumice sand. The sequence exposed along the Clackamas and Sandy Rivers was named the Sandy River Mudstone by Trimble (1963), who considered the mode of deposition to be lacustrine. However, sedimentary structures along the Clackamas River suggest a fluvial origin (C.D. Peterson, Portland State University, and A.R. Niem, Oregon State University, oral commun., 1989). Deeply weathered fluvial and loessal silts interbedded with gravels dominated by clasts of the Columbia River Basalt Group in the Tualatin basin were mapped as the Helvetia Formation by Schlicker and Deacon (1967). These sedimentary deposits are at least 240–275 m thick in the Portland basin, 350 m thick west of Beaverton, and 410 m thick beneath Hillsboro in the center of the Tualatin basin. The presence of clasts of granite and quartzite together with abundant quartz and mica and more locally derived clasts suggests that the greater part of these sedimentary materials was deposited by the ancestral Columbia River with some contribution by side streams draining the Cascade Range and the rising Tualatin Mountains.

South of the Portland basin, correlative sedimentary deposits are identified mainly in the subsurface, where they are known to water-well drillers as the so-called blue clay. In the northern Willamette Valley (pl. 2B), the contact between these deposits and the Columbia River Basalt Group is marked in some wells by a laterite. The sedimentary deposits increase in thickness northeastward, from 160 m in the Reichold Bagdanoff 23–28 well and Reichold

Werner 14–21 well to 265 m in the Oregon Natural Gas DeShazer 13–22 well and 300 m in the Damon Stauffer Farms 35–1 well. In the northern Willamette Valley and Tualatin basin, the sedimentary deposits are characterized on seismic profiles as a lower sequence with low-amplitude reflectors and an upper sequence with medium- to high-amplitude reflectors. Paleontologic analysis of borehole cuttings from the Tualatin basin indicates that this upper sequence probably is latest Pliocene or early Pleistocene in age (Unruh and others, 1994).

In the southern Willamette Valley south of the Salem Hills, a sequence of clay with intercalated sand and gravel was found to overlie marine Eocene strata along a surface of moderate relief (Niem and others, 1987) and is as much as 100 m thick near the center of the valley. Corehole DH 13–88 obtained by the Oregon State Highway Division at Corvallis penetrated 42 m of greenish-blue to blue-gray micaceous clay with minor interlayered sand, dark-brown organic clay, and poorly developed paleosols with rootlets in growth position, suggesting a fluvial origin (fig. 79). In another corehole at Corvallis, a multicolored paleosol is at the base of the clay unit. In corehole DH 14–90 between Sublimity and Stayton, the Columbia River Basalt Group is overlain by blue to dark-gray clay with intercalations of volcaniclastic sand and with paleosols with rootlets in growth position (fig. 80). Near Monroe, several coreholes penetrated a clay unit informally named the Monroe clay and dated as late Miocene to early Pliocene on the basis of palynology (Roberts and Whitehead, 1984). Roberts and Whitehead (1984) interpreted the Monroe clay as lacustrine in origin, in contrast to the fluvial interpretation for clays from the Oregon State Highway Division coreholes. Toward the center of the southern Willamette Valley, the clay is interbedded with sand and gravel that Graven (1990) interpreted as part of the main channel of the proto-Willamette River (figs. 81 and 82). However, more detailed study of water wells by Marshall Gannett (U.S. Geological Survey, oral commun., 1993) and Paul Crenna (Oregon State University, oral commun., 1993) shows that the coarser grained deposits are part of glaciofluvial fans from the Cascade Range. Drainage from a fan emerging from the drainage basin of the North Santiam River at Stayton (pl. 2B) appears to have flowed through a narrow water gap at the eastern margin of the Salem Hills now occupied by Mill Creek, an underfit stream. A channel beneath the present-day Willamette River west of the Salem Hills is filled by fine-grained sedimentary deposits rather than the sand-and-gravel fan facies found in the channel beneath Mill Creek. The main entry point is in the Eugene-Springfield area, where a 90-m-thick sequence of sand and gravel was called the Springfield delta by Frank (1973). A similar gravel fan is found near Salem at the north end of the Mill Creek watergap. Seismic profiles in the northern Willamette Valley and Tualatin basin show a prominent series of reflectors midway in the sedimentary sequence that are coarse clastic units in the Tualatin basin, based on water-well logs. Other side channels underlie the present North Santiam River and South Santiam River on the east side of the valley and Long Tom Creek at the southwestern corner of the valley.

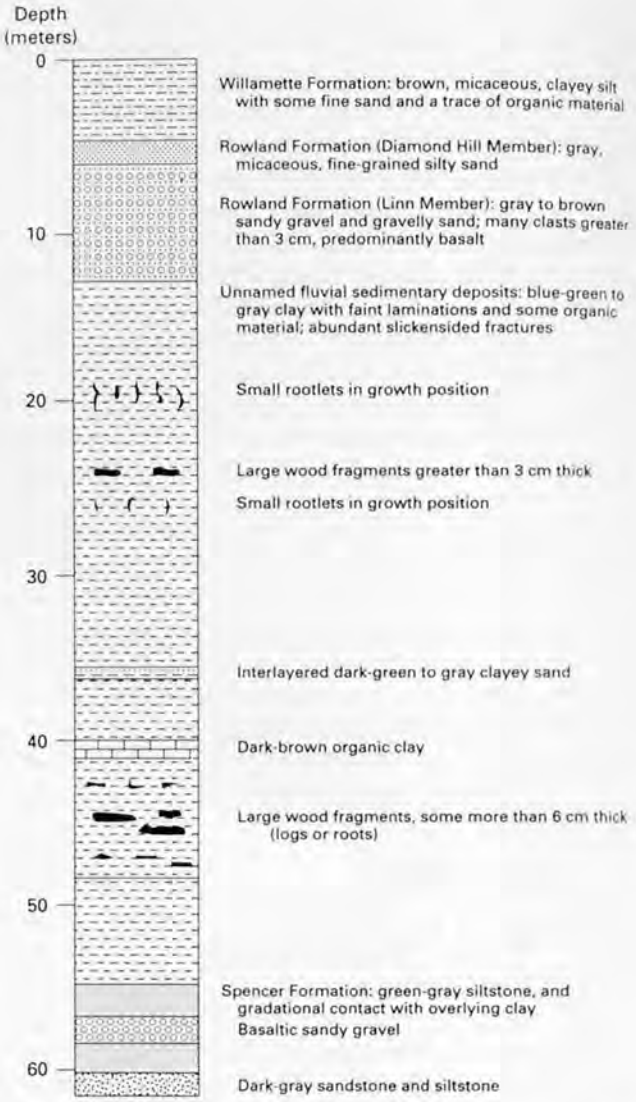

Figure 79. Graphic log of corehole DH 13–88, drilled on the southeast side of Corvallis, Oreg., just east of the intersection of State Highways 34 and 99W (see pl. 3 and fig. 82 for location of corehole). Total depth represented is 47.9 m.

TROUTDALE FORMATION

The moderately to well-indurated pebble to cobble conglomerate with a silt and sand matrix in the Portland basin is referred to the Troutdale Formation (Hodge, 1933; Trimble, 1963). The conglomerate clasts are predominantly derived from the Columbia River Basalt Group with significant percentages of exotic clasts such as quartzite and granite, indicating deposition by the ancestral Columbia River (ancestral Columbia River facies of the Troutdale Formation of Tolan and Beeson, 1984). The upper part of the ancestral Columbia River facies includes sandstone containing basaltic glass together with interbeds of conglomerate with clasts of high-alumina basalt derived from the Boring Lavas and the informally named High Cascade lavas, and the subordinate foreign clasts (Tolan and Beeson, 1984; Swanson, 1986).

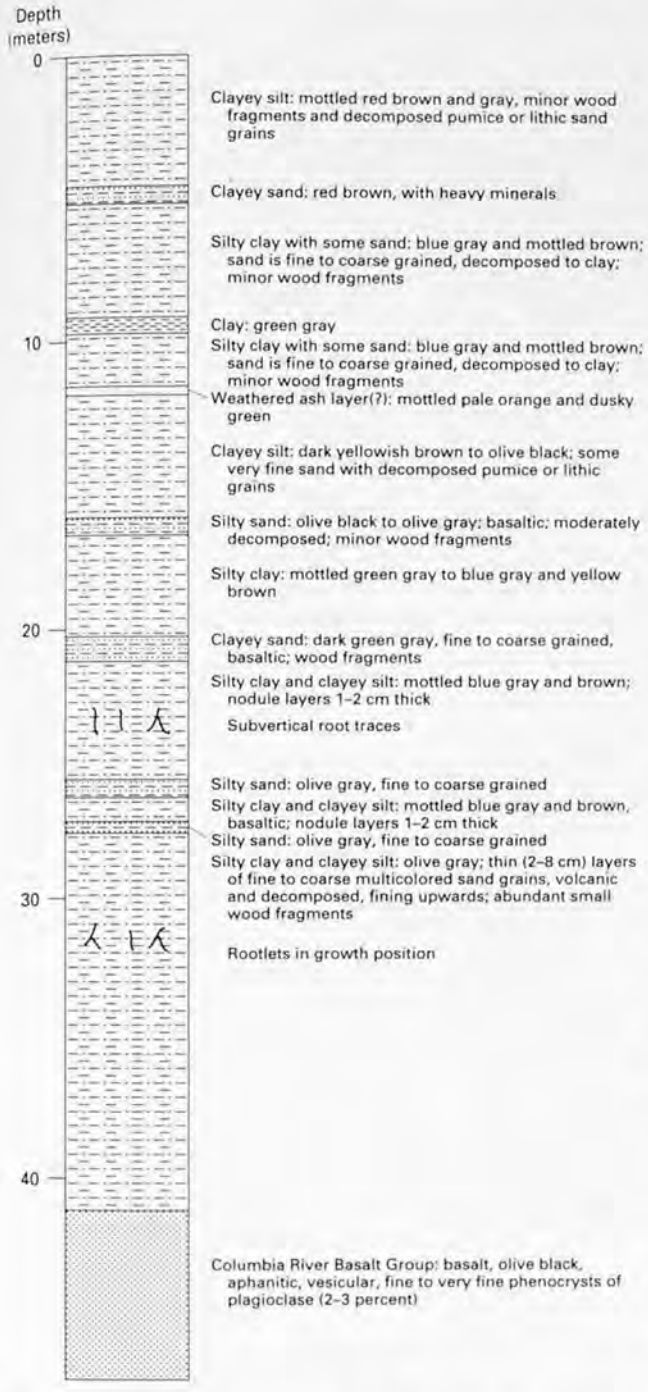

Figure 80. Graphic log of corehole DH 14–90, drilled 1.4 km west of Sublimity at State Highway 22 north of Mill Creek on the southern edge of the Waldo Hills, Oregon, showing unnamed nonmarine sedimentary deposits overlying the Columbia River Basalt Group.

Correlative conglomerate in the southeast part of the Portland basin contains a predominance of clasts derived from the Cascade Range (Tolan and Beeson, 1984; Hartford and McFarland, 1989). The Troutdale overlies the Sandy River Mudstone and locally may be interbedded with it. Plant fossils in the Troutdale are of early Pliocene age (Trimble, 1963), but the upper part of the formation could be younger.

BORING LAVA AND SNOW PEAK VOLCANO

Vents and flows of high-alumina, diktytaxitic, porphyritic olivine basalt and basaltic andesite with subordinate pyroclastic rocks, breccia, and ash in the Portland basin were named the Boring Lavas by Treasher (1942) and renamed the Boring Lavas by Allen (1975). These lavas intrude the Sandy River Mudstone and Troutdale Formation and form cones of interlayered cinders and lava (such as Mt. Sylvania and Mt. Scott in the middle of urban Portland) on an eroded surface of the Troutdale Formation (Trimble, 1963) as well as forming stocks from which the surrounding country rock has been eroded (Rocky Butte). East of Portland, high-alumina basalt flows overlie and are interbedded with the Troutdale Formation (Lowry and Baldwin, 1952; Tolan and Beeson, 1984; Tolan and others, 1989). The Boring Lavas are older than latest Pleistocene flood deposits (Allen, 1975). In the eastern Tualatin basin and the northern Willamette Valley, subsurface bodies visible on seismic lines as bowing up the Columbia River Basalt Group are interpreted as basalt intrusions correlated with the Boring Lavas. An intracanyon flow at Carver in the Clackamas River valley southeast of Portland has a potassium-argon age of 612±23 ka (R.A. Duncan, Oregon State University, oral commun. to I.P. Madin, 1989); other potassium-argon ages are as old as 5 Ma (Luedke and Smith, 1982; Swanson, 1986). The Boring Lavas of the Oregon City plateau are dated as 2.6 Ma (Swanson, 1986).

Snow Peak, just east of the study area, consists of nearly 1,000 m of basaltic andesite flows and breccia with minor basalt (Beaulieu, 1974). These rocks were dated by Verplanck (1985) as 3.3±0.6 Ma and 2.8±0.3 Ma, equivalent in age to the Boring Lavas. The shield volcano is deeply dissected by U-shaped valleys carved by glaciers.

PLEISTOCENE TERRACE GRAVELS

Sedimentary materials younger than the Boring Lavas, Troutdale Formation, and nonmarine fine-grained sedimentary deposits are described by McDowell (1991). Gravels in the eastern parts of the Willamette Valley and Portland basin are glaciofluvial, derived from the Cascade Range, whereas gravels on the west side of these basins are fluvial and derived from the Coast Range. Allison (1953) described three terrace-gravel units on the eastern margin of the southern Willamette Valley; from oldest to youngest, these are the Lacomb, Leffler, and Linn Gravels. The Lacomb and Leffler Gravels are preserved as high terraces at altitudes of 70–200 m along the edge of the valley (Allison, 1953; Allison and Felts, 1956). We do not separate the Lacomb and Leffler Gravels but instead refer to these units and other deeply weathered gravels as high-terrace gravels (fig. 83). Roberts (1984) suggested that the high-terrace gravels are the constructional top of his informally named Monroe clay. Subsequent erosion was accompanied by development of deep

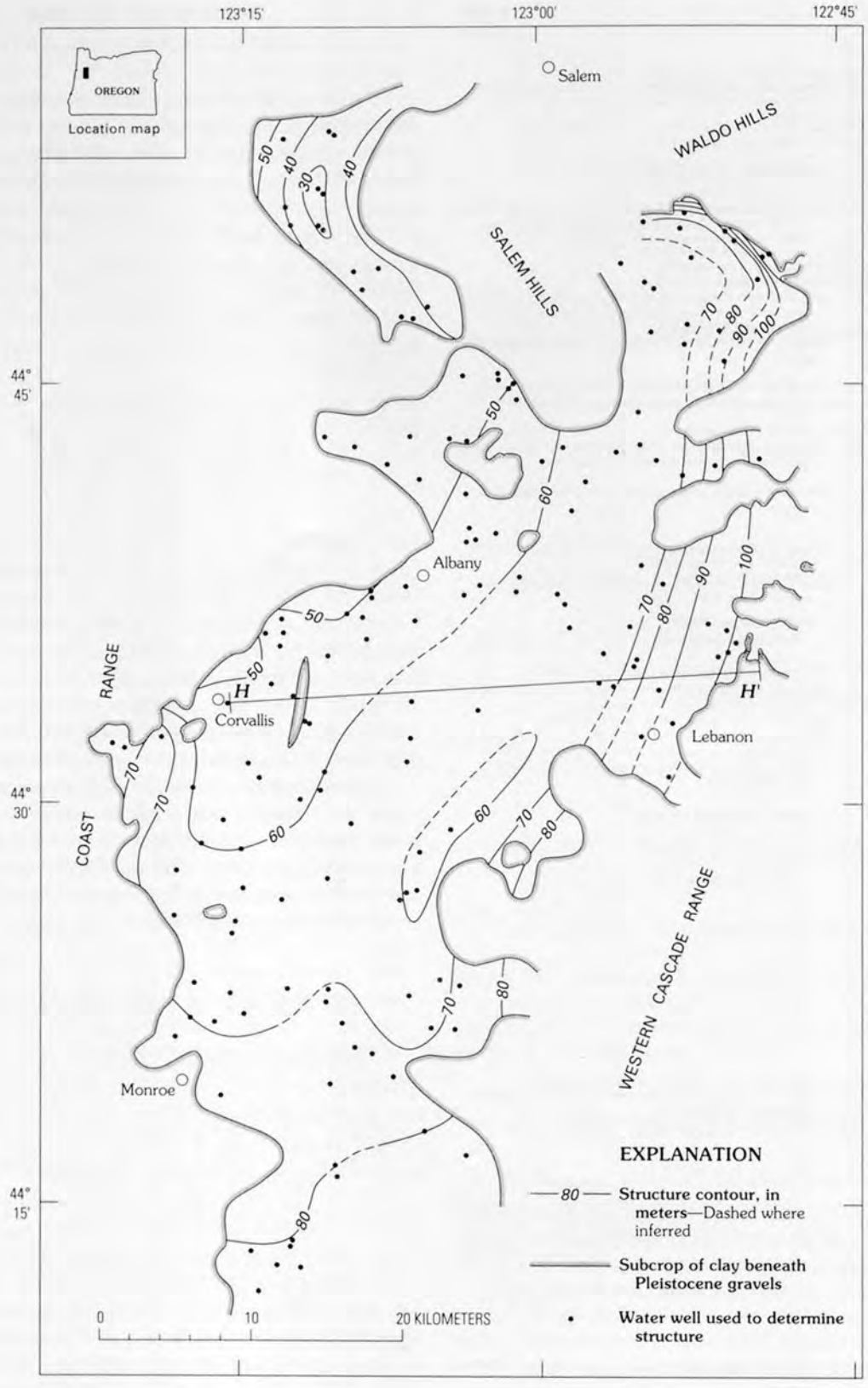

Figure 81. Structure contour map of the top of the nonmarine sedimentary deposits overlying the Columbia River Basalt Group, which is the contact with the base of the Pleistocene Rowland Formation (Balster and Parsons, 1969), in the southern Willamette Valley, Oregon. *H–H'* is the line of section for the cross section shown in figure 82.

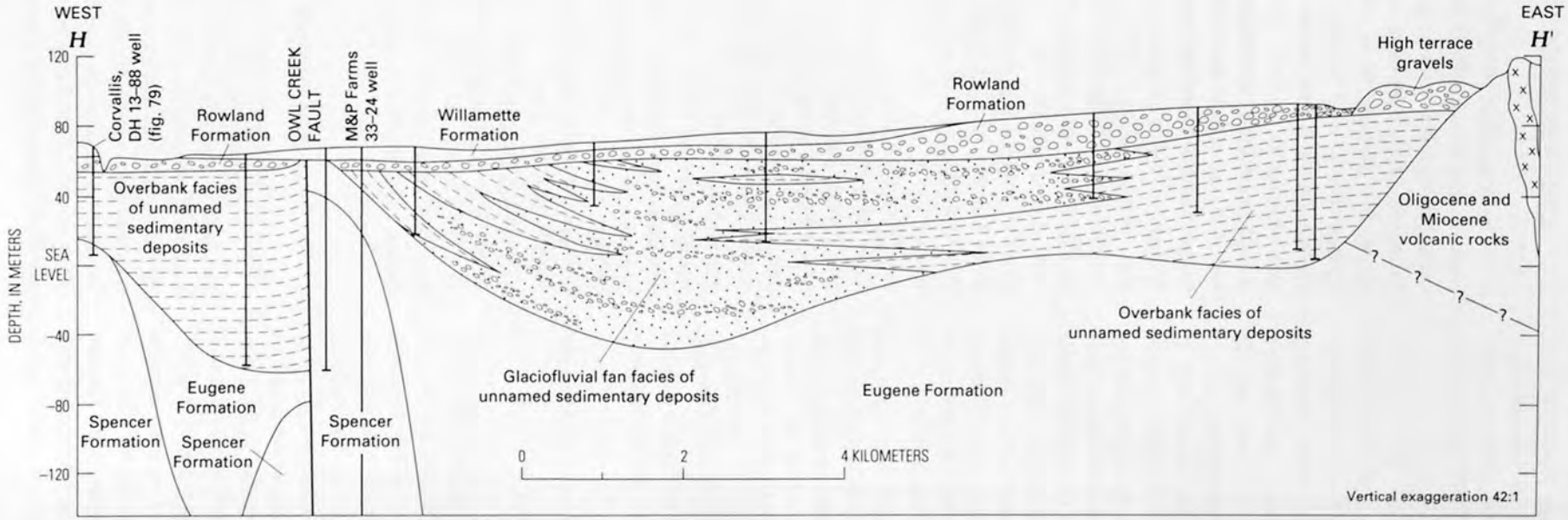

Figure 82. Structural cross section between Corvallis and Lebanon, Oreg., showing channel and overbank facies of unnamed fluvial sedimentary deposits, high-terrace gravels, late Pleistocene outwash deposits of the Rowland Formation, and catastrophic flood deposits of the Willamette Formation. Data are from water wells, engineering bore holes, and petroleum-exploration wells.

soils atop the Eola surface of Balster and Parsons (1968), evidence that the soils of the Eola surface are not correlative with the paleosol on top of the Spencer Formation near Corvallis or on top of the Columbia River Basalt Group in the northern Willamette Valley.

The materials forming the Linn Gravels, at or below the present Willamette Valley floor, were called the Rowland Formation by Balster and Parsons (1969) and divided into two members in the southern Willamette Valley: the Linn Member, predominantly silt, sand, and gravel, and the overlying Diamond Hill Member, predominantly sand and silt capped by a paleosol. The Linn Member is 6 m thick at Corvallis and thickens to about 20 m along the eastern edge of the valley. Allison (1953) suggested that the Linn Gravels are glacial outwash sediments derived from the Cascade Range, a view supported by a surface morphology of coalescing alluvial fans recognized by Piper (1942). The North Santiam, South Santiam, Willamette, McKenzie, and Calapooia Rivers all appear to have contributed to these deposits. Radiocarbon dates show that deposition of the Diamond Hill Member began before 36,000 years B.P. and continued past 28,500 years B.P. (McDowell and Roberts, 1987).

In the Portland basin, Trimble (1963) mapped the Springwater, Gresham, and Estacada Formations, consisting largely of glaciofluvial boulder and cobble gravels interbedded with mudflows and forming terraces along the Clackamas and Sandy Rivers. Madin (1990) found that the Estacada Formation includes several terraces, and he has recommended that Trimble's (1963) nomenclature be discontinued.

The relation between the Willamette Valley terraces and Pleistocene glacial sequences of the Cascade Range is poorly understood.

PORTLAND HILLS SILT

Poorly indurated quartz- and mica-bearing silt mantling hills around the Portland and Tualatin basins was named the Portland Hills Silt [Member] of the Troutdale Formation by Lowry and Baldwin (1952); this unit was subsequently raised to formational rank as the Portland Hills Silt by Baldwin (1964). The silt is more than 30 m thick in the Portland Hills but thinner elsewhere, and it is absent in the Red Hills of Dundee and farther south. Lentz (1981) demonstrated that the Portland Hills Silt is predominantly loess derived from the Columbia basin east of the Cascade Range. Lentz (1981) delineated as many as four silt units separated by paleosols, indicating that the loess accumulated over a considerable time span in the Quaternary. At one locality, the silt is apparently interbedded with what Lentz (1981) calls the Boring Lavas.

CATASTROPHIC FLOOD DEPOSITS

The Willamette Valley floor as far south as Eugene is mantled with horizontally bedded silt and gravel derived from the Columbia basin by glacial-outburst floods caused by the catastrophic drainage of Glacial Lake Missoula, an origin first recognized by Allison (1932, 1936, 1978). Treasher (1942) used the term "Willamette Valley terraces" for light brown, homogeneous silt interbedded with coarser grained deposits. Allison (1953) subsequently referred to these deposits as the Willamette Silts, and Baldwin and others (1955) called them the Willamette Silt. The unit contains boulders of exotic lithology found around the margins of the Willamette Valley, and a type section at Irish Bend was described by Allison (1953). Balster and Parsons (1969) used the name "Willamette Formation" for the unit and subdivided it into four members. The basal Wyatt Member consists of sand and silt that overlie the Rowland Formation unconformably as localized channel fills. The overlying Irish Bend Member resulted from multiple catastrophic floods that deposited silt in low-lying areas across much of the Willamette Valley (fig. 83). The coarse-grained equivalents of these silts in the northern Willamette Valley were called the River Bend Member (of the Willamette Formation) by Roberts (1984), and they consist of at least 40 rhythmically deposited beds of silt and fine sand, each apparently deposited by an individual catastrophic flood (Glenn, 1965). A paleosol separates the Irish Bend Member from the overlying Malpass Member, an extensive but discontinuous clay unit (Parsons and others, 1968; Balster and Parsons, 1969). The uppermost Greenback Member consists of silt accompanied by erratic boulders draped over the landscape at altitudes as high as 122 m by one catastrophic flood (fig. 8) (Allison, 1953). In the Portland basin, the flood deposits include boulder gravel, sandy gravel, and sand with a Columbia Basin provenance (Allen and others, 1986). The floods occurred later than 15,000 years B.P. (Baker and Bunker, 1985; Waitt, 1985), and a bog overlying flood deposits near Portland is dated as 13,000 years B.P. (Mullineaux and others, 1978; McDowell, 1991).

HOLOCENE DEPOSITS

During the Holocene, the Willamette River has incised the main Calapooyia-Senecal surface (fig. 83) and cut and deposited three additional surfaces, the Winkle, Ingram, and Horseshoe (Balster and Parsons, 1968). The surfaces reflect a change from a more braided channel pattern to the present meandering channel pattern (McDowell, 1991). Holocene sand, gravel, silt, and clay are largely confined to channels and flood plains of major rivers and their tributaries.

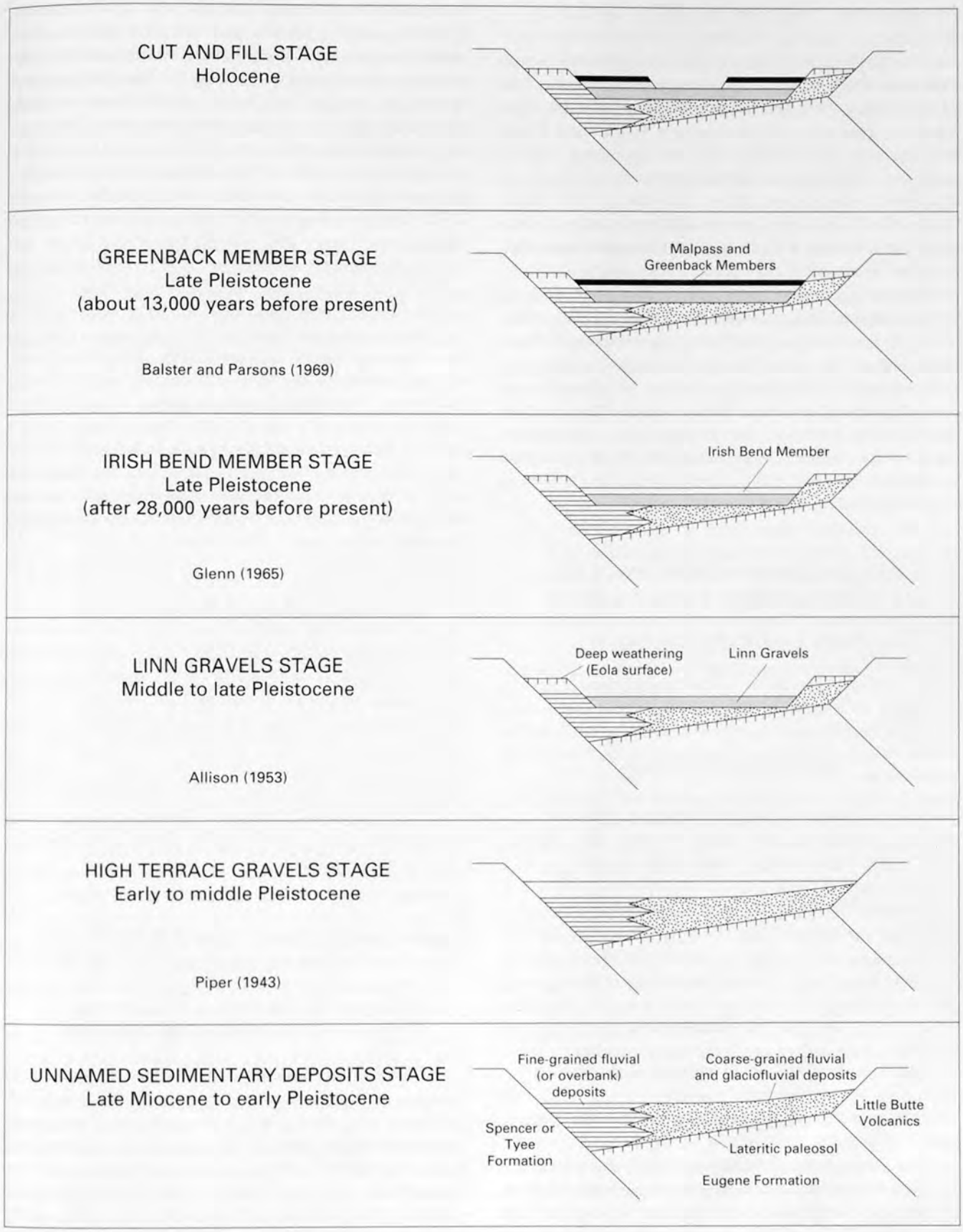

Figure 83. Depositional history of the southern Willamette Valley, Oregon, after Miocene time. Modified from Roberts (1984).

STRUCTURE

Faulting and folding have taken place in the Willamette Valley and Coast Range since the emplacement of the Siletz River Volcanics. Angular unconformities are common. The region has been near a subduction zone for the entire Cenozoic era, with plate convergence rates decreasing and the strike-slip component of subduction increasing from the Paleocene to the present (Wells and others, 1984; Riddihough, 1984). This history has resulted in clockwise rotation of structural blocks, with the amount of rotation decreasing from Eocene time to the present and from west to east.

In this chapter, we focus on deformation affecting the Columbia River Basalt Group and younger deposits. Older structures are examined briefly; they are important to our discussion only because in some places they are zones of weakness reactivated by younger faulting and thus they may have seismogenic potential. Faults cutting Oligocene and older strata but having unknown age relations to the Columbia River Basalt Group and younger deposits are discussed by Graven (1990) and Werner (1990). Most faults are shown on plate 2A and 2B and in figures 84 and 85.

DEFORMATION PREDATING THE COLUMBIA RIVER BASALT GROUP

COAST RANGE ANTICLINORIUM

Present-day exposures of the Siletz River Volcanics commonly correspond to basement highlands that existed during the time Eocene strata were deposited. The Tyee Formation onlapped a highland composed of the Siletz River Volcanics in the Valsetz area west of Dallas. The Siletz River Volcanics in the hanging wall of the Corvallis fault occupied a positive area that caused the informally named Miller sand of the Yamhill Formation to lens out toward the fault (Baker, 1988; Graven, 1990). This positive area provided detritus to the upper Eocene Spencer Formation (Goldfinger, 1990). In the northern Willamette Valley, strata as young as the Scotts Mills Formation (Oligocene and Miocene) were tilted to the east prior to the formation of the Columbia River Basalt Group, presumably reflecting uplift of the Coast Range, yet the Coast Range was low enough that intracanyon flows of the Columbia River Basalt Group were able to cross the range to the present-day coastline.

CORVALLIS FAULT

The northeast-trending Corvallis fault (fig. 84; pl. 2B) is at least 50 km long, and for part of its length, it is the western boundary of the southern Willamette Valley. The fault cannot be traced across the Willamette River to the Salem Hills, although the small-displacement Turner fault in the Salem Hills has the same trend and sense of displacement. Two recent gravity profiles show that the primary fault is a thrust that dips about 10° northwest (Goldfinger, 1990). Dips of strata in the hanging wall average 20° northwest, and beds in both the hanging wall and the footwall are overturned close to the fault, suggesting a fault-propagation fold geometry. Vertical separation on the Corvallis fault at seismogenic depths is about 6.7 km, a figure obtained by adding the separation on the fault at the surface and the separation implied by considering surface folding as caused by fault propagation (Yeats, 1988). Using a fault dip of 20°, the horizontal shortening is calculated as 11–13 km. The fault was active in late Eocene time, an interpretation based on isopachs on a map of the Miller sand that show thinning of the sand in the direction of the Corvallis fault (Baker, 1988) and on sedimentary breccia with clasts of the Siletz River Volcanics present within the Spencer Formation, adjacent to the fault west of Corvallis (Goldfinger, 1990). A younger high-angle fault parallel to the Corvallis thrust is exposed in a quarry 2 km northeast of Philomath and has left-lateral horizontal slickensides and mullion structure. The main fault trace is offset by several northwest-trending faults. Because this high-angle fault may displace Pleistocene sedimentary deposits, it is discussed further below.

EOLA HILLS-AMITY HILLS NORMAL FAULTS

A proprietary seismic profile shows that the Siletz River Volcanics and the lower part of the Yamhill Formation in the Eola Hills and Amity Hills are cut by two normal faults showing movement down to the east (fig. 85). This profile and a residual gravity map (Werner, 1990) suggest that the faults strike north-northeast. The Yamhill Formation increases in thickness eastward across the faults from 950 to 1,450 m. The Spencer Formation and the upper part of the Yamhill Formation are only slightly warped across the westernmost of the two faults.

DEFORMATION YOUNGER THAN THE COLUMBIA RIVER BASALT GROUP

COAST RANGE ANTICLINORIUM AND WILLAMETTE VALLEY SYNCLINORIUM

Flows of the Columbia River Basalt Group can be traced to the western margin of the northern Willamette Valley where they are exposed in an east-dipping homocline. Subaerial flows and invasive flows identical to those mapped in the Willamette Valley are found on the Oregon coast from Seal Rock north to the Columbia River. The absence of the Columbia River Basalt Group in the intervening Coast Range is due to younger warping of the Coast Range (Niem and Niem, 1985). As the Coast Range arched upward, the

Willamette Valley subsided and accumulated sediments of the proto-Willamette and proto-Columbia rivers and major tributary side streams. At Monroe, these sedimentary deposits are dated by palynology as late Miocene to early Pliocene (Roberts and Whitehead, 1984), but contact relations as young as 0.6 Ma with the Boring Lavas suggest that these sedimentary materials may be as young as Pleistocene. We suggest that the aggradation in the Willamette Valley and adjacent Columbia River valley was caused by a relative change in base level as the Coast Range was uplifted.

Farther east, the western Cascade Range underwent tilting (Priest, 1989). Beeson, Tolan, and Anderson (1989) recognized more than 1,200 m of uplift of the Cascade Range near the Columbia River, based on the structure of the Columbia River Basalt Group and overlying Troutdale Formation.

CORVALLIS FAULT

In the main Corvallis fault zone, horizontal slickensides are found in rocks as young as Oligocene intrusions, suggesting reactivation in a stress field compatible with north-south compression. In Corvallis and along the lower reaches of the Marys River, the contact between gravel possibly correlated with the Rowland Formation and the Willamette Formation dips 6°–12° east and southeast. The gravel is capped by the Quad surface of Balster and Parsons (1969), a probable continuation of their Calapooyia surface. Adjacent to the Corvallis fault, this surface is 30–40 m higher than it is farther east, suggesting to Balster and Parsons (1969) that the surface was uplifted by faulting. At the Mid Valley quarry between Philomath and Corvallis, the contact between the Willamette Formation and the underlying gravels is at an altitude of 107 m, near the highest elevation at which the Willamette Formation has been found (McDowell and Roberts, 1987). This contact is at an altitude of 68 m in the Willamette River channel east of the Mid Valley quarry. In addition, pre-Rowland Formation overbank facies deposits of the proto-Willamette River similar to those present at and east of the Willamette River (figs. 79, 81, and 82) are absent beneath the gravels at the Mid Valley quarry. These relations suggest eastward tilting or east-side-down faulting. Alternatively, the gravels at the Mid Valley quarry may be older than the Rowland Formation at the Willamette River.

In north Corvallis between Walnut Boulevard and a saddle at the entrance to Chip Ross Park, south of Jackson Creek, a scarp ranging from a few centimeters to 1 m in height marks the trace of the Corvallis fault. It has the same sense of displacement as the main fault, steeply dipping with the southeast side down, as based on relations exposed in a hand-dug pit. This scarp could be a slump rather than a fault. Low-sun-angle aerial photographs show northwest-trending scarps that may be related to left steps on the Corvallis fault. These scarps occur in areas of outcrops of the Siletz River Volcanics and high-terrace gravels. The neotectonic origin of these features is not confirmed (Goldfinger, 1990).

Goldfinger (1990) identified three earthquakes that have been felt along the general trend of the Corvallis fault, one of intensity III in 1957, one of intensity III–IV in 1961, and one of intensity V probably in 1946 or 1947 (incorrectly reported as May 12, 1942, by Berg and Baker, 1963).

OWL CREEK FAULT

The Owl Creek fault (figs. 82 and 84) strikes N. 10° E., has reverse separation with the east side up, and is associated with an anticline in the hanging wall. The Spencer Formation is 220 m thick on the crest of this fold but 550 m thick east of the fold, suggesting growth during Eocene time (Graven, 1990). Water-well data show that the bedrock surface is 115 m higher on the crest of the anticline than it is to the east and west (fig. 82). By comparison, the base of the Spencer Formation is 725 m higher on the crest of the anticline than it is to the east and west. In the upthrown block, proto-Willamette River overbank deposits dip east with respect to gravels of the Rowland Formation, and the Rowland Formation is eroded away near the fault so that the Willamette Formation rests directly on the Eugene Formation (fig. 82). Gravel in the Rowland Formation of Cascade Range provenance is exposed in the banks of the Willamette River at Corvallis, west of the fault, suggesting that the Rowland Formation was deposited over the Owl Creek structure, then uplifted and eroded from the hanging-wall block prior to the deposition of the Willamette Formation, which appears to postdate all faulting.

HARRISBURG ANTICLINE

A broad east-northeast-trending anticline between Corvallis and Eugene plunges east (fig. 84) and has about 100 m relief on the Eugene-Spencer Formation contact. The axis of the channel of the proto-Willamette River is warped upward about 50 m where it crosses the anticline at Harrisburg (fig. 86). There is no evidence of faulting associated with this anticline.

JEFFERSON ANTICLINE

A broad anticline (fig. 84, pl. 2B) north of Albany creates the concave-to-the-west map trace of the base of the Eugene Formation, as expressed by structure contours. There is no evidence of stratigraphic thinning of Eocene strata across the structure, indicating that the fold developed later. Topography resulting from anticlinal growth may have diverted flows of the Columbia River Basalt Group, particularly the Ginkgo flows of the Frenchman Springs Member of the Wanapum Basalt, northwestward around the anticline.

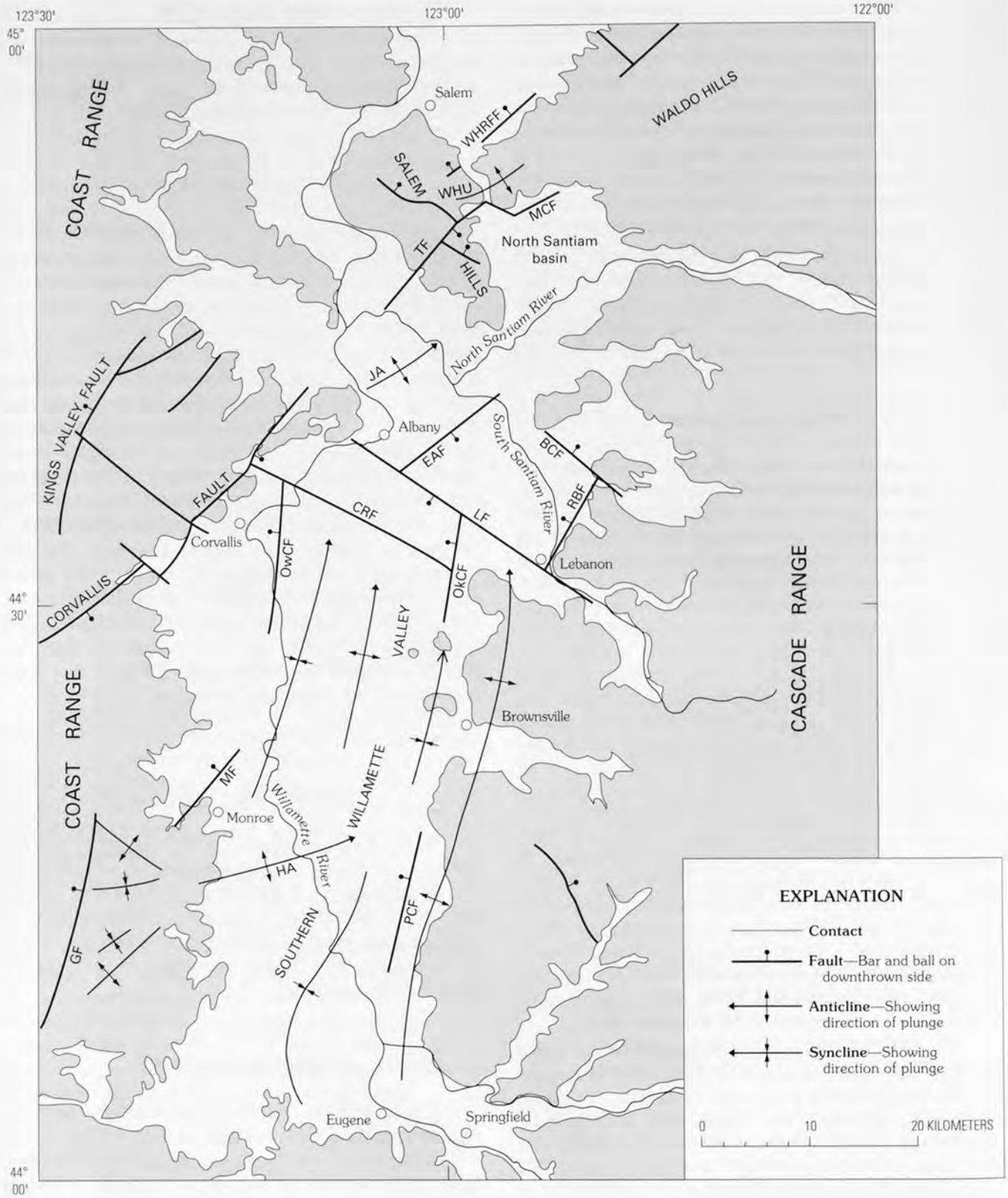

Figure 84. Tectonic map of the southern Willamette Valley, Oregon. Areas underlain by alluvial and fluvial deposits that postdate the Columbia River Basalt Group are unshaded; areas underlain directly by bedrock are shaded. BCF, Beaver Creek fault; CRF, Calapooia River fault; EAF, East Albany fault; GF, Glenbrook fault; HA, Harrisburg anticline; JA, Jefferson anticline; LF, Lebanon fault; MCF, Mill Creek fault; MF, Monroe fault; OwCF, Owl Creek fault; OkCF, Oak Creek fault; PCF, Pierce Creek fault; RBF, Ridgeway Butte fault; TF, Turner fault; WHRFF, Waldo Hills range-front fault; WHU, Waldo Hills uplift.

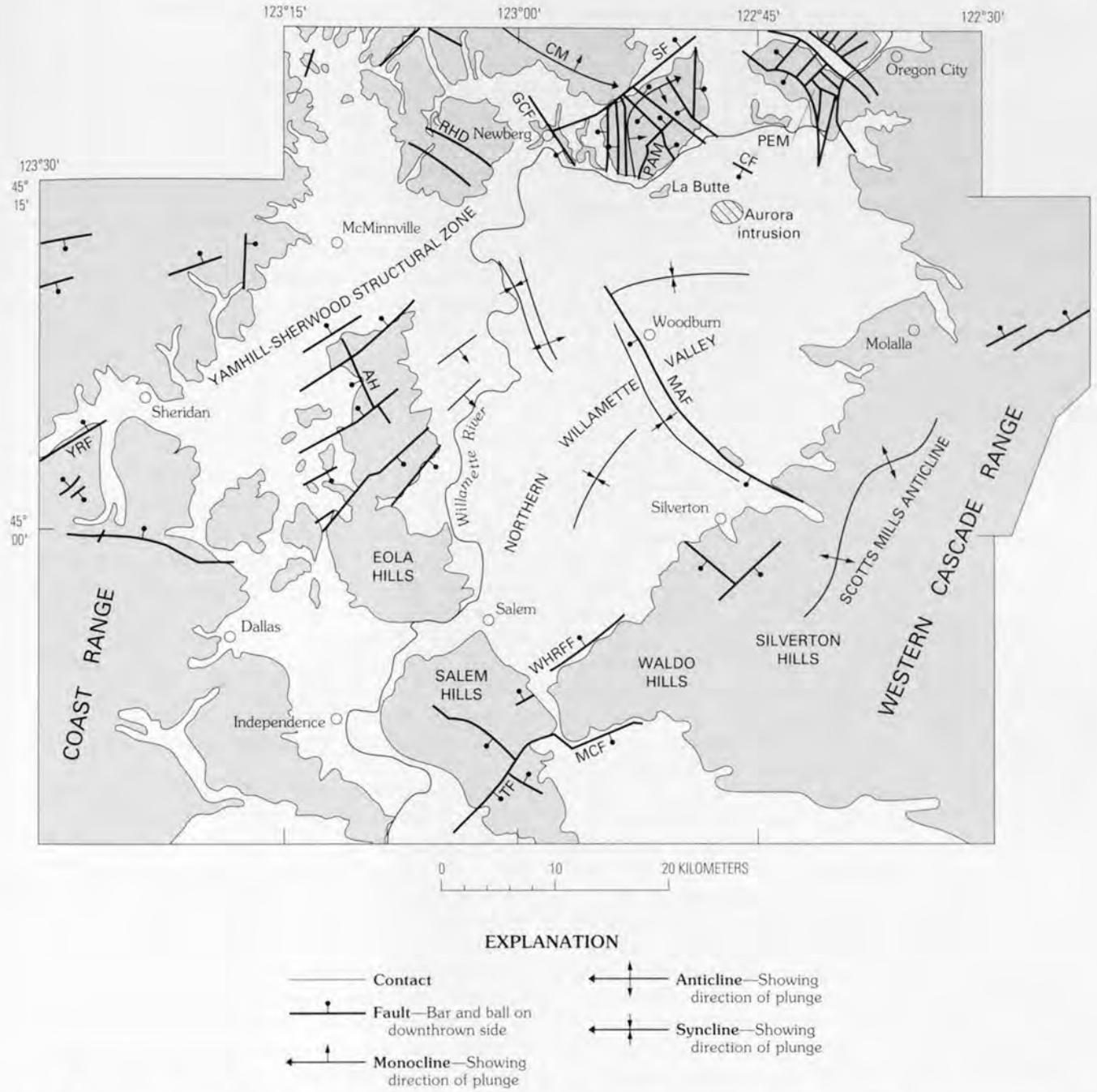

Figure 85. Tectonic map of the northern Willamette Valley, Oreg. Unshaded areas are underlain by alluvial and fluvial deposits that postdate the Columbia River Basalt Group. AH, Amity Hills; CM, Chehalem Mountains; PAM, Parrett Mountain; PEM, Petes Mountain; RHD, Red Hills of Dundee; CF, Curtis fault; GCF, Gales Creek fault; MAF, Mt. Angel fault; MCF, Mill Creek fault; SF, Sherwood fault; TF, Turner fault; WHRFF, Waldo Hills range-front fault; YRF, Yamhill River fault.

The axis of a channel of the proto-Willamette River west of the Salem Hills crosses a bedrock highland north and east of Albany including Spring Hill, Scravel Hill, and Hale Butte (fig. 81; pl. 3), and it is likely that this channel was warped upward across the Jefferson anticline. However, the base of the Rowland Formation does not appear to be warped (fig. 81). The Jefferson anticline may be a northeast continuation of the hanging-wall block of the Corvallis fault in which the Siletz River Volcanics are at the surface. The northwest-striking contact of the Siletz River Volcanics with younger rocks is expressed as a positive gravity anomaly in residual-gravity contours (Werner, 1990).

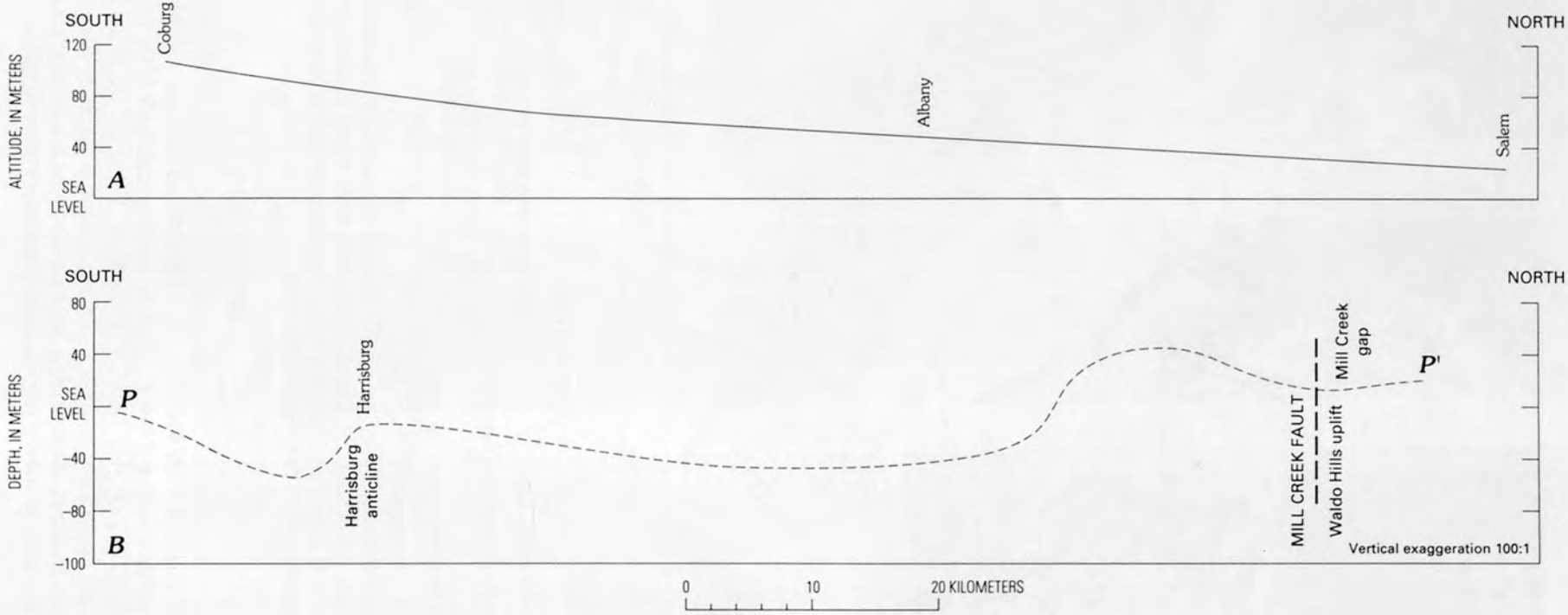

Figure 86. Longitudinal profiles of the modern and proto-Willamette Rivers, Oreg. *A*, profile of the modern river. *B*, profile of the proto-Willamette River showing deformation of the axis of the main stream channel. See plate 3 for location of line of section *P*–*P'*.

NORTH SANTIAM BASIN

The North Santiam River crosses a basin bounded by the Waldo Hills on the north, the Salem Hills on the west, and the western Cascade Range on the east. The minimum structural relief at the top of the Columbia River Basalt Group in the North Santiam basin is 260 m, based on the maximum depth to basalt in water wells in the basin and also the top of the Columbia River Basalt Group in the adjacent Waldo Hills. Except for the Mill Creek fault discussed below, no faults have been recognized in this basin, perhaps because of the difficulty of correlating horizons in the sedimentary deposits postdating the Columbia River Basalt Group across the basin.

MILL CREEK FAULT

The southern edge of the Waldo Hills is marked by a fault that displaces the Columbia River Basalt Group about 100 m (pl. 2B). The base of the Columbia River Basalt Group is exposed along the western end of the Waldo Hills near Turner, whereas the top of the group is near sea level in the North Santiam basin south of the range front. The Mill Creek fault may be the eastern extension of the Turner fault in the Salem Hills.

WALDO HILLS RANGE-FRONT FAULT

The northern range front of the Waldo Hills is marked by a pronounced northeast-trending aerial-photograph lineation that is on a trend with the Corvallis fault to the southwest. The contact between the Columbia River Basalt Group and underlying marine strata is exposed near the range front southeast of Salem; several wells also penetrate this contact (fig. 87). Northwest of the range front, water wells reach the top of the Columbia River Basalt Group, indicating vertical separation of at least 50 m. The fault may extend farther northeast than shown; vertical separation decreases toward the northeast. No clear evidence shows that the fault cuts strata younger than the Columbia River Basalt Group.

GALES CREEK-MOUNT ANGEL STRUCTURAL ZONE

The Gales Creek-Mount Angel structural zone is the southernmost of several northwest-trending, seismically active linear features in northwestern Oregon and southwestern Washington (Werner, 1990). Both the Gales Creek-Mount Angel structural zone and the Portland Hills-Clackamas River structural zone were active during formation of the Columbia River Basalt Group. The Mount Angel fault, part of the Gales Creek-Mount Angel structural zone, formed a barrier to three Silver Falls flows of the Frenchman Springs Member of the Wanapum Basalt (Beeson, Tolan, and Anderson, 1989).

Geological evidence exists for three segments of the Gales Creek-Mount Angel structural zone: the Gales Creek fault, the Newberg fault, and the Mount Angel fault, which have the same strike but are offset (fig. 85). The Gales Creek fault segment follows the Gales Creek valley between Gales Peak and David Hill, juxtaposing rocks equivalent to the Tillamook volcanics to the southwest with the Columbia River Basalt Group on the northeast. The fault has been extended south toward Gaston, where seismic profiles reveal a complex zone of deformation extending from Gaston to the base of the Chehalem Mountains. Modeling of a gravity profile across this zone suggests three fault segments having a total vertical separation, largely earlier than the Columbia River Basalt Group, of almost 3 km, down to the northeast (H.J. Meyer, Oregon Natural Gas Corp., oral commun., 1991). It is unclear whether this zone connects with the Newberg fault segment.

Werner (1990) mapped the Newberg fault on the basis of water-well data (fig. 88). North of the fault, the base of the Columbia River Basalt Group is exposed on the south side of the Chehalem Mountains and dips northeast. South of the fault, the top of the Columbia River Basalt Group is exposed in the Red Hills of Dundee and also dips northeast. The group is juxtaposed against Oligocene and Miocene marine strata along the fault, though the apparent sense of vertical offset is opposite that expressed in the Gaston area (Popowski, 1995). Gradient analyses of aeromagnetic and gravity data support the fault location. A seismic profile across the projection of the fault zone between Newberg and Woodburn shows no displacement of the top of the Columbia River Basalt Group (Werner, 1990).

The Mount Angel fault (fig. 85) was first mapped near Mount Angel by Hampton (1972) using water-well data. Based on additional data from seismic profiles and water wells, we extend the Mount Angel fault from the Waldo Hills northwest past Woodburn (figs. 89 and 90). Vertical offset of the top of the Columbia River Basalt Group increases to the southeast from 100 m in seismic section *A–A'* (fig. 91) to 200 m in seismic section *B–B'* (fig. 92), and at least 250 m in cross section *C–C'* (fig. 93). The presence of the Frenchman Springs Member of the Wanapum Basalt at the top of Mount Angel (M.H. Beeson, Portland State University, oral commun., 1990) indicates that the top of the Columbia River Basalt Group would have been close to the present summit prior to erosion, constraining offset to about 250 m. A seismic reflector within the overlying fluvial sequence is offset about 40 m and the dip of the fault is 60°–70° NE., based on seismic section *B–B'* (fig. 92). On the southwest side of the fault, the top of the Columbia River Basalt Group is warped into a shallow syncline that increases in prominence northward as offset on the Mount Angel fault decreases (fig. 88).

Evidence for the Mount Angel fault is limited in the Waldo Hills, although a Ginkgo intracanyon flow of the

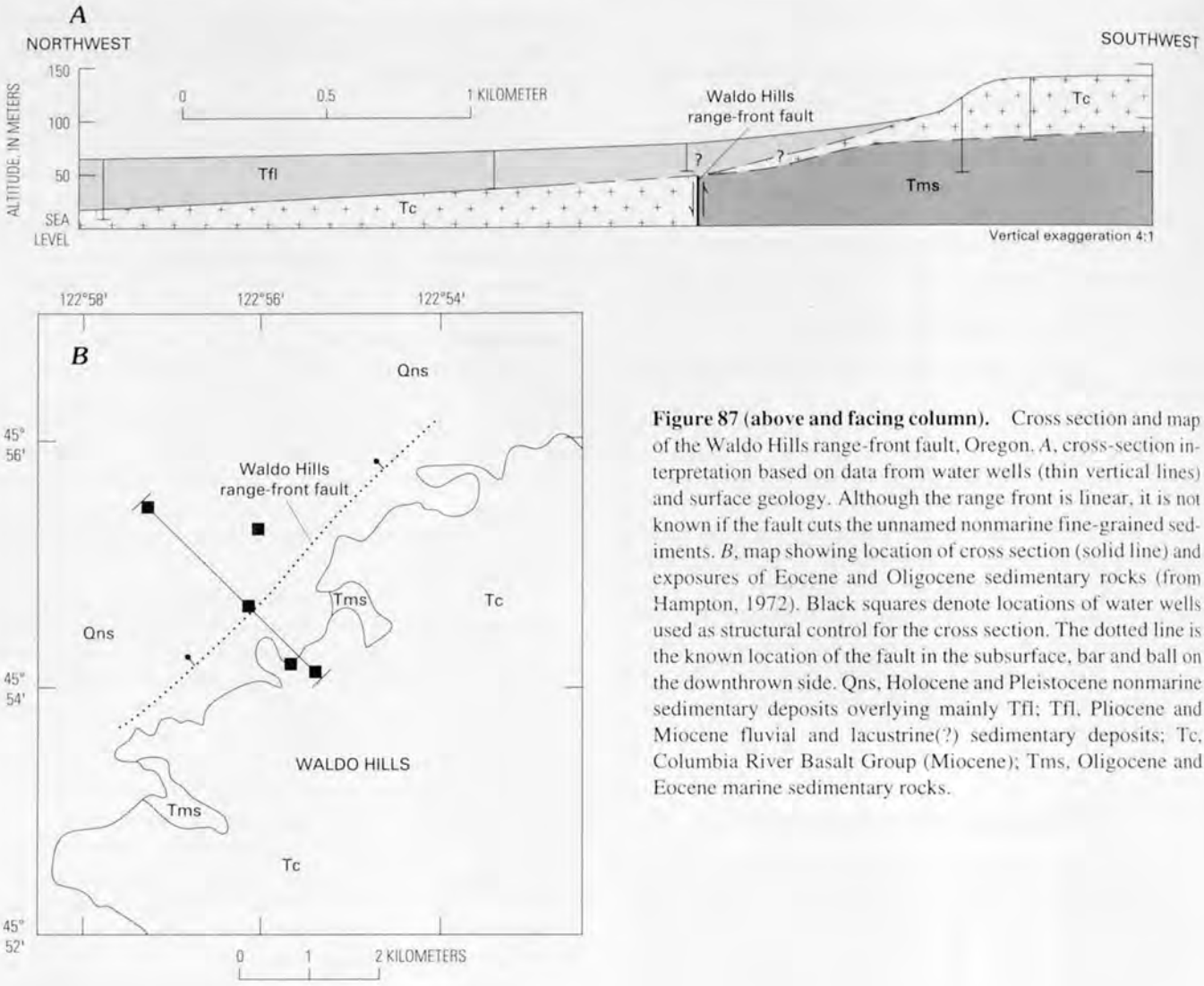

Figure 87 (above and facing column). Cross section and map of the Waldo Hills range-front fault, Oregon. *A*, cross-section interpretation based on data from water wells (thin vertical lines) and surface geology. Although the range front is linear, it is not known if the fault cuts the unnamed nonmarine fine-grained sediments. *B*, map showing location of cross section (solid line) and exposures of Eocene and Oligocene sedimentary rocks (from Hampton, 1972). Black squares denote locations of water wells used as structural control for the cross section. The dotted line is the known location of the fault in the subsurface, bar and ball on the downthrown side. Qns, Holocene and Pleistocene nonmarine sedimentary deposits overlying mainly Tfl; Tfl, Pliocene and Miocene fluvial and lacustrine(?) sedimentary deposits; Tc, Columbia River Basalt Group (Miocene); Tms, Oligocene and Eocene marine sedimentary rocks.

Columbia River Basalt Group in the Waldo Hills is offset about 1 km right laterally across the fault (M.H. Beeson, Portland State University, oral commun., 1990).

Six small earthquakes with m_c (m_c is coda-length magnitude) of 2.0, 2.5, 2.4, 2.2, 2.4, and 1.4 occurred on August 14, 22, and 23, 1990, near Woodburn (Werner and others, 1992). Epicenter locations (fig. 90) were determined using the broadband seismic station in Corvallis (epicentral distance, 68 km) and the Washington Regional Seismograph Network. Three earthquakes in 1980 and 1983 having m_c less than 1.7 occurred at the same locality. The waveforms for the six earthquakes are so similar that the locations of all events are considered to be much closer together than shown in figure 90. The preferred focal mechanism (fig. 94) is a right-lateral strike-slip fault (with a small normal component) striking north-south and dipping steeply to the west.

On March 25, 1993, an earthquake with m_c of 5.6 struck the Waldo Hills near the town of Scotts Mills (fig. 77) (Thomas and others, 1993), causing about $28 million in damage. The focal depth was 15 km. A preliminary determination of the focal mechanism has one nodal plane with a strike of N. 56° W. and a dip of 58° NE. A subset of aftershocks defines a plane with a west-northwest strike dipping 55°–60° NE. Rupture was by right-lateral strike slip and reverse slip, consistent with motion on the Mount Angel fault, although the earthquake occurred east of the southeast projection of the Mount Angel fault in the Waldo Hills.

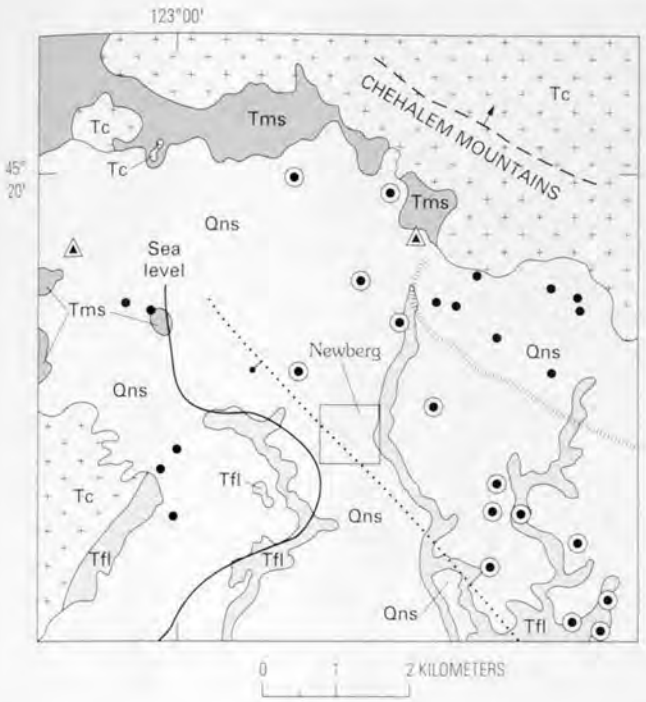

Figure 88. Buried trace of the Newberg fault, Newberg, Oreg., juxtaposing marine strata on the northeast against the Columbia River Basalt Group on the southwest. Sediments postdating the Columbia River Basalt Group do not appear to be faulted. Map-unit symbols are same as in figure 87.

YAMHILL-SHERWOOD STRUCTURAL ZONE

This northeast-trending zone (fig. 85) includes the Yamhill River fault of Baldwin and others (1955) and Brownfield (1982a, b), which juxtaposes the Nestucca Formation on the north against the Yamhill Formation on the south (pl. 2A) with maximum vertical separation greater than 300 m (Baldwin and others, 1955). The fault may continue along the northern end of the Amity Hills, based on a proprietary seismic profile. Farther northeast, the Sherwood fault between Parrett Mountain and the Chehalem Mountains has created 100–150 m of vertical separation in the Columbia River Basalt Group (Hart and Newcomb, 1965; Beeson, Tolan, and Anderson, 1989), though it is poorly expressed in aeromagnetic and gravity data. The Sherwood fault appears to be the southwest continuation of the northern margin of the Columbia trans-arc lowland through which the Columbia River Basalt Group traversed the Cascade Range (Beeson, Tolan, and Anderson, 1989). The structure may be part of the Yamhill-Bonneville lineament, which may have influenced the distribution of vents of the Boring Lavas in the Portland area (Allen, 1975).

NORTHERN WILLAMETTE DOWNWARP

The northern Willamette Valley generally trends northeast, but the northern end of the valley is underlain by an east-trending downwarp in which the top of the Columbia River Basalt Group is as deep as 500 m below sea level. The downwarp cuts across the northern extension of the Mount Angel fault but is most prominent east of the fault. The northern flank is steeper than the southern flank; this may indicate upwarping influenced by the emplacement of intrusions related to the Boring Lavas, such as the Aurora stock (pl. 2A). Sedimentary deposits postdating the Columbia River Basalt Group are warped to a lesser degree than the top of the group, as shown by proprietary seismic data. This downwarp may be part of a western extension of the Yakima fold belt, like other structures to the northeast, as suggested by Beeson, Tolan, and Anderson (1989).

FAULTS AT PARRETT MOUNTAIN, PETES MOUNTAIN, AND IN THE ADJACENT NORTHERN WILLAMETTE VALLEY

Faults at Parrett Mountain and Petes Mountain were mapped by Marvin H. Beeson and Terry L. Tolan of Portland State University (oral commun. to Ian P. Madin, Oregon Department of Geology and Mineral Industries, 1990) based on juxtaposition of flows of the Columbia River Basalt Group identified using geochemical data. Displacements are commonly tens of meters. To the south, seismic profiles show that the top of the Columbia River Basalt Group is

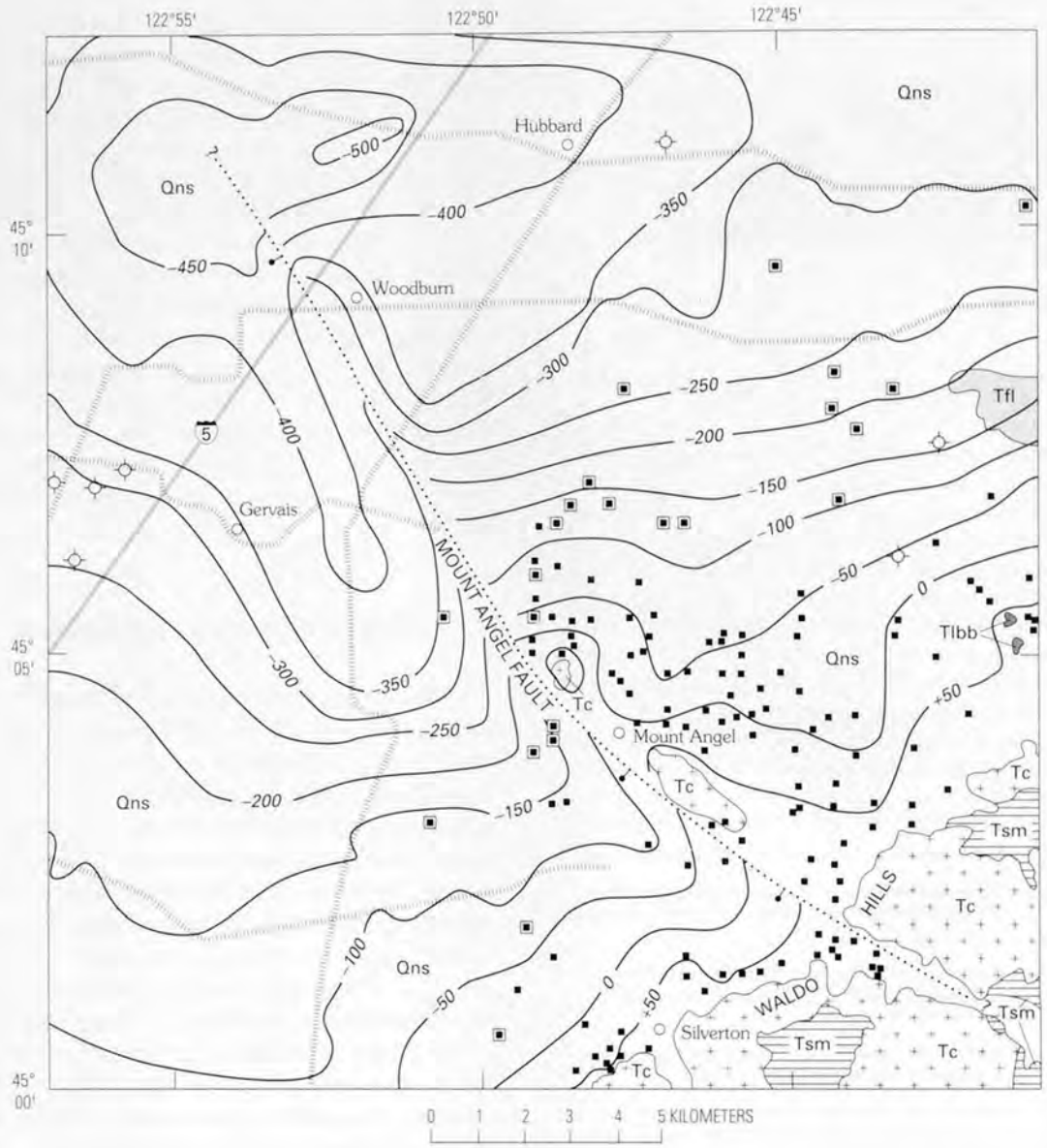

EXPLANATION

Contact

Concealed Fault—Bar and ball on downthrown side; queries mark limits of where the fault can be traced in the subsurface

-50 Structure contour on top of basalt—Datum is sea level

Seismic-reflection profile line

Petroleum-exploration well

Water well that reaches basalt

Deep water well that does not reach basalt

Figure 89. Structure contour map of the top of basalt units near Mount Angel, Oreg. The basalt is primarily the top of the Columbia River Basalt Group except near exposures of the Miocene basalt and basaltic andesite around the Mount Angel fault. Qns, Holocene and Pleistocene nonmarine sedimentary deposits; Tfl, Pliocene and Miocene fluvial and lacustrine(?) sedimentary deposits; Tc, Columbia River Basalt Group (Miocene); Tsm, Miocene and Oligocene Scotts Mills Formation of Miller and Orr (1988); Tlbb, Miocene basalt and basaltic andesite.

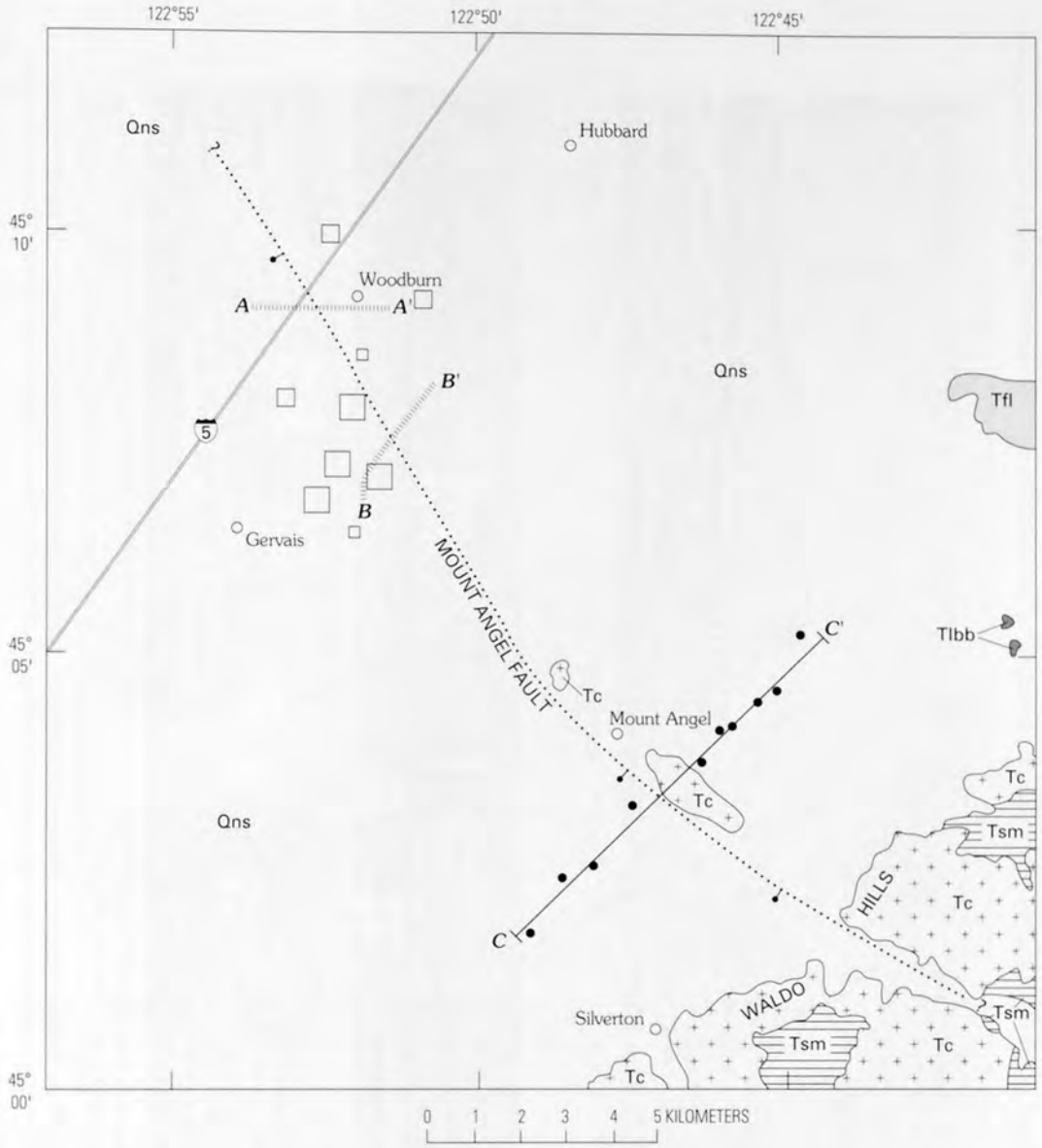

EXPLANATION

Contact

Concealed Fault—Bar and ball on downthrown side; queries mark limits of where the fault can be traced in the subsurface

Seismic-reflection profile lines for sections shown in figures 91 and 92

C — C' Line of cross section (fig. 93)—Dots show constraining water wells

EARTHQUAKE EPICENTERS

Magnitude 1.1–1.5

Magnitude 1.6–2.0

Magnitude 2.1–2.5

Figure 90. Locations of seismic and water-well cross sections, and epicenters of earthquakes that occurred between 1980 and 1990 near Woodburn, Oreg. Map-unit symbols are same as in figure 89.

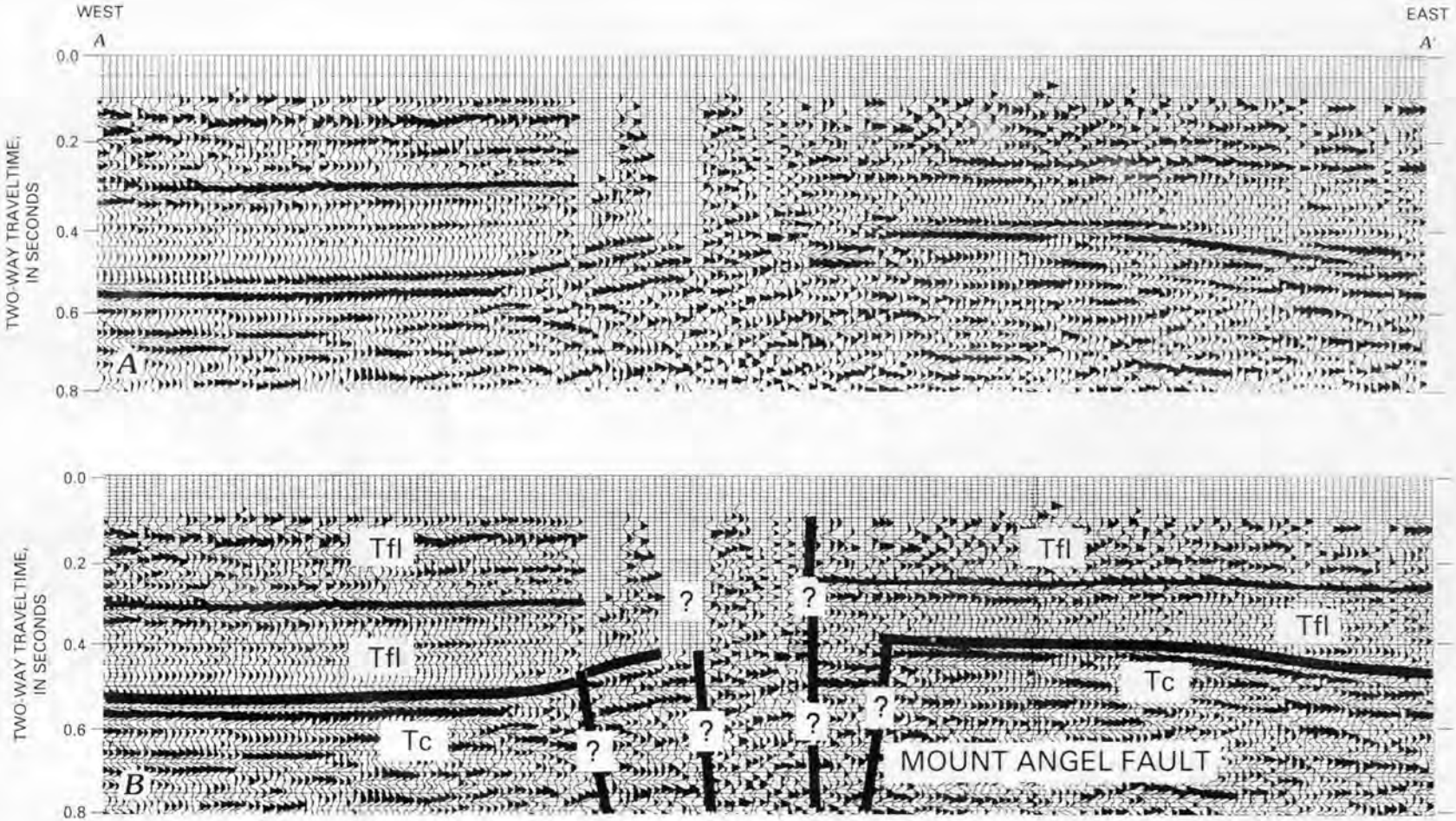

Figure 91. Seismic section *A–A'* across the Mount Angel fault, Willamette Valley, Oreg. *A*, uninterpreted section; *B*, interpreted section. Four strands of the Mount Angel fault are recognized. The prominent reflector within unit Tfl is higher on the northeast than on the southwest side of the fault. Queries denote possible faults. Map-unit symbols are same as in figure 89. Line of section is shown in figure 90.

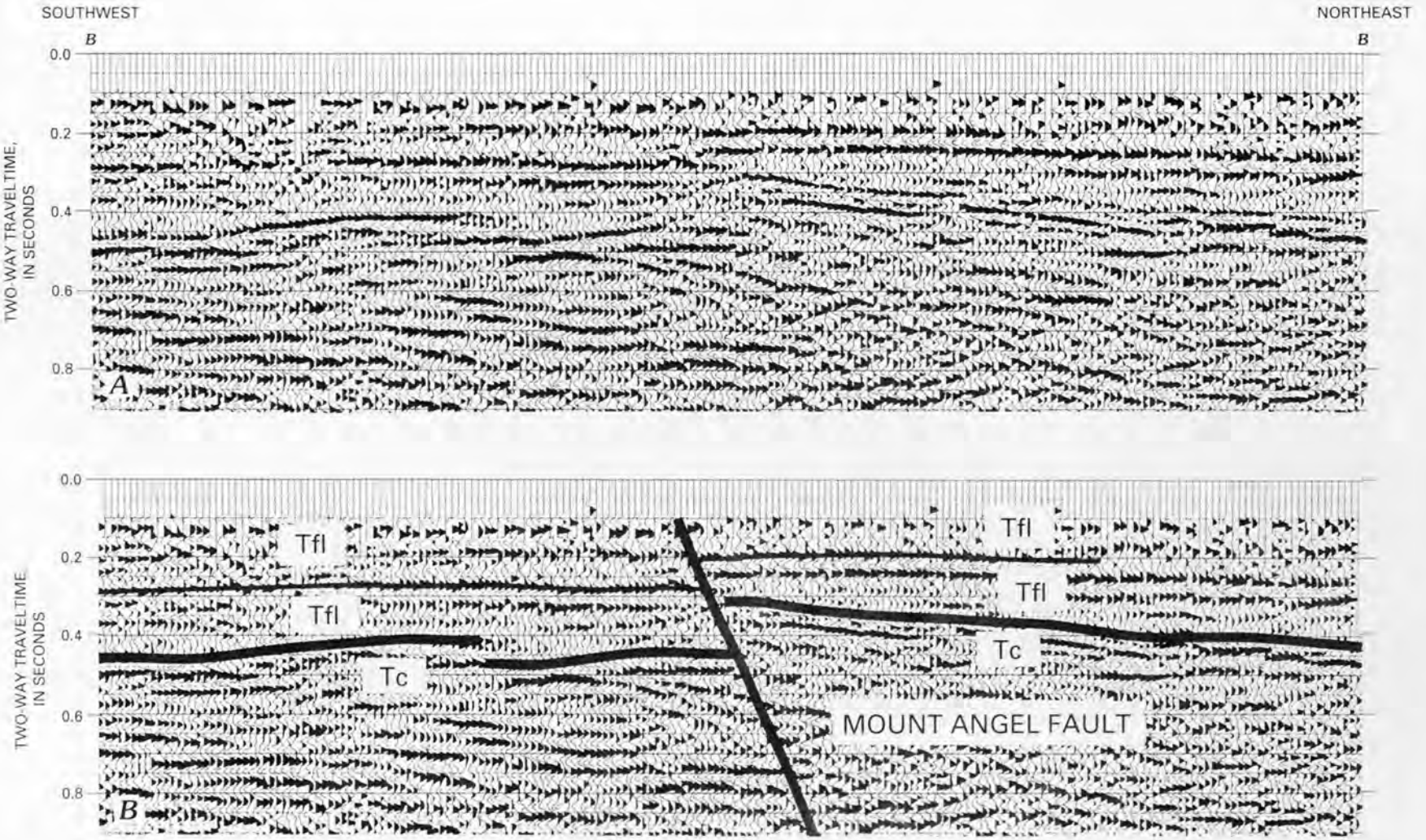

Figure 92. Seismic section *B–B'* across the Mount Angel fault, Willamette Valley, Oreg. *A*, uninterpreted section; *B*, interpreted section. The top of the basalt (unit Tc) is offset a greater amount than the unit Tfl reflector. Map-unit symbols are same as in figure 89. Line of section is shown in figure 90.

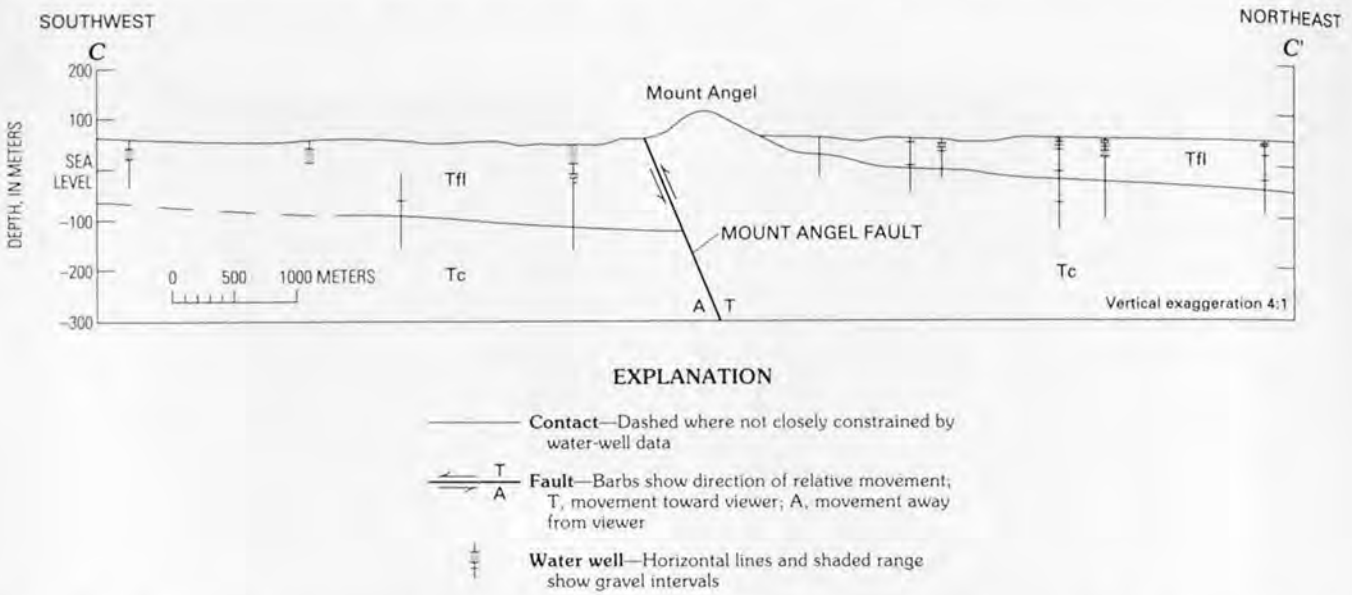

Figure 93. Cross section *C–C'* of the Mount Angel fault, Willamette Valley, Oreg., constrained by water wells. Only those parts of wells with useful well logs are shown. Base of unit Tc is not shown. The fault dip is based on seismic section *B–B'* (fig. 92). Map-unit symbols are same as in figure 89. Line of section is shown in figure 90.

faulted and has undergone upward bulging presumably related to emplacement of intrusions of the Boring Lavas (Werner, 1990). A fault (fig. 95), mapped by Glenn (1965) along the east bank of the Molalla River behind Swan Lake Farms near Canby, dips steeply to the north. A mudstone bed (fig. 95, unit I) beneath the unfaulted Willamette Formation is offset 1 m down to the north. The mudstone was correlated by Glenn (1965) with rocks now known as the Rowland Formation, although the characteristic paleosol at the top of what is now called the Diamond Hill Member is absent. Alternatively, the mudstone could be part of the pre-Rowland Formation fluvial sequence that is exposed east of Canby.

BEAVERTON FAULT ZONE

The Beaverton fault zone extends from beneath downtown Beaverton about 14 km westward along the northern flank of Cooper Mountain and the hills north of Farmington. The fault zone was originally mapped as a single fault with separation down to the north by Madin (1990) utilizing water wells. Proprietary seismic-reflection data and recently acquired aeromagnetic data (Snyder and others, 1993) show two separate traces in the area north of Cooper Mountain with a net vertical separation of 285 m down to the north. Beneath Aloha, the approximately horizontal flows of the Columbia River Basalt Group are offset 75 m down to the south; basalts of this age are south dipping at 260 m below sea level north of Cooper Mountain, whereas north-dipping flows are exposed at 100 m elevation on the northern flank of Cooper Mountain. A data gap in the seismic profile prevents precise location of the southern trace of the fault.

The westward extent of the fault zone is poorly constrained due to the paucity of deep water wells in the area north of Farmington but is interpreted to extend still farther along the northern flank of the Chehalem Mountains. Several(?) northeast-trending faults extending from the Chehalem Mountains to the Beaverton fault zone, interpreted on the basis of aeromagnetic data and water wells, are apparently truncated by the fault zone.

ELMONICA FAULT ZONE

Two subparallel faults, constrained by seismic-reflection profiles and aeromagnetic data, extend westward at least 11 km from Elmonica to the confluence of Rock and Beaverton Creeks south of Orenco (pl. 2A). The westward extent of the fault zone is unknown due to the paucity of deep water wells in the center of the basin, but interpretation of aeromagnetic data suggests the faults terminate east of Sewell.

The net vertical separation of the Columbia River Basalt Group is between 85 and 110 m down to the north. Separation on the northern trace increases westward, from about 10 m near Elmonica to 110 m south of Orenco, though possible intrusions of the Boring Lavas visible on seismic profiles complicate the structure. Seismic-reflection data show that folding of the reflectors in the upper part of the overlying sedimentary deposits increases westward; the reflectors are offset about 20 m near the mapped western end of the fault. Where the southern trace crosses seismic profiles, the vertical separation is about 75 m, and the reflectors in the overlying sedimentary deposits are not visibly offset.

HELVETIA FAULT

The northwest-trending Helvetia fault (pl. 2A) offsets the Columbia River Basalt Group from the McKay Creek valley southeastward to north of Orenco, based on water-well data. Separation is down to the southwest. The fault may extend northwestward into the Tualatin Mountains. Water wells west of Helvetia suggest as much as 100 m of vertical separation. The Helvetia fault has little aeromagnetic expression.

Undulation of the top of the Columbia River Basalt Group in the northern Tualatin basin suggests that similar faults may extend southeastward from the valleys containing the East and West Forks of Dairy Creek, though the data are inconclusive.

TUALATIN BASIN

The Columbia River Basalt Group is folded and faulted into a northwest-trending, fault-bounded, flat-bottomed basin southwest of the Tualatin Mountains and north of the Gales Creek and Newberg faults. The northeast-trending Sherwood fault (fig. 85) terminates the basin to the southeast, and the Helvetia fault and an unnamed fault on the flank of the Tualatin Mountains bound the basin to the northeast. The structure of the eastern part of the basin is complicated by the apparent intrusion of stocks composed of the Boring Lavas. Cooper Mountain and Bull Mountain, in the center of the basin southwest of Beaverton, are underlain by the Columbia River Basalt Group folded into two east-trending, doubly plunging anticlines.

Fill postdating the Columbia River Basalt Group consists of mudstone, siltstone, and sandstone with lenses of pebbly sand and gravel. The abundance of quartz and mica in these sedimentary deposits indicates a predominant source from the Columbia River, with a subordinate local source from the Columbia River Basalt Group in highlands flanking the basin. The floor of the basin is downwarped, and its axis is 200–300 m deep trending east-west. The thickest sequence of strata that postdates the Columbia River Basalt Group measures 410 m, near Hillsboro. Proprietary seismic data show that this dips much more gently than the underlying Columbia River Basalt Group.

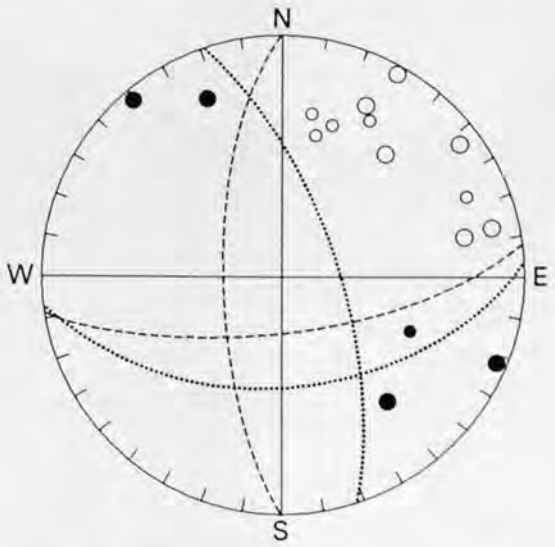

Figure 94. Composite focal mechanism for the August 1990 earthquake sequence at Woodburn, Oreg. (J.L. Nabelek, Oregon State University, written commun., 1990). Circles indicate dilatation and dots denote compression. Larger symbols indicate a stronger first motion. Three separate focal mechanisms based on wave-form analysis are indicated by solid, dashed, and dotted lines; the dashed-line focal mechanism is preferred. These mechanisms are compatible with first-motion solutions.

DISCUSSION AND CONCLUSIONS

AGE OF THE WILLAMETTE VALLEY AND COAST RANGE

The Willamette Valley is commonly referred to as a forearc basin. However, this statement is true only for the late Cenozoic after emplacement of the Columbia River Basalt Group. Strata that predate the Columbia River Basalt Group are part of a forearc basin, but this basin included the Coast Range as well as the Willamette Valley. For the most part, sedimentary facies deepen to the west across the Willamette Valley and Coast Range, as best documented by the facies boundary between the upper Eocene strandline deposits of the Spencer Formation and deeper water deposits of the Nestucca Formation. There were basaltic highlands to the west, but these did not join to form a continuous Coast Range.

The first-order structure of the Willamette Valley is an east-dipping homocline that developed after the deposition of the Oligocene and Miocene Scotts Mills Formation and prior to the emplacement of the Columbia River Basalt Group. The east dip of this homocline implies uplift of the Coast Range prior to the emplacement of the Columbia River Basalt Group, but this uplift is not clearly documented in facies changes of sedimentary rocks that predate the group. The flows of the Columbia River Basalt Group passed through the Cascade Range via the Columbia trans-arc lowland of Beeson, Tolan, and Anderson (1989) and continued to the coast as flows filling broad valleys in an incipient Coast Range. There was no marked tendency for these flows to follow the north-south trend of the modern Willamette Valley.

The fluvial deposits of the Willamette River and tributary drainages are the oldest strata to follow the present trend of the Willamette Valley. The top of the Columbia River Basalt Group beneath these deposits is commonly deeply weathered, suggesting that a long time elapsed after the emplacement of the group before these deposits began to

Figure 95. Swan Island fault exposed in the bank of the Molalla River, Willamette Valley, Oreg. The mudstone labeled unit I may be correlative with the Rowland Formation as described by Glenn (1965) at River Bend on the Willamette River, 5 km south-southwest of St. Paul; it is downdropped to the north. Unit II, the overlying Willamette Formation, is unfaulted. View to the northeast. Photograph courtesy of Jerry L. Glenn.

aggrade in the Willamette Valley. A channel cut to 150 m altitude between the Cooper and Bull Mountain uplifts and the Chehalem Mountains also suggests a substantial period of downcutting prior to sedimentation. Aggradation may have been a consequence of Coast Range uplift, raising the local base level for these fluvial sediments. Reactivation of the Gales Creek fault system and new faulting resulted in the deepening of the Tualatin basin. The Willamette Valley was downwarped, resulting in a flattening of homoclinal dips of older strata underneath the valley and, locally, a reversal of dip that produced broad synclines and anticlines.

AGE OF INITIATION OF ARC VOLCANISM EAST OF THE WILLAMETTE VALLEY

The general view is that Cascade arc volcanism began at about 43–42 Ma, based on the age of volcanic rocks at the base of the exposed sequence in the western Cascade Range. Data from wells in the Willamette Valley show that volcanic rocks of the Fisher Formation are underlain by the Yamhill Formation, which grades southeast from marine strata to volcanic and volcaniclastic rocks. The Yamhill Formation in the Willamette Valley contains early Narizian to late Ulatisian foraminifers, suggesting an age of 48–45 Ma. Coccoliths from the Yamhill Formation of the Coast Range are referred to Subzones CP 13c and CP 14a, with estimated ages of 47–42.5 Ma.

The underlying Tyee Formation shows no evidence of a nearby eastern volcanic source, suggesting that it predated the inception of a volcanic arc east of the Willamette Valley. Coccoliths from the Tyee Formation are referred to Subzones CP 12a and CP 12b, with an age estimated as 52.5–50 Ma. Thus, a volcanic arc was initiated later than 50 Ma, and arc volcanism occurred during deposition of the Yamhill Formation as early as 47 Ma. This 50–47 Ma age is coeval with the deposition of the Clarno Formation east of the Cascade Range, and the Yamhill-age arc volcanism may be part of the Clarno arc.

THE SOUTHERN WILLAMETTE VALLEY AS A BROAD STRIKE VALLEY

The older rocks of the western Cascade Range occur in an eastward-dipping homocline that strikes nearly north (Sherrod and Pickthorn, 1989). The outcrop belt is truncated at a low angle by the range front of the western Cascade Range such that the oldest sequence, dated at 45–35 Ma, is truncated in the southern Willamette Valley south of Lebanon, and the next oldest, dated at 35–25 Ma, is truncated against the Willamette Valley east of Salem. Facies boundaries between marine sedimentary rocks and volcaniclastic

rocks of late Eocene and Oligocene age strike north-northeast. This discordance between strike direction and the western Cascade Range front means that the outcrop belt of Eocene and Oligocene rocks cuts across the arc at a small angle so that the southern end of the outcrop belt consists of volcanic rocks and the northern end consists of sedimentary rocks (fig. 96).

The southern and eastern edges of the Willamette Valley appear to be controlled by the facies boundary between erosionally resistant volcanic and erosionally weak nonvolcanic rocks. The southern edge of the Willamette Valley corresponds to the northward termination of the Fisher Formation near Eugene. Volcanic rocks of the Little Butte Volcanics change facies to sedimentary rocks at the eastern margin of the southern Willamette Valley. Intrusive plugs in the Eugene Formation form isolated hills, including Peterson Butte and Bond Butte near the eastern edge of the valley.

The western edge of the valley is controlled by the contact between erosionally resistant sandstones of the Tyee Formation and the Spencer Formation on the west and erosionally weak fine-grained strata of the Eugene Formation to the east. Most of the valley is underlain by the Eugene Formation. The outcrop belt is wide because of a decrease in the east dip of the Eugene Formation accompanying downwarping of the Willamette Valley following emplacement of the Columbia River Basalt Group. The strike valley underlain by the Eugene Formation is a late Tertiary feature because it is covered by fluvial deposits of the Willamette River system.

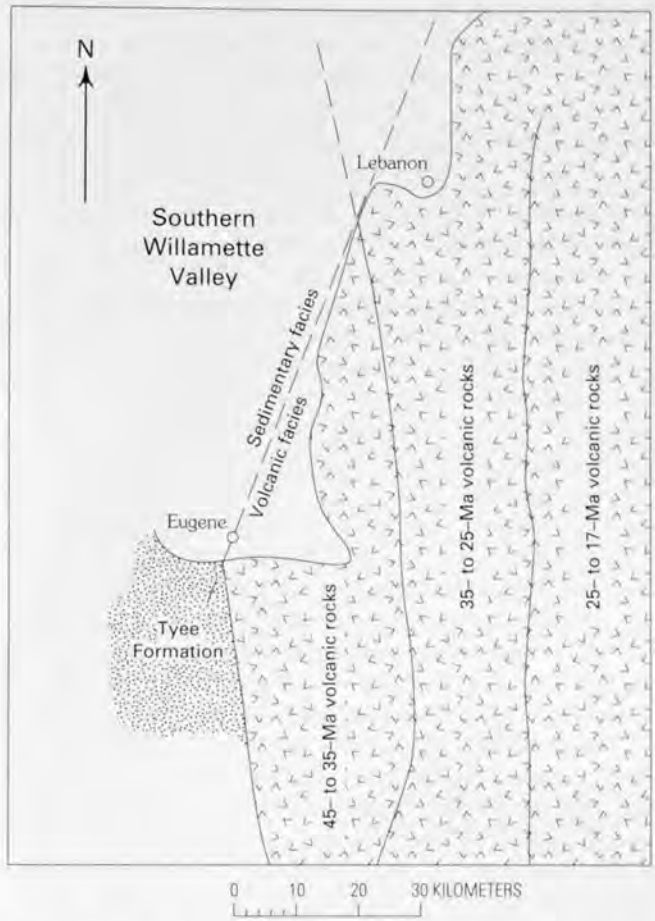

Figure 96. Map showing outcrop belts of western Cascade Range volcanic rocks (modified from Sherrod and Pickthorn, 1989) and the north-northeast-trending boundary between volcanic and sedimentary rocks (dashed line). The facies boundary controls the position of the eastern edge of the Willamette Valley; erosionally resistant volcanic rocks are to the east-southeast and weak sedimentary rocks, principally the Eugene Formation, are to the west-northwest beneath the valley.

STRUCTURAL CONTROL OF FAULT SYSTEMS

Western Oregon has undergone clockwise rotation from the Eocene through at least Miocene time, with greater rotations in the Coast Range than in the Cascade Range (Wells and Heller, 1988). This rotation has led to the development of faults with major displacement as early as the Eocene, the greatest measured displacement being on the Corvallis fault. Because these faults are zones of weakness, further movement is likely to reactivate them, even if their orientation is not parallel to the plane of maximum shear stress. The clearest example of this is the Corvallis fault, which was part of a low-angle fold-thrust system in Eocene time but was subsequently reactivated as a high-angle fault with a large component of strike slip (Goldfinger, 1990). The Gales Creek fault also had major vertical movement in Eocene time (H.J. Meyer, Oregon Natural Gas Corp., oral commun., 1991) and has been reactivated since middle Miocene time.

Werner and others (1991) compared the modern stress orientation in western Oregon using borehole breakouts with stress orientations based on earthquake focal mechanisms, alignment of volcanic vents, and orientation of conjugate faults. They found that the maximum horizontal compressive stress is oriented about north, confirming earlier studies based on less data. The fault-trend patterns in the Willamette Valley are predominantly northwest and northeast, and folds involving the section that postdates the Columbia River Basalt Group commonly strike east, in agreement with a north-south maximum horizontal compressive stress.

EARTHQUAKE HAZARD FROM CRUSTAL FAULTS IN THE WILLAMETTE VALLEY

The fluvial deposits of the Willamette River and its tributaries are cut by several faults with vertical separations as much as 250 m. In addition, these deposits are warped into broad folds that may be the surface expressions of faults at seismogenic depths. The fluvial deposits are poorly dated; paleobotanical evidence from fossil leaves and pollen favor

a late Miocene to Pliocene age, and the deposits in the Portland basin are older than the Boring Lavas, which is as young as 600 ka (Ian P. Madin, Oregon Department of Geology and Mineral Industries, oral commun., 1990). Roberts (1984) suggested that the deeply weathered high-terrace gravels of the southern Willamette Valley are the constructional top of the sequence formed by the Willamette River, and that this sequence is as young as Pleistocene.

Deposits that postdate the Columbia River Basalt Group in the Tualatin basin are cut by the Beaverton fault zone and the Helvetia fault, though some of the deformation could be attributed to intrusion of stocks, possibly of the Boring Lavas (Popowski, 1995). The Owl Creek fault (pl. 2B) cuts the Rowland Formation, which is late Pleistocene in age, beginning earlier than 36 ka and continuing past 28.5 ka. If the gravels at the Mid-Valley rock quarry between Corvallis and Philomath are part of the Rowland Formation, the Corvallis fault zone has undergone at least 40 m of vertical separation since the deposition of the Rowland Formation.

The Willamette Formation, dated as younger than 15–13 ka, shows no evidence of offset by faulting, including by the Owl Creek fault. However, seismicity on the Mount Angel fault at Woodburn indicates that this fault is active.

Because the vertical offsets of the proto-Willamette River deposits are no greater than a few hundred meters for deposits that are older than 600 ka, slip rates on Willamette Valley faults are probably small. A displacement of 300 m in 600,000 years represents a maximum average vertical slip rate of 0.5 mm/year. If the northwest- and northeast-trending faults are predominantly strike slip, the rate of 0.5 mm/year would be a minimum. However, the Mount Angel fault, with a maximum vertical offset of the top of the Columbia River Basalt Group of about 250 m, has only a 1-km lateral offset of a Ginkgo intracanyon flow of the Frenchman Springs Member of the Wanapum Basalt. There is no evidence of the amount of horizontal offset of other faults.

Faults in the Willamette Valley are relatively short in length. The mapped length of the Mt. Angel fault is about 24 km, the Waldo Hills range-front fault about 6 km, the Owl Creek fault about 15 km, and the Corvallis fault at least 35 km. The seismic moment of an earthquake with a slip of 1 m on a fault 30 km long in a crust in which the brittle-ductile transition is at 30 km would be 2.7×10^{26} dyne cm, assuming a shear modulus of 3×10^{11} dyne/cm.

It is premature to estimate the earthquake potential from crustal faults in the Willamette Valley because we do not know how much of a mapped fault would rupture in a single earthquake and we do not know what the slip would be in a single crustal earthquake. Earthquakes of moderate size have been generated in this century on the St. Helens seismic zone (Weaver and Smith, 1983), on the Portland frontal-fault structure (Yelin and Patton, 1991), and on the Mount Angel fault (Thomas and others, 1993), but we do not know if larger earthquakes are possible. Finally, we have no direct paleoseismological information about recurrence history on crustal faults in western Oregon.

REFERENCES CITED

Al-Azzaby, F.A., 1980, Stratigraphy and sedimentation of the Spencer Formation in Yamhill and Washington Counties, Oregon: Portland, Oreg., Portland State University, M.S. thesis, 104 p.

Al-Eisa, A.R.M., 1980, The structure and stratigraphy of the Columbia River Basalt in the Chehalem Mountains, Oregon: Portland, Oreg., Portland State University, M.S. thesis, 67 p.

Allen, J.E., 1975, Volcanoes of the Portland area, Oregon: Ore Bin, v. 37, no. 9, p. 145–157.

Allen, J.E., Burns, Marjorie, and Sargent, S.C., 1986, Cataclysms on the Columbia: Portland, Oreg., Timber Press, 211 p.

Allison, I.S., 1932, Spokane flood south of Portland, Oregon [abs.]: Geological Society of America Bulletin, v. 43, p. 133–134.

———1935, Glacial erratics in the Willamette Valley: Geological Society of America Bulletin, v. 46, p. 615–632.

———1936, Pleistocene alluvial stages in northwest Oregon: Science (new series), v. 83, p. 441–443.

———1953, Geology of the Albany quadrangle, Oregon: Oregon Department of Geology and Mineral Industries Bulletin 37, 18 p.

———1978, Late Pleistocene sediments and floods in the Willamette Valley: Ore Bin, v. 40, no. 11, p. 177–191 (part 1), no. 12, p. 193–202 (part 2).

Allison, I.S., and Felts, W.M., 1956, Reconnaissance geologic map of the Lebanon quadrangle, Oregon: Oregon Department of Geology and Mineral Industries Map QM–4, scale 1:62,500.

Anderson, R.W., 1963, Geology of the northwest quarter of the Brownsville quadrangle, Oregon: Eugene, University of Oregon, M.S. thesis, 62 p.

Armentrout, J.M., Hull, D.A., Beaulieu, J.D., and Rau, W.W., 1983, Correlation of Cenozoic stratigraphic units of western Oregon and Washington: Oregon Department of Geology and Mineral Industries Oil and Gas Investigations 7, 90 p.

Baker, L.J., 1988, The stratigraphy and depositional setting of the Spencer Formation, west-central Willamette Valley, Oregon—A surface-subsurface analysis: Corvallis, Oregon State University, M.S. thesis, 159 p.

Baker, V.R., and Bunker, R.C., 1985, Cataclysmic late Pleistocene flooding from Glacial Lake Missoula—A review: Quaternary Science Reviews, v. 4, p. 1–41.

Baldwin, E.M., 1948 [revised 1964], Geology of the Dallas and Valsetz 15-minute quadrangle, Polk County, Oregon: Oregon Department of Geology and Mineral Industries Bulletin 35, scale 1:62,500.

———1964, Geology of Oregon (2d ed.): Ann Arbor, Mich., Edwards Bros., Inc., 165 p.

———1974, Eocene stratigraphy of southwestern Oregon: Oregon Department of Geology and Mineral Industries Bulletin 83, 40 p.

Baldwin, E.M., Brown, R.D., Jr., Gair, J.E., and Pease, M.H., Jr., 1955, Geology of the Sheridan and McMinnville quadrangles, Oregon: U.S. Geological Survey Oil and Gas Investigations Map OM–155, scale 1:62,500.

Balster, C.A., and Parsons, R.B., 1968, Geomorphology and soils, Willamette Valley, Oregon: Corvallis, Oregon State University, Agricultural Experiment Station, Special Report 265, 31 p.

———1969, Late Pleistocene stratigraphy, southern Willamette Valley, Oregon: Northwest Science, v. 43, p. 116–129.

Beaulieu, J.D., 1974, Environmental geology of western Linn County, Oregon: Oregon Department of Geology and Mineral Industries Bulletin 84, 117 p.

Beeson, M.H., Fecht, K.R., Reidel, S.P., and Tolan, T.L., 1985, Regional correlations within the Frenchman Springs Member of the Columbia River Basalt Group—New insights into the middle Miocene tectonics of northwestern Oregon: Oregon Geology, v. 47, no. 8, p. 87–96.

Beeson, M.H., Johnson, A.G., and Moran, M.R., 1975, Portland environmental geology—Fault identification: Portland, Oreg., Portland State University, Geology Department, Earthquake Hazards Reduction Program Final Technical Report to U.S. Geological Survey, Contract 14–08–0001–14832, 107 p.

Beeson, M.H., and Tolan, T.L., 1990, The Columbia River Basalt Group in the Cascade Range—A middle Miocene reference datum for structural analysis: Journal of Geophysical Research, v. 95, p. 19547–19559.

Beeson, M.H., Tolan, T.L., and Anderson, J.L., 1989, The Columbia River Basalt Group in western Oregon—Geologic structures and other factors that controlled flow emplacement patterns, *in* Reidel, S.P., and Hooper, P.R., eds., Volcanism and tectonism in the Columbia River flood-basalt province: Geological Society of America Special Paper 239, p. 223–246.

Beeson, M.H., Tolan, T.L., and Madin, I.P., 1989, Geologic map of the Lake Oswego quadrangle, Clackamas, Multnomah, and Washington Counties, Oregon: Oregon Department of Geology and Mineral Industries Map GMS–59, scale 1:24,000.

Bela, J.L., 1979, Geologic hazards of eastern Benton County, Oregon: Oregon Department of Geology and Mineral Industries Bulletin 98, 122 p.

———1981, Geology of the Rickreall, Salem West, Monmouth, and Sidney 7½-minute quadrangle, Marion, Polk, and Linn Counties, Oregon: Oregon Department of Geology and Mineral Industries Map GMS–18.

Berg, J.W., Jr., and Baker, C.D., 1963, Oregon earthquakes, 1841 through 1958: Seismological Society of America Bulletin, v. 53, no. 1, p. 95–108.

Bird, K.J., 1967, Biostratigraphy of the Tyee Formation (Eocene), southwest Oregon: Madison, University of Wisconsin, Ph.D. dissertation, 187 p.

Bristow, M.M., 1959, The geology of the northwestern third of the Marcola quadrangle, Oregon: Eugene, University of Oregon, M.S. thesis, 70 p.

Brownfield, M.E., 1982a, Geologic map of the Grande Ronde quadrangle, Polk and Yamhill Counties, Oregon: Oregon Department of Geology and Mineral Industries Map GMS–24, scale 1:24,000.

———1982b, Geologic map of the Sheridan quadrangle, Polk and Yamhill Counties, Oregon: Oregon Department of Geology and Mineral Industries Map GMS–23, scale 1:24,000.

———1982c, Preliminary geologic map of the Ballston quadrangle, Oregon: Oregon Department of Geology and Mineral Industries Open-File Report 0–82–2, scale 1:24,000.

Brownfield, M.E., and Schlicker, H.G., 1981a, Preliminary geologic map of the Amity and Mission Bottom quadrangles, Oregon: Oregon Department of Geology and Mineral Industries Open-File Report 0–81–05, scale 1:24,000.

———1981b, Preliminary geologic map of the McMinnville and Dayton quadrangles, Oregon: Oregon Department of Geology and Mineral Industries Open-File Report 0–81–06, scale 1:24,000.

Bruer, W.G., Alger, M.P., Deacon, R.J., Meyer, H.J., Portwood, B.B., and Seeling, A.F. (project coordinators), 1984, Correlation section 24, northwest Oregon: American Association of Petroleum Geologists, Pacific Section.

Bukry, David, and Snavely, P.D., Jr., 1988, Coccolith zonation for Paleogene strata in the Oregon Coast Range, *in* Filewicz, M.V., and Squires, R.L., eds., Paleogene stratigraphy, west coast of North America: Society of Economic Paleontologists and Mineralogists, Pacific Section, West Coast Paleogene Symposium, v. 58, p. 251–263.

Chan, M.A., and Dott, R.H., Jr., 1983, Shelf and deep-sea sedimentation in Eocene forearc basin, western Oregon—Fan or non-fan?: American Association of Petroleum Geologists Bulletin, v. 67, no. 11, p. 2100–2116.

Clark, H.C., 1969, Remanent magnetization, cooling history, and paleomagnetic record of the Marys Peak sill, Oregon: Journal of Geophysical Research, v. 74, p. 3143–3160.

Committee for the Magnetic Anomaly Map of North America, 1987, Magnetic anomaly map of North America: Geological Society of America Decade of North American Geology Continent-Scale Map–003, scale 1:5,000,000.

Crouch, J.K., and Bukry, David, 1979, Comparison of Miocene provincial foraminiferal stages to coccolith zones in the California continental borderland: Geology, v. 7, p. 211–215.

Diller, J.C., 1896, A geological reconnaissance in northwestern Oregon: U.S. Geological Survey, 17th Annual Report, p. 441–520.

Duncan, R.A., 1982, A captured island chain in the Coast Range of Oregon and Washington: Journal of Geophysical Research, v. 87, no. B13, p. 10827–10837.

Fiebelkorn, R.B., Walker, G.W, MacLeod, N.S., McKee, E.H., and Smith, J.G., 1983, Index to K-Ar age determination for the State of Oregon: Isochron/West, no. 37, p. 3–60.

Frank, F.J., 1973, Ground water in the Eugene-Springfield area, southern Willamette Valley, Oregon: U.S. Geological Survey Water-Supply Paper 2018, 65 p.

Frank, F.J., and Collins, C.A., 1978, Ground water in the Newberg area, northern Willamette Valley, Oregon: Oregon Water Resources Department Ground Water Report No. 27, 77 p.

Gandera, W.E., 1977, Stratigraphy of the middle to late Eocene formations of southwestern Willamette Valley, Oregon: Eugene, University of Oregon, M.S. thesis, 75 p.

Glenn, J.L., 1965, Late Quaternary sedimentation and geological history of the north Willamette Valley, Oregon: Corvallis, Oregon State University, Ph.D. dissertation, 231 p.

Goldfinger, Chris, 1990, Evolution of the Corvallis fault and implications for the Oregon Coast Range: Corvallis, Oregon State University, M.S. thesis, 129 p.

Graven, E.P., 1990, Structure and tectonics of the southern Willamette Valley, Oregon: Corvallis, Oregon State University, M.S. thesis, 118 p.

Hammond, P.E., 1979, A tectonic model for the evolution of the Cascade Range, *in* Armentrout, J.M., Cole, M.R., and Ter Best, H.R., Jr., eds., Cenozoic paleogeography of the Western United States: Los Angeles, Society of Economic Paleontologists and Mineralogists, Pacific Section, p. 219–237.

Hammond, P.E., Anderson, J.L., and Manning, K.J., 1980, Guide to the geology of the upper Clackamas and North Santiam Rivers area, northern Oregon Cascade Range, *in* Oles, K.F., Johnson, J.G., Niem, A.R., and Niem, W.A., eds., Geologic field trips in western Oregon and southwestern Washington: Oregon

Department of Geology and Mineral Industries Bulletin 101, p. 133–167.

Hampton, E.R., 1972, Geology and ground water of the Molalla-Salem slope area, northern Willamette Valley, Oregon: U.S. Geological Survey Water-Supply Paper 1997, 83 p.

Harper, H.E., 1946, Preliminary report on the geology of the Molalla quadrangle, Oregon: Corvallis, Oregon State University, M.S. thesis, 29 p.

Hart, D.H., and Newcomb, R.C., 1965, Geology and ground water of the Tualatin Valley, Oregon: U.S. Geological Survey Water-Supply Paper 1697, 172 p.

Hartford, S.V., and McFarland, W.D., 1989, Lithology, thickness, and extent of hydrogeologic units underlying the East Portland area, Oregon: U.S. Geological Survey Water-Resources Investigations Report 88–4110, 23 p., 6 map sheets, scale 1:24,000.

Heller, P.L., and Dickinson, W.R., 1985, Submarine ramp facies model for delta-fed, sand-rich turbidite systems: American Association of Petroleum Geologists Bulletin, v. 69, p. 960–976.

Heller, P.L., Peterman, Z.E., O'Neil, J.R., and Shafiqullah, Muhammad, 1985, Isotopic provenance of sandstones from the Eocene Tyee Formation, Oregon Coast Range: Geological Society of America Bulletin, v. 96, no. 6, p. 770–780.

Hodge, E.T., 1933, Age of Columbia River and lower canyon [abs.]: Geological Society of America Bulletin, v. 44, p. 156–157.

Hoffman, C.W., 1981, A stratigraphic and geochemical investigation of ferruginous bauxite deposits in the Salem Hills, Marion County, Oregon: Portland, Oreg., Portland State University, M.S. thesis, 105 p.

Hoover, Linn, 1963, Geology of the Anlauf and Drain quadrangles, Douglas and Lane Counties, Oregon: U.S. Geological Survey Bulletin 1122–D, 62 p., 2 pls., scale 1:62,500.

Johnson, P.R., Zietz, Isidore, and Bond, K.R., 1990, U.S. West Coast revisited—An aeromagnetic perspective: Geology, v. 18, p. 332–335.

Keach R.W., II, Oliver, J.E., Brown, L.D., and Kaufman, Sidney, 1989, Cenozoic active margin and shallow Cascades structure—COCORP results from western Oregon: Geological Society of America Bulletin, v. 101, no. 6, p. 783–794.

Kleinpell, R.M., 1938, Miocene stratigraphy of California: Tulsa, Okla., American Association of Petroleum Geologists, 450 p., 22 pls.

Lentz, R.T., 1981, The petrology and stratigraphy of the Portland Hills Silt—A Pacific Northwest loess: Oregon Geology, v. 43, no. 1, p. 3–10.

Leonard, A.R., and Collins, C.A., 1983, Ground water in the northern part of Clackamas County, Oregon: Oregon Water Resources Department Ground Water Report 29, 85 p.

Lovell, J.P.B., 1969, Tyee Formation—Undeformed turbidites and their lateral equivalents, mineralogy, and paleogeography: Geological Society of America Bulletin, v. 80, no. 1, p. 9–22.

Lowry, W.D., and Baldwin, E.M., 1952, Late Cenozoic geology of the lower Columbia River Valley, Oregon and Washington: Geological Society of America Bulletin, v. 63, p. 1–24.

Luedke, R.G., and Smith, R.L., 1982, Map showing distribution, composition, and age of late Cenozoic volcanic centers in Washington and Oregon: U.S. Geological Survey Miscellaneous Investigations Series Map I–1091–D, scale 1:1,000,000.

Lux, D.R., 1982, K-Ar and ^{40}Ar–^{39}Ar ages of mid-Tertiary volcanic rocks from the western Cascade Range, Oregon: Isochron/West, no. 33, p. 27–32.

Maddox, Terrance, 1965, Geology of the southern third of the Marcola quadrangle, Oregon: Eugene, University of Oregon, M.S. thesis, 64 p.

Madin, I.P., 1990, Earthquake-hazard geology maps of the Portland metropolitan area, Oregon—Text and map explanation: Oregon Department of Geology and Mineral Industries Open-File Report 0–90–2, 21 p.

Magill, James, Cox, Allan, and Duncan, R.A., 1981, Tillamook Volcanic Series—Further evidence for tectonic rotation of the Oregon Coast Range: Journal of Geophysical Research, v. 86, no. B4, p. 2953–2970.

Mallory, V.S., 1959, Lower Tertiary biostratigraphy of the California Coast Ranges: Tulsa, Oklahoma, American Association of Petroleum Geologists, 416 p., 42 pls.

McDowell, P.F., 1991, Quaternary stratigraphy and geomorphic surfaces of the Willamette Valley, Oregon, *in* Morrison, R.B., ed., Quaternary nonglacial geology—Conterminous U.S.: Geological Society of America, Decade of North American Geology, v. K–2, p. 156–164.

McDowell, P.F., and Roberts, M.C., 1987, Field guidebook to the Quaternary stratigraphy, geomorphology and soils of the Willamette Valley, Oregon: Association of American Geographers, Annual meeting, Portland, Oreg., 1987, Field trip 3, 75 p.

McKeel, D.R., 1984, Biostratigraphy of exploratory wells, northern Willamette basin, Oregon: Oregon Department of Geology and Mineral Industries Oil and Gas Investigations 12, 19 p.

———1985, Biostratigraphy of exploratory wells, northern Willamette basin, Oregon: Oregon Department of Geology and Mineral Industries Oil and Gas Investigations 13, 17 p.

McWilliams, R.G., 1968, Paleogene stratigraphy and biostratigraphy of central-western Oregon: Seattle, University of Washington, Ph.D. dissertation, 140 p.

———1973, Stratigraphic and biostratigraphic relationships of the Tyee and Yamhill Formations in central-western Oregon: Ore Bin, v. 35, no. 11, p. 169–186.

———1980, Eocene correlations in western Oregon-Washington: Oregon Geology, v. 42, no. 9, p. 151–158.

Miller, P.R., and Orr, W.N., 1984a, Geologic map of the Scotts Mills quadrangle, Oregon: Oregon Department of Geology and Mineral Industries Map GMS–33, scale 1:24,000.

———1984b, Geologic map of the Wilhoit quadrangle, Oregon: Oregon Department of Geology and Mineral Industries Map GMS–32, scale 1:24,000.

———1988, Mid-Tertiary transgressive rocky coast sedimentation—Central western Cascade Range, Oregon: Journal of Sedimentary Petrology, v. 58, p. 959–968.

Molenaar, C.M., 1985, Depositional relationships of the Umpqua and Tyee Formations (Eocene), southwestern Oregon: American Association of Petroleum Geologists Bulletin, v. 69, no. 8, p. 1217–1229.

Mullineaux, D.R., Wilcox, R.E., Ebaugh, F.W., Fryxell, R., and Rubin, Meyer, 1978, Age of the last major scabland flood of the Columbia Plateau in eastern Washington: Quaternary Research, v. 10, no. 2, p. 67–70.

Newton, V.C., 1969, Subsurface geology of the lower Columbia and Willamette basins, Oregon: Oregon Department of Geology and Mineral Industries Oil and Gas Investigations 2, 121 p.

Niem, W.A., MacLeod, N.S., and Priest, G.R., 1987, Geology, *in* CH_2M-Hill, Superconducting super collider site proposal, University site, Oregon, v. 3, Geology and tunneling: Corvallis, Oreg., CH_2M Hill, p. 3–2 to 3–20.

Niem, A.R., and Niem, W.A., 1985, Oil and gas investigation of the Astoria basin, Clatsop and northernmost Tillamook Counties, northwest Oregon: Oregon Department of Geology and Mineral Industries Map OGI–14, 8 p., correlation chart, scale 1:100,000.

North American Commission on Stratigraphic Nomenclature, 1983, North American stratigraphic code: American Association of Petroleum Geologists Bulletin, v. 67, no. 5, p. 841–875.

Orr, W.N., and Miller, P.R., 1984, Geologic map of the Stayton NE quadrangle, Oregon: Oregon Department of Geology and Mineral Industries Map GMS–34, scale 1:24,000.

———1986, Geologic map of the Drake Crossing quadrangle, Marion County, Oregon: Oregon Department of Geology and Mineral Industries Map GMS–50, scale 1:24,000.

Parsons, R.B., Simmons, G.H., and Balster, C.A., 1968, Pedogenic and geomorphic relationships of associated Aqualfs, Albolls and Xerolls in western Oregon: Soil Science Society of America Proceedings, v. 32, p. 556–563.

Peck, D.L., Griggs, A.B., Schlicker, H.G., Wells, F.G., and Dole, H.M., 1964, Geology of the central and northern parts of the western Cascades, Oregon: U.S. Geological Survey Professional Paper 449, 56 p.

Phillips, W.M., Walsh, T.J., and Hagen, R.A., 1989, Eocene transition from oceanic to arc volcanism, southwest Washington, *in* Muffler, L.J.P., Weaver, C.S., and Blackwell, D.D., eds., Proceedings of workshop XLIV, Geological, geophysical, and tectonic setting of the Cascade Range: U.S. Geological Survey Open-File Report 89–178, p. 199–256.

Piper, A.M., 1942, Ground-water resources of the Willamette Valley, Oreg.: U.S. Geological Survey Water-Supply Paper 890, 194 p.

Poore, R.Z., 1976, Microfossil correlation of California lower Tertiary sections—A comparison: U.S. Geological Survey Professional Paper 743–F, 8 p., 2 pls.

———1980, Age and correlation of California Paleogene benthic foraminiferal stages: U.S. Geological Survey Professional Paper 1162–C, 8 p.

Popowski, T.A., 1995, Structure, subsurface geology, and neotectonic history of the Tualatin basin, northwestern Oregon: Corvallis, Oregon State University, M.S. thesis.

Price, Don, 1967, Geology and water resources in the French Prairie area, northern Willamette Valley, Oregon: U.S. Geological Survey Water Supply-Paper 1833, 98 p.

Priest, G.R., 1989, Volcanic and tectonic evolution of the Cascade volcanic arc, 44°00' to 44°52'30"N, *in* Muffler, L.J.P., Weaver, C.S., and Blackwell, D.D., eds., Proceedings of workshop XLIV, Geological, geophysical, and tectonic setting of the Cascade Range: U.S. Geological Survey Open-File Report 89–178, p. 430–489.

———1990, Volcanic and tectonic evolution of the Cascade volcanic arc, central Oregon: Journal of Geophysical Research, v. 95, no. B12, p. 19583–19599.

Priest, G.R., and Vogt, B.F., eds., 1983, Geology and geothermal resources of the central Oregon Cascade Range: Oregon Department of Geology and Mineral Industries Special Paper 15, 123 p.

Riddihough, R.P., 1984, Recent movements of the Juan de Fuca plate system: Journal of Geophysical Research, v. 89, no. B8, p. 6980–6994.

Roberts, A.E., 1953, A petrographic study of the intrusives at Marys Peak, Benton County, Oregon: Northwest Science, v. 27, p. 43–60.

Roberts, M.C., 1984, The late Cenozoic history of an alluvial fill—The southern Willamette Valley, Oregon, *in* Mahaney, W.C., ed., Correlation of Quaternary chronologies: Norwich, Great Britain, Geo Books, p. 491–504.

Roberts, M.C., and Whitehead, D.R., 1984, The palynology of a nonmarine Neogene deposit in the Willamette Valley, Oregon: Review of Palaeobotany and Palynology, v. 41, p. 1–12.

Schlicker, H.G., and Deacon, R.J., 1967, Engineering geology of the Tualatin Valley region, Oregon: Oregon Department of Geology and Mineral Industries Bulletin 60, 103 p.

Schlicker, H.G., and Finlayson, C.T., 1979, Geology and geologic hazards of northwestern Clackamas County, Oregon: Oregon Department of Geology and Mineral Industries Bulletin 99, 79 p.

Sherrod, D.R., and Pickthorn, L.B., 1989, Some notes on the Neogene structural evolution of the Cascade Range in Oregon, *in* Muffler, L.J.P., Weaver, C.S., and Blackwell, D.D., eds., Proceedings of Workshop XLIV, Geological, geophysical, and tectonic setting of the Cascade Range: U.S. Geological Survey Open-File Report 89–178, p. 351–368.

Sherrod, D.R., and Smith, J.G., 1989, Preliminary map of upper Eocene to Holocene volcanic and related rocks of the Cascade Range, Oregon: U.S. Geological Survey Open-File Report 89–14, 20 p., scale 1:500,000.

Snavely, P.D., Jr., and Baldwin, E.M., 1948, Siletz River Volcanic Series, northwestern Oregon: American Association of Petroleum Geologists Bulletin, v. 32, p. 806–812.

Snavely, P.D., Jr., MacLeod, N.S., and Wagner, H.C., 1968, Tholeiitic and alkalic basalts of the Eocene Siletz River Volcanics, Oregon Coast Range: American Journal of Science, v. 266, no. 6, p. 454–481.

Snavely, P.D., Jr., and Vokes, H.E., 1949, Geology of the coastal area between Cape Kiwanda and Cape Foulweather, Oregon: U.S. Geological Survey Oil and Gas Investigations Map 97, scale 1:62,500.

Snavely, P.D., Jr., and Wagner, H.C., 1961, Differentiated gabbroic sills and associated alkalic rocks in the central part of the Oregon Coast Range, Oregon, *in* Short papers in the geologic and hydrologic sciences: U.S. Geological Survey Professional Paper 424–D, p. 156–161.

Snavely, P.D., Jr., Wagner, H.C., and Lander, D.L., 1980, Interpretation of the Cenozoic geologic history, central Oregon continental margin—Cross-section summary: Geological Society of America Bulletin, v. 91, part 1, p. 143–146.

Snavely, P.D., Jr., Wagner, H.C., and MacLeod, N.S., 1964, Rhythmic bedded eugeosynclinal deposits of the Tyee Formation, Oregon Coast Ranges: Kansas Geological Survey Bulletin 169, p. 461–480.

Snyder, S.L., Felger, T.J., Blakely, R.J., and Wells, R.E., 1993, Aeromagnetic map of the Portland-Vancouver metropolitan area Oregon and Washington: U.S. Geological Survey Open-File Report 93–211, scale 1:100,000.

Sutter, J.F., 1978, K/Ar ages of Cenozoic volcanic rocks from the Oregon Cascades west of 120°30': Isochron/West, no. 21, p. 15–21.

Swanson, R.D., 1986, A stratigraphic-geochemical study of the Troutdale Formation and Sandy River Mudstone in the Portland basin and lower Columbia River Gorge: Portland, Oreg., Portland State University, M.S. thesis, 103 p.

Tabor, R.W., and Cady, W.M., 1978, The structure of the Olympic Mountains, Washington—Analysis of a subduction zone: U.S. Geological Survey Professional Paper 1033, 38 p.

Taylor, E.M., 1990, Volcanic history and tectonic development of the central high Cascade Range, Oregon: Journal of Geophysical Research, v. 95, p. 19611–19622.

Thayer, T.P., 1939, Geology of the Salem Hills and the North Santiam River basin, Oregon: Oregon Department of Geology and Mineral Industries Bulletin 15, 40 p.

Thomas, G.C., Crosson, R.S., Dewberry, S., Pullen, J., Yelin, T.S., Norris, R.D., Bice, W.T., Carver, D.L., Meremonte, M.E., Overturf, D.E., Worley, D.M., Sembera, E.D, and MacDonald, T.R., 1993, The 25 March 1993 Scotts Mills, Oregon earthquake—Aftershock analysis from combined permanent and temporary digital stations [abs.]: EOS [American Geophysical Union Transactions], v. 74, no. 43/Supplement, p. 201.

Tolan, T.L., and Beeson, M.H., 1984, Intracanyon flows of the Columbia River Basalt Group in the lower Columbia River Gorge and their relationship to the Troutdale Formation: Geological Society of America Bulletin, v. 95, no. 4, p. 463–477.

Tolan, T.L., Reidel, S.P., Beeson, M.H., Anderson, J.L., Fecht, K.R., and Swanson, D.A., 1989, Revisions to the estimates of the areal extent and volume of the Columbia River Basalt Group, *in* Reidel, S.P., and Hoover, P.R., eds., Volcanism and tectonism in the Columbia River flood-basalt province: Geological Society of America Special Paper 239, p. 1–20.

Treasher, R.C., 1942, Geologic history of the Portland area: Oregon Department of Geology and Mineral Industries, GMI Short Paper 7, 17 p.

Trimble, D.E., 1963, Geology of Portland, Oregon, and adjacent areas: U.S. Geological Survey Bulletin 1119, 119 p.

Turner, F.E., 1938, Stratigraphy and mollusca of the Eocene of western Oregon: Geological Society of America Special Paper 10, 130 p.

Unruh, J.R., Popowski, T.A., Wong, I.G., and Wilson, D.C., 1994, Implications of late Neogene to Quaternary folds and thrusts for deformation of the Cascadia fore-arc region, N.W. Oregon: Geological Society of America Abstracts with Programs, Annual Meeting, v. 26, no. 7, p. A–187.

Van Atta, R.D., and Kelty, K.B., 1985, Scappoose Formation, Columbia County, Oregon—New evidence of age and relation to Columbia River Basalt Group: American Association of Petroleum Geologists Bulletin, v. 69, p. 688–698.

Verplanck, E.P., 1985, Temporal variations in volume and geochemistry of volcanism in the western Cascades, Oregon: Corvallis, Oregon State University, M.S. thesis, 115 p.

Verplanck, E.P., and Duncan, R.A., 1987, Temporal variations in plate convergence and eruption rates in the Western Cascades, Oregon: Tectonics, v. 6, p. 197–209.

Vokes, H.E., Myers, D.A., and Hoover, Linn, 1954, Geology of the west central border area of the Willamette Valley, Oregon: U.S. Geological Survey Oil and Gas Investigations Map OM–150, scale 1:62,500.

Vokes, H.E., Snavely, P.D., Jr., and Myers, D.A., 1951, Geology of the southern and southwestern border area of the Willamette Valley, Oregon: U.S. Geological Survey Oil and Gas Investigations Map OM–110, scale 1:62,500.

Waitt, R.B., Jr., 1985, Case for periodic, colossal jökulhlaups from Pleistocene Glacial Lake Missoula: Geological Society of America Bulletin, v. 96, no. 10, p. 1271–1286.

Walker, G.W., and Duncan, R.A., 1989, Geologic map of the Salem 1° by 2° quadrangle, western Oregon: U.S. Geological Survey Miscellaneous Investigations Series Map I–1893, scale 1:250,000.

Wannamaker, P.E., Booker, J.R., Jones, A.G., Chave, A.D., Filloux, J.H., Waff, H.S., and Law, L.K., 1989, Resistivity cross section through the Juan de Fuca subduction system and its tectonic implications: Journal of Geophysical Research, v. 94, p. 14127–14144.

Weaver, C.S., and Smith, S.W., 1983, Regional tectonic and earthquake hazards implications of a crustal fault zone in southwestern Washington: Journal of Geophysical Research, v. 88, no. B12, p. 10371–10383.

Wells, F.G., and Waters, A.C., 1934, Quicksilver deposits of southwestern Oregon: U.S. Geological Survey Bulletin 850, 58 p.

Wells, F.G., 1956, Geology of the Medford quadrangle, Oregon-California: U.S. Geological Survey Geologic Quadrangle Map GQ–89, scale 1:96,000.

Wells, R.E., Niem, A.R., Macleod, N.S., Snavely, P.D, Jr., and Niem, W.A., 1983, Preliminary geologic map of the west half of the Vancouver (Washington-Oregon) 1° by 2° quadrangle, Oregon: U.S. Geological Survey Open-File Report 83–0591, scale 1:250,000.

Wells, R.E., Engebretson, D.C., Snavely, P.D., Jr., and Coe, R.S., 1984, Cenozoic plate motions and the volcano-tectonic evolution of western Oregon and Washington: Tectonics, v. 3, no. 2, p. 275–294.

Wells, R.E., and Heller, P.L., 1988, The relative contribution of accretion, shear, and extension to Cenozoic tectonic rotation in the Pacific Northwest: Geological Society of America Bulletin, v. 100, no. 3, p. 325–338.

Wells, R.E., Simpson, R.W., Bentley, R.D., Beeson, M.H., Mangan, M.T., and Wright, T.L., 1989, Correlation of Miocene flows of the Columbia River Basalt Group from the central Columbia River Plateau to the coast of Oregon and Washington, *in* Reidel, S.P., and Hooper, P.R., eds., Volcanism and tectonism in the Columbia River flood-basalt province: Geological Society of America Special Paper 239, p. 113–129.

Werner, K.S., 1990, I, Direction of maximum horizontal compression in western Oregon determined by borehole breakouts; II, Structure and tectonics of the northern Willamette Valley, Oregon: Corvallis, Oregon State University, M.S. thesis, 156 p.

Werner, K.S., Graven, E.P., Berkman, T.A., and Parker, M.J., 1991, Direction of maximum horizontal compression in western Oregon determined by borehole breakouts: Tectonics, v. 10, no. 5, p. 948–958.

Werner, K.S., Nabelek, J.L., Yeats, R.S., and Malone, S.D., 1992, The Mount Angel fault—Implications of seismic-reflection data and the Woodburn, Oregon, earthquake sequence of August 1990: Oregon Geology, v. 54, no. 5, p. 112–117.

Yeats, R.S., 1988, Late Quaternary slip rates on the Oak Ridge fault, Transverse Ranges, California—Implications for seismic risk: Journal of Geophysical Research, v. 93, p. 12137–12149.

Yelin, T.S., and Patton, H.J., 1991, Seismotectonics of the Portland, Oregon, region: Seismological Society of America Bulletin, v. 81, no. 1, p. 109–130.

ACTIVE STRIKE-SLIP FAULTING AND FOLDING OF THE CASCADIA SUBDUCTION-ZONE PLATE BOUNDARY AND FOREARC IN CENTRAL AND NORTHERN OREGON

By Chris Goldfinger,[1] LaVerne D. Kulm,[2] Robert S. Yeats,[1] Bruce Appelgate,[3] Mary E. MacKay,[3] *and* Guy R. Cochrane[4]

ABSTRACT

Three west-northwest-trending left-lateral strike-slip faults on the abyssal plain off central Oregon between lat 44°40'N. and lat 45°12'N. have been mapped using seismic reflection, sidescan sonar, data from ALVIN submersible dives, and SeaBeam bathymetry. These oblique faults, the Wecoma fault and faults B and C, intersect the north-south-striking structures of the active accretionary wedge. The faults cut the oceanic lithosphere of the subducting Juan de Fuca plate and appear to cross the plate boundary. The best studied of these, the Wecoma fault, extends 18 km northwestward across the abyssal plain from the deformation front. Displacement on this fault is 5.5± 0.8 km at the deformation front, decreasing to zero at the northwestern fault tip, based upon piercing-point offset. The Wecoma fault has been active for about 600±50 thousand years and has an average slip rate of 7–10 mm/year. The late Pleistocene-Holocene slip rate is 5–12 mm/year. These faults are active, as indicated by the offset of the youngest sedimentary units, the presence of surficial fault scarps, and the venting of deep source fluids. The Wecoma fault intersects the deformation front in a complex structural zone consisting of fault-bounded pop-ups (uplifted asymmetrical triangular plateaus), an embayment in the deformation front, and a local reversal of vergence in the basal thrust of the accretionary wedge.

Linear gullies and scarps in the Wecoma fault zone extend into the first several thrust ridges of the continental slope, suggesting that this fault remains active beneath the accretionary wedge. Changes in fold orientation and amount of shortening in the initial three to four thrust ridges of the accretionary wedge suggest that the strike-slip faults have influenced the development of coeval accretionary-wedge structures through differential slip of the downgoing plate.

Several west-northwest-trending deformation zones have been mapped on the continental slope off northern and central Oregon. The zones are composed of west-northwest-trending linear scarps, en echelon northwest to west-northwest-trending folds, and left-stepping and sigmoidally bent folds. Oblique folds are commonly fault-propagation and fault-bend folds developed above high-angle faults. Some of these active faults and folds striking north-northwest to west-northwest are refolding somewhat older north and north-northeast-trending folds. Deformation in these zones is consistent with a left-lateral sense of shear. Three of the zones adjoin the three abyssal-plain strike-slip faults, whereas at least one zone and possibly several others are restricted to the continental slope. We postulate that these are shear zones developed in the upper plate above the subducted strike-slip faults or, alternatively, that strike-slip faulting in the upper plate has propagated seaward into the subducting plate.

INTRODUCTION

The Cascadia subduction zone (fig. 97) off Oregon and Washington is one of the best studied subduction zones in the world. Its proximity to major United States ports and three decades of study by oceanographic institutions, government agencies, and industry have produced an extensive

[1]Department of Geosciences, Oregon State University, Corvallis, Oregon 97331.

[2]College of Oceanography, Oregon State University, Corvallis, Oregon 97331.

[3]School of Ocean and Earth Science and Technology, University of Hawaii, Honolulu, Hawaii 96822.

[4]Earth Sciences, University of California at Santa Cruz, California 95064.

data set for use in geologic and geophysical investigations. In recent years, attention has been focused on the anomalous seismic quiescence of much of the Cascadia subduction zone in comparison to other subduction zones. The moderate plate-convergence rate of 40 mm/year directed 062° (calculated from the Juan de Fuca-North America Euler vector of DeMets and others, 1990) and the relative youth of the subducting lithosphere (10–9 Ma, according to Wilson and others, 1984) characterize the Cascadia subduction zone as a Chilean-type convergent margin (Heaton and Kanamori, 1984). Because most Chilean-type margins have had great (*M* greater than 8.4) earthquakes in historical times, the Juan de Fuca-North America plate boundary should also be capable of generating great earthquakes. Geologic evidence for great earthquakes has been inferred from buried marsh deposits of the coastal bays of Washington (Atwater, 1987; Atwater and Yamaguchi, 1991), Oregon (Darienzo and Peterson, 1990), and northern California (Vick, 1988; Carver and others, 1989; Clarke and Carver, 1989). Rapid coseismic submergence in the bays, accompanied by tsunamis, is inferred from peat layers overlain by marine sands (Atwater, 1987). Presently, however, the Oregon Cascadia convergent margin may have the lowest incidence of plate-boundary seismicity of any subduction zone. Although earthquakes in the upper and lower plates are well monitored by the University of Washington seismic network, no thrust-type earthquakes at any magnitude level have been located on the plate interface (Ludwin and others, 1991). The absence of historical great earthquakes on the plate boundary can be explained by long recurrence intervals of 300–1,000 years or more (Atwater, 1987; Carver and others, 1989; Adams, 1990; Darienzo and Peterson, 1990; Atwater and Yamaguchi, 1991), yet the plate interface remains singularly quiet among the world's convergent margins.

The low seismicity of the Cascadia subduction zone has led investigators to explore a variety of hypotheses to explain the apparent seismic gap along the Cascadia margin (see Ando and Balasz, 1979; West and McCrumb, 1988; Sykes, 1989). Our investigation of the structure of the plate boundary and forearc off the Oregon coast was motivated in part by the discovery of three oblique strike-slip faults in the abyssal plain off central Oregon. These faults cut the subducting Juan de Fuca plate and cross the plate boundary, extending some distance into the overriding North America plate. To our knowledge, faults of this type have not previously been described from other subduction zones around the world, although strike-slip faulting restricted to the upper plate has been described in both orthogonal and oblique convergent settings (Lewis and others, 1988, and references therein; Geist and others, 1988). This discovery is almost certainly the result of the increased resolution of sea-floor mapping tools in recent years, but these faults may also represent something unique about this convergent margin. The discovery of these faults suggests that detailed structural investigations may offer new information about oblique subduction in general and the Cascadia subduction zone in particular.

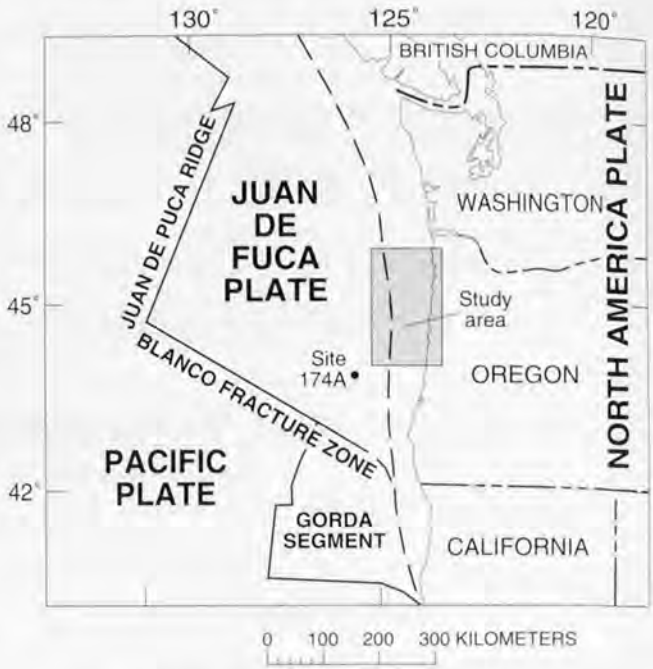

Figure 97. Index map showing tectonics of the Cascadia subduction zone. The dashed line is the plate-convergence boundary. The dot indicates Deep Sea Drilling Project site 174A.

The purpose of this chapter is to document the structural characteristics of the Wecoma fault, the largest and best known of the three strike-slip faults discovered on the abyssal plain off Oregon, and to discuss the relationship of this fault to new mapping of active tectonic features of the continental slope. The long-term goal of this study is to better define the active tectonics of the Cascadia subduction zone and thereby develop a better understanding of the regional tectonics and seismic hazards of the Pacific Northwest. The chapter concludes with a discussion of possible origins for the oblique faults, and the implications of the oblique faults and folds we have mapped for plate-boundary processes within the Cascadia convergent margin.

ACKNOWLEDGMENTS

We thank Richard Perry and Steven Mutula, U.S. National Oceanic and Atmospheric Administration (NOAA), National Ocean Survey, Rockville, Md., for preliminary copies of the SeaBeam bathymetry of the Oregon continental margin. They have also allowed us to publish a part of a three-dimensional-mesh diagram of the northern and central Oregon continental margin generated at their facility. We thank Sigmund Snelson and Dan Worrall of Shell Oil Company for the loan of seismic profiles of the Oregon and Washington continental shelf and for their efforts in locating these profiles in the company archives. We also thank Parke D. Snavely, Jr., Samuel H. Clarke, Jr.,

and Dan L. Orange for thorough reviews of the manuscript. The first two reviewers do not necessarily agree with all of our interpretations of oblique faults and folds on the upper continental slope or shelf; these conclusions are solely our responsibility. This research was supported by National Science Foundation grants OCE–8812731 (OSU) and OCE–8821577 (UH) and by the U.S. Geological Survey National Earthquake Hazards Reduction Program under award 14–08–001–G1800 (OSU). We thank the crews of the vessels *R.V. Wecoma*, *Digicon M.V. Geotide*, and *R.V. Atlantis II*, and also Margaret Mumford and Cheryl Hummon of Oregon State University for drafting the illustrations.

METHODS OF STUDY

We are studying the submerged plate boundary and forearc region off Oregon and Washington (fig. 97) using SeaMARC 1A and GLORIA sidescan sonar imagery, SeaBeam swath bathymetry, ALVIN submersible observations, and a dense network of single-channel and multichannel seismic (MCS) surveys. We are mapping the Oregon-Washington plate boundary and submarine forearc at a scale of 1:500,000. We have used about 30,000 km of seismic-reflection profiles collected by Oregon State University, the University of California at Santa Cruz, the University of Hawaii, the University of Washington, the Scripps Institution of Oceanography, the U.S. Geological Survey, NOAA, and the oil industry (fig. 98).

The seismic-reflection profiles vary widely in quality, depth of penetration, and navigational accuracy, ranging from single-channel sparker records navigated with Loran A to 144-channel digital profiles navigated with the Global Positioning System (GPS). Partly in preparation for the National Science Foundation's Ocean Drilling Program (ODP) Leg 146, a site survey consisting of closely spaced, high-resolution MCS lines, SeaMARC 1A sidescan mapping, SeaBeam swath bathymetry, and ALVIN submersible dives focused on the plate boundary and accretionary wedge at the proposed drilling sites near lat 45°N. (fig. 99). Within this 6,000-km^2 area, we were able to map submarine structures in considerable detail.

Within the ODP site-survey area (fig. 99), position information from the 144-channel reflection profiles was used as the datum for mapping that portion of the larger study area. Processing through time migration was carried out at the University of Hawaii. Several other U.S. Geological Survey 24-channel and Oregon State University single-channel lines also constrain the structural interpretations. The sidescan and bathymetric surveys were navigated with a combination of GPS and Transit satellite navigation, with Loran C tracking used between satellite fixes. Navigation of the deep-towed sidescan towfish was by the method described by Appelgate (1988). Where spatial misfits occurred, we adjusted the sidescan data to best fit the GPS-navigated MCS lines or the SeaBeam bathymetry where appropriate. SeaMARC 1A sidescan data were collected with a deep-towed 30-kHz system capable of imaging 2-km- or 5-km-swath widths having spatial resolutions of 1 m and 2.5 m, respectively. A magnetometer attached to the towfish recorded total field intensity over the sidescan tracks. Our technique with sidescan surveys was to cover the study area at the wider 5-km swath width, then return to areas of interest and conduct detailed surveys using the higher resolution 2-km swath. Sidescan processing, which included geometric and speed corrections, correction for towfish position, georeferencing of image pixels to a latitude-longitude grid, and image enhancement (as described in Appelgate, 1988), was done at the NOAA image-processing facility in Newport, Oreg. Outside the ODP site-survey area, navigational accuracy was more variable. Loran-A-navigated profiles have maximum errors on the order of 1–3 km, Loran C errors are about 0–1.5 km, and Transit satellite errors range from near zero up to hundreds of meters. The dense coverage of reflection profiles allowed adjustment of older tracklines where crossed by satellite-navigated lines.

STRIKE-SLIP FAULTS ON THE JUAN DE FUCA PLATE

Along the central Oregon convergent margin, the three west-northwest-trending left-lateral strike-slip faults (Wecoma fault and faults B and C in fig. 100) extend from the base of the continental slope 10–18 km northwestward across the abyssal plain. First imaged using SeaMARC 1A sidescan sonar in 1986, these faults were surveyed in detail in 1989 using a narrow-swath, high-resolution survey (Appelgate and others, 1992) and were crossed several times by MCS profiles in 1989. In reflection profiles of the abyssal plain, the three faults show vertical separation of both the oceanic basement and the 2- to 3-km-thick overlying sedimentary section (Appelgate and others, 1992; MacKay and others, 1992; this study). The faults strike 290°–295°, and all three are primarily strike-slip with a minor up-to-the-north component of displacement as evidenced by offset surface and subsurface features. In this paper, we discuss primarily the Wecoma fault because this fault is better covered by seismic and sidescan surveys. Faults B and C appear to be similar in structural style to the Wecoma fault, but the sparse data available on these faults presently precludes a detailed assessment of them.

CHARACTERISTICS OF THE WECOMA FAULT

The Wecoma fault is the longest and best developed of the three strike-slip faults on the abyssal plain (fig. 100). The general physiography of the Wecoma fault, its associated

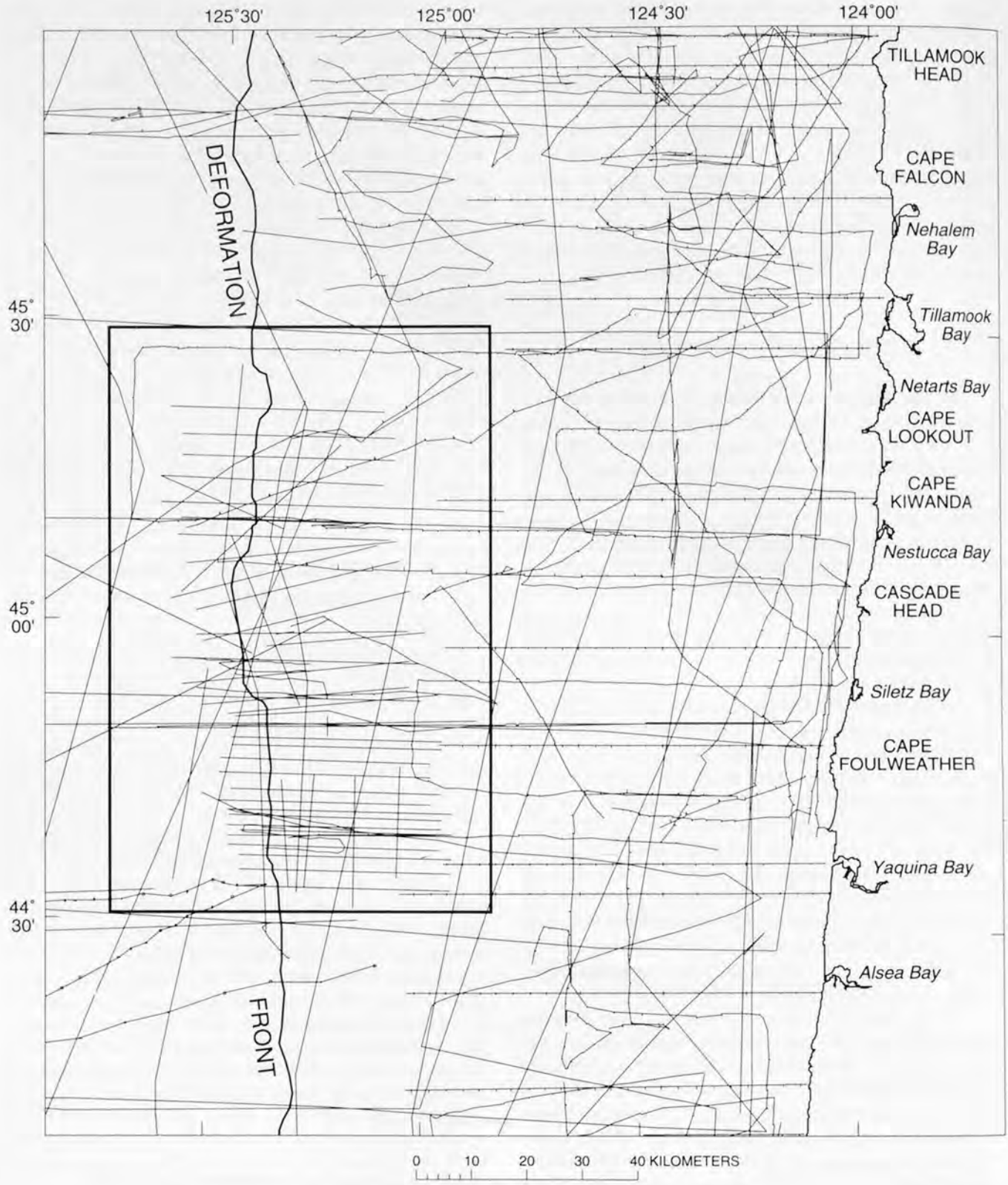

Figure 98. Trackline map of the northwestern Oregon coast showing the location of all seismic-reflection profiles used in this study. Trackline tick marks are hourly or quarter-hourly ship positions. The deformation front of the accretionary prism is shown. The box is the area in figure 99.

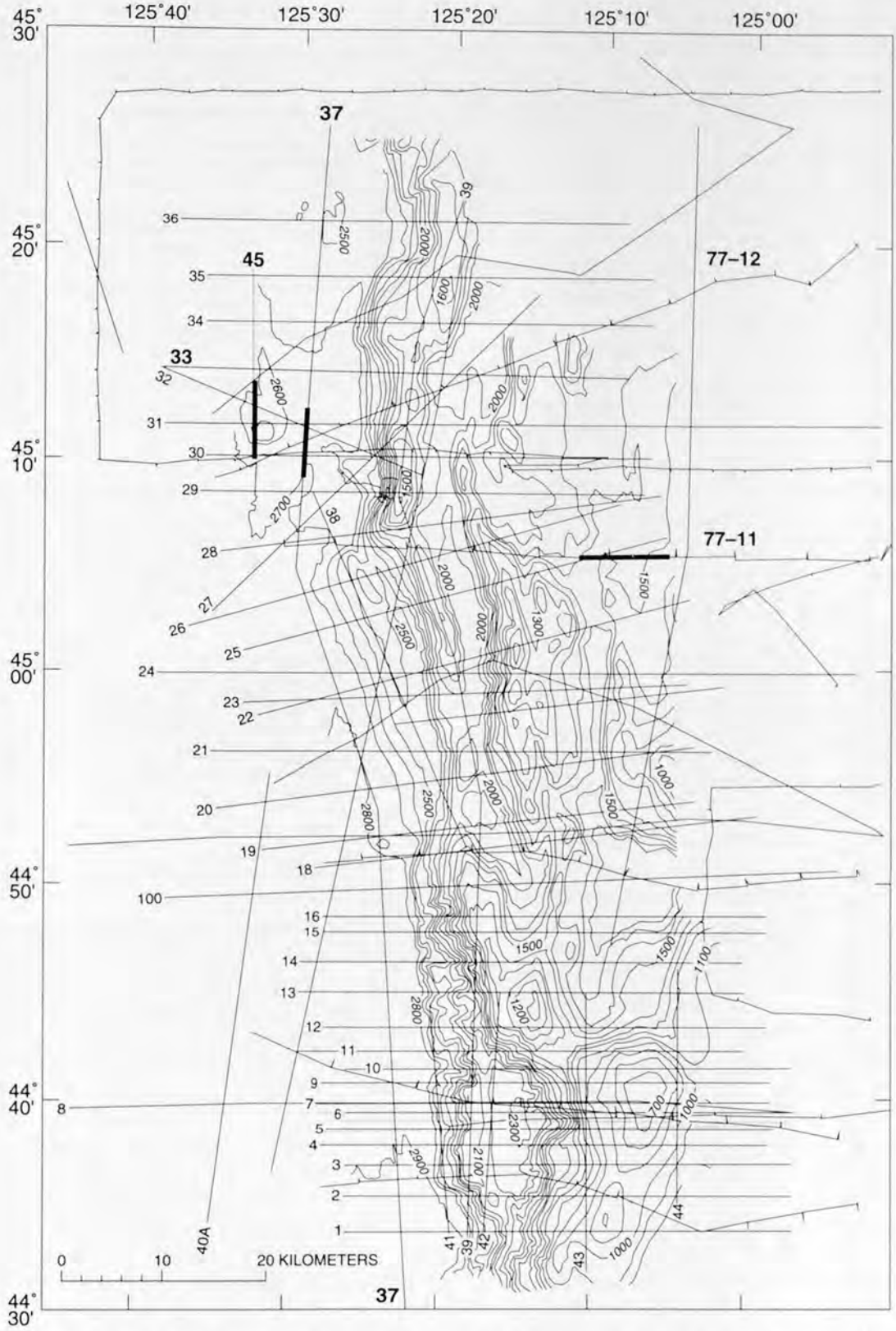

Figure 99. Map showing seismic-reflection tracklines and bathymetry in the Ocean Drilling Program (ODP) site-survey area off the northwestern Oregon coast. The location of this map is shown in figure 98. Depths are in meters; contour interval is 100 m. Bold-numbered lines are referred to in the text. Bold segments of lines 37, 45, and 77–11 are sections of profiles shown in figures 104, 105, and 117, respectively.

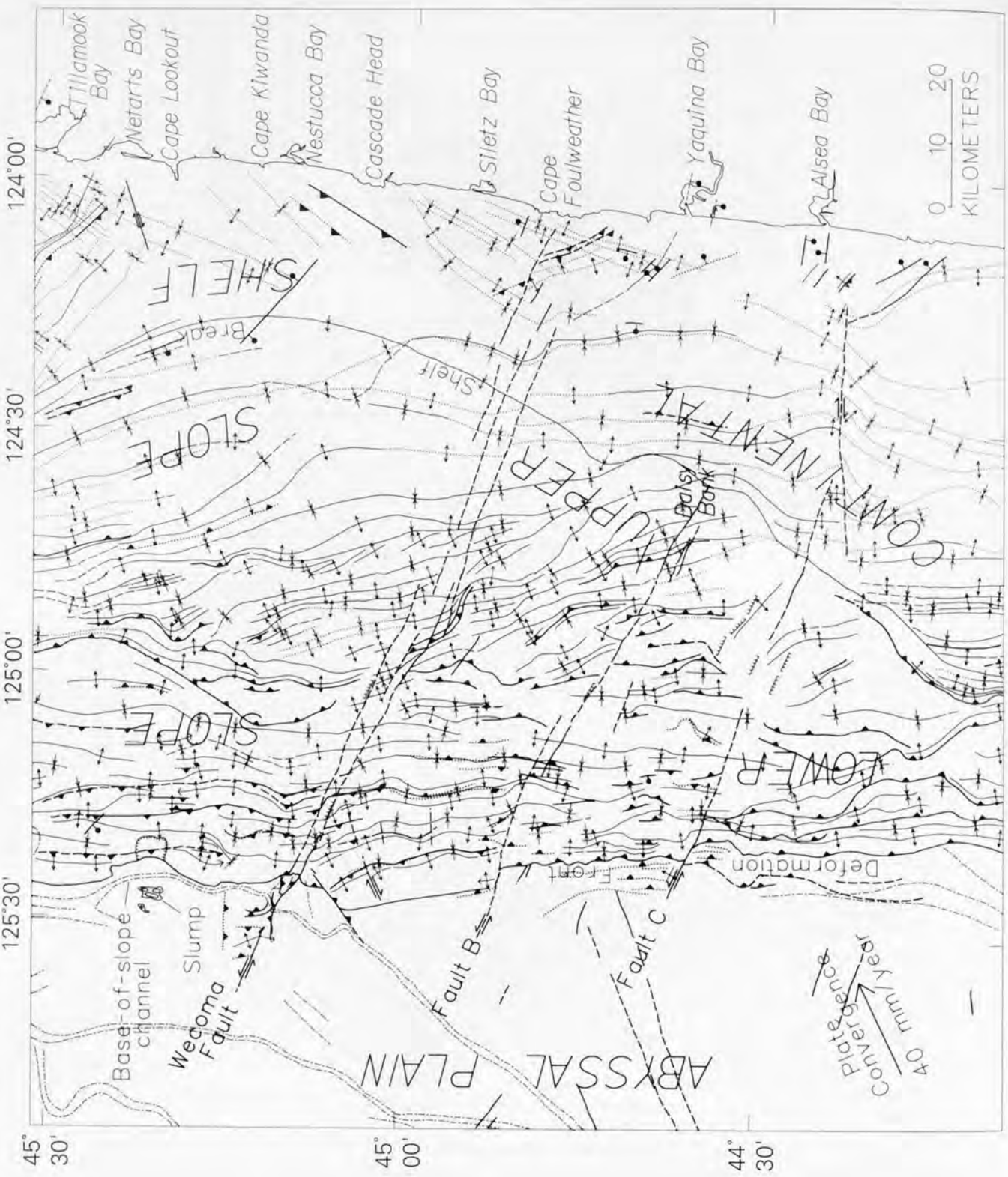
Tillamook Bay
Nehalem Bay
Cape Lookout
Cape Kiwanda
Nestucca Bay
Cascade Head
Siletz Bay
Cape Foulweather
Yaquina Bay
Alsea Bay
0 10 20
KILOMETERS
124°00'
124°30'
125°00'
125°30'
45° 30'
45° 00'
44° 30'
SHELF
Shelf Break
SLOPE
SLOPE
CONTINENTAL RISE
LOWER
ABYSSAL PLAIN
Daisy Bank
Deformation Front
Base-of-slope channel
Slump
Wedoma Fault
Fault B
Fault C
Plate Convergence
40 mm/year

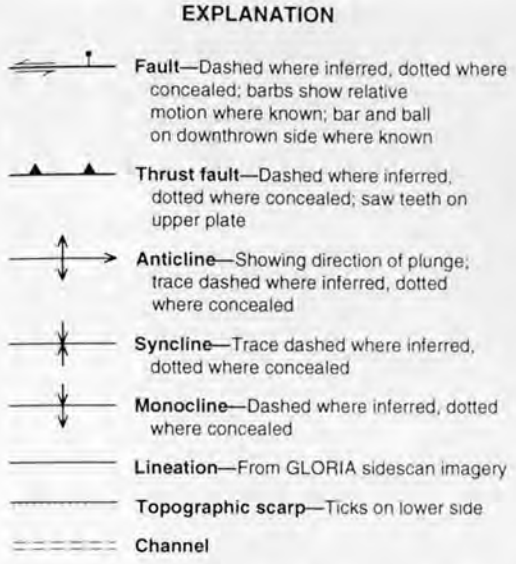

Figure 100 (facing page and above). Structure of the central Oregon continental margin. This map emphasizes active features; most structures shown cut or deform the sea floor. The deformation front is a thrust fault south of fault B and is the base of a seaward-dipping thrust ramp north of fault B. Structure offsets along faults are shown only where known. Missing offsets across faults may indicate (1) insufficient data, (2) no horizontal separation, or (3) horizontal separation not visible at this scale. Areas showing sets of structures intersecting and crossing other structures result from large age differences in the two structural sets.

structures, and the adjacent abyssal plain and accretionary wedge are shown in figure 101. The surface trace and morphologic features associated with the Wecoma fault, and the complex intersection of the fault with the deformation front are shown in figure 102. We have integrated all of the available geophysical data in a geologic structure map of the Wecoma fault on the abyssal plain and adjacent frontal accretionary wedge (fig. 103). Migrated MCS profiles of the Wecoma fault reveal that it is nearly vertical, in some places consisting of a main strand with little other deformation (figs. 104*A*, *B*), and in other places characterized by an upward-branching positive flower structure (fig. 105), as defined by Harding (1985). Blocks within the flower structure mostly show minor reverse motion. In both seismic and sidescan records, the displacement and surface expression of the Wecoma fault on the abyssal plain diminish toward the northwest. On the high-resolution 2-km sidescan swath, the trace of the fault is lost about 18 km west-northwest of the deformation front. An MCS profile (line 33 in fig. 99) crosses the along-strike projection of the fault 7 km west-northwest of the point at which the scarp disappears on the 2-km sidescan record. At the projected location, only minor deformation is seen, suggesting that this profile crosses near the fault tip. Two other crossing reflection profiles, located 3.7 km and 5.5 km west of the line-33 crossing of the fault, show that the fault does not extend west of long 125°41'W.

Seismic-reflection profiles indicate that the Wecoma fault is a structural break in the subducting Juan de Fuca plate. On MCS line 37 near the deformation front (fig. 104*A*, *B*), vertical separation of the basaltic oceanic crust is apparent, the northeastern block being upthrown (Appelgate and others, 1992; this study). Although the vertical separation of the basement seen in figure 104 is not large, identical vertical separation also occurs in the overlying stratigraphic units. A corresponding basement offset is required to produce the vertical separation of the sediments, thus, the observed basement offset cannot be a hummock on the basement surface.

The overall strike of the Wecoma fault from the base of the continental slope to its northwestern terminus is 293°, and the fault extends 18 km across the abyssal plain from the deformation front. The trace bends gently southward 7 km northwest of the deformation front, then abruptly terminates along the southern boundary of a structural upwarp (pressure ridge PR in figs. 102 and 105). Displacement is taken up by a second northwest-trending, right-stepping segment that originates on the northern flank of the upwarp and strikes northwest to its terminus (fig. 102; see also Appelgate and others, 1992). This upwarp was initially thought to be a mud volcano, but deep-towed seismic-reflection data shows internally coherent reflectors, suggesting a structural origin (Cochrane and Lewis, 1988). The upwarp gives much information about the timing and development of the Wecoma fault and is therefore discussed here in some detail. It is a complex structure that is bounded on the south by the southern strand of the Wecoma fault and on the other three sides by minor reverse faults, but it is best described as a doubly plunging north-northwest-trending anticline. The three-dimensional structure of the upwarp is shown in figure 106.

Magnetic modeling of the upwarp and the Wecoma fault indicates that the basaltic basement is also upwarped beneath the fold in the sedimentary section and is vertically offset about 100 m by the fault, north block up (Appelgate and others, 1992). Based on the involvement of the basement and the right step in the fault, we interpret the upwarp as a restraining-bend anticline (Sylvester, 1988) formed by compression across the right step in the Wecoma fault. Therefore, we refer to the upwarp as a pressure ridge. Alternatively, the ridge may be a truncated, early formed anticline of the type described by Wilcox and others (1973). If so, the anticline may have formed in the sedimentary section in response to left-lateral displacement of the underlying Juan de Fuca plate and then was partly truncated by two en echelon segments of the fault as they propagated upward with increasing fault motion. If this model is correct, the lack of a single throughgoing trace implies that the fault has not

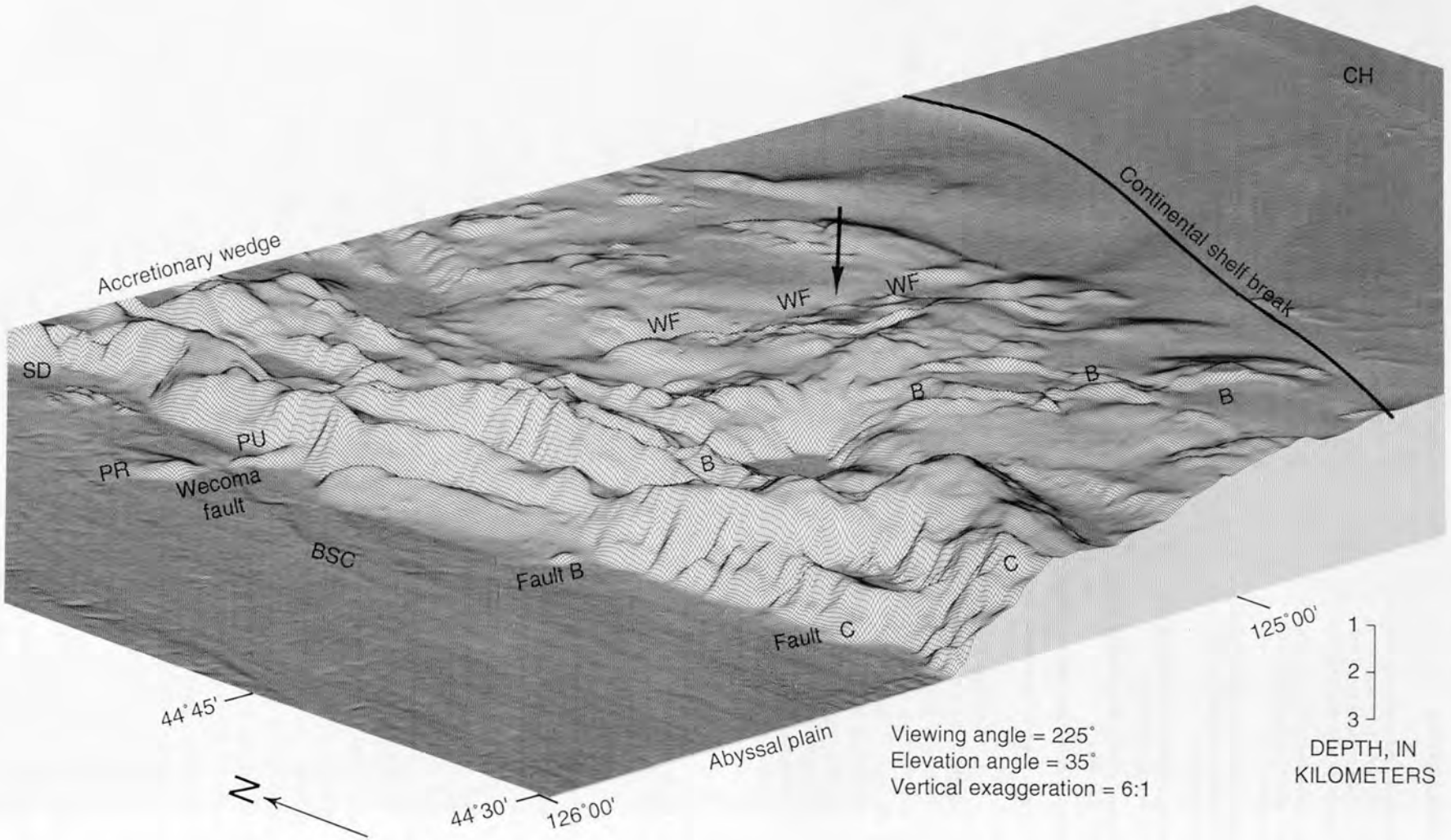

Figure 101. Perspective mesh plot of SeaBeam swath bathymetry data off the central and northern Oregon coast. View from the southwest showing the physiography of the abyssal plain and accretionary wedge near the Wecoma fault (WF) and faults B and C. Figure 100 shows map location of faults. BSC, base-of-slope channel; PR, pressure ridge; PU, pop-up plateau; SD, slump debris; CH, Cascade Head on the Oregon coast. Arrow shows location of figure 118. Diagram provided by the National Oceanic and Atmospheric Administration, National Ocean Survey.

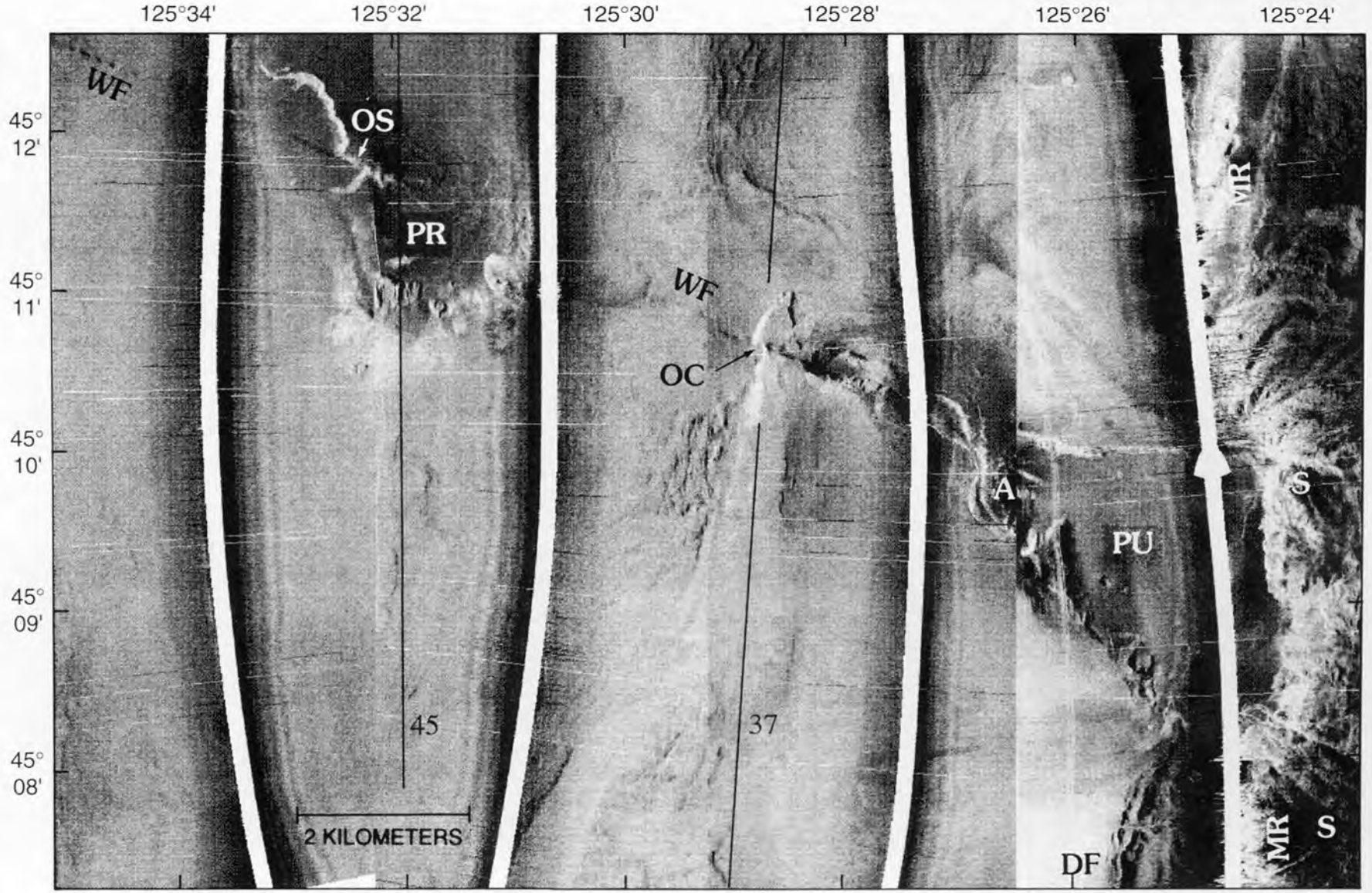

Figure 102. Mosaic of SeaMARC-1A 5-km swaths across the Wecoma fault off the central Oregon coast. PR, pressure ridge; WF, Wecoma fault; PU, the pop-up structure that marks the intersection of the Wecoma fault with the deformation front (DF); A, apex of pop-up corresponding to point A in figure 113; OC, offset channel; OS, offset slump scar; S, fault splays that occupy gullies on the seaward flank of the marginal ridge (MR). An embayment in the deformation front (discussed in text) is just east of PU. Numbered lines show locations of multichannel seismic survey (MCS) lines 37 and 45.

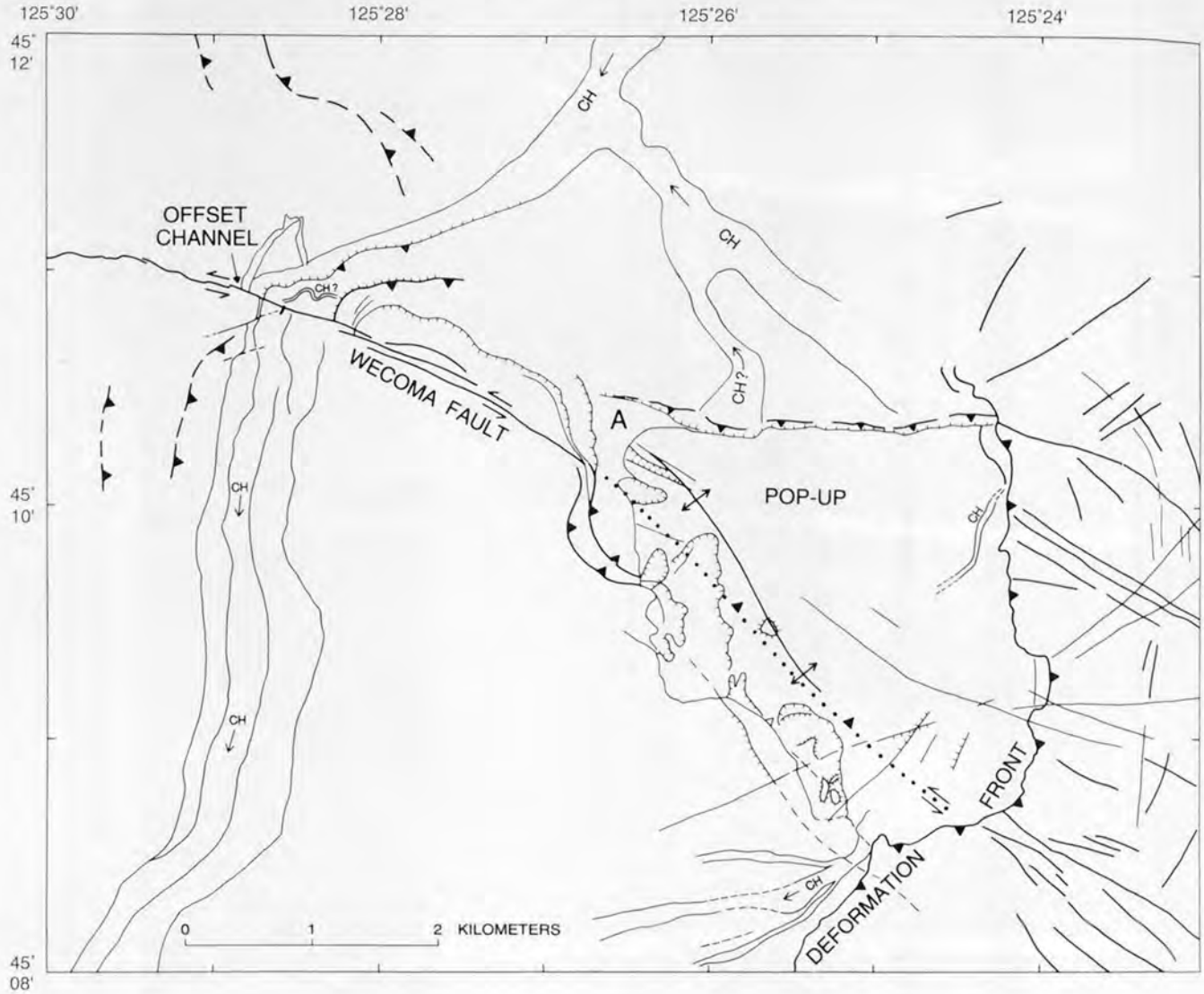

EXPLANATION

Fault—Dotted where concealed; barbs show relative motion where known; thinner lines show minor faults

Thrust fault—Dashed where inferred, dotted where concealed; sawteeth on upper plate

Anticline

Lineation—From SeaMARC 1A sidescan imagery

Topographic scarp—Ticks on lower side

Channel—Showing flow direction; dashed where inferred,queried where uncertain

Figure 103. Structure map of the western part of the Wecoma fault, adjacent abyssal plain, and frontal accretionary wedge off the central Oregon coast. Structure compiled from migrated and unmigrated seismic-reflection profiles, SeaBeam bathymetry, and SeaMARC 1A sidescan imagery. A, apex of pop-up (corresponds to A in fig. 113). Structures shown as offset only where known.

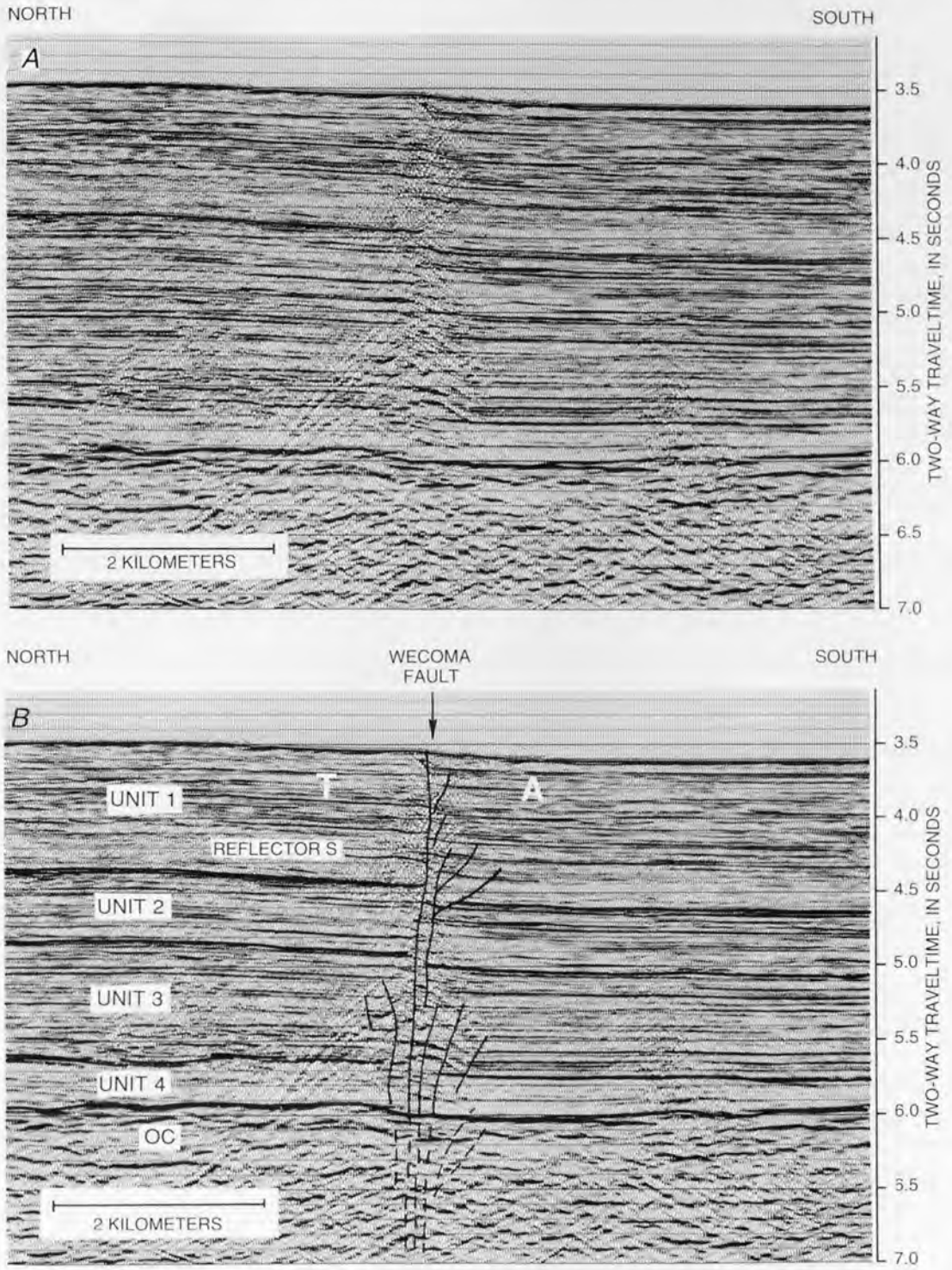

Figure 104. Migrated multichannel seismic line 37 crossing of the Wecoma fault between the pressure ridge and the deformation front off the central Oregon coast. The location of line 37 is shown in bold in figure 99. *A*, uninterpreted section; *B*, interpreted section. Note thickening of unit 1 and thinning of units 2 and 3 on the downthrown (right) block. OC, oceanic crust; T, block moving toward the viewer; A, block moving away from viewer.

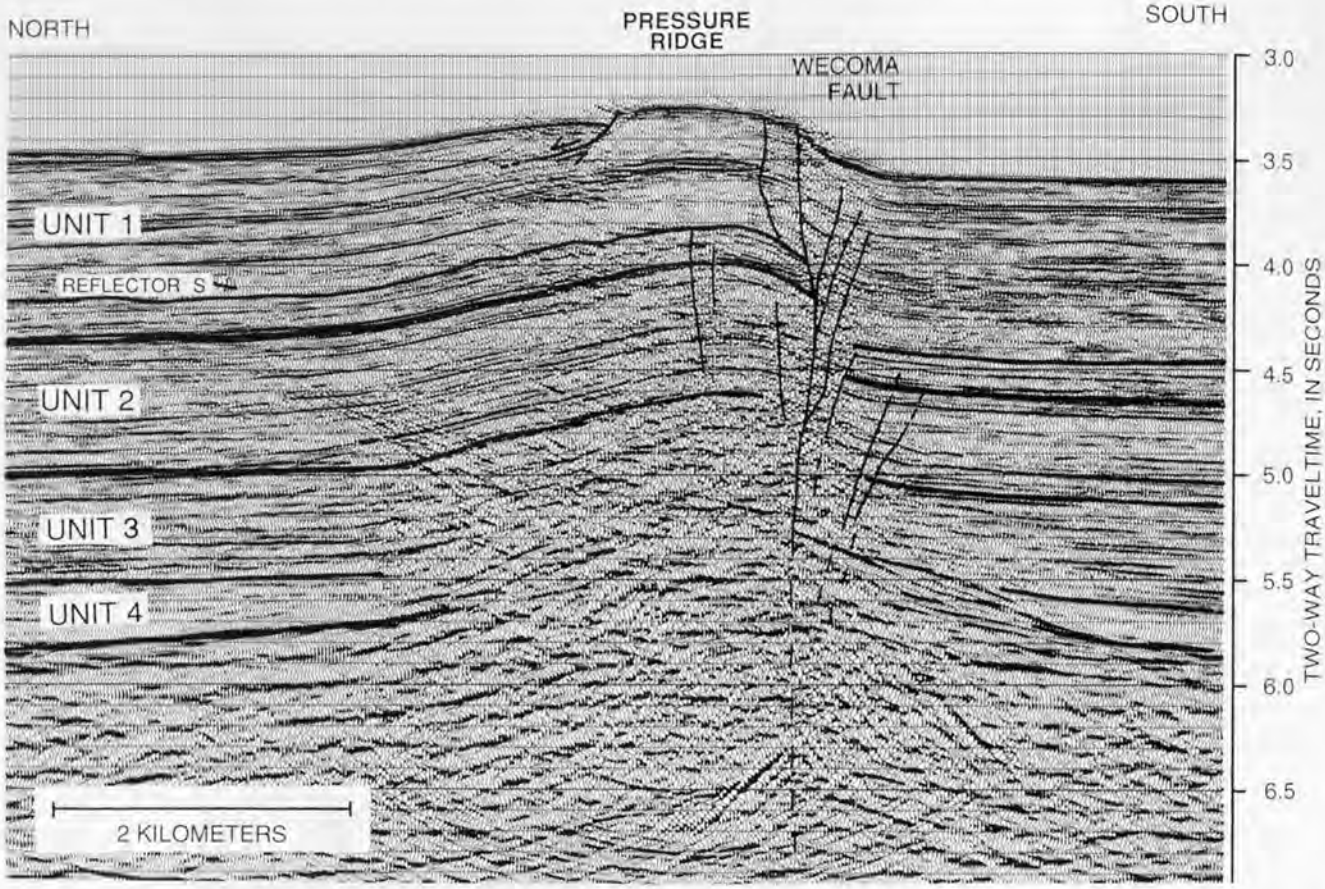

Figure 105. Part of multichannel seismic line 45 showing the Wecoma fault and the pressure-ridge anticline off the central Oregon coast. Location of line 45 is shown in bold in figure 99. Reflector S marks the stratigraphic point in the section above which seismic stratigraphic units thin over the ridge crest. Below reflector S, the stratigraphy does not show the influence of ridge growth. This profile crossed the fault just east of the eastern terminus of the northern strand of the Wecoma fault. A small normal fault is located just north of the Wecoma fault; barbs show direction of movement.

completed its final stage of development into a single throughgoing strand as modeled in clay experiments and observed in nature (Wilcox and others, 1973). An alternative explanation of the ridge is that the upwarp is related to the growth of the accretionary wedge (Cochrane and Lewis, 1988). If so, the ridge would be linked to the master décollement by an undetected basal fault. However, analysis of the growth history of the ridge, discussed below, indicates that it is roughly twice the age of the first ridge of the accretionary wedge and began its growth when it was 28–32 km west of the present deformation front, using the 40 mm/year Juan de Fuca-North America plate-convergence rate of DeMets and others (1990). The relative longevity of the ridge and the evidence for a basement upwarp suggest that the ridge's formation was unrelated to growth of the frontal thrusts of the accretionary wedge. However, recent growth probably has been augmented by horizontal compression due to the proximity of the plate boundary.

AGE, NET SLIP, AND AVERAGE SLIP RATE OF THE WECOMA FAULT

Stratigraphic relationships within the abyssal-plain sedimentary section near the Wecoma fault and the pressure ridge can be used to infer the growth history of the pressure ridge as well as the slip rate and horizontal separation on the Wecoma fault.

ABYSSAL-PLAIN STRATIGRAPHY

We have informally divided the abyssal-plain sedimentary section into four seismic-stratigraphic units on the basis of reflection character and stratigraphic coherence using the 1989 MCS data (fig. 104*B*). Unit 4 is a weakly reflecting layer that directly overlies the basaltic rocks of the oceanic crust. The poor reflectivity of this unit is probably due to its lithologic homogeneity, consisting of poorly stratified carbonate oozes, calcareous mudstone, and silt turbidites at the

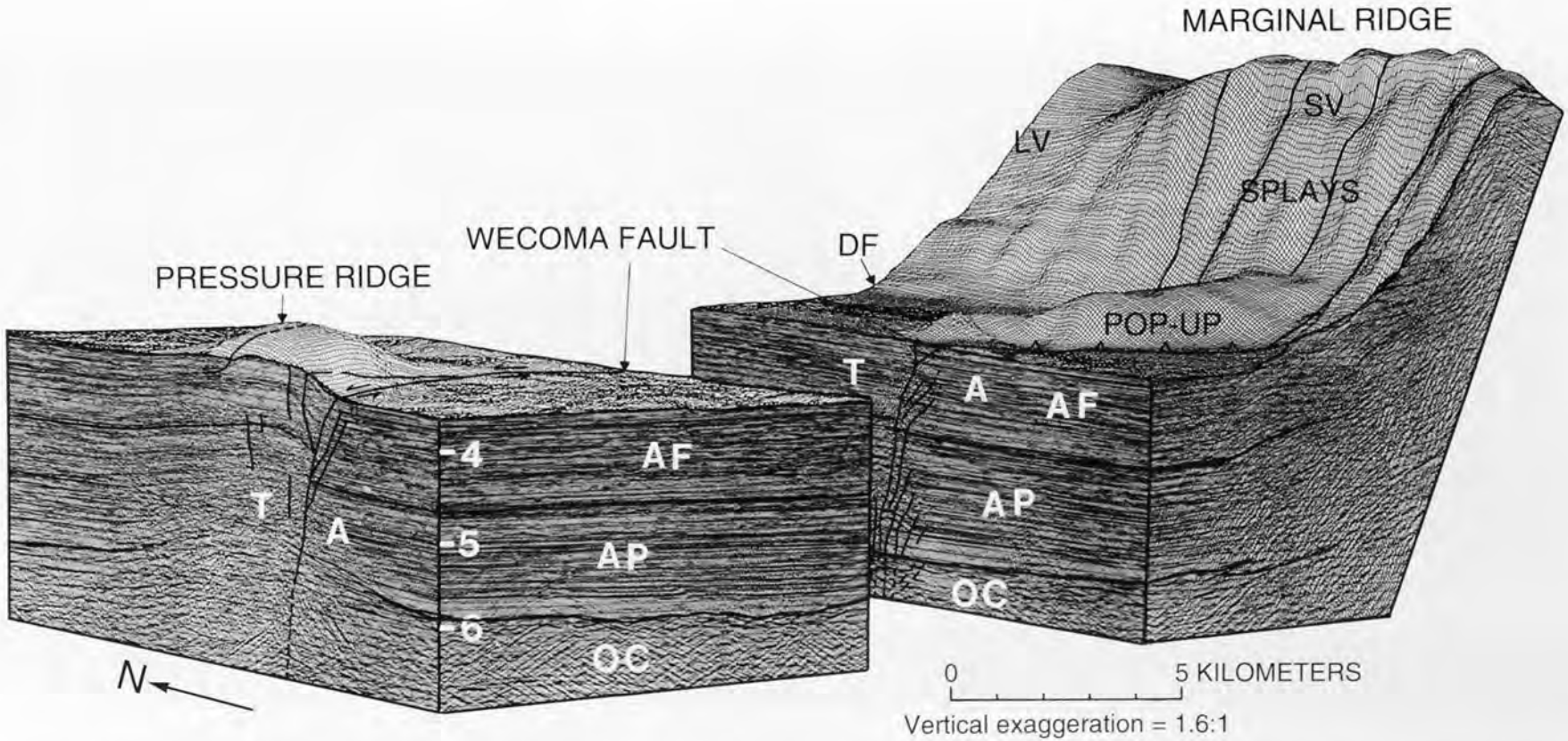

Figure 106. Composite block diagram of the pressure-ridge area and intersection of the Wecoma fault and the deformation front as viewed from the southwest. Other faults are also shown. Migrated seismic sections (two-way traveltime) are shown with selected reflectors enhanced. Vertical scale is two-way traveltime, in seconds. AP, abyssal plain section; AF, Astoria Fan (note thickening across the fault and thinning over the pressure ridge); OC, oceanic crust; A, motion away from viewer; T, motion toward viewer; SV, seaward vergence; LV, landward vergence; DF, deformation front.

National Science Foundation's Deep Sea Drilling Project (DSDP) drill site 174A on Astoria Fan (Kulm, Huene, and others, 1973). The thickness of the unit varies because it fills in the rough basement topography, but it averages about 300 m near the pressure ridge. Units 2 and 3 are defined somewhat arbitrarily on the basis of prominent reflectors and consist primarily of distal thin-bedded silty clay turbidites interbedded with hemipelagic clay (Kulm, Huene, and others, 1973). The units are an abyssal-plain sequence that is thought to have either a Klamath Mountains or Vancouver Island source (Kulm and Fowler, 1974). Units 2 and 3 both thicken uniformly eastward in response to increasing rates of sedimentation and the eastward slope of the 11–9 Ma crust presently being subducted (Wilson and others, 1984). Uppermost unit 1 is composed of overlapping lobes of the middle to late Pleistocene Astoria Fan (Kulm, Huene, and others, 1973). The lithology of unit 1 is dominated by thin- to thick-bedded medium to very fine grained sand intervals with sharp lower contacts grading upward into silts and silty clays (Kulm, Huene, and others, 1973). A capping fifth unit consists of 1–2 m of Holocene hemipelagic silt and clay (not visible in fig. 104*B*) (Nelson, 1976; this study).

TIMING CONSTRAINTS

Seismic profiles are notoriously poor at resolving stratigraphic and timing relationships in strike-slip fault zones. However, the closely spaced MCS lines near the Wecoma fault and the fortuitous presence of critical timing indicators allowed us to bracket the interval in the stratigraphic section at which vertical motion of both the fault and the pressure ridge began. On MCS line 37 (fig. 104*B*), unit 1 clearly shows thickening of the whole layer and also the individual acoustic intervals on the downthrown (south) side of the fault, indicating that the Wecoma fault has been active for most of the depositional history of the Astoria Fan. On line 45 (fig. 105), the same units thin across the pressure ridge, indicating that vertical development of the ridge occurred during the same time interval. Thickness trends in units lower in the section on both MCS lines are unaffected by the presence of the fault, indicating that they predate the Wecoma fault. Alternatively, Appelgate and others (1992) have interpreted apparent stratigraphic pinchouts against the pressure ridge as suggesting an early history for the basement upwarp, inferring that ridge formation occurred shortly after the formation of the crust at the spreading ridge (see unit 4 in fig. 105). However, the morphology of the basement upwarp as determined from magnetic modeling and MCS profiles matches that of the folded sedimentary section, indicating that folding occurred following deposition of most of the sedimentary section. Additionally, the pinchout of unit 4 is only observed on some reflection profiles of the upwarp, whereas on others it is clearly an artifact. We therefore now interpret this apparent pinchout as a side echo of the upwarped basement superimposed on unit 4. Oregon State University MCS line 30 and U.S. Geological Survey line 77–12, neither of which cross the upwarp, show this superimposed side echo clearly (see fig. 99 for locations of these lines).

On close inspection, the division between prefaulting and synfaulting units, reflector S, can be identified at a depth of 4.30 seconds on line 37 (fig. 104*B*, abyssal plain, upthrown side) and 3.82 seconds on line 45 (fig. 105, top of the pressure ridge). Reflector S was identified by examining the thickness of each stratigraphic subunit on these two lines and picking the reflector that separated units showing fault-related thickness trends from those that did not. Units 2 and 3 show the reverse thickness relationship, with thinner units on the downthrown side of the fault. This relationship is maintained along the length of the fault, suggesting that the fault was not active in a vertical sense during unit 2 and 3 deposition or that the sense of vertical motion was south block up. Because the reflectors consistently show a south-block-down separation, we can attribute these thickness changes across the fault to left-lateral strike-slip displacement of the eastward-thickening wedges of sediment (that is, left slip moves thinner wedges of sediment eastward on the southern side of the fault relative to the north side). Note that not all reflectors need show any vertical separation on seismic profiles of strike-slip faults and, in fact, some in figure 105 do not even though other evidence discussed below demonstrates 5–6 km of net slip on the fault. Growth of the pressure-ridge anticline appears to have been coeval with slip on the Wecoma fault, as the seismic reflector in both lines 37 and 45 (reflector S) that separates prefaulting and synfaulting sediments can be correlated over the intervening distance on MCS line 32. The high quality of the data allows correlation over tens of kilometers with a high degree of confidence.

In order to establish the time at which fault motion began, we have correlated a prominent seismic reflector at the base of the Astoria Fan with the same interval drilled at DSDP site 174A, 70 km southwest of the pressure ridge (figs. 97 and 107). Fortuitously, during the initial survey for site 174A, a seismic-reflection profile was made that provides a direct tie between the drill site and the pressure-ridge anticline (Kulm and others, 1973, fig. 2, line A–C). The change in reflection character above this reflector (fig. 104*B*, base of unit 1) can also be traced from the pressure ridge to the drill site. At the drill site, the profound lithologic change between the sand turbidites of the fan and the silt turbidites of the abyssal plain sequence was observed at the depth of this reflector in the cores (fig. 107). Matching reflectors with their respective lithologic changes in the cores also allows accurate calculation of seismic-interval velocities at the drill site.

Ingle (1973) plotted the coiling directions of the planktonic foraminifer *Globigerina pachyderma* in the cores from site 174A (fig. 108). Notable are three dextral coiling events at depths below the surface of 0–40 m, 125–135 m, and 238–295 m. The earliest of these three events brackets the

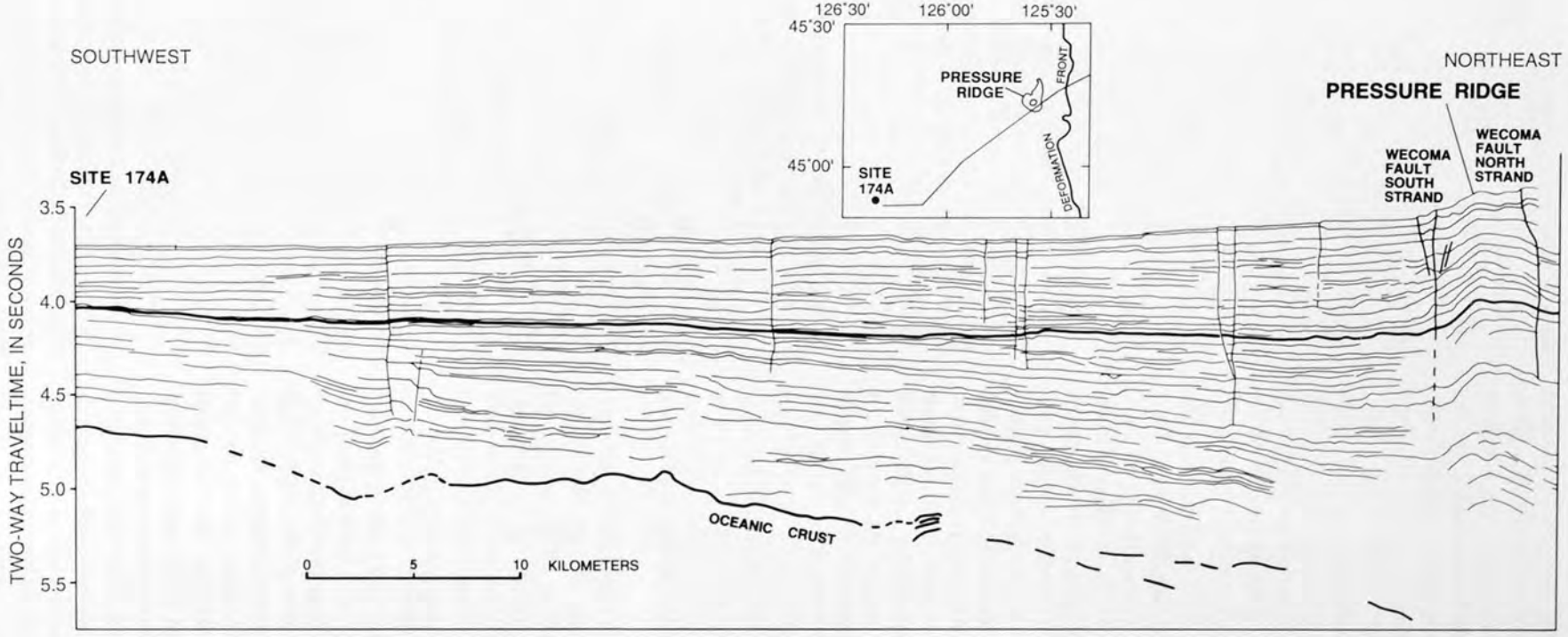

Figure 107. Line drawing of a single-channel reflection profile (Oregon State University cruise YALOC 70, Leg 5) linking Deep Sea Drilling Project drill site 174A to the pressure-ridge anticline and the Wecoma fault off the central Oregon coast. Upper heavy line marks the base of the Astoria Fan at the drill site. Lower heavy line is the top of the basaltic crust, dated by micropaleontologic techniques at 760±50 ka. Inset shows trackline of the seismic profile linking the drill site with the pressure ridge.

depth at which the base of the Astoria Fan section was found in the hole (284 m). J.C. Ingle (Stanford University, written commun., 1991) has related these dextral coiling events to regional northeastern Pacific paleo-oceanographic events, which are dated with magnetostratigraphy and tephrochronology. By this method, the upper and lower bounds of the lowest coiling event are dated at 600 ka and 800 ka, respectively. Interpolating from these bracketing ages with sedimentation rates, the age of the base of the Astoria Fan section at site 174A is 760±50 ka, with the margin of error reflecting uncertainties in using uniform sedimentation rates and in the precision of determining the age of the coiling events.

To estimate the age of this same reflector near the Wecoma fault, we infer that there is no significant time transgression between site 174A and the pressure ridge. We make this inference because no significant onlap or offlap relationships were observed within several hundred vertical meters of the base of the fan (fig. 107); the reflector is nearly horizontal, and the trend of the seismic section is about perpendicular to the sediment transport direction. Using an average sedimentation rate of 110 cm per 1,000 years calculated from the age, thickness, and seismic velocity of the fan section at the Wecoma fault, the age of reflector S, and thus the age of vertical motion on the Wecoma fault, is estimated to be 600±50 ka. Although additional uncertainties exist in sedimentation rates, age correlation of the base of the fan, and seismic velocities, we use the same margin of error here because we are unable to quantify them independently.

RETRODEFORMATION OF FAULT MOVEMENT

We have taken advantage of the geometry of the abyssal-plain units in order to calculate the net slip on the Wecoma fault. Sedimentary units strike mostly north-south and thicken uniformly eastward, resulting in eastward-thickening sedimentary wedges. Slip on the Wecoma fault has cut and juxtaposed these wedges so that thickness changes across the fault are pronounced. On MCS line 37, units 2 and 3 (fig. 104*B*) are thinner on the southern (downthrown) side. We attribute this abrupt thinning across the fault to be the result of left-lateral translation of the eastward-thickening wedges making up these two units (we assume negligible differential loading of the units due to thickness changes in unit 1). In order to estimate the horizontal separation along the Wecoma fault, we have restored the abyssal-plain section by reversing the left-lateral motion on the fault (fig. 109). The blocks were translated right-laterally until the eastward-thickening wedges of sediment matched. Using this method, the thickness match across the fault was made simultaneously with 18 individual reflectors within units 2 and 3, reducing the error inherent in picking only a few reflectors. The horizontal distance needed to restore the section is 5.5±0.8 km.

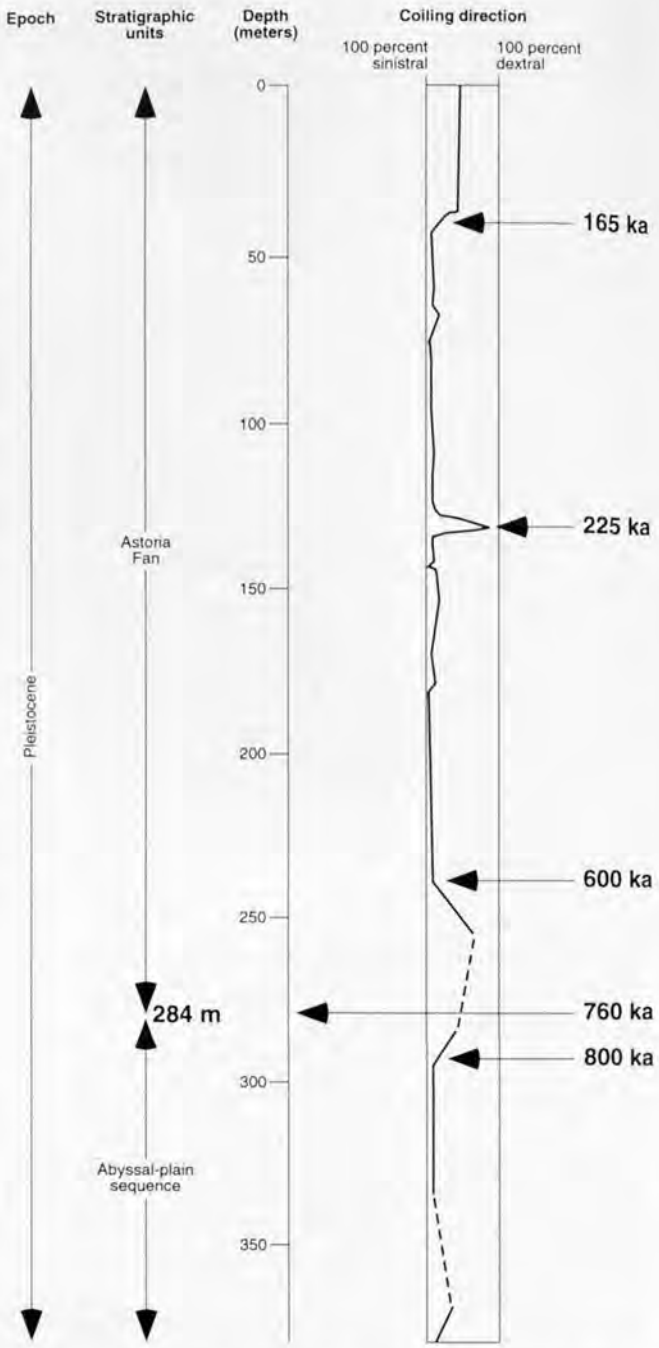

Figure 108. Coiling directions of *Globigerina pachyderma* in cores from Deep Sea Drilling Project site 174A off the central Oregon coast. Lowermost dextral coiling event is dated by tephrochronology. Plot is dashed where inferred. Modified from Ingle (1973, fig. 4).

We also plotted isopachs of units 2 and 3 as an alternative method for determining horizontal separation. Figure 110 is a pseudo-isopach plot (contours in two-way traveltime) of unit 2, following smoothing of the data and removal of a velocity artifact from the pressure-ridge area. The plot reveals a pattern of left offsets of individual

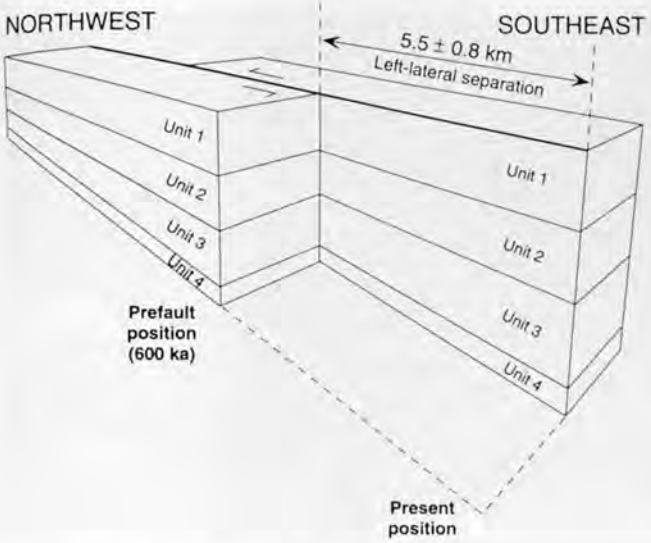

Figure 109. Diagram illustrating the method used in retrodeformation of the Wecoma fault located off the central Oregon coast. Fault motion was reversed graphically by moving seismic time sections on both sides of the fault until eastward-thickening sediment wedges of units 2 and 3 matched across the fault. The technique indicates a present horizontal separation of the units of 5.5±0.8 km. Barbs show relative motion.

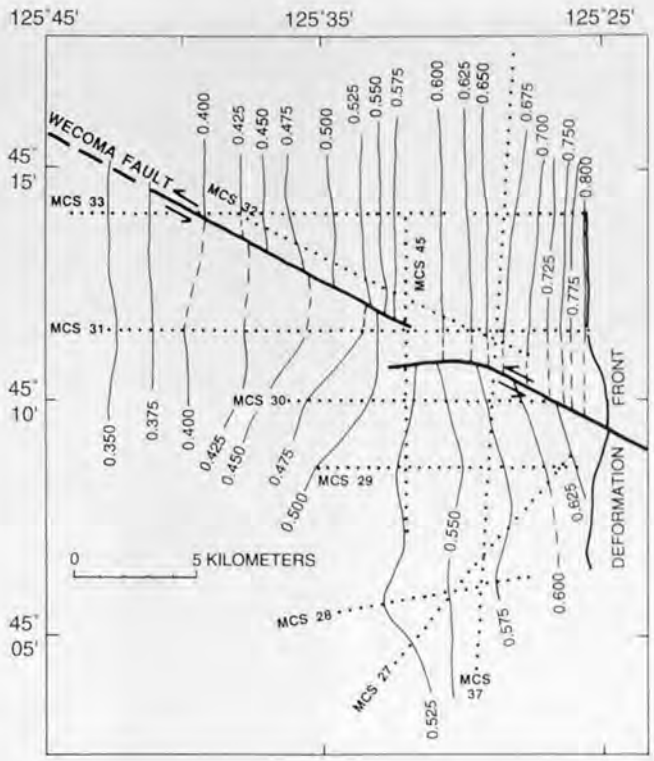

Figure 110. Pseudo-isopach plot of abyssal-plain unit 2 off the central Oregon coast. Contours are in units of two-way traveltime (seconds) rather than thickness; see figure 104 for unit designations. Note westward-decreasing left offset of unit 2 by the Wecoma fault (barbs show direction of movement). The average offset of the 0.625, 0.600, and 0.575 contours is about 4 km. Contours dashed where inferred. Dots are control points along multichannel seismic (MCS) profiles. Line numbers correspond to the tracklines shown in figure 99.

contours decreasing northwestward to zero at the fault tip 17–20 km seaward of the deformation front. The offset of the contours near the deformation front is 3.7±0.5 km, determined by averaging the three easternmost contours. We attribute this somewhat different result to poor constraint on the contours south of the fault and to disruption of thickness trends near the adjacent pop-up. Additionally, the isopach offset depends on only 3 piercing points, whereas the retrodeformation uses 18. We thus infer that the retrodeformation method is the better method of estimating horizontal separation, and we use the value 5.5± 0.8 km in the slip-rate calculations below. Neglecting the 100 m of vertical separation, this value represents the net slip on the Wecoma fault near the deformation front.

A potential source of error in the use of time versus thickness is the possibility of lateral velocity changes in the selected units. However, lateral velocity changes, if present, are most likely to be oriented normal to the deformation front and thus have negligible effect on restoration of the sedimentary section. Unfortunately, the youngest unit (fig. 104*B*, unit 1) cannot be used for an independent estimate of net slip during deposition of the youngest part of the fan section because vertical movement on the Wecoma fault has influenced thickness of this unit.

Using the previously calculated age of the fault and the net-slip estimate above, we calculated that the average slip rate of the Wecoma fault since its inception 600±50 thousand years ago has been 7–10 mm/year near the present deformation front. This rate depends on the estimated age of the fault, which may include a margin of error that is too small, as discussed above. Thus, the calculated slip rate may have a larger error than calculated here.

LATE PLEISTOCENE-HOLOCENE SLIP RATE

SeaMARC 1A sidescan imagery shows that the Wecoma fault offsets a late Pleistocene distributary channel and an older slump scar on the Astoria Fan (OC and OS in fig. 102; offset channel in fig. 111) left laterally. Horizontal separations are about 120±5 m and 350±10 m, respectively (Appelgate and others, 1992; this study). These crosscutting relations can be used to obtain an independent estimate of the slip rate during latest Pleistocene and Holocene time. The offset channel in particular offers the best opportunity for estimating the Holocene slip rate. The channel is blocked 18 km upstream (to the north) by slump debris from a 32 km^3 slope failure (figs. 100 and 101, labeled SD). The slump is apparently a bedding-plane slide from the western flank of the leading landward-vergent accretionary thrust ridge. We

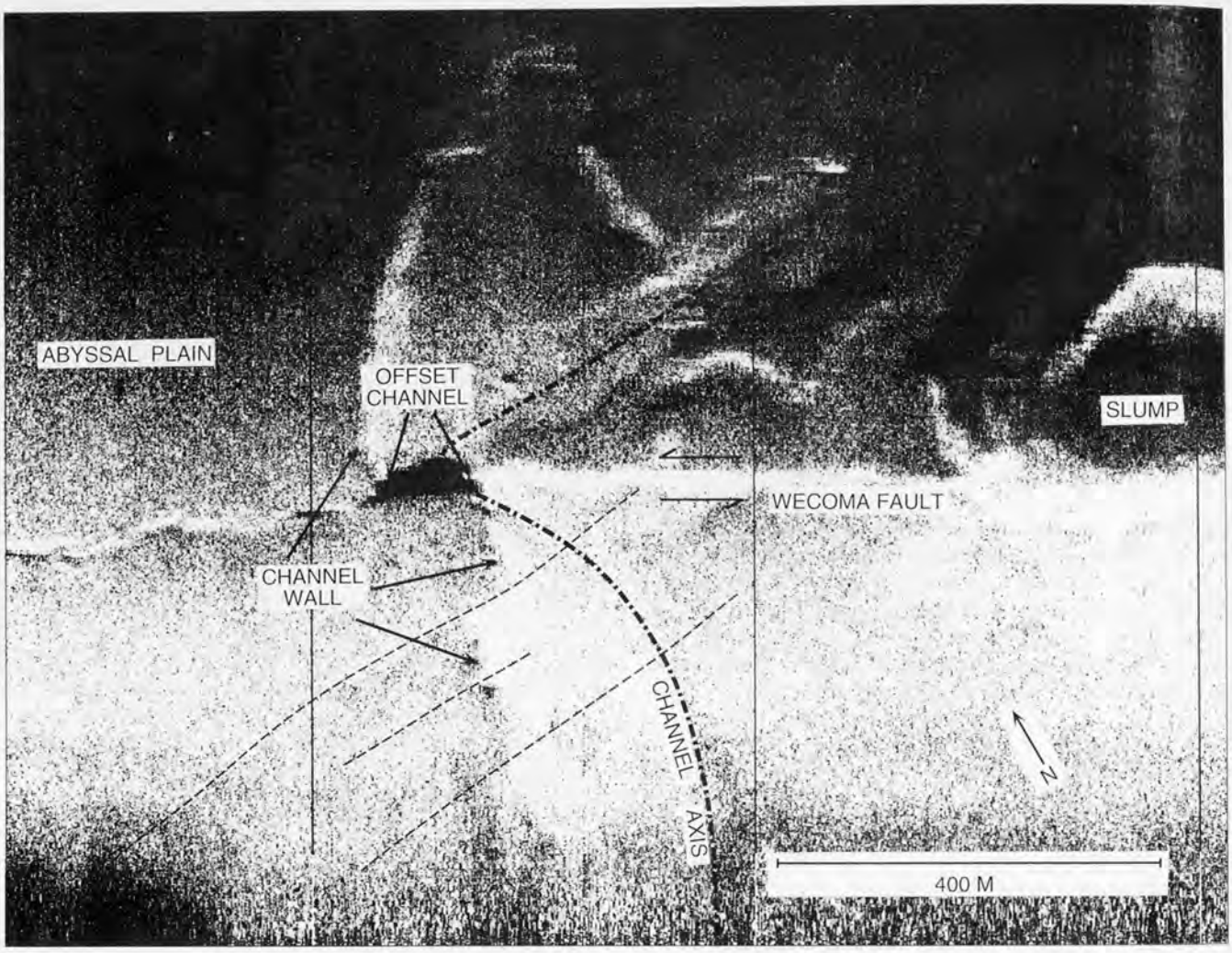

Figure 111. High-resolution SeaMARC 1A sidescan image of the Wecoma fault offsetting the western bank of a late Pleistocene distributary channel on the southeastern part of the Astoria Fan. Horizontal separation is 120±10 m. Light tones represent high backscatter; insonification (direction of sonar illumination) is from the south. Vertical scarps (highest backscatter at right-center of image) are the result of strike-slip juxtaposition of irregular sea-floor topography. The fault strike is 293°. Barbs show relative motion. Minor faults (dashed lines) that also offset the channel wall are interpreted as part of the surface expression of the flower structure shown in figure 106.

estimate the age of this slump to be 24–10 ka, based on a ^{14}C date from a gravity core taken from a sediment drape on top of one of the slump blocks and also on onlapping relations observed on a high-resolution seismic record. In the reflection profile, the slump debris rests directly on the sea-floor reflector with no visible sediment onlap or ponding around the slump blocks. Using a composite late Pleistocene-Holocene sedimentation rate derived from Nelson (1968) and from this study, we estimated that sediment accumulation following the slump could not continue for more than about 24,000 years without depositing a thick-enough unit to be detectable on the MCS profile, thus setting a maximum age for the slump. We derived the minimum age for the slump from the ^{14}C age of sediment at the bottom of the gravity core. The core sampled only postslump hemipelagic sediment and, thus, the 10,300 radiocarbon-years-before-present (R.C.Y.B.P.) date from the lowermost part of the core sets the minimum age of the slump at about 10 ka.

Because the fault is older than either the slump or the channel, a slip rate can be estimated from the channel offset shown in figure 111. The channel wall must have been cut prior to blockage of the channel by the slump, establishing the minimum age of the slump at about 10 ka. Similarly, a maximum age for the channel wall is constrained to be the same as the maximum age of the slump. Channel cutting should have ceased or been greatly reduced following the blockage; thus, younger fault motion would offset the channel wall, as presently observed, without modification by erosion. If channel cutting and fault motion were simultaneous, the high frequency of late Pleistocene turbidity currents

carrying large quantities of sand and gravel (Duncan 1968; Nelson, 1968; Griggs and others, 1970) should have eroded the offset to something other than the crisp separation seen in sidescan images (fig. 111). Seismic-reflection records showing the truncation of deep-sea channel walls (Griggs and Kulm, 1973), and numerous sediment hiatuses in cores from the axial part of these channels (Griggs and Kulm, 1970) document the erosive character of the coarse-grained late Pleistocene turbidity currents in this region. Therefore, the age of the channel wall is probably 24–10 ka, consistent with incision during the last episode of high turbidity-current activity during the latest Pleistocene sea-level low stand. Using this age range, we calculated a latest Pleistocene-Holocene slip rate of 5–12 mm/year, one comparable to the 7–10 mm/year average rate calculated from the net horizontal displacement since inception of the fault.

INTERSECTION OF THE WECOMA FAULT AND THE ACCRETIONARY WEDGE

The complex structure of the area where the Wecoma fault intersects the initial thrust ridge indicates that this fault is not simply overridden by the accretionary prism. High-resolution SeaMARC 1A sidescan records of the intersection zone on the abyssal plain show that this area is dominated by a nested series of uplifted asymmetrical triangular plateaus, called pop-ups, bounded by reverse faults (figs. 102, 103, 112, and 113). The single trace of the Wecoma fault separates into several diverging splays at the western tip of the largest of the pop-ups (A), and the largest of these splays is the southern bounding fault of the pop-up. Sidescan and MCS records suggest that the main trace is buried by slump debris along much of its length in this area (Appelgate and others, 1992). The pop-up plateaus appear to be the result of a complex interaction between the strike-slip fault and the evolving deformation front. The model we prefer to explain their development is shown in figure 113. The plateaus were uplifted between divergent splays of the main strike-slip fault and possibly were driven westward by horizontal compression because of their proximity to the plate boundary. Appelgate and others (1992) suggested that the high vertical scarps between the offset channel and the western tip of the pop-up (fig. 102) are the result of 2.5 km of left-lateral displacement of a part of the pop-up.

INFLUENCE OF THE WECOMA FAULT ON THE ACCRETIONARY WEDGE

The eastern end of the pop-up directly abuts the western flank of the first accretionary ridge of the North America plate (MR in fig. 102). On the western side of the initial thrust ridge, the plate boundary forms an embayment corresponding to the width of the adjacent pop-up on the abyssal plain (Appelgate and others, 1992). A seaward-vergent thrust segment occupies the area of the embayment in an overall landward-vergent thrust setting described by MacKay and others (1992). This configuration suggests that the local reversal of vergence in the leading accretionary ridge may be related to the effects of the strike-slip fault subducting beneath the wedge. The mechanism for this vergence reversal may be a local reduction in pore fluid pressure due to fluid venting by the Wecoma fault. Such a pressure loss would increase the basal shear stress along the décollement, promoting development of the seaward-vergent segment (Tobin and others, 1993). The ridge formed less than 300,000 years ago, based upon microfossil evidence from rocks dredged from the ridge (Carson, 1977). The embayment is bounded by linear gullies that cut upslope into the initial thrust ridge, and other such gullies lie within the embayment (fig. 102). We interpret these linear gullies as fault splays related to slip on the Wecoma fault. Observations and samples from the submersible ALVIN confirm that the linear gullies visible in sidescan records are zones of active oblique faulting. Several dives (fig. 114) showed that bedding is extensively sheared, with multidirectional slickensided surfaces and mullions (fig. 115). Shear planes striking west-northwest, roughly parallel to the Wecoma fault, were observed in these gullies. Linear west-northwest-trending scarps along the strike of the Wecoma fault are also present on the eastern flank of the initial thrust ridge, the crest of which has a small left-lateral offset (fig. 116). These lineations follow the Wecoma fault trend and are interpreted as fault scarps because (1) they lack the dendritic drainage pattern commonly observed in nearby erosional gullies, (2) they strike at an angle to the bathymetric contours, and (3) they originate at the highest point on the marginal ridge. MCS line 29 crosses the area of these scarps and shows a strong vertical disruption of the marginal ridge that we interpret as the cause of the sea-floor scarps.

Rocks collected with the ALVIN submersible from the gullies on the seaward flank of the marginal ridge consist of sheared siltstone, sandstone, and pebble-to-cobble conglomerate (Sample and others, 1993; Tobin and others, 1993) that probably originated on the Astoria Fan and were recemented with a secondary carbonate cement (Kulm and Suess, 1990). The carbonate cement, derived from fluids venting from the shear zones, bonds the sheared sedimentary fragments into an angular breccia that fills the bottoms of the gullies. Isotopic analyses of these pore-fluid-derived carbonate cements show that cements in the fault zone differ significantly from those elsewhere in the young accretionary wedge. Fault-zone cements from the Wecoma fault have depleted $\delta^{18}O$ values ranging from –4 to –13‰ (permil) Peedee Belemnite (PDB) and $\delta^{13}C$ values from –1 to –25‰ PDB (Sample and others, 1993). Cements from an accretionary-wedge thrust fault on the first thrust ridge 38 km to the south have $\delta^{18}O$ values ranging from +4 to +7‰ PDB and $\delta^{13}C$ values from

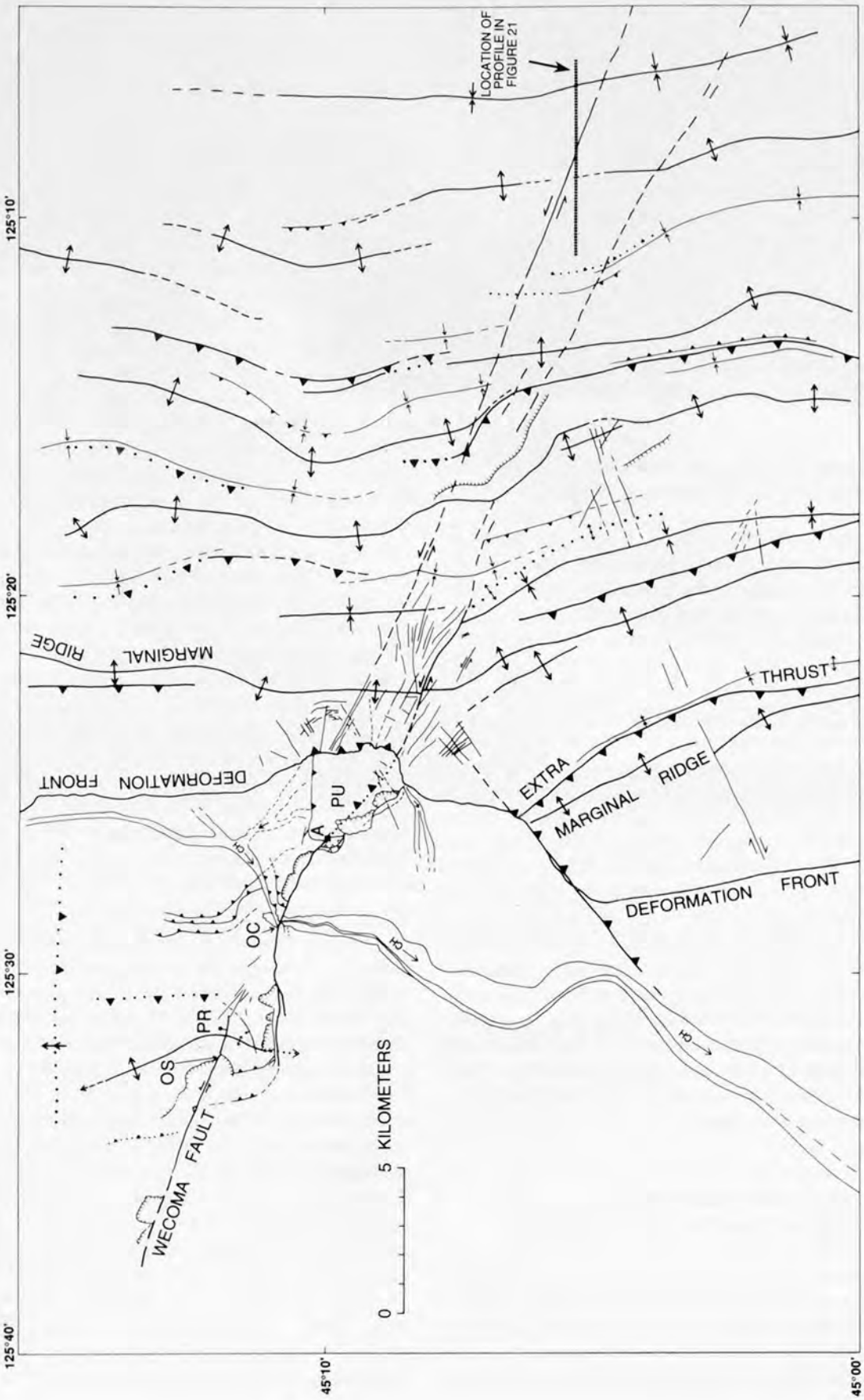
LOCATION OF PROFILE IN FIGURE 21
125°10'
125°20'
125°30'
125°40'
45°10'
45°00'
MARGINAL RIDGE
DEFORMATION FRONT
THRUST
EXTRA MARGINAL RIDGE
DEFORMATION FRONT
PU
OC
PR
OS
WECOMA FAULT
5 KILOMETERS
0

EXPLANATION

Fault—Dashed where inferred, dotted where concealed; barbs show relative motion where known; bar and ball on downthrown side where known; smaller symbols indicate minor faults

Thrust fault—Dashed where inferred, dotted where concealed; sawteeth on upper plate; smaller symbols indicate minor thrust faults

Anticline—Showing direction of plunge; trace dashed where inferred, dotted where concealed; smaller symbols indicate minor anticlines

Syncline—Trace dashed where inferred; smaller symbols indicate minor synclines

Monocline—Trace dotted where concealed

Lineation—From SeaMARC 1A sidescan imagery

Topographic scarp—Ticks on lower side

←CH **Channel**—Showing flow direction; dashed where inferred

Figure 112 (above and facing page). Structural interpretation of the intersection zone and pop-up structure at the intersection of the Wecoma fault and the deformation front. OS, offset scarp; PR, pressure ridge; OC, offset channel; PU, pop-up; A, apex of pop-up (corresponds to A in figure 113).

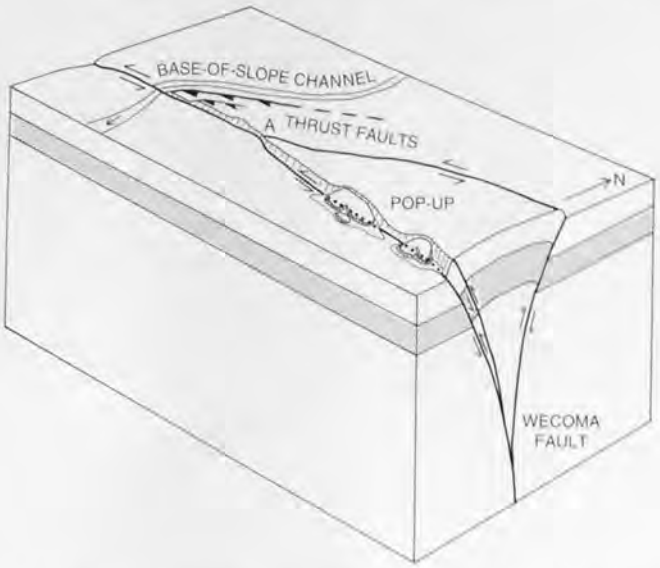

Figure 113. Block diagram illustrating structure of the pop-up at the intersection of the Wecoma fault and the deformation front. Blocks within the flower structure of the Wecoma fault are forced upward and westward by increasing horizontal compression as subduction progresses. Apex A corresponds to A in figure 112. Arrow in channel shows flow direction. Barbs show relative motion on faults. Sawteeth are on upper plates of thrust faults; faults are dashed where inferred, dotted where concealed. Modified from Sylvester (1988, fig. 22*C*).

–30 to –52‰ PDB (Kulm and Suess, 1990). Sample and others (1993) attributed the isotopic ratios within the Wecoma fault zone to higher fluid temperatures near the Wecoma fault, perhaps as high as 100°C, and a probable thermogenic methane source. The source of these fluids probably lies deeply buried within the sedimentary deposits of the abyssal-plain accretionary wedge. In contrast, isotopic ratios from the thrust fault are best explained by fluids derived from a relatively shallow biogenic methane source (Kulm and Suess, 1990).

The evidence from fluid chemistry, sidescan images, and seismic profiles indicates that the leading edge of the accretionary wedge is disrupted and offset by the Wecoma fault. We have studied sidescan images, SeaBeam bathymetry, and seismic profiles of the frontal accretionary wedge in order to determine the extent to which these effects can be observed on the continental slope. In high-resolution SeaMARC 1A sidescan images (fig. 116), scarps and shear zones are observed to affect the bathymetric expression of several thrust ridges 8–15 km landward of the deformation front. The scarps are subparallel to the Wecoma fault and lie along the projected trend of the fault into the accretionary wedge. Using detailed image-enhancement techniques, we observed that the Wecoma fault zone is composed of several subparallel west-northwest-trending linear scarps and shear zones. These linear features are clearly fault scarps cutting across the erosional spurs and gullies of the main escarpment at nearly right angles. The seawardmost synclinal basin of the accretionary wedge is cut by both a northern and southern strand of the Wecoma fault. Eight kilometers southeast of the second thrust ridge and 22 km southeast of the deformation front, the projected trend of the Wecoma fault is crossed by U.S. Geological Survey line 77–11 (figs. 99 and 117). This reflection record shows a near-vertical fault at the western edge of a bathymetric bench near the projected position of the Wecoma fault. A surficial bump or scarp overlies the fault, which affects the uppermost flat-lying sediments of a broad basin. Reflectors deeper in the section show a sharp dip reversal and loss of coherence. The dip reversal might be resolved as a basin if the line were migrated, but we think it is too abrupt and the radius of curvature of the beds too short for this interpretation. Thus, we interpret this feature as a vertical fault, possibly the landward extension of the Wecoma fault.

Having found possible evidence for an upper-plate continuation of the Wecoma fault 10–20 km southeastward into the accretionary wedge, we searched for evidence of either termination or continuation of this fault as well as faults B and C higher on the continental slope. We used academic, U.S. Geological Survey, NOAA, and industry seismic-reflection profiles as well as GLORIA long-range sidescan images and NOAA SeaBeam high-resolution bathymetry now available from the abyssal plain landward to about the continental-shelf break in northern Oregon.

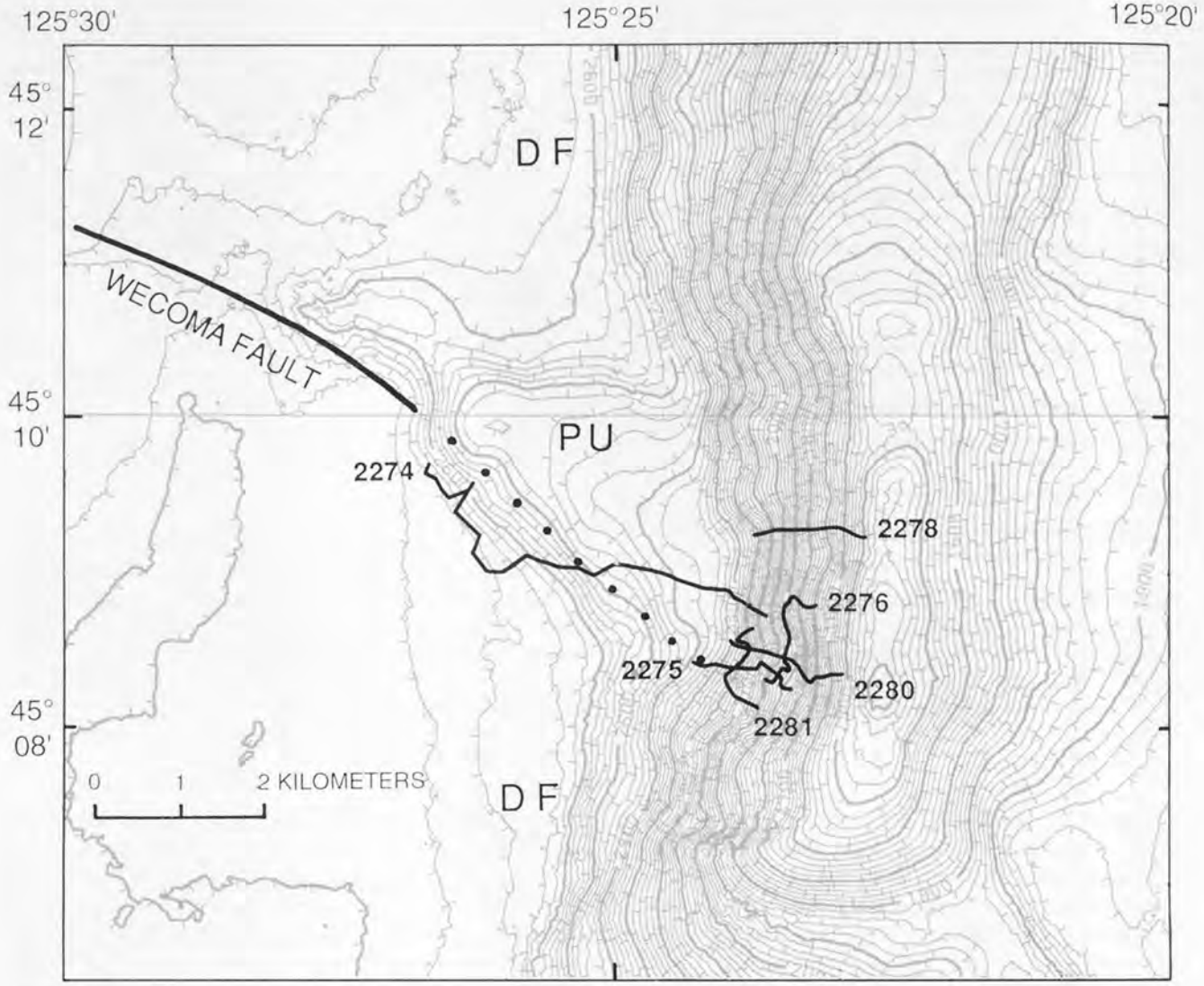

Figure 114. Bathymetry and ALVIN submersible tracklines near the intersection of the Wecoma fault and the deformation front. Several dives focused on the gullies visible on the SeaBeam bathymetry and SeaMARC 1A sidescan images (see also fig. 102). PU, pop-up; DF, deformation front. Contour interval is 20 m. Ticks face downslope. Tracklines show dive numbers. Wecoma fault dotted where concealed.

We observed that several prominent west-northwest/east-southeast bathymetric trends cross the continental slope off central Oregon (fig. 101). These trends are composed of north-northwest- to west-northwest-trending folds and scarps 5–40 km in length. They appear prominently on the slope because they cross the north- to northwest-trending grain of the accretionary wedge obliquely and because the deformation within these zones is more intense than in the surrounding wedge. In several places, the oblique folds are accretionary-wedge folds whose axes have been sigmoidally bent to the northwest, whereas others are fault-bend and fault-propagation folds overlying steeply dipping oblique faults. In map view, SeaBeam bathymetry and GLORIA images show left-stepping sigmoidal bending of fold axes along these trends, left offsets of fold axes, and linear west-northwest-trending scarps (fig. 118). These features were mapped using continuous GLORIA long-range sidescan on the continental slope and continuous SeaBeam bathymetry on the slope and outermost shelf. The deformation of accretionary-wedge structures observed in the perspective SeaBeam mesh plot (fig. 101) and in map view (fig. 118) has a variety of forms but, generally, older structures are systematically disrupted and younger structures have developed along these throughgoing zones to the extent that they are bathymetrically well expressed.

Three of the west-northwest-trending slope deformation zones (WF, B, and C in fig. 101) adjoin the Wecoma fault and faults B and C and have similar trends. The zones

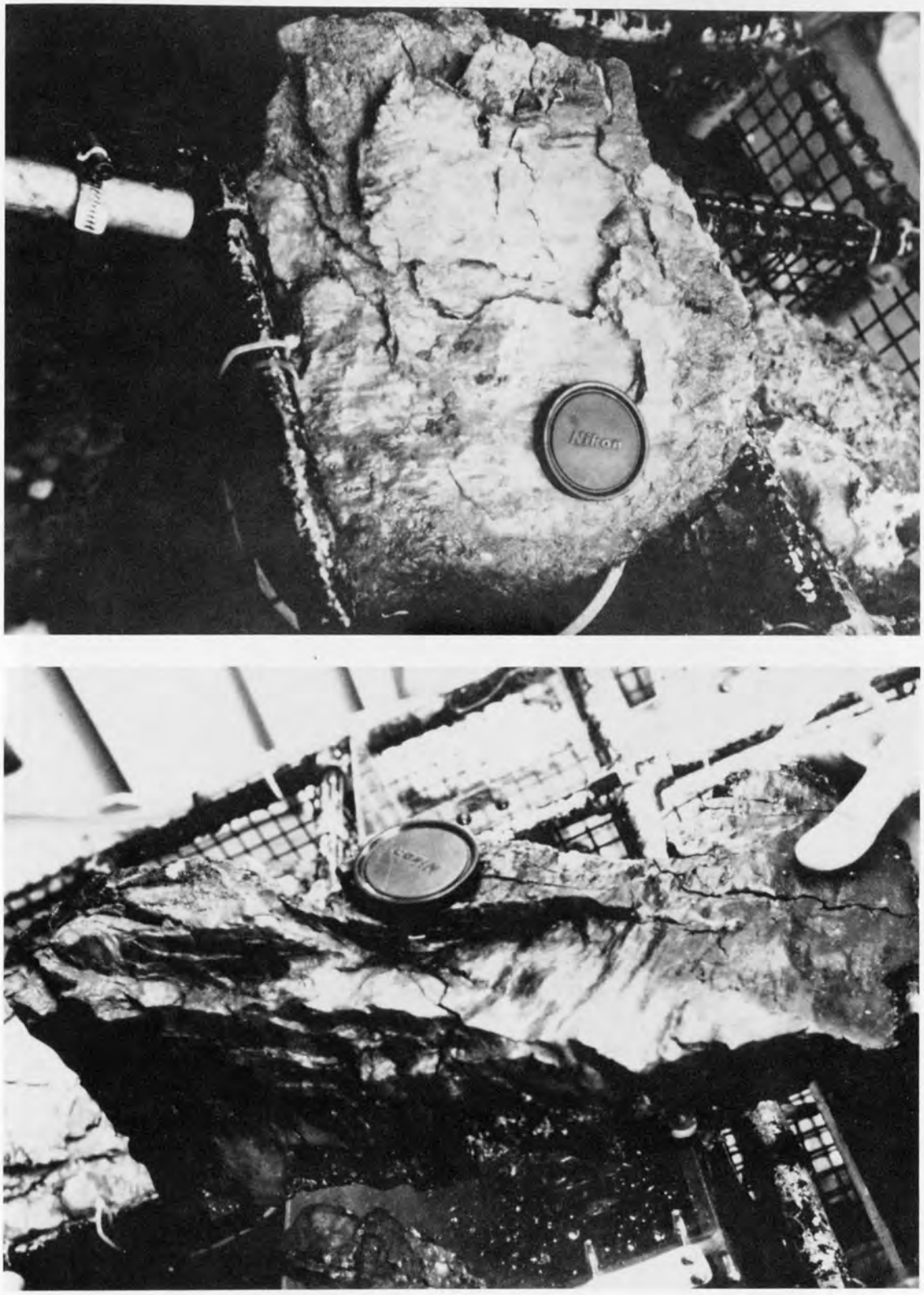

Figure 115. Sandy siltstone samples collected using the ALVIN submersible from one of the fault-occupied gullies on the seaward flank of the first accretionary ridge near the intersection of the Wecoma fault and the deformation front. Note slickensided surfaces and mullions.

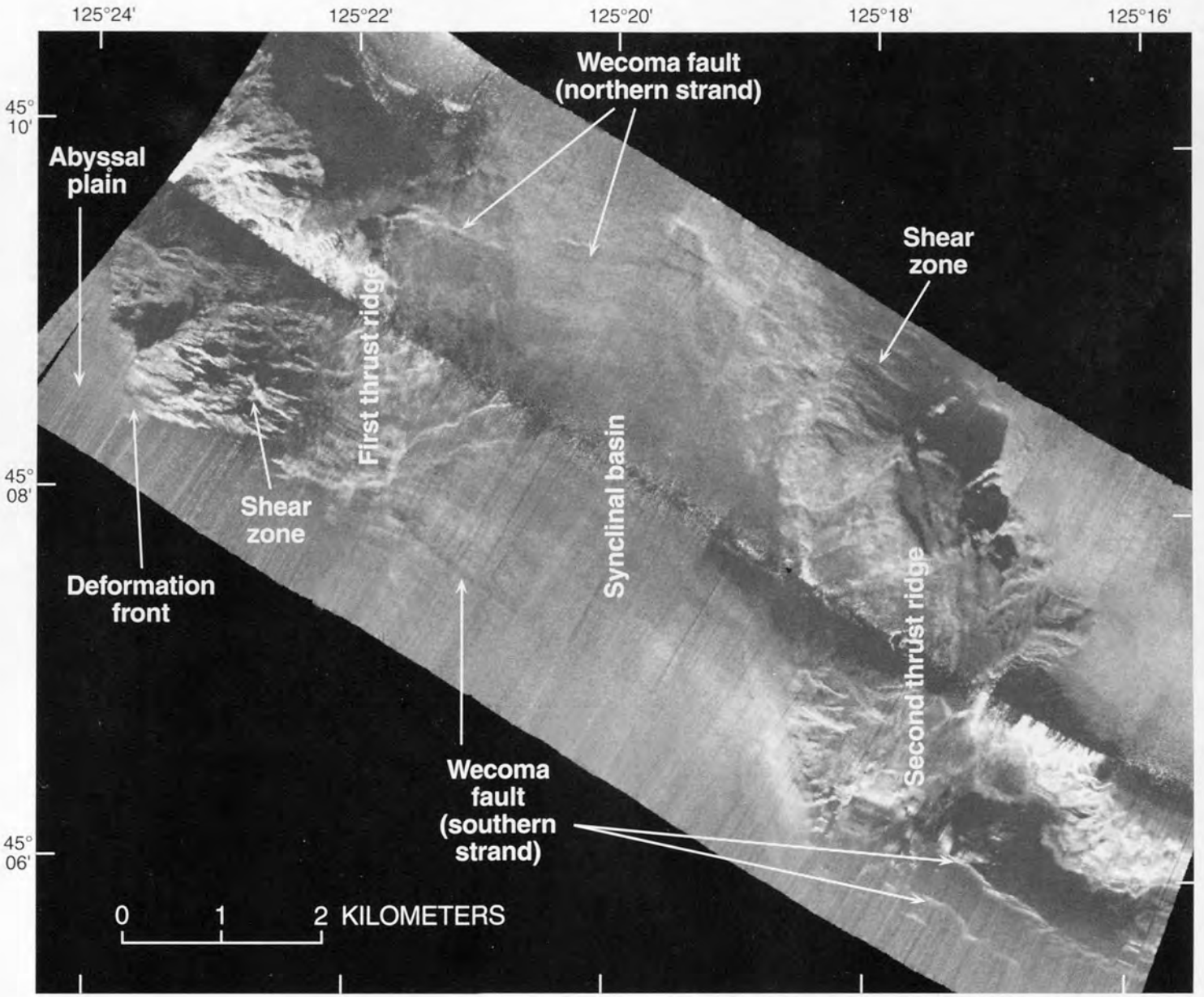

Figure 116. SeaMARC 1A sidescan image of the Wecoma fault crossing the accretionary wedge. The northern strand of the Wecoma fault cuts the first thrust ridge and synclinal basin and develops into a shear zone at the second thrust ridge. The southern strand is a shear zone at the first thrust ridge and cuts the first synclinal basin as a single splay and the second thrust ridge as two splays. See figure 120 for location of image.

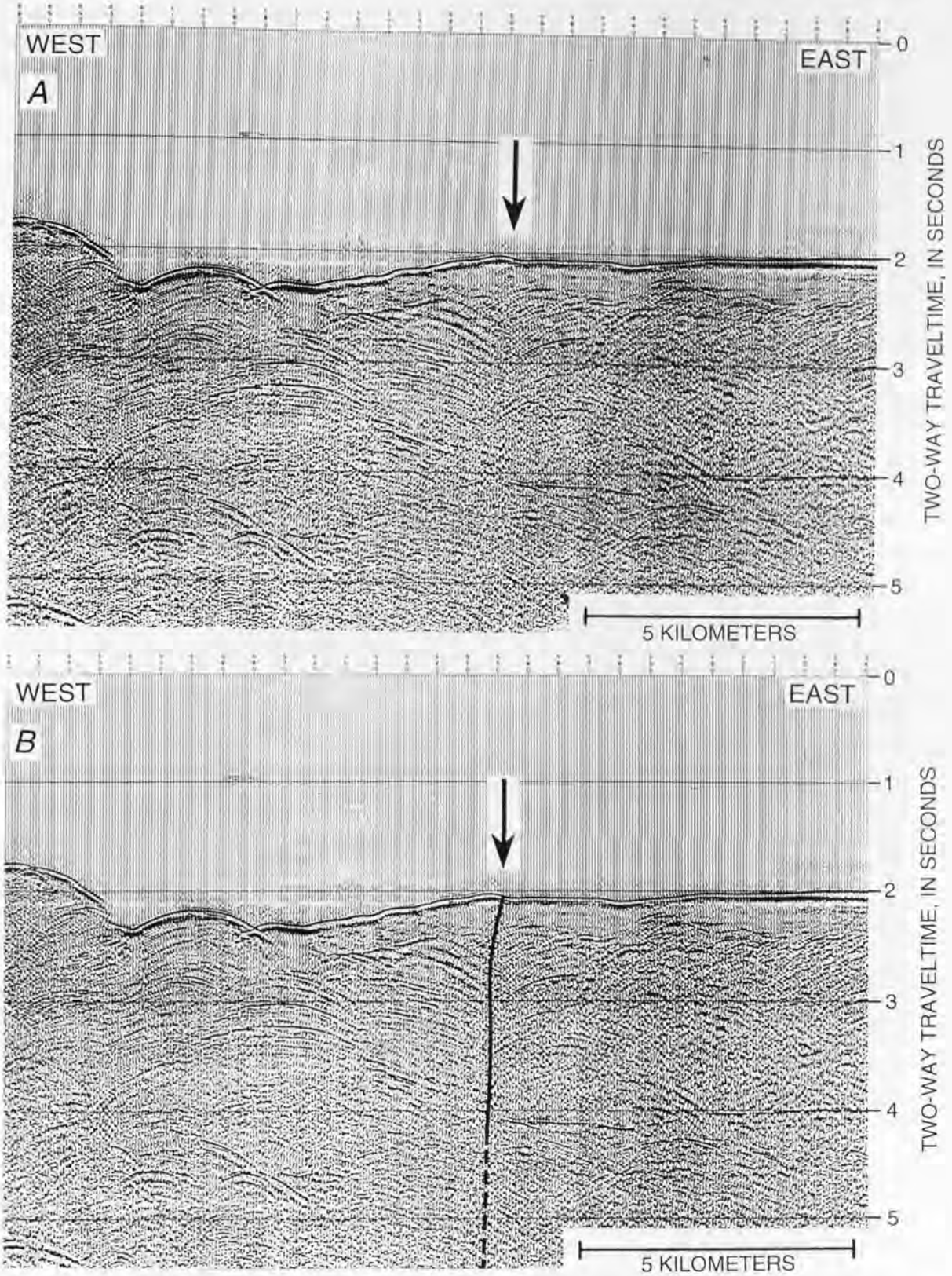

Figure 117. Unmigrated 24-channel seismic profile of the Wecoma fault on the lower continental slope, 26 km landward of the deformation front. Arrow shows fault location. *A*, uninterpreted section; *B*, interpreted section. Note near-vertical trace, the sharp dip reversals across the fault, and the up-to-the-west (north block up) surface expression. The vertical exaggeration is 2.7:1. See figures 103 and 119*A* for location. From Snavely and McClellan (1987, line 77–11).

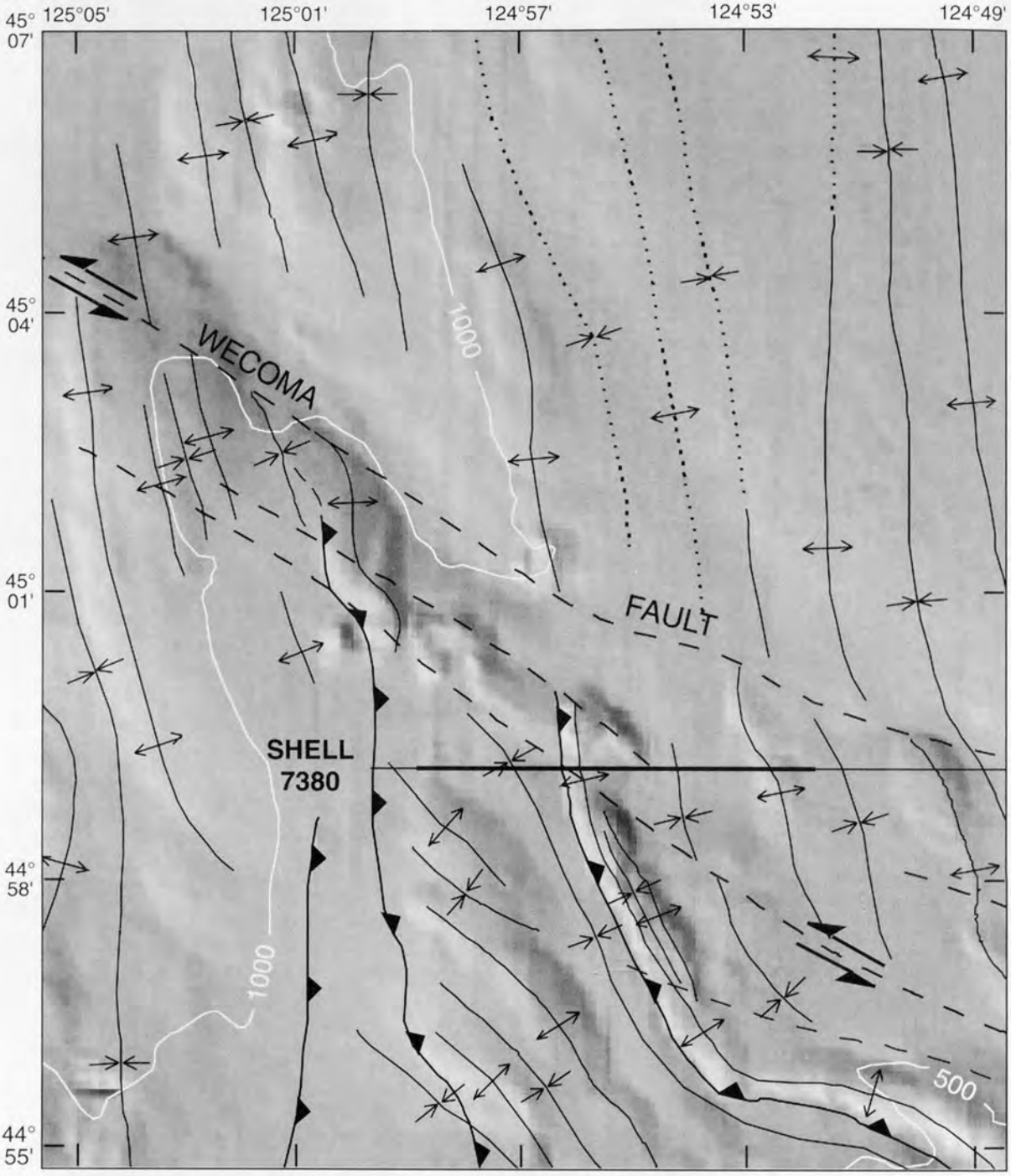

EXPLANATION

Fault—Dashed where inferred; barbs show relative motion where known

Thrust fault—Sawteeth on upper plate; dashed where inferred

Anticline—Trace dotted where concealed

Syncline—Trace dotted where concealed

−500− **Bathymetric contour**

begin on the middle to lowermost part of the slope and continue southeastward to the shelf break, where bathymetric expression dies out (figs. 100 and 101). Zone WF in figure 101 extends southeastward from the area where scarps and offsets related to the Wecoma fault were mapped with sidescan imagery (fig. 116). This deformation zone is crossed by several seismic-reflection lines, including four Oregon State University lines, two U.S. Geological Survey lines, and two industry lines in our data set. The profiles clearly show the oblique folds observed on the SeaBeam bathymetry, and most also show that the deformation zone includes several major and many minor high-angle faults. Several profiles reveal that the oblique folds that define the bathymetric deformation zone are fault-bend and fault-propagation folds, both landward and seaward vergent, developed above high-angle faults. Detailed mapping suggests that some of these oblique folds are superimposed on somewhat older northwest- to north-northwest-trending folds. Those that overlie high-angle faults show by their trends that the underlying faults also trend northwest to west-northwest. In seismic-reflection crossings, the high-angle faults are commonly expressed as a nearly vertical main trace with a flower structure in the upper section (fig. 119*A–D*). Development of oblique folds and faults decreases or becomes more distributed southeastward (landward) toward the upper slope and outermost shelf within the deformation zone.

FAULT ORIENTATION AND THE REGIONAL TECTONIC SETTING

The Wecoma fault strikes 293° on the abyssal plain, the same as faults B and C (fig. 100). This orientation is virtually the same as the 295° strike of the Blanco fracture zone, the transform fault that separates the Juan de Fuca and Pacific plates and forms the boundary between the Gorda and main segments of the Juan de Fuca plate (fig. 97). Detailed mapping of the continental slope off Washington and Oregon has also documented an additional six oblique deformation zones with similar strikes, three of which adjoin abyssal-plain strike-slip faults (Chris Goldfinger and L.D. Kulm, unpub. data, 1993). All these features, including the Blanco fracture zone, are oriented along small circles of rotation of the Juan de Fuca plate with respect to the Pacific plate. It is presently unknown if this is coincidental or if there is a fundamental relationship between plate motion and the orientation of the strike-slip faults. An attractive explanation for this similarity might be that the strike-slip faults are reactivated minor transforms, formerly generated at the spreading ridge, that are currently responding to the subduction-related stress field at the deformation front. Detailed reconstructions of the spreading history of the Juan de Fuca plate by Wilson and others (1984), however, indicate that the Juan de Fuca ridge (fig. 97) was oriented nearly north-south at the time the presently subducting crust was generated. Any relict transforms generated at that time should be oriented east-west, making it unlikely that reactivated faults are responsible for the observed structures. Although the reflection profiles have been interpreted to include the possibility of a long (more than 6 million years) history for the Wecoma fault (Appelgate and others, 1992), our preferred interpretation suggests that the faults are on the order of 600,000 years old, eliminating a spreading-ridge origin. The youth of these faults and their proximity to and influence on the plate boundary suggest that they are a subduction-related phenomenon as opposed to relict structures or structures related to regional Juan de Fuca plate stresses. Indeed, limited seismological evidence that suggests the regional stress field may be roughly north-south in much of the Juan de Fuca plate (Spence, 1989) is incompatible with the orientation and slip direction of the abyssal-plain strike-slip faults.

STRIKE-SLIP FAULTS AND THE ACCRETIONARY WEDGE

We have shown that the Wecoma fault influences the seawardmost accretionary wedge. Seismic and sidescan records show that the intersection of the fault and the deformation front is a complex zone of interaction between the frontal thrust and the strike-slip fault. Strands of the fault extend into the seawardmost three or four thrust ridges on sidescan records, and these observations are supported by direct observation from ALVIN and analysis of carbonate material derived from venting fluids on the marginal ridge.

In addition to seismic-reflection and sidescan evidence, we observed significant differences in the style and growth history of the youngest thrust ridges near the Wecoma fault. Considerably more shortening has occurred on equivalent structures immediately south of the projection of the Wecoma fault than to the north. Both fault-bend and fault-propagation folds are better developed to the south, and an

Figure 118 (facing page). Shaded relief plot of SeaBeam bathymetry and structure of a part of the central continental slope off the central Oregon coast crossed by the Wecoma fault. The fault is expressed as a wide zone consisting of several fault strands and intervening fault-related folds. The sigmoidal patterns and offsets of fold axes indicate left-lateral offset on the Wecoma fault. The bold segment of the Shell 7380 trackline is profiled in figure 119*B*. The area shown is located by the arrow in figure 101.

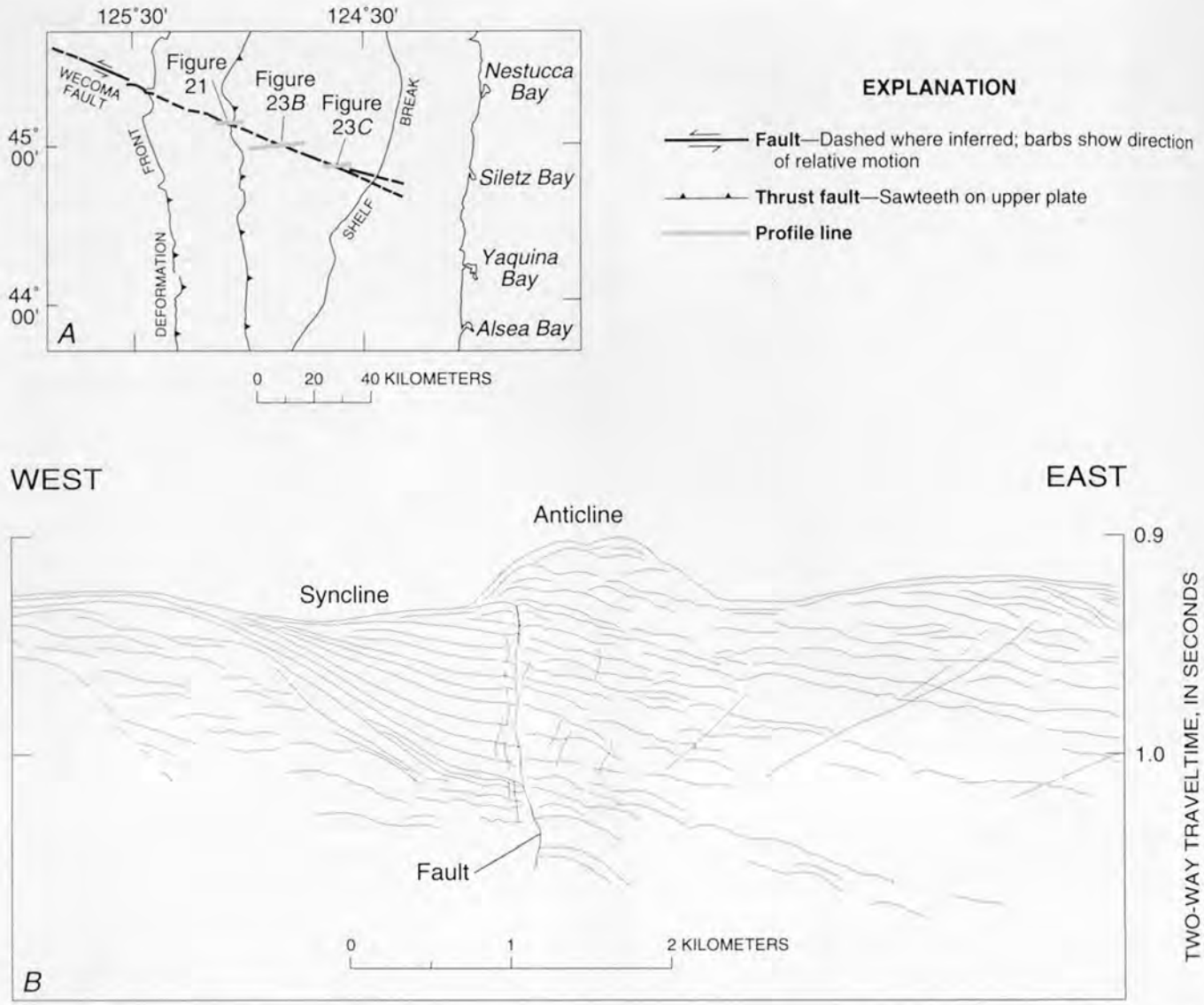

Figure 119 (above and facing page). Seismic profiles showing the Wecoma fault and deformation zone off the central Oregon coast. *A*, location of seismic profiles shown on figures 117 and 119*B–D*. *B*, line drawing of part of Shell 7380 trackline. This single-channel sparker record crosses the Wecoma fault and deformation zone and shows a northwest-trending anticline and a truncated syncline separated by a high-angle fault, the central of three mapped strands of the Wecoma fault. Other dipping faults may be minor splays. The anticline is typical of young oblique structures in the deformation zone. *C*, unmigrated single-channel seismic profile of a strike-slip fault within the Wecoma fault deformation zone on the upper continental slope. Arrow shows fault location. *D*, interpreted version of profile in figure 119*C*. Note near-vertical fault and sharp dip reversals of reflectors. Oregon State University line SP–56. Vertical exaggeration is 2.0:1.

additional thrust ridge is present to the south that is not present to the north (fig. 120). This change in fold and thrust development across the Wecoma fault is clear on reflection profiles and can also be seen in the bathymetry, which shows an abrupt bathymetric change across the fault (fig. 120; see also MacKay and others, 1992). This change corresponds to the scarp discussed above and shown in figure 116. Much of the bathymetric change is due to the abrupt increase in development of the thrust ridges on the southern side.

The structure map of this area (fig. 103) shows that other changes in accretionary-wedge structures also occur along this bathymetric trend and escarpment. Some fold axes and thrust faults step or bend to the left, whereas others terminate altogether. The left offsets and sigmoidal bending are consistent with a left-lateral shear zone. Similar relationships between trench-parallel accretionary-wedge structures and a conjugate set of strike-slip faults have been mapped in the Shumagin segment of the

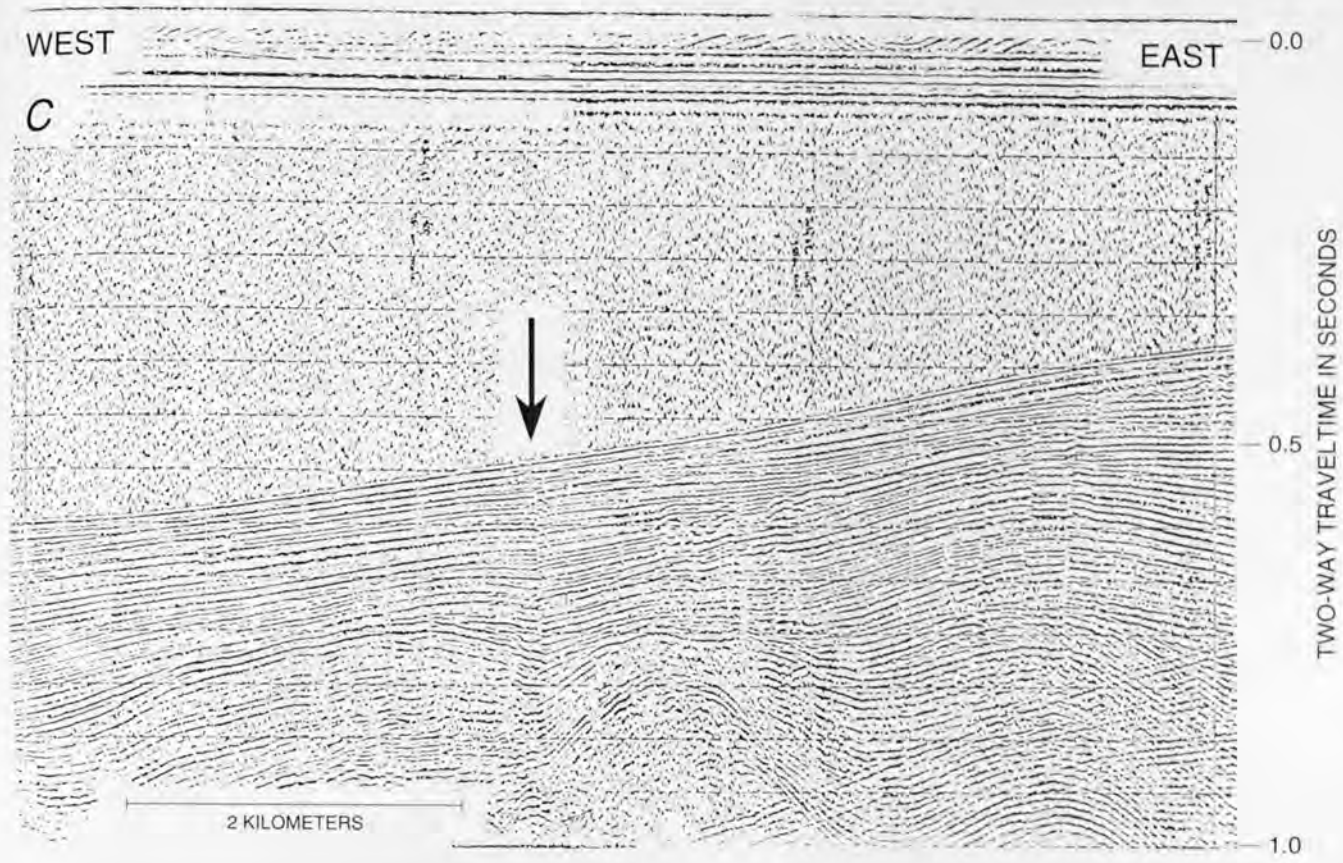
WEST
EAST
C
0.0
0.5
1.0
TWO-WAY TRAVELTIME IN SECONDS
2 KILOMETERS

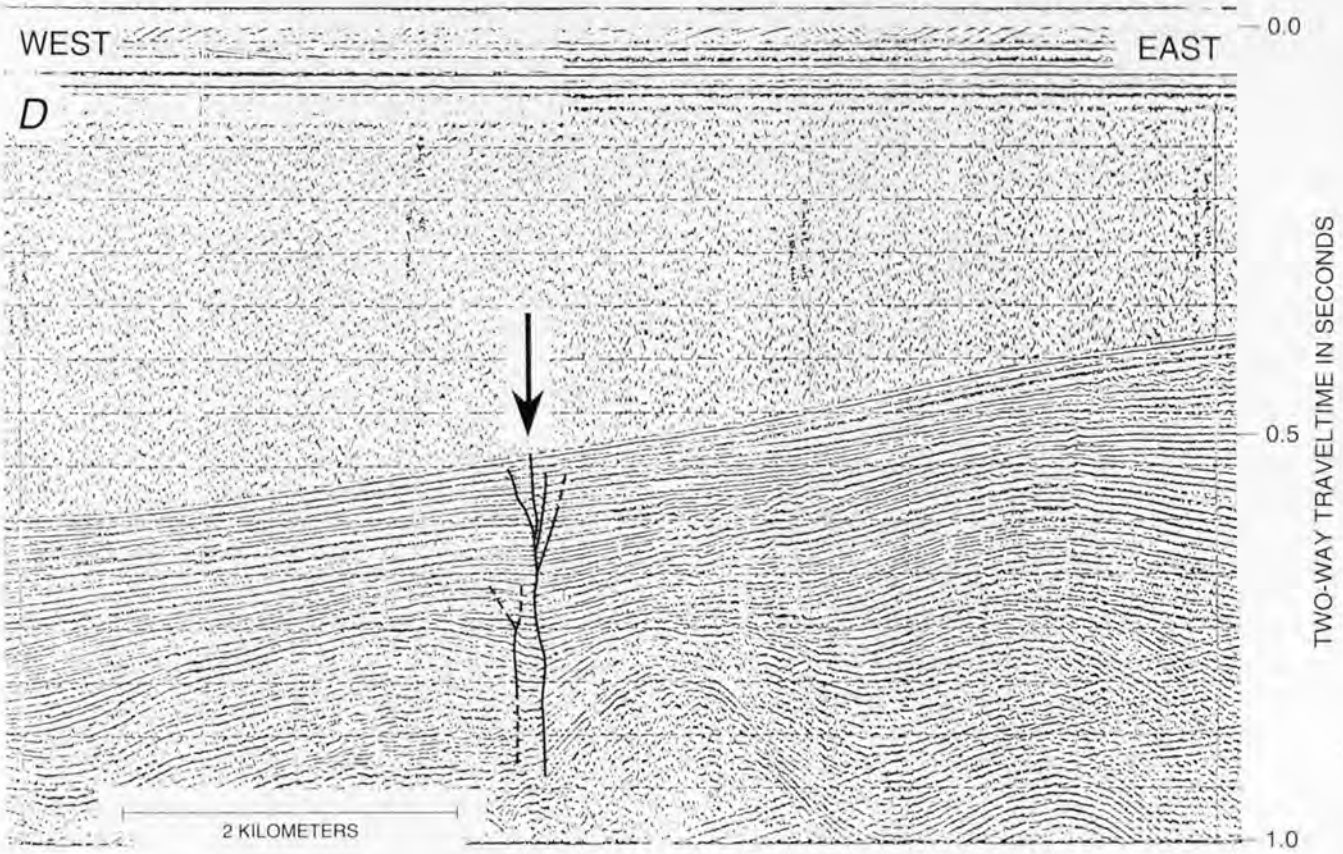
WEST
EAST
D
0.0
0.5
1.0
TWO-WAY TRAVELTIME IN SECONDS
2 KILOMETERS

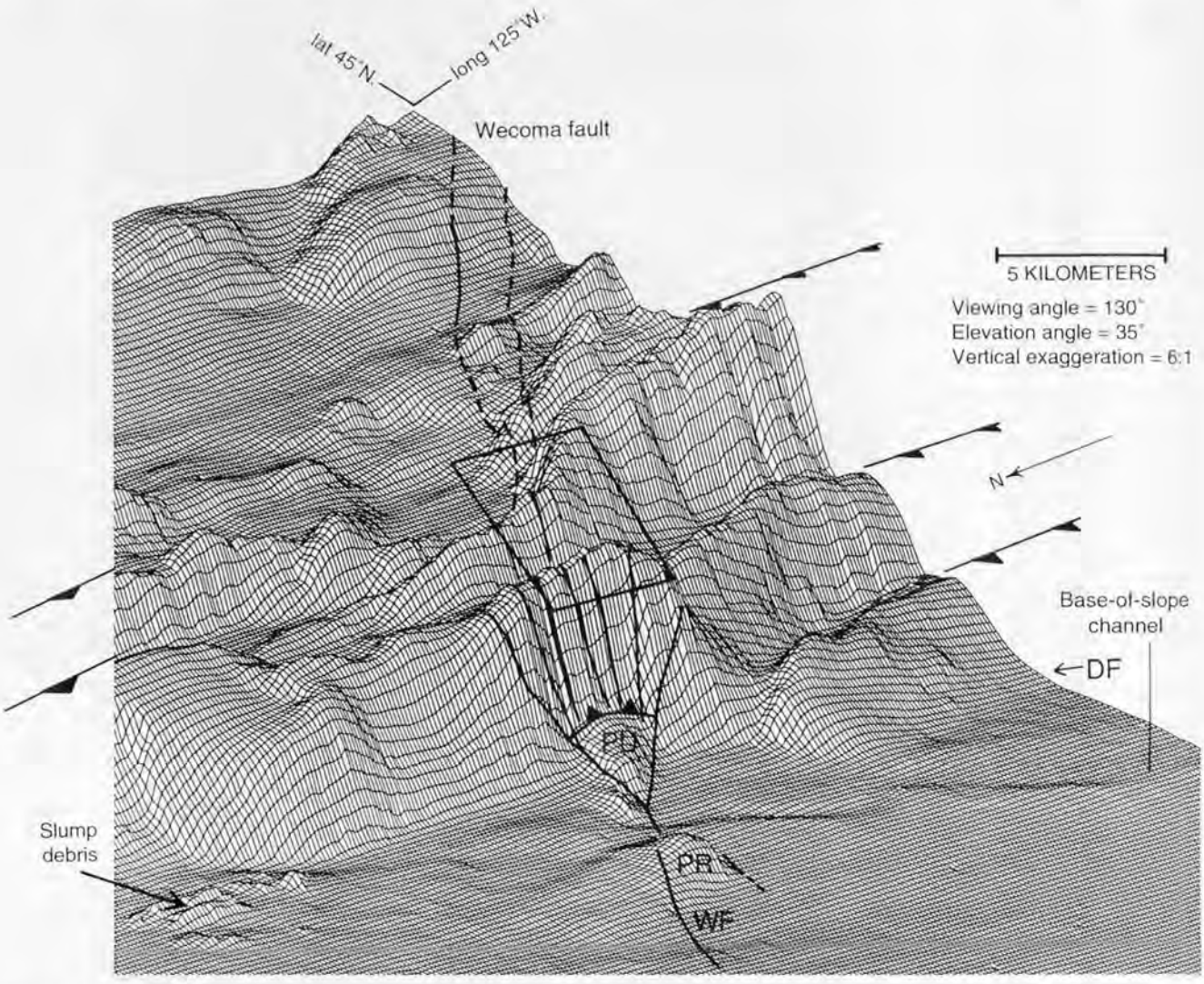

Figure 120. SeaBeam-bathymetry perspective view along the strike of the Wecoma fault as it crosses from the abyssal plain into the accretionary wedge. Grid spacing is 250 m. Note the morphologic change in the thrust ridges from the south block to the north block across the Wecoma fault. Note also the extra thrust ridge on the south block that has no correlative to the north. Parallelogram shows location of figure 116. Solid and dashed lines are faults; solid lines with sawteeth are thrust faults (sawteeth on upper plate). PR, pressure ridge; PU, pop-up; DF, deformation front; WF, Wecoma fault.

Aleutian forearc (Lewis and others, 1988). The projected trend of the Wecoma fault also coincides with an abrupt change in strike of the seaward thrust ridges. North of the fault, the ridges strike about north-south; south of the fault, the strike is 340°. The differences in thrust-ridge development across the projection of the Wecoma fault also support the presence of an active left-lateral shear zone. Given the plate convergence rate of 40 mm/year (DeMets and others, 1990) and a simple calculation of the shortening on these structures, we estimate that the four westernmost thrust ridges must have formed during the 600±50 thousand years that the Wecoma fault has been active. We postulate that the difference in shortening is due to a local change in the subduction rate across the fault resulting from subduction of the active Wecoma fault. Using the net slip of 5.5±0.8 km and the 600±50 ka age of the Wecoma fault, the difference in subduction across the fault has been 8.4–10.0 km, or 41–44 percent of the 19–24 km of normal convergence that has occurred during the life span of the Wecoma fault. Figure 121 illustrates this geometric result and shows that the effective local convergence rate is 28 percent greater south of the Wecoma fault than to the north. We postulate that increased convergence south of the fault due to this difference has caused the extra shortening in the seaward thrust ridges and probably also the early development of the extra thrust ridge (fig. 120).

KINEMATICS OF OBLIQUE FAULT-ACCRETIONARY WEDGE INTERACTION

We suggest three hypotheses to explain the possible interactions of the abyssal-plain faults and the accretionary wedge: (1) the strike-slip faults extend from the abyssal plain beneath the accretionary wedge and are the source of the deformation zones; (2) the strike-slip faults originate within the North America plate and propagate into the subjacent subducted slab and seaward into the abyssal plain; and (3) the deformation zones on the slope are unrelated to the abyssal-plain faults.

If the strike-slip faults originate in the Juan de Fuca plate (hypothesis 1), the deformation zones in the accretionary wedge may have developed in response to strike-slip motion of the Juan de Fuca plate beneath the accretionary wedge and thick Tertiary shelf sequence. If so, the presence of such deformation in both the overriding and downgoing plates presents a problem in reconciling strike-slip motion and oblique convergence over the last 600,000 years. Oblique convergence of about 24 km directed 062° has occurred over the past 600,000 years, according to the plate vectors of DeMets and others (1990). During that time, the points at which the three strike-slip faults on the abyssal plain intersect the present deformation front should have moved some 20 km to the north (neglecting the unknown amount of advance of the deformation front), yet we observed little or no offset between the abyssal plain and accretionary-wedge segments of these faults. The discrepancy could be due to a very recent slowdown or cessation of subduction. Although cessation is unlikely given the preponderance of geologic and geophysical evidence, a significant slowdown cannot be ruled out and could reduce the missing component of convergence (Riddihough, 1984). Three structural explanations might also be considered: (1) the existence of right-lateral strike-slip faults in the upper plate to the east of the youngest accretionary thrusts. Such faults can decouple the seaward part of the accretionary complex and accommodate the margin-parallel component of oblique convergence (Fitch, 1972; Jarrard, 1986; Karig and others, 1986). Snavely (1987) has mapped such a feature (the Fulmar fault) on the Oregon shelf. More than 200 km of dextral slip occurred on this fault, primarily in the Eocene, but minor offsets of younger units may indicate continued or renewed activity (Snavely and others, 1985; Snavely, 1987); (2) a right-lateral component on the accretionary thrusts themselves could accommodate the missing north-south convergence component, distributing the expected offset of the strike-slip faults over many crossing structures. The deformation zones on the continental slope do show a tendency to step or bend to the south, a requirement of this mechanism; or (3) the subducted strike-slip faults leave progressive deformation behind in the upper plate as they pass beneath it

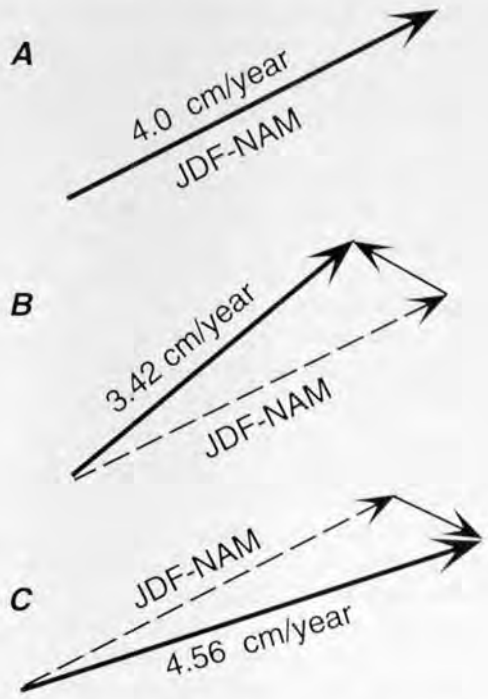

Figure 121. Vector diagram of the inferred local effect of Wecoma-fault slip on the plate convergence vector. *A*, regional Juan de Fuca-North America (JDF–NAM) plate vector of DeMets and others (1990), oriented 062°. *B*, JDF-NAM vector (dashed) on the north block of the Wecoma fault. The short arrow is the local vector due to motion on the Wecoma fault, oriented 292°. The new resultant, with a strike of 051°, and convergence rate are shown by the bold arrow. *C*, JDF-NAM vector (dashed) on the south block of the Wecoma fault. The short arrow is the local vector due to motion on the fault. The new resultant, oriented 072°, and convergence rate are shown with the bold arrow. Increased convergence south of the fault may be responsible for the greater shortening and topographic expression of the thrust faults south of the Wecoma fault. Calculated from the Euler pole of DeMets and others (1990), North America fixed.

to the northeast. Two oblique deformation zones limited to the accretionary wedge have been mapped on the continental slope and shelf, one in northern Oregon off the Tillamook Bay area and one off southern Oregon northwest of Cape Blanco. This process might be analogous to the trail of volcanoes left on a lithospheric plate as it passes over a fixed mantle hot spot. As the Juan de Fuca plate is subducted, lower plate faults leave behind a trail of deformation in the accretionary wedge as they pass obliquely beneath the North America plate.

If the strike-slip faults originate within the upper plate (hypothesis 2), several problems with hypothesis 1 are avoided. Because not all the mapped deformation zones on

the slope have abyssal-plain counterparts, an upper-plate origin does not require a separate explanation for those structures. It is also more mechanically reasonable to envision faults in the thicker upper plate propagating across a locked interface into the thin, relatively warm subducting plate than the reverse. The apparent incompatibility of west-northwest-trending left-lateral faults with the focal solutions and inferred north-south principal stress of Spence (1989) for the Juan de Fuca plate is resolved if the abyssal-plain faults are only the western extensions of faults that originate within the upper plate to the east. If this is the case, the regional stress field in the oceanic plate might coexist with a somewhat different stress field within the upper plate and near the deformation front, with a transition somewhere seaward of the abyssal-plain faults. Lastly, a domain of subparallel left-lateral strike-slip faults should rotate clockwise through time (Freund, 1974; Ron and others, 1984; Scotti and others, 1991). Such rotations as a result of progressive slip on these faults were suggested by Goldfinger and others (1992) and could resolve the question of the offset across the deformation front expected in hypothesis 1 because clockwise rotation of the upper plate could make up the missing north-south component of plate convergence.

Hypothesis 3, that there is no connection between the slope deformation zones and the abyssal-plain faults, must be considered, as data positively linking these structures is not available at present. However, the trends, shear sense, and youth of these structures all strongly suggest at least a genetic connection, if not a physical one. If these structures are not directly linked, they may be separate but similar responses by the interacting plates to interplate subduction stresses.

CONCLUSIONS

Three west-northwest-trending left-lateral strike-slip faults in the Cascadia subduction zone off the central Oregon coast offset both the oceanic basement and sedimentary cover of the Juan de Fuca plate. The Wecoma fault, the largest of the three faults, has a measured net slip of 5–6 km at the plate boundary, dying out in the Juan de Fuca plate 18 km to the northwest of its intersection with the deformation front. Two independent estimates of the slip rate on this fault during two time periods show similar rates of 5–12 mm/year for the period 24–10 ka, and 7–12 mm/year over the 600,000-year life span of the fault. The Wecoma fault intersects the deformation front in a complex area of structural pop-ups and an embayment in the deformation front. Sidescan images show that scarps and linear gullies extend along the projected strike of the subducted Wecoma fault about 15 km into the accretionary wedge. Slip on the Wecoma fault beneath the North America plate has influenced the development of the initial thrust ridges in the accretionary wedge. Three deformation zones in the accretionary wedge lie along the landward projections of the three abyssal-plain faults. These zones are composed of west-northwest- to northwest-trending folds, sigmoidally bent fold axes, and west-northwest-trending linear scarps. The style of deformation in these zones is consistent with left-lateral shear zones superimposed on the structural grain of the accretionary wedge. We postulate that these deformation zones are the result of subduction of the active strike-slip faults or, alternatively, that the shear zones originate in the upper plate and propagate across the plate boundary into the Juan de Fuca plate. The orientation of the Wecoma fault and the other strike-slip faults along small circles of rotation of the Juan de Fuca-Pacific plate system is not yet understood.

REFERENCES CITED

Adams, John, 1990, Paleoseismicity of the Cascadia subduction zone—Evidence from turbidites off the Oregon-Washington margin: Tectonics, v. 9, no. 4, p. 569–583.

Ando, Masataka, and Balazs, E.I., 1979, Geodetic evidence for aseismic subduction of the Juan de Fuca plate: Journal of Geophysical Research, v. 84, no. B6, p. 3023–3028.

Appelgate, T.B., 1988, Tectonic and volcanic structures of the southern flank of Axial volcano, Juan de Fuca Ridge—Results from a SeaMARC I sidescan sonar survey: Corvallis, Oregon State University, M.S. thesis, 161 p.

Appelgate, T.B., Goldfinger, Chris, MacKay, M.E., Kulm, L.D., Fox, C.G., Embley, R.W., and Meis, P.J., 1992, A left-lateral strike-slip fault seaward of the central Oregon convergent margin: Tectonics, v. 9, no. 3, p. 465–477.

Atwater, B.F., 1987, Evidence for great Holocene earthquakes along the outer coast of Washington State: Science, v. 236, no. 4804, p. 942–944.

Atwater, B.F., and Yamaguchi, D.K., 1991, Sudden, probably coseismic submergence of Holocene trees and grass in coastal Washington State: Geology, v. 19, no. 7, p. 706–709.

Carson, Bobb, 1977, Tectonically induced deformation of deep-sea sediments off Washington and northern Oregon—Mechanical consolidation: Marine Geology, v. 24, no. 4, p. 289–307.

Carver, G.A., Vick, G.S., and Burke, R.M., 1989, Late Holocene paleoseismicity of the Gorda segment of the Cascadia subduction zone: Geological Society of America Abstracts with Programs, v. 21, no. 5, p. 64.

Clarke, S.H., Jr., and Carver, G.A., 1989, Late Cenozoic structure and seismic potential of the southern Cascadia subduction zone [abs.]: EOS [American Geophysical Union Transactions], v. 70, no. 43, p. 1331–1332.

Cochrane, G.R., and Lewis, B.T.R., 1988, Deep-tow seismic reflection records from the Oregon lower slope: EOS [American Geophysical Union Transactions], v. 69, no. 43, p. 1442–1443.

Darienzo, M.E., and Peterson, C.D., 1990, Episodic tectonic subsidence of late Holocene salt marshes, northern Oregon central Cascadia margin: Tectonics, v. 9, no. 1, p. 1–22.

DeMets, Charles, Gordon, R.G., Argus, D.F., and Stein, Seth, 1990, Current plate motions: Geophysical Journal International, v. 101, no. 2, p. 425–478.

Duncan, J.R., 1968, Late Pleistocene and postglacial sedimentation and stratigraphy of deep-sea environments off Oregon: Corvallis, Oregon State University, Ph.D. dissertation, 222 p.

Fitch, T.J., 1972, Plate convergence, transcurrent faults, and internal deformation adjacent to southeast Asia and the western Pacific: Journal of Geophysical Research, v. 77, no. 23, p. 4432–4460.

Freund, Raphael, 1974, Kinematics of transform and transcurrent faults: Tectonophysics, v. 21, p. 93–134.

Geist, E.L., Childs, J.R., and Scholl, D.R., 1988, The origin of summit basins of the Aleutian Ridge—Implications for block rotation of an arc massif: Tectonics, v. 7, no. 2, p. 327–341.

Goldfinger, Chris, Kulm, L.D., Yeats, R.S., Appelgate, T.B., MacKay, M.E., and Moore, G.F., 1992, Transverse structural trends along the Oregon convergent margin—Implications for Cascadia earthquake potential and crustal rotations: Geology, v. 20, no. 2, p. 141–144.

Griggs, G.B., and Kulm, L.D., 1970, Sedimentation in Cascadia deep-sea channel: Geological Society of America Bulletin, v. 81, no. 5, p. 1361–1384.

———1973, Origin and development of Cascadia deep-sea channel: Journal of Geophysical Research, v. 78, no. 27, p. 6325–6339.

Griggs, G.B., Kulm, L.D., Waters, A.C., and Fowler, G.A., 1970, Deep-sea gravel from Cascadia Channel: Journal of Geology, v. 78, no. 5, p. 611–619.

Harding, T.P., 1985, Seismic characteristics and identification of negative flower structures, positive flower structures, and positive structural inversion: American Association of Petroleum Geologists Bulletin, v. 69, no. 4, p. 582–600.

Heaton, T.H., and Kanamori, Hiroo, 1984, Seismic potential associated with subduction in the Northwestern United States: Seismological Society of America Bulletin, v. 74, no. 3, p. 993–941.

Ingle, J.C., 1973, Neogene foraminifera from the northeastern Pacific Ocean, Leg 18, Deep Sea Drilling Project: Washington, D.C., U.S. Government Printing Office, Initial Reports of the Deep Sea Drilling Project, v. XVIII, p. 517–567.

Jarrard, R.D., 1986, Terrane motion by strike-slip faulting of forearc slivers: Geology, v. 14, no. 9, p. 780–783.

Karig, D.E., Sarewitz, D.R., and Haeck, G.D., 1986, Role of strike-slip faulting in the evolution of allochthonous terranes in the Philippines: Geology, v. 14, no. 10, p. 852–855.

Kulm, L.D., and Fowler, G.A., 1974, Oregon continental margin structure and stratigraphy—A test of the imbricate thrust model, *in* Burke, C.A., and Drake, C.L., eds., The geology of continental margins: New York, Springer-Verlag, p. 261–284.

Kulm, L.D., Prince, R.A., and Snavely, P.D., Jr., 1973, Site survey of the northern Oregon continental margin and Astoria Fan: Washington, D.C., U.S. Government Printing Office, Initial Reports of the Deep Sea Drilling Project, v. XVIII, p. 979–987.

Kulm, L.D., and Suess, Erwin, 1990, The relation of carbonate deposits to fluid venting processes—Oregon accretionary prism: Journal of Geophysical Research, v. 95, no. B6, p. 8899–8915.

Kulm, L.D., Huene, Roland von, and the shipboard scientific party, 1973, Initial Reports of the Deep Sea Drilling Project: Washington, D.C., U.S. Government Printing Office, v. XVIII, p. 97–168.

Lewis, S.D., Ladd, J.W., and Bruns, T.R., 1988, Structural development of an accretionary prism by thrust and strike-slip faulting—Shumagin region, Aleutian Trench: Geological Society of America Bulletin, v. 100, no. 5, p. 767–782.

Ludwin, R.S., Weaver, C.S., and Crosson, R.S., 1991, Seismicity of Washington and Oregon, *in* Slemmons, D.B., Engdahl, E.R., Zoback, M.D., and Blackwell, D.D., eds., Neotectonics of North America: Boulder, Colo., Geological Society of America, Decade Map Volume 1, p. 77–98.

MacKay, M.E., Moore, G.F., Cochrane, G.R., Moore, J.C., and Kulm, L.D., 1992, Landward vergence, oblique structural trends, and tectonic segmentation in the Oregon margin accretionary prism: Earth and Planetary Science Letters, v. 109, p. 477–491.

Nelson, C.H., 1968, Marine geology of Astoria deep-sea fan: Corvallis, Oregon State University, Ph.D. dissertation, 287 p.

———1976, Late Pleistocene and Holocene depositional trends, processes and history of Astoria deep-sea fan, northeast Pacific: Marine Geology, v. 20, p. 129–173.

Riddihough, Robin, 1984, Recent movements of the Juan de Fuca plate system: Journal of Geophysical Research, v. 89, no. B8, p. 6980–6994.

Ron, Hagai, Freund, Raphael, Garfunkel, Zvi, and Nur, Amos, 1984, Block rotation by strike-slip faulting—Structural and paleomagnetic evidence: Journal of Geophysical Research, v. 89, no. B7, p. 6256–6270.

Sample, J.C., Reid, M.R., Tobin, H.J., and Moore, J.C., 1993, Carbonate cements indicate channeled fluid flow along a zone of vertical faults at the deformation front of the Cascadia accretionary wedge (northwest U.S.A. coast): Geology, v. 21, p. 507–510.

Scotti, Oona, Nur, Amos, and Estevez, Raul, 1991, Distributed deformation and block rotation in 3D: Journal of Geophysical Research, v. 96, no. B7, p. 12225–12243.

Snavely, P.D., Jr., 1987, Tertiary geologic framework, neotectonics, and petroleum potential of the Oregon-Washington continental margin, *in* Scholl, D.W., Grantz, Arthur, and Vedder, J.G., eds., Geology and resource potential of the continental margin of western North America and adjacent ocean basins—Beaufort Sea to Baja California: Houston, Tex., Circum-Pacific Council for Energy and Mineral Resources, Earth Science Series, v. 6, no. 6, p. 305–335.

Snavely, P.D., Jr., and McClellan, P.H., 1987, Multichannel seismic-reflection data collected in 1976 off of the Washington-Oregon coast: U.S. Geological Survey Open-File Report 87-607, 3 p.

Snavely, P.D., Jr., Wagner, H.C., and Lander, D.L., 1985, Land-sea geologic cross section of the southern Oregon continental margin: U.S. Geological Survey Miscellaneous Investigations Series Map I–1463, scale 1:125,000.

Spence, William, 1989, Stress origins and earthquake potential in Cascadia: Journal of Geophysical Research, v. 94, p. 3076–3088.

Sykes, L.R., 1989, Great earthquakes of 1855 and 1931 in New Zealand—Evidence for seismic slip along downgoing plate boundary and implications for seismic potential of Cascadia subduction zone [abs.]: EOS [American Geophysical Union Transactions], v. 70, no. 43, p. 1331.

Sylvester, A.G., 1988, Strike-slip faults: Geological Society of America Bulletin, v. 100, no. 11, p. 1666–1703.

Tobin, H.J., Moore, J.C., MacKay, M.E., Orange, D.L., and Kulm, L.D., 1993, Fluid flow along a strike-slip fault at the toe of the Oregon accretionary prism—Implications for the geometry of frontal accretion: Geological Society America Bulletin, v. 105, no. 5, p. 569–582.

Vick, G.S., 1988, Late Holocene paleoseismicity and relative sea level changes of the Mad River slough, northern Humboldt Bay, California: Arcata, Calif., Humboldt State University, M.S. thesis, 87 p.

West, D.O., and McCrumb, D.R., 1988, Coastline uplift in Oregon and Washington and the nature of Cascadia subduction-zone tectonics: Geology, v. 16, no. 2, p. 169–172.

Wilcox, R.E., Harding, T.P., and Seely, D.R., 1973, Basic wrench tectonics: American Association of Petroleum Geologists Bulletin, v. 57, no. 1, p. 74–96.

Wilson, D.S., Hey, R.N., and Nishimura, Clyde, 1984, Propagation as a mechanism of reorientation of the Juan de Fuca Ridge: Journal of Geophysical Research, v. 89, no. B11, p. 9215–9225.

WESTERN WASHINGTON EARTHQUAKE FOCAL MECHANISMS AND THEIR RELATIONSHIP TO REGIONAL TECTONIC STRESS

By Li Ma,[1] Robert Crosson,[1] *and* Ruth Ludwin[1]

ABSTRACT

Tectonic stress in western Washington has been investigated by inverting earthquake focal mechanisms to ascertain principal-stress directions. A total of 191 well-constrained focal mechanisms were determined from data collected by the Washington Regional Seismograph Network for 3 spatially distinct groups of earthquakes: (1) shallow (crustal) Puget Sound; (2) deep (subcrustal) Puget Sound; and (3) shallow (crustal) Mount St. Helens events. Although focal mechanisms clearly differ among the three groups, it is less obvious whether significant differences in the tectonic stress regime are required to produce the observed focal-mechanism variations.

Comparing crustal earthquakes (depth less than 30 km) in the North America plate between the Puget Sound and Mount St. Helens regions, the single best fitting stress model for Puget Sound has a nearly north-south σ_1 (maximum principal compressive stress) orientation with an east-west σ_3 (minimum principal compressive stress) orientation, whereas the best fitting model in the Mount St. Helens area has north-northeast σ_1 orientation and east-southeast σ_3 orientation. At all confidence levels examined, the allowable stress orientations for these two regions overlap. Therefore, we conclude that reorientation of stress in the Mount St. Helens region is neither required nor precluded by the data. A uniform north-south compressive tectonic stress in the crust can adequately explain all of the observed focal mechanisms in western Washington.

In the subducted Juan de Fuca plate, or slab, the state of stress is more complex. The orientations of P (apparent compressional) and T (apparent tensional) axes, derived from focal mechanisms of subcrustal earthquakes (depths greater than 30 km), do not cluster around a single direction, although T-axis orientations weakly correlate with the general easterly direction of plate subduction. Inversion to ascertain the stress orientation indicates that no single set of stress directions adequately fits the observed focal mechanisms for subcrustal earthquakes within the subducted slab. The diversity of orientations of P and T axes of these intraslab earthquakes may be consistent with the model of an arched slab beneath Puget Sound that produces variations in the slab stress state.

The north-south compressive tectonic stress in the North America plate and the dramatic change in stress state between it and the subducted Juan de Fuca slab indicate that the crustal stress is not controlled in a simple fashion by the processes causing plate convergence and subduction. We suggest that the magnitude of plate coupling stress is significantly lower than the level of regional tectonic stress from other causes.

INTRODUCTION

Only a few geophysical methods provide direct insight into the state of tectonic stress. Stress measurements using borehole techniques reflect only near-surface conditions and few have been made in the Pacific Northwest. Geodetic strain measurements provide information on changes and rates of change of stress indirectly through measurements of strain but, again, only limited measurements have been made in the Pacific Northwest (Lisowski and others, 1987; Savage and Lisowski, 1991). Earthquakes reflect strain within the Earth through slip on fault surfaces. This process is controlled by stress and the yield properties of rock. By making reasonable assumptions about the relationships between stress and fault slip, we can infer the state of stress at midcrustal and greater depths through the study of earthquake focal mechanisms. For each earthquake, we can estimate the orientations of P and T axes, which are the apparent maximum and minimum principal-stress directions for that event. We are ultimately interested in the orientations of σ_1 and σ_3, the maximum and

[1]Geophysics Program, AK-50, University of Washington, Seattle, WA 98195.

minimum principal-stress components, respectively. For various reasons, P and T orientations for any given earthquake may depart significantly from the true σ_1 and σ_3 directions. With a relatively large number of earthquakes, statistical uncertainty in our ability to determine stress can be reduced. Midcrustal and subcrustal earthquakes are relatively abundant in western Washington. Using data obtained by the Washington Regional Seismograph Network (WRSN), a powerful observational tool, we analyze focal mechanisms to establish the orientation of regional tectonic stress.

In the Pacific Northwest, we expect the tectonics to be strongly influenced by the subduction of the Juan de Fuca plate beneath the North America plate along the Cascadia subduction zone (CSZ) (for example, see Atwater, 1970; Riddihough, 1984). In subduction zones where the convergent plates are strongly coupled, the backarc is expected to be characterized by tectonic compression normal to the arc (for example, see Uyeda and Kanamori, 1979). Because tectonic stress is the underlying physical source of earthquakes, understanding regional tectonic stress in the Pacific Northwest is very important. At shallow depths (less than 30–40 km), most subduction zones worldwide have earthquakes caused by direct slip between the two plates (interplate earthquakes). Stresses interpreted from these earthquakes are consistent with compression in the direction of plate convergence. At greater depths, earthquakes within the descending plate, or slab, commonly indicate downdip tension or other stresses within the slab (for example, see Isacks and Molnar, 1971).

Interplate (between plates) earthquakes have never been recorded along the CSZ, although active plate convergence is widely accepted by scientists. Previous focal-mechanism studies indicate the prevalence of north-south compressive tectonic stress orientation based on earthquakes in both western and eastern Washington (Crosson, 1972; Malone and others, 1975; Yelin and Crosson, 1982; Crosson, 1983). This prevalent north-south compression is not easily interpreted in terms of our understanding of plate convergence in a N. 50° E. direction (Riddihough, 1984), or with the N. 70° E. principal-stress direction predicted from a simple mechanical model of plate interaction (Savage and others, 1981). If the plates are strongly coupled, we expect focal mechanisms of crustal earthquakes to indicate compression in the direction of convergence. The north-south σ_1 orientation obtained from focal mechanisms also does not agree with the northeastward principal compressive strain derived from the geodetic observations of Savage and others (1981), Lisowski and others (1987), and Savage and Lisowski (1991), although strain rates measured so far in the Pacific Northwest are generally of low magnitude compared to those in many other tectonically active regions.

The earthquake and geodetic observations might be reconciled by noting that the geodetic measurements are sensitive to small changes in strain, whereas earthquakes should reflect the absolute ambient levels of stress in the crust (Sbar, 1982). Thus, strain-rate measurements may reflect small incremental changes in stress superimposed upon a much larger ambient tectonic stress field, and the two types of measurements need not agree in orientation. The concept implies that the northeast-directed strain found by Savage and others (1981), Lisowski and others (1987), and Savage and Lisowski (1991), which is consistent with the expected orientation due to subduction, is small in magnitude relative to the background ambient tectonic stress that focal mechanisms indicate is directed north-south. This does not necessarily mean that large subduction earthquakes cannot be produced by this relatively low level of coupling stress, but rather that the stress due to subduction may be low in magnitude compared to regional ambient tectonic stress.

In the Mount St. Helens region, focal mechanisms from earthquakes along the St. Helens seismic zone (Weaver and Smith, 1983) show rotation of P axes from north to the northeast relative to other regions in western Washington. This rotation was interpreted by Weaver and Smith (1983) to indicate a σ_1 affected more strongly by plate coupling in this region, suggesting a variation in plate coupling from north to south along the CSZ. In this chapter, we further examine this important issue, which bears directly on earthquake hazards.

Our understanding of the stresses producing intraslab earthquakes (that is, earthquakes occurring within the subducting Juan de Fuca slab) is far from clear. Because the Puget Sound region is vulnerable to hazards from subcrustal earthquakes, we may expect to learn more about the origin and nature of these hazards through the study of intraslab focal mechanisms. Although past focal-mechanism studies have suggested changes in orientation of stress from the subducted slab to the overlying North America plate, the extent of this difference has not been clearly quantified. Furthermore, although downdip extensional stress has been associated with slab earthquakes (Taber and Smith, 1985), not all intraslab earthquakes reflect this type of stress, as we illustrate in this chapter. Thus, an objective of this study is to clarify some of the uncertainties in interpretation of intraslab focal mechanisms and to learn if a coherent stress model can be determined from these earthquakes.

ACKNOWLEDGMENTS

We thank John Gephart of Cornell University for providing the original computer programs for this analysis and for assistance in their use. This study was supported by the U.S. Geological Survey under grants 14–08–0001–G1080, 14–08–0001–G1390, and 14–08–0001–G1803.

METHOD OF STRESS DETERMINATION

Stress is usually described in terms of three mutually perpendicular axes, which are called principal-stress axes. The orientation of these axes is determined by the perpendicular directions corresponding to maximum (σ_1) and minimum (σ_3) compressive stresses. The third axis, corresponding to intermediate stress (σ_2), is determined by the orientation of the other two axes. In conventional focal-mechanism studies, it is common to use the pattern of P and T axes as estimated by individual focal mechanisms to infer the orientation of the regional tectonic principal-stress axes. Scattered directions of axes may be averaged either qualitatively or quantitatively to establish the preferred directions of σ_1 and σ_3. A possible difficulty with this approach became clear when McKenzie (1969) pointed out that if slip occurs on preexisting zones of weakness, there may be substantial difference between the orientations of seismic P and T axes and the true principal axes of stress. As the Earth's crust is commonly believed to have many fractures, faults, and zones of varying strength, the simplified interpretation of P and T axes may lead to erroneous conclusions about the true orientation of tectonic stress. McKenzie (1969) established the theoretical basis for analyzing this problem. Several investigators, among them Angelier (1979), subsequently developed quantitative methods of analyzing large amounts of geologic data, such as fault-movement striations, to correctly estimate regional stress. Such methods are necessarily limited to near-surface conditions. Ellsworth and Zhonghuai (1980) extended these methods to the analysis of focal mechanisms.

Gephart and Forsyth (1984) and Gephart (1985, 1990a, b) developed a complete and self-consistent method of using a group of focal mechanisms to find the orientation of the regional tectonic stress axes along with a quantitative indicator of the relative magnitudes of the principal stresses. Their method is based on McKenzie's (1969) principle and makes use of a scalar rotational misfit between the theoretical stress orientation that is currently being tested and the stress orientation required to activate the observed fault planes. The sum of misfits is the objective function that is minimized to achieve a best fitting stress model, as well as to establish the statistical scatter of possible solutions. The actual slip plane for each earthquake may either be assigned or selected objectively by the processing algorithm. Formal statistical confidence limits are established for possible tectonic stress orientations that are consistent with the observed focal mechanisms. A central assumption of this method is that the magnitudes and directions of principal stresses do not change over a region from which the earthquakes to be analyzed are selected. Therefore, the method may be viewed as a test of the hypothesis that a single uniform regional stress explains all observed focal mechanisms.

SELECTION OF DATA

The WRSN comprises over 120 short-period vertical-component stations in Washington and northern Oregon (Qamar and others, 1987). Real-time signals sent to a central recording facility have been digitally recorded since 1980. Two horizontal-component Wood-Anderson seismographs are also operated as part of the network. Although the network operated for about 10 years prior to 1980, only data acquired after that time have been used for this study because of the quality improvement resulting from digital-data acquisition. This improvement is particularly important for focal-mechanism studies because *P*-wave polarities, the main part of our data set, are generally clearly identifiable from digital data, whereas they are commonly obscured on the older analog film records.

The following criteria were used to initially select earthquakes for focal-mechanism studies: (1) an azimuthal gap of station coverage of 100° or less, (2) an unweighted root-mean-square traveltime residual of 0.3 second or less, and (3) a coda magnitude of 1.0 or greater. Earthquake locations determined in normal preliminary processing (for example, Qamar and others, 1987) were used for this study. All earthquakes with eight or more identified polarities were examined for possible inclusion in the data set; seismograms of promising events were reread for polarities, and known polarity reversals were corrected. Focal mechanisms were then constructed by hand fitting, and acceptable solutions were retained for the inversion analysis. If a nodal plane could be rotated 20° or more, or the solution was deemed poorly constrained due to polarity discrepancies or other factors, the earthquake was rejected. Subcrustal earthquakes (within the subducted Juan de Fuca slab) are rarer than crustal earthquakes (Crosson, 1983) and relatively few of their focal mechanisms have been determined, so special effort was made to include all from this group. A total of 191 high-quality focal mechanisms were ultimately retained for further analysis. These mechanisms and their associated polarity data are listed in the "Focal Mechanism Listings and Plots" section at the end of this chapter. The data set is divided into three spatial groups: (1) shallow Puget Sound earthquakes; (2) deep (subcrustal) Puget Sound earthquakes; and (3) shallow Mount St. Helens region earthquakes. Each group was individually analyzed, and we discuss the significance of our results in light of regional stress orientation.

Figure 122 is an east-west cross section of western Washington showing hypocenters of earthquakes used in this study. The grouping of subcrustal (deeper than 30 km) earthquakes, constituting what is termed the Wadati-Benioff zone, is clearly separated from the shallower crustal earthquakes. Subcrustal seismicity is within the subducting slab and not at the plate interface. The slab dip angle varies from between 10° and 12° in the Puget Sound area to between 15° and 20° north and south of Puget Sound (Green and others, 1986; Keach and others, 1986; Crosson and Owens, 1987).

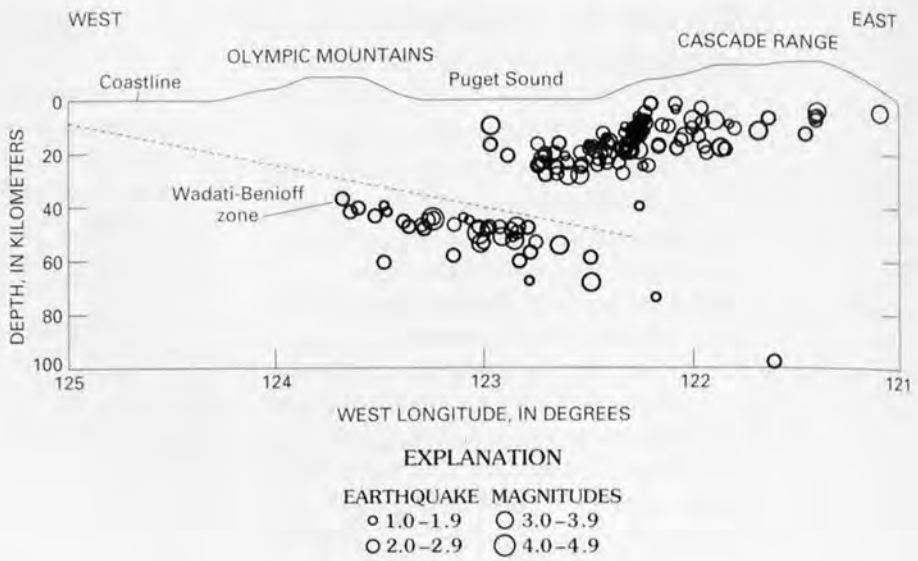

Figure 122. Cross section across western Washington showing hypocenters of earthquakes used in this study projected onto an east-west plane. Dashed line shows approximate top of subducted Juan de Fuca plate.

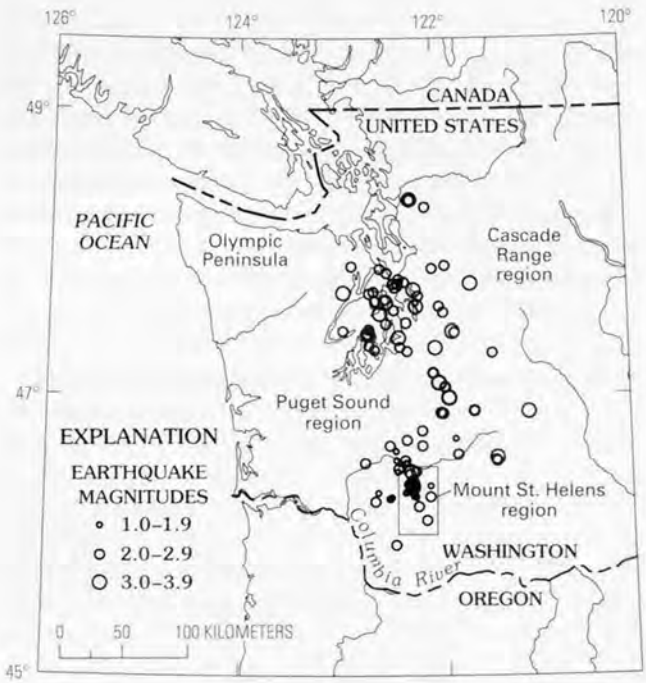

Figure 123. Epicenters of all crustal earthquakes in the focal-mechanism data set used for this study. Different velocity models are used for locations of earthquakes in the regions labeled Cascade Range, Puget Sound, and Mount St. Helens. Velocity models and model areas are given in Ludwin and others (1991). All earthquakes used for the study of the Mount St. Helens region are located within the boxed area.

Figure 124. Lower-hemisphere, equal-area focal mechanisms of the 17 largest Washington crustal earthquakes used in this study. Magnitudes ranged from 3.0 to 3.6. Numbers refer to earthquakes listed in tables 19 and 20. Dots are earthquake epicenters. Compressional quadrants are shaded. The T axis of each mechanism runs through the middle of the compressional quadrant, and the P axis is in the middle of the tensional quadrant. An explanation of earthquake focal mechanisms can be found in Fowler (1990).

FOCAL MECHANISMS

CRUSTAL EARTHQUAKES

Crustal earthquake focal mechanisms (hypocentral depths less than 30 km; fig. 123) were divided into two groups. The shallow Puget Sound group numbered 76 earthquakes in the central Puget Sound and western Cascade Range regions. The shallow Mount St. Helens group was composed of 73 earthquakes in the Mount St. Helens region (fig. 123). Of the combined 149 earthquakes, 17 were larger than magnitude 3.0 (fig. 124). Focal mechanisms for earthquakes located in the Puget Sound region have P axes varying generally from north-northwest to north-northeast and are of both thrust and strike-slip type. Only two of the earthquakes shown in figure 124 are in the Mount St. Helens group (events 48 and 140; table 20). Of these, event 48 has a mechanism similar to that of the 1981 Elk Lake, Wash., main shock (Grant and others, 1984). Both of these earthquakes have strike-slip mechanisms that are typical of this region but less common in the Puget Sound region.

Figure 125 summarizes the shallow Puget Sound group data set with lower hemisphere, equal-area composite plots of the P and T axes. The figure shows that most P axes are nearly north-south and that T axes are more uniformly distributed in a zone around the equator of the projection.

In the Mount St. Helens region, 52 of the 73 earthquakes were along the northern part of the St. Helens seismic zone (Weaver and Smith, 1983) and the remainder were scattered throughout the rest of the region. In our analysis, we assumed that the slip planes of these 52 earthquakes were constrained to align approximately with the strike of the seismic zone. P axes in the Mount St. Helens region tend to be oriented northeast (fig. 126), indicating apparent stress rotation due either to the existence of the St. Helens seismic zone itself or to larger regional tectonic variations.

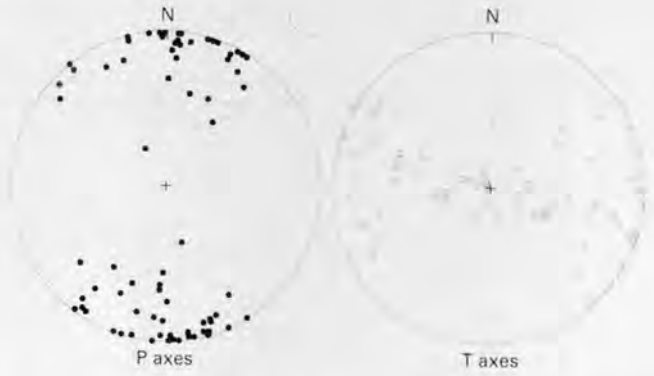

Figure 125. Lower hemisphere, equal-area composite projections of P and T axes for the 76 crustal earthquakes in the shallow Puget Sound data set.

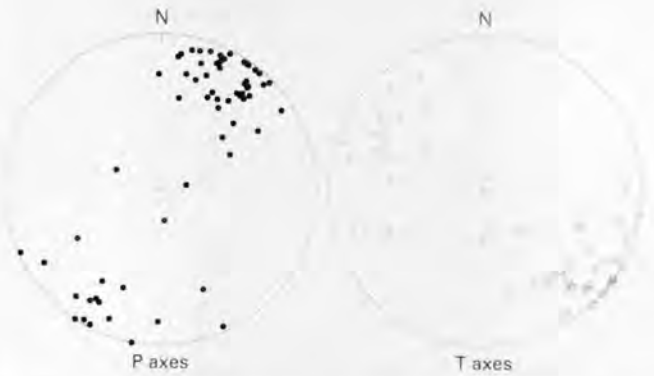

Figure 126. Lower hemisphere, equal-area composite projections of P and T axes for the 73 crustal earthquakes in the Mount St. Helens region data set.

SUBCRUSTAL EARTHQUAKES

Most subcrustal earthquakes were on the western side of Puget Sound and beneath the eastern side of the Olympic Peninsula (fig. 127). Focal mechanisms for selected large subcrustal earthquakes are shown in figure 128. Events 3 and 116 (table 21) were larger than magnitude 4.0, and the remaining events were between magnitudes 3.0 and 3.9. Both events 3 and 116 have vertical P axes and nearly horizontal T axes. Although these two normal earthquakes suggest an extensional environment beneath the convergent plate margin, in agreement with Taber and Smith (1985), the two earthquakes have very different apparent stress orientations. Event 3, in the northeastern corner of the Olympic Peninsula and at a depth of 48.5 km, has a nearly north-south T axis. On the other hand, event 116, at the southern end of the Olympic Peninsula, has a southeast-oriented T axis. A careful examination of the focal mechanisms shown in figure 128 reveals the lack of any obvious consistency in the subcrustal group. It is difficult to generalize about the state of stress within the subducted slab except to note that there may be a prevalence of horizontal T axes.

As another way to view this variability, plots of P and T axes for all subcrustal earthquakes are plotted in figure 129. P axes vary in plunge from near vertical to near horizontal and azimuths vary from northeast to southeast and from northwest to southwest. Because there are no P axes oriented north-south, as with the crustal earthquakes, we conclude qualitatively that these data are not consistent with the north-south compression noted earlier for crustal earthquakes and that there is a major change in stress state from the subducted Juan de Fuca slab to the overlying North America plate.

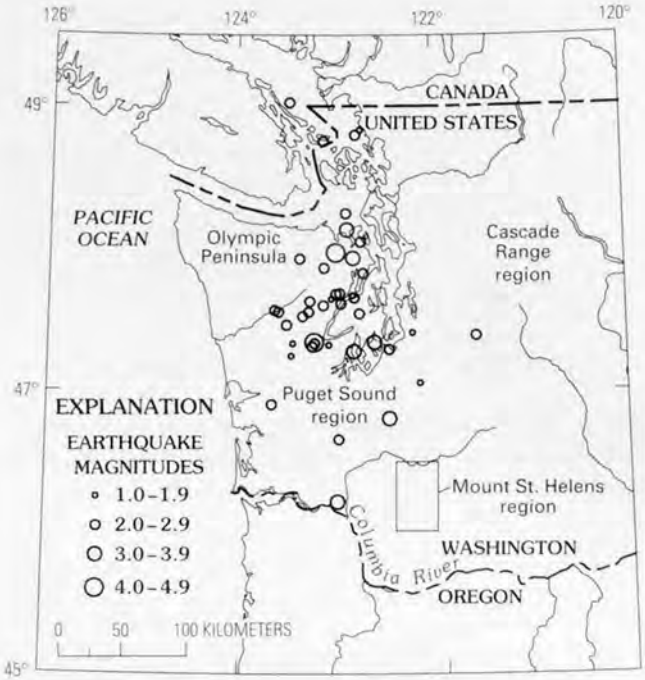

Figure 127. Epicenters of all subcrustal (also called deep or intraslab) earthquakes in western Washington used in this study.

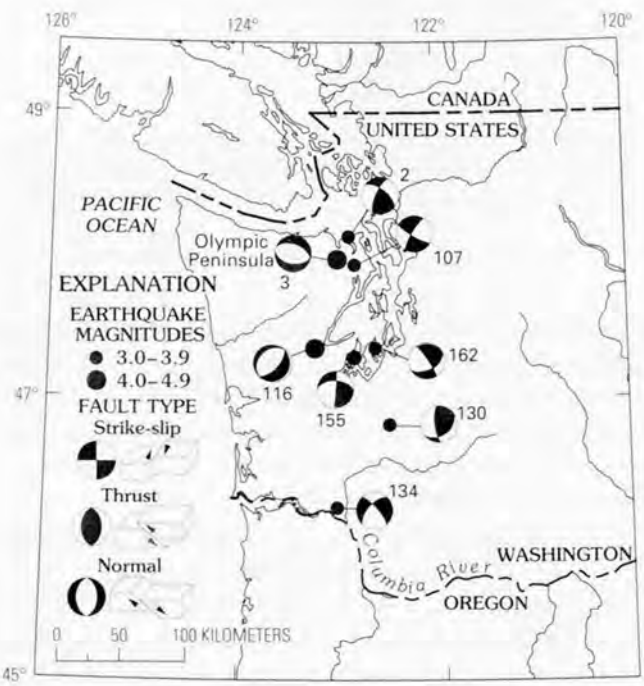

Figure 128. Lower hemisphere, equal-area focal mechanisms of eight larger magnitude subcrustal, or intraslab, earthquakes in western Washington. This figure illustrates the variability of focal mechanisms within the intraslab earthquake group. Numbers refer to earthquakes listed in table 21. Dots are earthquake epicenters.

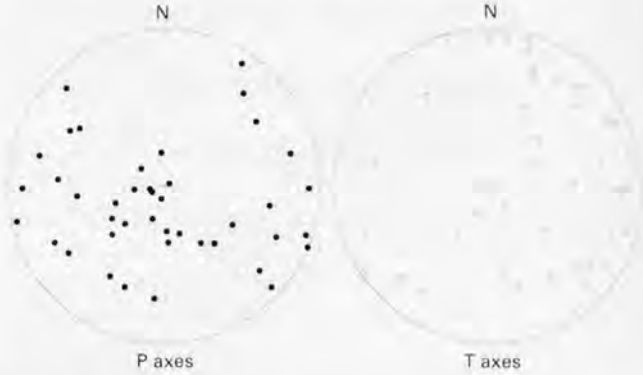

Figure 129. Lower hemisphere, equal-area composite projections of P and T axes for the 42 subcrustal (intraslab) Puget Sound earthquakes shown in figure 127.

STRESS ANALYSIS

We applied the inversion technique of Gephart and Forsyth (1984) separately to the three groups (shallow Puget Sound, Mount St. Helens region, and subducted slab) of focal mechanisms in western Washington. The output of the inversion calculations includes the best fitting principal-stress-axis orientations for σ_1, σ_2, and σ_3, the distribution of acceptable orientations for each axis at the specified confidence level, and the best fitting R value where R is defined as:

$$R = \frac{(\sigma_1 - \sigma_2)}{(\sigma_1 - \sigma_3)}.$$

Thus, R is a measure of whether the intermediate principal stress is near the maximum ($R \sim 0$) or the minimum ($R \sim 1$) principal stresses. In addition, the mean value of misfit for the best fitting values is given as an angular rotation (Gephart and Forsyth, 1984). The inversion calculations involve a modified grid-search method where we may predefine the allowable search ranges to increase efficiency.

SHALLOW PUGET SOUND GROUP RESULTS

For this data set, we limited the grid-search values for σ_1 used in the inversion because there is a general consistency in the P and T axes distributions. The azimuth ranges selected were from N. 60° W. to N. 60° E. and from S. 57° E. to S. 63° E. The allowed range of plunge was set from 1° to 51°. An angular increment of 5° between grid points was used for both azimuth and plunge. The result of setting these parameters is that 11,000 discrete stress orientations are tested for each R value, where R varies between 0.1 and 1.0 in steps of 0.1.

Table 18. Best-fit principal-stress-orientation models of western Washington earthquakes based on inversion analyses of focal mechanisms.

[σ_1, maximum compressive stress; σ_2, intermediate compressive stress; σ_3, minimum compressive stress. Azimuth measured clockwise from north; plunge measured down from the horizontal. R, ratio comparing the intermediate compressive stress to the maximum and minimum compressive stresses ($1 \geq R \geq 0$). Misfit, mean rotational difference between individual focal mechanisms and modeled stress orientations]

Earthquake group	Number of events	σ_1		σ_2		σ_3		R	Misfit
		Azimuth	Plunge	Azimuth	Plunge	Azimuth	Plunge		
Shallow Puget Sound	76	356°	1°	262°	72°	86°	18°	0.6	12.6°
Shallow Mount St. Helens	73	203°	1°	106°	81°	293°	9°	0.7	9.1°
Subcrustal Puget Sound	42	245°	51°	13°	26°	117°	26°	0.1	19.9°

For the shallow Puget Sound data set, the best fitting model is (azimuth, plunge): $\sigma_1 = 356°, 1°$; $\sigma_2 = 262°, 72°$; and $\sigma_3 = 86°, 18°$ (table 18). Azimuth is expressed in degrees counterclockwise from north, and plunge is in degrees below horizontal. The value of R yielding the best fit is 0.6. Figure 130 shows the allowable σ_1 orientations at both 50-percent and 95-percent confidence levels. In agreement with our intuition based on the distributions of P and T axes, the best fitting σ_1 is nearly horizontal and oriented north-south, with only a narrow range of possible σ_1 axes in the 50-percent confidence limit plot (fig. 130). For the best fitting stress-axis model, the 76 earthquakes have an average misfit of 12.6°, and all but 15 have misfits of less than 20°, suggesting that the single north-south compression model is a good representation of the regional stress. This result supports and refines previous findings for the region (Crosson, 1972; Crosson and Frank, 1975; Crosson and Lin, 1975; Malone and others, 1975; Rogers, 1979; Sbar, 1982; Yelin, 1982; Yelin and Crosson, 1982). To test the stability of the inversion to outlier data, the computations were repeated after individually removing focal mechanisms with misfits greater than 20°. The results were virtually unchanged, suggesting that our data set is large enough to produce stable and robust results.

MOUNT ST. HELENS REGION GROUP RESULTS

A total of 73 focal mechanisms was included in the Mount St. Helens region data set. We used the same orientation grid constraints as described for the shallow Puget Sound group, and the same increments for R. Although the inversion technique will normally select the appropriate slip plane using a minimum rotation criterion, when external knowledge of the slip plane is available, it can (and should) be specified explicitly. The existence of a nearly linear zone of epicenters more than 50 km long extending from Mount St. Helens to the north-northwest allowed us to select the slip plane in 59 of the earthquakes analyzed under the assumption that this is a strike-slip crustal fault zone. For this group, nodal planes with strikes within 15° of north were judged to be aligned along the St. Helens seismic zone and were selected as fault planes.

The single best fitting model found for all 73 Mount St. Helens focal mechanisms is (azimuth, plunge): $\sigma_1 = 203°, 1°$; $\sigma_2 = 106°, 81°$; $\sigma_3 = 293°, 9°$; and $R = 0.7$ (table 18). The allowable σ_1 axis orientations at the 50-percent and 95-percent confidence levels are shown in figure 131. The average misfit for all earthquakes in this example is 9.1°, and nine events have misfits greater than 20°. At both 95-percent and 50-percent confidence levels, the allowable P-axis orientations for the shallow Mount St. Helens region overlap those for the shallow Puget Sound region.

SUBDUCTED-SLAB GROUP RESULTS

If we assume that McKenzie's (1969) theory of uniform stress causing slip on preexisting faults can be equally applied to earthquakes at subcrustal depths, then the

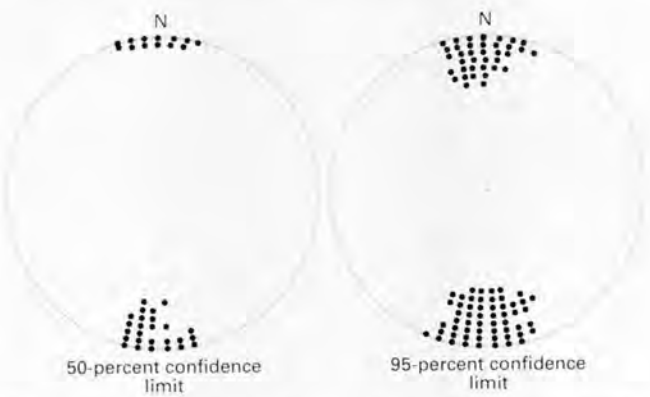

Figure 130. Lower hemisphere, equal-area plots showing the distribution of maximum principal compressive stress (σ_1) axes. Stress was determined from focal mechanisms using 76 shallow Puget Sound earthquakes and Gephart and Forsyth's (1984) method. The best fitting model is listed in table 18. The distribution of acceptable axes is shown at the 50-percent and 95-percent confidence limits.

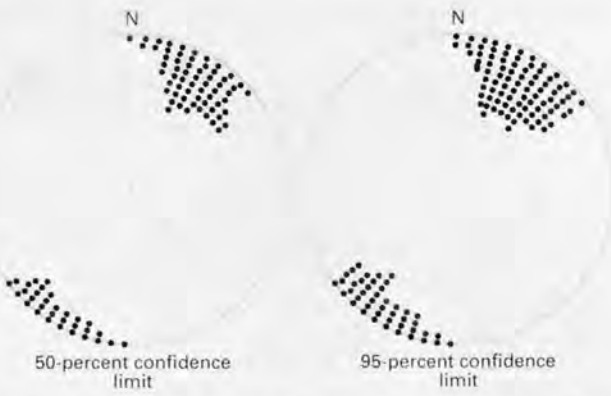

Figure 131. Lower hemisphere, equal-area plots showing the distribution of maximum principal compressive stress (σ_1) axes. Stress was determined from focal mechanisms using 73 shallow Mount St. Helens area earthquakes and Gephart and Forsyth's (1984) method. The best fitting model is listed in table 18. The distribution of acceptable axes is shown at the 50-percent and 95-percent confidence limits.

inversion method can be used to investigate the stress state in the subducted Juan de Fuca slab. Composite plots of P and T axes from focal mechanisms of subcrustal earthquakes in the Puget Sound area (fig. 129) do not show a clustered distribution of P and T axes so, for subcrustal earthquakes, a stress grid with σ_1 directions covering the entire focal sphere was used.

The best fitting model for subcrustal earthquakes is (azimuth, plunge): $\sigma_1 = 245°, 51°$; $\sigma_2 = 13°, 26°$; $\sigma_3 = 117°, 26°$; and $R = 0.1$ (table 18). The allowable σ_1 axis orientations at the 50-percent and 95-percent confidence levels are shown in figure 132. The low value of R means that the intermediate and maximum principal stresses are close in magnitude, with the minimum principal stress significantly smaller than the other two. This result generally agrees with the expected extensional stress state along the top surface of a bending slab (Isacks and Molnar, 1971). Furthermore, the scatter of allowable solutions at the 50-percent and 95-percent confidence levels indicates that the single stress-orientation model does not satisfactorily explain the range of focal mechanisms observed. We suggest the slab is in a heterogeneous stress state, perhaps resulting from the complications in slab geometry noted by Crosson and Owens (1987) and Weaver and Baker (1988). It is certain from these results, however, that the state of stress in the subducted slab is significantly more complex and different than the state of stress in the continental crust of the North America plate.

DISCUSSION OF RESULTS

The results of this study, based on a substantial amount of high-quality digital data, confirm the general north-south horizontal tectonic compression in the North America plate of Washington, as first suggested by Crosson (1972). Although the best fitting stress model for the shallow Mount St. Helens area has σ_1 rotated about 27° to the northeast relative to the shallow Puget Sound region, the overlap of preferred stress models at the 95-percent confidence level suggests that a rotation of tectonic stress between these two regions is not required. However, such a rotation is also not precluded by the data.

Our results offer an alternative explanation to the suggestion by Weaver and Smith (1983) that the rotation of stress indicates a change in stress coupling along the subduction zone. In the absence of evidence to the contrary, we should assume that a more uniform north-south regional tectonic compressive stress is predominant and can explain the focal-mechanism data while introducing the fewest complicating assumptions. The apparent rotation of stress in the shallow Mount St. Helens area is likely to be a result of preferred slip on a preexisting zone of crustal weakness. We note that north-south compression is the predominant tectonic characteristic along the west coast of the United States (Zoback and Zoback, 1980; Sbar, 1982). Because of the rather limited size of the Juan de Fuca plate in relation to the extensive San Andreas and Queen Charlotte right-lateral transform fault systems that form most of the remainder of the western plate boundary of North America, it appears that the stress state of the North America plate in western Washington is influenced mainly by the large-scale interaction between the Pacific and North America plates (Zoback and Zoback, 1980).

The accumulation of tectonic strain recorded by geodetic measurements (Savage and others, 1981; Lisowski and others, 1987; Savage and Lisowski, 1991) appears to conflict with the north-south compression interpreted from the focal-mechanism analysis. It is important to note, however, that the geodetically observed strain rate is very low (less than 0.10 μstrain per year) (Lisowski and others, 1987; Savage

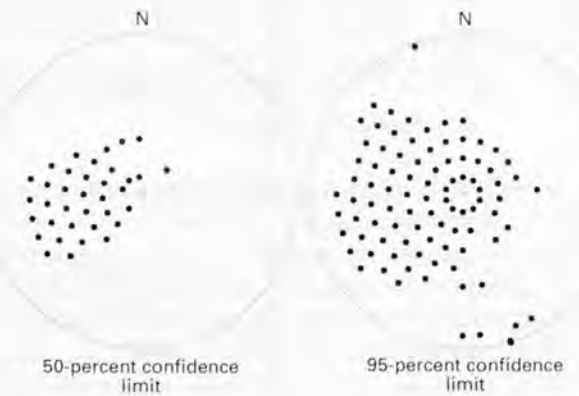

Figure 132. Lower hemisphere, equal-area plots showing the distribution of maximum critical compressive stress (σ_1) axes. Stress was determined from focal mechanisms using 42 subcrustal Puget Sound earthquakes and Gephart and Forsyth's (1984) method. The best fitting model is listed in table 18. The distribution of acceptable axes is shown at the 50-percent and 95-percent confidence limits.

and Lisowski, 1991) and that strain measurements reflect only incremental changes in stress, whereas focal mechanisms probably reflect the regional ambient stress. Furthermore, geodetic measurements may reflect inelastic deformation, so that the principal-strain axes determined from geodetic measurements need not reflect the deep state of stress. If the explanation for the difference between the orientation of stress determined from geodetic measurements and from focal mechanisms lies in the relative magnitudes of ambient and incremental stress, then clearly the plate-coupling (incremental) stress producing the observed strain must be much smaller in magnitude than the ambient tectonic stress that causes most intraplate earthquakes.

The stress state in the Juan de Fuca slab appears to be complicated and is not well described by a single stress model. The initial assumption of Gephart and Forsyth's (1984) method, that slip occurs on preexisting planes of weakness, may not apply to the slab. However, the wide scatter of P- and T-axis directions suggests an inhomogeneous stress field. From the composite plots of P and T axes (fig. 129), it is difficult to even estimate directions of apparent compression and tension. However, there are two clear characteristics: (1) no P axes are oriented north-south with shallow plunge angles; (2) T axes are generally oriented northeast or southeast with shallow plunge angles. The differences between the P and T axes of subcrustal (fig. 129) and crustal earthquakes (figs. 125 and 126) indicate that there is little direct mechanical coupling between the crust and the deeper part of the subducted slab. Rather, the slab stress distribution appears to be generated largely by processes inside the slab itself (for example, bending stresses or stresses induced from phase changes). Although the implication of these results in terms of intraslab earthquake hazards is not clear at this time, understanding the slab stress state should lead to improved estimates of source parameters of future slab earthquakes. The general spatial coincidence of the crustal and subcrustal earthquake groups in the Puget Sound region (fig. 122) is puzzling in view of the clear difference in stress states that we have found from this study.

The variety of the directions of tensional axes in different parts of the slab might result from superposition of down-dip tension with stress resulting from the arching of the Juan de Fuca plate under the Puget Sound area. To test this possibility, we examined the slab stress-axis orientations in light of the best available knowledge of slab geometry. Most T axes, as shown in figure 133, seem to lie in the plane of the plate arch or in a down-dip direction. For higher magnitude earthquakes, this tendency may be even more pronounced. For example, five of the eight earthquakes with magnitudes of 3.0 or greater had T axes that closely parallel the arched slab. These results suggest that the arching could produce tensional stress due to bending of the slab. The configuration of P axes shown in figure 134 is quite different, with P axes tending to be normal to the slab surface. A qualitative comparison of figures 133 and 134 suggests a general control of the intraslab earthquakes by slab bending or slab geometry.

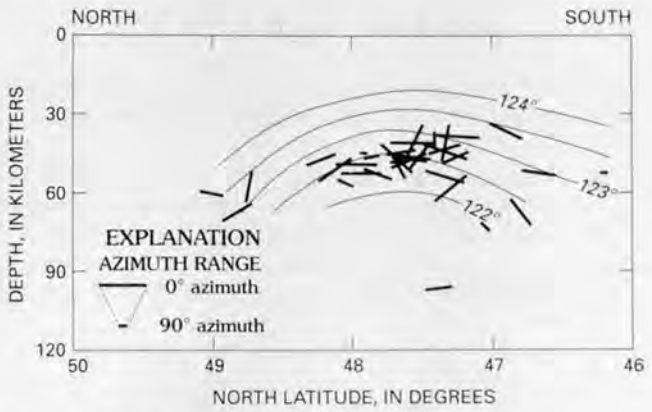

Figure 133. T axes of the 42 subcrustal western Washington earthquakes used in the study projected onto a north-south cross section. The numbered curves are approximate contours at equal longitude values (from the model of Crosson and Owens, 1987).

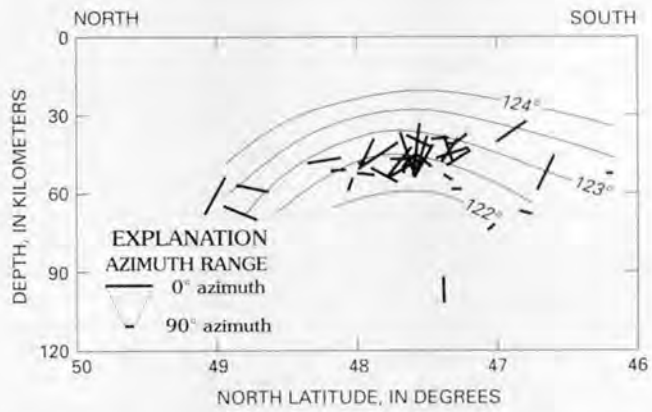

Figure 134. P axes of the 42 subcrustal western Washington earthquakes used in the study projected onto a north-south cross section. The numbered curves are approximate contours at equal longitude values (from the model of Crosson and Owens, 1987).

CONCLUSIONS

Our studies indicate that the Washington part of the North America plate is likely to be in a state of uniform regional north-south compressive tectonic stress that does not directly reflect the active subduction along the Cascadia subduction zone. Plate-coupling stress between the Juan de Fuca and North America plates may be of much lower magnitude than the regional north-south compressive stress. Based on focal-mechanism data, a rotation of principal stress directions is not required near Mount St. Helens, although such a rotation is not excluded by the data. The state of stress in the subducted Juan de Fuca plate is distinctly different from and more complex than the stress state in the overlying North America plate. The lack of a uniform stress state in the subducted slab indicates that plate-geometry variations may be important in controlling slab stress and seismicity. In view of the apparent stress decoupling of crustal and subcrustal earthquakes in the Puget Sound region, the spatial coincidence of these two zones remains enigmatic.

REFERENCES CITED

Angelier, J., 1979, Determination of the mean principal directions of stresses for a given fault population: Tectonophysics, v. 56, no. 3–4, p. T17–T26.

Atwater, Tanya, 1970, Implications of plate tectonics for the Cenozoic tectonic evolution of western North America: Geological Society of America Bulletin, v. 81, no. 12, p. 3513–3535.

Crosson, R.S., 1972, Small earthquakes, structure, and tectonics of the Puget Sound region: Seismological Society of America Bulletin, v. 62, no. 5, p. 1133–1171.

———1983, Review of seismicity in the Puget Sound region from 1970 through 1978, *in* Yount, J.C., and Crosson, R.S., eds., Proceedings of Workshop XIV, Earthquake hazards of the Puget Sound region, Washington: U.S. Geological Survey Open-File Report 83–19, p. 6–18.

Crosson, R.S., and Frank, D.G., 1975, The Mt. Rainier earthquake of July 18, 1973, and its tectonic significance: Seismological Society of America Bulletin, v. 65, no. 2, p. 393–401.

Crosson, R.S., and Lin, Jia-Wen, 1975, A note on the Mt. Rainier earthquake of April 20, 1974: Seismological Society of America Bulletin, v. 65, no. 2, p. 549–556.

Crosson, R.S, and Owens, T.J., 1987, Slab geometry of the Cascadia subduction zone beneath Washington from earthquake hypocenters and teleseismic converted waves: Geophysical Research Letters, v. 14, no. 8, p. 824–827.

Ellsworth, W.L.L., and Zhonghuai, X., 1980, Determination of the stress tensor from focal mechanism data [abs.]: EOS [American Geophysical Union Transactions], v. 61, no. 46, p. 1117.

Fowler, C.M.R., 1990, The solid Earth—An introduction to global geophysics: New York, Cambridge University Press, 472 p.

Gephart, J.W., 1985, Principal stress directions and the ambiguity in fault plane identification from focal mechanisms: Seismological Society of America Bulletin, v. 75, no. 2, p. 621–625.

———1990a, FMSI—A FORTRAN program for inverting fault/slickenside and earthquake focal mechanism data to obtain the regional stress tensor: Computers and Geosciences, v. 16, no. 7, p. 953–989.

———1990b, Stress and the direction of slip on fault planes: Tectonics, v. 9, no. 4, p. 845–858.

Gephart, J.W., and Forsyth, D.W., 1984, An improved method for determining the regional stress tensor using earthquake focal mechanism data—Application to the San Fernando earthquake sequence: Journal of Geophysical Research, v. 89, no. 11, p. 9305–9320.

Grant, W.C., Weaver, C.S., and Zollweg, J.E., 1984, The 14 February 1981 Elk Lake, Washington, earthquake sequence: Seismological Society of America Bulletin, v. 74, no. 4, p. 1289–1309.

Green, A.G., Clowes, R.M., Yorath, C.J., Spencer, C.P., Kanasewich, E.R., Brandon, M.T., and Brown, A.S., 1986, Seismic reflection imaging of the subducting Juan de Fuca plate: Nature, v. 319, no. 6050, p. 210–213.

Isacks, Bryan, and Molnar, Peter, 1971, Distribution of stresses in the descending lithosphere from a global survey of focal-mechanism solutions of mantle earthquakes: Geophysics and Space Physics Reviews, v. 9, no. 1, p. 103–174.

Keach, R.W., II, Potter, C.J., Oliver, J.E., and Brown, L.D., 1986, Cenozoic active margin and shallow Cascades structure—COCORP results from western Oregon [abs.]: San Antonio, Tex., Geological Society of America Abstracts with Programs, v. 18, no. 6, p. 652.

Lisowski, Michael, Savage, J.C., Prescott, W.H., and Dragert, Herb, 1987, Strain accumulation along the Cascadia subduction zone in western Washington [abs.]: EOS [American Geophysical Union Transactions], v. 68, no. 44, p. 1240.

Ludwin, R.S., Weaver, C.S., and Crosson, R.S., 1991, Seismicity of Washington and Oregon, *in* Slemmons, D.B., Engdahl, E.R., Zoback, M.D., and Blackwell, D.D., eds., Neotectonics of North America: Boulder, Colo., Geological Society of America, Decade Map Volume 1, p. 77–98.

Malone, S.D., Rothe, G.H., and Smith, S.W., 1975, Details of microearthquake swarms in the Columbia basin, Washington: Seismological Society of America Bulletin, v. 65, no. 4, p. 855–864.

McKenzie, D.P., 1969, The relation between fault plane solutions for earthquakes and the directions of the principal stresses: Seismological Society of America Bulletin, v. 59, no. 2, p. 591–601.

Qamar, A.I., Ludwin, R.S., Crosson, R.S., and Malone, S.D., 1987, Earthquake hypocenters in Washington and northern Oregon, 1982–1986: Washington Department of Natural Resources, Division of Geology and Earth Resources, Information Circular 84, 78 p.

Riddihough, R.P., 1984, Recent movements of the Juan de Fuca plate system: Journal of Geophysical Research, v. 89, no. B8, p. 6980–6994.

Rogers, G.C., 1979, Earthquake fault plane solutions near Vancouver Island: Canadian Journal of Earth Sciences, v. 16, no. 3, part 1, p. 523–531.

Savage, J.C., and Lisowski, Michael, 1991, Strain measurements and the potential for a great subduction earthquake off the coast of Washington: Science, v. 252, no. 5002, p. 101–103.

Savage, J.C., Lisowski, Michael, and Prescott, W.H., 1981, Geodetic strain measurements in Washington: Journal of Geophysical Research, v. 86, no. B6, p. 4929–4940.

Sbar, M.L., 1982, Delineation and interpretation of seismotectonic domains in western North America: Journal of Geophysical Research, v. 87, no. B5, p. 3919–3928.

Taber, J.J., and Smith, S.W., 1985, Seismicity and focal mechanisms associated with the subduction of the Juan de Fuca plate beneath the Olympic Peninsula, Washington: Seismological Society of America Bulletin, v. 75, no. 1, p. 237–249.

Uyeda, S., and Kanamori, Hiroo, 1979, Back-arc opening and the mode of subduction: Journal of Geophysical Research, v. 84, no. B3, p. 1049–1061.

Weaver, C.S., and Baker, G.E., 1988, Geometry of the Juan de Fuca plate beneath Washington and northern Oregon from seismicity: Seismological Society of America Bulletin, v. 78, no. 1, p. 264–275.

Weaver, C.S., and Smith, S.W., 1983, Regional tectonic and earthquake hazards implications of a crustal fault zone in southwestern Washington: Journal of Geophysical Research, v. 88, no. B12, p. 10371–10383.

Yelin, T.S., 1982, The Seattle earthquake swarms and Puget basin focal mechanisms and their tectonic implications: Seattle, University of Washington, M.S. thesis, 96 p.

Yelin, T.S., and Crosson, R.S., 1982, A note on the south Puget Sound basin magnitude 4.6 earthquake of 11 March 1978 and its aftershocks: Seismological Society of America Bulletin, v. 72, no. 3, p. 1033–1038.

Zoback, M.L., and Zoback, M.D., 1980, State of stress in the conterminous United States: Journal of Geophysical Research, v. 85, no. 11, p. 6113–6156.

FOCAL-MECHANISM LISTINGS AND PLOTS

All focal mechanisms used in this study are listed and plotted here. The mechanisms were constructed by hand from polarity data reread from the original digital seismograms. An explanation of earthquake focal mechanisms can be found in Fowler (1990). All focal-mechanism plots shown here are lower hemisphere, equal-area stereonet projections. Symbols represent the first motion of vertical-component *P*-wave arrivals. Symbols that intersect at the center, such as Xs and asterisks, represent compression; symbols open in the middle, such as octagons and triangles, represent dilatation for vertical-component *P*-wave arrivals. The strength of first motion is indicated as follows: strong compression is shown as an asterisk, less strong compression as a large X, weaker compression as a smaller asterisk, and weakest compression as a small ×; strong dilatation is shown as an octagon, less strong dilatation as a triangle, weaker dilatation as a small octagon, and weakest dilatation as a small triangle. Corrections have been made for stations known to have been reversed. Takeoff angles at the focal sphere were computed using a local velocity model with a linear increase in velocity with depth, approximating the regional velocity model used for the earthquake locations. This procedure smoothes the distribution of takeoff angles. A small square in the center of any symbol shows that the ray leaves the source at an upgoing angle. The T axis of each mechanism runs through the middle of the compressional quadrant, whereas the P axis is in the middle of the tensional quadrant. The tables and plots are separated into the three regions analyzed in the study. The event numbers are sequential in time. For planes A and B in the focal mechanisms, the azimuth gives the angular distance in degrees measured counterclockwise from north to the dip direction (this means that the azimuth is 90° from the strike of the plane), and the plunge angle gives the dip of the plane in degrees below the horizontal.

Table 19. Shallow Puget Sound region earthquake data.

Event number	Date (year, month, day)	Latitude	Longitude	Depth (kilometers)	Magnitude	P axis		T axis		Plane A		Plane B	
						Azimuth	Plunge	Azimuth	Plunge	Azimuth	Plunge	Azimuth	Plunge
14	820102	47.37	122.39	14.47	2.7	162	4	72	6	207	83	117	89
17	820123	46.61	121.43	3.33	3.2	180	45	90	0	215	60	325	60
26	820303	45.99	122.44	11.78	2.1	30	0	120	0	345	90	75	90
29	820310	46.74	122.20	16.71	2.4	192	4	285	38	322	61	65	67
30	820310	47.33	122.71	26.79	2.9	16	0	106	0	331	90	61	90
38	820404	46.57	122.48	19.53	1.9	182	38	89	4	218	61	322	68
41	820414	47.71	122.52	27.28	3.4	6	8	101	33	138	61	238	73
55	820718	46.58	121.39	6.48	2.9	5	0	95	0	320	90	50	90
58	820926	46.87	121.12	3.25	3.4	192	20	285	8	330	70	237	82
61	821015	47.59	122.63	27.52	3.0	38	18	284	51	89	40	334	71
63	821112	47.69	122.69	24.54	2.8	6	0	96	30	137	69	235	69
67	821211	47.53	122.73	20.22	2.3	5	17	101	18	143	65	233	89
70	821218	47.89	122.53	23.17	2.8	10	5	190	85	100	40	280	50
71	821220	46.59	121.42	5.26	2.7	15	37	108	4	158	61	56	68
72	821231	47.19	122.08	14.27	2.4	26	36	132	21	175	48	76	81
73	830124	47.11	121.99	6.62	3.0	342	15	162	75	72	30	252	60
75	830131	46.67	122.33	17.91	2.2	358	0	88	66	110	50	246	50
78	830303	47.64	121.94	2.35	2.9	346	0	76	0	301	90	31	90
80	830313	46.24	122.69	15.40	2.9	18	0	108	0	333	90	63	90
81	830315	46.52	122.79	24.05	2.7	36	46	127	0	182	59	71	60
84	830407	46.63	122.42	16.07	1.9	20	0	110	0	335	90	65	90
85	830409	46.74	121.82	8.27	1.8	170	7	272	60	289	46	56	58
90	830424	46.54	121.45	4.97	2.7	354	0	84	0	309	90	39	90
92	830504	48.34	122.10	8.68	2.9	2	30	266	10	40	61	137	77
94	830516	47.49	122.58	24.17	2.0	335	67	65	0	134	49	356	49
95	830519	47.64	122.50	23.48	2.0	28	0	118	62	143	51	273	51
97	830521	47.36	121.49	11.69	2.8	163	11	256	14	299	72	30	88
99	830525	47.78	121.71	10.72	3.0	180	16	275	16	317	67	231	90
100	830605	46.54	122.73	23.73	2.3	198	36	291	4	341	62	239	69
102	830726	46.69	122.54	17.35	2.2	199	3	98	75	274	44	123	50
103	830728	46.06	122.81	16.06	2.4	20	0	110	57	139	54	261	54
104	830728	46.07	122.74	15.65	2.3	176	3	79	68	244	46	106	52
106	830819	47.43	122.74	23.12	2.2	214	23	96	47	259	37	150	76
108	830901	47.77	122.72	19.20	2.5	163	0	73	30	212	69	114	69
110	830904	47.89	122.63	22.78	2.6	164	5	344	85	254	40	74	50
111	830914	47.09	121.93	19.02	2.2	161	60	295	22	353	29	220	69
113	830929	47.34	122.72	27.12	2.7	184	2	276	40	312	61	57	65
115	831023	46.56	122.35	17.28	2.5	212	7	111	58	272	47	147	59
119	831216	47.34	122.03	12.91	3.0	214	8	305	10	350	77	80	89
120	840104	47.68	122.58	18.83	2.8	216	13	119	28	261	60	165	80
122	840111	46.91	121.64	5.94	2.2	202	28	105	13	240	61	336	80
124	840219	47.35	122.35	15.83	2.4	160	10	347	80	249	35	71	55
126	840314	47.84	122.36	22.68	2.7	170	4	350	86	260	41	80	49
127	840323	47.75	122.69	19.07	2.9	174	0	84	0	39	90	309	90
131	840427	47.65	122.03	9.77	2.9	147	0	57	13	193	81	101	81
132	840602	47.49	122.71	21.49	3.6	216	4	308	22	350	72	84	78
133	840602	47.50	122.72	22.60	2.8	26	8	290	38	75	58	332	70
135	840619	47.72	122.99	8.78	3.0	0	0	90	0	315	90	45	90
139	840724	47.77	122.45	21.28	2.7	4	7	118	73	111	40	261	54
143	840905	47.92	122.04	17.37	2.2	322	5	212	76	38	42	244	51

Table 19. Shallow Puget Sound region earthquake data—Continued

Event number	Date (year, month, day)	Latitude	Longitude	Depth (kilometers)	Magnitude	P axis		T axis		Plane A		Plane B	
						Azimuth	Plunge	Azimuth	Plunge	Azimuth	Plunge	Azimuth	Plunge
146	840920	47.55	122.34	26.52	2.7	26	4	293	37	76	62	333	68
148	841029	47.85	122.43	18.35	2.0	168	3	264	62	284	49	54	54
151	841120	47.95	121.98	16.64	2.0	310	13	212	30	355	59	258	79
153	841130	47.76	122.24	23.72	2.7	178	28	85	6	218	66	315	75
154	841204	46:55	122.37	19.94	1.7	228	29	137	2	268	68	6	72
156	841220	47.88	122.46	22.65	2.2	5	5	102	54	127	51	246	59
157	850121	46.91	122.02	12.80	2.7	176	3	296	84	272	42	81	48
158	850123	47.77	122.47	18.39	2.6	181	6	295	75	285	41	79	52
159	850123	47.83	122.48	18.44	2.2	177	6	300	79	277	40	79	52
160	850129	47.48	121.83	17.55	2.7	359	3	262	67	67	47	289	52
163	850321	47.64	122.22	7.86	3.0	160	12	257	29	295	60	31	79
164	850330	46.70	122.20	15.98	2.8	148	21	246	21	287	60	197	90
165	850330	46.69	122.20	16.69	2.6	155	0	65	0	20	90	290	90
167	850417	47.70	122.25	23.94	1.9	184	18	297	50	314	40	68	71
169	850426	48.41	122.31	18.21	3.0	182	35	2	55	272	10	92	80
170	850430	48.40	122.32	18.16	2.4	32	0	302	0	257	90	167	90
172	850509	46.57	121.84	9.84	2.7	196	1	14	89	286	44	106	46
176	850616	47.44	121.87	17.03	3.1	314	6	49	37	84	60	187	69
177	850621	46.51	122.37	20.02	1.8	212	40	310	9	359	56	255	70
178	850706	47.77	122.27	17.97	3.1	157	13	54	44	206	49	98	70
182	850914	47.43	122.38	19.85	3.0	334	15	240	14	17	69	107	89
183	851006	47.93	122.90	19.96	2.8	322	0	52	70	71	48	213	48
184	851014	46.37	122.68	20.16	1.5	32	12	134	44	162	50	270	70
185	851017	47.46	123.00	15.87	2.6	178	0	268	67	289	49	67	49
186	851106	46.89	121.99	7.61	2.3	3	12	248	64	66	39	292	61
191	851227	46.97	121.94	7.02	3.0	346	3	255	19	32	74	299	79

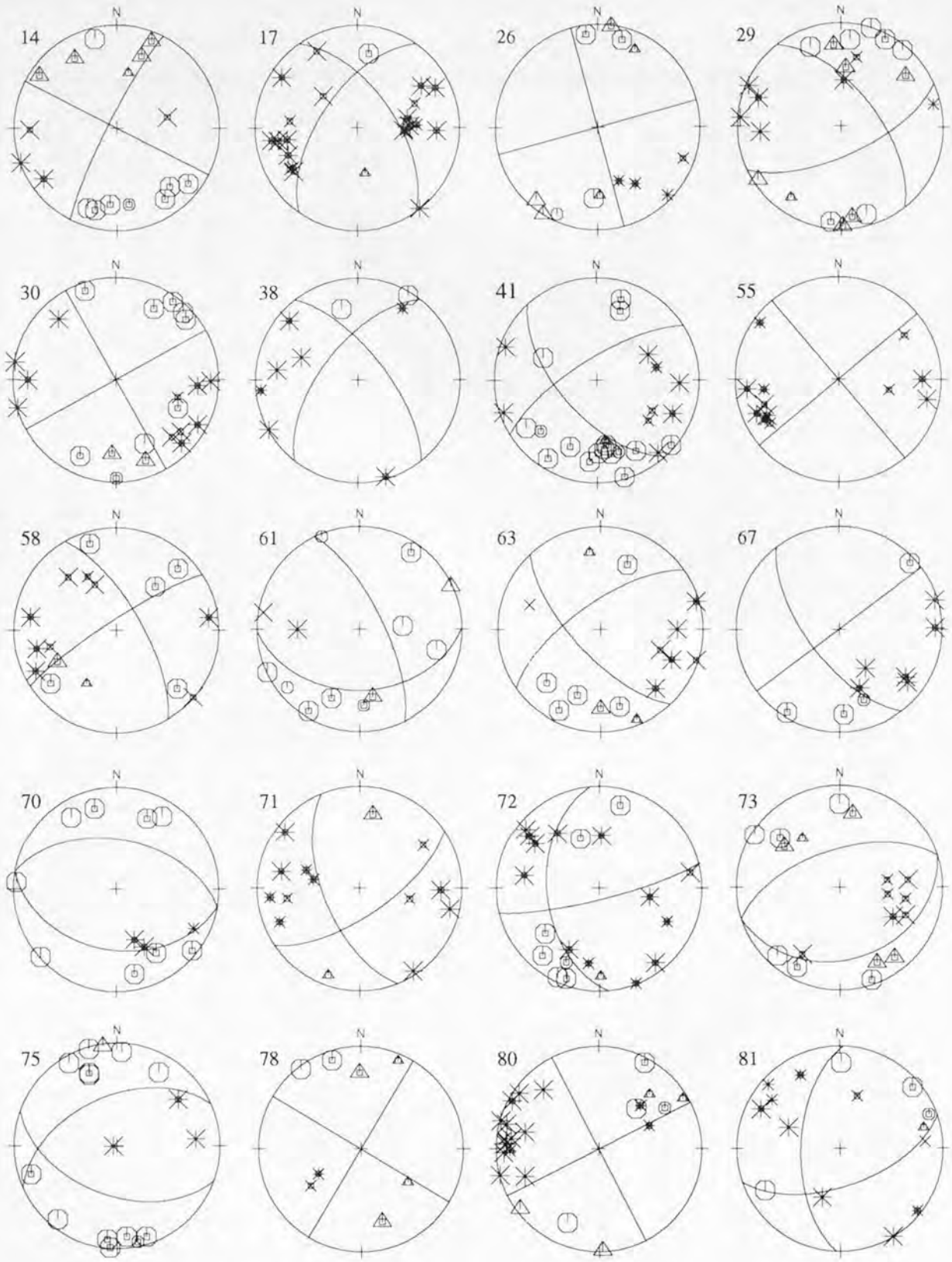

Figure 135 (above and next three pages). Lower hemisphere, equal-area projections of shallow Puget Sound earthquake focal mechanisms.

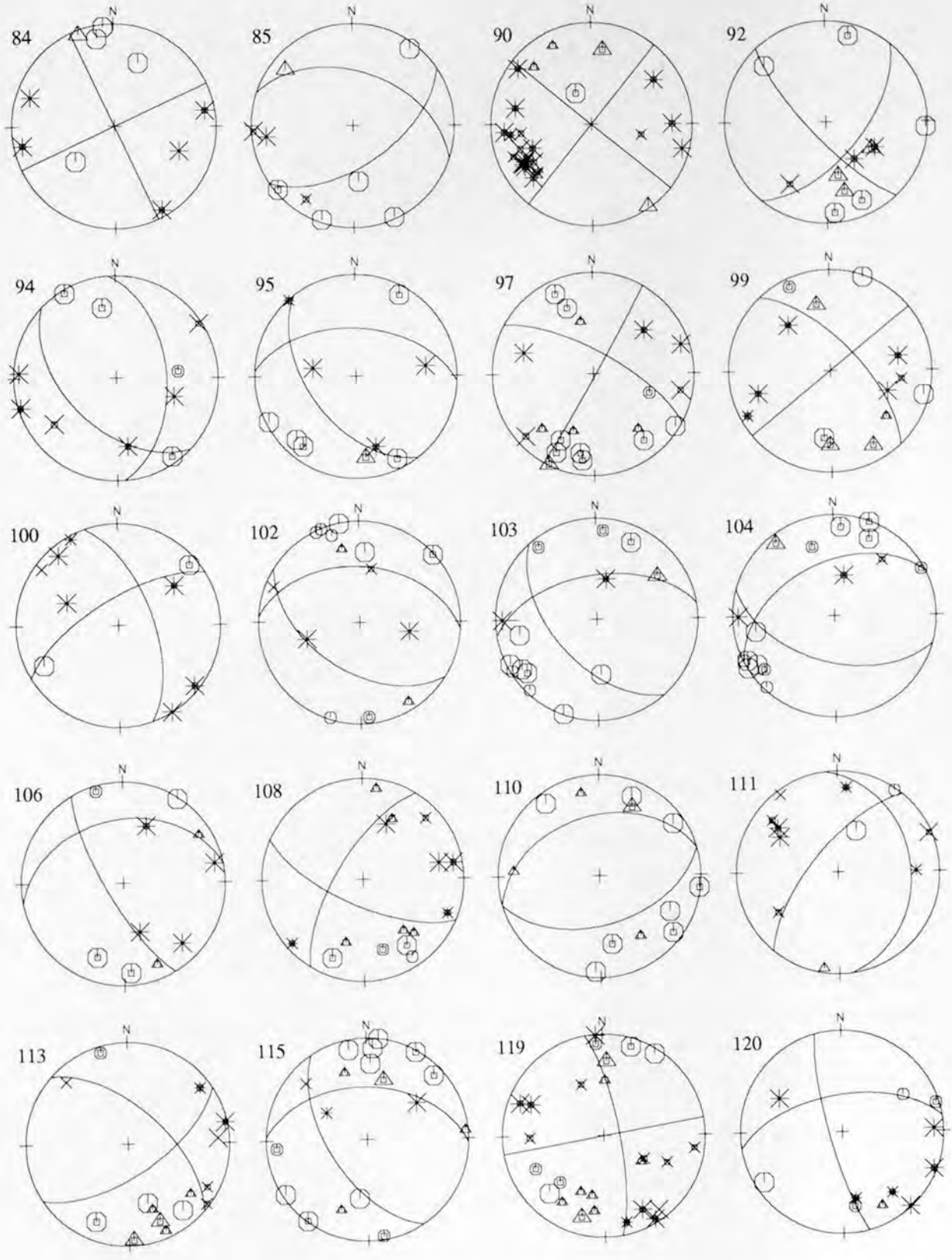

Figure 135. Lower hemisphere, equal-area projections of shallow Puget Sound earthquake focal mechanisms—Continued

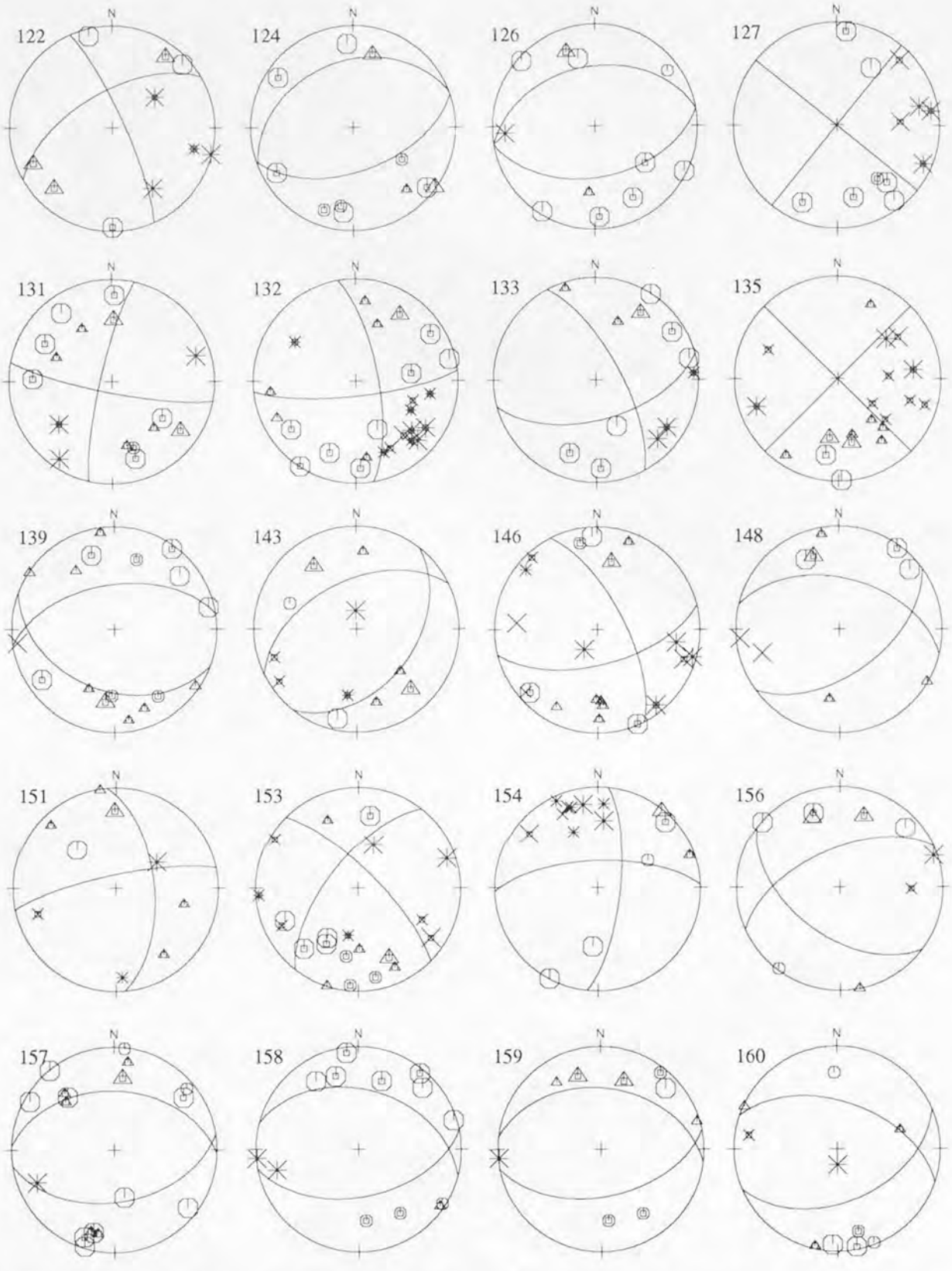

Figure 135. Lower hemisphere, equal-area projections of shallow Puget Sound earthquake focal mechanisms—Continued

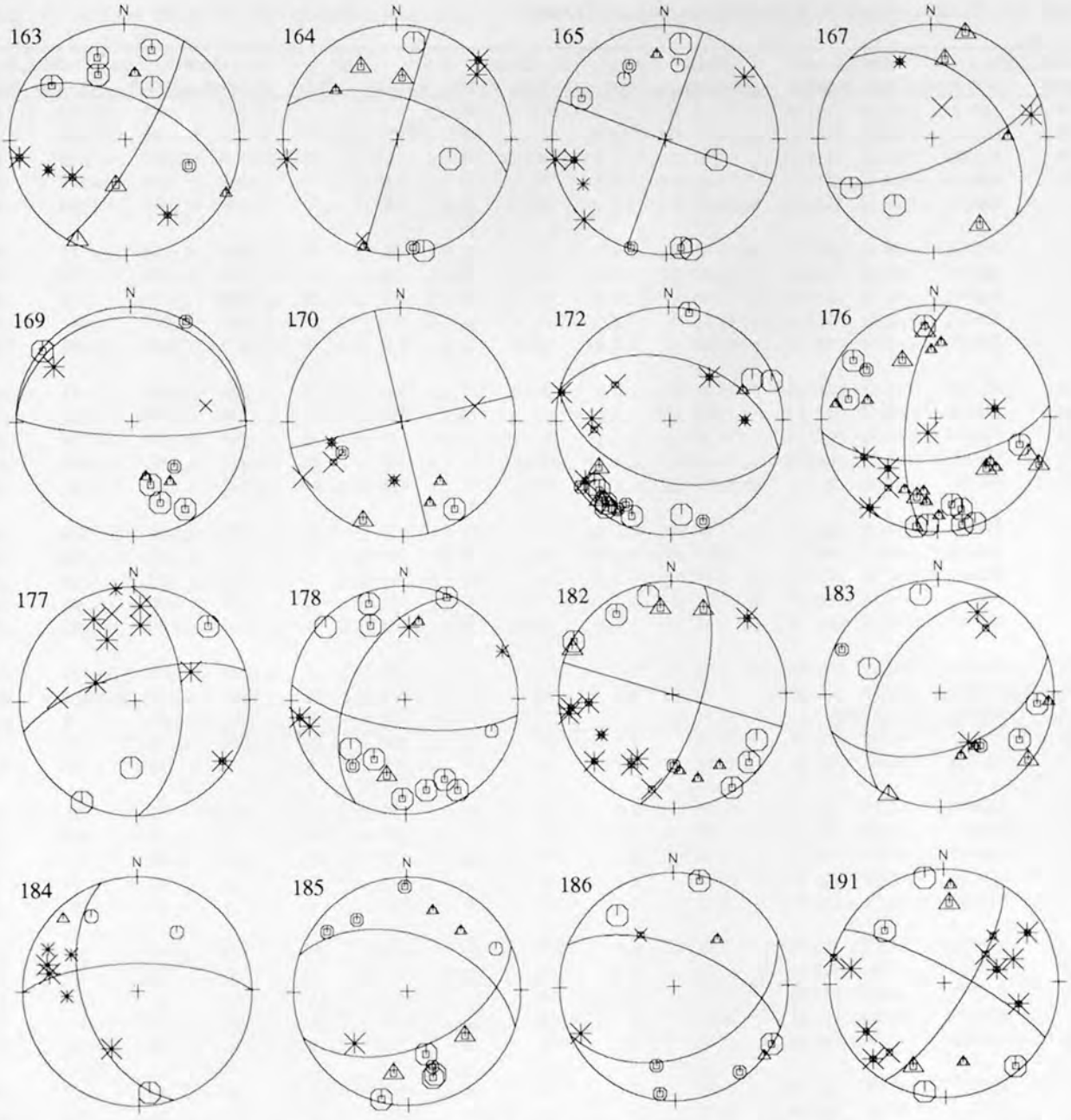

Figure 135. Lower hemisphere, equal-area projections of shallow Puget Sound earthquake focal mechanisms—Continued

Table 20. Shallow Mount St. Helens region earthquake data.

Event number	Date (year, month, day)	Latitude	Longitude	Depth (kilometers)	Magnitude	P axis		T axis		Plane A		Plane B	
						Azimuth	Plunge	Azimuth	Plunge	Azimuth	Plunge	Azimuth	Plunge
16	820123	46.39	122.28	9.45	2.9	40	0	130	0	355	90	85	90
18	820127	46.42	122.26	8.09	2.1	43	16	155	53	170	41	288	68
19	820208	46.52	122.28	4.02	2.3	246	4	342	57	6	50	129	57
20	820217	46.41	122.32	10.61	1.7	34	0	124	0	349	90	79	90
21	820301	46.40	122.30	10.97	2.7	35	34	151	33	184	38	94	90
22	820301	46.42	122.30	11.33	1.8	212	19	108	35	255	50	157	80
23	820301	46.40	122.30	11.48	1.0	44	4	136	22	178	72	272	78
24	820302	46.39	122.30	11.40	2.0	40	20	143	33	178	51	274	82
25	820302	46.41	122.29	11.61	1.8	213	3	307	50	337	55	91	60
27	820303	46.39	122.30	11.13	1.5	20	4	110	4	155	84	65	90
28	820306	46.38	122.28	11.24	2.6	28	28	134	27	171	49	81	89
32	820316	46.41	122.33	12.65	1.7	24	4	291	34	73	64	333	70
33	820316	46.40	122.27	11.22	2.1	33	0	123	0	348	90	78	90
34	820320	46.39	122.33	11.60	2.4	208	21	306	20	347	60	257	89
35	820326	46.40	122.31	11.61	1.9	47	35	166	34	197	36	108	90
36	820401	46.38	122.25	11.94	2.2	38	12	135	30	173	60	270	78
37	820402	46.27	122.29	10.90	1.2	56	6	147	7	191	81	282	89
39	820410	46.38	122.31	8.88	2.2	240	40	144	8	274	57	18	69
40	820412	46.38	122.28	12.01	2.0	35	0	125	0	350	90	80	90
42	820417	46.37	122.25	9.14	1.7	45	0	135	0	0	90	90	90
43	820426	46.43	122.26	9.69	2.7	201	14	299	29	336	59	73	80
44	820521	46.41	122.07	2.92	1.5	75	75	255	15	345	30	165	60
45	820526	46.41	122.31	11.94	1.8	35	0	125	0	350	90	0	90
46	820527	46.36	122.26	7.52	1.7	34	0	124	0	349	90	79	90
47	820528	46.40	122.32	11.56	1.7	45	0	135	0	0	90	90	90
48	820531	46.39	122.32	12.04	3.0	42	20	139	19	181	62	91	90
49	820531	46.40	122.28	11.76	1.8	27	32	139	31	173	42	83	90
50	820605	46.43	122.29	10.44	1.5	298	65	116	25	204	20	27	70
51	820606	46.41	122.25	10.86	1.0	45	0	135	0	0	90	90	90
52	820606	46.38	122.25	5.45	1.4	45	0	135	0	0	90	90	90
53	820704	46.35	122.30	9.26	1.2	212	33	328	34	359	39	90	89
54	820712	46.30	122.30	11.45	1.1	45	0	135	0	0	90	90	90
56	820724	46.31	122.26	9.25	1.2	18	14	284	14	61	70	156	90
57	820819	46.40	122.25	9.68	2.3	38	20	136	20	177	61	267	90
59	821008	46.28	122.08	0.77	2.2	168	75	348	15	78	30	258	60
60	821009	46.39	122.31	8.91	1.7	58	26	312	29	96	49	5	88
64	821113	46.39	122.29	10.97	1.8	62	47	318	12	87	48	198	69
65	821116	46.31	122.30	10.58	1.9	38	0	128	0	353	90	83	90
66	821128	46.34	122.28	11.93	2.6	13	23	126	43	150	41	254	78
68	821212	46.38	122.30	14.80	2.2	26	5	116	4	161	84	71	89
69	821212	46.28	122.50	15.85	1.9	8	13	98	0	144	81	52	81
74	830129	46.36	122.34	11.50	1.3	154	5	248	36	285	61	26	69
77	830208	46.44	122.33	9.25	1.2	40	13	133	12	177	72	86	89
79	830309	46.40	122.29	11.36	1.1	200	35	299	12	345	56	245	75
82	830318	46.41	122.24	7.65	1.5	40	12	132	11	176	74	86	89
83	830320	46.12	122.13	9.12	2.0	207	5	299	22	341	71	75	78
86	830412	46.41	122.33	10.31	1.5	18	25	120	25	160	51	256	82
87	830412	46.39	122.31	8.61	2.0	32	30	123	1	171	68	73	70
88	830420	46.41	122.32	9.48	2.3	218	16	124	15	261	68	351	89
89	830420	46.41	122.33	9.27	2.3	38	10	130	11	174	75	264	89

Table 20. Shallow Mount St. Helens earthquake data—Continued

Event number	Date (year, month, day)	Latitude	Longitude	Depth (kilometers)	Magnitude	P axis		T axis		Plane A		Plane B	
						Azimuth	Plunge	Azimuth	Plunge	Azimuth	Plunge	Azimuth	Plunge
93	830506	46.41	122.23	7.41	2.3	38	0	128	0	353	90	83	90
96	830519	46.39	122.30	8.98	1.5	40	18	136	18	178	64	268	90
98	830521	46.38	122.37	9.32	1.9	180	18	87	10	222	70	314	84
109	830902	46.33	122.53	15.94	1.0	49	45	306	13	76	49	185	70
112	830915	46.53	122.45	15.31	2.3	16	6	110	36	147	61	249	70
114	831002	46.46	122.33	9.20	2.2	38	0	128	28	169	71	267	71
117	831101	46.34	122.29	9.95	2.0	155	32	259	21	300	51	205	83
118	831213	46.37	122.26	9.42	1.8	238	15	332	16	15	68	105	89
123	840111	46.41	122.28	6.52	1.7	27	0	117	0	342	90	72	90
129	840404	46.43	122.32	9.21	2.4	24	10	135	64	141	41	274	59
138	840716	46.49	122.30	15.25	2.8	210	6	303	25	344	68	79	77
140	840805	46.52	122.32	11.26	3.1	22	20	290	6	64	71	157	80
144	840908	46.29	122.28	7.00	1.4	210	22	117	8	251	69	345	81
145	840915	46.50	122.40	13.36	1.1	26	12	119	12	162	73	72	90
147	841016	46.43	122.31	10.58	1.2	0	25	180	65	90	20	270	70
149	841103	46.41	122.32	11.24	1.9	0	25	180	65	90	20	270	70
150	841103	46.41	122.31	11.57	1.1	12	38	106	5	156	60	53	68
166	850414	46.40	122.25	8.03	2.1	25	8	291	26	71	66	335	78
171	850430	46.41	122.30	10.95	2.0	37	27	143	29	180	49	271	89
174	850523	46.21	122.21	0.72	2.5	190	0	10	90	100	45	280	45
179	850801	46.26	122.52	16.91	1.4	13	7	277	40	63	57	318	68
181	850905	46.33	122.23	7.16	2.5	9	11	101	11	145	74	55	90
188	851117	46.43	122.33	11.06	2.9	45	0	135	0	0	90	90	90

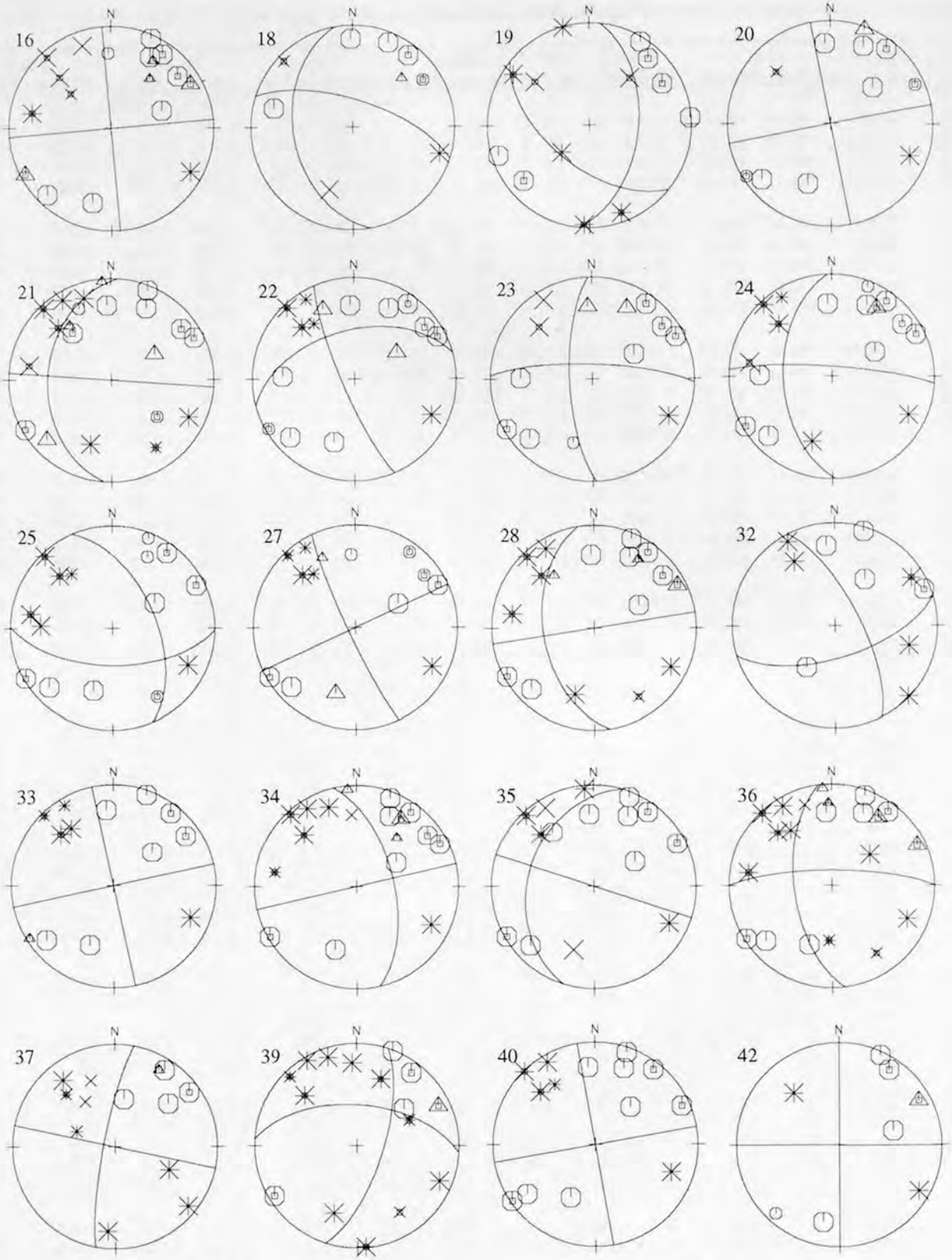

Figure 136 (above and next three pages). Lower hemisphere, equal-area projections of shallow Mount St. Helens region earthquake focal mechanisms.

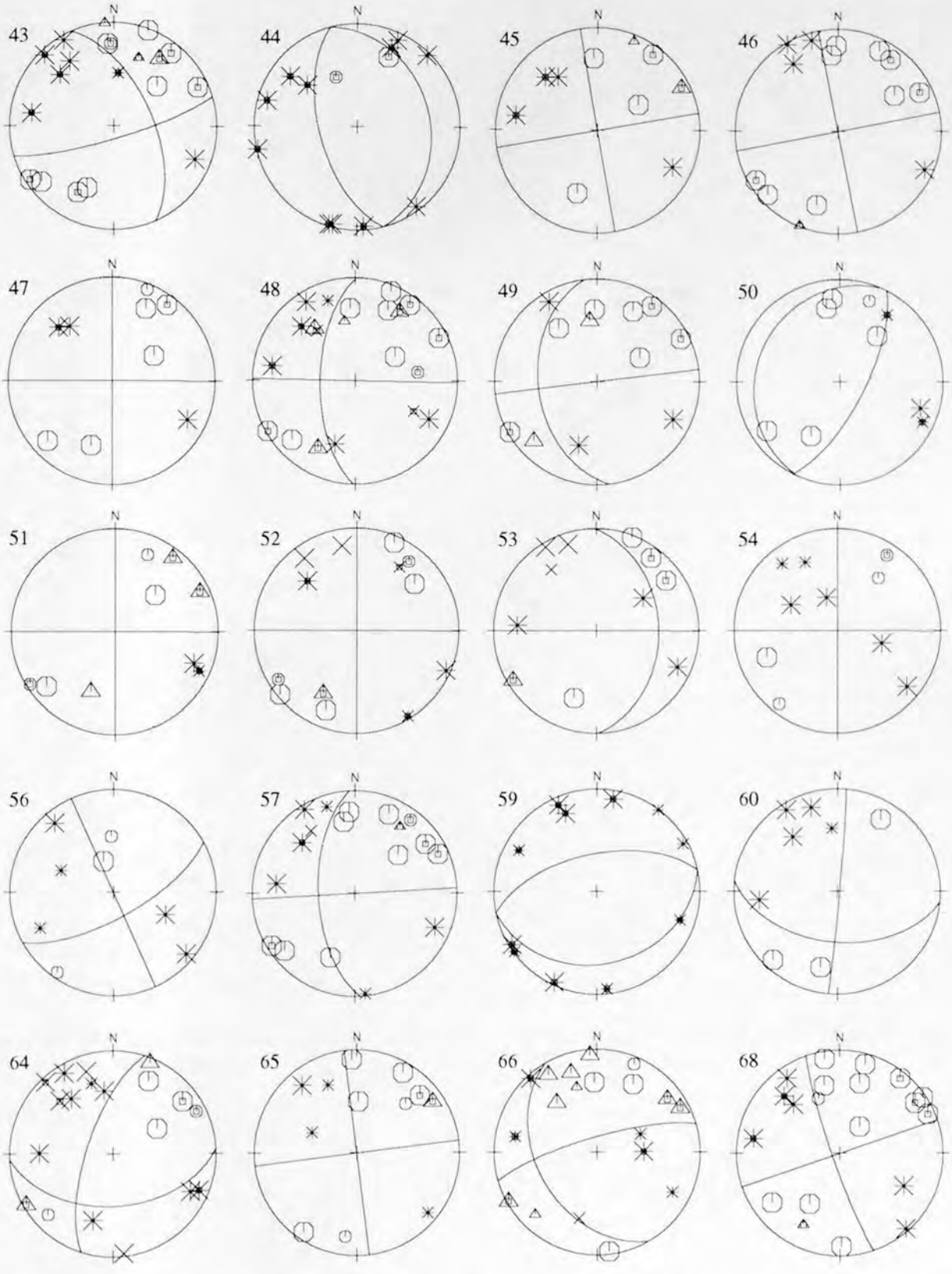

Figure 136. Lower hemisphere, equal-area projections of shallow Mount St. Helens region earthquake focal mechanisms—Continued

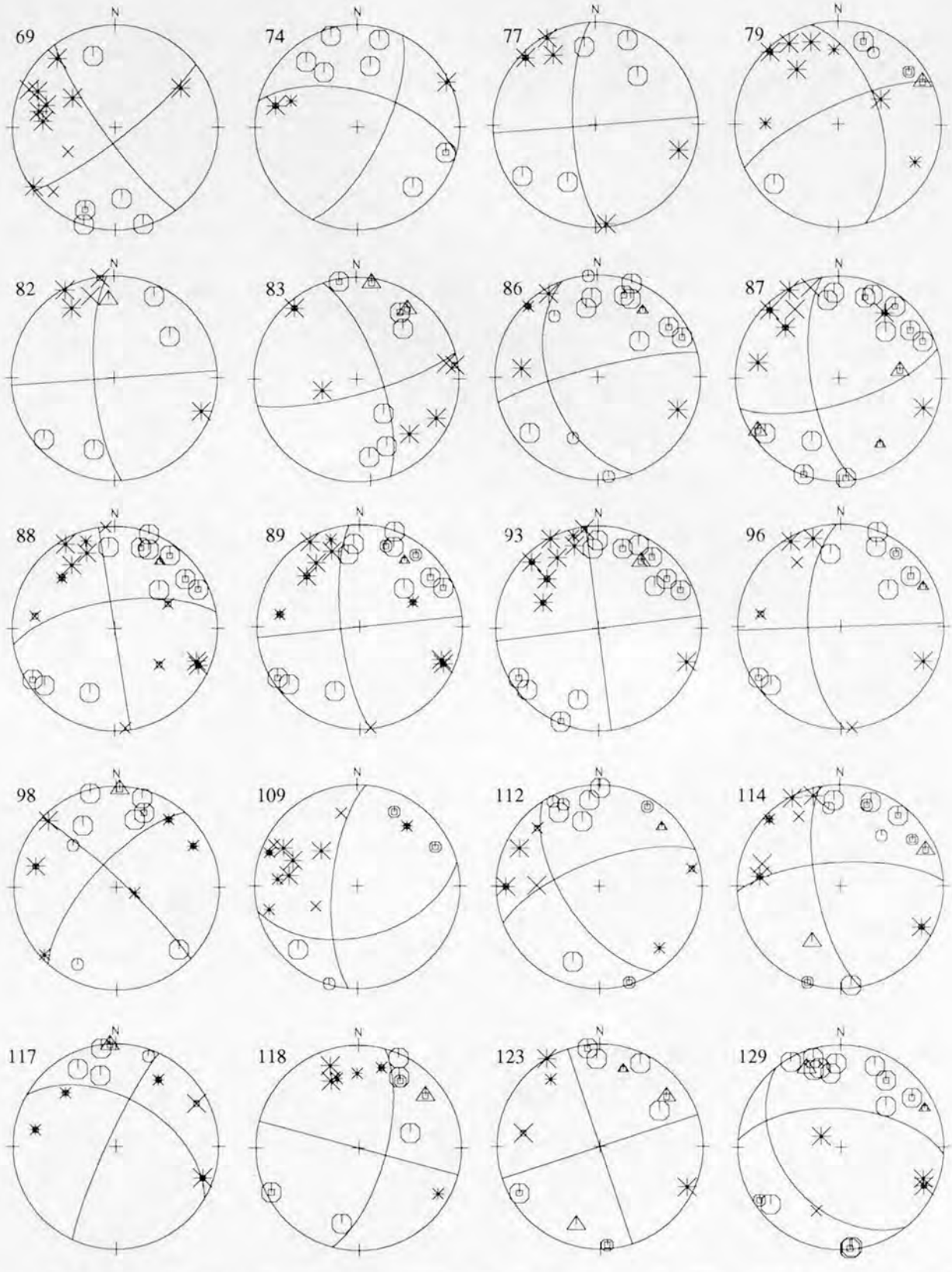

Figure 136. Lower hemisphere, equal-area projections of shallow Mount St. Helens region earthquake focal mechanisms—Continued

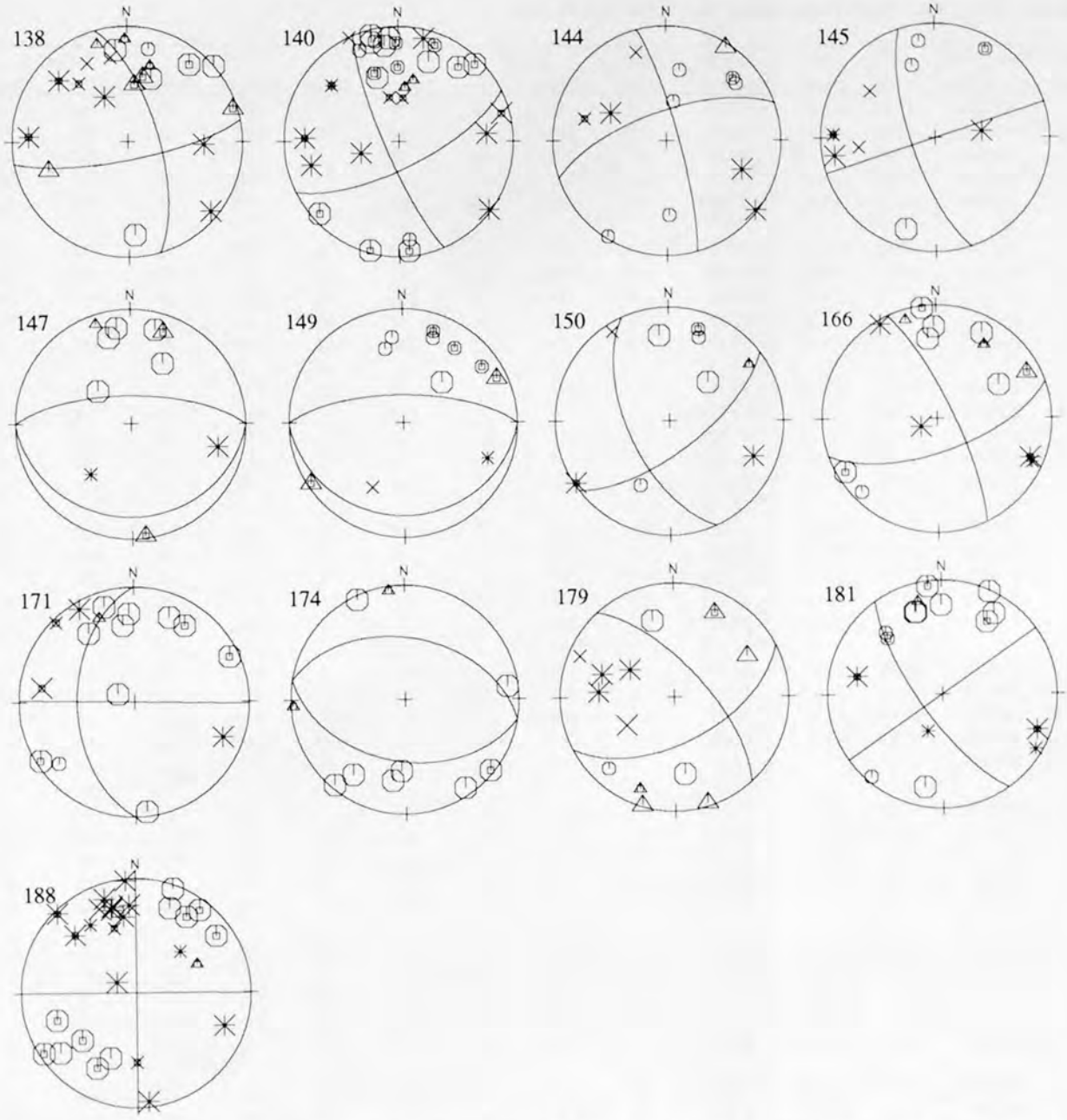

Figure 136. Lower hemisphere, equal-area projections of shallow Mount St. Helens region earthquake focal mechanisms—Continued

Table 21. Subcrustal (slab) Puget Sound region earthquake data.

Event number	Date (year, month, day)	Latitude	Longitude	Depth (kilometers)	Magnitude	P axis		T axis		Plane A		Plane B	
						Azimuth	Plunge	Azimuth	Plunge	Azimuth	Plunge	Azimuth	Plunge
1	800204	47.39	121.65	96.35	2.4	55	85	236	5	326	40	146	50
2	800416	48.19	122.90	50.10	3.8	258	6	164	36	307	61	205	70
3	800608	47.97	123.10	48.54	4.2	272	84	15	1	99	44	291	47
4	800816	47.39	123.26	43.11	2.3	228	55	111	17	238	38	358	68
5	800906	47.54	123.42	46.16	2.8	173	68	62	8	175	41	315	56
6	801106	47.91	123.17	45.56	2.9	201	34	106	8	238	61	338	73
7	801130	47.35	123.34	43.81	2.6	130	20	32	20	171	61	81	90
8	810111	47.39	123.47	40.58	1.8	90	7	209	76	194	39	349	53
9	810704	47.86	122.73	52.11	2.8	303	31	47	22	88	51	353	84
10	810705	47.56	123.68	39.13	2.0	55	27	216	62	164	19	318	72
11	810722	47.96	123.43	44.18	2.3	227	64	89	20	205	29	346	67
12	810804	47.69	123.13	43.85	1.9	0	71	123	11	194	37	46	57
13	810821	47.62	123.67	40.52	2.8	180	85	0	5	90	40	270	50
15	820114	48.10	122.81	55.95	2.7	254	65	74	25	164	20	344	70
31	820313	47.06	122.17	72.53	1.9	266	45	86	45	356	90	176	90
62	821101	47.55	123.38	45.61	2.5	197	74	40	15	139	31	305	60
76	830205	46.67	123.04	52.22	2.2	158	65	43	11	159	39	295	60
91	830425	47.28	123.56	38.31	1.9	99	31	7	4	138	66	237	71
101	830708	47.76	123.02	47.12	2.4	144	55	281	27	332	25	208	75
105	830802	47.66	122.87	48.48	2.3	254	85	74	5	164	40	344	50
107	830828	48.00	122.87	51.50	3.9	75	16	345	0	119	79	211	79
116	831031	47.35	123.29	43.36	4.3	316	75	134	15	223	30	44	60
121	840105	47.44	122.28	38.77	1.9	108	4	287	86	198	41	18	49
125	840223	47.65	123.04	46.32	2.2	117	48	16	10	143	50	255	66
128	840328	47.33	123.13	42.89	1.9	136	50	249	18	299	40	185	71
130	840408	46.80	122.49	67.03	3.3	286	20	44	53	55	36	173	71
134	840604	46.29	123.04	52.60	3.7	184	31	88	10	221	61	319	76
136	840621	48.30	122.97	46.47	2.0	132	7	225	21	266	70	0	80
137	840708	47.57	122.81	46.69	2.2	307	35	128	55	35	10	217	80
141	840812	47.73	123.02	46.32	2.2	112	0	22	43	166	61	58	61
142	840902	48.75	123.20	57.01	2.6	317	12	137	78	47	33	227	57
152	841121	46.98	123.69	35.67	2.8	211	36	326	30	1	40	267	86
155	841217	47.31	122.91	46.30	3.2	236	29	131	25	272	50	4	88
161	850306	48.90	122.82	66.48	1.8	41	21	145	32	179	51	275	83
162	850318	47.37	122.64	53.30	3.5	276	34	20	20	63	50	326	81
168	850426	47.31	122.48	57.83	2.5	271	12	170	42	320	52	214	71
173	850521	47.66	123.22	47.22	2.8	113	22	213	24	253	56	344	89
175	850523	47.67	123.31	47.04	2.0	33	6	125	21	167	71	261	80
180	850822	47.67	122.91	50.27	1.8	244	25	62	65	336	20	153	70
187	851115	47.51	123.59	42.13	2.7	270	76	90	14	180	31	0	59
189	851202	49.06	123.58	59.40	2.3	173	62	60	12	179	40	310	61
190	851204	48.86	122.87	59.14	2.2	240	60	22	24	81	25	305	71

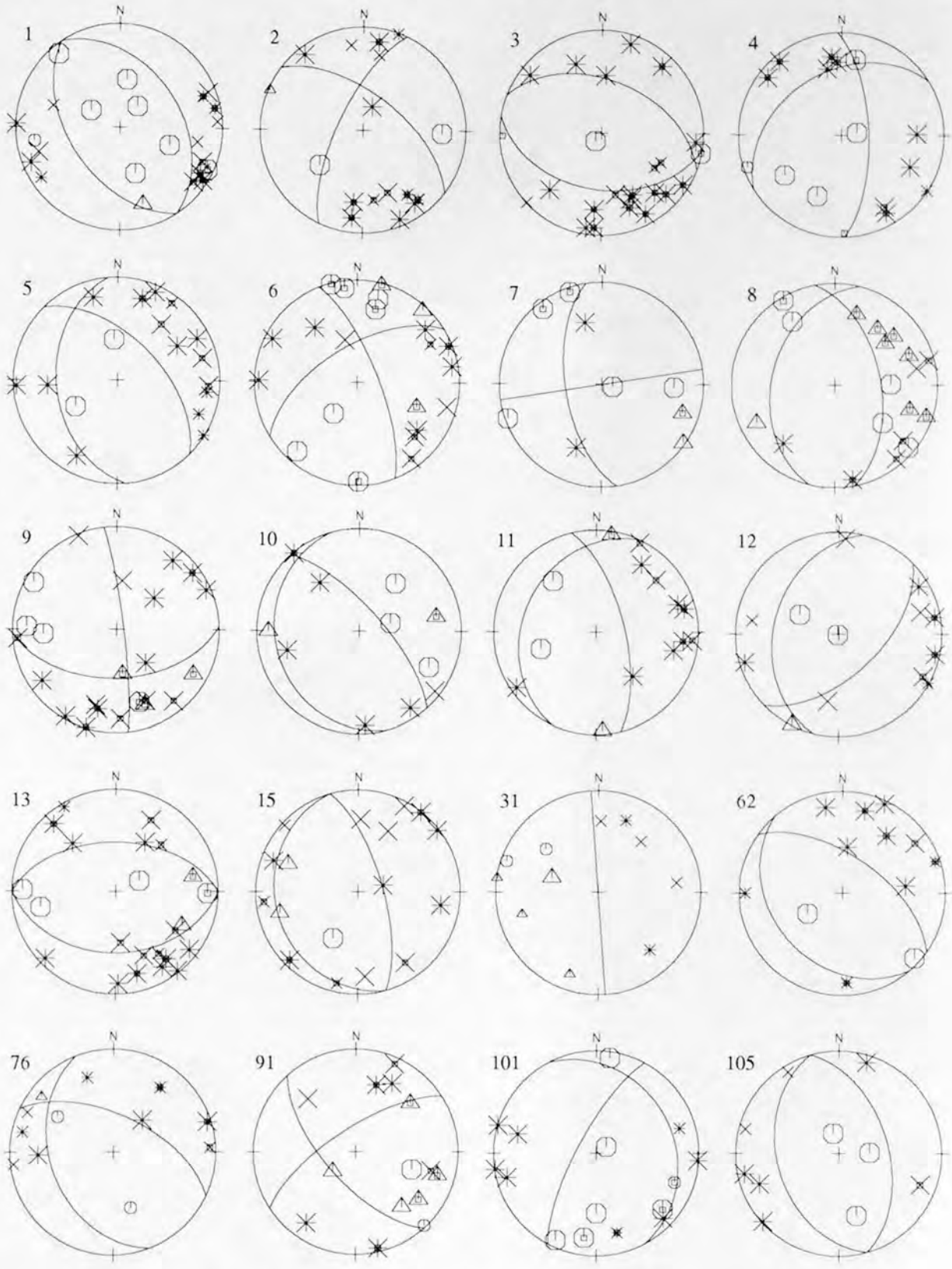

Figure 137 (above and next two pages). Lower hemisphere, equal-area projections of subcrustal (slab) Puget Sound earthquake focal mechanisms.

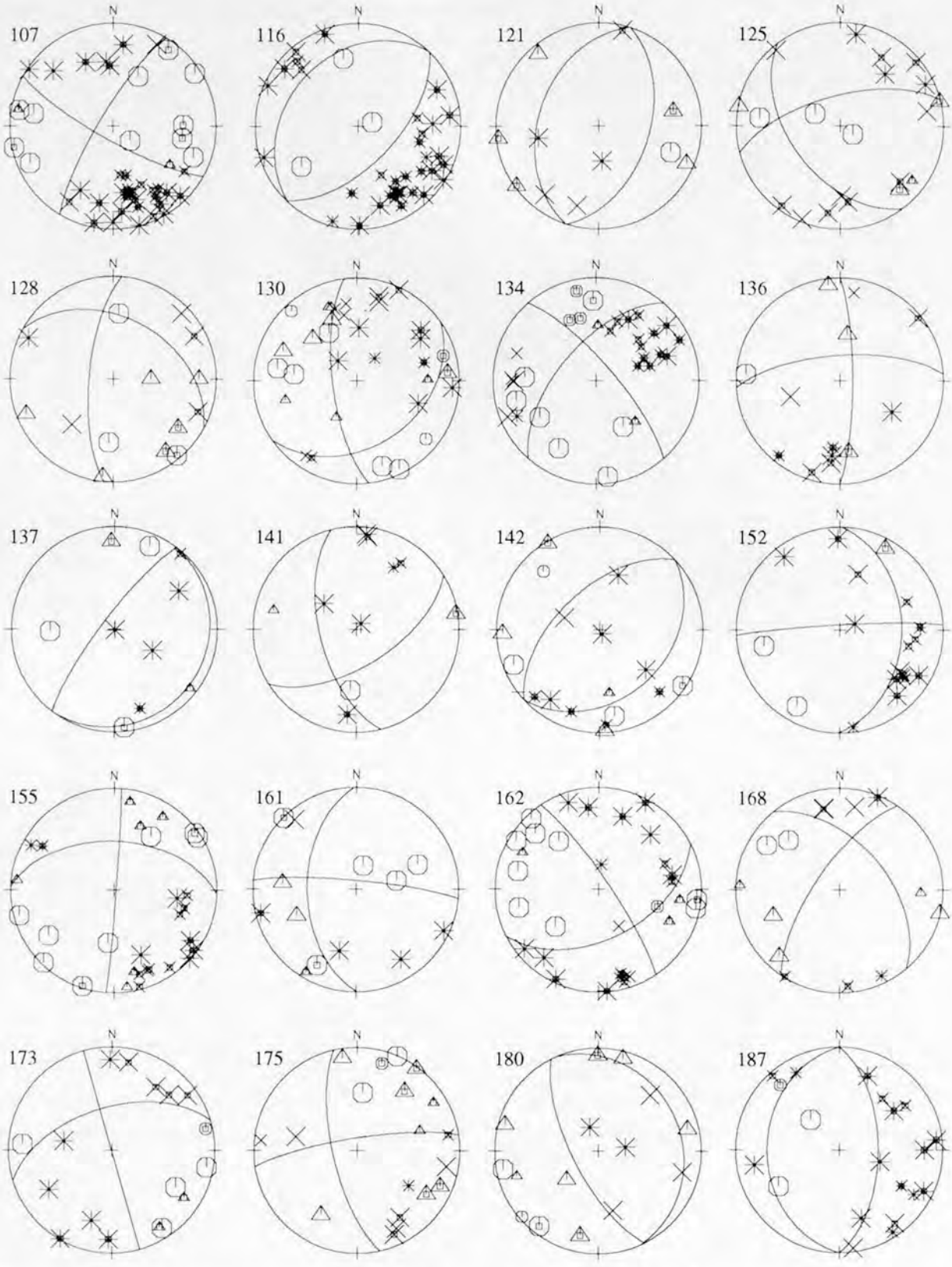

Figure 137. Lower hemisphere, equal-area projections of subcrustal (slab) Puget Sound earthquake focal mechanisms—Continued

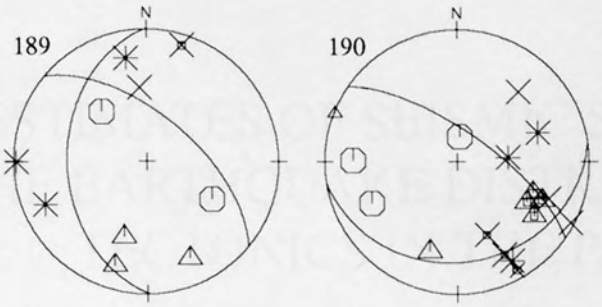

Figure 137. Lower hemisphere, equal-area projections of subcrustal (slab) Puget Sound earthquake focal mechanisms—Continued

ESTIMATES OF SEISMIC SOURCE REGIONS FROM THE EARTHQUAKE DISTRIBUTION AND REGIONAL TECTONICS IN THE PACIFIC NORTHWEST

By Craig S. Weaver[1] *and* Kaye M. Shedlock[2]

ABSTRACT

The tectonic and geologic setting of the Pacific Northwest is that of an active subduction zone. West of the Cascade Range, there are three distinct earthquake source regions: (1) at the interface between the Juan de Fuca and North America plates; (2) within the subducting Juan de Fuca and Gorda plates; and (3) within the crust of the overlying North America plate. East of the Cascade Range, earthquakes occur only in the North America plate. The record of historical seismicity in the region indicates few earthquakes of magnitude 7 or greater; all of these events are thought to have been within the subducting part of the Juan de Fuca or Gorda plates, within the crust of the North America plate, or off northern California in the flat-lying section of the Gorda plate. This limited historical record is used for nearly all estimates of the earthquake hazards in the region. Unfortunately, the distribution of seismicity determined using the modern seismic network is not in accord with the location of many of the largest historical earthquakes.

The best understood earthquake source zone is within the subducting Juan de Fuca and Gorda plates. Most of the historically damaging earthquakes of the Pacific Northwest have been in this zone, and data from these events has served as the cornerstone for earthquake-hazards assessments in the Puget Sound region. Generally, this type of event is thought to be caused by gravitational forces within the subducting plate where the dip increases from about 10° to more than 25°. Interpretation of the currently available data, including earthquake hypocenters and geophysical imaging of the subducting plates, indicates that these earthquakes should be expected along the strike of the entire subduction zone. Because of the known plate geometry, most of these events are expected to be at depths of 45–60 km and to have magnitudes as least as large as those already experienced in the region (magnitude 7+). The rate of occurrence of these earthquakes is unknown but, in Oregon and Washington, six events since 1870 had estimated magnitudes of 6 or greater.

With the exception of the Mendocino triple junction area, no earthquakes recorded by modern seismic networks have been located on the interface between the Juan de Fuca and North America plates, and in the history of European settlement in the Pacific Northwest, no known large event can be associated with most of the interface. However, the late Holocene geologic record of subsidence in coastal intertidal marshes provides evidence consistent with the occurrence of great subduction-related earthquakes. The available geologic record suggests that the return period for these events is irregular, varying from 100 years to longer than 1,200 years; the length of the coast interpreted to have subsided during a particular event is sufficient to have generated earthquakes of magnitude 8 or greater. Some studies have suggested that the entire coast from northern California to central British Columbia could slip in a single earthquake of magnitude 9 or greater. Even though there are many unknown details concerning intraplate earthquakes, the general understanding of large-scale plate-tectonic processes allows a reliable estimation of the potential source zone for subduction earthquakes. The source zone for these events is very great, including the entire coast from the deformation front offshore to about the coastline.

The source zone for crustal earthquakes is very poorly known. The historical record includes events greater than magnitude 7 in central Vancouver Island, the North Cascades of Washington, and offshore northern California. Geologic mapping has found evidence of surface displacements that are consistent with those expected to accompany a magnitude 7 or greater earthquake in the shallow crust of the central Puget Sound basin. Until the tectonic causes of these earthquakes are better understood, it is not possible to reliably determine the source zones for these crustal events.

[1]U.S. Geological Survey, Geophysics Program AK–50, University of Washington, Seattle, WA 98195.

[2]U.S. Geological Survey, Box 25046, MS 966, Federal Center, Denver, CO 80225.

INTRODUCTION

The first step in assessing earthquake hazards and risks within a region requires that the nature and distribution of earthquake sources be understood. During the past 10 years, considerable study in the Pacific Northwest has been focused on determining the distribution of earthquake sources and on placing these sources within the regional tectonic setting. Two examples illustrate how successful these studies have been in changing the assessment of earthquake hazards in the Pacific Northwest. First, in 1975, Hopper and others (1975) suggested that the Juan de Fuca plate might be attached to the North America plate (fig. 138), thereby making it unlikely that great thrust earthquakes (magnitude 8 or larger) would occur on the interface between the two plates. At present, most earth scientists routinely accept convergence between the two plates and, as a consequence, most further accept the interpretation that subduction-zone earthquakes on this plate interface will be at least magnitude 8.0 (for example, Heaton, 1990); some scientists even argue for earthquakes greater than magnitude 9.0 (Heaton and Hartzell, 1987). The most compelling evidence that has caused this change in earthquake-hazards assessments is found in the intertidal marshes along the coast. At some sites in Willapa Bay on the Washington coast, at least eight discrete episodes of subsidence of the intertidal marsh surface are recorded in the geologic section of the last 4,000 years (Grant and others, 1989). Each episode of subsidence is thought to have been the result of a subduction-zone earthquake (Atwater, 1987); thus, subduction-zone earthquakes appear frequently in the geologic record (see Atwater, this volume; and Rogers and others, this volume, for more discussion).

As a second example of how source studies have changed earthquake-hazard assessments, Perkins and others (1980) issued a revised estimate of the maximum horizontal ground acceleration for Oregon and Washington in which the maximum expected earthquake magnitude was estimated for subregions of the two states. In the southern Washington Cascade Range near Mount St. Helens, the estimate used for the maximum expected magnitude was 5.1. By 1985, the St. Helens seismic zone had been identified, and several studies had concluded that a maximum-magnitude event of 6.8 should be adopted for engineering-design purposes in the region of this zone. Both of these changes in the assessment of earthquake hazards relied heavily on understanding the regional tectonic framework, with the second example nearly completely dependent on seismicity studies.

Because of the subduction-zone regime, there are three distinct sources of earthquakes in the Pacific Northwest: (1) crustal earthquakes that occur within the overriding North America plate, (2) intraplate earthquakes that occur within the subducting Juan de Fuca and Gorda plates, and (3) interplate earthquakes that are expected to occur at the interface between the Juan de Fuca (and Gorda) plate and the North America plate (subduction, or thrust, events). West of the Cascade Range, the distribution of earthquake source types reflects a combination of the geometry of the subducting Juan de Fuca and Gorda plates, crustal structure within the overriding North America plate, and tectonic interactions among the North America, Pacific, and Juan de Fuca plates. East of the Cascade Range, it is likely that the earthquake distribution reflects the tectonics and structure of only the North America plate.

Of the three source types, crustal earthquakes in the North America plate and events within the subducting plate (we refer to the latter as intraplate events, or Benioff-zone earthquakes) have been the basis of earthquake-hazard assessments for the Pacific Northwest (for example, Algermissen, 1988). In Washington and Oregon, where the historical record is thought to be complete since the 1870's at magnitude 6 and greater (Ludwin and others, 1991), there were two earthquakes that certainly occurred in the crust and six earthquakes that are either considered or known to have occurred within the subducting plate. One of the anomalies of the Cascadia subduction zone is that, with the exception of the Mendocino triple junction (where the North America, Pacific, and Gorda plates meet) (Oppenheimer and others, 1993), there are no large historical earthquakes that are thought to have had their source on the plate interface. In most subduction zones, it is this interface that produces the great (magnitude 8+) thrust events, like the earthquake that struck the Prince William Sound area of southern Alaska in 1964. Recently, efforts have been made to incorporate at least the possibility of great thrust-zone earthquakes in the Pacific Northwest into a regional hazards analysis (Algermissen, 1988).

This chapter focuses on the extent of the three earthquake source regions of the Cascadia subduction zone. In defining the source regions, we have relied on recent compilations of earthquake catalogs for Oregon and Washington, studies of regional seismotectonics, investigations of coastal-marsh stratigraphy and determinations of the depth and dip of the Juan de Fuca and Gorda plates beneath the North America plate. It is clear that intraplate earthquakes, the most frequently observed large-magnitude (6+) events in the historical record of Oregon and Washington, are understood well enough that the source region expected to produce such events in the future can be specified with great confidence. Despite uncertainty surrounding the details of how and when great subduction-zone thrust events may occur on the interface, there is clearly a growing acceptance of the past occurrence of these events. As the general forces that produce these earthquakes are understood from comparative studies with other subduction zones, the potential source regions can be defined fairly accurately. Finally, because the causes of large-magnitude historical crustal earthquakes remain obscure, the parts of Washington and Oregon that may be subject to their effects remain uncertain. As noted elsewhere (Rogers and others, this volume; Shedlock and Weaver, 1989), reducing the uncertainty surrounding the

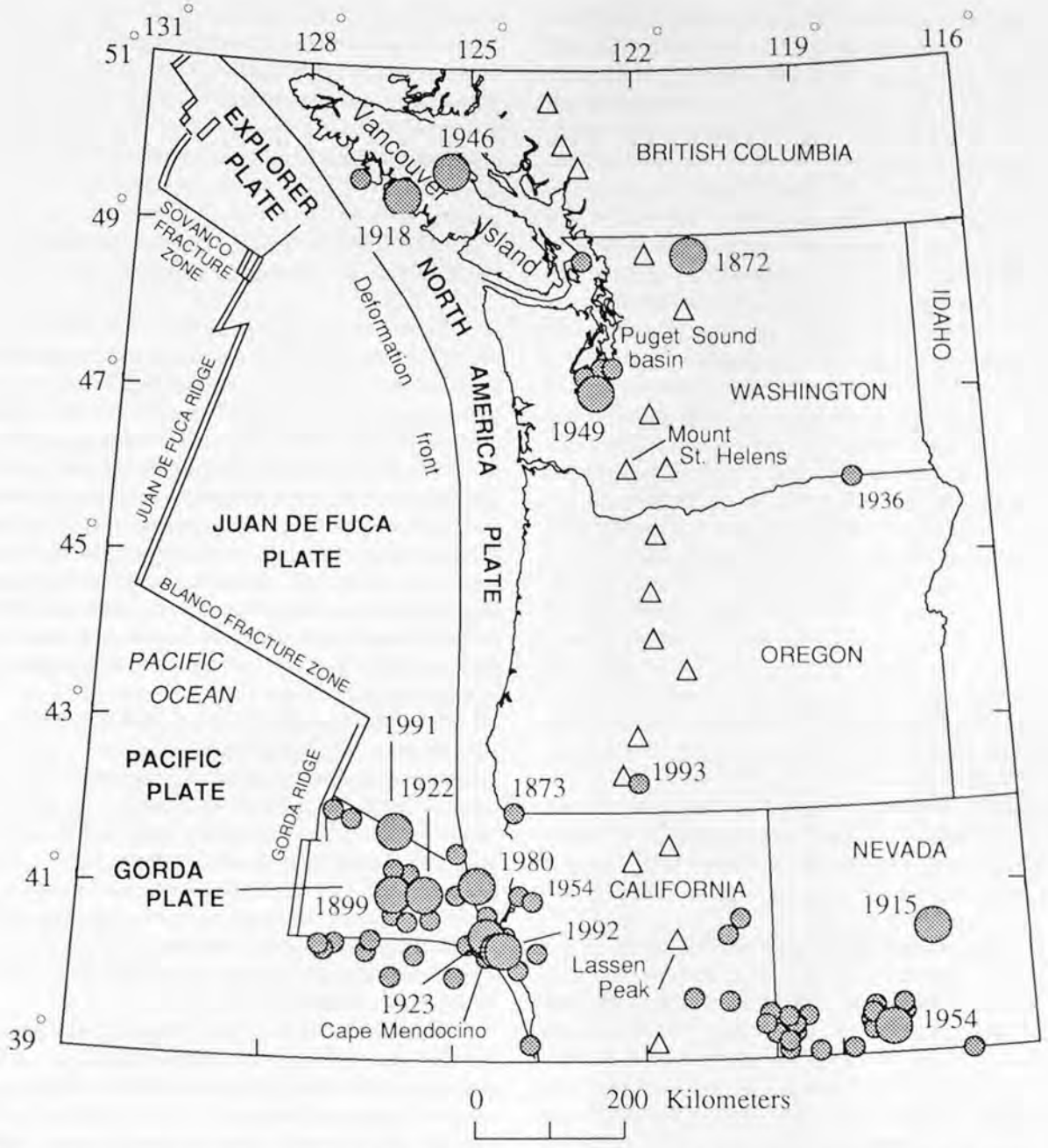

Figure 138. Locations of earthquakes in the Pacific Northwest having estimated magnitudes greater than 6 from 1870 to 1993. Small circles are earthquakes with magnitudes 6.0–6.9; large circles denote magnitudes greater than 7.0. The year of occurrence is shown for earthquakes greater than magnitude 7 and for four events greater than magnitude 6.0 discussed in the text. Triangles show Quaternary stratovolcanoes in the Cascade Range. Parallel lines indicate spreading ridges.

occurrence of great subduction-zone events and determining whether the urban centers in the Puget Sound basin and the Willamette Valley as well as those east of the Cascade Range are subject to magnitude 7, shallow (less than 20 km) crustal earthquakes will require significant investments of time and effort for new experiments, research, and modeling.

This chapter differs from recent review articles on the earthquake distribution in this region in that we give an overview of the distribution in the entire Juan de Fuca-North America plate system. Our plots of seismicity combine the reviews of Ludwin and others (1991), who summarized seismicity in Oregon and Washington, and Uhrhammer (1991) and Hill and others (1991), who discussed the seismicity of northern and central California, respectively. To complete our historical perspective, we combine the catalog of earthquakes greater than magnitude

6 for California (Ellsworth, 1990) with similar-sized events listed by Ludwin and others (1991) for Washington and Oregon and events listed by Rogers (1983a) for southern British Columbia. The scope of our review broadens that of Weaver and others (1990), who discussed the crustal earthquake distribution associated with the Cascade Range from Lassen Peak, Calif., to Mount Baker, Wash.

A comment concerning the terminology used in this chapter. Unfortunately for most readers, seismologists use several magnitude scales to measure the strength of an earthquake at its source (magnitudes are distinct from the earthquake-shaking effects at specific sites, which are measured by intensity). The different magnitude scales reflect the fact that most scales are appropriate for only a small part of the wide range of possible magnitudes. Although we specify the appropriate magnitude scale for particular earthquakes (local magnitude, M_L; body-wave magnitude, m_b; surface-wave magnitude, M_S; moment magnitude, M_W; or coda magnitude, M_c), to avoid confusion we have tried to deemphasize the differences between the various scales and commonly use only the term "magnitude." Generally, magnitudes greater than 8 are determined using seismic moment, magnitudes greater than about 5 but less than 8 are calculated using either body or surface waves, magnitudes less than about 5.5 usually are determined using a local magnitude (sometimes called a Wood-Anderson magnitude, after the instrument used to generate the seismogram), and magnitudes less than about 4.5 tend to be calculated from the coda length of the event. More discussion of the magnitude scales and definitions of seismologic terms can be found in the glossary to this volume.

ACKNOWLEDGMENTS

This chapter was improved by the thoughtful comments of Ivan Wong, Garry Rogers, and Timothy Walsh. Two of the editors, Timothy Walsh and Albert Rogers, showed unusual patience during revision of the original manuscript. Barbara Hillier helped refine the language throughout the chapter. The figures were drafted by Karen Meagher of the U.S. Geological Survey in Seattle.

EARTHQUAKE DISTRIBUTION

One of the significant problems in assessing the earthquake hazards of the Pacific Northwest is the discordance between the historical earthquake record and the record available from modern seismic instrumentation (starting about 1950). The historical record is essential because in Washington and Oregon, only the 1965 event near Seattle exceeded magnitude 6 since the World Wide Standard Seismic Network began recording in 1962; since then, the largest event was the September 1993 Klamath Falls earthquake of magnitude 6.0 in Oregon. Thus, one goal of any earthquake-hazards assessment program must be to place the historical, larger magnitude earthquakes in the tectonic framework. This task is difficult in western Oregon and Washington because of the lack of known surface faults with Pleistocene to Holocene offsets (Rogers and others, this volume).

EARTHQUAKES GREATER THAN MAGNITUDE 6

Earthquakes that occurred from 1870 through September 1993 that are estimated to be larger than magnitude 6 are restricted to a relatively small area of the Pacific Northwest. In mapping the earthquakes (fig. 138), we did not include events along the offshore ridge system other than those near the Gorda plate. The likelihood that all events greater than magnitude 6 will be felt or noted decreases with increasing distance from the coast to the offshore ridges and fracture zones. For the northwestern United States, the seismic catalogs are thought to be complete for magnitude 6 earthquakes since 1870 (Ellsworth, 1990; Ludwin and others, 1991); in British Columbia, the catalog of magnitude 6 events is complete from 1899 (G.C. Rogers, Geological Survey of Canada, written commun., 1990).

At the southern end of the Juan de Fuca-North America plate system, these larger earthquakes have occurred both onshore and offshore in northern California and east of Lassen Peak in Nevada. Large earthquakes are found in the historical record from northwestern Washington and central Vancouver Island but are notably absent in nearly all of Oregon (fig. 138). Within this distribution, the most important events that must be incorporated into hazard assessments are those earthquakes greater than magnitude 7 (nine events total, excluding the two events in Nevada) and a few events of magnitude less than 7.

The 1872 North Cascades earthquake in north-central Washington is generally considered the largest historical earthquake in the Pacific Northwest (Milne, 1956), with an estimated felt-area magnitude of 7.4 (Malone and Bor, 1979). It was felt over an area of more than 1,010,000 km^2, including Washington, northern and central Oregon, northern Idaho, western Montana, and southern British Columbia. The earthquake was followed by an extensive aftershock sequence (Milne, 1956). Study of damage reports suggests that the maximum intensity exceeded VII and may have been as high as IX on the Modified Mercalli intensity (MMI) scale (Milne, 1956). Because the available historical data does not unequivocally allow the location and depth of the earthquake to be determined, both remain subjects of discussion. The location shown in figure 138 was determined by Malone and Bor (1979) based on the intensity pattern; these authors also summarized other possible locations of the event. Hopper and others (1982) suggested a shallow crustal depth based upon the intensity reports and the extensive aftershock

sequence. A shallow depth for the 1872 earthquake is consistent with the depths determined from all instrumentally located earthquakes (since 1970) near the epicenter proposed by Malone and Bor (1979); all calculated hypocentral depths are shallower than 25 km.

The 1949 southern Puget Sound earthquake (M_S 7.1) is one of five earthquakes (the others were in 1909, 1939, 1946, and 1965) of magnitude 6 or greater known to have occurred in the Puget Sound basin (fig. 138). The 1949 and 1965 (m_b 6.5) earthquakes caused significant damage in the Puget Sound region (Murphy and Ulrich, 1951; Nuttli, 1952; Algermissen and others, 1965) and most of the major earthquake damage documented in the Pacific Northwest. These two events had instrumentally determined hypocentral depths of 54 km (1949) and 60 km (1965) (Baker and Langston, 1987; Algermissen and others, 1965). No aftershocks were felt or recorded after the 1949 earthquake; instruments available at the time would have detected events larger than magnitude 4.5 (M_L). Similarly, no aftershocks were felt following the 1965 earthquake, and an examination of seismograms recorded on stations operating within the region failed to identify any aftershocks greater than magnitude 2.5 (M_c). Because these large earthquakes did not produce felt aftershocks, Rogers (1983a) noted that lack of aftershocks is one possible way of estimating whether historical earthquakes were within the crust (where felt aftershocks would be expected) or within the subducting plate.

Large earthquakes occurred in central Vancouver Island in 1918 and 1946 (fig. 138). The 1918 event was about magnitude 7 and had an extensive aftershock sequence (Cassidy and others, 1988). The 1946 event of magnitude 7.3 (M_S) occurred in the middle to lower crust (about 15–25 km deep) and had almost no aftershocks (Rogers and Hasegawa, 1978). Because of the sparse population of central Vancouver Island during these earthquakes, the value of the damage was not large. As these events were within the crust of the North America plate (Cassidy and others, 1988), they raise serious questions as to the possibility of similar future events in the heavily populated urban areas in the Pacific Northwest.

Large earthquakes off the northern California coast have been frequent during the last 120 years (fig. 138) and have caused structural damage to onshore facilities. Five events are estimated to have been of magnitude 7 or greater; the largest offshore event of felt-area magnitude 7.3 occurred in 1923, and shaking from this shock damaged chimneys in the small towns north of Cape Mendocino (Toppozada and others, 1981; Ellsworth, 1990). In 1980, a magnitude 7.0 (M_S) event occurred within the Gorda plate just west of the deformation front (fig. 138). Although there was relatively little damage to most structures, a highway overpass with five people collapsed; fortunately no one was injured (Simon, 1981).

The most damaging earthquake in northern California through September 1993 was the April 25, 1992, Cape Mendocino event of magnitude 7.1 (M_S). Damage from the earthquake has been estimated at between $48 million and $66 million, but there were no deaths. Although the occurrence of magnitude 7 events is not unusual in the Cape Mendocino area (fig. 138), this event is particularly noteworthy because it appears to provide direct evidence of faulting on the plate interface and it generated a small tsunami along the western coast of North America (Oppenheimer and others, 1993). However, because this earthquake occurred at the Mendocino triple junction, the tectonic setting is complex, and considerably more study is required before the implications of this sequence can be integrated into regional earthquake-hazards assessments.

Three other notable earthquakes are in the historical record. An event estimated to have a felt-area magnitude of at least 6.75 (Toppozada and others, 1981) occurred in 1873 near the Oregon-California border (fig. 138). The earthquake was felt over most of western Oregon and as far south as Sacramento, Calif., but was felt with MMI VIII only in a small area near the estimated epicenter (Toppozada and others, 1981). There is no mention in contemporary newspaper accounts of felt aftershocks accompanying the main shock. This suggests either that the event was sufficiently far offshore that no aftershocks were felt or that it was deep, possibly within the subducting Gorda plate where aftershocks are not necessarily expected. The second event is the 1936 Milton-Freewater earthquake, the largest known event in eastern Washington. Maximum intensity was reported as MMI VII (Coffman and others, 1982), and the magnitude was calculated by Gutenberg and Richter (1954) as 5.75 (M_S). Noson and others (1988) estimated a magnitude of 6.4 for this earthquake based on the felt area. Because all earthquakes located since 1970 in eastern Washington occurred in the crust, the 1936 event is also assumed to be crustal. Numerous aftershocks were felt. The 1954 Eureka event occurred further inland in northern California than most other large earthquakes. That earthquake was estimated to be of magnitude 6.5 (Ellsworth, 1990); one person was killed, and there was considerable nonstructural damage.

The greatest earthquake losses in the Pacific Northwest were caused by the 1949 and 1965 events. Eight people were killed in the 1949 earthquake (Ulrich, 1949), and six died in the 1965 event (Algermissen and others, 1965). In terms of 1984 dollars, $150 million damage occurred in 1949; the 1965 event caused an estimated $50 million damage (Noson and others, 1988). As noted above, the 1992 Cape Mendocino earthquake caused between $48 million and $66 million damage. In 1993, two earthquake sequences in Oregon did considerable damage. A magnitude 5.6 event occurred in March 1993 about 40 km southeast of Portland. Despite being a moderate-magnitude earthquake in a relatively lightly populated area along the Cascade Range foothills, this earthquake still caused more than $28 million damage (Madin and others, 1993). The second sequence took place in September 1993 near Klamath Falls in southern Oregon. Two events of magnitude 5.8 and 6.0 occurred about three

hours apart; two people died from shaking effects, and preliminary estimates of damage exceeded $5 million. Most of the damage was to older, unreinforced-masonry buildings in the downtown section of Klamath Falls.

The effects of the 1949 and 1965 earthquakes are currently used as the basis for engineering design, emergency-response planning, and damage and loss estimates in the Puget Sound region (Hopper and others, 1975). Since Hopper and others' (1975) report was issued, the population of the Puget Sound region has increased by more than 600,000, and many new buildings have been constructed. More important, the 1975 study considered only the effects of deep earthquakes and did not consider the effects of either a shallow crustal earthquake (like the 1872 event) or a great megathrust earthquake. Thus, there is wide agreement by scientists that an updated study of earthquake sources, the hazards posed by these sources, and revised estimates of earthquake losses are urgently needed in the Pacific Northwest. Perhaps the 1993 earthquakes in Oregon will convince residents of Oregon and Washington of the need to update earthquake hazards and risk assessments in the region.

SUMMARY OF INSTRUMENTAL SEISMICITY

Although a few seismic stations have operated in the Pacific Northwest since 1900 (Rogers, 1983a; Ludwin and others, 1991), 1960 is commonly assumed to be the beginning of the modern instrumental-recording period for the region. By 1960, the distribution of seismic stations and the population density facilitated the reporting and location of earthquakes greater than magnitude 4 so that since then, for Washington and Oregon, the earthquake catalog is considered complete for events greater than magnitude 4.0 (M_L) (Ludwin and others, 1991); in California, the catalog has been complete at this magnitude level since at least 1960 (Uhrhammer, 1991). Since 1960, the number of seismic stations operating in the Pacific Northwest has greatly increased so that by 1990, much of the region was routinely monitored for earthquake activity less than magnitude 2.5 (M_c). Details of the evolution of the seismic network can be found elsewhere (for example, Ludwin and others, 1991; Weaver and others, 1982, 1990; Rogers, 1983b; Eaton, 1989). The distribution of short-period (1 Hz) seismic stations operating in late 1993 is shown in figure 139. Most of the stations in British Columbia are operated by the Geological Survey of Canada, stations in Oregon and Washington are nearly all operated by the University of Washington, and most of the stations in California are part of the U.S. Geological Survey network.

For a plate-wide perspective of instrumentally recorded seismicity, we selected well-located earthquakes that occurred from 1980 through April 1990 that were greater than magnitude 2.0 (M_c), and that met the following statistical criteria: calculated hypocentral standard errors of less than ±3 km, at least six P waves used in the solutions, and a root mean square of the traveltime residuals less than 0.35 s. Most hypocenter solutions considerably exceed these criteria. Because of the significant earthquakes in 1992 and 1993, we added all located events greater than magnitude 5 from April 1990 through September 1993 to our initial catalog selections. For Washington and Oregon, our hypocentral data are from the University of Washington earthquake catalog, and for California, the data is from catalogs maintained by the U.S. Geological Survey. Hypocentral catalogs compiled by the Geological Survey of Canada for British Columbia are incorporated into the University of Washington catalog.

In plotting the seismic distribution of the combined catalog (figs. 140 and 141), we subdivided our data into two depth ranges, 0–30 km and deeper than 30 km. Earthquakes deeper than 30 km are nearly all within the subducting Juan de Fuca plate system (fig. 140). Earthquakes shallower than 30 km (fig. 141) are within the North America plate in Washington or Oregon; however, along the northern California coast, most of the shallow seismicity is probably within the subducting Gorda plate (Hill and others, 1991; Eaton, 1989). Inland from the California coast, the shallow earthquakes are within the North America plate.

It is clear that the distribution of both the shallow and deep earthquakes is not uniform across the Pacific Northwest. The deep events are concentrated beneath northwestern Washington and northwestern California, with a sparser distribution of events beneath southwestern Washington and northern Oregon (fig. 140). The absence of deep events beneath the southwestern Oregon coast may result in part from a lack of seismic stations (compare fig. 140 with fig. 139); however, as noted earlier, earthquakes greater than magnitude 4 would have been instrumentally recorded since about 1960. Events of this magnitude would have been felt along the Oregon coast throughout the 20th century, so there is little doubt that at the magnitude 4 level, this part of the subducting Juan de Fuca and Gorda plates is seismically quiet.

The distribution of crustal earthquakes is likewise not uniform across the Pacific Northwest (fig. 141). Weaver and others (1990) used the changes in the crustal seismicity pattern to divide the Cascade Range and adjacent areas into four segments; in this chapter, we expand those segments westward to the coast. In the northernmost segment, from Mount Baker to Mount Rainier, nearly all of the well-located crustal earthquakes are confined to the region between the eastern Olympic Mountains and the Quaternary Cascade Range stratovolcanoes; there were few events east of the stratovolcanoes. The second segment defined by Weaver and others (1990), from Mount Rainier to Mount Hood, is the most seismically active part of the crust. In southern Washington, the St. Helens seismic zone (SHZ) is a particularly prominent north-northwest-striking alignment of earthquakes. Although there is a hiatus of activity east of the SHZ, in general, seismicity continues in

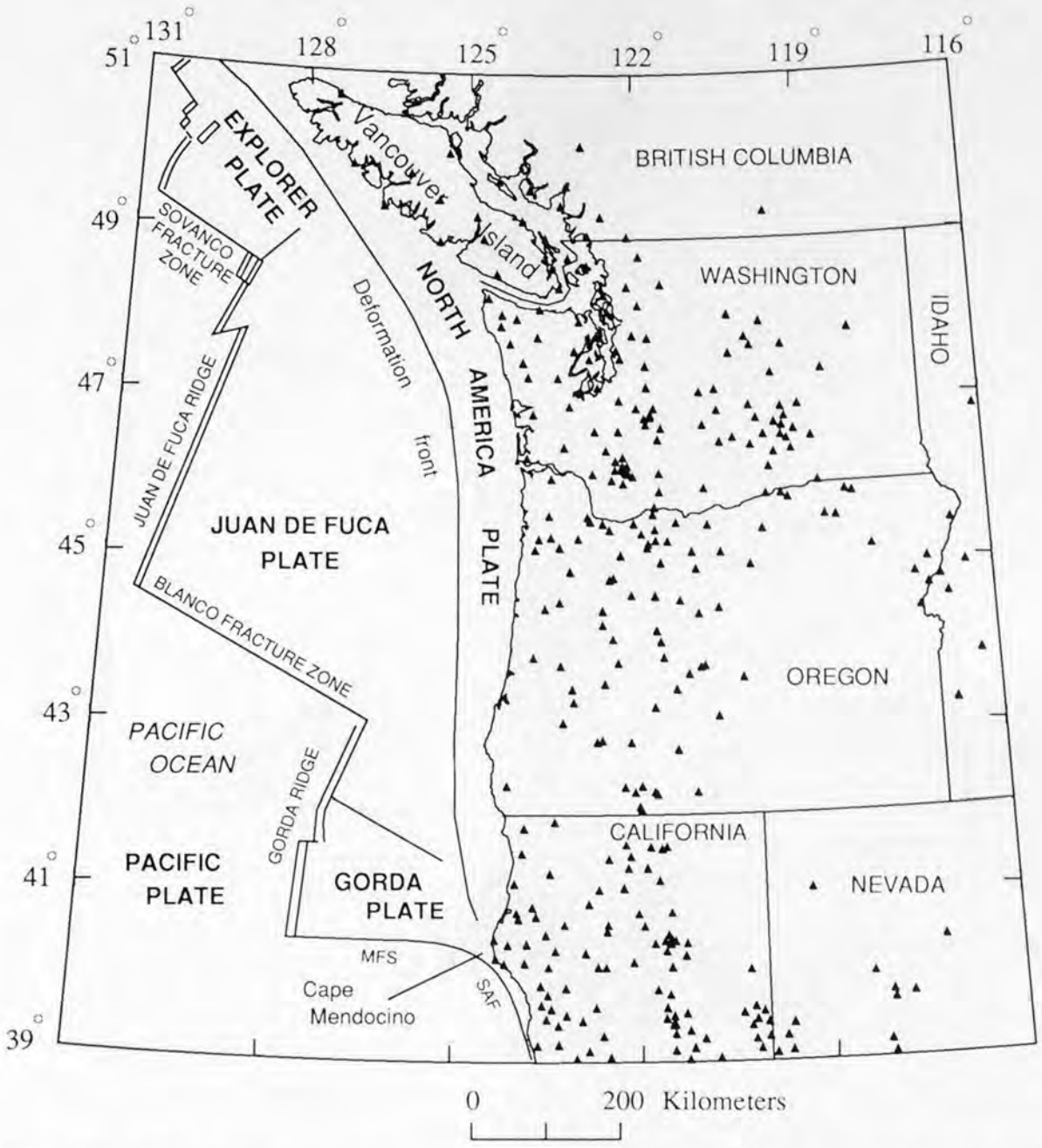

Figure 139. Regional short-period seismic stations (triangles) operating in the Pacific Northwest and southwestern British Columbia. MFS, Mendocino fracture zone; SAF, San Andreas fault.

a broad zone from the area immediately west of the SHZ into southeastern Washington. The third segment, from south of Mount Hood to just north of Mount Shasta, is seismically very quiet except for the 1993 earthquakes east of the Cascade Range volcanoes near Klamath Falls. This segment has not been monitored continuously, but very few earthquakes were observed during the two years (1980–82) of continuous operation of a 32-station network or since stations were reinstalled in the central Oregon Cascade Range in 1987 (Ludwin and others, 1991). There is a marked increase in earthquake activity in the fourth segment, between Mount Shasta and Lassen Peak and also along the northern California coast.

CRUSTAL THICKNESS AND PLATE GEOMETRY

The composition of the crust of the Pacific Northwest has been investigated using geologic and geophysical methods, but there are few reversed, high-resolution refraction or wide-angle reflection profiles for the region. Mooney and

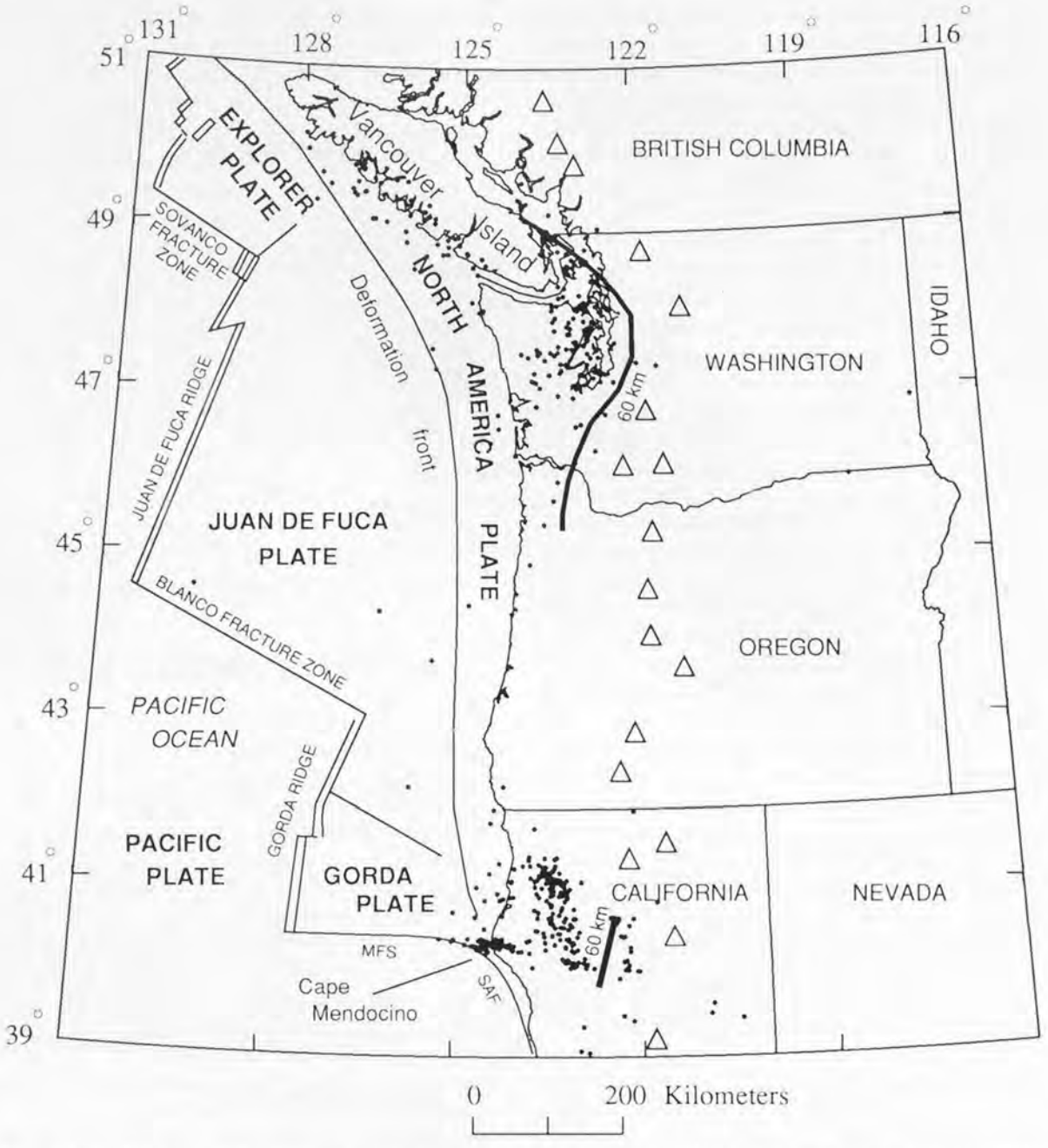

Figure 140. Distribution of earthquakes (dots) deeper than 30 km in the Pacific Northwest from 1980 to September 1993. The heavy lines show the approximate easternmost extent of earthquakes at a depth of 60 km (Weaver and Baker, 1988). Triangles show Quaternary stratovolcanoes in the Cascade Range. MFS, Mendocino fracture zone; SAF, San Andreas fault.

Weaver (1989) summarized the existing studies with a contour map of estimated crustal thickness beneath Washington, Oregon, and northern California. Using this map as a working hypothesis for the configuration of the Moho (see the glossary), two noteworthy features can be seen. The first is the pronounced eastward increase in crustal thickness from 16 km at the continental margin to about 40 km beneath the western flank of the Cascade Range. Gravity modeling along two profiles in Oregon and interpretations of electrical and magnetic data collected by the Electromagnetic Sounding of the Lithosphere and Beyond (EMSLAB) experiment (EMSLAB Group, 1988) along a profile perpendicular to the northern Oregon coast are consistent with crustal thickening.

The second major feature is the presence of thick crust beneath the Cascade Range, the Puget Sound basin, and the Columbia Plateau. Crustal thickness is estimated to be at least 38 km over this entire region and locally reaches 46 km in the southern Oregon Cascade Range. There is a gradual

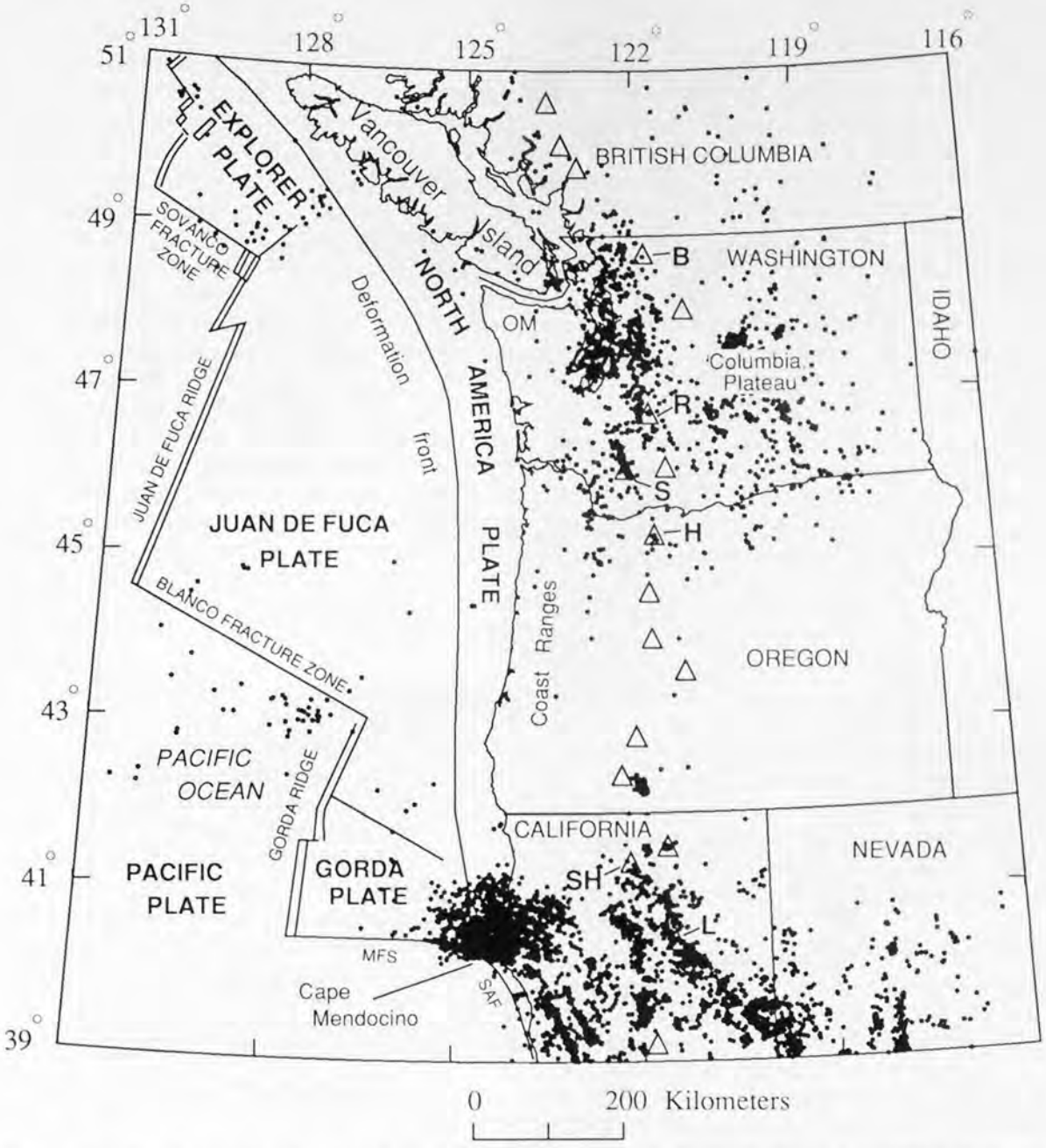

Figure 141. Distribution of earthquakes (dots) shallower than 30 km in the Pacific Northwest from 1980 to September 1993. SHZ is the St. Helens seismic zone. Triangles show Quaternary stratovolcanoes in the Cascade Range. B, Mount Baker; R, Mount Rainier; S, Mount St. Helens; H, Mount Hood; SH, Mount Shasta; L, Lassen Peak; OM, Olympic Mountains; MFS, Mendocino fracture zone; SAF, San Andreas fault.

eastward thinning of the crust beneath southeastern Oregon and northeastern California. The Moho shallows at about a 36-km depth beneath most of northeastern Washington (Potter and others, 1986).

The geometry of the subducting Juan de Fuca and Gorda plates has been partly inferred from the locations of earthquakes occurring within the plates; commonly, these events are referred to as Benioff-zone earthquakes. In the historical record of large-magnitude earthquakes, it is these events that are most frequently observed. Disregarding the concentration of earthquakes off Cape Mendocino, since 1870 at least six large earthquakes are either known or thought to have been within the subducting plate. These events occurred in 1873 along the coast near the Oregon-California border and in 1909, 1939, 1946, 1949, and 1965 within the Puget Sound basin (fig. 142). The distribution of intraplate earthquake hypocenters (largely those shown in fig. 140) indicates that the subducting Juan de Fuca plate

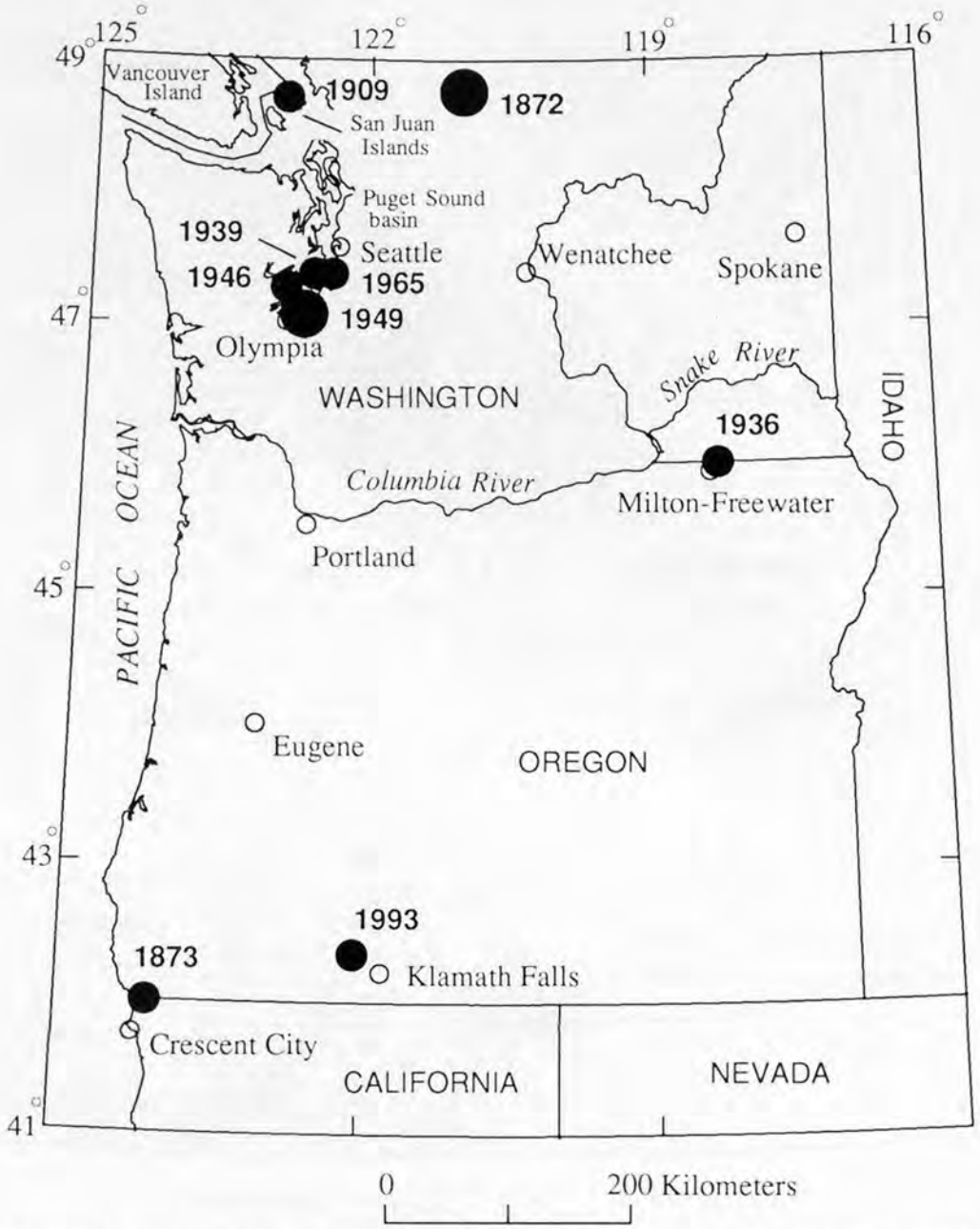

Figure 142. Locations of major earthquakes in Oregon and Washington. Small circles are earthquakes with magnitudes estimated between 6.0 and 6.9; large circles are earthquakes with magnitudes estimated as greater than 7. The 1872, 1936, and 1993 earthquakes were crustal, whereas all others are either known or thought to have been within the subducting plate system.

arches upward beneath the southern and central Puget Sound basin; beneath southwestern Washington, the plate dips to the east-southeast, changing to a northeast dip beneath northwest Washington (Weaver and Baker, 1988). The structure of the arch can be seen in figure 140, where we have indicated the eastern extent of the location of hypocenters at 60-km depth (from Weaver and Baker, 1988). Although much of the shallow plate geometry beneath Oregon is either poorly resolved or unknown, it appears that the average dip of the plate (between the deformation front and the position where the plate reaches 60 km depth) must be greater in northern Oregon than in Washington.

In Washington and northern California, there is general agreement between areas of the thickest crust (greater than 38 km) and areas of crustal seismicity in the North America plate. Clearly, however, there are areas where this association does not hold, particularly from the Oregon Cascade Range eastward—recall that the shallow seismicity mapped

off the northern California coast is within the Gorda plate. Thus, the segmentation of the crustal seismicity pattern is probably not directly related to crustal thickness. Unfortunately, the structure of the crust is too poorly known in this region to determine if the composition of the middle to upper crust may play a role in the distribution of crustal seismicity.

The segmentation of the crustal-seismicity pattern also does not match the variation of the geometry of the Juan de Fuca plate. The crustal seismicity in the Puget Sound area lies above the arch in the Juan de Fuca plate, yet relatively sharp variations in the distribution of the earthquakes suggest the importance of unknown crustal structure rather than variations of the subducting plate geometry. Guffanti and Weaver (1988) noted that the high-seismicity segment, between Mount Rainier and Mount Hood, was on the southeastern edge of the plate arch, whereas the seismically quiet segment in Oregon was inland from the section of the Juan de Fuca plate that has an increase in plate dip. However, in suggesting these associations, Guffanti and Weaver did not incorporate the historical seismicity. In particular, when the 1872 earthquake (fig. 142) is considered, it is clear that seismic-moment release in north-central Washington dominates all of the crustal seismicity south of the Canadian border (Shedlock and others, 1989).

This last observation points to an important difference between seismicity in Oregon and Washington and that throughout California (including the subduction regime). In Oregon and Washington, seismicity shows a temporal variation on the scale of at least a few decades (Ludwin and others, 1991) whereas in California, Hill and others (1991) noted that a few years of microearthquake monitoring coupled with known mapped faults provides a good representation of the long-term (decades to a few centuries) seismicity pattern. The 1993 Klamath Falls earthquakes, occurring in an area lacking any significant known historical seismicity (Ludwin and others, 1991), have served as the most recent reminder of the limitations of the earthquake catalogs in Oregon and Washington with respect to understanding seismic source zones and earthquake hazards.

ESTIMATES OF THE SOURCE REGIONS

PROBABLE ZONE FOR INTRAPLATE EARTHQUAKES

The geometry of the subducting plate (shown by the 60-km-depth line in fig. 140) illustrates how large earthquakes in the historical record (1949, 1965) can be related directly to the plate configuration (Weaver and Baker, 1988). The T-axis from the focal mechanism calculated by Baker and Langston (1987) for the 1949 south Puget Sound earthquake of magnitude 7.1 (M_S) is oriented to the east-southeast, and the 20° plunge of the T-axis was shown by Weaver and Baker (1988) to agree well with the plate dip angle determined from the earthquake hypocenters. Therefore, Weaver and Baker (1988) concluded that the 1949 earthquake resulted from down-dip tensional forces within the subducting Juan de Fuca plate, an interpretation consistent with observations for many earthquakes in this depth range in other subduction zones (Isacks and Molnar, 1971). Rogers (1983a) reached a similar conclusion concerning the forces responsible for the 1965 south Seattle earthquake and a smaller event of magnitude 5.1 (m_b) in 1976 off the southeastern end of Vancouver Island. Both events were at a depth of about 60 km, and focal mechanisms calculated for both earthquakes indicated normal faulting with the T axes striking northeast and plunging down dip (Rogers, 1983a).

Based on the agreement between the dip of the Juan de Fuca plate as inferred from earthquake hypocenters determined from the modern seismographic network and the dip of the T axes calculated for the larger magnitude historical earthquakes, we can confidently predict the intraplate earthquake source region for the entire plate (fig. 143). We expect that future large-magnitude (about 7) intraplate earthquakes will occur within the Juan de Fuca plate system in the depth range of the 1949 and 1965 events. Although the depths of these events are considered to be well known, we have chosen to bracket our source region at a shallower depth. An examination of the University of Washington seismic catalog for the years 1970 through 1990 shows that all of the intraplate earthquakes greater than magnitude 4 were below 45 km and that none have been located deeper than the 1976 event (60 km). Therefore, we have used the depth range of 45–60 km for our estimate of the probable source region for intraplate events.

We emphasize that this probable source region represents the likely areal extent within which an earthquake may occur; the actual dimensions of the fault area associated with an earthquake of approximate magnitude 7 would be expected to be similar to the 40-km-long fault length estimated for the 1949 earthquake (Baker and Langston, 1987). The queried area in southern Oregon (fig. 143) represents the region of unknown plate geometry where no intraplate earthquakes have been located either because any events that did occur were not large enough to be detected by the existing seismic network or because no events have occurred. We note that expansion of the existing seismic network (fig. 139) in southern Oregon will greatly help to resolve the long-standing question concerning whether this part of the Juan de Fuca plate is currently truly aseismic. In northern California, Benioff-zone earthquakes also allow the plate depth to be estimated from the subduction-zone trench eastward to the western edge of the Cascade Range (Cockerham, 1984; Walter, 1986), so we have shown (fig. 143) the probable source region here between the same depth limits as in Washington and northern Oregon.

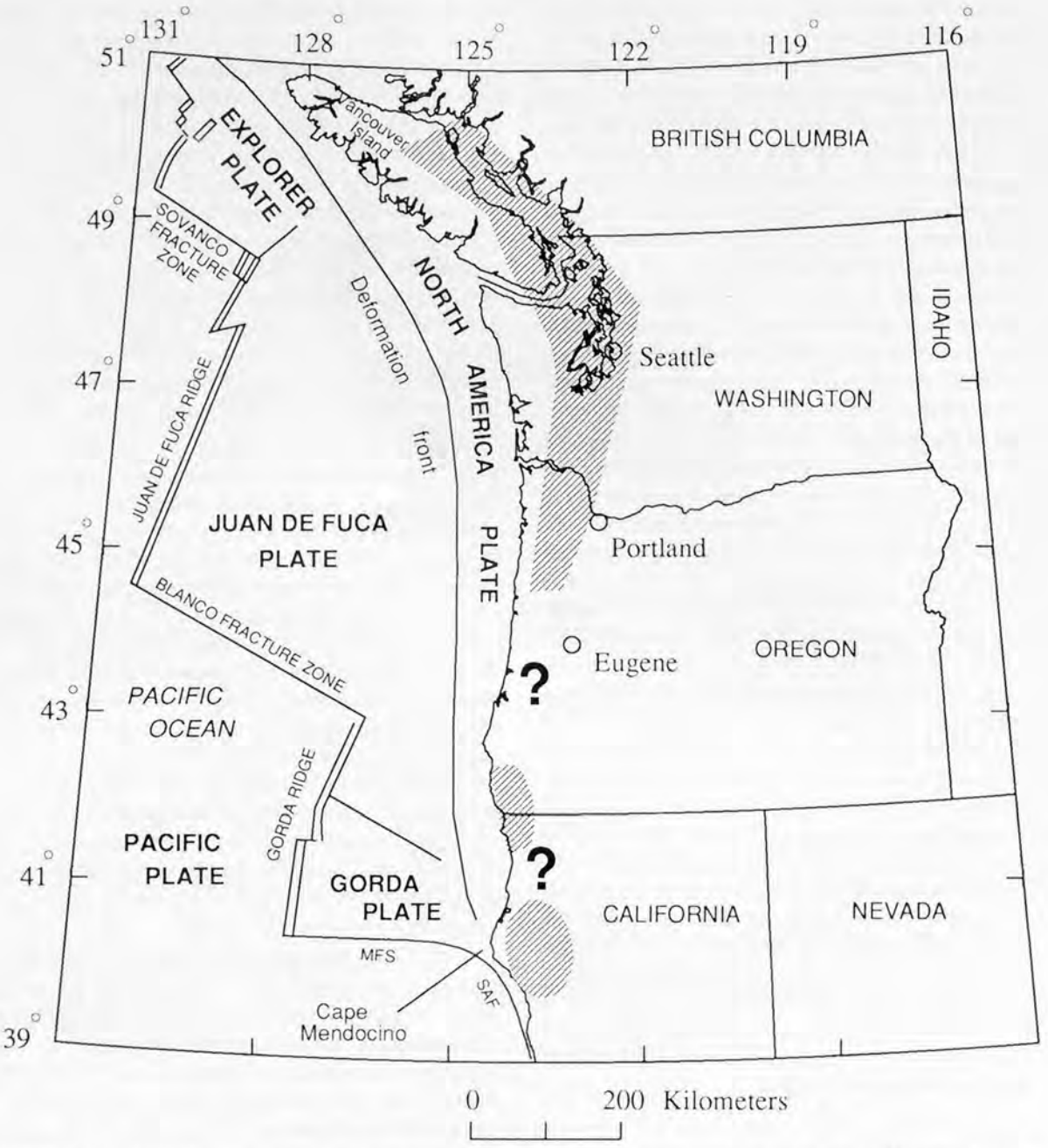

Figure 143. Probable source regions for intraplate, down-dip tensional earthquakes in the Pacific Northwest. Large-magnitude earthquakes (7–7.5) are expected anywhere within the patterned areas. Question marks indicate areas where no earthquakes were located within the Juan de Fuca plate and where the plate geometry is uncertain. MFS, Mendocino fracture zone; SAF, San Andreas fault.

POSSIBLE SOURCE REGIONS FOR SUBDUCTION-ZONE EARTHQUAKES

At nearly all convergent margins around the world, magnitude 8+ earthquakes are known to occur; the Cascadia subduction zone is unusual in that there is no such earthquake in the historical record. However, recent studies of subduction-zone characteristics (Heaton and Kanamori, 1984; Heaton and Hartzell, 1986), crustal-strain accumulation in Washington (Savage and others, 1981), crustal earthquakes in southwestern Washington (Weaver and Smith, 1983), and the stratigraphy of coastal marshes along the Washington and Oregon coasts (Atwater, 1987; Atwater, this volume; Grant and others, 1989) have all either concluded directly or inferred that the Cascadia subduction zone should be regarded as capable of generating great interface earthquakes.

The geologic evidence from the coastal marshes is particularly compelling for the occurrence of past great subduction-zone earthquakes. The evidence is multiple

buried peat horizons in many bays along the coast (Atwater, this volume). The preferred interpretation is that each buried peat layer represents a previous surface soil horizon that was suddenly submerged during a great earthquake. Subsequently, intertidal deposits accumulated on the submerged soils until the deposits reached a level allowing the development of a new marsh surface. At some sites in Willapa Bay, Wash., fine-grained sand is deposited directly on the submerged soils. Atwater (1987; this volume) and Grant and others (1989) interpreted these sands as having been deposited by tsunamis, and because they lie directly on submerged peat layers, they are further interpreted as having been locally generated by the same earthquake that produced the subsidence.

The marsh data indicate that the return period for great earthquakes in the late Holocene has been irregular, varying from less than 100 years to more than 1,200 years (Atwater, this volume; Grant and others, 1989). At many sites along the coast from Humboldt Bay, Calif., to the Copalis River, Wash., considerable field evidence indicates that the last event occurred about 300 years ago; both carbon-14 and tree-ring dating techniques are in reasonable agreement on this date (Atwater, this volume). Much uncertainty remains concerning both the repeat time for these great earthquakes and the probable magnitude. Both issues require showing synchronous submergence of specific marsh horizons at multiple sites on the coast. Although, geologic techniques may never demonstrate proof of synchronous motion for a given marsh horizon at many sites, they may be able to rule out the possibility that the entire subduction zone from Cape Mendocino to central Vancouver Island slipped in a single earthquake.

The area where great subduction-zone earthquakes occur is not in doubt, in that the shallow-dipping interface between the subducting plate and the overlying plate is the fault plane. The issues concerning the source area for subduction-zone earthquakes relate to whether or not the entire length of the Cascadia subduction zone generates these earthquakes and to the width of the fault zone that slips. A minimum length was provided by Heaton and Kanamori (1984). On the basis of regression analysis of plate age and convergence rate against the observed magnitude of interface earthquakes in other subduction zones, they suggested that in the Cascadia subduction zone, an event of about magnitude 8.3 (M_w) would be expected given the plate age and convergence rate measured there. Such an earthquake might be expected to rupture a length of about 150–200 km along the subduction zone. After comparing additional plate parameters such as offshore bathymetry and gravity and the historical rate of moderate (magnitude 5.7+) earthquakes, Heaton and Hartzell (1986) suggested that the entire length of the Cascadia subduction-zone (1,100 km) from Cape Mendocino to central Vancouver Island might rupture in one great event of magnitude 9 or greater (M_w).

Although, as noted above, all of the marsh data is not completely analyzed, the great extent of the coast where evidence of rapid subsidence has now been documented (fig. 144) indicates that very large parts of the coast (at least several hundred to many hundreds of kilometers) were affected by prehistoric earthquakes. The impressive number of sites where multiple buried peat sequences of similar age have now been found (fig. 144) suggests that the most likely cause of the marsh subsidence is coseismic surface deformation during a great earthquake. Because of the extent of the marsh data along the coast and the arguments of tectonic setting raised by Heaton and Hartzell (1986), we believe that the entire length of the Cascadia subduction zone is capable of generating great earthquakes, even though it is not yet clear if the entire length fails during a single event.

The second issue in estimating source areas concerns the width of the rupture area perpendicular to the coast. Two models, one in which the rupture is largely offshore and one in which it is largely beneath the continent, bracket the range of probable source-area widths. In the first model, the rupture extends from the deformation-front trench down-dip along the interface to a depth of 30–40 km. Because of the plate geometry, this width varies along the subduction zone from a maximum beneath northwestern Washington (about 200 km) to less than 100 km beneath central Oregon and areas further south (fig. 140). If the end of the fault rupture zone were as deep as 40 km, then a significant part of the rupture area would be beneath Washington (fig. 145), whereas if the rupture ends at about a 30-km depth, the eastern extent of the fault-rupture area would be near the coast practically everywhere. In the second model, in areas like the Cascadia subduction zone that have a very high rate of sedimentation offshore, Byrne and others (1988) have argued that as these sediments are subducted, they allow very poor coupling between the two plates from the trench landward, possibly as far as the coast. In this model, the potential source area capable of generating subduction-zone interface earthquakes is greatly reduced, consisting approximately of the area from about the coast inland to where the subducting plate begins to dip steeply eastward, perhaps at a depth of 50–60 km (Byrne and others, 1988). Because of the plate geometry, this area is particularly small south of the arch beneath Puget Sound (fig. 140).

In our map of the source areas for great subduction-zone earthquakes (fig. 145), we have shown the fault-zone width extending from the deformation front offshore to just beneath the coastline. We chose this fault width because of deformation-modeling results that indicate that it is difficult to explain the pattern of sudden subsidence recorded in the coastal-marsh stratigraphy without the rupture area extending offshore (Savage and others, 1981). The patterned areas in figure 145 illustrate the large source areas for these events. Based on the record from other subduction zones, interface earthquakes can be expected to occur anywhere within these source areas. The two hypothesized earthquakes would fill the entire subduction zone; however, other possibilities have been discussed by Heaton and Hartzell (1986). To date, the geologic record from coastal intertidal marshes does not rule

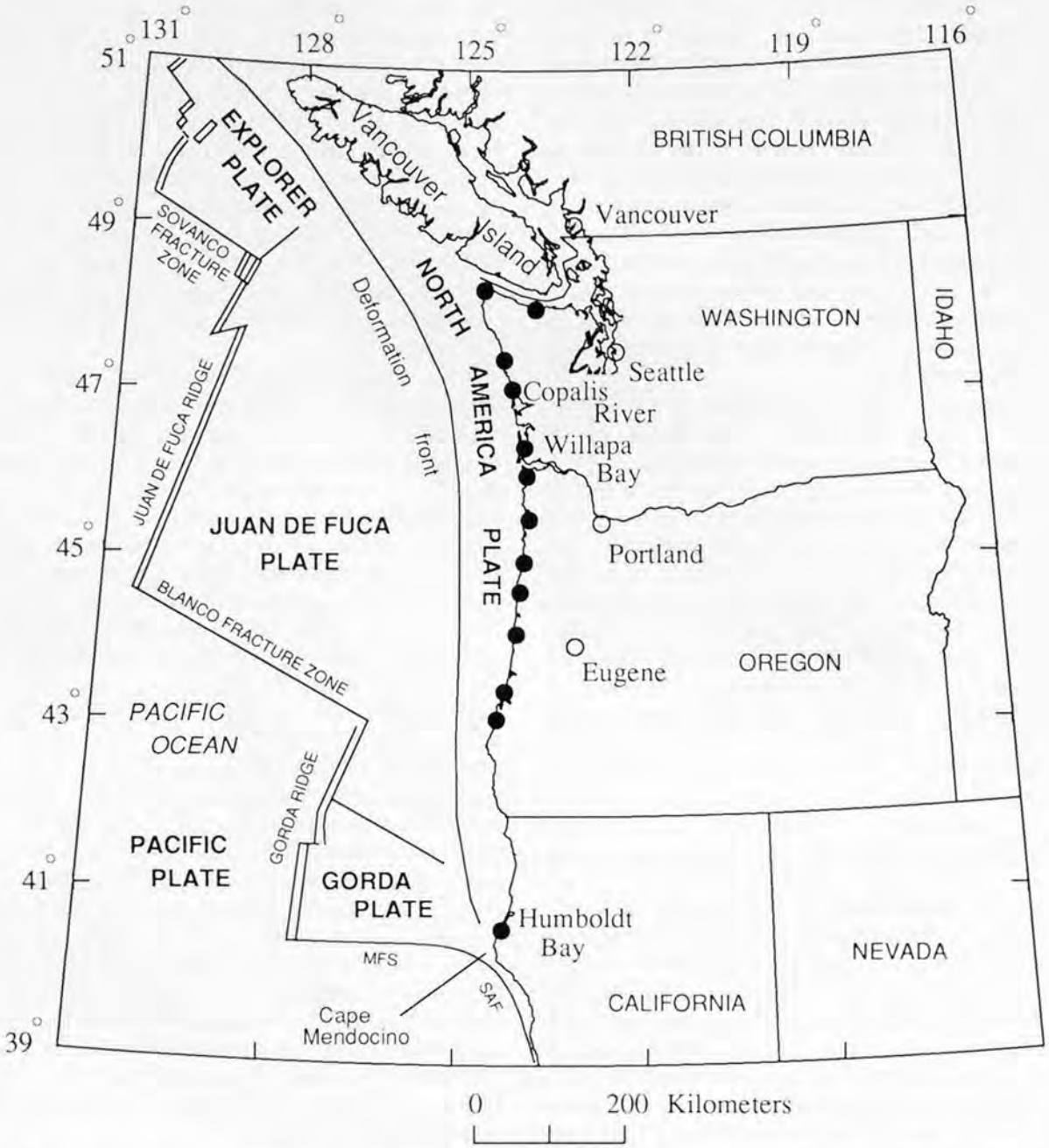

Figure 144. Sites in Washington, Oregon, and northern California (dots) where coastal-marsh stratigraphy studies have found evidence of sudden subsidence. Compiled from Grant and others (1989). MFS, Mendocino fracture zone; SAF, San Andreas fault.

out the possibility that the entire length of the subduction zone can fail in one very great earthquake. However, the same data do not yet allow unequivocal interpretations of whether the zone might break in a series of smaller earthquakes of approximate magnitude 8–8.5 (M_w).

The very large area involved in any subduction-zone earthquake indicates the need for large-scale studies of the properties of the Cascadia subduction zone. For example, greatly expanded regional strain studies would help address the issue of whether the plate boundary breaks in a single great earthquake or in a series of smaller ones. A second issue is that of the eastern extent of the fault. Clearly, if the eastern limit of the fault zone for a great subduction event was further westward than the limit shown in figure 145, then it is possible that this would produce lower levels of strong ground shaking in the major urban areas.

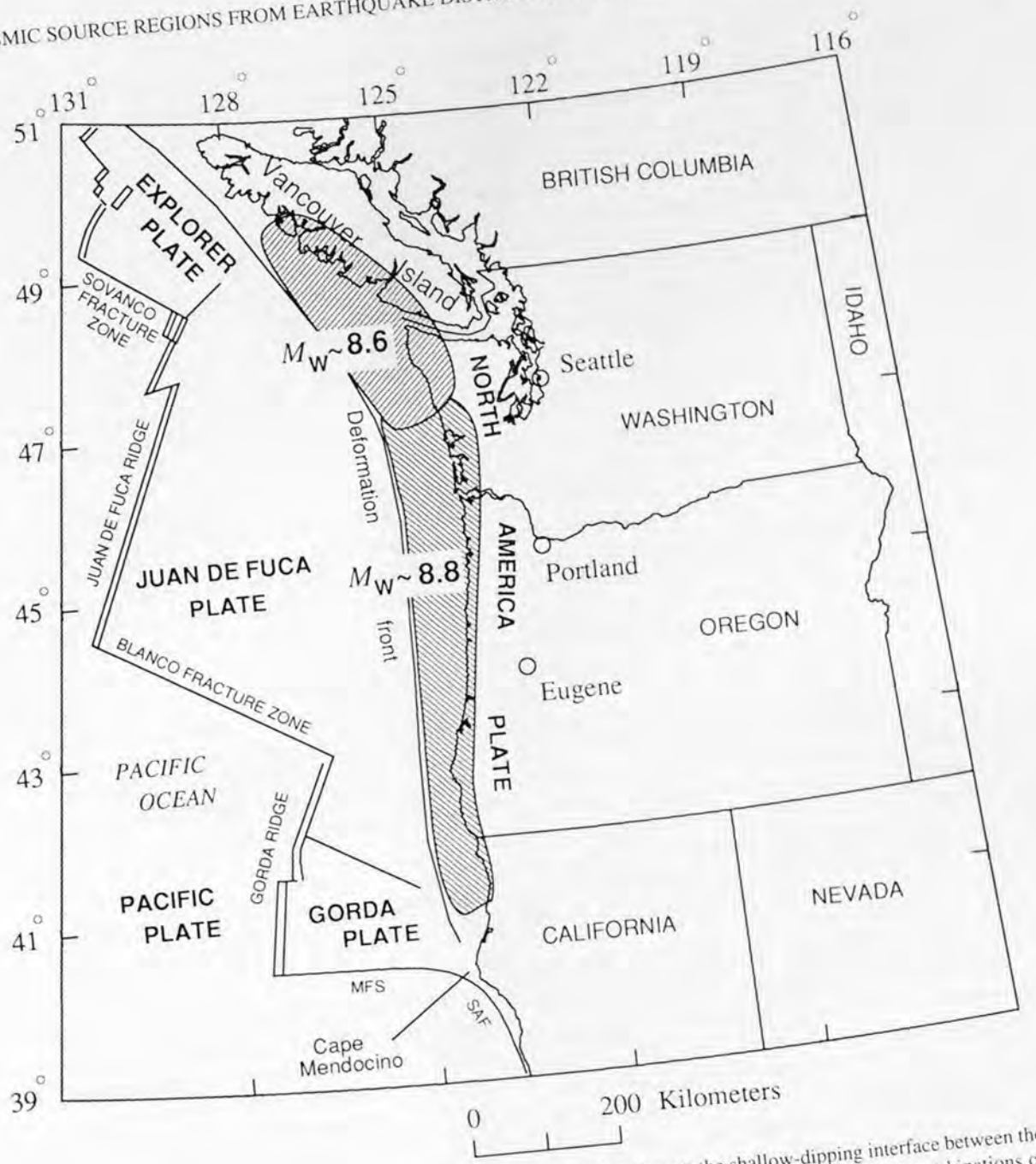

Figure 145. Source areas (patterned) for two possible interplate earthquakes on the shallow-dipping interface between the Juan de Fuca and North America plates. Approximate moment magnitude for each event is shown. Other combinations of source areas are also possible. MFS, Mendocino fracture zone; SAF, San Andreas fault.

KNOWN SOURCE REGIONS OF LARGE CRUSTAL EARTHQUAKES

The known areas of large-magnitude (7+) crustal earthquakes in the North America plate in the Pacific Northwest are limited to central Vancouver Island and the northern Cascade Range (fig. 138). The Vancouver Island events were probably related to the stress regime generated by the interaction of the Explorer plate with the North America plate (Rogers, 1983b). The cause of the 1872 event remains uncertain in that it occurred in an area with very little contemporary seismicity and no obvious surface-fault expression (Malone and Bor, 1979).

These large crustal earthquakes raise the question of whether they might occur within the urban areas of western Washington and Oregon. Unfortunately, the sparsity of

known Quaternary faults (Gower and others, 1985) and the current seismicity distribution does little to answer this question. In the Puget Sound basin, crustal earthquakes do not occur along simple, linear fault zones but appear to be distributed throughout the crust (fig. 141). Zollweg and Johnson (1989) have recently interpreted a sequence of earthquakes on the western margin of the northern Cascade Range as evidence of a south-dipping fault zone, the first such zone identified in northwestern Washington. Nevertheless, it remains impossible to infer the possibility of, or argue conclusively against, a future magnitude 7+ shallow crustal earthquake in the Puget Sound area.

Mapped Quaternary faults in the Puget Sound basin are sparse (Gower and others, 1985), although shallow-reflection data may indicate Quaternary faults within Puget Sound (Harding and others, 1988). Combined with the apparent sparsity of Quaternary faults, the available seismicity record in the Puget Sound basin is usually interpreted as suggesting that the expected maximum-magnitude crustal earthquake is less than that expected in southern Washington (Ludwin and others, 1991). However, observations of uplift on late Holocene terraces by Bucknam and others (1992), coupled with supporting evidence for the generation of tsunamis in Puget Sound (Atwater and Moore, 1992) and landslides into lowland lakes (Schuster and others, 1992; Jacoby and others, 1993), strongly indicate that magnitude 7 events have occurred in the crust of the Puget Sound basin. Once again, the limited earthquake history makes it difficult to meld the new findings for the Puget Sound basin directly into earthquake-hazards assessments. Many additional geologic investigations are needed to attempt to estimate possible recurrence of large crustal earthquakes in the Puget Sound basin.

In contrast to the earthquake distribution in the Puget Sound basin, much of the earthquake activity in southwestern Washington occurs along the SHZ, a right-lateral strike-slip fault zone that is defined for more than 130 km (Ludwin and others, 1991; Weaver and Smith, 1983). Two earthquakes greater than magnitude 5 have occurred on the SHZ since 1960: in 1961, a magnitude 5.1 (M_L) event occurred south of Mount St. Helens and, in 1981, a magnitude 5.5 (M_L) event occurred on the SHZ north of the volcano. Mount St. Helens directly overlies the SHZ where a small (a few kilometers) right-stepping offset occurs (Weaver and others, 1987). Several studies have assumed that the magmatic system beneath Mount St. Helens prevents the entire 130-km length from rupturing in a single earthquake (Weaver and Smith, 1983). We compared possible source areas along the SHZ north of Mount St. Helens with observations of both fault area and magnitudes calculated from earthquakes on other strike-slip fault zones and concluded that an earthquake in the magnitude range of 6.2–6.8 was the expected maximum-magnitude event for the SHZ north of Mount St. Helens.

Our map of crustal earthquake source areas (fig. 146) shows the regions where these earthquakes occurred in the historical record including the SHZ, the northern end of the San Andreas fault system in California, and the central Puget Sound basin near Seattle, where paleoseismic evidence of uplift has recently been found. The large area in north-central Washington illustrates the uncertainty about the epicentral position of the 1872 earthquake. Although Malone and Bor (1979) concluded that the event probably was on the northeastern flank of the Cascade Range, other studies (Milne, 1956) have suggested that the event was near the United States-Canada border. A problem highlighted by this map is that modern seismicity distribution gives no indication of the past large crustal earthquakes in central Vancouver Island and the North Cascades.

Figure 146 does emphasize the advantage of both accurate locations and an understanding of the seismotectonics responsible for crustal earthquakes because, on the SHZ, it is possible to relate a large earthquake to a specific structure, as opposed to having to consider equally likely that the event may occur throughout a given area. We emphasize that figure 146 represents a very incomplete assessment of the source regions of large crustal events. Considerable study of regional geology, local Quaternary studies, and data from regional-scale strain networks, as discussed by Shedlock and Weaver (1989), will be required to reduce the uncertainty in defining source regions for large crustal earthquakes in the Pacific Northwest.

INTERPRETATION AND DISCUSSION OF SOURCE REGIONS

Our definition of the source areas for the three types of earthquakes expected in the Pacific Northwest has relied heavily on historical and instrumental seismicity with reference to the regional tectonic setting. This reliance is most clear with respect to the area of possible intraplate earthquakes. Our existing understanding of the geometry of the Juan de Fuca plate system is sufficient for us to think that events like the 1949 south Puget Sound earthquake may occur anywhere along the length of the subducting plate system. Current interpretations of marine seismic-reflection data (Hyndman and others, 1990; Couch and Riddihough, 1989; Snavely, 1988) show that everywhere offshore, the Juan de Fuca plate is dipping eastward at shallow angles (less than 10°). Onshore, even in areas where the Juan de Fuca plate is currently seismically quiet, inversion of teleseismic *P*-wave arrival times has been interpreted to show that below depths of 40–60 km, the subducting plate is nearly vertical beneath the Cascade Range (Michaelson and Weaver, 1986; Rasmussen and Humphreys, 1988). Furthermore, Crosson and Owens (1987) have suggested that teleseismic waveforms recorded near the central Washington

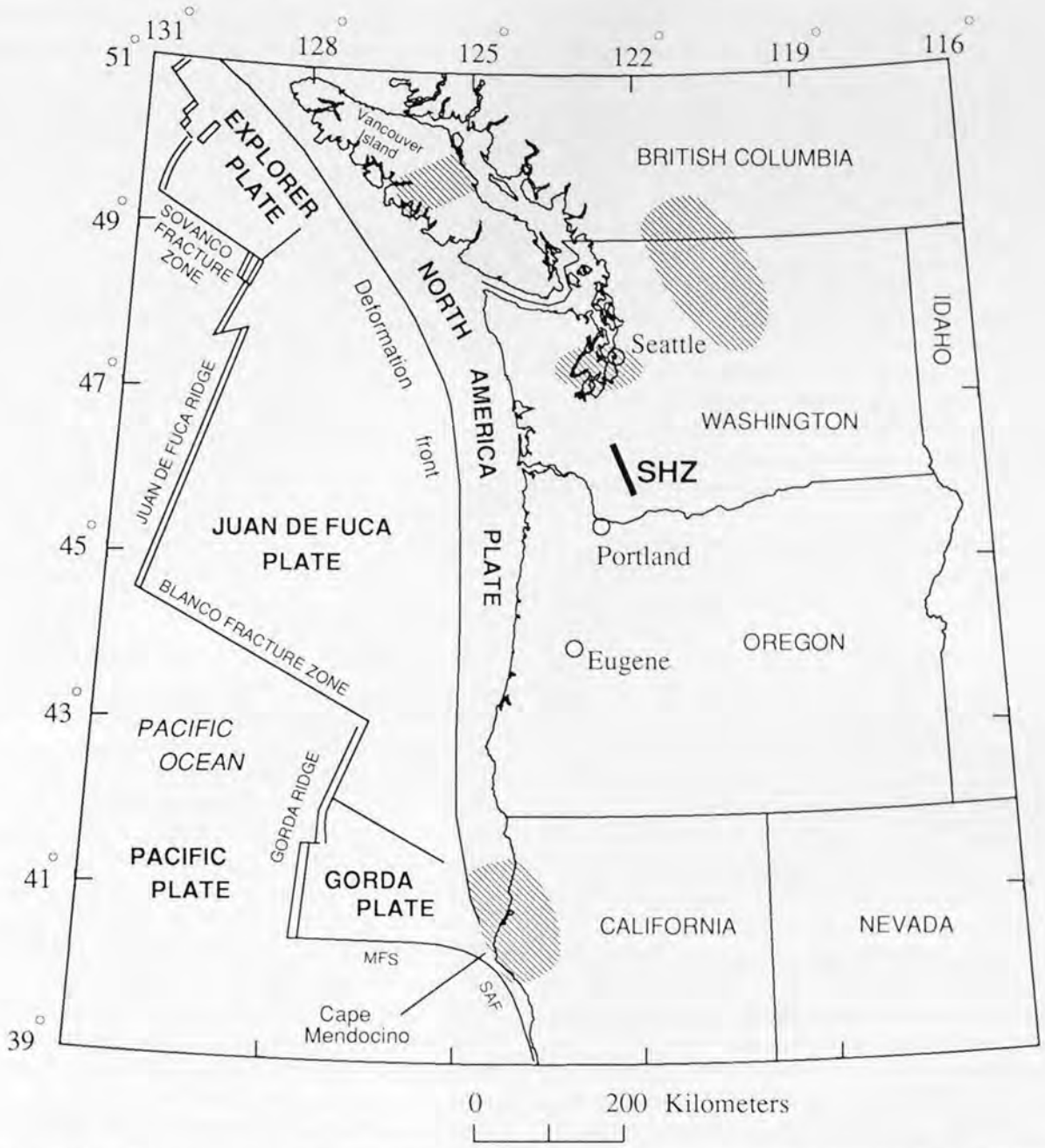

Figure 146. Known source areas (patterned) for crustal earthquakes greater than a magnitude of about 6.5. SHZ, St. Helens seismic zone; MFS, Mendocino fracture zone; SAF, San Andreas fault.

coast are compatible with the hypothesis that the Juan de Fuca plate is continuous (that is, not faulted or offset) south of the arch beneath northwestern Oregon. Thus, despite variations in the dip of the upper part of the plate, the known or interpreted characteristics of the Juan de Fuca plate argue strongly for the existence of a subducting plate capable of producing intraplate tensional stresses along the down-dip axis of the plate (see Spence, 1987, for a discussion of plate stresses). Indeed, if the 1873 earthquake at the Oregon-California border (fig. 138) was an intraplate earthquake, as suggested by Ludwin and others (1991), then the currently seismically quiet part of the subducting plate system had the second largest Benioff-zone earthquake in historical times.

Any link between the segmented nature of the crustal-earthquake distribution and sources for either subduction-zone events or crustal earthquakes is unclear. With respect to crustal earthquakes, the segmentation outlined by Weaver and others (1990) is similar to the division of the Cascade Range suggested by Guffanti and Weaver (1988). These authors used differences in the distribution and composition

of late Cenozoic volcanic vents (less than 5 Ma) to divide the Cascade Range into five segments. These volcanic segments were the same as those suggested here, except that Guffanti and Weaver (1988) had two segments in northern California. In fact, isostatic residual-gravity anomalies (Blakely and Jachens, 1990) and the variations in the volume of Quaternary volcanism (Sherrod and Smith, 1990) in the Cascade Range can be used to divide the Cascade Range into segments identical to those of Guffanti and Weaver (1988). Apparently, the segmentation suggested by the seismicity pattern in the Pacific Northwest must be reflecting the same regional tectonic framework that fundamentally shaped the distribution and volume of late Cenozoic volcanism. The components of this tectonic framework (variations in crustal stress, changes in crustal structure) have left their mark in the middle and upper crust, expressed today by the gravity field and, to a lesser extent, by regional heat flow (Blackwell and others, 1990).

The link between the regional seismotectonic fabric and late Cenozoic volcanism is likely to be particularly important in assessing the earthquake hazards in areas of the Pacific Northwest with few earthquakes in the available historical record. The Portland, Oreg., area is a clear example of the need to understand this link. A recent study of seismicity in the region around Portland has concluded that there may be a series of en echelon strike-slip fault zones southwest of the SHZ (Yelin and Patton, 1991). The Portland Hills fault, a few kilometers west of downtown Portland, shows at least Pliocene offsets (Sherrod and Pickthorn, 1989) and is nearly parallel to the possible en echelon seismic zones.

The Portland area has a history of moderate-magnitude earthquakes (about 5+). A recent earthquake in the heavily urbanized area occurred in 1962 (the most recent moderate-magnitude event occurred southeast of Portland in 1993 along the foothills of the Cascade Range; see Rogers and others, this volume). The 1962 earthquake was probably a normal faulting event (Yelin and Patton, 1991), compatible with the hypothesis that the Portland basin formed by crustal extension. Localized crustal extension may also explain the occurrence of late Cenozoic basaltic volcanism in the Portland urban area, far west of the Cascade Range axis. In contrast to this result favoring crustal extension, the preliminary focal mechanism calculated for the 1993 earthquake southeast of Portland has a combination of thrust and strike-slip motion (Madin and others, 1993), with a north-striking direction of maximum horizontal compression. These two focal mechanisms underscore the ambiguous relation among contemporary seismicity distribution, structural features such as the Portland basin and the Portland Hills fault zone, and basaltic volcanism. It is clear that the area warrants continued seismic monitoring to determine more completely the seismotectonic relations and the associated earthquake hazards.

The segmentation interpreted from the seismicity pattern may provide additional justification for assumptions that are made for modeling ground shaking from crustal earthquakes. In areas where faults are not well exposed at the surface, a region must be divided into subregions with different source characteristics (for example, Algermissen and others, 1982). Commonly, these divisions reflect geologic boundaries and the maximum-magnitude earthquake expected within each subregion. If seismic segmentation is related to broad regional processes or structures, then these processes or structures will be a further constraint that can be used in determining subregions for ground-motion modeling. In addition, the segmentation may determine boundaries for the use of different modeling techniques. For example, across southwestern Washington and northwestern Oregon, the definition of discrete seismic zones (as defined by earthquakes) will likely provide a framework within which maximum-magnitude events can be estimated from an interpretation of seismicity patterns, geologic mapping, and crustal-structure studies. In northwestern Washington, however, the lack of recognized seismic zones makes likely a continued reliance largely on an areal approach to hazard estimation. Clearly, a more complete characterization of the crustal structure and regional tectonics is the key to understanding the generation of the two widely disparate seismicity patterns found in northwestern and southwestern Washington. A second point concerns the possible segmentation of the Cascadia subduction-zone thrust interface. If any of the processes responsible for the segmentation observed across the Cascade Range are the result of the direct interaction of the Juan de Fuca plate system with the North America plate, then perhaps some fundamental rupture length along the coast might reflect this segmentation.

We emphasize that the source regions we have shown for the three earthquake types are part of a major revision of the understanding of earthquake hazards facing the Pacific Northwest. As noted by Heaton and Hartzell (1987), great subduction-zone earthquakes will have shaking effects that are felt over much of western Washington, western Oregon, northwestern California, and southwestern British Columbia. With these earthquakes will likely come locally generated tsunamis that will wash over many of the coastal communities, with only minutes of warning (Heaton and Hartzell, 1987). The possibility of these great subduction earthquakes alone is enough to warrant a thorough reexamination of building codes and earthquake-preparedness programs throughout the region. We believe that it is critically important that this reexamination begin immediately in urban areas in the Willamette Valley such as Eugene, Salem, and Portland because these cities were not included in earlier studies undertaken in the Puget Sound region (Hopper and others, 1975) that at least have allowed local governments to

be aware of some of the potential problems from earthquakes. The fact that Willamette Valley cities have not had the larger magnitude earthquakes found in other parts of the Pacific Northwest (Puget Sound, North Cascades, northern California) should not be a justification for delaying reassessments of hazards. As the March 1993 event southeast of Portland has clearly shown, many cities in Oregon are particularly vulnerable, even to relatively small ground motions caused by moderate earthquakes. We reiterate that the short-term seismic record in the Pacific Northwest cannot be viewed as representative of the long-term risk of large earthquakes. The September 1993 earthquakes near Klamath Falls (Rogers and others, this volume), occurring in an area essentially without historical seismicity, have served to emphasize the shortcomings of the historical record in the Pacific Northwest. Also, our judgment that the entire part of the subducting Juan de Fuca plate capable of producing intraplate earthquakes like those of 1949 and 1965 in the Puget Sound basin, coupled with the uncertainty surrounding the extent of the areas where large crustal earthquakes should be expected, gives added urgency for a region-wide reexamination of the hazards posed by earthquakes.

Finally, there may be other potential seismic source zones in the Pacific Northwest that may ultimately be important in earthquake-hazard assessments. One such zone is west of the deformation front (fig. 138), in the nearly flat-lying part of the Juan de Fuca and Gorda plates. Earthquakes in this part of the tectonic plates were referred to as "oceanic intraplate" by Astiz and others (1988). This zone is particularly active off the coast of northern California. But, as noted above, oceanic intraplate earthquakes in the historical record have caused relatively little damage to onshore facilities. Nevertheless, as the collapse of the highway bridge during the 1980 Eureka earthquake indicated, these events must be acknowledged in hazards assessments along the northern coast of California. Earthquakes are sparse within the Juan de Fuca plate west of the deformation front off the Oregon and Washington coasts (Spence, 1989). Because so few earthquakes are known off the Oregon and Washington coasts and the tectonic setting of these intraplate events is very uncertain, it is not yet possible to assess how important events west of the deformation front may be in the overall earthquake-hazards assessment of the Pacific Northwest. However, if the historical record of damage resulting from earthquakes in this zone in northern California is similar for Oregon and Washington, combined with the fact that the distance between the deformation front and the coastline steadily increases northward from Cape Mendocino, then it is likely that oceanic intraplate events will be considerably less important in most of the Pacific Northwest as compared with the three zones discussed in this chapter.

SUMMARY

In the convergent-margin setting of the Cascadia subduction zone, three distinct earthquake sources are possible: (1) earthquakes at the interface between the Juan de Fuca and North America plate; (2) earthquakes within the crust of the overlying North America plate; and (3) earthquakes within the subducting Juan de Fuca plate. The probable source region for earthquakes within the Juan de Fuca plate is the best known, as we are able to combine the historical data from the 1949 and 1965 earthquakes with the modern instrumental record. The latter data have been used to infer the geometry of the Juan de Fuca plate, whereas the historical data have been used to deduce that the large-magnitude earthquakes occur at least in part in response to down-dip tensional forces within the subducting plate. We suggest that the entire subduction zone, at depths between 45 and 60 km, is capable of producing these events.

Despite many unresolved issues surrounding great subduction-zone interface earthquakes, the available geologic record, combined with the plate-tectonic setting, is interpreted as evidence that these events have occurred in the late Holocene along the coast. Because these events occur on the shallow-dipping part of the plate interface, their general location is well known. Subduction-zone earthquakes represent a major threat to the population of the Pacific Northwest, one that has not been integrated into current hazard assessments. A program to accomplish this integration must consider the large size of the source region for these earthquakes. The possibility of large crustal earthquakes in the Pacific Northwest urban areas also remains very poorly studied.

REFERENCES CITED

Algermissen, S.T., 1988, Estimation of ground shaking in the Pacific Northwest, *in* Hays, W.W., ed., Proceedings of Conference XLII, Workshop on evaluation of earthquake hazards and risk in the Puget Sound and Portland areas: U.S. Geological Survey Open-File Report 88–541, p. 43–51.

Algermissen, S.T., Harding, S.T., Steinbrugge, L.V., and Cloud, W.K., 1965, The Puget Sound, Washington, earthquake of 29 April, 1965: Washington, D.C., U.S. Coast and Geodetic Survey, 51 p.

Algermissen, S.T., Perkins, D.M., Thenhaus, P.C., Hanson, S.L., and Bender, B.L., 1982, Probabilistic estimates of maximum acceleration and velocity in rock in the contiguous United States: U.S. Geological Survey Open-File Report 82–1033, 99 p.

Astiz, Luciana, Lay, Thorne, and Kanamori, Hiroo, 1988, Large intermediate depth earthquakes and the subduction process: Physics of the Earth and Planetary Interiors, v. 53, no. 1/2, p. 80–166.

Atwater, B.F., 1987, Evidence for great Holocene earthquakes along the outer coast of Washington State: Science, v. 236, no. 4804, p. 942–944.

Atwater, B.F., and Moore, A.L., 1992, A tsunami about 1000 years ago in Puget Sound, Washington: Science, v. 258, no. 5088, p. 1614–1617.

Baker, G.E., and Langston, C.A., 1987, Source parameters of the 1949 magnitude 7.1 south Puget Sound, Washington, earthquake as determined from long-period body waves and strong ground motions: Seismological Society of America Bulletin, v. 77, no. 5, p. 1530–1557.

Blackwell, D.D., Steele, J.L., Frohme, M.K., Murphy, C.F., Priest, G.R., and Black, G.L., 1990, Heat flow of the Oregon Cascade Range and its correlation with regional gravity, Curie point depths, and geology: Journal of Geophysical Research, v. 95, no. B12, p. 19475–19493.

Blakely, R.J., and Jachens, R.C., 1990, Volcanism, isostatic residual gravity, and regional tectonic setting of the Cascade volcanic province: Journal of Geophysical Research, v. 95, no. B12, p. 19439–19451.

Bucknam, R.C., Hemphill-Haley, Eileen, and Leopold, E.B., 1992, Abrupt uplift within the past 1700 years at southern Puget Sound, Washington: Science, v. 258, no. 5088, p. 1611–1614.

Byrne, D.E., Davis, D.M., and Sykes, L.R., 1988, Loci and maximum size of thrust earthquakes and the mechanics of the shallow region of subduction zones: Tectonics, v. 7, no. 4, p. 833–857.

Cassidy, J.F., Ellis, R.M., and Rogers, G.C., 1988, The 1918 and 1957 Vancouver Island earthquakes: Seismological Society of America Bulletin, v. 78, no. 2, p. 617–635.

Cockerham, R.S., 1984, Evidence for a 180-km-long subducted plate beneath northern California: Seismological Society of America Bulletin, v. 74, no. 2, p. 569–576.

Coffman, J.L., Hake, C.A. von, and Stover, C.W. (editors), 1982, Earthquake history of the United States: Washington, D.C., U.S. National Oceanic and Atmospheric Administration and U.S. Geological Survey Publication 41-1, Revised edition, 270 p.

Couch, R.W., and Riddihough, R.P., 1989, The crustal structure of the western continental margin of North America, *in* Pakiser, L.C., and Mooney, W.D., eds., Geophysical framework of the continental United States: Boulder, Colo., Geological Society of America Memoir 172, p. 103–128.

Crosson, R.S., and Owens, T.J., 1987, Slab geometry of the Cascadia subduction zone beneath Washington from earthquake hypocenters and teleseismic converted waves: Geophysical Research Letters, v. 14, no. 8, p. 824–827.

Eaton, J.P., 1989, Dense microearthquake network study of northern California earthquakes, Chap. 13 *of* Litehiser, J.J., ed., Observatory seismology—A centennial symposium for the Berkeley seismographic stations: Berkeley, University of California Press, p. 199–224.

Ellsworth, W.L., 1990, Earthquake history, 1769–1989, *in* Wallace, R.E., ed., The San Andreas fault system, California: U.S. Geological Survey Professional Paper 1515, p. 153–187.

EMSLAB Group, 1988, The EMSLAB electromagnetic sounding experiment: EOS [American Geophysical Union Transactions], v. 69, no. 7, p. 89–99.

Gower, H.D., Yount, J.C., and Crosson, R.S., 1985, Seismotectonic map of the Puget Sound region, Washington: U.S. Geological Survey Miscellaneous Investigations Series Map I–1613, 15 p., scale 1:250,000.

Grant, W.C., Atwater, B.F., Carver, G.A., Darienzo, M.E., Nelson, A.R., Peterson, C.D., and Vick, G.S., 1989, Radiocarbon dating of late Holocene coastal subsidence above the Cascadia subduction zone—Compilation for Washington, Oregon, and northern California [abs.]: EOS [American Geophysical Union Transactions], v. 70, no. 43, p. 1331.

Guffanti, MaryAnn, and Weaver, C.S., 1988, Distribution of late Cenozoic volcanic vents in the Cascade Range—Volcanic arc segmentation and regional tectonic considerations: Journal of Geophysical Research, v. 93, no. B6, p. 6513–6529.

Gutenberg, Beno, and Richter, C.F., 1954, Seismicity of the Earth (2d ed.): Princeton, N.J., Princeton University Press, 654 p.

Harding, S.H., Urban, T.C., and Diment, W.H., 1988, Evidence of recent tectonic deformation in the Puget Sound from seismic-reflection profiles [abs.]: EOS [American Geophysical Union Transactions], v. 69, no. 44, p. 1314.

Heaton, T.H., 1990, Calm before the quake?: Nature, v. 343, no. 6258, p. 511–512.

Heaton, T.H., and Kanamori, Hiroo, 1984, Seismic potential associated with subduction in the Northwestern United States: Seismological Society of America Bulletin, v. 74, no. 3, p. 993–941.

Heaton, T.H., and Hartzell, S.H., 1986, Source characteristics of hypothetical subduction earthquakes in the Northwestern United States: Seismological Society of America Bulletin, v. 76, no. 3, p. 675–708.

———1987, Earthquake hazards on the Cascadia subduction zone: Science, v. 236, no. 4798, p. 162–168.

Hill, D.P., Eaton, J.P., Ellsworth, W.L., Cockerham, R.S., Lester, F.W., and Corbett, E.J., 1991, The seismotectonic fabric of central California, *in* Slemmons, D.B., Engdahl, E.R., Zoback, M.D., and Blackwell, D.D., eds., Neotectonics of North America: Boulder, Colo., Geological Society of America, p. 107–132.

Hopper, M.G., Algermissen, S.T., Perkins, D.M., Brockman, S.R., and Arnold, E.P., 1982, The earthquake of December 14, 1872, in the Pacific Northwest [abs.]: Seismological Society of America, Annual meeting, 1982.

Hopper, M.G., Langer, C.J., Spence, W.J., Rogers, A.M., and Algermissen, S.T., 1975, A study of earthquake losses in the Puget Sound, Washington, area: U.S. Geological Survey Open-File Report 75–375, 298 p.

Hyndman, R.D., Yorath, C.J., Clowes, R.M., and Davis, E.E., 1990, The northern Cascadia subduction zone at Vancouver Island—Seismic structure and tectonic history: Canadian Journal of Earth Sciences, v. 27, no. 3, p. 313–329.

Isacks, Brian, and Molnar, Peter, 1971, Distribution of stresses in the descending lithosphere from a global survey of focal-mechanism solutions of mantle earthquakes: Geophysics and Space Physics Reviews, v. 9, no. 1, p. 103–174.

Jacoby, G.C., Williams, P.L., and Buckley, B.M., 1992, Tree ring correlation between prehistoric landslides and abrupt tectonic events in Seattle, Washington: Science, v. 258, no. 5088, p. 1621–1623.

Ludwin, R.S., Weaver, C.S., and Crosson, R.S., 1991, Seismicity of Washington and Oregon, *in* Slemmons, D.B., Engdahl, E.R., Blackwell, D.D., and Schwartz, D.P., eds, Neotectonics of North America: Boulder, Colo., Geological Society of America, Decade of North American Geology, p. 77–98.

Madin, I.P., Priest, G.R., Mabey, M.A., Malone, Steve, Yelin, T.S., and Meier, Dan, 1993, March 25, 1993, Scotts Mills

earthquake—Western Oregon's wake-up call: Oregon Geology, v. 55, no. 3, p. 51–57.

Malone, S.D., and Bor, S.S., 1979, Attenuation patterns in the Pacific Northwest based on intensity data and the location of the 1872 North Cascades earthquake: Seismological Society of America Bulletin, v. 69, no. 2, p. 531–546.

Michaelson, C.A., and Weaver, C.S., 1986, Upper mantle structure from teleseismic *P*-wave arrivals in Washington and northern Oregon: Journal of Geophysical Research, v. 91, no. B2, p. 2077–2094.

Milne, W.G., 1956, Seismic activity in Canada west of the 113th meridian, 1841–1951: Ottawa, Canada, Dominion Observatory Publication, v. 18, no. 7, p. 119–127.

Mooney, W.D., and Weaver, C.S., 1989, Regional crustal structure and tectonics of the Pacific coastal States, California, Oregon, and Washington, *in* Pakiser, L.C., and Mooney, W.D., eds., Geophysical framework of the continental United States: Boulder, Colo., Geological Society of America Memoir 172, p. 129–161.

Murphy, L.M., and Ulrich, F.P., 1951, United States earthquakes 1949: U.S. Department of Commerce, Coast and Geodetic Survey, no. 748, 64 p.

Noson, L.L., Qamar, A.I., and Thorsen, G.W., 1988, Washington State earthquake hazards: Washington Division of Geology and Earth Resources, Information Circular 85, 77 p.

Nuttli, O.W., 1952, The western Washington earthquake of April 13, 1949: Seismological Society of America Bulletin, v. 42, no. 1, p. 21–28.

Oppenheimer, D.H., Beroza, G.C., Carver, G.A., Dengeler, Lori, Eaton, J.P., Gee, Lind, Gonzalez, F.I., Jayko, A.S., Li, W.H., Lisowski, Michael, Magee, M.E., Marshall, G.A., Murray, M.H., McPherson, Robert, Romanowicz, Barbara, Satake, Karji, Simpson, R.W., Somerville, P.G., Stein, R.S., and Valentine, David, 1993, The Cape Mendocino, California, earthquakes of April 1992—Subduction at the triple junction: Science, v. 261, no. 5120, p. 433–438.

Perkins, D.M., Thenhaus, P.C., Hanson, S.L., Ziony, J.I., and Algermissen, S.T., 1980, Probabilistic estimates of maximum seismic horizontal ground motion on rock in the Pacific Northwest and the adjacent outer continental shelf: U.S. Geological Survey Open-File Report 80–471, 40 p.

Potter, C.J., Sanford, W.E., Yoos, T.R., Prussen, E.L., Keach, W.R, Oliver, J.E., Kaufman, Sidney, and Brown, L.D., 1986, COCORP deep seismic reflection transverse of the interior of the North American cordillera, Washington and Idaho—Implications for orogenic evolution: Tectonics, v. 5, no. 7, p. 1007–1025.

Rasmussen, J.R., and Humphreys, E.D., 1988, Tomographic image of the Juan de Fuca plate beneath Washington and western Oregon using teleseismic *P*-wave travel times: Geophysical Research Letters, v. 15, no. 12, p. 1417–1420.

Rogers, G.C., 1983a, Some comments on the seismicity of the northern Puget Sound-southern Vancouver Island region, *in* Yount, J.C., and Crosson, R.S., eds., Proceedings of Workshop XIV, Earthquake hazards of the Puget Sound region, Washington: U.S. Geological Survey Open-File Report 83–19, p. 19–39.

———1983b, Seismotectonics of British Columbia: Vancouver, University of British Columbia, Ph.D. dissertation, 247 p.

Rogers, G.C., and Hasegawa, H.S., 1978, A second look at the British Columbia earthquake of June 23, 1946: Seismological Society of America Bulletin, v. 68, no. 3, p. 653–675.

Savage, J.C., Lisowski, Michael, and Prescott, W.H., 1981, Geodetic strain measurements in Washington: Journal of Geophysical Research, v. 86, no. B6, p. 4929–4940.

Schuster, R.L., Logan, R.L., and Pringle, P.T., 1992, Prehistoric rock avalanches in the Olympic Mountains, Washington: Science, v. 258, no. 5088, p. 1620–1621.

Shedlock, K.M., and Weaver, C.S., 1989, Rationale and outline of a program for earthquake hazards assessment in the Pacific Northwest, *in* Hays, W.W., ed., Proceedings of Conference XLVIII, 3d annual workshop on earthquake hazards in the Puget Sound, Portland area: U.S. Geological Survey Open-File Report 89–465, p. 2–10.

Shedlock, K.M., Weaver, C.S., Oppenheimer, David, and King, G.C.P., 1989, Seismic deformation in the Pacific Northwest [abs.]: EOS [American Geophysical Union Transactions], v. 70, no. 43, p. 1330.

Sherrod, D.R., and Pickthorn, L.B., 1989, Some notes on the Neogene structural evolution of the Cascade Range in Oregon, *in* Muffler, L.J.P., Weaver, C.S., and Blackwell, D.D., eds., Proceedings of Workshop XLIV, Geological, geophysical, and tectonic setting of the Cascade Range: U.S. Geological Survey Open-File Report 89–178, p. 351–368.

Sherrod, D.R., and Smith, J.G., 1990, Quaternary extrusion rates from the Cascade Range, Northwestern United States and southern British Columbia: Journal of Geophysical Research, v. 95, no. B12, p. 19465–19474.

Simon, R.B., 1981, Intensity survey for 8 November 1980 Eureka, California earthquake [abs.]: Earthquake Notes, v. 52, no. 1, p. 44.

Snavely, P.D., Jr., 1987, Tertiary geologic framework, neotectonics, and petroleum potential of the Oregon-Washington continental margin, *in* Scholl, D.W., Grantz, Arthur, and Vedder, J.G., eds., Geology and resource potential of the continental margin of western North America and adjacent ocean basins—Beaufort Sea to Baja California: Houston, Tex., Circum-Pacific Council for Energy and Mineral Resources, Earth Science Series, v. 6, no. 6, p. 305–335.

Spence, William, 1987, Slab pull and the seismotectonics of subducting lithosphere: Reviews of Geophysics and Space Physics, v. 25, no. 1, p. 55–69.

———1989, Stress origins and earthquake potential in Cascadia: Journal of Geophysical Research, v. 94, p. 3076–3088.

Toppozada, T.R., Real, C.R., and Parke, D.L., 1981, Preparation of isoseismal maps and summaries of related effects of pre-1900 California earthquakes: California Division of Mines and Geology Open-File Report 81–11, 101 p.

Uhrhammer, R.A., 1991, Seismicity of northern California, *in* Slemmons, D.B., Engdahl, E.R., Zoback, M.D., and Blackwell, D.D., eds., Neotectonics of North America: Boulder, Colo., Geological Society of America, p. 99–106.

Ulrich, F.P., 1949, Reporting the Northwest earthquake [article in Building Standards Monthly, June 1949], Reprinted in 1986 *in* Thorson, G.W., comp., The Puget lowland earthquakes of 1949 and 1965—Reproduction of selected articles describing damage: Washington Division of Geology and Earth Resources Information Circular 81, p. 19–23.

Walter, S.R., 1986, Intermediate-depth focus earthquakes associated with Gorda plate subduction in northern California: Seismological Society of America Bulletin, v. 76, no. 2, p. 583–588.

Weaver, C.S., and Baker, G.E., 1988, Geometry of the Juan de Fuca plate beneath Washington and northern Oregon from seismicity: Seismological Society of America Bulletin, v. 78, no. 1, p. 264–275.

Weaver, C.S., Grant, W.C., and Shemeta, J.E., 1987, Local crustal extension at Mount St. Helens, Washington: Journal of Geophysical Research, v. 92, no. B10, p. 10170–10178.

Weaver, C.S., Green, S.M., and Iyer, H.M., 1982, Seismicity of Mount Hood and structure as determined from teleseismic *P* wave delay studies: Journal of Geophysical Research, v. 87, no. B4, p. 2782–2792.

Weaver, C.S., Norris, R.D., and Jonientz-Trisler, C., 1990, Results of seismological monitoring in the Cascade Range, 1960–1989—Earthquakes, eruptions, avalanches and other curiosities: Geoscience Canada, v. 17, no. 3, p. 158–162.

Weaver, C.S., and Smith, S.W., 1983, Regional tectonic and earthquake hazards implications of a crustal fault zone in southwestern Washington: Journal of Geophysical Research, v. 88, no. B12, p. 10371–10383.

Yelin, T.S., and Patton, H.J., 1991, Seismotectonics of the Portland, Oregon region: Seismological Society of America Bulletin, v. 81, no. 1, p. 109–130.

Zollweg, J.E., and Johnson, P.A., 1989, The Darrington seismic zone in northwestern Washington: Seismological Society of America Bulletin, v. 79, no. 6, p. 1833–1845.

Edited by John Synnefakis and Barbara Hillier
Graphics prepared by Carol A. Quesenberry and Mari Kauffmann
Plates prepared by Patricia L. Wilber and Michael Kirtley
Photocomposition by Carol A. Quesenberry, Mari Kauffmann, and Shelly Fields
Book design by Carol A. Quesenberry

☆ U.S. GOVERNMENT PRINTING OFFICE: 1996 - 774-045 / 20058 REGION NO. 8